Fall 2017

Impact of vertical internals on the hydrodynamics and heat transfer coefficient in a gas-solid fluidized bed

Haidar Moafaq Taofeeq

Department: Chemical and Biochemical Engineering

IMPACT OF VERTICAL INTERNALS ON THE HYDRODYNAMICS AND HEAT TRANSFER COEFFICIENT IN A GAS-SOLID FLUIDIZED BED

by

HAIDAR MOAFAQ TAOFEEQ

A DISSERTATION

Presented to the Faculty of the Graduate School of the

MISSOURI UNIVERSITY OF SCIENCE AND TECHNOLOGY

In Partial Fulfillment of the Requirements for the Degree

DOCTOR OF PHILOSOPHY
in
CHEMICAL ENGINEERING

2017

Approved by
Muthanna Al-Dahhan, Advisor
Joontaek Park
Sutapa Barua
Fateme Rezaei
Kakkattukuzhy Isaac

PUBLICATION DISSERTATION OPTION

This dissertation consists of following seven articles that may be submitted for publishing in the future:

Paper I, pages 10-78. The impact of vertical internals on the key hydrodynamic parameters in a gas-solid fluidized bed using an advance optical fiber probe.

Paper II, pages 79-147. Heat transfer and hydrodynamics in a gas-solid fluidized bed with vertical immersed internals.

Paper III, pages 148-210. Flow regimes in gas-solid fluidized bed with vertical internals.

Paper IV, pages 211-281. Effect of vertical internals on the pressure drop in gas–solid fluidized.

Paper V, pages 282-316. Comparison between the new mechanistic and the chaos scale-up methods for gas-solid fluidized beds.

ABSTRACT

This research studied the impact of the dense vertical immersed heat exchanging tubes on the gas and solids hydrodynamic characteristics, flow regime, pressure drop, and heat transfer in a 0.14 m inside diameter gas-solid fluidized bed column of. Two sizes of vertical internal tube bundles (0.0127 and 0.0254 m) of circular arrangement have been implemented to represent the heat exchange tubes covering 25% of the column cross-sectional area. The experimental work was achieved at different operating conditions and various solids particle types that differ in average particle size, solids density, particles shape, and particles sphericity. The experimental measurements were performed using various kinds of measurement techniques such as advanced optical fiber probe for local solids and bubble hydrodynamics measurements, differential pressure transducer for pressure fluctuation measurements, advanced fast response heat transfer probe for local heat transfer coefficient measurements, probe-single ended and probe-differential pressure transducers for measuring the pressure fluctuations and pressure drop inside the bed.

It was found that the immersed vertical tubes have a significant effect on the studied hydrodynamics parameters (solids velocity, solids and gas holdups, bubbles velocity, bubble frequency, and bubble chord length), flow regime, pressure drop and heat transfer coefficients inside the gas-solid fluidized bed. In which, the vertical internals improve the heat transfer performance, increase the heat transfer coefficient, reduce the pressure drop, affect the flow regimes and their transition velocities, as well as enhance the performance of the gas-solid fluidization process by improving the studied local hydrodynamic characteristics.

ACKNOWLEDGMENTS

First of all, I would like to thank my God (ALLAH) for his mercy, kindness and so many blessings in my life.

Throughout my studying and staying here at Missouri University of Science and Technology, many people have supported me both academically and personally and inspired me. I would like to deeply thank and expression of gratitude to my advisor, Professor Muthanna H. Al - Dahhan, first, for gave me an opportunity to conduct this research under his supervision. Second, he encouraged, helped, and supported me morally and financially through my PhD studying. Without his guidance and continual help, this thesis would not have been possible.

I would also like to acknowledge the members of my committee, namely, Dr. Joontaek Park, Dr. Sutapa Barua, Dr. Fateme Rezaei and Dr. Kakkattukuzhy Isaac, for taking interest in my work and examining my dissertation.

I would like to thank and appreciate the opportunity that has given to me by the higher committee for education development in Iraq (HCED) and Nahrain University to complete my PhD degree in United States.

Special thanks to my friends and colleagues in Iraq and here in the Untied States for their continued and untiring support during tough times.

I express a deep sense of appreciation to family in Iraq (my parents and sisters) for their support and encouragement throughout my studying years. Finally, thanks to my wife and my kids, who stood by my side all the time during my studying period, for believing in me and for supporting my ideas and dreams. They were always the breath of fresh air that sailed me through my long PhD Journey.

TABLE OF CONTENTS

LIST OF ILLUSTRATIONS

Paper IV

Paper V

LIST OF TABLES

NOMENCLATURE

Symbol	Description
Ar	Archimedes number of the solid particles
D	inside column diameter (m)
Dc	inside column diameter (m)
Di	Internal diameter (m)
d_p	particle mean diameter or average particle diameter (μm)
D_T	tube diameter (m)
g	gravitational force (m/s^2)
H	Static bed height (mm)
L_e	Effective distance (m)
h	heat transfer coefficient (W/m^2 K)
L	column height (m)
r	radial position (m)
R	radius of the column (m)
Re_c	Reynolds number of solid particles at transition fluidized velocity (U_c)
Re_{mf}	Reynolds number of solid particle at minimum fluidized velocity (U_{mf})
u	superficial gas velocity (m/s)
U_B	bubble velocity (m/s)
U_c	transition velocity or turbulent transition velocity (m/s)
U_{mb}	minimum bubbling velocity (m/s)
U_{mf}	minimum fluidization velocity (m/s)
u_{mf}	minimum fluidized velocity (m/s)

U_{slug}	minimum slugging velocity (m/s)
V_{avg}	Average voltage, volts
V_i	Voltage from the probe tips, volts
V_{max}	Maximum voltage, volts
V_{min}	Minimum voltage, volts
Vp	Particles velocity (m/s)
z	Axial distance (m)
Δp	pressure drop (KPa)
θ	Azimuthal distance (m)
μ	gas viscosity (Kg/m.s)
μ_g	gas viscosity (Kg/m.s)
ρ	gas density (Kg/m^3)
ρ_f	fluid density (Kg/m^3)
ρ_g	gas density (Kg/m3)
ρ_p	solid particle density or solid density (Kg/m^3)
ρ_s	Solid particle density (Kg/m^3)

Greek Letters

t	Delay time, sec
ε	gas holdup
ε_s	solid holdup
θ	Azimuthal distance (m)
μ	viscosity (Kg/m.s)

ρ	Density (Kg/m^3)
φ	sphericity

Subscripts and Superscripts

B	bubble
c	minimum turbulent fluidization
Inversion	inversion point
mb	minimum bubbling
mf	minimum fluidization
p	particle
f	fluid
s	solid
slug	minimum slugging

Abbreviations

%PR	Percentage pressure drop
$\overline{V_p}$	cross-sectional average particles velocity
$\overline{\varepsilon_s}$	cross-sectional average solid holdup
$\overline{\mathrm{BF}}$	cross-sectional average bubble rise velocity frequency
$\overline{\mathrm{BMS}}$	cross-sectional average bubble mean size
$\overline{\mathrm{BRV}}$	cross-sectional average bubble rise velocity
Eu	Euler number
FCC	fluid catalytic cracking

Fr	Froude number
ID	inside diameter
KE	Kolmogorov entropy
MRD	Mean relative deviation
SD	standard deviation

1. INTRODUCTION

In the recent years, energy request is expanding because of increasing energy utilization in the US, China, India, and other developing nations. The question emerges with respect to the accessibility of extra energy sources. Parallel with that, there are expanding worries about atmosphere changes, and also contamination and the ecological impacts of petroleum derivatives. Therefore, governments worldwide are continually searching for a safe and economic energy source. Coal use represents up 16 % of U.S. energy consumption while natural gas represents up to 29 % in 2015 as appeared in Figure 1.1. Sustainable power source utilization of U.S. about contributed up to 10 % where 49 % of them was biomass, which was consumed by different industrial applications to produce heat and steam. Biomass is likewise utilized for delivering transportation energies (ethanol and biodiesel) and for giving private and business space warming. Biomass is one of the choices among sustainable power sources (Figure 1.1) and is the fourth biggest essential energy resource on the planet, after coal, oil, and gas. One of the routes for using coal, petroleum gas and biomass is its conversion to syngas gas (a blend of CO and H_2) by gasification (partial or complete oxidation). For all these processes and other vast number of industrial processes, gas-solid fluidized beds have found applications.

For example, the fluidized bed is considered one of the most promising reactors to gasify coal and biomass and to convert them to syngas gases. Additionally, one route of converting syngas gas to fuel is by utilizing fluidized beds at high temperature via high-temperature Fisher-Tropsch (FT). In addition, fluidized bed reactors have been widely utilized in many industrial applications, such as drying of solids, combustion, catalytic reactions, gasification, coating, and many other processes (Mohanty et al. 2009). Today

high-pressure fluidized beds are considered the reactors of choice for cleaner coal utilization for combustion and for gasification to generate syngas.

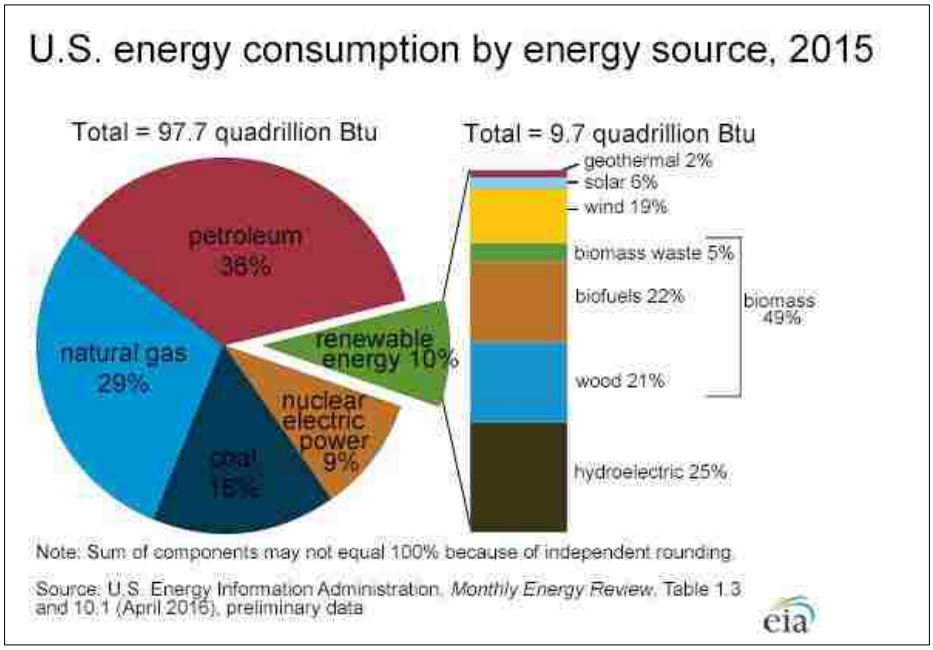

Figure 1.1. U.S. energy consumption by energy source (Source: U. S. energy information administration)

Consequently, the gas–solid fluidization beds have been implemented in various commercial processes due to their several advantages such as; excellent gas–solid mixing, which leads to high contact efficiency between gas and solid phases, the local temperature distribution and heat transfer rate are high, as well, comparing with another chemical process, which utilizes solid catalysts, the particles size used in the fluidized bed is much smaller than that which is used in fixed-bed systems. These beds affords less resistance to the diffusion of gas through solid particles (less pressure drop) and yields a high mass transfer (Mathew, Begum, and Anantharaman 2014).

Generally, in the chemical industry, there are two types of processes that utilized fluidized bed reactors, catalytic and non-catalytic gas-solid fluidized bed reactors. In catalytic gas-solid fluidized bed reactors, the solid particles are not engaged in the chemical reaction, e.g. chemical cracking of high molecular weight hydrocarbons to produce different chemical substances. For the non-catalytic reactors, the particles are involved through the chemical reaction, e.g. biomass combustion and coal gasification (Halvorsen 2005). In these types of chemical reactors, the heat transfer is essential to keep the reactor operates under optimum operation conditions and to control the reaction rate of these processes. Therefore, it is completely essential to control the operating temperature in order to ensure reliable efficiency, high yield, and excellent conversion rate. Subsequently, the implementation of heat transfer immersed surfaces with different types (plates, tubes, and baffles), various arrangements and orientation methods inside the fluidized bed reactors (vertical and horizontal) are required (Grace and Harrison 1968; Ozawa et al. 2002; Ozawa et al. 2004; Maurer, Wagner, van Ommen, et al. 2015; Maurer, Wagner, Schildhauer, et al. 2015).

In the recent decades, many types of research have been conducted experimentally and numerically to study the effect of different types and configurations of immersed surfaces on the performance and hydrodynamics of the gas-solid fluidized beds. Volk et al. (1962) is considered the first work that studied the impact of vertical internals in a gas-solid fluidized bed. They reported that the difficulties of the scale-up process could be solved by using vertical internals inside the gas-solid fluidized bed reactor. Glass and Harrison (1964) investigated the gas-solid fluidized bed with horizontal internals using the photographic technique. They concluded that the horizontal immersed tubes could improve

the fluidization quality by reducing the bubble size and thus the heat transfer from bed to immersed surface could be improved. Grace and Harrison (1968) utilized various kinds of internals orientations (vertical, horizontal and inclined) inside the fluidized beds. They found that the vertical and horizontal arrangements are useful, while the inclined orientation has some drawbacks such as excessive gas bypassing, heat transfer reduction and short circuiting of gas bubbles along the undersides of the inclined surfaces. Ramamoorthy and Subramanian (1981); Yates et al. (1984) and Olowson (1994) used different sizes, orientations, and types of internals in beds of different solid particles. They found that the using the immersed surfaces can improve the fluidization process by reducing the bubble size and improve the contact between the gas and dense phase, as well as increase the residence time of the gas phase inside the bed. Law et al. (2003) investigated the effect of vertical immersed baffles on the drying and mixing of Geldart D type powder inside gas-solid fluidized bed dryer. They deduced that the vertical immersed baffles could enhance the contact efficiency between gas and solid particles. In which, the heat and mass transfer rates inside the fluidized bed dryer can be improved accordingly. Yurong et al. (2004) investigated the hydrodynamics of gas-solid fluidized bed with and without vertical internals using computational fluid dynamics simulation. They reported that the using of horizontally immersed tubes as heat-exchange surfaces is essential to absorb the generated heat through the chemical reaction in order to keep the bubbling fluidized bed reactors operate under optimum conditions. Rüdisüli et al. (2012b); Rüdisüli et al. (2012a); Maurer et al. (2015a); Maurer et al. (2015b) and Verma et al. (2016) used different size, tube-to-tube spaces and tube configurations (square and triangular) to investigate the impact of vertical internals on the bubble hydrodynamic characteristics using experimental and

simulation methods. Furthermore, they found that the vertical internals has a significant influence on the bubble hydrodynamic properties, in which the implementation of vertical internals lead to reduce the bubble size, improve the bubble frequency and increase or decrease the bubble rise velocity.

1.1. RESEARCH MOTIVATIONS

Recently, the immersed tubes have been implemented in fluidized bed industrial applications due to many advantage effects on these fluidization processes as mentioned above. The immersed tubes can modify the flow structure of the gas-solid patterns and therefore the hydrodynamic properties of gas and solid phases, flow regimes, heat transfer and pressure drop are typically changed. In general, the utilization of such internals inside the gas-solid fluidized beds has many benefits:

(1) Reducing the bubble size by controlling the bubble growth and minimizing the number of coalescence between bubbles. Therefore, the contact between the gas phase and dense phase would improve consequently (Volk, Johnson, and Stotler 1962; Grace and Harrison 1968). Additionally, the bubble size reduction can decrease the carryover of the solids from the bed and make the fluidization more “smoother” and enhance the heat and mass transfer rates between solid particles, fluidizing gas and immersed surfaces (Yates et al. 1984 and Law et al. 2003).

(2) The internal surfaces can suppress the cross-circulation of solids phase inside the bed, and thus the back mixing of gas phase can be reduced (Grace and Harrison 1968 and Olowson 1994).

(3) The immersed tubes can divide the bed into many small fluidized bed sections, each one can serve as an individual fluidization unit. Consequently, the reaction conversion inside the fluidized bed reactor would be enhanced (Law et al. 2003).

(4) The use of the immersed surfaces can decrease the pressure drop inside the bed, slugging behavior, bed fluctuations and particle elutriation. Moreover, local solids circulation is improved (Ramamoorthy and Subramanian 1981).

Among different orientations of immersed surfaces, it has reported by many experimental and numerical studies that the implementing of vertical tube internals in gas-solid fluidized beds has several advantages such as; (1) The simplicity in design in compared to other geometries. (2) The installation, removal and emptying the bed is comfortable. (3) The dead spots that occurred in other catalytic reactors can be obviated. (4) The occupied volume of vertical internals is considered small in compared to other orientations. (5) Since the bubbles pass the vertical internals tangentially, the tube erosion can minimize by 50% in contrast with horizontal geometry (Rüdisüli et al. 2012b).

Due to many advantages of utilizing vertical immersed tubes inside gas-solid fluidized beds that mentioned earlier, the interest in studying the hydrodynamics of various types of fluidized bed reactors with vertical internals has been increased. Additionally, the complexity of the fluidization system with vertical immersed tubes still considered a big challenge and needed more effort to understand. As well, the experimental investigations available in the literature, that studying the impact of the vertical internals on hydrodynamic characteristics inside the fluidized beds are rare, particularly for Geldart B particles and at laboratory scale (Rüdisüli et al. 2012a). Therefore, the focus of this work is to address this need.

1.2. RESEARCH OBJECTIVES

The overall objective of this work is to advance the understanding of using vertical immersed tubes (internals) to represent the heat-exchange tubes and studying their impacts on the hydrodynamic characteristics, flow regimes, pressure drop and heat transfer in gas-solid fluidized beds. Thus, the objectives of this study are the following:

- Developing simple and reliable methods for calibrating and validating the optical fiber probe for solids holdup and velocity measurements. The solid holdup calibrating method can be used for measuring the solids holdup by correlating the normalized voltage signal that is related to solids concentration in front of the probe to solids holdup. Furthermore, calibrating the effective distance between the two tips of the optical fiber probe which is essential to ensure the proper measurements of both bubbles and solids particle velocities. Then, implementing the optical fiber probe technique which can measure simultaneously the solids holdup, solids velocity and gas hydrodynamic characteristics such as bubble rise velocity, bubble frequency, and bubble mean size in the studied gas-solid fluidized beds.
- Studying the effect of vertical immersed heat exchanging tubes (internals) on solids and bubbles hydrodynamic parameters inside the fluidized bed by the means of the fiber optical probe.
- Investigating the impact of different sizes of the vertical internals on the flow regimes and their transition velocities using differential pressure transducer technique.
- Studying the effect of vertical internals and solid physical properties on the pressure drop at the wall and radial location pressure drop along the bed using probe-differential pressure transducer.

- Investigating the influence of the vertical immersed tubes on heat transfer and gas hydrodynamics using simultaneously advanced fast response heat transfer probe and the optical fiber probe in glass beads solid particles of Geldart A type. Additionally, studying the effect of operating conditions (superficial gas velocity and the location of the heat transfer probe inside the fluidized bed axially and radially) on the heat transfer coefficient and gas hydrodynamics. Furthermore, studying the effect of vertical tube diameter on the heat transfer coefficient inside the fluidizing bed of Geldart B type.
- Assessing the scale up of gas-solid fluidized bed using chaos scale-up approach that proposed by Schouten et al. (1996) for the selected experimental conditions that based on our new mechanistic scale-up methodology of matching the radial profiles of gas holdups.

1.3. DISSERTATION OUTLINE

This dissertation consists of the following sections:

- Section 1 introduces fluidized bed reactors and their uses, highlights the importance of using vertical immersed tubes in gas-solid fluidized bed reactors, and presents the motivation and objectives of this study.
- Paper I. The Impact of Vertical Internals on the Key Hydrodynamic Parameters in a Gas-Solid Fluidized Bed Using an Advance Optical Fiber Probe
- Paper II. Heat Transfer and Hydrodynamics in a Gas-Solid Fluidized Bed with Vertical Immersed Internals.
- Paper III. Flow Regimes in Gas-Solid Fluidized Bed with Vertical Internals.

- Paper IV. Effect of Vertical Internals on the Pressure Drop in Gas–solid Fluidized.
- Paper V. Comparison Between the New Mechanistic and the Chaos Scale-Up Methods for Gas-Solid Fluidized Beds.

PAPER

I. THE IMPACT OF VERTICAL INTERNALS ON THE KEY HYDRODYNAMIC PARAMETERS IN A GAS-SOLID FLUIDIZED BED USING AN ADVANCE OPTICAL FIBER PROBE

Haidar Taofeeq[1] and Muthanna Al-Dahhan[2*]

Multiphase Reactors Engineering and Applications Laboratory (mReal)

Department of Chemical & Biochemical Engineering

Missouri University of Science & Technology, Rolla, MO 65409 USA

ABSTRACT

The effect of a circular configuration of intense vertical immersed tubes on the hydrodynamic parameters has been investigated in a gas-solid fluidized bed of 0.14 m inside diameter. The experiments were performed using glass beads solid particles of 365 μm average particle size, with a solid density of 2500 Kg/m^3 which (Geldart B). An advanced optical fiber probe technique was used to study the behavior of six essential local hydrodynamic parameters (i.e., local solids holdup, particles velocity, gas holdup, bubble rise velocity, bubble frequency, and bubble mean chord length) in the presence of vertical immersed tubes. The experimental measurements were carried out at six radial positions and three axial heights, which represent the three key zones of the bed: near the distributor plate, the middle of the fluidizing bed, and near the freeboard of the column. Furthermore, four superficial gas velocities (u/u_{mf} = 1.6, 1.76, 1.96, and 2.14) were employed to study the effect of operating conditions. The experimental results demonstrated that the vertical internals had a significant effect on all the studied local hydrodynamic characteristics such

that when using internals, both the solids holdup and bubble mean chord length decreased, while the particles velocity, gas holdup, bubble rise velocity, and bubble frequency increased. The measured values of averaged bubble rise velocities and averaged bubble chord lengths at different axial heights and superficial gas velocities have been compared with most used correlations available in the literature. It was found that the measured values are in good agreement with values calculated using predicted correlation for the case without vertical internals. While, the absolute percentage relative error between the measured and calculated values of these two hydrodynamic parameters indicate large differences for the case of vertical internals.

Keywords: Vertical internals, hydrodynamic parameters, optical fiber probe, gas-solid fluidized bed

* Corresponding Author: aldahhanm@mst.edu

1. INTRODUCTION

Gas-solid fluidized bed systems have been widely used in industrial processes. Many commercial applications can be found in the chemical, petroleum, pharmaceutical, biochemical, and food industries, heat transfer operations, and catalytic reactions. This is due to their excellent particle mixing, high heat and mass transfer rates, which can enhance chemical reaction conversions; and chemical process efficiency (Olowson 1994; Yurong et al. 2004; Ozawa et al. 2004).

In general, there are two types of processes in the chemical industry that use fluidized bed contractors: catalytic fluidized bed and non-catalytic fluidized bed reactors. In catalytic fluidized bed reactors, the solid particles are not involved in the chemical reaction (e.g., chemical cracking of oil to produce different chemical substances). However, in gas-solid non-catalytic fluidized bed reactors, the particles undergo a chemical reaction (e.g., biomass combustion and coal gasification) (Halvorsen 2005). In these types of chemical reactors, heat transfer is necessary to keep the operating reactor under desirable operating conditions and to regulate the reaction rate of these processes. Therefore, it is essential to control the temperature to ensure reliable efficiency, high yield, and the proper conversion rate. Consequently, immersed surfaces or internals of different types (e.g., plates, tubes, and baffles) and various configurations and methods of orientation inside fluidized bed reactors (e.g., vertical and horizontal) are required and have been employed (Grace and Harrison 1968; Ozawa et al. 2002, 2004; Maurer et al. 2015a, b).

In addition to the benefit of the immersed internals for temperature adjusted and control, they have many other advantages on the fluidization processes. The immersed tubes can modify the flow structure of the gas-solid patterns, which typically alters the

hydrodynamic parameters. Generally, the internals inside gas-solid fluidized beds has the following many beneficial effects. First, it reduces the bubble size by controlling the bubble growth and minimizes the total amount of coalescence, which improves the contact between the gas phase and the dense phase (Volk, Johnson, and Stotler 1962; Grace and Harrison 1968). In addition, a decrease in bubble size can reduce the carryover of the solids from the bed and make the fluidization "smoother," while also increasing the heat and mass transfer rates between the solid particles and the fluidizing gas (Yates et al. 1984; Law et al. 2003). Second, the internal tubes can suppress the cross-circulation patterns of the solids phase inside the bed (Grace and Harrison 1968). Moreover, the back-mixing of the gas phase can be reduced (Olowson 1994). Third, immersed internal tubes can divide the bed into many small fluidized bed sections, such that each can serve as an individual fluidization unit, which improves the chemical reaction conversion inside the fluidized bed reactors (Law et al. 2003). Fourth, using the internals can reduce the following: the pressure drop inside the bed, slugging behavior, fluctuations in bed height, and particle elutriation. Moreover, local solids circulation is improved (Ramamoorthy and Subramanian 1981).

Many types of research have been conducted experimentally and numerically to study the impact of different types and configurations of immersed surfaces on the hydrodynamics behavior in gas-solid fluidized beds (Rüdisüli et al. 2012b). Table 1.1 lists the sources of the experimental and numerical investigations that have been reported in the literature using different internals in gas–solid fluidized bed systems. Most of these works studied the effect of different shapes, sizes, and configurations of the internals on the global and some local hydrodynamic parameters such as gas holdup, bubble rise velocity, axial particle velocity, bubble size, and bubble frequency.

Table 1.1: Sources of experimental and numerical studies that have been reported in the literature using different internals in gas-solid fluidized beds

Year	Author	Technique used	Internals Configuration	Internals Size & number of internals	Material	Particle Diameter (d_p)	Particle Density (ρ_p)	Measuring System (Vessel size) & Studied Parameters
1962	Volk et al.	Pressure taps at the wall	Vertical	1.875 inches (18 and 36 internals)	Iron ore	110 µm 33 µm 27 µm	2,963 kg/m^3 3,300 kg/m^3 2,851 kg/m^3	-Fluidized bed (0.6 m) -Overall gas holdup
1964	Glass and Harrison	Camera	Horizontal	2 cm & 5 cm	Sand particles; glass ballotini	0.01 cm 0.05 cm	-	- Fluidized bed -Bubble cord length
1968	Grace and Harrison	Pressure drop measurements and camera	Vertical, horizontal, & inclined	0.63 cm & 7.8 cm (4, 8, 42, 44 and 80 internals)	Sand; silver sand; magnesite; glass ballotini	135 µm 148 µm 274 µm 284 µm	2,800 kg/m^3 2,600 kg/m^3 3,000 kg/m^3 2,500 kg/m^3	- 3 fluidized beds of 2-D (7.6 cm × 1.9 cm, 45.7 cm × 1.9 cm and 27.9 cm × 27.9 cm) - Overall gas holdup & bubble mean diameter
1981	Ramamoorthy and Subramanian	Liquid tracer	Vertical springs/rods	Springs (0.035-0.09) cm (1-9 internals); rods (0.0565) cm (1-3 internals)	Sand particles	(-0.4+0.35) mm (-0.63+0.5) mm (-1.0+0.8) mm	2,600 kg/m^3	-Fluidized bed (9.2 cm) -Axial solid diffusivity, Overall gas holdup, effective bubble size, and bubble degree of interactions

Table 1.1: Sources of experimental and numerical studies that have been reported in the literature using different internals in gas-solid fluidized beds. (cont.)

1984	Yates et al.	X-ray imaging	Vertical	6.4 mm (1-3 internals)	Alumina powder	270 µm	-	-Square cross-section fluidized bed (0.3 m x 0.15 m) -Bubble shape, bubble velocity, and bubble volume
1994	Olowson	Capacitance and pilot-static pressures probes	Horizontal	20 mm (2, 3, and 4 internals)	Silica sand	0.7 mm	2,600 kg/m^3	-Pressurized fluidized bed (0.2 m x 0.3 m) -Bed expansion ratio, overall gas holdup, mean bubble frequency, mean bubble rise velocity, and mean pierced length of bubbles
2002	Ozawa et al.	Neutron radiography	Vertical	25 mm	Silica-sand (99.7% SiO_2); silica-sand (89.5% SiO_2)	218 µm 62 µm	2,555 kg/m^3 2,310 kg/m^3	-Rectangular fluidized-bed (300 mm width, 720 mm height, and 100 mm depth) -Local gas holdup, bubble frequency, equivalent bubble diameter, and bubble rise velocity

Table 1.1: Sources of experimental and numerical studies that have been reported in the literature using different internals in gas-solid fluidized beds. (cont.)

2003	Law et al.	-	Vertical	0.15 m x 0.1 m (2 internals)	Paddy rice	d_v = 3.13 mm, d_{sv} = 2.18 mm	-	-Fluidized bed dryer (0.15 m x 0.61 m) - Mixing and drying characteristics
2004	Yurong et al.	Numerical simulation using computational fluid dynamics	Horizontal	51 mm	-	1.0 mm	1,600 kg/m^3	-Fluidized bed (31.5 cm x 31.5 cm) -Axial and radial particle velocity, granular temperature, bubble frequency, and bed expansion
2012 b	Rüdisüli et al.	Pressure transducer & optical probe	Vertical	10 mm 15 mm 20 mm (12, 16, 24 and 37 internals)	Aluminum oxide	289 µm	1,350 kg/m^3	-Fluidized bed (0.145 m) -Pressure fluctuations, bubble size, bubble rise velocity, and bubble frequency
2012 c	Rüdisüli et al.	Optical probe	Vertical	15 mm (12 and 16 internals)	Aluminum oxide	289 µm	1,350 kg/m^3	-Fluidized bed -Bubble frequency, bubble size and bubble rise velocity
2015 a	Maurer et al.	X-ray tomography	Vertical	1 cm (4 internals) & 2 cm (12 internals)	Aluminum oxide	289 µm	1,350 kg/m^3	-Fluidized bed -Overall gas holdup

Table 1.1: Sources of experimental and numerical studies that have been reported in the literature using different internals in gas-solid fluidized beds. (cont.)

2015 b	Maurer et al.	X-ray tomography & optical probe	Vertical	1 cm (4 internals) & 2 cm (12 internals)	Aluminum oxide	289 µm	1,350 kg/m^3	-Fluidized bed -Bubble volume, equivalent bubble diameter, hydraulic bubble diameter, and bubble rise velocity
2016	Verma et al.	Numerical simulation using computational fluid dynamics	Vertical	15 mm (12, 16, 24 and 37 internals)	Aluminum oxide	289 µm	1,350 kg/m^3	-Fluidized bed -Equivalent bubble diameter, bubble distribution, average bubble rise velocity, and average axial solid velocity

The first work that studied the effect of internals on scale-up process in a fluidized bed was Volk, Johnson, and Stotler (1962). They reported that the problem of scale-up could be solved by employing vertical internals within the gas-solid fluidized bed reactor. Glass and Harrison (1964) investigated the bubble sizes in fluidized bed with horizontal internals using a photographic approach. They concluded that the internals could enhance the fluidization quality by reducing the bubble size, which would lead to improving the heat transfer between the bed and the surface of the internals. Grace and Harrison (1968) studied different ways to orient the internals (e.g., vertically, horizontally, and inclined) inside the fluidized bed. They reported that the vertical and horizontal orientations are valuable, but the inclined orientation has some disadvantages, such as excessive gas bypassing, heat transfer reduction, and short-circuiting of gas bubbles along the undersides of the inclined surfaces. Ramamoorthy and Subramanian (1981), Yates et al. (1984), and Olowson (1994) used various sizes, orientations, and types of internals in beds of different solid particles. They found that using the internals can improve the fluidization process by reducing the size of the bubbles and enhancing the contact between the gas and dense phases as well as increasing the residence time of the gas phase inside the bed. Law et al. (2003) studied the effect of vertical baffles on the drying and mixing of Geldart D powder inside a fluidized bed dryer. They deduced that the vertical baffles could modify the contact efficiency between the gas and solid particles and that the heat and mass transfer rates inside the fluidized bed dryer could be enhanced accordingly. Yurong et al. (2004) investigated the gas and solid hydrodynamic parameters of fluidized beds with and without internals, using numerical simulation (computational fluid dynamics). They concluded that using horizontally immersed internals as heat exchange surfaces is necessary for absorbing

the heat generated by the chemical reaction to keep the bubbling fluidized bed reactors working under desirable operating conditions. Different sizes, tube-to-tube spaces, and tube arrangements (i.e., square and triangular) to study the effect of vertical internals on the bubble hydrodynamic characteristics (i.e., bubble size, bubble rise velocity, bubble frequency, and bubble holdup) using different techniques have been investigated (Rüdisüli et al. 2012a, 2012b; Maurer et al. 2015a, b; Verma et al. 2016). All of these researchers reported that vertical internals have a significant effect on the bubble hydrodynamic parameters, such as the reduction of the bubble size, improving the bubble frequency, and increasing or decreasing the bubble rise velocities.

Accordingly, harnessing the power of vertical internals in gas-solid fluidized beds has many advantages: (1) the difficulty of scaling-up fluidized bed reactors can be reduced by using vertical internals (Volk, Johnson, and Stotler 1962); (2) the design is simple compared with other complex geometry; (3) the installation, removal, and emptying of the bed is physically easy; (4) dead spots can be obviated; (5) the volume occupied by the vertical internals is considered small compared with other orientations; (6) the internals provide high heat transfer efficiency (Grace and Harrison 1968); and (7) because the bubbles pass the vertical internals tangentially, the tube erosion can be reduced by 50% in contrast with using horizontal geometry (Rüdisüli et al. 2012b). However, there is still a major disadvantage of using vertical internals which is related to the creation of complex interaction among the gas-solid phases and the internals which complicate the hydrodynamics. In addition, the complexity of the fluidization system with vertical internals is still considered a big challenge, where more understanding is needed. Consequently, while the addition of the vertical internals inside fluidized bed reactors has

been recommended as a desirable option, they present a considerable challenge where the flow pattern and phases interactions have been still not yet properly understood. These cause a technical difficulties to plant designers and investors (Yurong et al. 2004).

Therefore, due to the many aforementioned advantages of using vertical internals inside gas-solid fluidized beds, the investigations of the hydrodynamic characteristics of different types of internals and of fluidized bed reactors has increased. A survey of the literature shows that there are few studies on the effect of vertical internals on hydrodynamics parameters that studied the local parameters such as local solid and gas holdups and particles velocity inside fluidized beds, particularly for Geldart B particles and at a laboratory scale (Rüdisüli et al. 2012a). Also, such literature survey shows that there is no integrated study that investigate together the local gas and solids holdups, velocities, and bubble properties at various radial and axial locations inside the beds. Additionally, to the best of our knowledge, the literature does not discuss measurements of the local solid holdup with vertical internals in a fluidized bed system. Accordingly, in this work, the impact of vertical internals on the local hydrodynamic parameters of solids holdup, gas holdup, particle velocity, bubble rise velocity, mean bubble size, and bubble frequency has been investigated in a gas-solid fluidized bed of 0.14 m inside diameter using an advanced optical fiber probe technique. The hydrodynamic parameters were measured radially and axially to give a clear presentation of the influence of the vertical internals on the fluidization mechanism. Such obtained knowledge and data are valuable as a benchmark data to validate computational fluid dynamics (CFD) models and simulations.

2. EXPERIMENTAL SETUP

The experimental setup consisted of a laboratory-scale fluidized bed column with 0.14 m inside diameter and 1.84 m height. The column was constructed from Plexiglas®, and the plenum was built from aluminum. The column and the plenum were placed on the top of a stainless steel base. Industrial-scale compressors were used to supply compressed air to the column at pressures up to 1.38 MPa. Omega flow meters were used to control the flow rate. A schematic diagram of the experimental setup, including the fluidized bed column with vertical internals, is provided in Figure 2.1. The gas phase was introduced through a sparger tube in the plenum section and then through a distributor mounted between the column and plenum. The gas distributor was made of a porous polyethylene sheet, with a pore size of 15-40 μm. The sparger tube was plugged at one end and had 14 holes, all facing downward with respect to the column. The column was electrically grounded to minimize electrostatic effects. Also, a rigid metallic structure was used to support the column and reduce the mechanical vibrations, as shown in Figure 2.2.

In the current study, a circular configuration of internals was used that occupy 25% of the cross-sectional area. These intense internals have been used to represent progress of high exothermic reaction where intense heat exchanging surfaces are needed to control the reaction temperature in high temperature industrial processes such as Fisher-Tropsch, Ammonia synthesis, and methanol synthesis (Bartholomew and Farrauto 2010; A. Pinto 1978; Tijm, Waller, and Brown 2001). The schematic diagram with dimensions of the internal support is shown in Figure 2.3. The circular arrangement featured uniformly distributed internals over the cross-sectional area of the fluidized bed column. This circular configuration of the internals was selected to maintain equal spacing between the internals

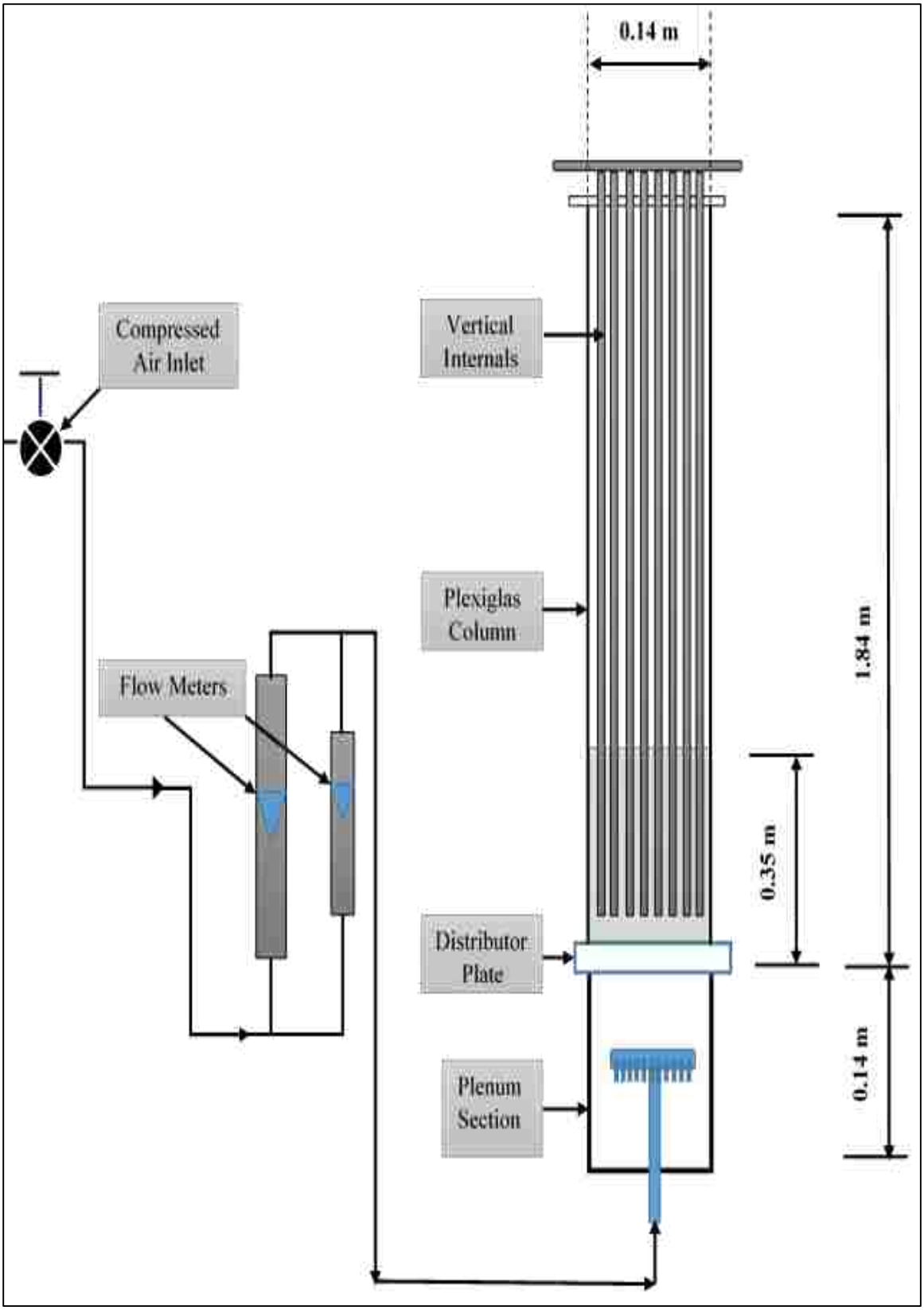

Figure 2.1. Schematic diagram of the 0.14 m inside diameter fluidized bed column with vertical internals.

Figure 2.2. Photo of the fluidized-bed column with vertical internals.

and the wall of the fluidized bed column. The photo of the internal configuration and its support is shown in Figure 2.4. The configuration of the internals consisted of 30 Plexiglas® vertical internals with a 0.5 in. inside diameter and 1.84 m height, covering 25% of the column cross-sectional area. The internals were secured in the column using four supports (honeycombs), which also minimized the vibration of the internals during the experiments. The distance between the distributor plate and the lower end of the vertical internals was 0.09 m.

The experiments were conducted at relative gas velocities (u/u_{mf}) of 1.6, 1.78, 1.96, and 2.14, where u is the superficial gas velocity and u_{mf} is the minimum fluidized velocity. The minimum fluidized velocity for both cases of with and without internals is 0.4 m/s. This is because static bed height in both cases (with and without internals) were maintained similar of 0.35 m. To compare the experimental results between the column with and without internals, the ratio of u/u_{mf} was kept similar and the superficial gas velocity of the column with and without internals was calculated based on the cross-sectional area of the column available for the flow. For the case with internals, the superficial gas velocity was calculated based on the free cross-sectional area available for the flow, which represented 75% of the cross-sectional area of the column.

Optical probe measurements were taken at three axial levels (H/D = 0.75, 1.5, and 2.0) above the gas distributor, and at six radial positions (r/R = 0.0, 0.2, 0.4, 0.6, 0.8, and 1.0). The solid particles used in this work were glass beads of 365 μm average particle size and 2500 Kg/m^3 density which represent Geldart B type of particles, and the static bed height was 0.35 m as mentioned earlier. More details about the solid can be found in Table 2.1.

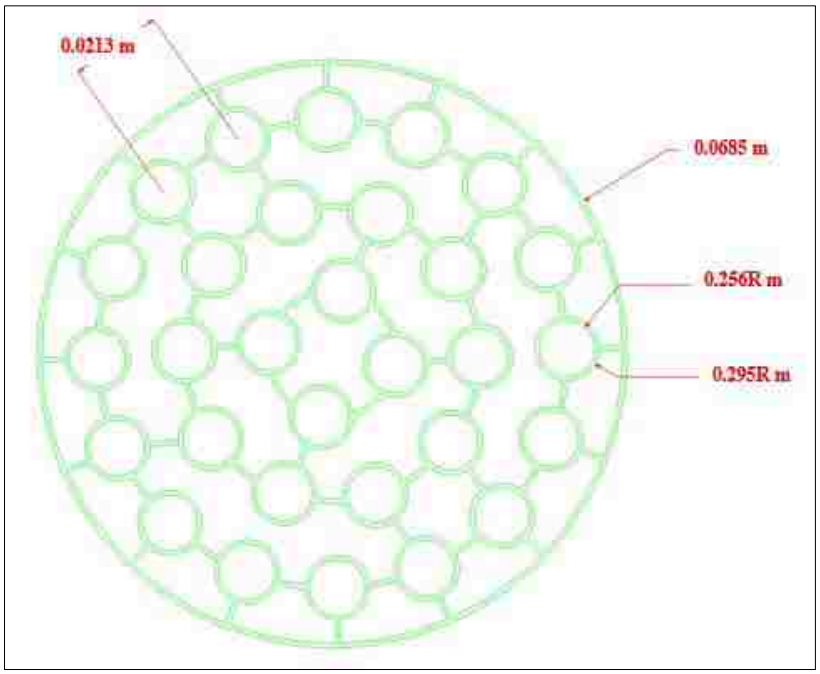

(a)

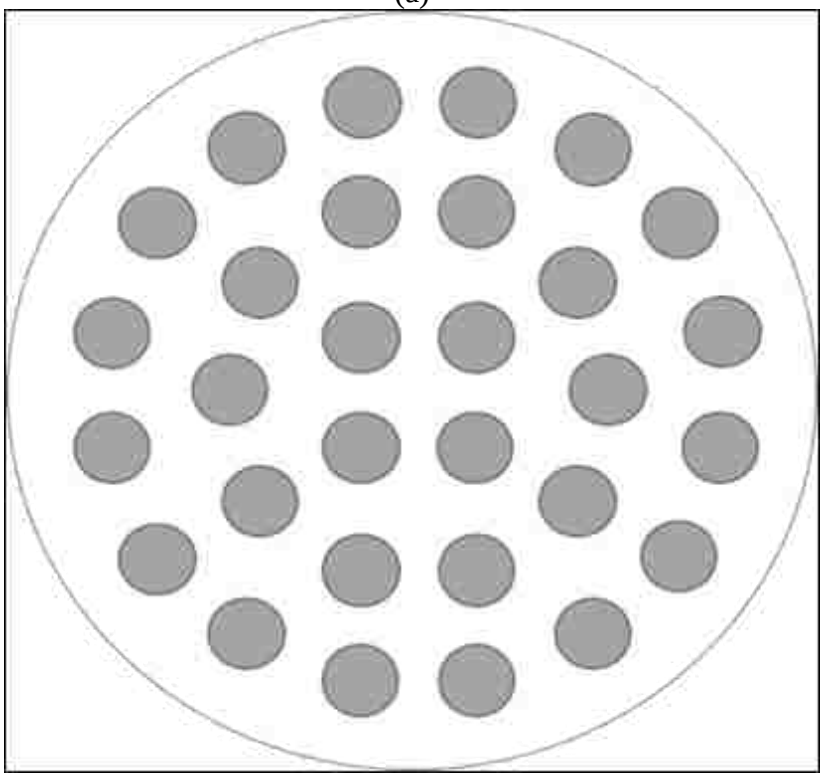

(b)

Figure 2.3. (a) Schematic of the 0.0127 m (0.05 in.) internals support (honeycomb), with all dimensions in meter, and (b) the configuration of the 0.0127 m internals used in the present work.

Figure 2.4. Photo of the internals configuration and its support.

Table 2.1. Physical properties of glass bead solid particles used in this work that represented Geldart B type of particles.

Particle mean diameter (μm)	365
Particle density (Kg/m^3)	2500
Static bed height (m)	0.35
Sphericity factor (φ)	0.90
Particle size distribution (μm)	300-430
Minimum fluidization velocity with and without internals (m/s)	0.4

3. ADVANCED OPTICAL FIBER PROBE TECHNIQUE

The Advanced optical fiber probe used in this work was model PV-6, which was manufactured by the Institute of Process Engineering, Chinese Academy of Sciences, Beijing, China (Figure 3.1.a). We implemented the probe by developing the needed signal processing algorithms to obtain through calibration the quantity related to local solids concentration and then solids holdup, particle velocity, and bubble hydrodynamic characteristics simultaneously (Appendix A). The optical probe was 3 mm in diameter and consisted of two sub-probes, each with an active tip area of 1 mm × 1 mm cross-section. The effective distance between the two tips was 2.12 mm which was calibrated using our newly developed calibration method (Appendix A). Each tip was composed of light-emitting and receiving fibers of 15 μm in diameter arranged in an alternating array. The two discrete optical bundles had separate channels for signal processing. The probe works on the principle of the back-reflection of light, such that the receiving light reflected by the solid particles is multiplied by the photomultiplier and converted into voltage signals. The voltage signals are further amplified and fed into a personal computer. To ensure the validity and repeatability of the sampled signals, the sampling time was 65 s and the frequency was 2 KHz. The measurements were repeated at least five times at each position for which the mean, variance, standard deviation and reproducibility of the measurements have been quantified. The reproducibility of the results was found to be less than of 5% and the error bars represented by the standard deviation were shown for each measurement. The chosen probe sample frequency (f) in HZ was based on the following equation recommended by the manufacturer (Institute of Process Engineering, Chinese Academy of Sciences, Beijing, China):

$$T < \frac{t}{20} = \frac{L_e}{20V} \quad (1)$$

where T is the sampling cycle, and T = 1/f; t is the time for the particles to pass between the two tips of the probe; L_e is the distance between the two tips of the probe (effective distance); and V is the particle velocity.

To make the error of the particle velocity measurements less than 5% within t, t should be no less than 20 times the sampling rate (i.e., the sampling cycle (T) should be smaller than t/20). Before the experiments, the optical probe was calibrated in our laboratory for local solids holdup measurements using dropping/trapping calibration method described by Zhang et al. (1998), and modified by us (Appendix A). The purpose of calibrating the optical probe is to convert the voltage signal that is related to the solids concentration to the solids holdup. The measuring signal in Volt obtained by the probe has been converted into dimensionless averaged voltage as per following equation:

$$V_{avg} = \frac{1}{n}\sum_{i=1}^{n} V_{i_{norm}} = \frac{V_i - V_{\min}}{V_{\max} - V_{\min}} \quad (2)$$

where V_{inorm} is the normalized voltage for each point in the signal, V_i represents each point in the voltage signal, V_{min} is the minimum point in the voltage signal, and V_{max} is the maximum point in the voltage signal.

The new calibration method for solids holdup measurements has been developed in our laboratory based on the trapping/dropping method that was first proposed by Zhang et al. (1998). In this method, the solid particles flow in a vertical Plexiglas tube which suitable for probe reflection light measurements at different flow rate which cover a range of solids holdup from 0 to 0.6 using syringe pump. At the inlet and exit of the tube there are two solenoid valves to trap the flowing solid particles. For each flow rate, the related voltage

signal is recorded and converted to a normalized averaged voltage signal (Equation 2). The mass of the trapped solids for each flow rate is measured by a balance and converted to volume fraction based on the volume of tube between the two solenoid valves (Appendix A). The measured solids volume fraction is a meaningful hydrodynamic parameter as solid holdup that is corresponding to the normalized averaged voltage signal estimated by Equation 2. Eventually, the calibration curve correlates the solids holdup with the normalized averaged voltage signal and hence the fitted line is obtained to be used in the actual experimental solids holdup measurements (Figure 3.1.b).

Figure 3.1.a. Optical fiber probe PV-6 and its data acquisition system.

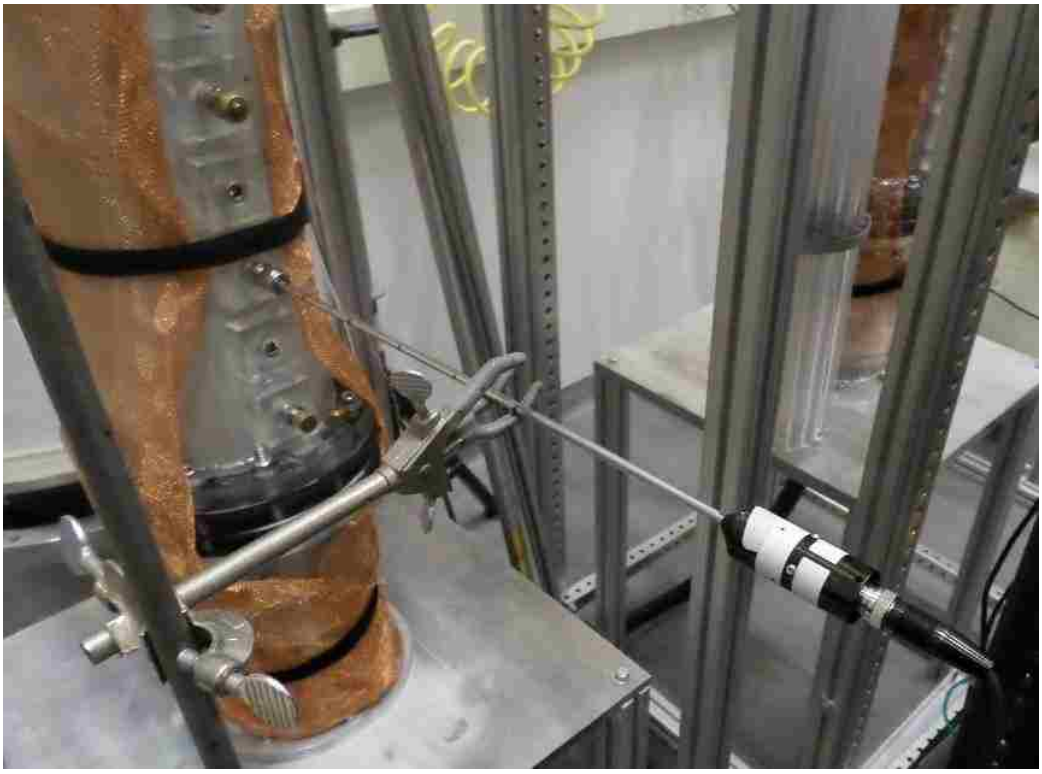

Figure 3.1.b. The insertion of the optical fiber probe in the bed.

Additionally, the optical fiber probe was calibrated for particles velocity measurements using our developed stepping motor and a high-speed camera to adjust or determine the effective distance between the two tips (L_e) of the probe or to validate the value of L_e if it is provided by the manufacturer. The cross-correlation method was used to estimate the time lag between the two generated signals of the two tips for particles velocity measurements. More details about the calibration and validation processes of the effective distance and the use of the cross-correlation method can be found in Appendix A.

The signals for both tips are divided into groups of data points. In our work, the recorded signal during 65 s at 2 KHz (131072 sample points) is divided into 255 groups of data point of 514 points for each group. The cross-correlation method has been applied on each corresponding group of data points for the two tips to estimate the time shift (time

lag) between the two signals of that group. For each time shift (time lag, τ_i) the particles velocity ($V_{p,i}$) has been calculated as per Equation 3.a

$$V_{p,i} = \frac{L_e}{\tau_i} \quad (3.\ a)$$

Where L_e is the effective distance between the two tips.

The particles velocity in the gas-solid fluidized bed move upward and downward. The optical fiber probe can measure both the upward and downward particles velocity where the direction of the particles can be specified from the sign of cross-correlation coefficient obtained at the maximum cross-correlation coefficient where the time shift (time shift) is also defined (Wang et al. 2008). The arithmetic average of the distribution of the particles velocity of all groups is calculated using Equation 3.b to get the averaged particles velocity for that particular condition (mean of distribution can be also estimated as another alternative).

$$V_p = \frac{1}{255}\sum_1^{255} V_{p,i} \quad (3.\ b)$$

As the optical probe has two sub-fiber probes, it allows for the estimation of the bubble rise velocity, bubble size, and the number of bubbles (bubble frequency). In this case the same signals of the two tips of the optical fiber probe will be processed differently to obtain bubble velocity according to the bubble linking algorithm described by van Dijk (2007) and Rüdisüli et al. (2012). For the bubble chord length and bubble frequency, same signal of the only lower tip has been used. The bubble rise velocity then is estimated as follows:

$$U_B = \frac{L_e}{\bar{\tau}} \quad (4)$$

where L_e is the effective distance between the two tips of the optical probe, and $\bar{\tau}$ is the bubble liking time shift (time lag) obtained using the cross-correlation function

between the signals of the two tips with bubble linking algorithm implementation. In this case, the bubble linking algorithm method uses the least sum of squared residuals regression analysis between the signals of the two tips described by van Dijk (2007) and Rüdisüli et al. (2012) as per Equation 5.

$$SSD(i) = \sum_{j=1}^{n}[A(j) - B(j+i)]^2 \;\; for\; 0 \leq i \leq \frac{L_e\, f}{u_{mf}} \qquad (5)$$

In this case A(j) is designated to the signals of the upper tip of the probe. The B(j + i) is the signal of the lower tip of the probe where i is the value between zero and (L_e f/u_{mf}) (Rüdisüli et al. 2012). Therefore, with increment of (i) between these two limits, we will obtain a new time series for B(i + j) for each i where j varies from 1 to n (if the whole signal is divided into segments and implement the same steps of estimations, distribution bubble velocity can be obtained where the mean average can bed estimated). Here n is the total

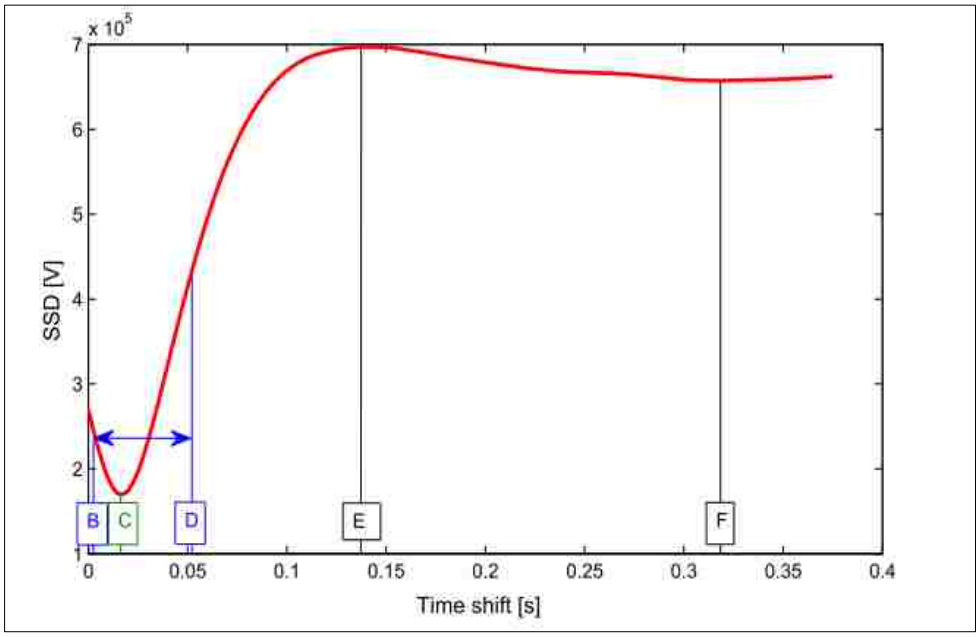

Figure 3.2. The relation between bubble linking time shift and sum of squares (SSD) at different signal peak fits (Rüdisüli et al., 2012).

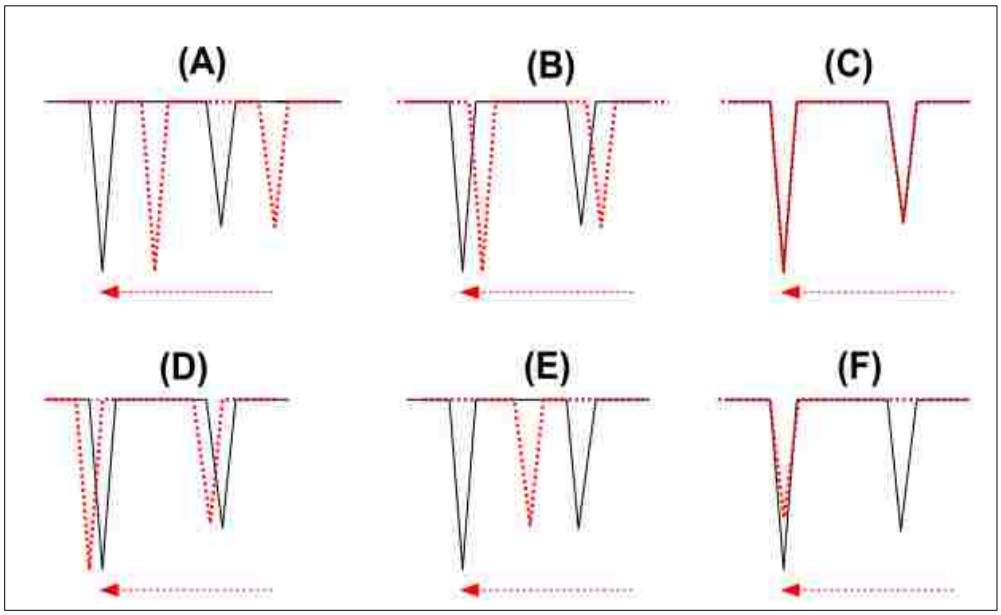

Figure 3.3. Different signal peak fit of the optical probe signals from the upper tip (dotted red line) and lower (full black line) probe tip to calculate the SSD according to Eq. (5). The coverage of the optical probe signals is divided into the Phases A–F in Figure 3.2 (Rüdisüli et al., 2012).

data points of the new time series of B(i + j). Hence, for each A(j) and B(i + j) we will obtain corresponding $\bar{\tau}_i$ using cross-correlation function where $\bar{\tau}_i$ is obtained at maximum value of the cross correlation coefficients. With this calculations we will obtain a series of SSD(i) [Equation 5] and corresponding $\bar{\tau}_i$. SSD(i) is the least sum of squares as a function of (i) which means $\bar{\tau}_i$. By plotting SSD(i) and $\bar{\tau}_i$ as shown in Figure 3.2, the $\bar{\tau}$ (bubble linking time shift) can be determined at the minimum represented by phase [c] in Figure 3.2 which represent the best fit between the two signals as shown in Figure 3.3. This value will be used in Equation 4 to estimate the bubble velocity at that particular condition. This bubble linking time lag $(\bar{\tau})$ is different from that obtained for particles velocity discussed earlier. More details about the bubble linking algorithm method can be found in van Dijk (2007) and Rüdisüli et al. (2012).

Figures 3.2 and 3.3 are discussed as follows:

- Phase A (which is not appeared in Figure 3.2): In this phase, the two peaks indicate that they are generated from the same bubble, when it first passes the lower tip and thereafter the upper one.
- Phase B: The SSD starts to decrease (as in Figure 3.2), which indicates the two signals have combined coverage.
- Phase C: The two signals indicate a best fit between them, in which the SSD(i) at its minimum value and the time shift $\bar{\tau}$ can be taken to calculate the bubble rise velocity in Equation 4.
- Phase D: In this phase, a temporal shift between the two signals is occurred, in which the value of SSD(i) starts to increase and the combined converge between the two signals is decreased.
- Phase E: In this phase, the combined coverage between the two signals is further decreases due to the increase of the shift between the two signals until the SSD(i) reached it maximum value, which indicate the minimum combined coverage between the two signals.
- Phase F: After the SSD(i) reaches its maximum value in Phase E, the SSD(i) start to decrease and the combined coverage between the two signals still indicates a larger shift between the two signals.

Once the bubble velocity is estimated, the bubble chord length can be obtained from the duration of the contact time (Δt) of the bubble with the lower tip of the optical probe as follows:

$$d_B = U_B * \Delta t \tag{6}$$

The contact time Δt is demonstrated in Figure 3.4. in this case the signal from the lower tip of the probe is only used because the generated signal from the upper tip of the probe may be influenced by the lower tip. In which, the lower tip can affect the shape of the bubble and thus can reflect on the bubble chord length measurement precision. To determine Δt from the signal of the lower tip of the probe, threshold voltage that can separate the voltage signals generated by the solids from that generated by the gas phase needs to be determined. This means that the threshold represents the boundary between the solids phase and the gas phase in the recording signal. This threshold can be determined by plotting the signal histograms as shown in Figure 3.5.a where each bar is called peak. In this figure, the highest peak (bar of the histogram) represents the maximum solids peak when the probe detects solids phase. Hence, the voltages beyond the maximum voltage peak till the maximum range of the data acquisition voltage of 5 represent the solids phase (the range of the data acquisition signal is 0-5 volt). The difference between the 5 volts and the value of this maximum peak can be defined. If the same difference is mapped on the left side of the maximum peak, the threshold can be determined as shown in Figure 3.5.a (Schweitzer et al., 2001). In this case the range between the voltage of the maximum peak and the voltage of the threshold represents the peaks (bars) of both solids and bubbles detected at the same time (which reflects the clusters of solids and gas) called emulsion peaks. Therefore, in order to check if the probe is in contact with solids or bubbles, the threshold voltage which delimits the two peaks (solids and bubble phases) of the histogram. The threshold value and the maximum peak is a function of the fluidization velocity. In which, the number of bubble peaks is high at higher fluidization velocity. Accordingly, the threshold voltage is demonstrated further on Figure 3.5.b where the area above the

threshold represents the contact time of the solids phase, while the lower area represents the contact time of the bubbles (gas phase) with the lower tip of the probe.

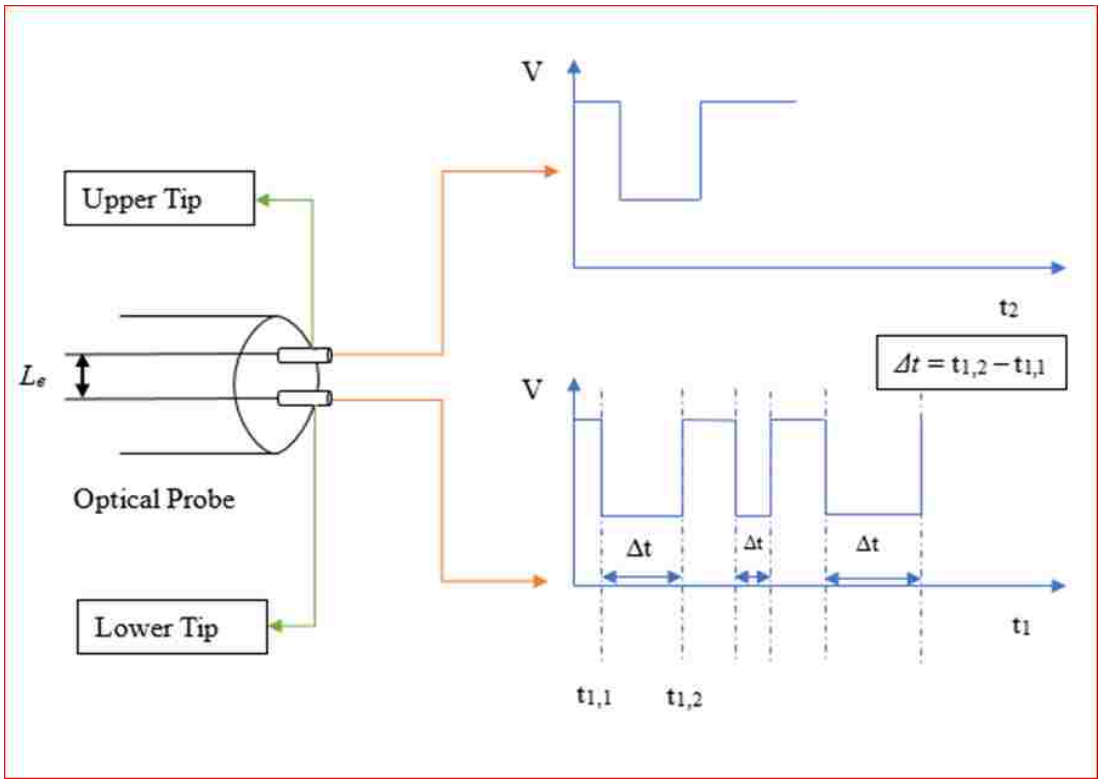

Figure 3.4. Schematic representation of the method of estimating the bubble chord length from the lower tip voltage signal

Therefore, after the signal breaks into two parts as shown in Figure 3.5.b where each one represents the corresponding phase. The signal is then normalized into 0 and 1 values to estimate the bubble frequency and bubble size. The 1 value represents the solids phase (above the threshold) and the 0 values represents the gas phase (below the threshold). The normalized signal below the threshold will be used to determine Δt in Equation 6. In this case the normalized signal consists of varying width Δt of the block of zeros as shown

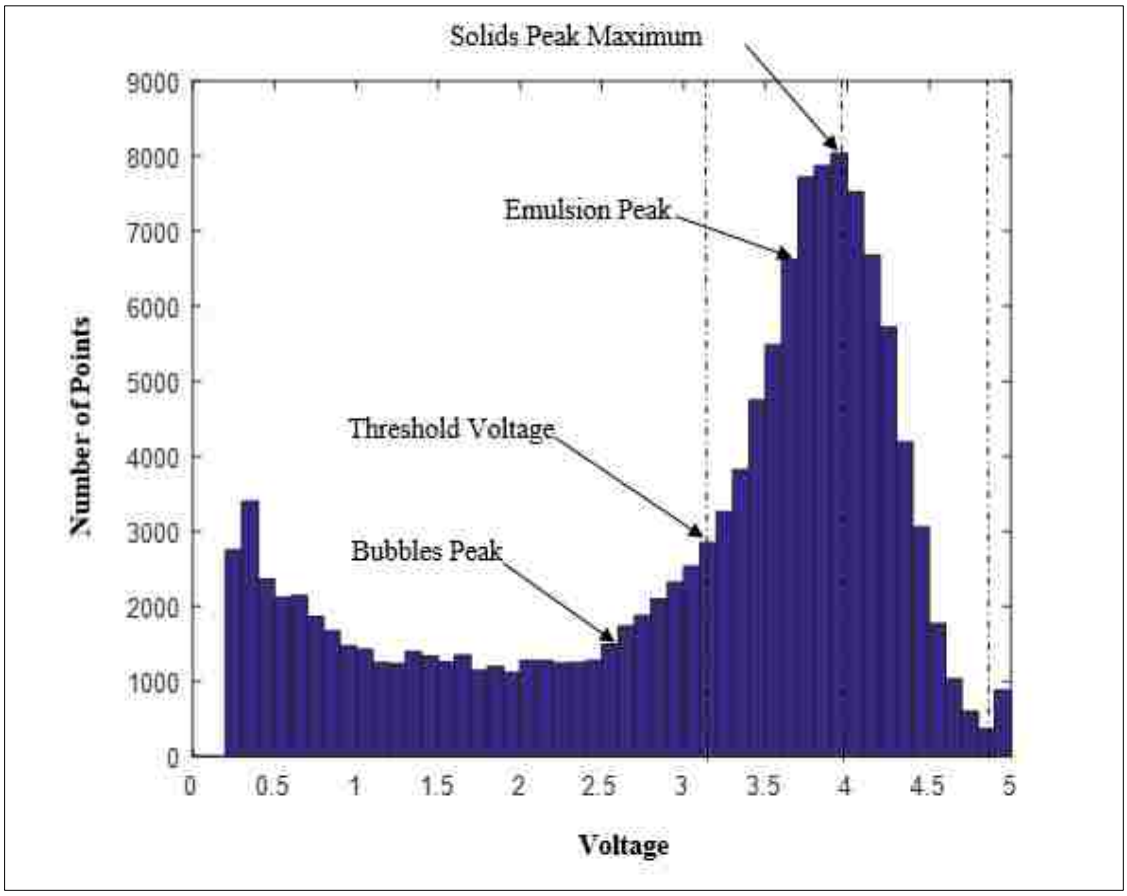

Figure 3.5.a. The typical histogram of the voltage signal.

in Figure 3.4. The mean of Δt will be estimated by arithmetic average of the Δt with respect to the number of blocks which represent the number of bubbles. Thus, the bubble chord length can be now estimated from Equation 6. Another approach is by using the distribution of Δt along with or without distribution of bubble velocity (U_B) to obtain the distribution of bubble chord length. In this case either arithmetic-average or the mean of the distribution can be estimated which represent the average or the mean bubble chord length (d_B). The bubble frequency in this case is obtained by counting the number of blocks that are detected in the lower part of the signal after normalization per unit time of the recorded signal which is 65 s (Number of bubbles/time of the recorded signal (65 s)).

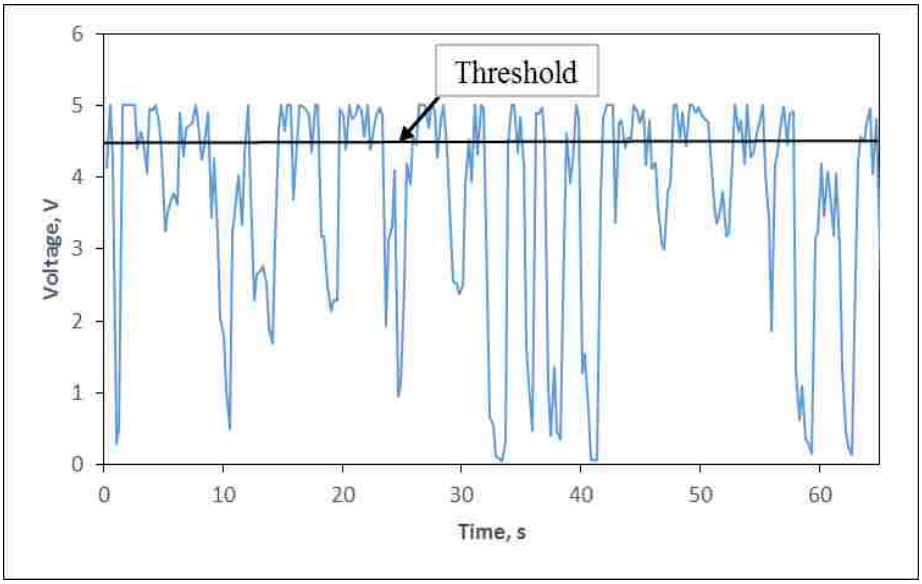

Figure 3.5.b. The typical signal of the lower tip of the probe with the indication of the threshold.

4. RESULTS AND DISCUSSION

4.1 HYDRODYNAMIC PARAMETERS OF THE SOLID PARTICLES

4.1.1 Solids Holdup. The solids holdup is considered one of the important hydrodynamic parameters in the design, scale-up, and operation of gas-solid fluidized bed reactors in which the amount of gas entering the fluidized bed reactor and the distribution of the gas phase within the bed of solid particles affect the performance of the reactors. Furthermore, the solids holdup can influence the chemical reaction rate, chemical conversion, heat and mass transfers, and particle mixing in fluid catalytic cracking reactors (Maurer et al. 2015a). Accordingly, the measurements of the locals solid holdup are essential to ensure that the operation and reaction functionality of gas-solid fluidized bed reactors are working appropriately and efficiently. In the present work, the radial profiles of the solids holdup were measured with and without internals at three axial heights (i.e.,

near the distributor, in the middle of the fluidizing bed, and near the freeboard of the column) and at six radial positions as mentioned earlier.

The radial profiles of the solids holdup were presented at different superficial gas velocities and axial heights in Figure 4.1. The figure shows that with the presence of vertical internals, the variation of the radial profiles of the solids holdup with the axial height, as follows. At H/D = 0.75, which represents the bed section near the distributor, solids holdup is low near the central region of the column and increases toward the wall for all the superficial gas velocities. This trend becomes obvious the solids holdup decreases furthermore at the wall region with increasing superficial gas velocities, as in the case of u/u_{mf} = 2.14 where the solids holdup with internals is lower at the center of the bed region compared to that without internals. Same finding has been shown for all the axial heights. At H/D = 1.5, which represents approximately the middle of the bed when it is fluidizing, the radial profiles of the solids holdup for the case of with and without internals appear to be similar with small variation at low superficial gas velocities, as in the case of u/u_{mf} = 1.6 and 1.76. The differences in the magnitude of the solids holdup increases with the increase in the superficial gas velocity, as in the case of u/u_{mf} = 1.96 and 2.14. Also it is lower at the central region of the bed and lower noticeably lower in the case of without internals. The difference in the solids holdup in the case of the presence of internals is small near the wall and high near the central region of the bed compared to the case of without internals. At H/D = 2.0, which represents the axial position near the freeboard of the column, same trends have been found as these for H/D = 1.5. Generally, it can be concluded from the behavior of the radial profiles of the solids holdup at the different axial heights mentioned above and with the presence of vertical internals that the solids holdups are

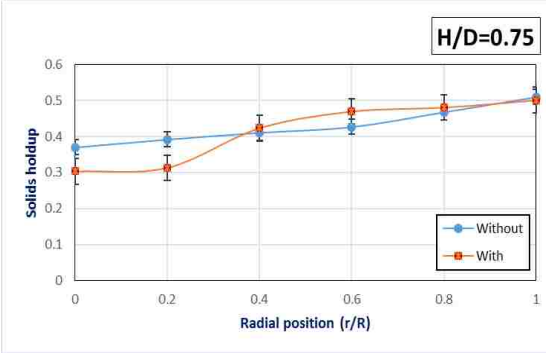

Radial profiles of solids holdup at u/u_{mf} = 1.6 and H/D = 0.75, with and without internals.

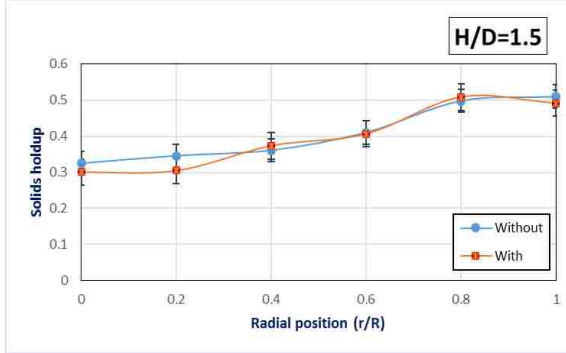

Radial profiles of solids holdup at u/u_{mf} = 1.6 and H/D = 1.5, with and without internals.

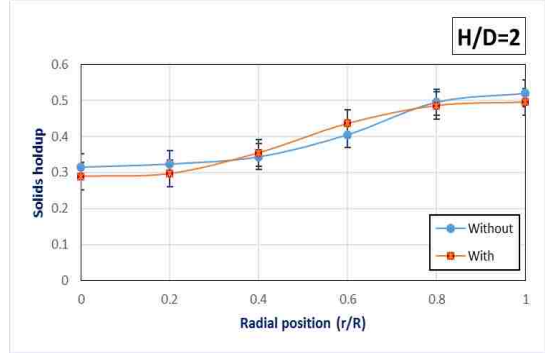

Radial profiles of solids holdup at u/u_{mf} = 1.6 and H/D = 2, with and without internals.

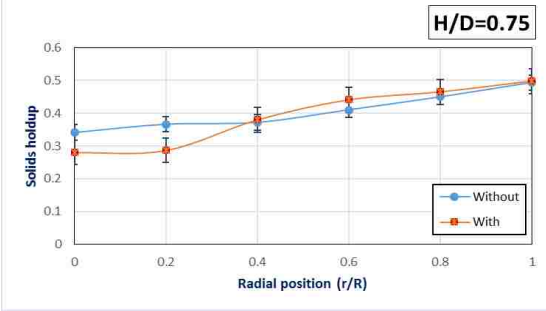

Radial profiles of solids holdup at u/u_{mf} = 1.76 and H/D = 0.75, with and without internals.

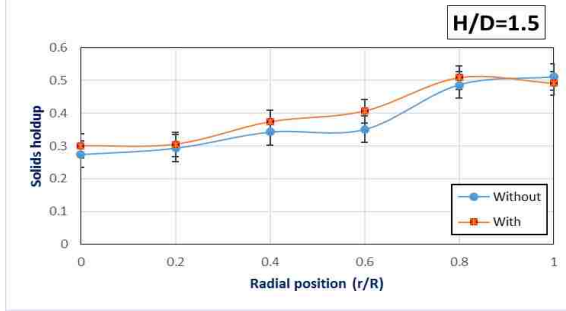

Radial profiles of solids holdup at u/u_{mf} = 1.76 and H/D = 1.5, with and without internals.

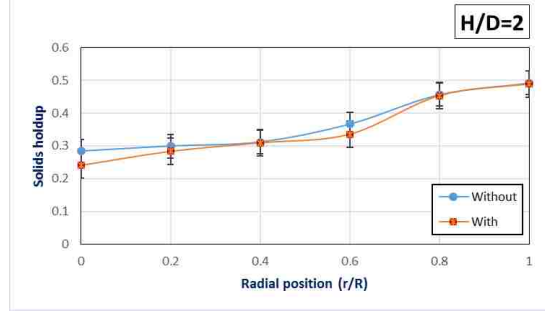

Radial profiles of solids holdup at u/u_{mf} = 1.76 and H/D = 2, with and without internals.

Figure 4.1. Radial profiles of the solids holdup at different axial heights and superficial gas velocities (u/u_{mf}), with and without internals.

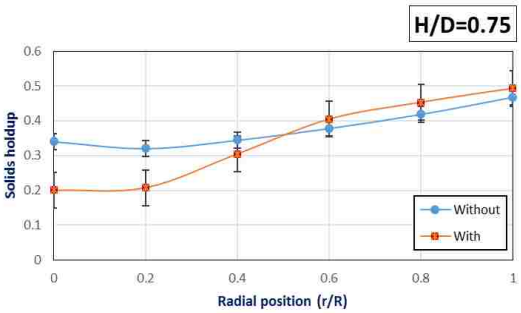

Radial profiles of solids holdup at u/u_{mf} = 1.96 and H/D = 0.75, with and without internals.

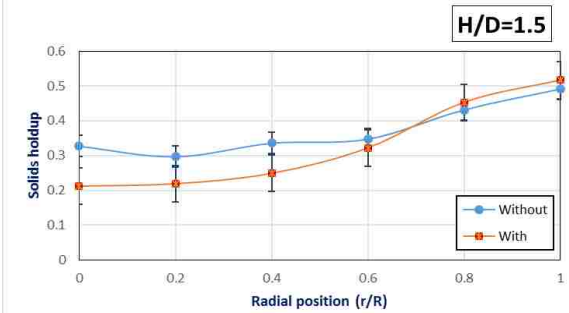

Radial profiles of solids holdup at u/u_{mf} = 1.96 and H/D = 1.5, with and without internals.

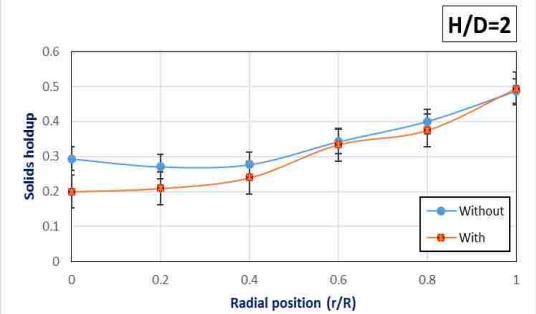

Radial profiles of solids holdup at u/u_{mf} = 1.96 and H/D = 2, with and without internals.

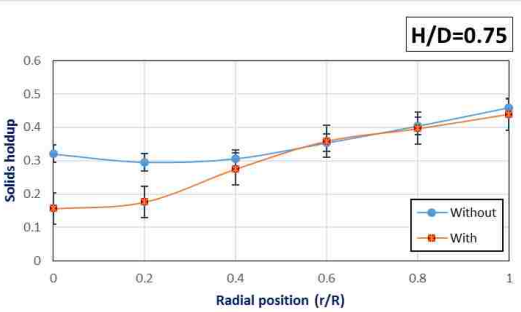

Radial profiles of solids holdup at u/u_{mf} = 2.14 and H/D = 0.75, with and without internals.

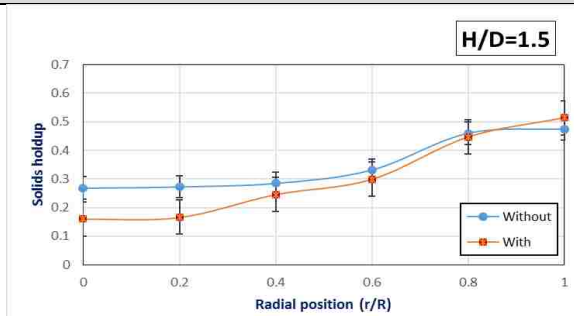

Radial profiles of solids holdup at u/u_{mf} = 2.14 and H/D = 1.5, with and without internals.

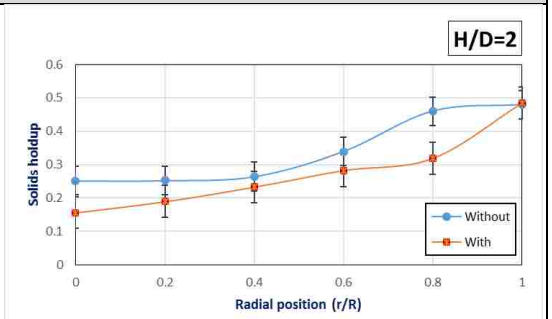

Radial profiles of solids holdup at u/u_{mf} = 2.14 and H/D = 2, with and without internals.

Figure 4.1. Radial profiles of the solids holdup at different axial heights and superficial gas velocities (u/u_{mf}), with and without internals. (cont.)

noticeably lower compared to these without internals near the central region of the column with not clear differences at the wall region (within the error bars). This behavior can be explained because the solids circulation within the bed enhanced due to the presence of vertical internals particularly at the regions away from the sparger region, and the gas holdup significantly increases. Furthermore, the contact between the solids and gas phases would increase, so the particle mixing and heat and the mass transfer rates would be enhanced accordingly.

To further clarify the influence of the vertical internals on the solids holdup. The cross-sectional average solid holdup ($\overline{\varepsilon_s}$) was calculated for each radial profile of solids holdup at different axial heights, using Eq. 7. In addition, $\overline{\varepsilon_s}$ was plotted versus the superficial gas velocity (u/u_{mf}) at different axial heights, as illustrated in Figures 4.2.

$$\overline{\varepsilon_s} = \frac{1}{A_c}\int_0^{2\pi}\int_0^R \epsilon_s(r,\theta) r dr d\theta = \frac{2}{R^2}\int_0^R \epsilon_s(r) r dr \qquad (7)$$

where A_c is the cross-sectional area (πR^2), r is the radial position, R is the column radius, and Θ is the azimuthal distance.

As shown in Figures 4.2, $\overline{\varepsilon_s}$ decreased with the case of internals at all axial heights and superficial gas velocities. In which, the decrease percentage of $\overline{\varepsilon_s}$ at different axial heights and superficial gas velocities is as follows: at H/D = 0.75, the decrease percentage at different superficial gas velocities (1.6, 1.76, 1.96, and 2.14) is 3.29%, 3.32%, 9.13%, and 15.71% respectively. At H/D = 1.5, the decrease percentage at different superficial gas velocities (1.6, 1.76, 1.96, and 2.14) is 2.65%, 1.02%, 11.6%, and 12.57%, respectively. At H/D = 2, the decrease percentage at different superficial gas velocities (1.6, 1.76, 1.96, and 2.14) is 1.9%, 4.47%, 10.59%, and 18.78%, respectively. Additionally, it was found from the percentage decrease of $\overline{\varepsilon_s}$ listed above, that this value increases with increasing

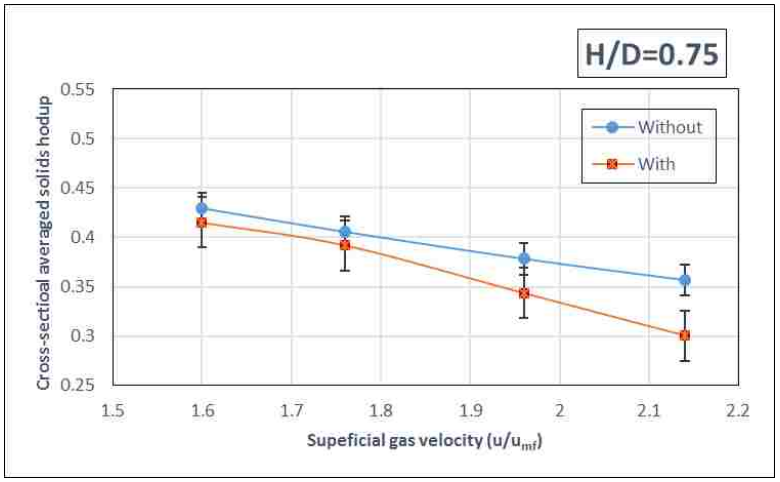

(a)

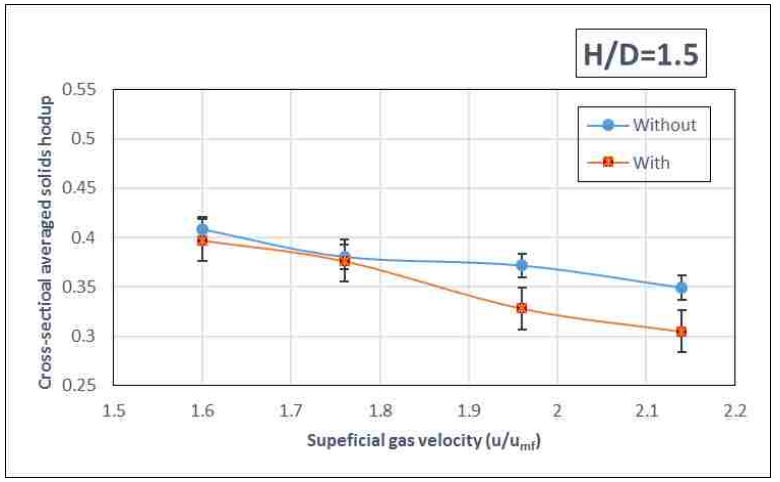

(b)

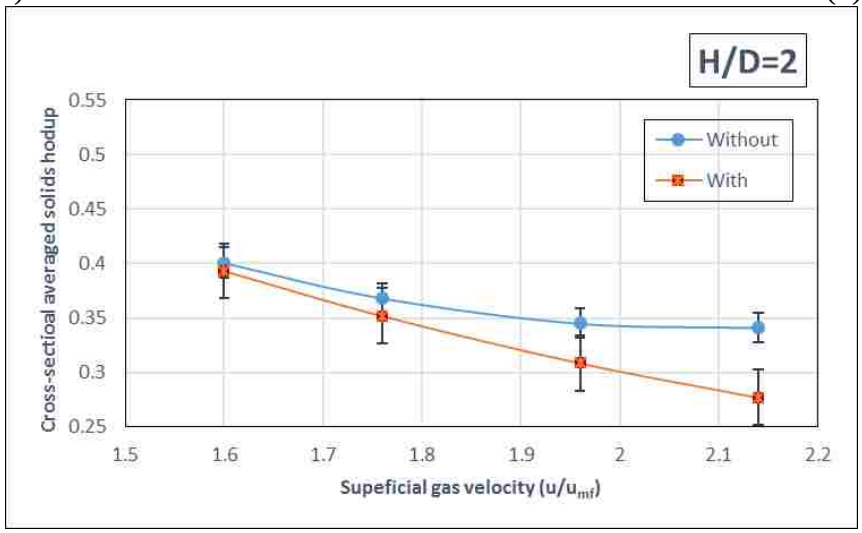

(c)

Figure 4.2. Cross-sectional averaged solids holdup ($\overline{\varepsilon_s}$), with and without internals, at different axial heights and superficial gas velocities, (a) H/D = 0.75, (b) H/D = 1.5, and (c) H/D = 2.

the axial height and with increasing the superficial gas velocity. As well, it clearly appeared that the decrease percentage of $\overline{\varepsilon_s}$ is significantly increased at (u/u_{mf} = 2.14) for all the axial heights.

Accordingly, it can be concluded that the presence of vertical internals inside the gas-solid fluidized bed leads to a decrease in the local radial profiles and average cross-sectional solids holdup particularly at higher superficial gas velocity. Likewise, the local radial profiles and average cross-sectional gas holdup increase. This variations in the gas holdup enhance the mixing rate, local solid circulation, heat and mass transfer rates, and the residence time of bubbles inside the bed, which would consequently improve the chemical reaction rate, chemical conversion, and products yield (Maurer et al. 2015a; Rüdisüli et al. 2012b).

4.1.2 Particles Velocity. The particles velocity is an important hydrodynamic parameter for the design, operation, and scale-up of a gas-solid fluidized bed. It has been reported by many studies that the particles velocity plays a significant role in the heat and mass transfer characteristics inside fluidized beds (Bhusarapu et al. 2005; Zhu et al. 2008). In this work, the effects of the vertical internals on the particles velocity were experimentally studied for the first time in a gas-solid fluidized bed. The impact of the vertical internals on the radial profiles of the particles velocity at different superficial gas velocities and axial heights were taken into consideration.

It is important to mention that the inversion point of the particles velocity from positive to negative magnitude has been found within the radial position of r/R = 0.6-0.7 as stated by many experimental works in the literature that studied the particles velocity in gas-solid fluidized beds particularly with the use of the advanced techniques such as

radioactive particle tracking and positron emission particle tracking (Laverman et al. 2012; Tebianian et al. 2015; Tebianian et al. 2016; Efhaima 2016). The radial profiles of particles velocities at different axial heights and superficial gas velocities for the cases of with and without internals are illustrated in Figure 4.3. In this figure, it is clearly shown that the particles velocity is positive in the central region of the bed (r/R = 0) and negative near the wall of the column (r/R = 1.0). This indicates that the solid particles move upward in the central region of the bed, because the gas phase in forms of bubbles tend to move toward the center and away from the column walls. While, the solid particles move downward near the wall of the column due to the back mixing of solids near the wall. In addition, Figure 4.3 shows that the radial profiles of particles velocities significantly increased in the case of internals near the center of the column (the upward particles velocity) and increase near the wall region (the downward particles velocity). This behavior is clearly represented in Figure 4.3 for all the axial heights and superficial gas velocities, except H/D = 0.75 and for all the superficial gas velocities used. In which, at this axial level the particles velocity has been decreased in the case of vertical internals due to the influence of the sparger region and the lower end of the vertical internals bundle that works to suppress the moving of solid particles when they collide with the lower surface of the vertical internals bundle.

At higher axial height (H/D = 1.5 and 2), it is noteworthy that the increase in the particles velocity is related to the magnitude of the particle velocity, regardless of the direction of the solid particles. This increment of change in the particles velocity may be explained by the decrease in the cross-sectional area available for flowing gas due to the presence of the vertical immersed tubes, which causes that the local bubble velocity to increase particularly in the upper section of the bed when the bubble size increases due to

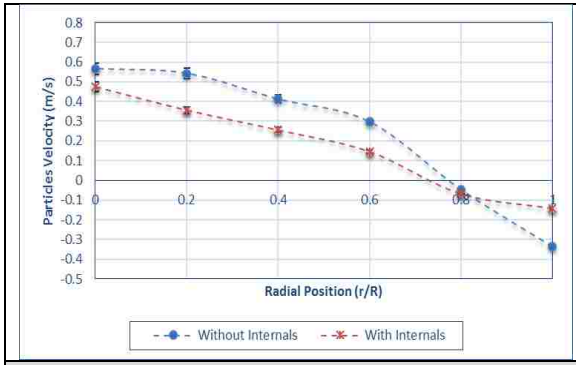

Radial profiles of particles velocities at u/u_{mf} = 1.6 and H/D = 0.75, with and without internals.

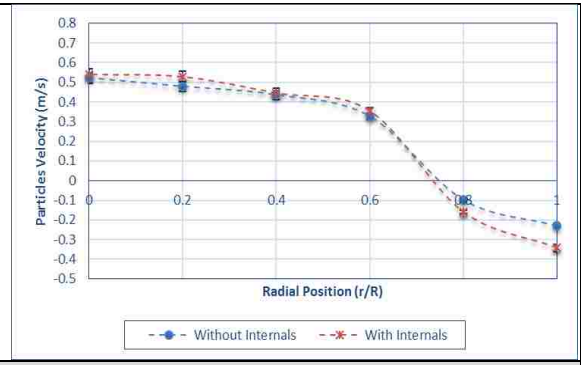

Radial profiles of particles velocities at u/u_{mf} = 1.6 and H/D = 1.5, with and without internals.

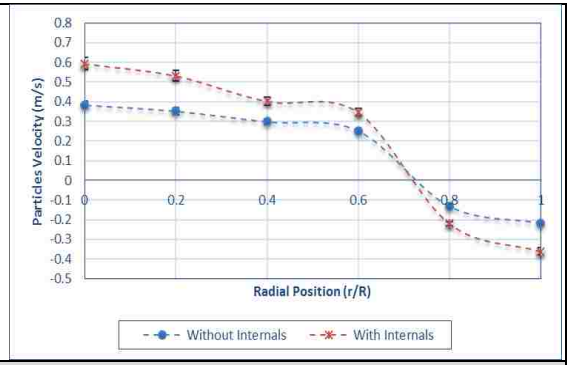

Radial profiles of particles velocities at u/u_{mf} = 1.6 and H/D = 2, with and without internals.

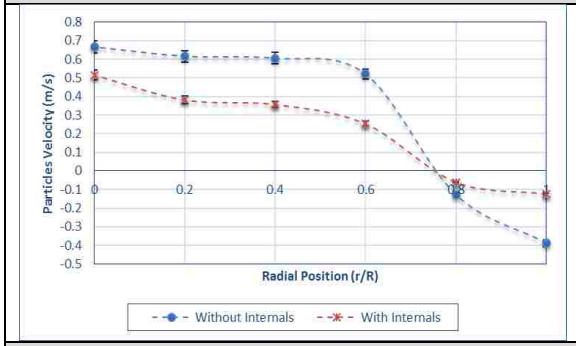

Radial profiles of particle velocities at u/u_{mf} = 1.76 and H/D = 0.75, with and without internals.

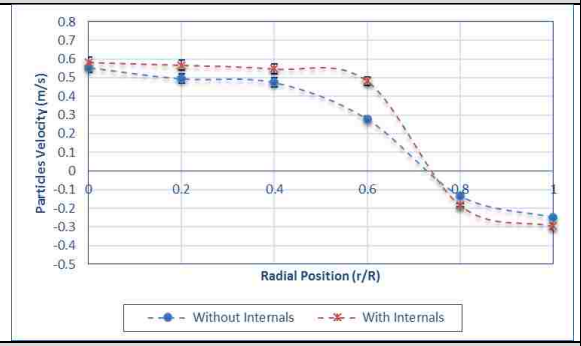

Radial profiles of particle velocities at u/u_{mf} = 1.76 and H/D = 1.5, with and without internals.

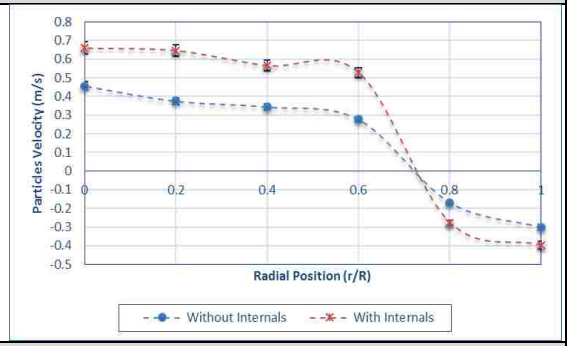

Radial profiles of particle velocities at u/u_{mf} = 1.76 and H/D = 2, with and without internals.

Figure 4.3. Radial profiles of particles velocities at different axial heights and superficial gas velocities (u/u_{mf}), with and without internals.

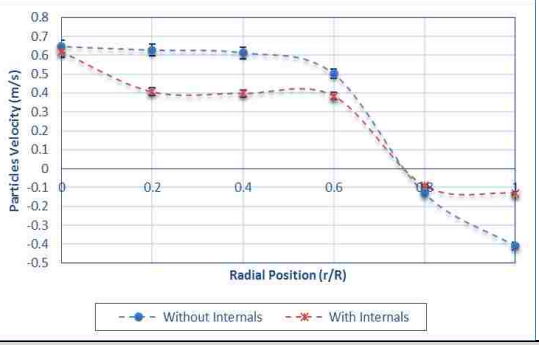	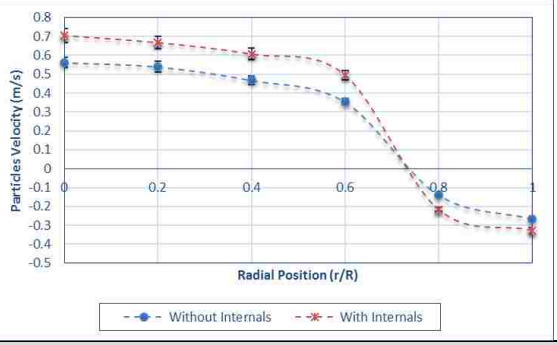	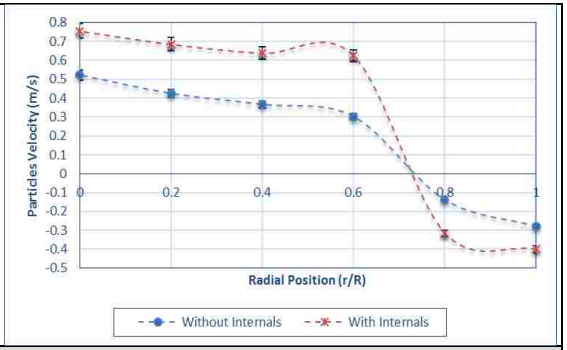
Radial profiles of particle velocities at u/u_{mf} = 1.96 and H/D = 0.75, with and without internals.	Radial profiles of particle velocities at u/u_{mf} = 1.96 and H/D = 1.5, with and without internals.	Radial profiles of particle velocities at u/u_{mf} = 1.96 and H/D = 2, with and without internals.
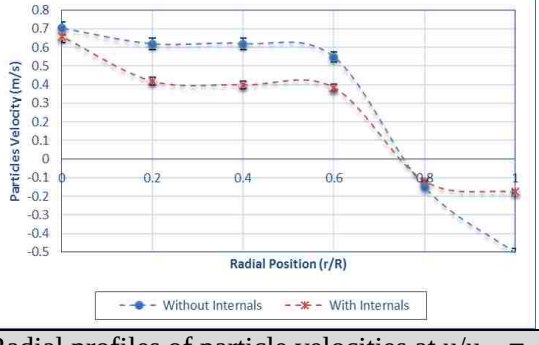	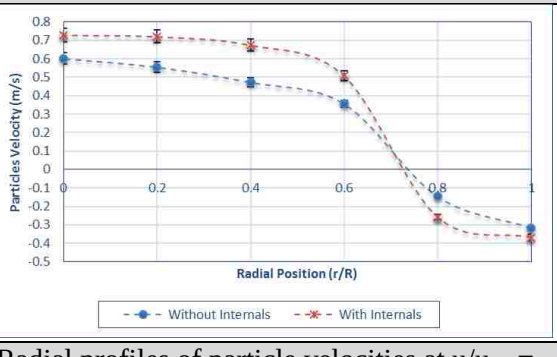	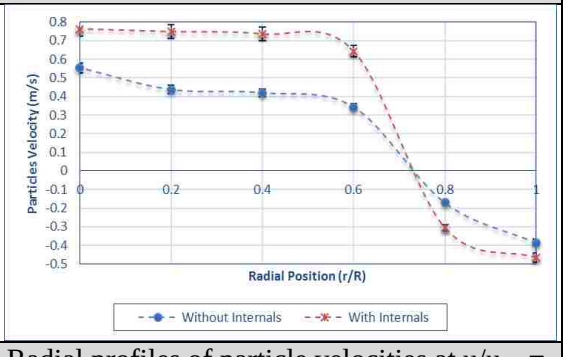
Radial profiles of particle velocities at u/u_{mf} = 2.14 and H/D = 0.75, with and without internals.	Radial profiles of particle velocities at u/u_{mf} = 2.14 and H/D = 1.5, with and without internals.	Radial profiles of particle velocities at u/u_{mf} = 2.14 and H/D = 2, with and without internals.

Figure 4.3. Radial profiles of particles velocities at different axial heights and superficial gas velocities (u/u_{mf}), with and without internals. (cont.)

the coalescence phenomena between the bubbles. This increase leads to a rise in the drift velocity of the bubbles, which affects the particles velocity accordingly. The enhancement in the magnitude of the particles velocity in either direction improves the local solid mixing and the heat transfer rate inside the bed.

Additionally, it is clearly noticed from Figure 4.3 that the percentage of increase of particles velocity in the case of vertical internals is a function of the axial height and superficial gas velocity. In which, for both axial heights (H/D = 1.5 and 2) the particles velocity in the case of vertical internals increase with increasing the superficial gas velocity with respect to the case of without vertical internals. The percentage of increase of particles velocity at different superficial gas velocities and for the case of vertical internals is as follows: at H/D = 1.5, the percentage of increase of particles velocity for upward (at r/R = 0) and downward particles velocity (at r/R = 0) at different superficial gas velocities (u/u_{mf} = 1.6, 1.76, 1.96, 2.14) is 3.4%, 4.7%, 20.1%, 17.4% and 33.4%, 15.4%, 6.1%, 14.2%, respectively. At H/D = 1.5, the percentage of increase of particles velocity for upward (at r/R = 0) and downward particles velocity (at r/R = 0) at different superficial gas velocities (u/u_{mf} = 1.6, 1.76, 1.96, 2.14) is 35.4%, 30.7%, 30.9%, 27.3% and 35.4%, 30.75%, 30.3%, 17.26%, respectively.

4.2 HYDRODYNAMIC PARAMETERS OF THE BUBBLES

In gas-solid fluidization systems the gas phase dictates the hydrodynamics of the beds. Hence, the knowledge of the bubble characteristics, such as local radial profiles of the gas holdup, bubble rise velocity, bubble frequency, and bubble chord length, are essential in the design and scale-up of gas-solid fluidized beds. Furthermore, the bubble

dynamic parameters play an important role in the operation of such reactors, as these parameters are influential factors in the performance of these types of gas-solid systems. Thus, understanding the behavior of such hydrodynamic properties can help improve the comprehension of the working mechanism of gas-solid fluidized bed reactors, especially when the immersed surfaces reside inside the bed, which make the gas-solid behavior more complex. Accordingly, the effect of the vertical internals on the local gas holdup and the bubble hydrodynamic characteristics is discussed in this section.

4.2.1 Local Radial Profiles of Gas Holdup. The gas holdup is considered one of the most important hydrodynamic parameters for scale-up, design, and operation of catalytic fluidized bed. Since it dictates the other hydrodynamic parameters inside the gas-solid fluidized bed (Al-Dahhan et al. 2014). Furthermore, the gas holdup can affect the performance of chemical reaction as well as the heat and mass transfers, and the particles mixing inside the bed (Maurer et al. 2015a). Therefore, the knowledge of the local gas holdup is important to ensure that the desirable reaction rate and conversion of gas-solid fluidized bed reactors are achieved properly. We discussed earlier the radial profiles of the studies holdups and hence the gas holdup radial profiles can be estimated as follows:

$$\varepsilon_{g,r} = 1 - \epsilon_{s,r} \tag{8}$$

Thus, the radial profiles of the gas holdup were obtained with and without internals at three axial heights (i.e., near the distributor, in the middle of the fluidizing bed, and near the freeboard of the column) and at six radial positions as mentioned earlier.

Figure 4.4 shows the radial profiles of the gas holdup at different superficial gas velocities and axial heights. The effects of the vertical internals on the radial profiles of the gas holdup vary radially and with the axial heights following the opposite trends discussed

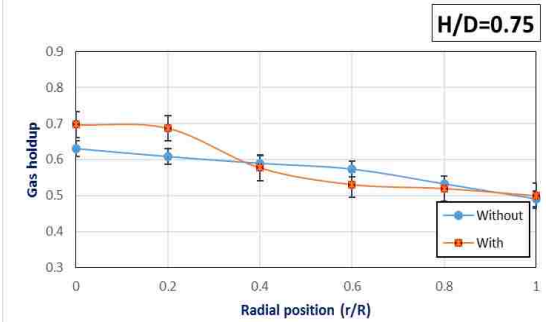

Radial profiles of gas holdup at u/u_{mf} = 1.6 and H/D = 0.75, with and without internals.

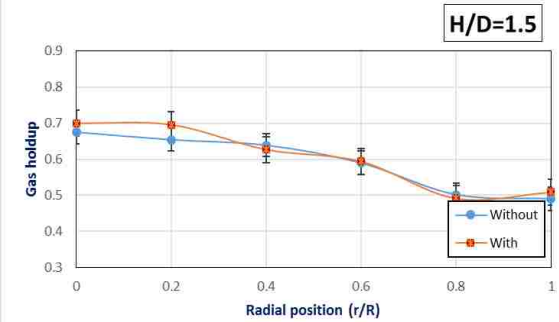

Radial profiles of gas holdup at u/u_{mf} = 1.6 and H/D = 1.5, with and without internals.

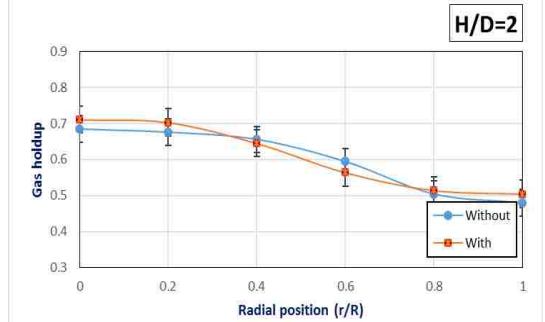

Radial profiles of gas holdup at u/u_{mf} = 1.6 and H/D = 2, with and without internals.

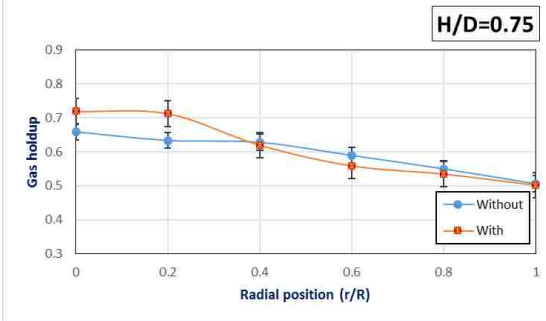

Radial profiles of gas holdup at u/u_{mf} = 1.76 and H/D = 0.75, with and without internals.

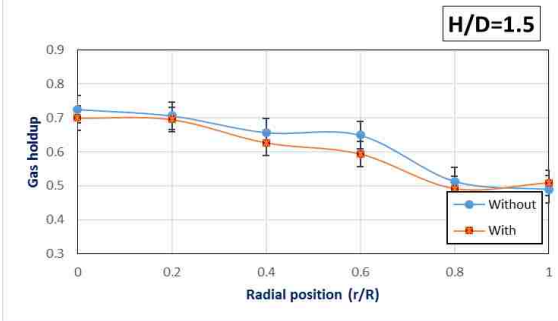

Radial profiles of gas holdup at u/u_{mf} = 1.76 and H/D = 1.5, with and without internals.

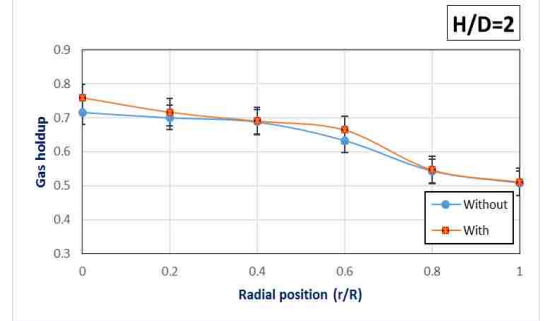

Radial profiles of gas holdup at u/u_{mf} = 1.76 and H/D = 2, with and without internals.

Figure 4.4. Radial profiles of the gas holdup at different axial heights and superficial gas velocities (u/u_{mf}), with and without internals.

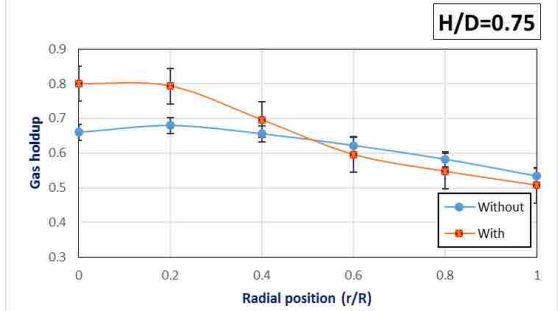

Radial profiles of gas holdup at u/u_{mf} = 1.96 and H/D = 0.75, with and without internals.

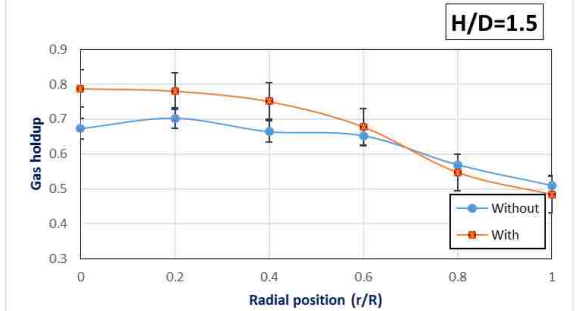

Radial profiles of gas holdup at u/u_{mf} = 1.96 and H/D = 1.5, with and without internals.

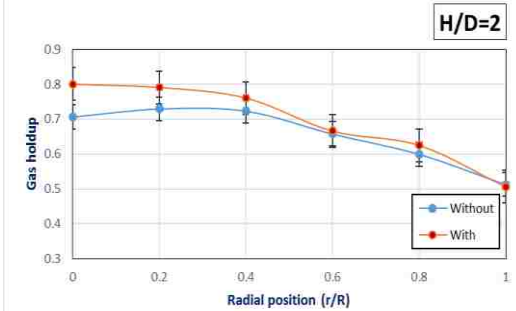

Radial profiles of gas holdup at u/u_{mf} = 1.96 and H/D = 2, with and without internals.

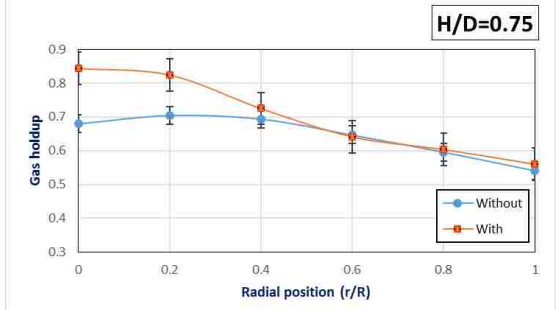

Radial profiles of gas holdup at u/u_{mf} = 2.14 and H/D = 0.75, with and without internals.

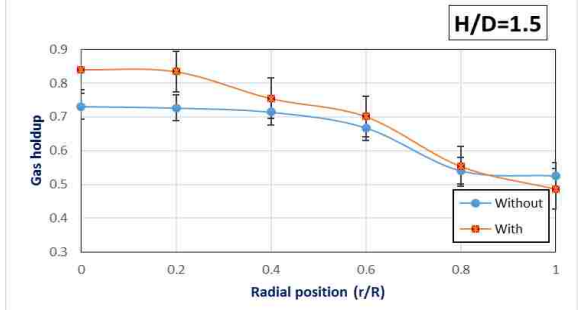

Radial profiles of gas holdup at u/u_{mf} = 2.14 and H/D = 1.5, with and without internals.

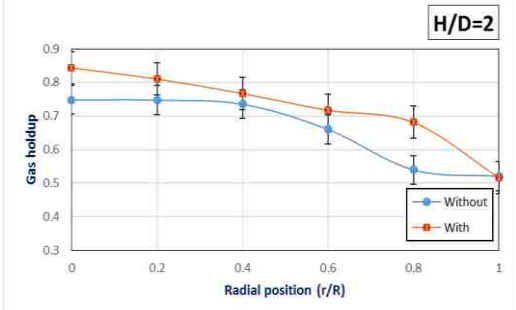

Radial profiles of gas holdup at u/u_{mf} = 2.14 and H/D = 2, with and without internals.

Figure 4.4. Radial profiles of the gas holdup at different axial heights and superficial gas velocities (u/u_{mf}), with and without internals. (cont.)

earlier for solids holdups radial profiles. At H/D = 0.75, the gas holdup is larger near the central region of the column and decreases toward the wall region of the bed for all the superficial gas velocities and for other axial heights as well H/D = 1.5 and 2. This trend become more significant with increasing superficial gas velocities, as in the case of u/u_{mf} = 2.14. At H/D = 1.5, the radial profiles of the gas holdup appeared to close to each other and within the error bars for the case of with and without vertical internals for u/u_{mf} = 1.6 and 1.76. But the differences in gas holdup between the presence of internals and without internals increase with increasing the superficial gas velocity, as in the case of u/u_{mf} = 1.96 and 2.14. The gas holdups are larger with internals as compared to those without internals within the central region of the bed. However, they are close to each other at the wall region because most of bubble attempt to move toward this region and away from drag force effect of the wall as in the case of without internals. Also, the bubble chord lengths decrease with the presence of internals as will be demonstrated in the following sections. These cause enhanced solids circulation and increased center line solids velocity with internals. At H/D = 2.0, the same trends have been found as that at the H/D = 1.5 that discussed above. In general, it can be deduced that with the presence of vertical internals the gas holdups increase within the central region of the bed and as compared to those without internals and it is larger in this region as compared to the wall region.

4.2.2 Bubble Rise Velocity. The bubble rise velocity (BRV) is considered one of the most important bubble properties in the gas-solid fluidizing system, in which the BRV of formed bubbles is essential to estimate the residence time and bubble distribution inside gas-solid fluidized bed reactors. The BRV is a function of the bubble size, operating conditions, solids properties. and design parameters. The placement of the vertical internals

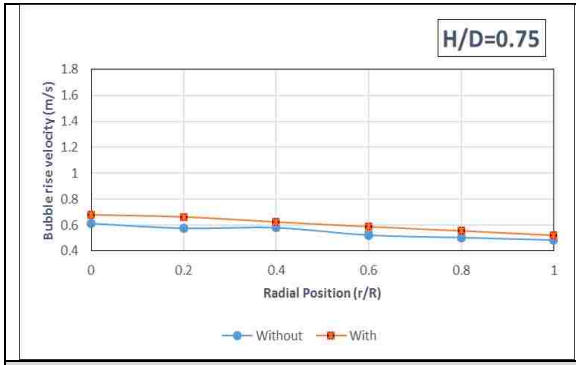

Radial profiles of bubble rise velocity at (u/u_{mf}=1.6) and (H/D=0.75) with and without internals

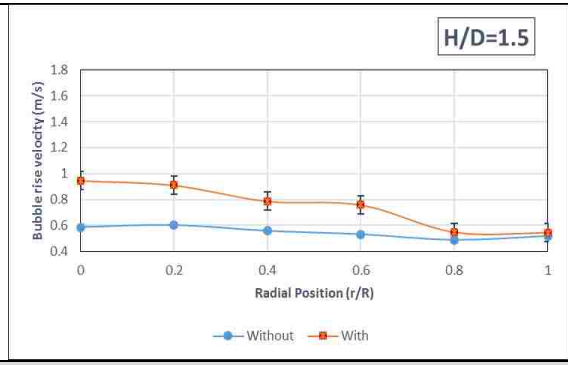

Radial profiles of bubble rise velocity at (u/u_{mf}=1.6) and (H/D=1.5) with and without internals

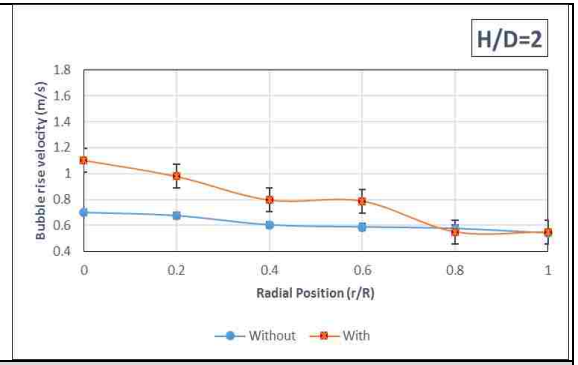

Radial profiles of bubble rise velocity at (u/u_{mf}=1.6) and (H/D=2) with and without internals

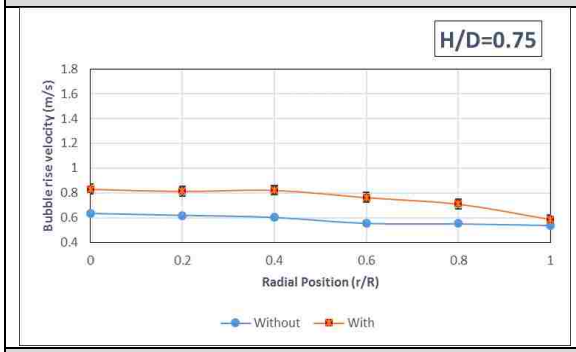

Radial profiles of bubble rise velocity at (u/u_{mf}=1.76) and (H/D=0.75) with and without internals

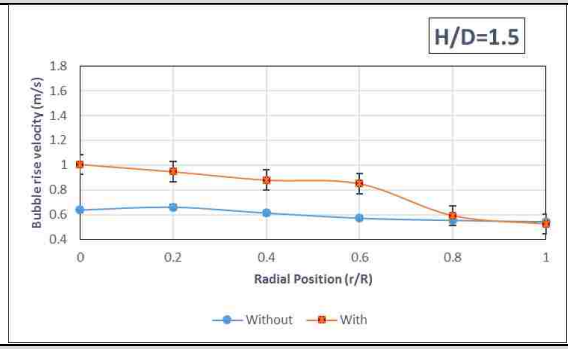

Radial profiles of bubble rise velocity at (u/u_{mf}=1.76) and (H/D=1.5) with and without internals

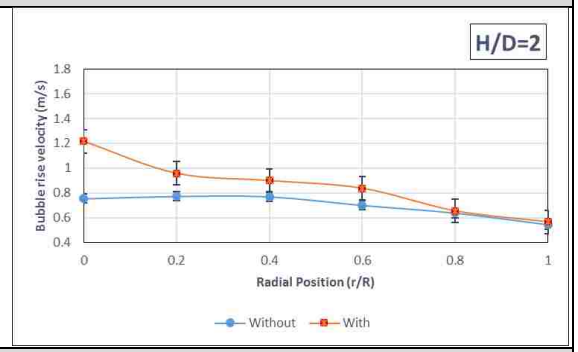

Radial profiles of bubble rise velocity at (u/u_{mf}=1.76) and (H/D=2) with and without internals

Figure 4.5. Radial profiles of bubble rise velocity at different axial heights and superficial gas velocities (u/u_{mf}) with and without internals.

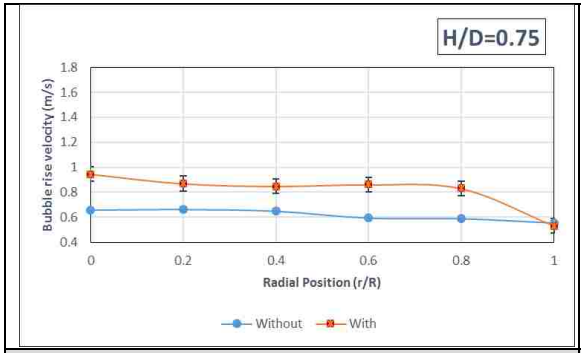

Radial profiles of bubble rise velocity at (u/u_{mf}=1.96) and (H/D=0.75) with and without internals

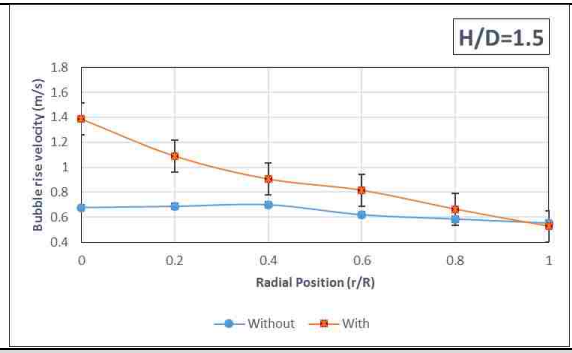

Radial profiles of bubble rise velocity at (u/u_{mf}=1.96) and (H/D=1.5) with and without internals

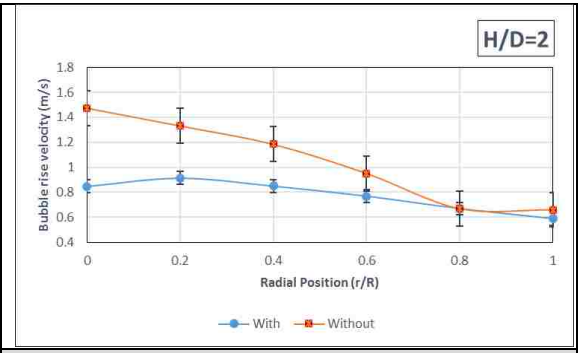

Radial profiles of bubble rise velocity at (u/u_{mf}=1.96) and (H/D=2) with and without internals

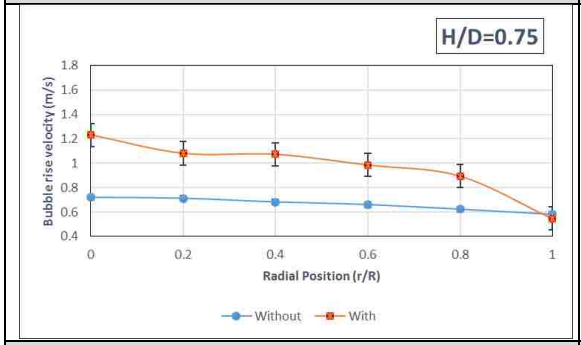

Radial profiles of bubble rise velocity at (u/u_{mf}=2.14) and (H/D=0.75) with and without internals

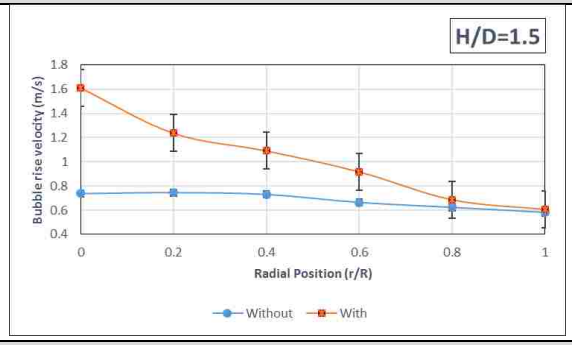

Radial profiles of bubble rise velocity at (u/u_{mf}=2.14) and (H/D=1.5) with and without internals

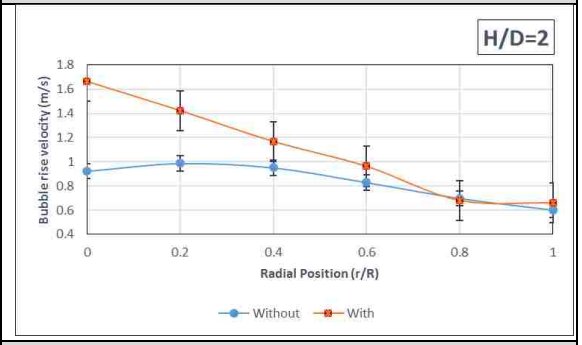

Radial profiles of bubble rise velocity at (u/u_{mf}=2.14) and (H/D=2) with and without internals

Figure 4.5. Radial profiles of bubble rise velocity at different axial heights and superficial gas velocities (u/u_{mf}) with and without internals. (cont.)

inside the gas-solid fluidized bed influences the movement, splitting, and coalescence of the bubbles (Rüdisüli et al. 2012a, b) and hence the BRV as it affects the local gas holdup. Figure 4.5 demonstrates he effect of the vertical internals on the radial profiles of the BRV at three axial heights and four superficial gas velocities (u/u_{mf}). As shown in Figure 4.5, the radial profiles of the BRV vary with the axial height and superficial gas velocity, such that for all heights (H/D = 0.75, 1.5, and 2) the BRV in the case of with internals is lower near the wall region of the bed and increases toward the central region of the bed which is similar trend of the case without internals. Also for all heights the BRV are larger for the case of with internals compared to those without internals at the central region of the bed and the differences increase at higher u/u_{mf} such as 1.96 and 2.14. At the wall region, the differences in BRVs for the case of with and without internals are not significant and within the error bars. These findings are consistent and in relation with the findings discussed earlier of solids velocity and gas holdups. At H/D = 1.5 (the middle zone of the fluidizing bed) and at a low superficial gas velocity (u/u_{mf} = 1.76), the radial profile of the BRV in the case with internals was close to that without internals that there was a small increase in the local BRV in the central region and a decrease in the wall region. Subsequently, with an increase in the superficial gas velocity (u/u_{mf} = 1.76, 1.96, and 2.14), the radial profiles of the BRV are higher than for the case without internals, particularly in the radial positions in the range $r/R \geq 0.6$. At H/D = 2.0 (which represents the zone near the freeboard of the column) and for all the superficial gas velocities tested, the radial profiles of the BRV are higher with the presence of internals for most of the radial positions, but not at the wall region. In other words, the local BRV was larger in the case of vertical internals in the radial positions from $r/R \geq 0.8$. Generally, it can be concluded from the behavior of the

radial profiles of the BRV that the local BRVs at various axial heights increase with vertical internals in the core region of the bed and there is not much difference near the wall region due to the effect of the dragging force and solids circulation.

The cross-sectional average bubble rise velocity ($\overline{BRV}$) was calculated using Eq. 7 and plotted versus the axial height at different superficial gas velocities, as shown in Figures 4.6. In Figure 4.6 a, which displays results at a low superficial gas velocity (u/u_{mf} = 1.6), there is clear difference in the $\overline{BRV}$ between the cases of with and without internals as well as this difference is larger with increase the axial heights. For the other larger gas velocities and at all the axial heights the BRVs are larger with the presence of the internals compared to those without internals. This due to the nature of the effects of the internals on the behavior of the radial profiles of the gas holdup and solids velocity as explained by Rüdisüli et al. (2012a). Generally, the increase in the BRV and $\overline{BRVs}$ due to the use of vertical internals agreed with the results reported in the literature (Grace and Harrison 1968; Yates et al. 1984; Gallucci et al. 2002), in which it has been reported that the bubbles in the case of vertical tubes tend to elongate and move faster in their vertical pathways, especially for the case of large solid particles (i.e., Geldart B). These aforementioned studies also stated that the BRV increases with an increase in the number of vertical immersed tubes.

The percentage of increase of $\overline{BRV}$ for case with internals has been calculated with respect to case without internals. It was found that the percentage of increase of $\overline{BRV}$ is as follows: at u/u_{mf} = 1.76 and at three axial heights (H/D = 0.75, 1.5, and 2.14) the percentage of increase of $\overline{BRV}$ is %22.7, %25.3, and %14.41. At u/u_{mf} = 1.96 and at three axial heights (H/D = 0.75, 1.5, and 2.14) the percentage of increase of $\overline{BRV}$ is %24.1, %29.1, and %29.

At u/u_{mf} = 2.14 and at three axial heights (H/D = 0.75, 1.5, and 2.14) the percentage of increase of $\overline{BRV}$ is %31.6, %33.6, and %23.8. Apparently, the percentage of increase of $\overline{BRV}$ increase when the superficial gas velocity increases from 1.76 to 1.96, as well as the percentage of increase of $\overline{BRV}$ becomes higher when the superficial gas velocity reached 2.14.

The measured $\overline{BRV}$ at different axial heights and superficial gas velocities for the case of with and without internals has been compared with the commonly used formula for estimating the bubble rise velocity (BRV) in a bubbling fluidized beds (Equation 9) by Davidson and Harrison (1963):

$$\overline{u_b} = 0.711\sqrt{g.\overline{d_b}} \quad (9)$$

where, $\overline{u_b}$:represents the average bubble rise velocity, $\overline{d_b}$ is the average bubble size, and g is the gravitational acceleration.

The $\overline{d_b}$ can be estimated from the correlation predicted by Chan et al., (1987) which is shown in Equation 10:

$$\overline{d_b} = 1.43\,\overline{BCL} \quad (10)$$

Where, $\overline{BCL}$:represents the Average bubble chord length that would be discussed in the coming section. The measured and calculated averaged bubble rise velocity for the case of without and with vertical internals are illustrated in Table 4.1 and 4.2, respectively. From the values of absolute percentage relative differences that listed in Tables 4.1 and 4.2, it can be concluded that the measured and calculated values of averaged bubble rise velocities are in good agreement for the case without internals. While, for the case with internals the absolute percentage relative differences are relatively high comparing with case without internals. The reason of this difference is may return to the fact that these

Table 4.1. The measured and calculated averaged bubble rise velocity for the case of without internals.

Measured Averaged Bubble rise velocity		**u/u_{mf} = 1.6**	**u/u_{mf} = 1.76**	**u/u_{mf} = 1.96**	**u/u_{mf} = 2.14**
	H/D = 0.75	0.54	0.58	0.61	0.66
	H/D = 1.5	0.54	0.59	0.63	0.68
	H/D = 2	0.61	0.69	0.77	0.83
Calculated Averaged Bubble rise velocity		**u/u_{mf} = 1.6**	**u/u_{mf} = 1.76**	**u/u_{mf} = 1.96**	**u/u_{mf} = 2.14**
	H/D = 0.75	0.51	0.58	0.58	0.62
	H/D = 1.5	0.557065	0.60	0.63	0.68
	H/D = 2	0.63	0.69	0.72	0.81
% Absolute Relative difference		**u/u_{mf} = 1.6**	**u/u_{mf} = 1.76**	**u/u_{mf} = 1.96**	**u/u_{mf} = 2.14**
	H/D = 0.75	5.2	0.17	4.8	6.2
	H/D = 1.5	1.9	0.86	0.2	1.2
	H/D = 2	4.3	0.21	6.4	2.0

Table 4.2. The measured and calculated averaged bubble rise velocity for the case of with internals.

Measured Averaged Bubble rise velocity		**u/u_{mf} = 1.6**	**u/u_{mf} = 1.76**	**u/u_{mf} = 1.96**	**u/u_{mf} = 2.14**
	H/D = 0.75	0.6	0.75	0.81	0.96
	H/D = 1.5	0.74	0.79	0.89	1.02
	H/D = 2	0.79	0.83	1.04	1.09
Calculated Averaged Bubble rise velocity		**u/u_{mf} = 1.6**	**u/u_{mf} = 1.76**	**u/u_{mf} = 1.96**	**u/u_{mf} = 2.14**
	H/D = 0.75	0.44	0.47	0.50	0.51
	H/D = 1.5	0.42	0.50	0.59	0.62
	H/D = 2	0.56	0.60	0.64	0.70
% Absolute Relative Difference		**u/u_{mf} = 1.6**	**u/u_{mf} = 1.76**	**u/u_{mf} = 1.96**	**u/u_{mf} = 2.14**
	H/D = 0.75	25.7	36.6	38.4	46.6
	H/D = 1.5	42.7	37.3	33.9	38.6
	H/D = 2	28.7	27.3	38	35.6

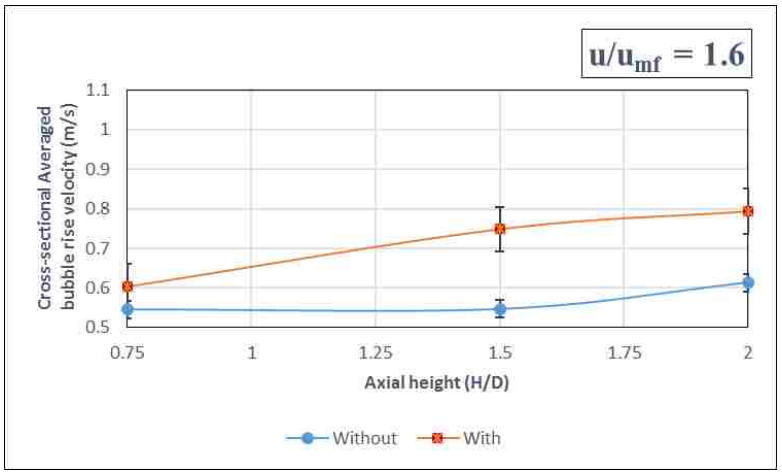

(a)

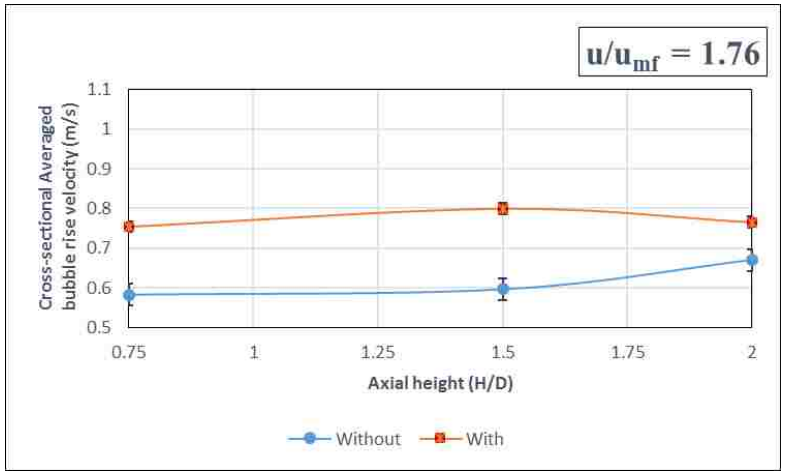

(b)

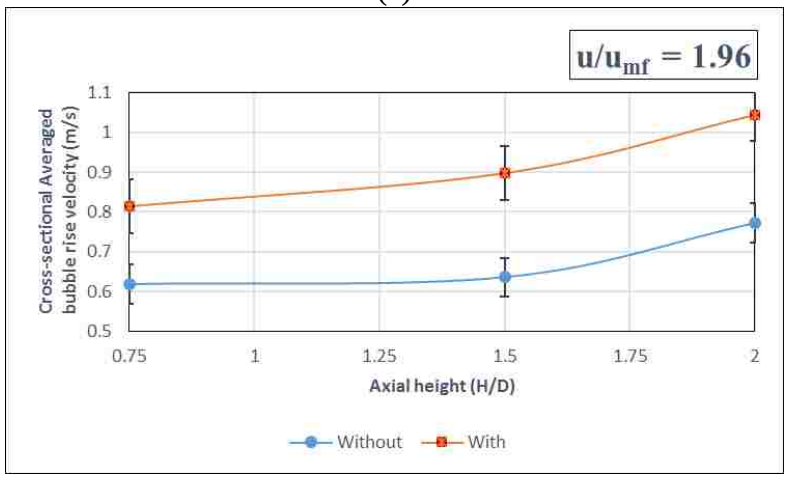

(c)

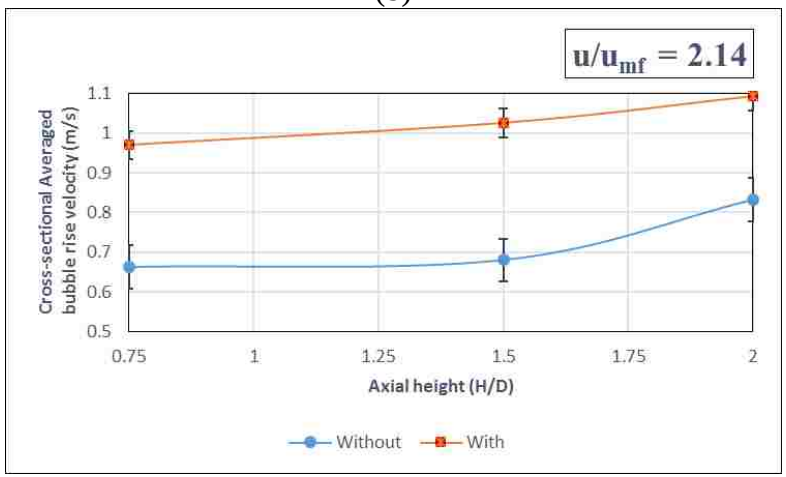

(d)

Figure 4.6. Cross-sectional average bubble rise velocity ($\overline{BRV}$), with and without internals, at different axial heights and superficial gas velocities, (a) u/u_{mf} = 1.6, (b) u/u_{mf} = 1.76, (c) u/u_{mf} = 1.96, and (d) u/u_{mf} = 2.14.

equations (9 and 10) were established for the case of without immersed tubes. In which, these hydrodynamic parameters (bubble rise velocity and bubble size) were measured in the gas-solid fluidized bed system without immersed internals. Accordingly, there is a need to develop a new correlation or formula to account for the effects of the presence of the internals on these parameters.

4.2.3 Bubble Frequency. The bubble frequency or the number of analyzed bubbles per time is considered a significant hydrodynamic parameter in the gas-solid fluidized bed because it reflects the gas phase behavior and distribution in the form of bubbles through the bed of solid particles. The vertical internals have a considerable impact on the bubble frequency in the gas-solid bubbling fluidized bed as reported by Rüdisüli et al. (2012a), who state that the bubble rate is strongly dependent on the radial position in the bed. Therefore, the effect of the vertical internals on the bubble frequency was studied in the present work at different radial positions, axial heights, and superficial gas velocities, so as to understand the bubble distribution in the gas-solid fluidized bed system with vertical immersed tubes.

The radial profiles of the bubble frequency for both cases (i.e., with and without internals) are presented in Figure 4.7, at different axial heights and superficial gas velocities. Figure 4.7 clearly shows that for the case with internals, the radial profiles of the bubble frequency are a function of the axial height and the superficial gas velocity. The following conclusions can be drawn. At H/D = 0.75 and for all the superficial gas velocities tested, the bubble frequency is larger in the radial positions of $r/R \geq 0.7$, except for the highest superficial gas velocity ($u/u_{mf} = 2.14$), at which the entire radial profile of the bubble frequency was higher than in the case without internals. At H/D = 1.5 there is not

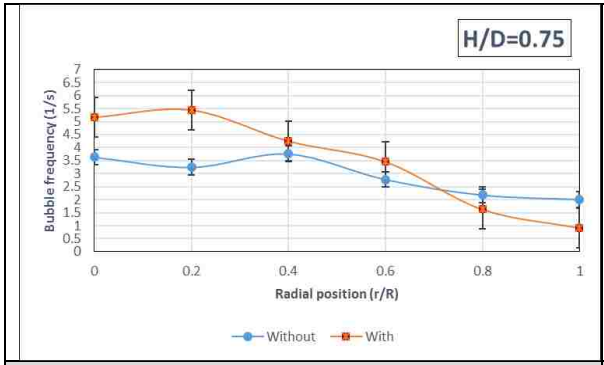

Radial profiles of bubble frequency at (u/u_{mf}=1.6) and (H/D=0.75) with and without internals

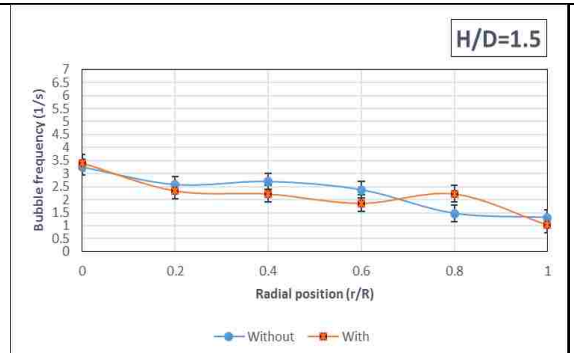

Radial profiles of bubble frequency velocity at (u/u_{mf}=1.6) and (H/D=1.5) with and without internals

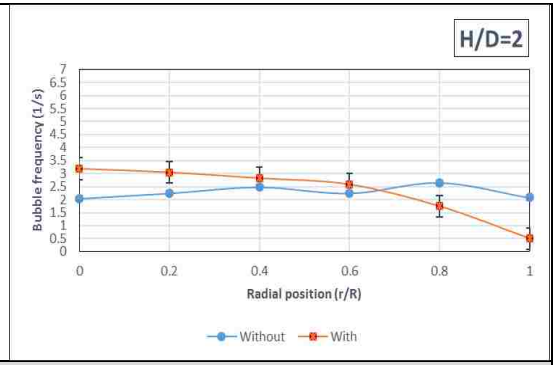

Radial profiles of bubble frequency at (u/u_{mf}=1.6) and (H/D=2) with and without internals

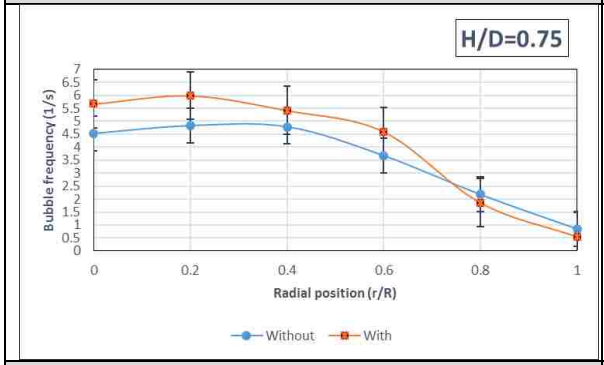

Radial profiles of bubble frequency at (u/u_{mf}=1.76) and (H/D=0.75) with and without internals

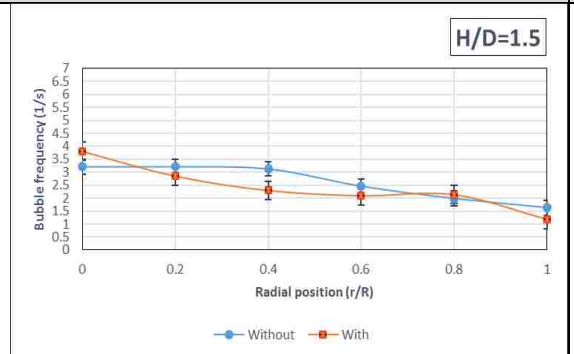

Radial profiles of bubble frequency at (u/u_{mf}=1.76) and (H/D=1.5) with and without internals

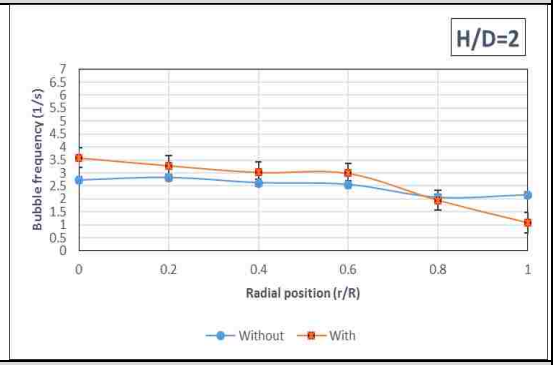

Radial profiles of bubble frequency at (u/u_{mf}=1.76) and (H/D=2) with and without internals

Figure 4.7. Radial profiles of bubble frequency at different axial heights and superficial gas velocities (u/u_{mf}) with and without internals.

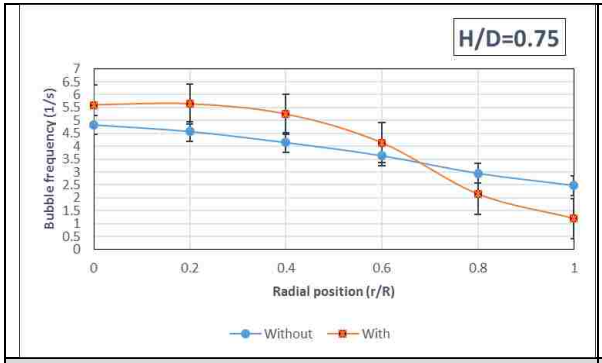

Radial profiles of bubble frequency at (u/u_{mf}=1.96) and (H/D=0.75) with and without internals

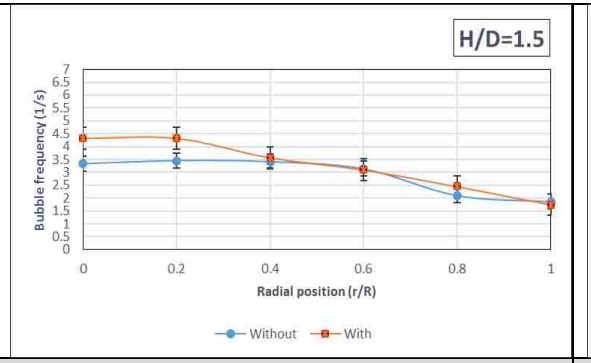

Radial profiles of bubble frequency at (u/u_{mf}=1.96) and (H/D=1.5) with and without internals

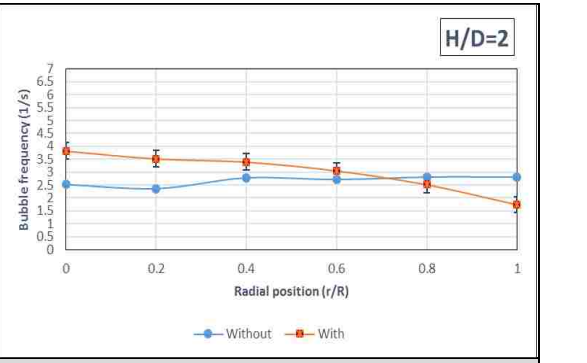

Radial profiles of bubble frequency at (u/u_{mf}=1.96) and (H/D=2) with and without internals

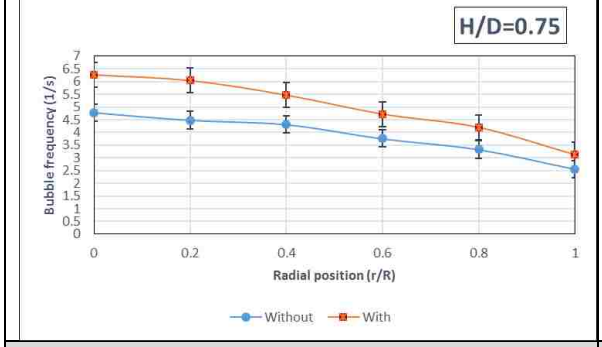

Radial profiles of bubble frequency at (u/u_{mf}=2.14) and (H/D=0.75) with and without internals

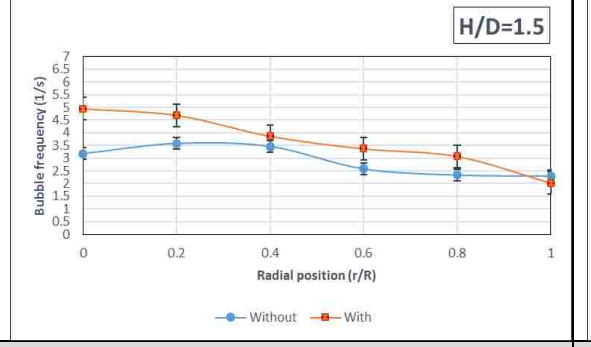

Radial profiles of bubble frequency at (u/u_{mf}=2.14) and (H/D=1.5) with and without internals

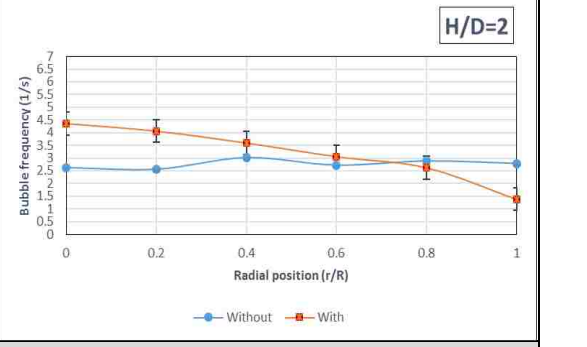

Radial profiles of bubble frequency at (u/u_{mf}=2.14) and (H/D=2) with and without internals

Figure 4.7. Radial profiles of bubble frequency at different axial heights and superficial gas velocities (u/umf) with and without internals. (cont.)

much difference in the bubble frequency between the presence of internals and without internals for u/u_{mf} = 1.6 and 1.76. However, for u/u_{mf} = 1.96 and 2.14, the bubble frequencies are larger with internals at the central region of the bed without much differences with those at the wall region. At H/D = 2 and for all the superficial gas velocities tested, the bubble frequencies were higher than in the case without internals within the radial positions from $r/R \geq 0.7$ and lower near the wall region. Consequently, it is clear that the radial profiles of the bubble frequency shown in Figures 4.7 are (1) similar to the radial profiles of the BRV represented in Figure 4.5, especially at H/D = 0.75 and 2.0 and (2) are slightly different at the axial height of H/D = 1.5 at a high superficial gas velocity. This indicates that both the bubble frequency and BRV are related. Also, the distribution of the bubbles inside the bed is strongly affected by the gas velocity at the axial heights and radial positions inside the bed. Furthermore, depending on the free cross-sectional area available for the gas to flow, the amount of gas in the form of bubbles entering the column is less in the case of with internals in order to have similar u/u_{mf}. However, with vertical internals inside the bed, the bubbles tend to move faster, and the bubble frequency increases due to the action caused by the internals lower ends, in which the presence of immersed tubes leads to enhanced bubble splitting, reduced bubble coalescence, and minimized bubble size as a result of the splitting process caused by the lower edges of the vertical tubes (Ramamoorthy and Subramanian 1981; Rüdisüli et al. 2012a, b; Maurer et al. 2015b).

To further understand the effect of the vertical internals on the bubble frequency at different axial heights and various operating gas velocities, the cross-sectional average bubble frequency ($\overline{BF}$) was calculated using Eq. 7 and plotted versus the superficial gas velocity, as illustrated in Figure 4.8. It can be seen that the $\overline{BF}$ is larger at H/D = 0.75 for

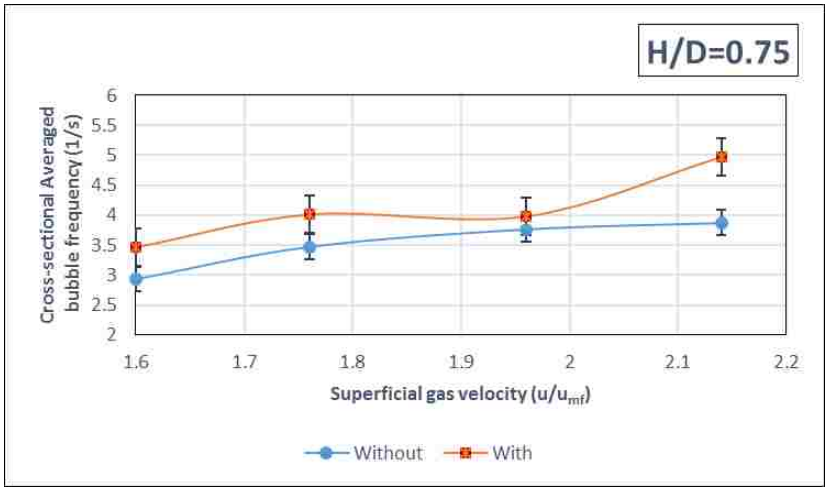

(a)

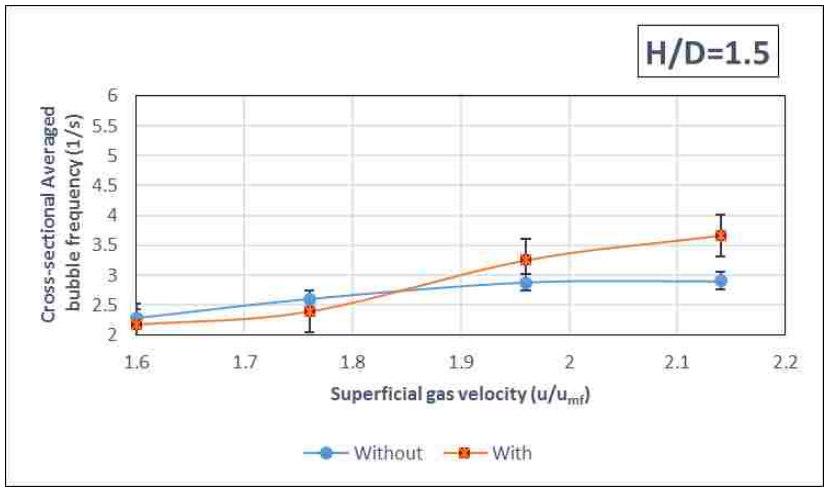

(b)

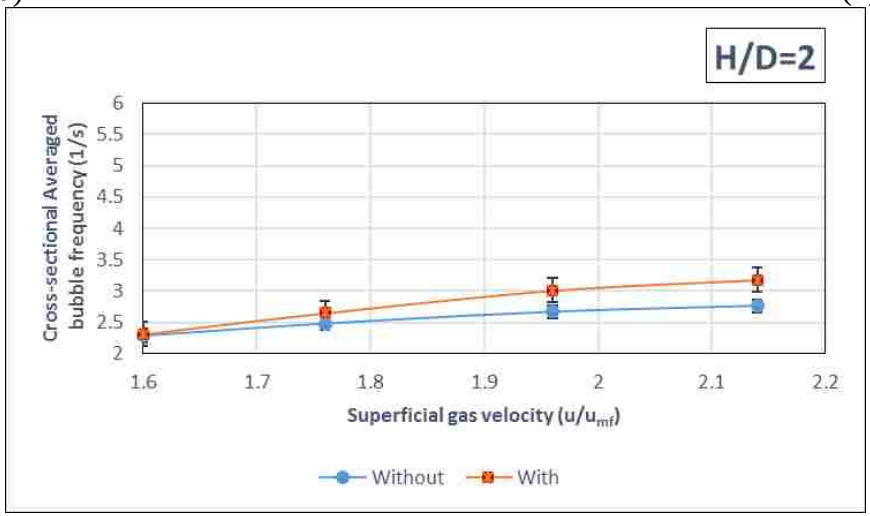

(c)

Figure 4.8. Cross-sectional average bubble frequency ($\overline{BF}$), with and without internals, at different axial heights and superficial gas velocities, (a) H/D = 0.75, (b) H/D = 1.5, and (c) H/D = 2.

both cases (i.e., with and without internals) because this zone is near the distributor level when the bubbles first formed and were small and rising vertically. However, because of the effect of the immersed tubes, which work as bubble splitters and as a bubble coalescence reducer, the bubble frequency rose in the case of internals, as shown in Figure 4.8 a. In which, the percentage of increase of $\overline{BF}$ in the case with vertical internals with different superficial gas velocities (1.6, 1.76, 1.96, and 2.14) is %15.5, %13.51, %5.5, and %22.1, respectively. As the bubbles moved up, they tended to coalesce in the zones between the vertical tubes, and the bubble frequency becomes a function of the superficial gas velocity, as shown in Figure 4.8 b. At H/D = 1.5 (middle zone of the fluidizing bed), there is not much difference between with and without internals beds, the bubble frequency at a low superficial gas velocity (u/u_{mf} =1.6 and 1.76) and it larger at with internals higher at higher superficial gas velocity (u/u_{mf} = 1.96 and 2.14). The percentage of increase of $\overline{BF}$ in the case with vertical internals with different superficial gas velocities (1.96 and 2.14) is %11.3 and %20.7, respectively. It is noteworthy that the bubble frequency at this level for both cases (i.e., with and without internals) was lower than at H/D = 0.75 due to the coalescence between the raised bubbles. Eventually, when the bubbles reached the top zone of the fluidizing bed, the bubble frequency slightly increased compared with H/D = 1.5 for both cases (i.e., with and without internals), as presented in Figure 4.8 c. Also, the bubble frequency was higher than in the case without internals for all the superficial gas velocities due to the reduction of bubble coalescence as a result of the presence of the internals. In which, the percentage of increase of $\overline{BF}$ in the case with vertical internals with different superficial gas velocities (1.6, 1.76, 1.96, and 2.14) is %1, %6.3, %11.3, and %13,

respectively. It can be noticed that the percentage of increase of $\overline{BF}$ in the case with vertical internals is high at the higher superficial gas velocity at all the axial height.

4.2.4 Bubble Chord Length. The bubble chord length or bubble chord diameter is a substantial hydrodynamic parameter in the design, scale-up, operation, and performance of gas-solid fluidized bed reactors. The bubble chord length is also a function of the operating conditions, solids properties, and design parameters. Therefore, in this work, the bubble chord length distribution was measured using an optical fiber probe and was correlated to the bubble frequency to evaluate the bubble mean chord length, which represents the chord length of the detected bubbles per the number of bubbles. Rüdisüli et al., (2012d) showed that the chord length of the bubble that is measured by using two tips optical fiber probe can be taken as a representative bubble size in the bed with ± 10% percentage error. As mentioned earlier, the measurements of the bubble hydrodynamic characteristics were carried out at various axial levels and radial positions, and the experiments were conducted at four superficial gas velocities to facilitate the understanding of the hydrodynamic behavior of gas bubbles inside a gas-solid fluidized bed with vertical immersed tubes.

The radial profiles of the bubble mean chord length (BMCL) are plotted in Figure 4.9 at different axial heights and superficial gas velocities for the cases with and without internals. Figure 4.9 shows that the bubble mean chord length in the case of vertical internals smaller for all radial positions, axial heights, and superficial gas velocities used compared to that without internals. The BMCL is smaller due to the effect of the vertical immersed tubes, which led to a reduction in the bubble size by splitting them and increasing the bubble frequency. The decrease in the BMCL found in this study agrees with other

works (Glass and Harrison 1964; Yates et al. 1984; Rüdisüli et al. 2012a, b; Maurer et al. 2015a). Furthermore, at H/D = 0.75, the BMCL reduction is high near the wall region and lower toward the center of the bed, while at H/D = 1.5 and 2, the reduction in the BMCL is noticeable for all radial profiles and superficial gas velocities. In general, the BMCL is smaller in the case of vertical internals because the large bubbles split, and a maximum bubble size reduction of 55% was obtained at H/D = 0.75, r/R = 0.8, and u/u_{mf} = 2.14, in which the bubble size was reduced to about half of its size in the case without internals.

The cross-sectional average bubble mean size $\overline{BMCL}$ was calculated using Eq. 7 for different axial heights and superficial gas velocities for the two cases (i.e., with and without internals). In addition, the percentage of the reduction in bubble mean chord length in the case of internals was evaluated and is plotted in Figure 4.10 based on the values of the $\overline{BMCL}$. As shown in Figure 4.10, the percentage reduction of the $\overline{BMCL}$ clearly varies based on the axial height of H/D = 1.5, in which the values of the percentage reduction of $\overline{BMCL}$ are ranged from 12% to 40%. However, in comparison, the percentage of the reduction of the $\overline{BMCL}$ are ranged from 24% to 33% for H/D = 0.75 and from 19% to 25% for H/D = 2. Moreover, the percentage of bubble size reduction is larger in the zone near the distributor level (H/D = 0.75) with respect to the top zone of the fluidizing bed (H/D = 2) for all the superficial gas velocities because the vertical internals faced downward, which reduced the bubble size. In contrast, the trend of the bubble size reduction at H/D = 0.75 is not uniform and varied irregularly with the superficial gas velocity due to the chaotic nature of the sparger zone.

The bubble size at different axial heights and superficial gas velocities for the case of with and without internals has been calculated using the correlation proposed by Chan

et al., (1987) which shown earlier in Equation 10 that mentioned earlier. The average bubble size that estimated using Chan et al., (1987) at different axial heights and for each superficial gas velocity has been compared with the empirical correlation proposed by Darton et al. (1977) for the case of with and without vertical internals (Equation 11):

$$\overline{d_b} = 0.54\,(u - u_{mf})^{0.4}\,H_s^{0.8}\,g^{-0.2} \qquad (11)$$

The average bubble size that estimated using Chan et al., (1987) and Darton et al. (1977) for each superficial gas velocity and for the case of without and with vertical internals are listed in Table 4.3 and 4.4. It is clearly shown from the values of absolute

Table 4.3. The averaged bubble size calculated using Chan et al., (1987) and Darton et al. (1977) at different superficial gas velocities for the case of without internals.

Averaged Bubble size using Chan et al., (1987)	**u/u_{mf} = 1.6**	**u/u_{mf} = 1.76**	**u/u_{mf} = 1.96**	**u/u_{mf} = 2.14**
	0.06	0.07	0.08	0.10
Averaged Bubble size using Darton et al. (1977)	**u/u_{mf} = 1.6**	**u/u_{mf} = 1.76**	**u/u_{mf} = 1.96**	**u/u_{mf} = 2.14**
	0.07	0.09	0.10	0.107
% Absolute Relative difference	**u/u_{mf} = 1.6**	**u/u_{mf} = 1.76**	**u/u_{mf} = 1.96**	**u/u_{mf} = 2.14**
	10	15	17	5.1

Table 4.4. The averaged bubble size calculated using Chan et al., (1987) and Darton et al. (1977) at different superficial gas velocities for the case of with internals.

Averaged Bubble size using Chan et al., (1987)	**u/u_{mf} = 1.6**	**u/u_{mf} = 1.76**	**u/u_{mf} = 1.96**	**u/u_{mf} = 2.14**
	0.047	0.057	0.068	0.077
Averaged Bubble size using Darton et al. (1977)	**u/u_{mf} = 1.6**	**u/u_{mf} = 1.76**	**u/u_{mf} = 1.96**	**u/u_{mf} = 2.14**
	0.073	0.09	0.1	0.1
% Absolute Relative Difference	**u/u_{mf} = 1.6**	**u/u_{mf} = 1.76**	**u/u_{mf} = 1.96**	**u/u_{mf} = 2.14**
	54	60	46	38

percentage relative difference that the averaged bubble size calculated by Chan et al., (1987) and Darton et al. (1977) equation are in good agreement for the case without internals as listed in Table 4.3, in which the maximum absolute percentage relative difference can reach about 17%. While, for the case of with vertical internals, the absolute percentage relative difference is high and range from 38% to 60%. The values of absolute percentage relative difference are shown that these correlations are not applicable for the case of vertical internals as in the case of estimating the average bubble rise velocity, since these correlations were established for the gas-solid fluidized bed without the presence of vertical immersed tubes.

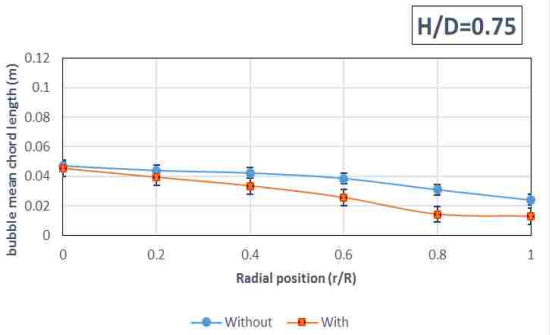

Radial profiles of bubble mean chord length at u/u_{mf} = 1.6 and H/D = 0.75, with and without internals.

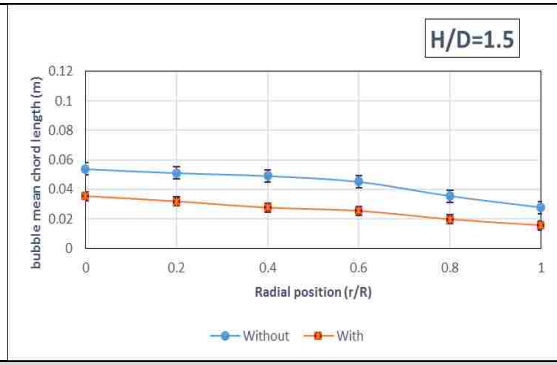

Radial profiles of bubble mean chord length velocity at u/u_{mf} = 1.6 and H/D = 1.5, with and without internals.

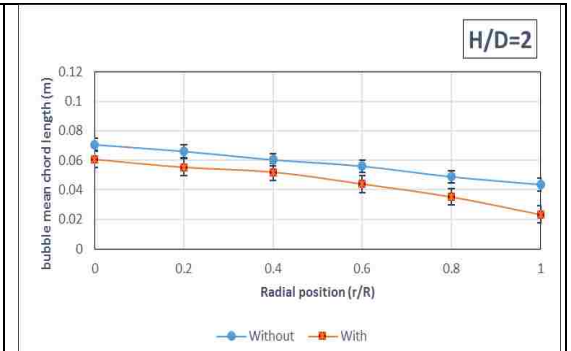

Radial profiles of bubble mean chord length at u/u_{mf} = 1.6 and H/D = 2, with and without internals.

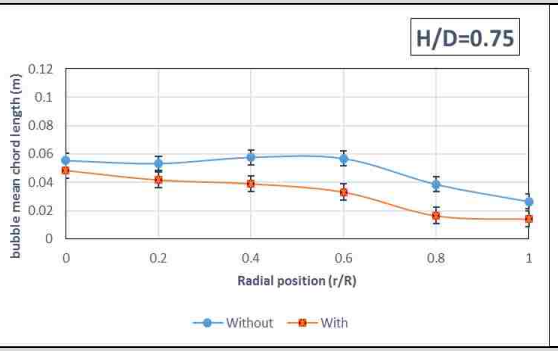

Radial profiles of bubble mean chord length at u/u_{mf} = 1.76 and H/D = 0.75, with and without internals.

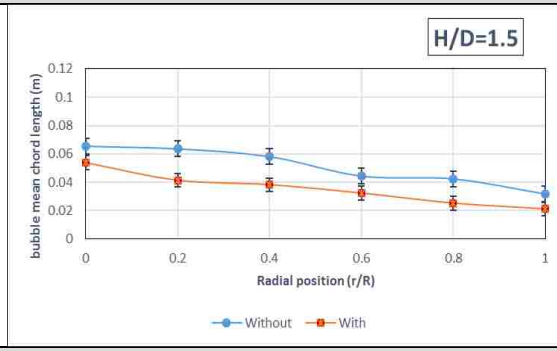

Radial profiles of bubble mean chord length at u/u_{mf} = 1.76 and H/D = 1.5, with and without internals.

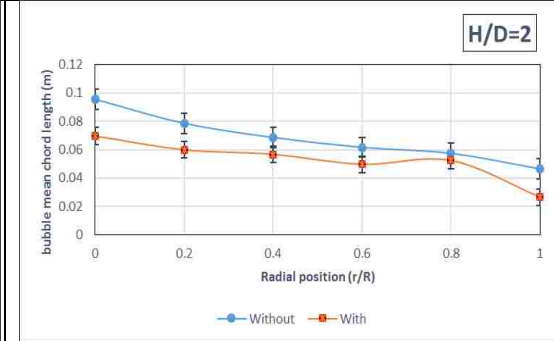

Radial profiles of bubble mean chord length at u/u_{mf} = 1.76 and H/D = 2 with and without internals.

Figure 4.9. Radial profiles of the bubble mean chord length at different axial heights and superficial gas velocities (u/u_{mf}), with and without internals.

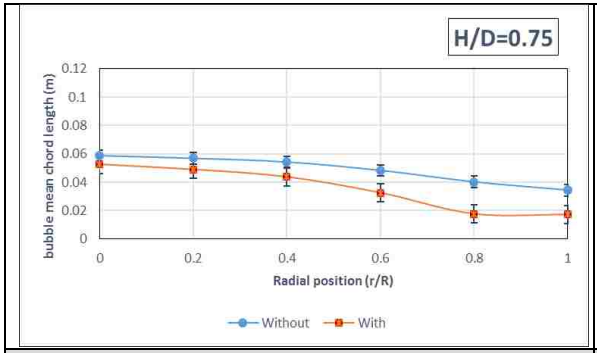

Radial profiles of bubble mean chord length at u/u_{mf} = 1.96 and H/D = 0.75, with and without internals.

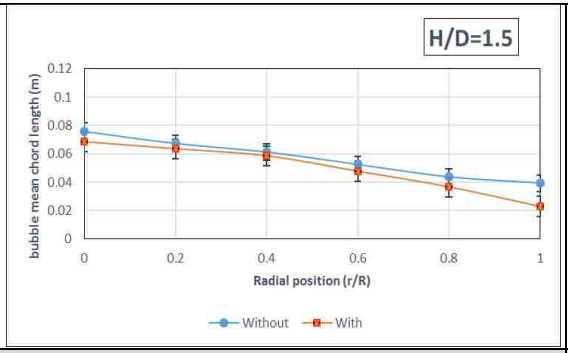

Radial profiles of bubble mean chord length at u/u_{mf} = 1.96 and H/D = 1.5, with and without internals.

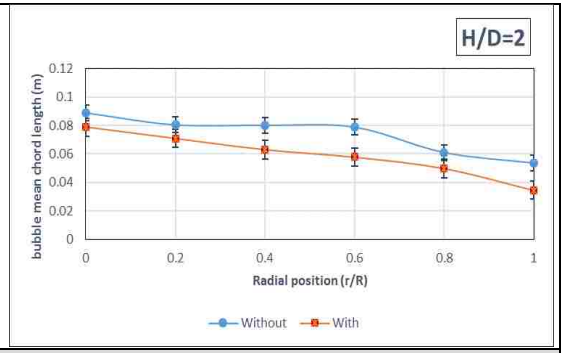

Radial profiles of bubble mean chord length at u/u_{mf} = 1.96 and H/D = 2, with and without internals.

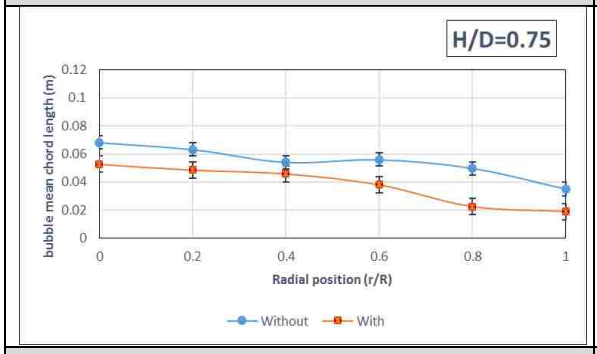

Radial profiles of bubble mean chord length at u/u_{mf} = 2.14 and H/D = 0.75, with and without internals.

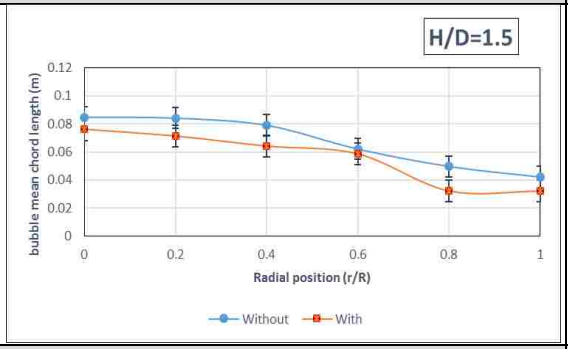

Radial profiles of bubble mean chord length at u/u_{mf} = 2.14 and H/D =1.5, with and without internals.

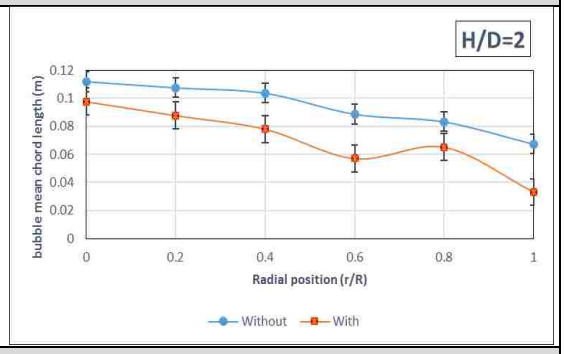

Radial profiles of bubble mean chord length at u/u_{mf} = 2.14 and H/D = 2, with and without internals.

Figure 4.9. Radial profiles of the bubble mean chord length at different axial heights and superficial gas velocities (u/u_{mf}), with and without internals. (cont.)

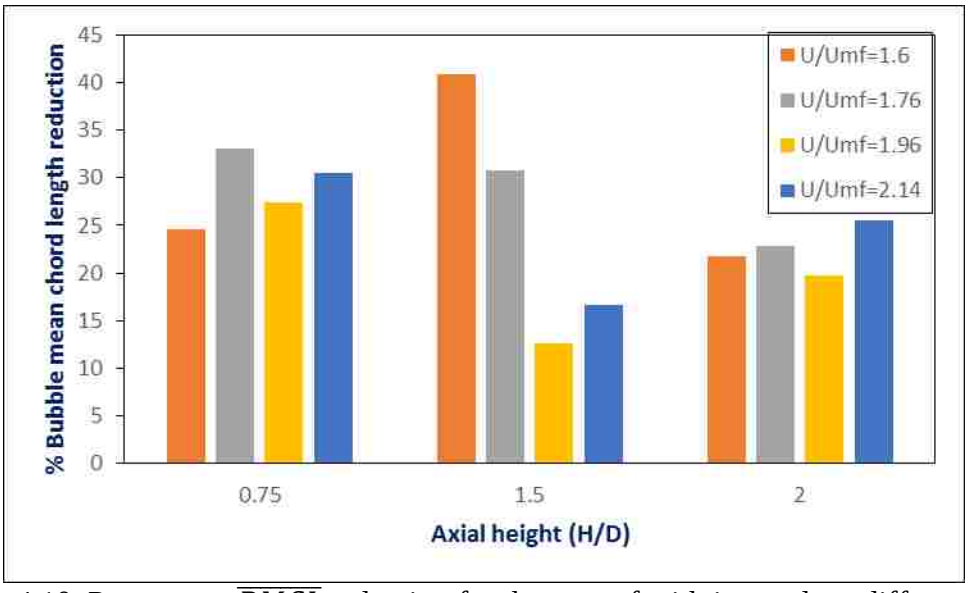

Figure 4.10. Percentage $\overline{BMCL}$ reduction for the case of with internals at different axial heights and superficial gas velocities.

5. REMARKS

The impact of the vertical immersed tubes on the gas and solid hydrodynamic parameters has been investigated in a gas-solid fluidized bed of 0.14 m inside diameter. The experimental measurements were performed using an advanced optical fiber probe technique, enabling the simultaneous measurement of six essential local hydrodynamic parameters: local solids holdup, particles velocity, gas holdup, bubble rise velocity, bubble frequency, and bubble mean chord length. The circular configuration of dense vertical internals (occupying 25% of the cross-sectional area) was employed to represent the vertical heat exchange tubes inside a conventional gas-solid fluidized bed reactor. Different radial positions (r/R), axial heights (H/D), and superficial gas velocities (u/u_{mf}) were chosen to illustrate the influence of the vertical internals on the behavior of the studied hydrodynamic characteristics inside the bed. It was experimentally demonstrated that the vertical internals had a considerable effect on the six hydrodynamic properties examined

in this study, such that the presence of vertical immersed tubes inside the bed acted as a bubble splitter and bubble coalescence reducer, thus leading to an increase in the gas holdup and hence a decrease in the solid holdup, increasing in the upward and downward particle velocities, local gas holdup, bubble rise velocity, and bubble frequency, while the bubble mean chord length decreased. The averaged bubble rise velocity and the calculated averaged bubble size have been compared with the correlations available in the literature. It was found for these hydrodynamic parameters (averaged bubble rise velocity and calculated averaged bubble size) that the correlations used for the case of without internals are applicable with low absolute percentage relative differences, while for the case of vertical internals, the absolute percentage relative differences indicate the inapplicability of these empirical correlations when the used gas-solid fluidized bed with vertical immersed tubes. The vertical internals help to improving the hydrodynamics inside the gas-solid fluidized bed because the influence of these immersed internals enhanced the gas-solid mixing and the heat and mass transfer rates, so that the gas residence time and the local gas-solid interaction would increase accordingly.

ACKNOWLEDGEMENTS

The authors would like to thank the Multiphase Reactors Engineering and Applications Laboratory (mReal) for funding and support.

NOMENCLATURE

D	inside column diameter (m)
d_p	particle mean diameter or average particle diameter (μm)
H	axial height (m)

H_s	static bed height (m)
g	gravitational acceleration
r	radial position (m)
R	radius of the column (m)
u	superficial gas velocity (m/s)
U_B	bubble velocity (m/s)
u_{mf}	minimum fluidized velocity (m/s)
V_p	particle velocity (m/s)
ρ_p	solid particle density or solid density (Kg/m^3)

Greek Letters

εs	solid holdup
ρ	density (Kg/m3)
φ	sphericity factor

Subscripts and Superscripts

B	bubble
mf	minimum fluidization
p	particle
f	fluid
s	solid

Abbreviations

$\overline{d_b}$	averaged bubble size
$\overline{V_p}$	cross-sectional average particles velocity
$\overline{\varepsilon_s}$	cross-sectional average solid holdup
$\overline{\mathrm{BF}}$	cross-sectional average bubble rise velocity frequency
$\overline{\mathrm{BMCL}}$	cross-sectional average bubble mean chord length
$\overline{\mathrm{BRV}}$	cross-sectional average bubble rise velocity

REFERENCES

A. Pinto. 1978. Ammonia Production Process, issued 1978.

Al-Dahhan, M., S. Aradhya, F. Zaid, N. Ali, and T. Aljuwaya. 2014. "Scale-up and On-Line Monitoring of Gas-Solid Systems Using Advanced and Non-Invasive Measurement Techniques." *Procedia Engineering* 83. Elsevier B.V.: 469–76. doi:10.1016/j.proeng.2014.09.080.

Bartholomew, Calvin H., and Robert J. Farrauto. 2010. *Fundamentals of Industrial Catalytic Processes: Second Edition*. *Fundamentals of Industrial Catalytic Processes: Second Edition*. doi:10.1002/9780471730071.

Bhusarapu, Satish, Muthanna H. Al-Dahhan, Milorad P. Duduković, Steven Trujillo, Timothy J. O'Hern, Milorad P Dudukovic, Steven Trujillo, and Timothy J O Hern. 2005. "Experimental Study of the Solids Velocity Field in Gas - Solid Risers." *Industrial and Engineering Chemistry Research* 44 (25): 9739–49. doi:10.1021/ie050297f.

Chan, I. H., C. Sishtla, and T. M. Knowlton. 1987. "The Effect of Pressure on Bubble Parameters in Gas-Fluidized Beds." *Powder Technology*.

Darton, Rc, Rd LaNauze, Jf Davidson, and D Harrison. 1977. "Bubble Growth due to Coalescence in Fluidised Beds." *Transcripts of the Institute of Chemical Engineering* 55: 274–80. http://ci.nii.ac.jp/naid/80014839677/.

Davidson, J. F., and D. Harrison. 1963. *Fluidized Particles*. First ed. Cambridge, New York: Cambridge University Press.

Efhaima, Abdelsalam. 2016. "Scale-up Investigation and Hydrodynamics Study of Gas-Solid Fluidized Bed Reactor Using Advanced Non- Invasive Measurement Techniques." PhD Thesis, Missouri University of Science and Technology.

Gallucci, K., N. Jand, P. U. Foscolo, and M. Santini. 2002. "Cold Model Characterisation of a Fluidised Bed Catalytic Reactor by Means of Instantaneous Pressure Measurements." *Chemical Engineering Journal* 87 (1): 61–71. doi:10.1016/S1385-8947(01)00202-9.

Glass, D. H., and D. Harrison. 1964. "Flow Patterns near a Solid Obstacle in a Fluidized Bed." *Chemical Engineering Science* 16 (12): 1001–2. doi:10.1016/0009-2509(64)85112-5.

Grace, J. R., and D. Harrison. 1968. "The Effect of Internal Baffles in Fluidized Beds: A Guide to Design." In *Inst. Chem. Eng. Symp. Ser.*

Halvorsen, B. 2005. “An Experimental and Computational Study of Flow Behaviour in Bubbling Fluidized Beds.” PhD thesis, The Norwegian University of Science and Technology, Norway. http://teora.hit.no/dspace/handle/2282/301.

Laverman, J. A., X. Fan, A. Ingram, Van Sint M Annaland, D. J. Parker, J. P K Seville, and J. A M Kuipers. 2012. “Experimental Study on the Influence of Bed Material on the Scaling of Solids Circulation Patterns in 3D Bubbling Gas-Solid Fluidized Beds of Glass and Polyethylene Using Positron Emission Particle Tracking.” *Powder Technology* 224. Elsevier B.V.: 297–305. doi:10.1016/j.powtec.2012.03.011.

Law, Chung Lim, Siti Masrinda Tasirin, Wan Ramli Wan Daud, and Derek Geldart. 2003. “Effect of Vertical Baffles on Particle Mixing and Drying in Fluidized Beds of Group D Particles.” *China Particuology* 1 (3): 115–18. doi:10.1016/S1672-2515(07)60121-3.

Maurer, Simon, Evert C Wagner, Tilman J Schildhauer, J. Ruud van Ommen, Serge M A Biollaz, and Robert F Mudde. 2015. “X-Ray Measurements of Bubble Hold-up in Fluidized Beds with and without Vertical Internals.” *International Journal of Multiphase Flow* 74. Elsevier Ltd: 118–24. doi:10.1016/j.ijmultiphaseflow.2015.03.009.

Maurer, Simon, Evert C Wagner, J. Ruud van Ommen, Tilman J Schildhauer, Sinan L Teske, Serge M A Biollaz, Alexander Wokaun, and Robert F Mudde. 2015. “Influence of Vertical Internals on a Bubbling Fluidized Bed Characterized by X-Ray Tomography.” *International Journal of Multiphase Flow* 75. Elsevier Ltd: 237–49. doi:10.1016/j.ijmultiphaseflow.2015.06.001.

Olowson, P.A. 1994. “Influence of Pressure and Fluidization Velocity on the Hydrodynamics of a Fluidized Bed Containing Horizontal Tubes.” *Chemical Engineering Science* 49 (15): 2437–46.

Ozawa, M, H. Umekawa, S. Furui, K. Hayashi, and N. Takenaka. 2002. “Bubble Behavior and Void Fraction Fluctuation in Vertical Tube Banks Immersed in a Gas-Solid Fluidized-Bed Model.” *Experimental Thermal and Fluid Science* 26 (6–7): 643–52. doi:10.1016/S0894-1777(02)00178-4.

Ozawa, M, H Umekawa, S Furui, K Hayashi, and N Takenaka. 2004. “Quantitative Flow Visualization of Fluidized-Bed Heat Exchanger by Neutron Radiography.” In *Applied Radiation and Isotopes*, 61:715–24. doi:10.1016/j.apradiso.2004.03.099.

Ramamoorthy, S., and N. Subramanian. 1981. “Axial Solids Mixing and Bubble Characteristics in Gas-Fluidized Beds with Vertical Internals.” *Chemical Engineering Journal* 22 (3): 237–42.

Rüdisüli, Martin, Tilman J. Schildhauer, Serge M.A. Biollaz, and J. Ruud van Ommen. 2012. "Monte Carlo Simulation of the Bubble Size Distribution in a Fluidized Bed with Intrusive Probes." *International Journal of Multiphase Flow* 44 (September): 1–14. doi:10.1016/j.ijmultiphaseflow.2012.03.009.

Rüdisüli, Martin, Tilman J. Schildhauer, Serge M. A. Biollaz, and J. Ruud Van Ommen. 2012a. "Radial Bubble Distribution in a Fluidized Bed with Vertical Tubes." *Industrial and Engineering Chemistry Research* 51 (42): 13815–24. doi:10.1021/ie3004418.

Rüdisüli, Martin, Tilman J Schildhauer, Serge M A Biollaz, and J. Ruud van Ommen. 2012. "Bubble Characterization in a Fluidized Bed by Means of Optical Probes." *International Journal of Multiphase Flow* 41: 56–67. doi:10.1016/j.ijmultiphaseflow.2012.01.001.

Rüdisüli, Martin, Tilman J Schildhauer, Serge M A Biollaz, and J. Ruud Van Ommen. 2012b. "Bubble Characterization in a Fluidized Bed with Vertical Tubes." *Industrial and Engineering Chemistry Research* 51 (12): 4748–58. doi:10.1021/ie2022306.

Schweitzer, J. M., J. Bayle, and T. Gauthier. 2001. "Local Gas Hold-up Measurements in Fluidized Bed and Slurry Bubble Column." *Chemical Engineering Science* 56 (3): 1103–10. doi:10.1016/S0009-2509(00)00327-4.

Tebianian, Sina, Kristian Dubrawski, Naoko Ellis, Ray A. Cocco, Roy Hays, S. B. Reddy Karri, Thomas W. Leadbeater, et al. 2015. "Investigation of Particle Velocity in FCC Gas-Fluidized Beds Based on Different Measurement Techniques." *Chemical Engineering Science* 127. Elsevier: 310–22. doi:10.1016/j.ces.2015.01.049.

Tebianian, Sina, Kristian Dubrawski, Naoko Ellis, Ray A. Cocco, Roy Hays, S.B. Reddy Karri, Thomas W. Leadbeater, et al. 2016. "Comparison of Particle Velocity Measurement Techniques in a Fluidized Bed Operating in the Square-Nosed Slugging Flow Regime." *Powder Technology* 296 (August). Elsevier B.V.: 45–52. doi:10.1016/j.powtec.2015.08.040.

Tijm, P. J A, F. J. Waller, and D. M. Brown. 2001. "Methanol Technology Developments for the New Millennium." *Applied Catalysis A: General* 221 (1–2): 275–82. doi:10.1016/S0926-860X(01)00805-5.

van Dijk, R. 2007. "Bubble Size Reduction in Fluidized Beds by Varying Particle Size Distribution Using High Throughput Experimentation." Diss. MA thesis. Delft University of Technology (TU Delft).

Verma, Vikrant, Tingwen Li, Jean-François Dietiker, and William A. Rogers. 2016. "Hydrodynamics of Gas–solids Flow in a Bubbling Fluidized Bed with Immersed Vertical U-Tube Banks." *Chemical Engineering Journal* 287. Elsevier B.V.: 727–43. doi:10.1016/j.cej.2015.11.049.

Volk, W., C. A. Johnson, and H. H. Stotler. 1962. “Effect of Reactor Internals on Quality of Fluidization.” *Chemical Engineering Progress* 58 (3): 44–47.

Wang, Qicheng, Kai Zhang, Kuanli Yang, and Jianchun Jiang. 2008. “Particle Velocity in a Dense Gas-Solid Fluidized Bed.” *International Journal of Chemical Reactor Engineering* 6.

Yates, J.G., D.J. Cheesman, T.A. Mashingaidze, C. Howe, and G Jefferis. 1984. “The Effect of Vertical Rods on Bubbles in Gas Fluidized Beds.” In *Engineering Foundation*, 103–10. New York.

Yurong, He, Lu Huilin, Sun Qiaoqun, Yang Lidan, Zhao Yunhua, Dimitri Gidaspow, and Jacques Bouillard. 2004. “Hydrodynamics of Gas-Solid Flow around Immersed Tubes in Bubbling Fluidized Beds.” *Powder Technology* 145 (2): 88–105. doi:10.1016/j.powtec.2004.04.047.

Zhang, H., P. M. Johnston, J. X. Zhu, H. I. De Lasa, and M. A. Bergougnou. 1998. “A Novel Calibration Procedure for a Fiber Optic Solids Concentration Probe.” *Powder Technology* 100 (2–3): 260–72. doi:10.1016/S0032-5910(98)00147-8.

Zhu, Haiyan, Jesse Zhu, Guozheng Li, and Fengyun Li. 2008. “Detailed Measurements of Flow Structure inside a Dense Gas-Solids Fluidized Bed.” *Powder Technology* 180 (3): 339–49. doi:10.1016/j.powtec.2007.02.043.

II. HEAT TRANSFER AND HYDRODYNAMICS IN A GAS-SOLID FLUIDIZED BED WITH VERTICAL IMMERSED INTERNALS

Haidar Taofeeq[1] and Muthanna Al-Dahhan[2*]

Multiphase Reactors Engineering and Applications Laboratory (mReal)

Department of Chemical & Biochemical Engineering

Missouri University of Science & Technology, Rolla, MO-65409 USA

ABSTRACT

An investigation of the influence of a bundle of intense vertical immersed tubes on the local heat transfer coefficients and related gas hydrodynamics of bubble frequency and gas holdup was conducted in a gas-solid fluidized bed of 0.14 m inside diameter. The heat transfer coefficient and bubble frequency and gas holdup were measured using an advanced non-invasive fast response heat transfer probe and sophisticated optical fiber probe techniques, respectively. A circular configuration of 30 vertical immersed tubes of 0.0127 m diameter occupying 25% of the cross-sectional area was employed. Glass bead solid particles with an average particle size of 210 μm and 2500 Kg/m^3 solid density which representing Geldart A type was used. The experiments were performed at different superficial gas velocities, axial heights, and radial positions. It was found that the local heat transfer coefficient and local gas hydrodynamics are directly related, such that the immersed heat exchanger tubes enhanced the heat transfer by increasing the bubble frequency and local gas holdup. The current common correlations available in the literature do not predict well our results. Hence, a new correlation that account for the effect of bubble frequency and gas holdup in addition to other parameters have been developed. The effective dimensionless groups have been correlated with a good mean relative deviation value of 4.84% between the experimental and predicted values.

Keywords: Vertical immersed internals, hydrodynamic parameters, heat transfer, gas-solid fluidized bed

* Corresponding Author: aldahhanm@mst.edu

1. INTRODUCTION

Gas-solid fluidized beds are largely employed in numerous industrial applications, such as petroleum refining, chemicals synthesis, food and pharmaceutical production, physical operations, and power generation. For catalytic reactions, drying, coating, and combustion, due to their high heat transfer efficiency and good gas, particles mixing (Martin 1984; White, Mathur, and Saxena 1986; Hu, Cheng, and Fan 1998; Stefanova et al. 2011). Heat transfer in these units is one of the key parameters that affect their design, scale-up, operation, and performance (Sunderesan and Clark 1995; Stefanova et al. 2007a; Pisters and Prakash 2011; Yao et al. 2015). It is accomplished by the contact of the bed particles and the flowing gas with the heat exchanger surfaces, which usually they are vertical or horizontal bundle of tubes, plates, or coils. Understanding and properly quantifying the bed-to-surface heat exchange or heat transfer coefficients and the related heat transfer mechanism are required for their proper design, scale-up, operation, performance, and safety of the fluidized bed for physical and chemical operations when the control of temperature is considered as an essential need (Baeyens and Goossens 1973; Fox, Grewal, and Moen 1999; Rasouli, Golriz, and Hamidi 2005). Three types of heat transfer mechanism between the bed and the heat exchanging surfaces exist which are particle convection, gas convection, and radiation. The overall heat transfer coefficient is the addition of the heat transfer coefficients of these types of heat transfer which his expressed as follows:

$$H_{overall} = \delta_d \, h_p + (1-\delta_d) h_g + h_{rad} \qquad (1)$$

where δ_d is a fraction of time during which any point on the heat transfer surface is occupied by particle packets, $\delta_d \, h_p$ is the particle convection component, $(1-\delta_d) h_g$ is the gas

convection component, and h_{rad} is the radiation component (Kim et al. 2003). However, many chemical processes using fluidized beds operate at temperatures below 500 °C, where the radiation is of less significance (Stefanova et al. 2007a, b). These types of heat transfer mechanism are affected by the hydrodynamics of the bed.

Hence, several researchers have investigated theoretically and experimentally the behavior of heat transfer and hydrodynamics in fluidized beds as well as examined different designs and operating parameters to study the heat transfer coefficient inside different configurations of gas-solid fluidized bed vessels (Wu et al. 1991; Li, Huang, and Qian 1995; Seo et al. 2011). For processes with high exothermic reaction, intense heat exchanging tubes are needed such as Fisher-Tropsch, Ammonia synthesis, and methanol synthesis (Bartholomew and Farrauto 2010; A. Pinto 1978; Tijm, Waller, and Brown 2001). Futhermore, these investigations have found that the heat transfer coefficient is affected by the following parameters (White, Mathur, and Saxena 1986; Doherty et al. 1986; Leming et al. 1995; Hu, Cheng, and Fan 1998; Sundaresan and Kolar 2002):

a. Physical properties of the solids and the gases inside the bed, including solid particles size, solids density, specific heat capacity, and the thermal conductivity, and fluid density, viscosity, and thermal conductivity.
b. Operating conditions, such as temperature, pressure, and superficial gas velocity.
c. Distributor design and heat transfer surfaces, including their geometry and location as well as the orientation of the internals relative to the fluidizing gas flow direction.

Martin (1984) reported that the maximum heat transfer coefficient apparently depends on the physical properties (mainly the thermal conductivity) of the gas and the volumetric heat capacity of the solids, but this seems to be independent of the thermal

conductivity of the solid. A number of experimental studies have examined the impact of the bundle of immersed tubes (internals) on the heat transfer coefficients in gas-solid fluidized beds. Borodulya et al. (1984) investigated the influence of square, inline, and horizontal tube bundles with different center-to-center spacing (pitch) in a pressurized gas-solid fluidized bed with large solid particles. They found that the heat transfer coefficient is insensitive to the vibration in the horizontal and vertical pitch. Wiman and Almstedt (1997) used two configuration types of horizontal tube bundles in a pressurized gas-solid fluidized bed. They concluded that the local heat transfer coefficient was higher for the tube bank configuration with a short distance between the tubes of the bundle than for those with more densely packed tubes. Kim et al. (2003) studied the heat transfer and bubble characteristics in a fluidized bed with an immersed horizontal tube bundle. They found that the average heat transfer coefficient reaches its maximum value with increasing superficial gas velocity and then decreases. Lechner, Merzsch, and Krautz (2014) constructed a horizontal tube bundle with various tube diameters, horizontal and vertical spacing, and alignment inside a fluidized bed with solid particles of Geldart A. The reduction in the heat transfer coefficient due to the existence of the tube bank is represented by the tube bundle reduction factor, which was derived using the dimensionless geometric number of the horizontal tube bundles. The tube bundle reduction factor is a key parameter to show the reduction in the heat transfer coefficient. The results show that the reduction of the heat transfer coefficient, compared to a case using only a single tube, occurred because of the particles and gas flow disturbances caused by the immersed tubes.

Many researchers have reported the advantages of inserting vertical immersed heat exchanging tubes inside gas-solid fluidized beds for heat exchanging needs. The addition

of vertical internals inside the fluidized bed can minimizes the pressure drop, slugging phenomena, bed height fluctuations, and solid particles erosion which have positive impact on the heat transfer in gas-solid fluidized beds (Grace and Harrison 1968; Ramamoorthy and Subramanian 1981; Rüdisüli et al. 2012a, 2012b). In addition, the vertical internals can reduce the size of the bubbles, which can lead to improving the mass and heat transfer rates inside the bed. Therefore, studying the effects of vertical heat exhchanging internal bundles on the heat transfer coefficients and the hydrodynamic related parameters can improve the understanding of the relationship between the heat transfer along with the related hydrodynamics of gas-solid fluidized bed reactors. Such advancementcan can help improving the design, scale-up, operation, performance, and safety of these types of reactors.

However, there is little published work and experimental findings in the literature on the impact of vertical heat exhchanging internal bundles on heat transfer coefficients, in particular, related to the combined knowledge of the local heat transfer coefficient and the related hydrodynamic characteristics inside gas-solid fluidized beds such as bubble characteristics in terms of bubble frequency and local gas holdup. Recently, Kagumba (2013) reported the integrated relationship between the heat transfer coefficient from the surface of immersed vertical internal to the flowing gas and liquid phases and the bubble frequency in gas-liquid bubble column. Since, there is an analogy between gas-liquid bubble column and gas-solid fluidized bed (Krishna et al., 1993) it is interested to understand and explore such relationship between heat transfer coefficient and bubble frequency in gas-solid fluidized beds where there is no study that has addressed this integrated investigation in gas-solid fluidized bed with vertical internals orientation.

Accordingly, the present work focuses on investigating the influence of a bundle of intense vertical immersed heat exhchanging tubes on the local heat transfer coefficient and local bubble dynamic characteristics in terms of bubble frequency and gas holdup inside the gas-solid fluidized bed column at different radial and axial positions using a non-invasive advanced, fast-response, heat transfer probe, that was flash mounted on the surface of the vertical immersed tubes to measure heat transfer coefficient and advanced fiber optical probe to measure bubble frequency and gas holdup, respectively. This will provide useful knowledge on the integrated relationship between the heat transfer coefficient and bubble dynamics in terms of the bubble frequency and gas holdup.

2. EXPERIMENTAL SETUP

The experimental setup consisted of a fluidized bed column with an inside diameter of 0.14 m and 1.84 m height. The column was constructed from Plexiglas®, and the plenum was made from aluminum. The column and plenum were placed on the top of a stainless steel base. Industrial-scale compressors were used to supply compressed air to the column at pressures up to 1.38 MPa. Omega flow meters were used to adjust the flow rate. A schematic diagram of the fluidized bed column with vertical internals is provided in Figure 2.1. The gas phase was introduced through a sparger tube in the plenum and then through a distributor mounted between the column and the plenum. The gas distributor was made of a porous polyethylene sheet and had a pore size of 15-40 μm. The sparger tube was plugged at one end and had 14 holes, all facing downward with respect to the column. The column was electrically grounded to minimize electrostatic effects. A rigid, metallic

structure was used to support the column and to eliminate mechanical vibrations, as shown in Figure 2.2.

In the current study, a circular arrangement of vertical internals was used. The configuration of the internals consisted of 30 Plexiglas® vertical internals with a 0.0127 m inside diameter and 1.84 m height, covering 25% of the column's cross-sectional area. These intense internals have been used to represent the needed internals for high exothermic reaction where intense heat exchanging surfaces are required to control the reaction temperature as mentioned earlier. The schematic diagram of the internal support and internals is shown in Figure 2.3. The circular configuration features uniformly distributed the internals over the cross-sectional area of the fluidized bed column. This circular configuration of the internals maintained equal spacing between the internals and the wall of the fluidized bed column. A photo of the internals and its configuration is shown in Figure 2.4. The internals were secured in the column by four supports (honeycombs), which also minimized the vibration of the internals during the experiments. The distance between the distributor plate and the lower end of the vertical internals was 0.09 m.

The experiments were conducted at relative gas velocities (u/u_{mf}) of 1.4, 1.6, 1.78, 1.96, 2.14, 2.3, and 2.5 (where u is the superficial gas velocity and u_{mf} is the minimum fluidizing velocity). Therefore, to compare the experimental results between the column with and without internals similar of u/u_{mf} have been used in this work. The superficial gas velocity of the column without internals was calculated based on the cross-sectional area of the column when it was not occupied with the internals. In contrast, for the case with

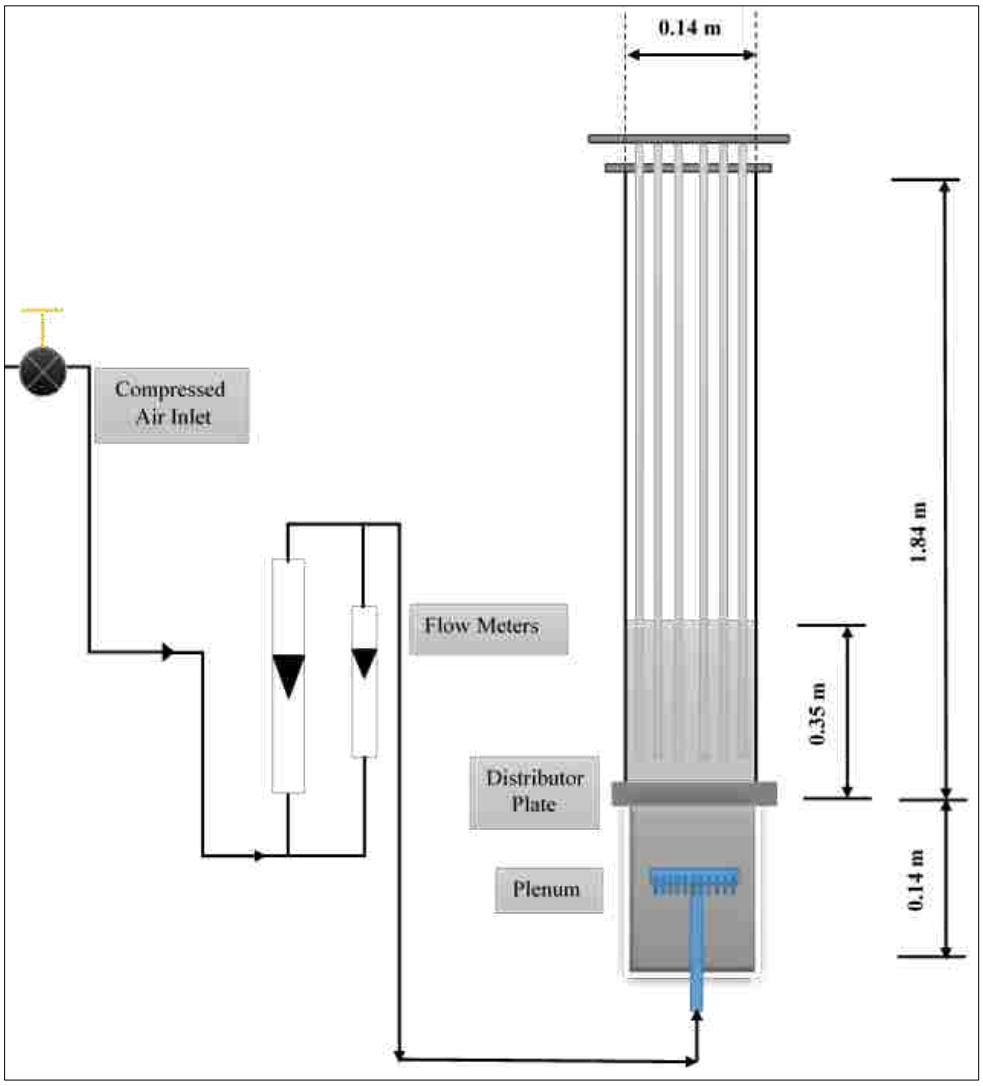

Figure 2.1. Schematic diagram of 0.14 m ID fluidized bed column with internals.

internals, the superficial gas velocity was calculated based on the free cross-sectional area available for the flow, which represented 75% of the cross-sectional area of the column. For both cases, the difference between the minimum fluidized velocities was taken into consideration. The minimum fluidization velocities for the case of with and without vertical internals were measured using the pressure drop measurements along the bed at different superficial gas velocities, in which the pressure drop has been increased with increasing

Figure 2.2. Photo of the fluidized bed column with internals.

the superficial gas velocity until it reaches the maximum value and then start to be constant. The corresponding superficial gas velocity at the point when the pressure drop reach its maximum value is represented the minimum fluidization velocity. This experiment was done for both the cases of with and without internals.

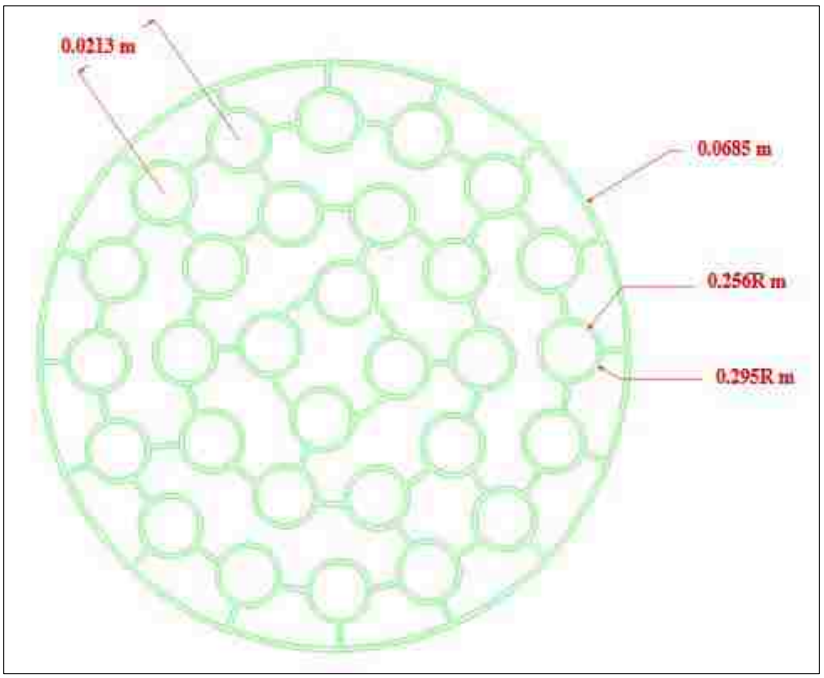

(a)

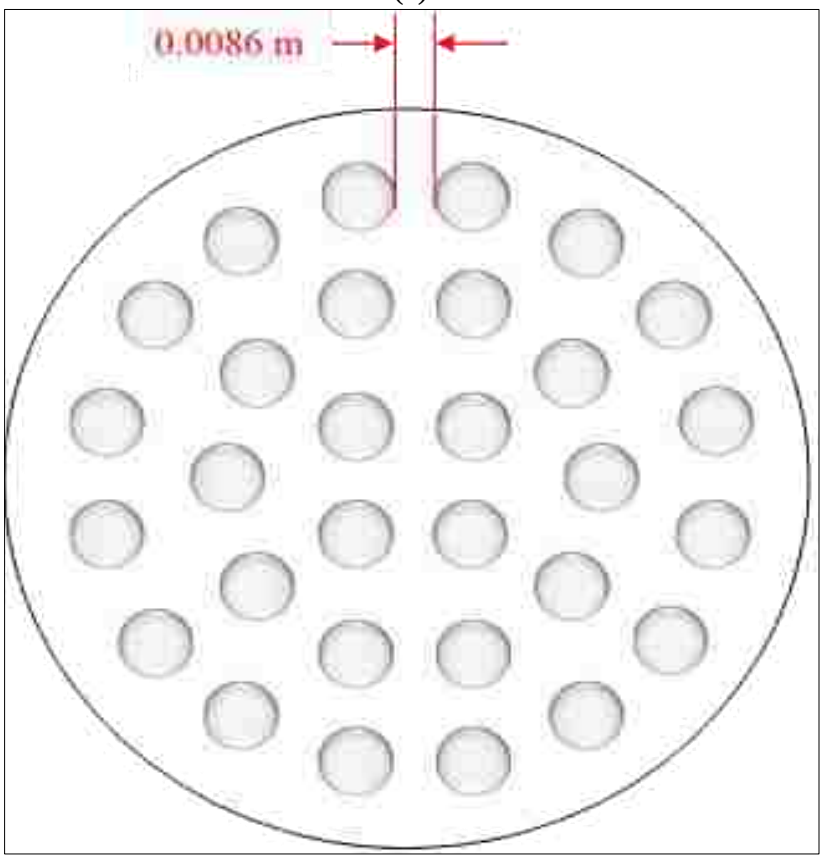

(b)

Figure 2.3. Schematic of the internals and support (honeycomb) used in this work.

Figure 2.4. Photo of the internals and its configuration.

The non-invasive heat transfer probe was flash mounted on the surface of three of the tube internals at three different heights of H/D = 0.75, 1.5, and 2 from the distributor as it will be discussed in the following section. The locations of these tubes were varied at r/R= 0.2, 0.6, and 0.8 to measure radial heat transfer coefficients. Therefore, the optical probe measurements of gas holdup and bubble frequency were acquired at H/D = 0.75, 1.5, and 2.0 above the gas distributor and the measurements were carried out also at the same three radial positions (r/R = 0.2, 0.6, and 0.8) consistent with the radial locations of the heat transfer probe. The solid particles used in this work were glass beads of 210 μm average particle size and 2500 Kg/m^3 density that represent Geldart A type with the static

bed height of 0.35 m for all the beds of with and without internals. The minimum fluidized velocity was measured to be 0.112 m/s for the case without internals, while for the case with internals, the minimum fluidizing velocity u_{mf} was 0.161 m/s. This could be due to the nature of Geldart A particles which tend to agglomerate and form cluster that affect the pressure drop along the height of the bed of solid particles. Hence, the used superficial gas (u) velocity through the free area to flow varies from condition to condition to maintain same u/u_{mf}.

3. EXPERIMENTAL TECHNIQUES

3.1. NON-INVASIVE ADVANCED HEAT TRANSFER PROBE

The measurements of the local heat transfer coefficients were carried out using three heat transfer probes that were built as a part of three vertical internals made from stainless steel and placed at different axial positions (H/D = 0.75, 1.5, and 1.75). Additionally, each internal could be moved at three radial positions (r/R = 0.2, 0.6, and 0.8) within the whole bundle of the vertical internals, as shown in Figure 3.1. It is worth noting that the three heat transfer probes were worked simultaneously, so that the heat transfer coefficients at the three axial heights and three radial positions were recorded simultaneously. The heat transfer probe consisted of a Micro-Foil® heat transfer sensor (RDF Corp., model 27134-1). The Micro-Foil® sensor was flash mounted on the outer surface of a brass cylinder of 12.7 mm outer diameter and 62 mm length. The Micro-Foil® sensor is considered one of the best techniques for measuring the heat transfer coefficient for various multiphase flow systems due to its many beneficial characteristics, such as its fast response, high sensitivity, low thermal impedance, thin size (least disturbance to heat

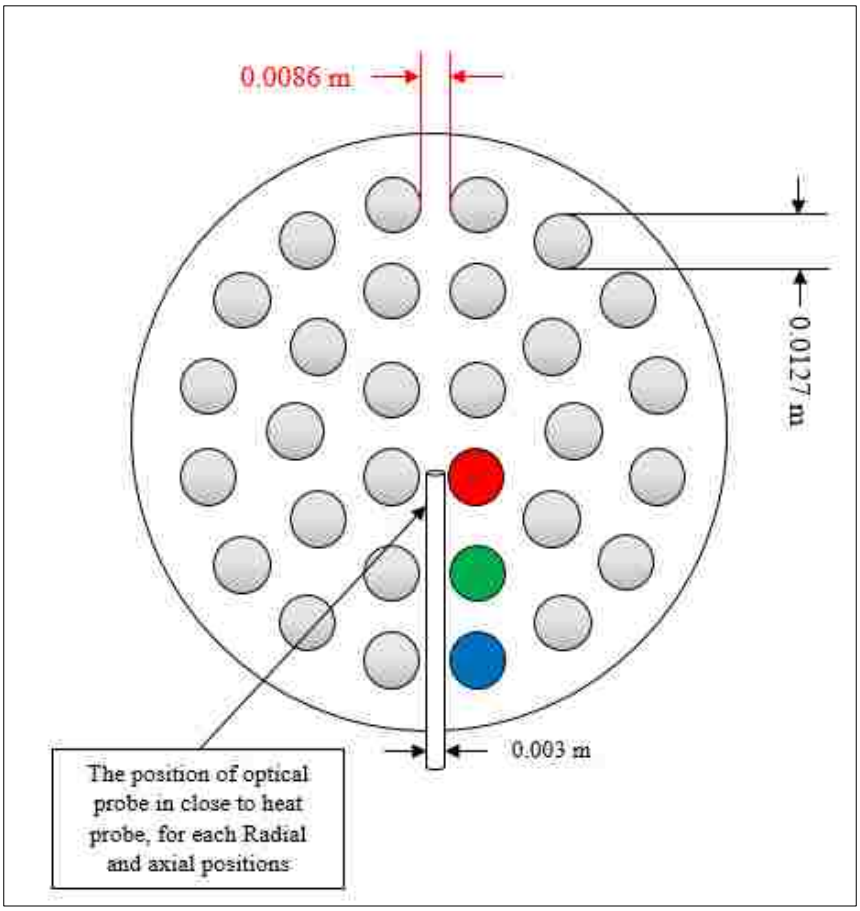

Figure 3.1. Radial positions of the three stainless steel vertical internals that contain built-in heat transfer probes; the blue internal is at r/R = 0.2, the green internal is at r/R = 0.6, the red internals is at r/R = 0.8, and the insertion of the optical probe are shown.

flow), flexibility, and wide temperature range. The Micro-Foil® sensor includes a built-in heat flux sensor and thermocouple to simultaneously measure the local heat flux (q_i) and the surface temperature (T_{si}) of the heat transfer probe. The heat element cartridge (Chromalox, model CIR- 1012) was installed inside the brass cylinder, which is a heat source. Photo and schematic of the heat transfer probe are shown in Figure 3.2. The electric power was supplied to the heating element through a DC power supply. The bed temperature (bulk temperature) was measured using five copper-constantan thermocouples (Omega Inc., model TQSS-18U-12), three of which were contiguous to the heat probes at

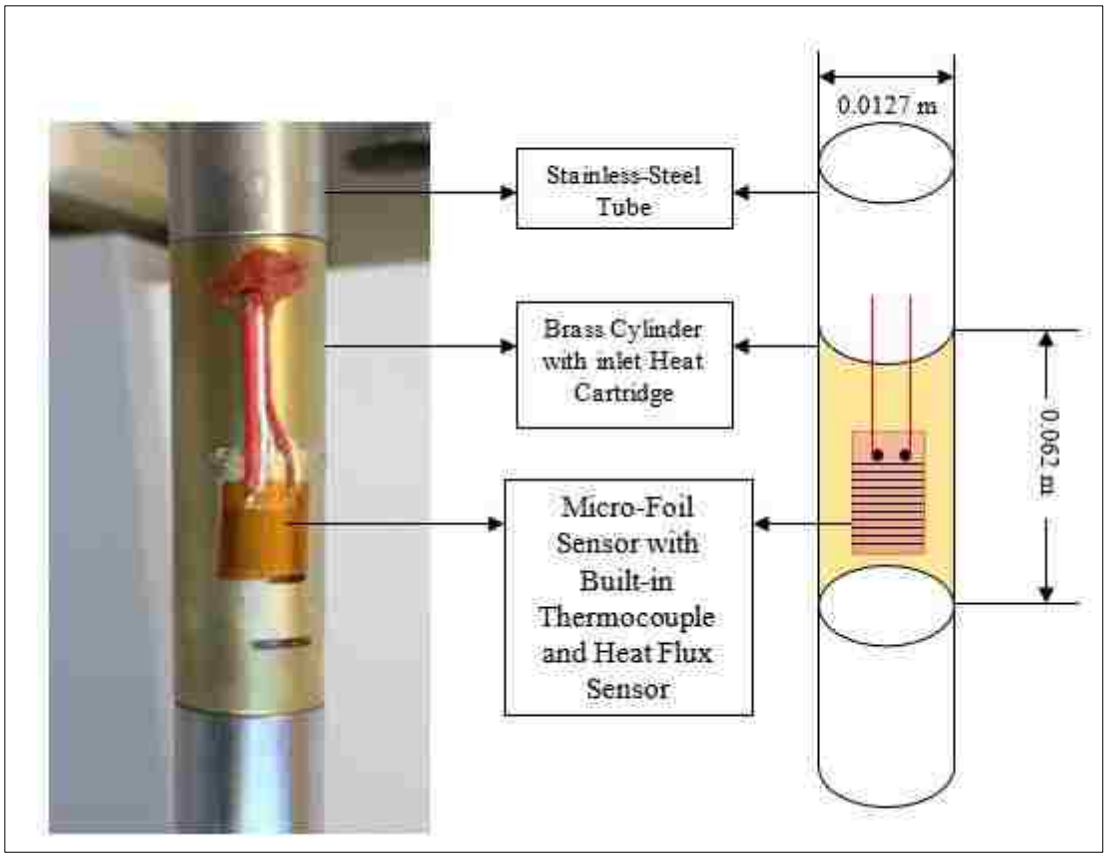

Figure 3.2. Photo and schematic of the non- invasive advanced heat transfer probe.

(r/R = 0.2, 0.6, and 0.8) and at (H/D = 0.75, 1.5, and 2), with the other two installed at various axial and radial positions (r/R = 0.0 and 1.0) and at (H/D = 0.5 and 2.25). The heat flux voltage signal was generated in the micro voltage range. An amplifier (JH Technology, Inc., model JH4300) was connected to the heat flux sensor before the voltage signal was received by the data acquisition system (DAQ, model NI-9205). The surface temperature sensor and the bed thermocouples were connected to another data acquisition system (DAQ, model NI-9213). The heat transfer measurement system is shown in Figure 3.3. The heat flux signals and the signals from the thermocouples were recorded at 25 Hz for about 160 s and repeated five times to ensure their reproducibility. The reproducibility of the

results was found to be less than of 5%, and the error bars were shown for each measurement.

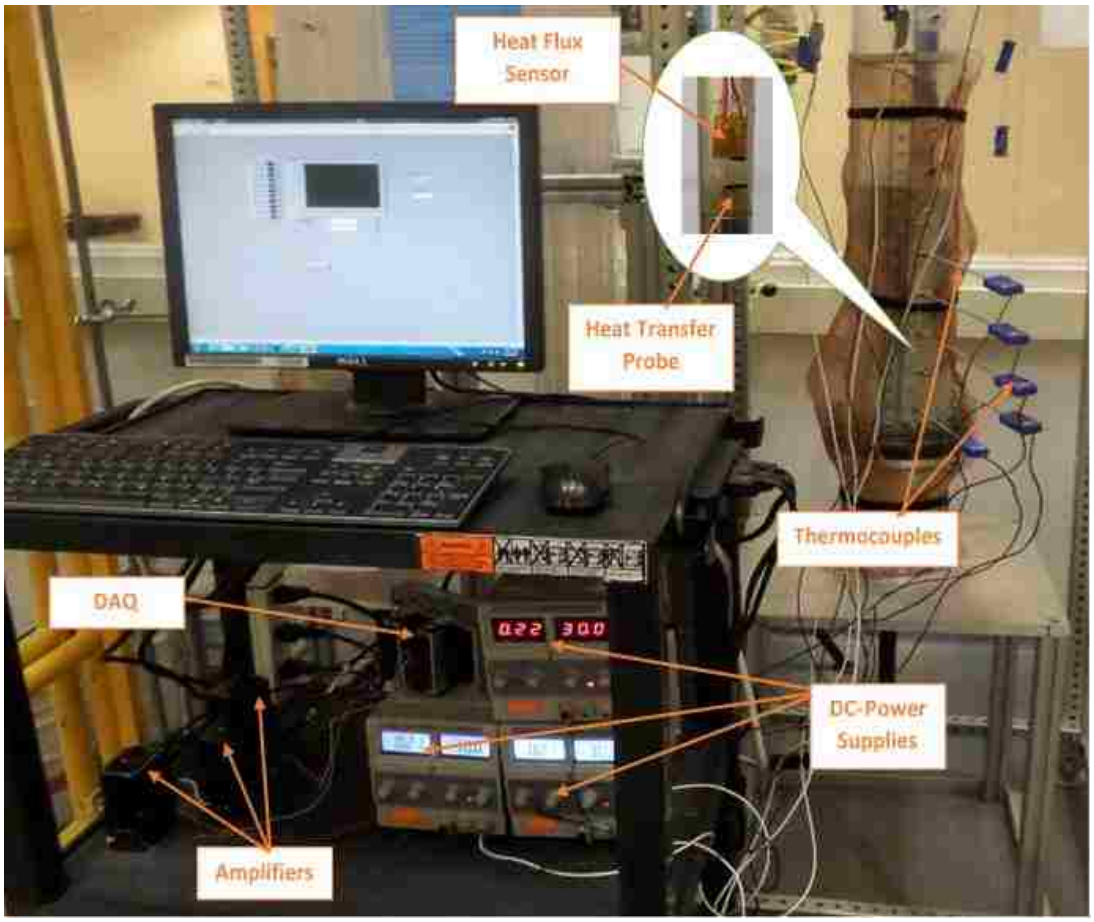

Figure 3.3. Photo of the heat transfer measurement system and the fluidized bed column.

The instantaneous local heat transfer coefficient was determined by the direct measurement of the heat flux and the difference between the surface and the bulk temperatures at a given time as follows (Abdulmohsin, Abid, and Al-Dahhan 2011; Abdulmohsin and Al-Dahhan 2012):

$$h_i = \frac{q_i}{T_{si}-T_{bi}} \quad (2)$$

where h_i is the instantaneous local heat-transfer coefficient (W/m^2 K), q_i is the instantaneous heat flux across the sensor (W/m^2), T_{si} is the instantaneous surface temperature of the heat transfer probe (K), and T_{bi} is the instantaneous bulk temperature of the bed (K). The time-averaged heat-transfer coefficient (h_{ave}) at a given location was then calculated by averaging the instantaneous-heat-transfer coefficient measurements over the sampling period of 160 s.

$$h_{ave} = \frac{1}{n}\sum_{i=1}^{n} \frac{q_i}{T_{si}-T_{bi}} \quad (3)$$

where n is the total number of the sample data points (n = 4,000 over the sampling period).

3.2. ADVANCED OPTICAL FIBER PROBE TECHNIQUE

The optical fiber probe used in this work was model PV-6, which was developed by the Institute of Process Engineering, Chinese Academy of Sciences, Beijing, China (Figure 3.4) (Aradhya et al., 2016; Al-Dahhan et al. 2017; Aradhya et al., 2017). As per our request, the probe and its electronics have been made to be able to simultaneously measure local solids concentrations and bubble hydrodynamic characteristics according to the algorithms and data processing that we developed in our laboratory (Multiphase reactors engineering and applications (mReal). The optical probe was 3 mm in diameter and consisted of two sub-probes, each with an active tip area of 1 mm × 1 mm in cross-section. The effective distance between the two tips was 2.12 mm as it was calibrated for solids velocity measurements. Each tip was composed of light-emitting and receiving fibers 25 μm in diameter arranged in an alternating array. The two separate optical bundles had separate channels for signal processing. The probe works on the principle of the back

reflection of light, where the receiving light that is reflected by the solid particles is multiplied by the photomultiplier and converted into voltage signals. The voltage signals are further amplified and fed into a personal computer. To ensure the repeatability of sampled signals, the sampling time was 65 s, at a frequency of 2000 Hz, and the measurements were repeated at least five times at each position. The reproducibility of the results was found to be less than of 5% and the error bars were shown for each measurement.

Figure 3.4. The insertion of the optical fiber probe PV-6 in the bed.

Before the experiments, the optical probe was calibrated in our laboratory for local solids holdup measurements using our modified dropping/trapping calibration method

(Zhang et al., 1998). The purpose of calibrating the optical probe is that because the signal is related to solids concentrations in front of the window of the probe and hence there is a need to relate the generated voltage signal to solids holdup (volume fraction of solids) which are useful hydrodynamic parameters from which gas holdup can be estimated. When the solids holdup measured, the gas holdup can be estimated since the gas holdup ($\varepsilon_g = 1-\varepsilon_s$). Also, we have developed a special calibration method by equating the measured known solids velocity to thee solids velocity that can be measured by the probe to determine the distance between the two sub-probes before employing the probe for any related hydrodynamics measurements such as solids velocity and bubble characteristics such as bubble rise velocity, bubble chord length, and bubble frequency. More details about our developed simple and reliable calibration methods can be found in Taofeeq, Aradhya, and Al-Dahhan (n.d.). In this work, the optical fiber probe was used to measure the number of bubbles per sampling time (bubble frequency) that passed the first tip of the probe and the local gas holdup which are key parameters affecting heat transfer coefficients inside the gas-solid fluidized bed. It is worthy to mention that Taofeeq and Al-Dahhan (paper I) have used this probe to investigate in more details the effects of the vertical internals on the solids velocity, solids and gas holdups, and bubbles dynamics (bubble rise velocity, bubble frequency, and bubble chord length) which are the focus of that manuscript.

In this work the bubble frequency is determined from the signal of lower tip of the probe because the generated signal from upper tip of the probe may already be influenced by the lower tip. The threshold of lower tip signal should be specified properly in order to estimate the bubble frequency. The threshold represents the boundary between the dense phase (solids phase) and gas phase in the recording signal, in which the area above the

threshold represents the contact time of solids phase, while the lower area represents the contact time of the bubble (gas phase) with the lower tip of the probe. More details about the threshold and its measurement can be found in Taofeeq and Al-Dahhan (paper I) and (Schweitzer et al., (2001). After the signal break into two parts, each one represents the related phase. The lower part of the signal which represents the gas phase (bubbles pass the tip of the probe) can be used to calculate the bubble frequency. The bubble frequency is estimated by determining the number of peaks that are detected in the lower part of the signal per unit time of the recorded signal which is 65 s (Number of bubbles/time of the recorded signal). The algorithms and data processing for estimating the threshold and then the bubble frequency have been developed and implemented in our laboratory (mReal).

4. RESULTS AND DISCUSSION

The heat transfer coefficients and local gas holdup and bubble frequency were experimentally measured at three axial heights as mentioned earlier (H/D = 0.75, 1.5, and 2), three radial positions (r/R = 0.8, 0.6, and 0.2), and seven values of u/u_{mf} (u/u_{mf} = 1.4, 1.6, 1,76, 1.96, 2.14, 2.3, and 2.5). Moreover, the axial heights were chosen to cover three key axial levels inside the bed, in which H/D = 0.75 was the axial level near the distributor plate where the bubbles entered and dispersed throughout the bed; H/D = 1.5 was the middle section of the fluidizing bed, where the bubbles passed the entering zone and rose through vertical pathways between the immersed tubes; and H/D = 2.0 was the axial level near the freeboard of the column where the bubbles reached their maximum size and left the bed. The three radial positions were chosen to cover three principal radial positions: near the wall region (r/R = 0.8), near the central region of the bed (r/R = 0.2), and near the

middle of the radius (r/R = 0.6) or near the inversion point of the time averaged particles velocity (Efhaima 2016), as well as it represents the radial position between the wall and the central region. The superficial gas velocity and hence the ratio (u/u_{mf}) were selected to cover the bubbling flow regime for the Geldard A solid particles, as mentioned by Nedeltchev et al. (2012). Consequently, the effect of the superficial gas velocity, axial height, and radial position on both the heat transfer coefficient and gas holdup and bubble frequency for the two cases (i.e., with and without immersed tubes) is discussed in this section. In addition, it is worth to mention that the experimental measurements of the heat transfer coefficients and gas holdup and bubble frequency are local measurements which present knowledge of how the local mechanism of heat transfer and these hydrodynamics are interrelated.

4.1. THE EFFECT OF SUPERFICIAL GAS VELOCITY IN TERMS OF U/U_{MF}

The effect of the superficial gas velocity in terms of u/u_{mf} (where u_{mf} = 0.112 m/s for without internals and 0.161 m/s for with internals) on the heat transfer coefficient at different axial heights and radial positions for the two cases (i.e., with and without immersed tubes) is represented in Figures 4.1-4.3. These Figures show that the heat transfer coefficients rose with the increasing superficial gas velocity in terms of u/u_{mf} for all the radial and axial positions. Furthermore, the heat transfer coefficients are larger in the case of the vertical immersed tubes in comparison to those without internals. The averaged percentage larger of the averaged heat transfer coefficient at different superficial gas velocities with the presence of vertical internals at r/R = 0.2 is 9.6%, 17.2%, and 18.7% at H/D = 0.75, 1.5, and 2, respectively. The increase in the heat transfer coefficient is a

function of the axial height and radial position, in which the heat transfer coefficient radially increased from the wall zone toward the central region of the bed and axially increased with an increase in H/D. To explain the increase in the heat transfer coefficient in the case of vertical immersed tubes, the effect of the superficial gas velocity (u/u_{mf}) on the bubble characteristics in terms of local gas holdup and bubble frequency for the cases with and without immersed tubes is presented in Figures 4.4 and 4.5.

Based on Figure 4.4, for the case without internals, there is clear trend of increasing in the bubble frequency with an increase in the superficial gas velocity in terms of u/u_{mf}. In addition, the increase in bubble frequecy varies with the radial and axial positions inside the bed. In which, the bubble frequency increase from the wall region toward the center of the column due to the effect of drag forces of the wall in which the bubbles tend to move toward the center region in their vertical pathways. Additionally, the bubble frequency was found to be less with the axial height due to the coalescence mechanism of the bubbles when they rise inside the bed. For the case of vertical internals, the bubble frequecy has almsot the same trends comapring with that of the case without internals. Furthermore, the augmentation of the bubble frequency is clearly shown with the presence of vertical internals inside the bed for all the axial and radial positions and all the superficial gas velocities. The change in the bubble frequency in the case with vertical internals can be explained by the mechanism of bubble splitting due to the existence of immersed tubes near the lower end of the vertical tube bundle as well as the vertical tubes working to reduce the bubble coalescence at the higher axial level, in which the bubbles elongate and move in the space between the internals (Ramamoorthy and Subramanian 1981; Rüdisüli et al. 2012a, b; Maurer et al. 2015b). It was found that the percentage of increase of bubble

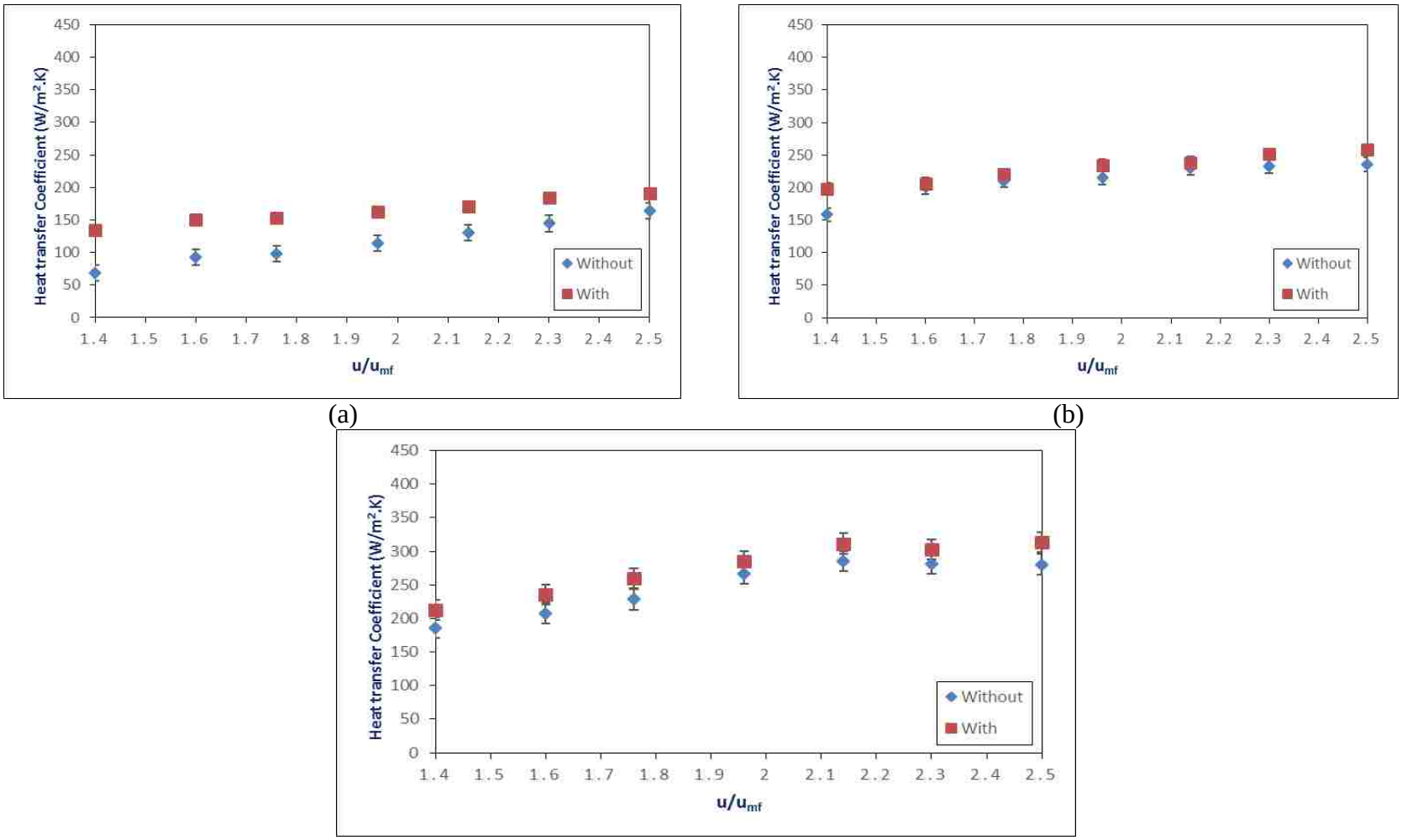

Figure 4.1. Heat transfer coefficient versus different superficial gas velocities in terms of u/u_{mf} at H/D = 0.75 and for the cases with and without internals, (a) r/R = 0.8, (b) r/R = 0.6, and (c) r/R = 0.2.

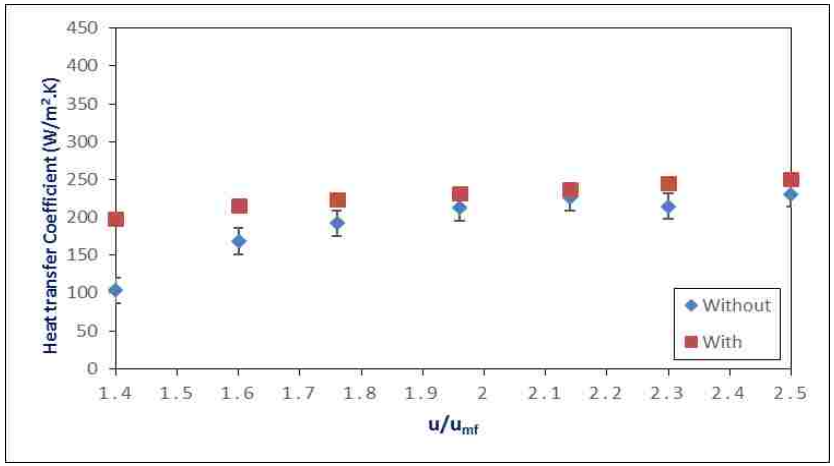

(a)

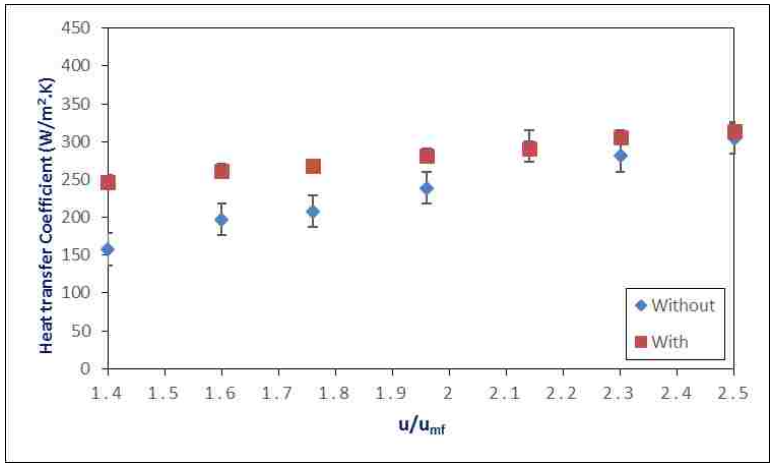

(b)

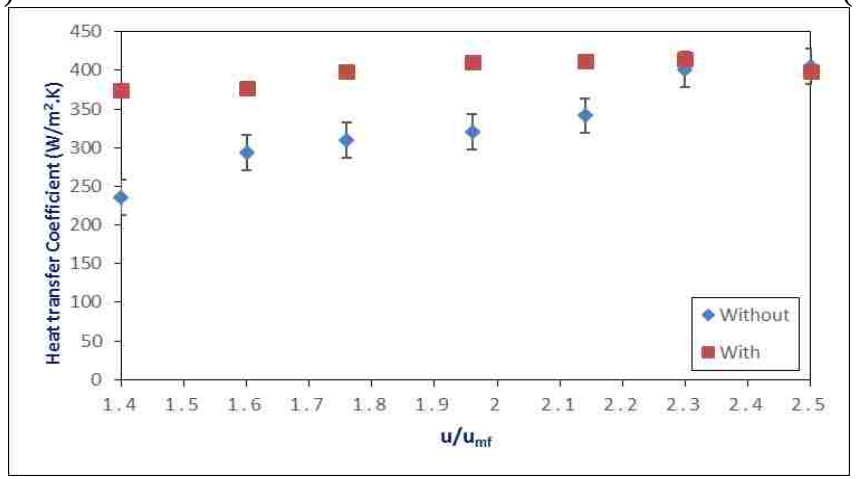

(c)

Figure 4.2. Heat transfer coefficient versus different superficial gas velocities in terms of u/u_{mf} at H/D = 1.5 and for the cases with and without internals, (a) r/R = 0.8, (b) r/R = 0.6, and (c) r/R = 0.2.

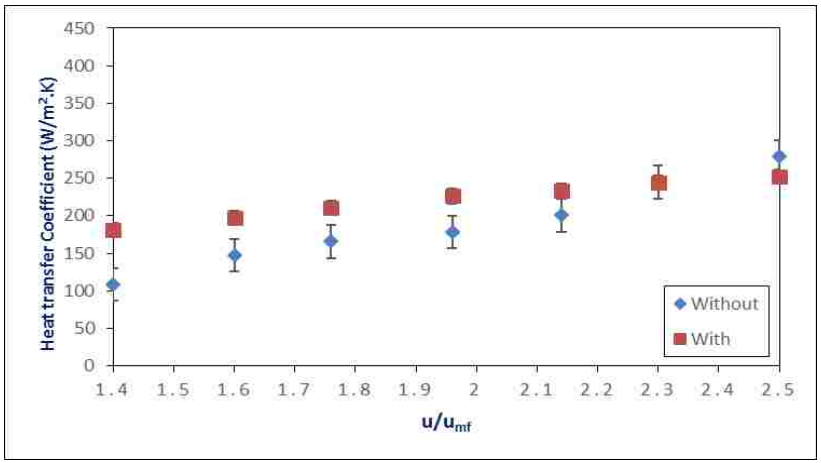

(a)

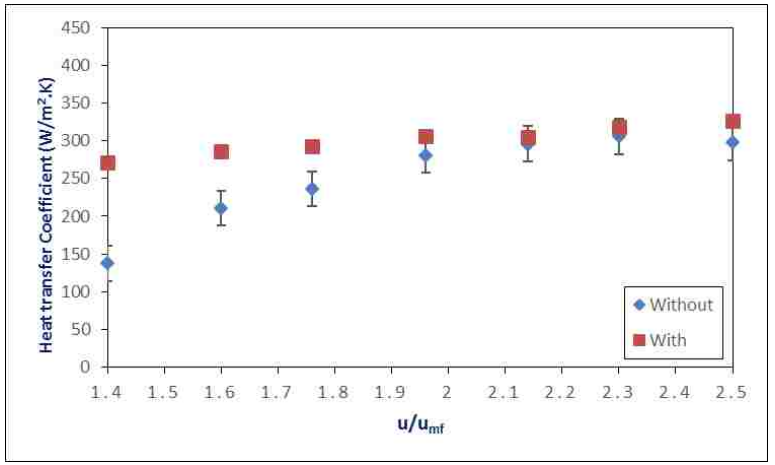

(b)

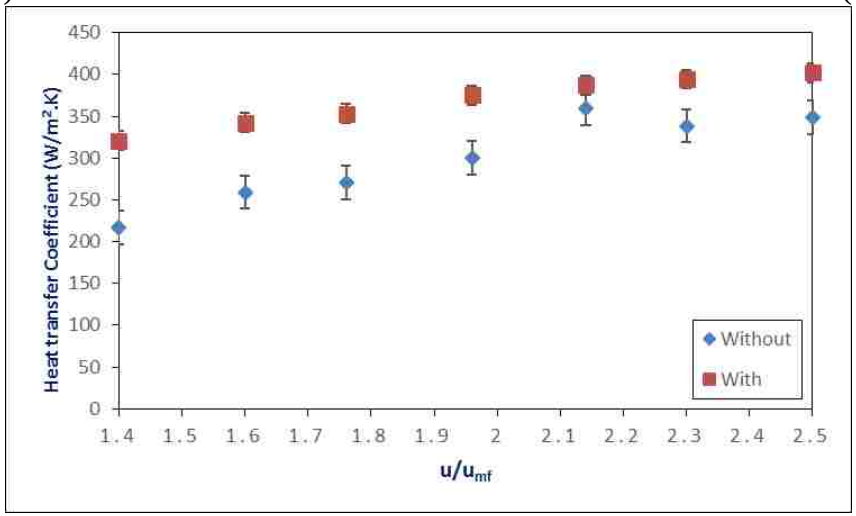

(c)

Figure 4.3. Heat transfer coefficient versus different superficial gas velocities in terms of u/u_{mf} at H/D = 2.0 and for the cases with and without internals, (a) r/R = 0.8, (b) r/R = 0.6, (c) r/R = 0.2.

frequency in the case of vertical internals (at u/u_{mf} =2.5 and r/R = 0.2) is 16.7%, 15.6%, and 15% at H/D = 0.75, 1.5, and 2, respectively.

Figure 4.5 illustrates the local gas holdup at different axial heights and radial positions. It shows that the gas holdup rose with the increasing of u/u_{mf} in the case with and without vertical immersed tubes. The increase of gas holdup has been demonstrated at all the axial and radial positions as well as for all the range of u/u_{mf} used in this work. Moreover, the gas holdup in the case of the vertical immersed tubes was higher than that of the case without internals. This is consistent with the trend in bubble frequency and with the literature (Maurer et al. 2015a). The percentage increase of local gas holdup in the case of vertical internals and at u/u_{mf} = 2.5 and r/R = 0.2 is 7.7%, 6.2, and 9% at H/D = 0.75, 1.5, and 2, respectively.

This change in the gas holdup with the presence of vertical internal tubes reflected the change in the amount of gas entering the bed to maintain same u/u_{mf} for both with and without internals. Since the u_{mf} for the case with internals is higher than that without internals, the superficial gas velocity (u) based on the free cross-sectional area available for flow is higher in the presence of immersed vertical tubes and thus the bubble rise velocity and particles velocity are larger. This affects the heat transfer coefficients since the related hydrodynamic parameters inside the bed have been affected accordingly. Thus, it can be concluded that the heat transfer coefficient is directly related to the bubble frequency and gas holdup inside the bed. The enhancement in the heat transfer inside the gas-solid fluidized bed with vertical internals was reported in the literature by Glass and Harrison (1964) Grace and Harrison (1968), Law et al. (2003), and Maurer et al. (2015a). Generally, it can be deduced from Figures 4.1-4.5 that the heat transfer coefficient, bubble

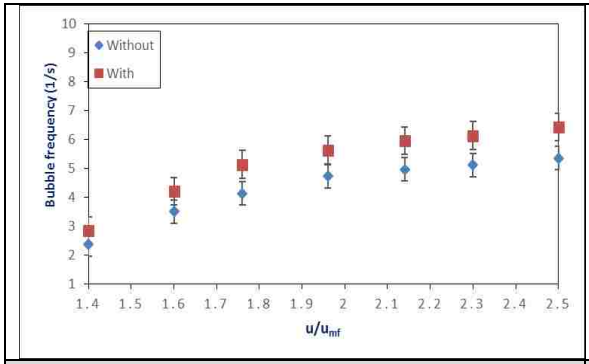

Bubble frequency versus superficial gas velocity at r/R = 0.8 and H/D = 0.75, with and without internals.

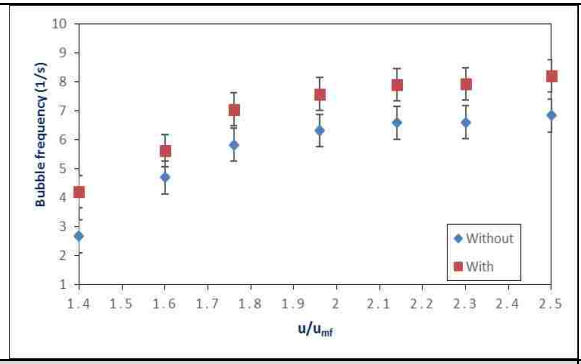

Bubble frequency versus superficial gas velocity at r/R = 0.6 and H/D = 0.75, with and without internals.

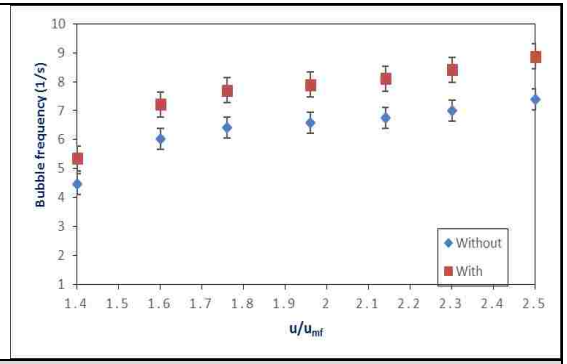

Bubble frequency versus superficial gas velocity at r/R = 0.2 and H/D = 0.75, with and without internals.

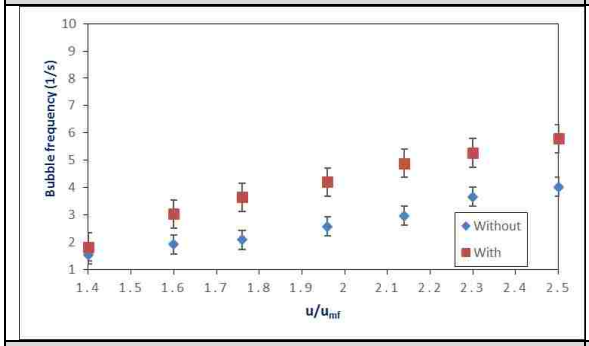

Bubble frequency versus superficial gas velocity at r/R = 0.8 and H/D = 1.5, with and without internals.

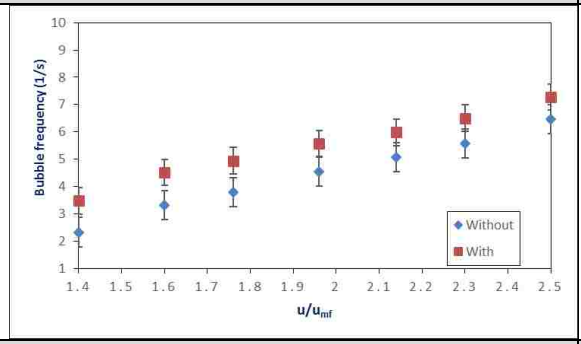

Bubble frequency versus superficial gas velocity at r/R = 0.6 and H/D = 1.5, with and without internals.

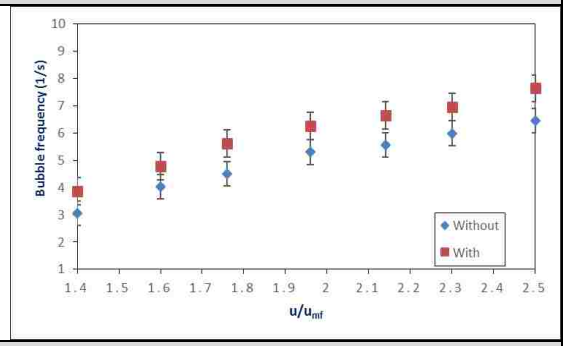

Bubble frequency versus superficial gas velocity at r/R = 0.2 and H/D = 1.5, with and without internals.

Figure 4.4. Variation in bubble frequency with superficial gas velocity in terms of u/u_{mf} at different axial heights and radial positions, with and without internals.

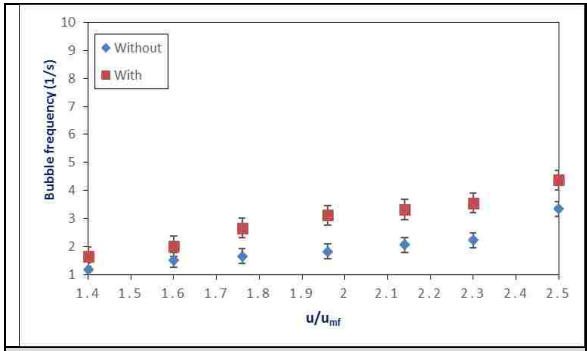

Bubble frequency versus superficial gas velocity at r/R = 0.8 and H/D = 2.0, with and without internals.

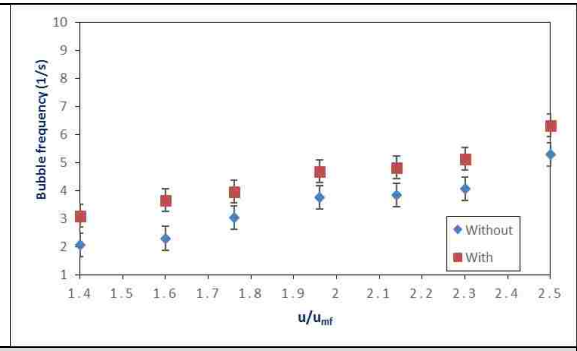

Bubble frequency versus superficial gas velocity at r/R = 0.6 and H/D = 2.0, with and without internals.

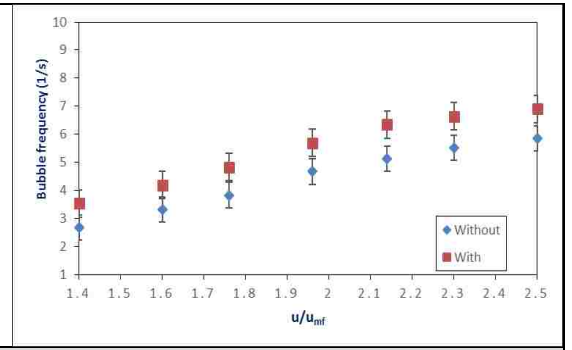

Bubble frequency versus superficial gas velocity at r/R = 0.2 and H/D = 2.0, with and without internals.

Figure 4.4. Variation in bubble frequency with superficial gas velocity in terms of u/u_{mf} at different axial heights and radial positions, with and without internals. (cont.)

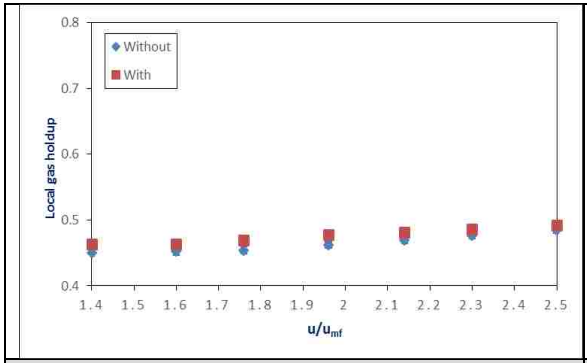

Gas holdup versus superficial gas velocity at r/R = 0.8 and H/D = 0.75, with and without internals.

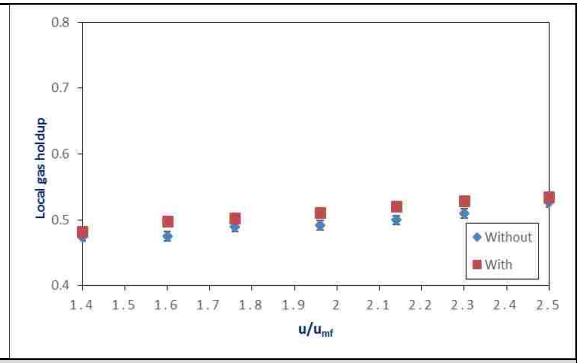

Gas holdup versus superficial gas velocity at r/R = 0.6 and H/D = 0.75, with and without internals.

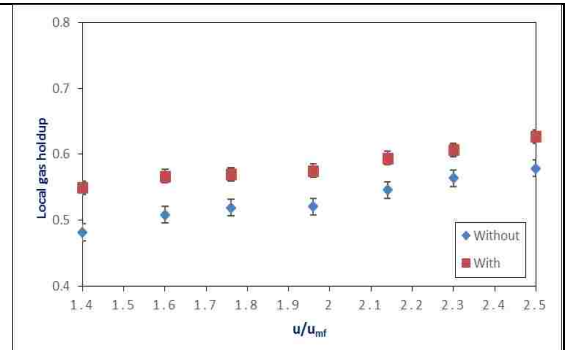

Gas holdup versus superficial gas velocity at r/R = 0.2 and H/D = 0.75, with and without internals.

Figure 4.5. Variation in gas holdup with superficial gas velocity in terms of u/u_{mf} at different axial heights and radial positions, with and without internals.

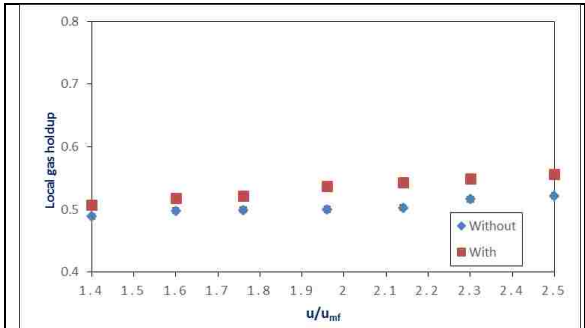

Gas holdup versus superficial gas velocity at r/R = 0.8 and H/D = 1.5, with and without internals.

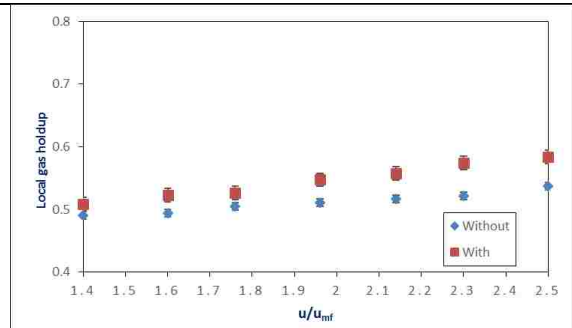

Gas holdup versus superficial gas velocity at r/R = 0.6 and H/D = 1.5, with and without internals.

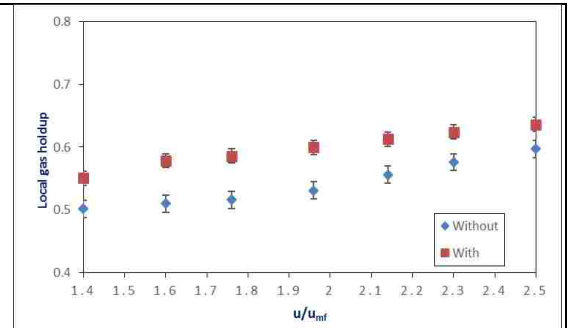

Gas holdup versus superficial gas velocity at r/R = 0.2 and H/D = 1.5, with and without internals.

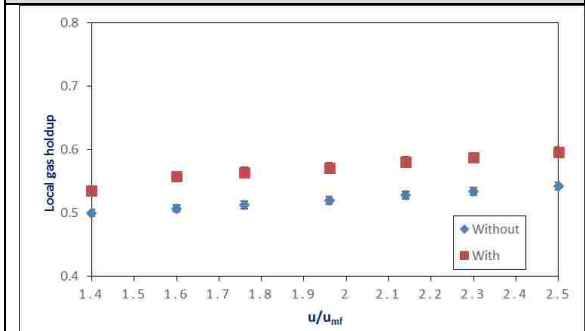

Gas holdup versus superficial gas velocity at r/R = 0.8 and H/D = 2.0, with and without internals.

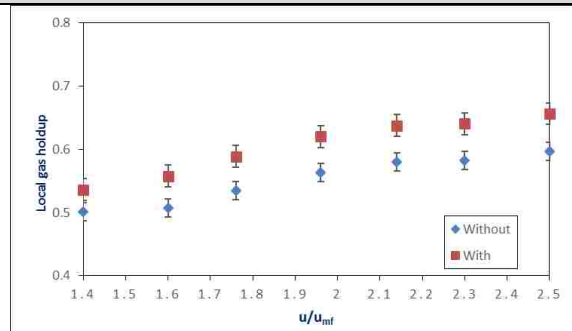

Gas holdup versus superficial gas velocity at r/R = 0.6 and H/D = 2.0, with and without internals.

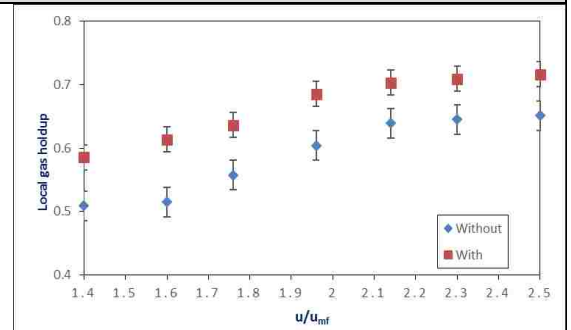

Gas holdup versus superficial gas velocity at r/R = 0.2 and H/D = 2.0, with and without internals.

Figure 4.5. Variation in gas holdup with superficial gas velocity in terms of u/u_{mf} at different axial heights and radial positions, with and without internals. (cont.)

frequency, and gas holdup rise with increasing superficial gas velocity and with the presence of vertical immersed tubes. Furthermore, the heat transfer coefficient is directly related to the bubble frequency and gas holdup in both cases of with and withotu vertical immersed tubes, in which the rate of change of both the bubble frequency and gas holdup leads to an increase in the convective heat transfer that occurs due to the contact of the gas phase in the form of bubbles and moving solids with the heating surface. The increase in bubble frequency would lead to increase in the rate of frequent replacement of solids layer that covers the heat surface. In which, the solids frequency near the heat surafce would increse and also lead to improve the heat transfer coefficents as mentioned by Mickley and Fairbanks (1955) in their heat transfer mechnisum inside the gas-solid fluidized bed. They mentioned that the increasing bubble frequency causes an increase in the particle convective heat transferdue to an increase in the number of solid particles that reach and contact the surface of the heating probe.

4.2. THE VARIATION OF HEAT TRANSFER, BUBBLE FREQUENCY AND LOCAL GAS HOLDUP AT DIFFERENT RADIAL POSITIONS

The radial positions were selected at three important radial zones: near the column wall (r/R = 0.8), near the middle of the radius (r/R = 0.6) as well near the inversion point of the time averaged particles velocity (Efhaima 2016), and near the center of the bed (r/R = 0.2), as shown in Figure 3.2. Three superficial gas velocities were selected to study the heat transfer in relation to the variation in radial profiles (u/u_{mf} = 1.76, 2.14, and 2.5). The radial profiles of the heat transfer coefficients at different axial heights and for the two cases (i.e., with and without vertical immersed tubes) are illustrated in Figure 4.6. The left side of Figure 4.6 represents the radial profiles of the heat transfer coefficient at three axial

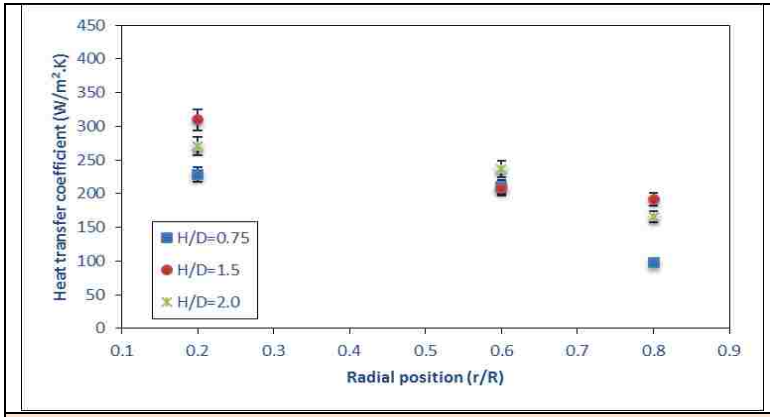

Radial profiles of the heat transfer coefficients at different axial heights, where u/u_{mf} = 1.76 for the case without immersed tubes.

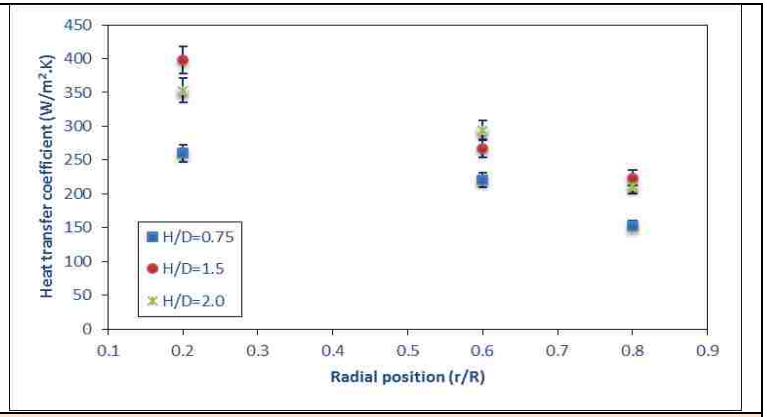

Radial profiles of the heat transfer coefficients at different axial heights, where u/u_{mf} = 1.76 for the case with immersed tubes.

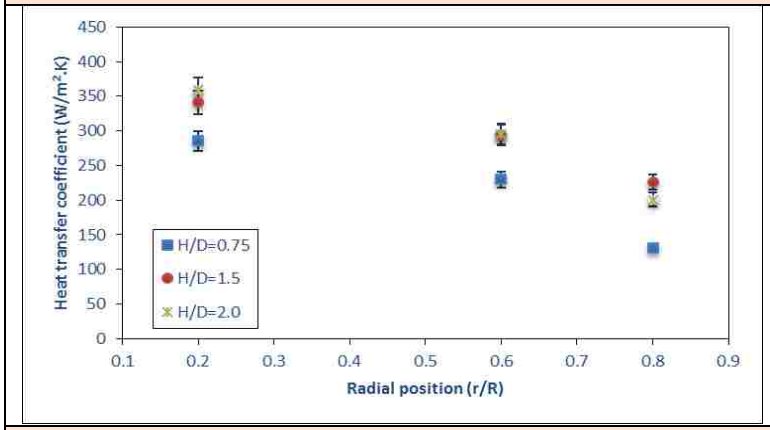

Radial profiles of the heat transfer coefficients at different axial heights, where u/u_{mf} = 2.14 for the case without immersed tubes.

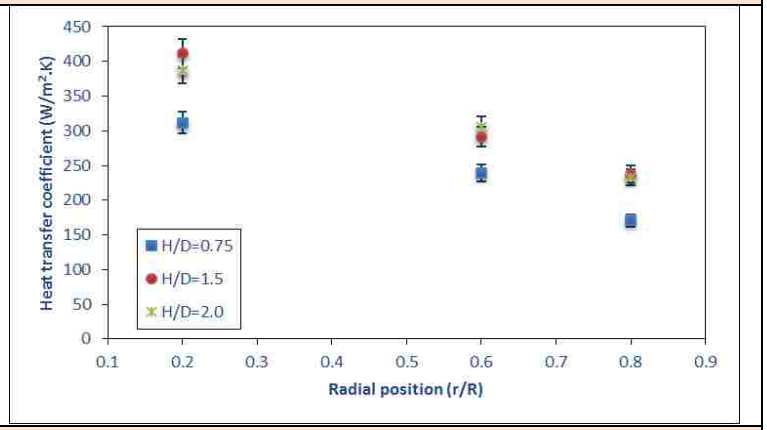

Radial profiles of the heat transfer coefficients at different axial heights, where u/u_{mf} = 2.14 for the case with immersed tubes.

Figure 4.6. Radial profiles of heat transfer coefficients at different axial heights and three superficial gas velocities in terms of u/u_{mf} for the case without immersed tubes (left side) and with immersed tubes (right side).

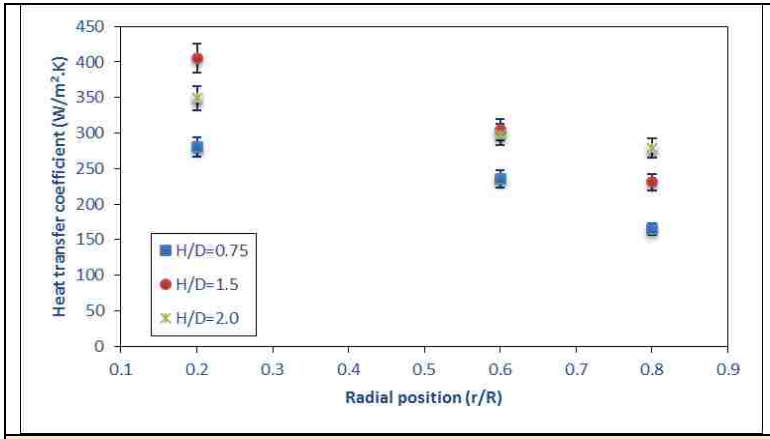

Radial profiles of the heat transfer coefficients at different axial heights, where u/u_{mf} = 2.5 for the case without immersed tubes.

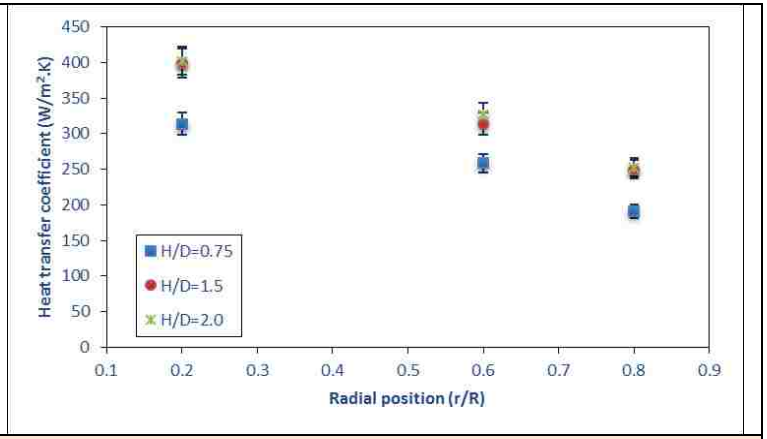

Radial profiles of the heat transfer coefficients at different axial heights, where u/u_{mf} = 2.5 for the case with immersed tubes.

Figure 4.6. Radial profiles of heat transfer coefficients at different axial heights and three superficial gas velocities in terms of u/u_{mf} for the case without immersed tubes (left side) and with immersed tubes (right side). (cont.)

levels: (H/D = 0.75, 1.5, and 2.0) for the case without immersed heat exchanging tubes, while the right side of Figure 4.6 represents the radial profiles of the heat transfer coefficient at the same three axial levels (H/D = 0.75, 1.5, and 2.0) for the case with immersed tubes. It can be seen from Figure 4.6 that the local heat transfer coefficients increase from the wall toward the center of the bed for all the axial heights and the superficial gas velocities in terms of u/u_{mf}. This result concurs with the results reported by Pisters and Prakash (2011) and Stefanova et al. (2007a, 2011). Furthermore, Figure 4.6 illustrates that for all the axial heights and superficial gas velocities in terms of u/u_{mf}, the local values of the heat transfer coefficients in the case with vertical immersed tubes are higher than those for the case without immersed tubes.

The average percentage increase in the heat transfer coefficient from near the wall to the center region at $u/u_{mf} = 2.5$ for the case of with and without internals was found to be (for the case of internals: 39%, 37%, and 37% at H/D = 0.75, 1.5, and 2, respectively) and (for the case of without internals: 41%, 43%, and 20% at H/D = 0.75, 1.5, and 2, respectively). It can be notice that the percentage of increase of the heat transfer coefficient from near the wall region to the center region are almost equal for the case of with and without internals except at H/D = 2 (higher axial level). The reason for this change may be explained by the reduction of bubble frequency at higher axial level in the case of without internals due to the coalescence phenomena between the bubbles when they rise up inside the bed and then they disengagement from the bed. While, for the case of with internals the coalescence phenomena is considered less due to the presence of vertical internals which reduces the coalescence process by reducing the contact between them in their vertical pathways. In another meaning, the vertical internals help to stabilize the moving of bubble

at their radial position and suppress the tendency of bubbles to move toward the central region of the bed.

The radial profiles of the bubble and gas holdup are plotted in Figures 4.7 and 4.8, respectively. Figures 4.7 and 4.8 show the radial profiles of both the local bubble frequency and local gas holdup at three axial heights and three selected superficial gas velocities, which were used to reflect the radial profiles of the heat transfer coefficients in Figure 4.6. Also, Figures 4.7 and 4.8 illustrate for both cases (i.e., with and without immersed tubes), in which the left side illustrates the case without immersed tubes, and the right side demonstrates the case with immersed tubes. The magnitudes of both the bubble frequency and local gas holdup are clearly higher near the central region of the bed and lower toward the column wall. Also, the local values of the bubble frequency and gas holdup are larger in the case with immersed tubes (right side) compared with the case without immersed tubes (left side) for all the axial heights and superficial gas velocities. The trends of both the bubble frequency and local gas holdup shown in Figures 4.7 and 4.8 are similar to those of the local heat transfer coefficients displayed in Figure 4.6. The similar tendencies of the radial profiles of the local heat transfer coefficients, local bubble frequency, and local gas holdup demonstrate the direct relationship between the heat transfer and the hydrodynamics of the gas phase, which is represented by the number of bubbles and gas concentration. In addition, the obvious relationship between these three parameters demonstrates the enhancement of the local heat transfer coefficient when using vertical immersed tubes, which results from increasing the bubble frequency and local gas holdup.

It was found that the percentage increase in the local bubble frequency with the presence of vertical internals was higher near the wall ($r/R = 0.8$) and less near the

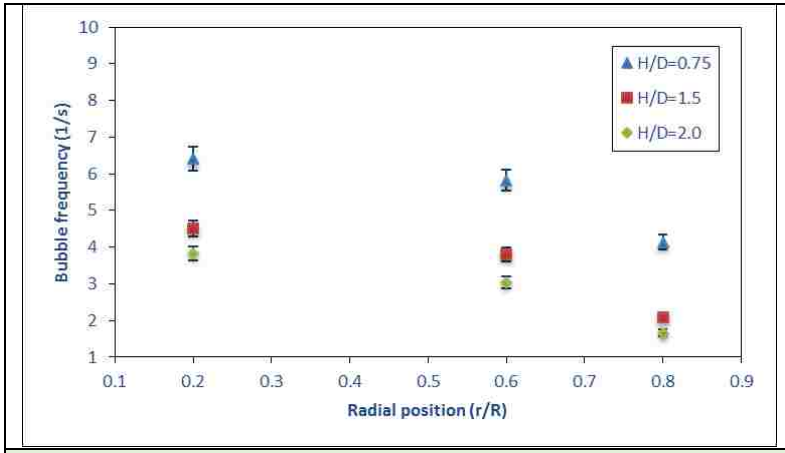

Radial profiles of the bubble frequency at different axial heights, where u/u_{mf} = 1.76 for the case without immersed tubes.

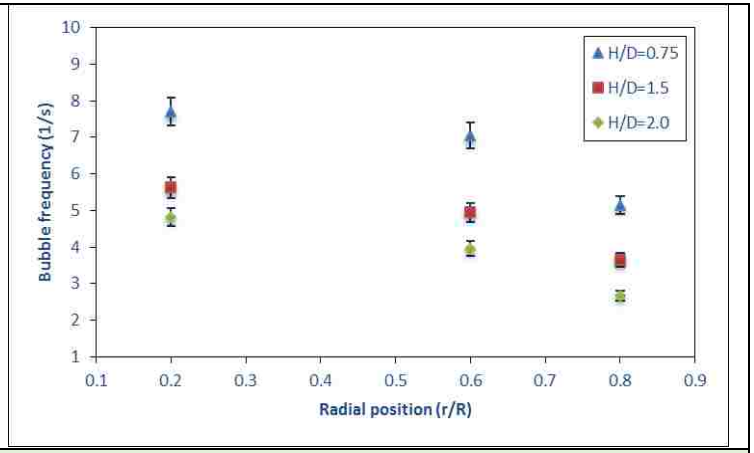

Radial profiles of the bubble frequency at different axial heights, where u/u_{mf} = 1.76 for the case with immersed tubes.

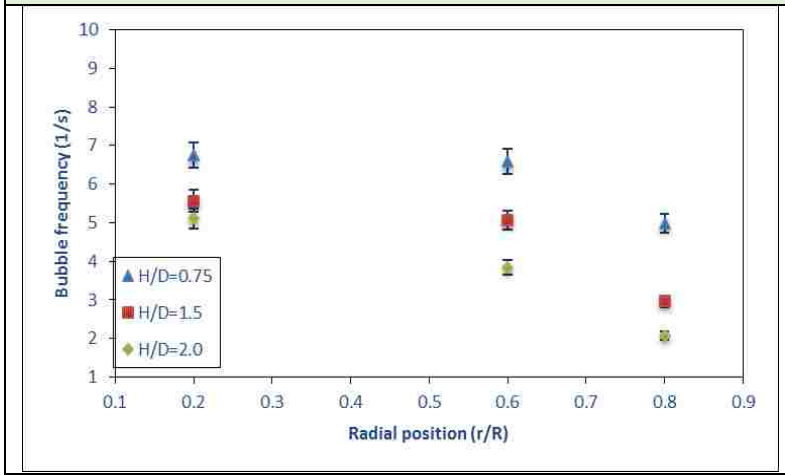

Radial profiles of the bubble frequency at different axial heights, where u/u_{mf} = 2.14 for the case without immersed tubes.

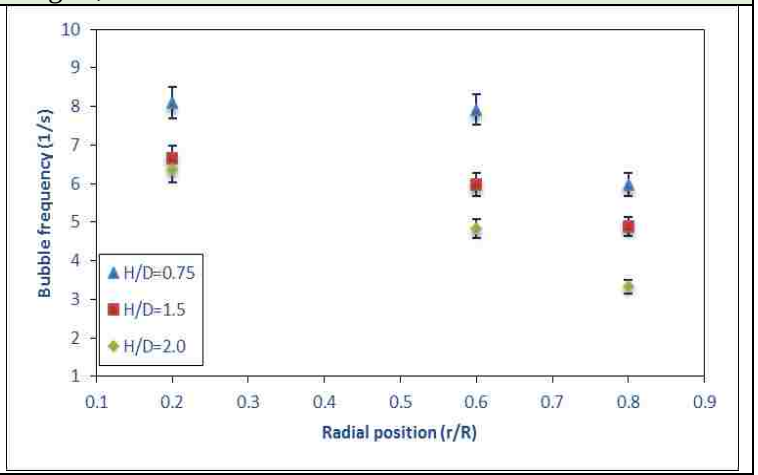

Radial profiles of the bubble frequency at different axial heights, where u/u_{mf} = 2.14 for the case with immersed tubes.

Figure 4.7. The radial profiles of bubble frequenct at different axial heights and three superficial gas velocities in terms of u/u_{mf} for the case without immersed tubes (left side) and with immersed tubes (right side)

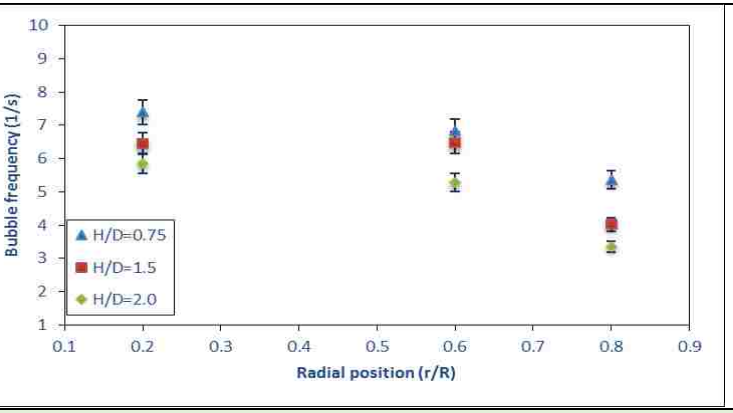

Radial profiles of the bubble frequency at different axial heights, where u/u_{mf} = 2.5 for the case without immersed tubes.

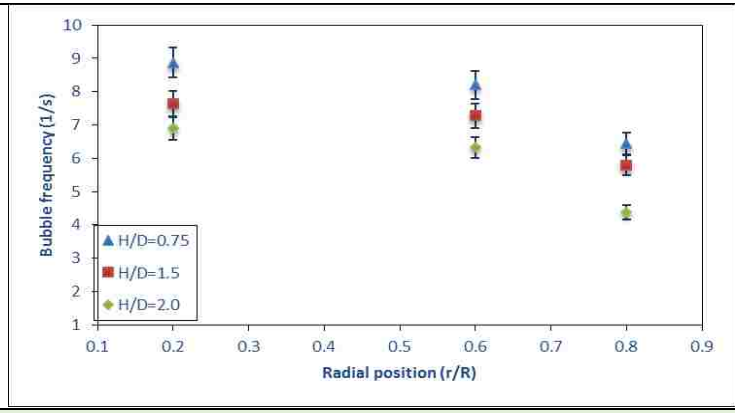

Radial profiles of the bubble frequency at different axial heights, where u/u_{mf} = 2.5 for the case with immersed tubes.

Figure 4.7. The radial profiles of bubble frequency at different axial heights and three superficial gas velocities in terms of u/u_{mf} for the case without immersed tubes (left side) and with immersed tubes (right side). (cont.)

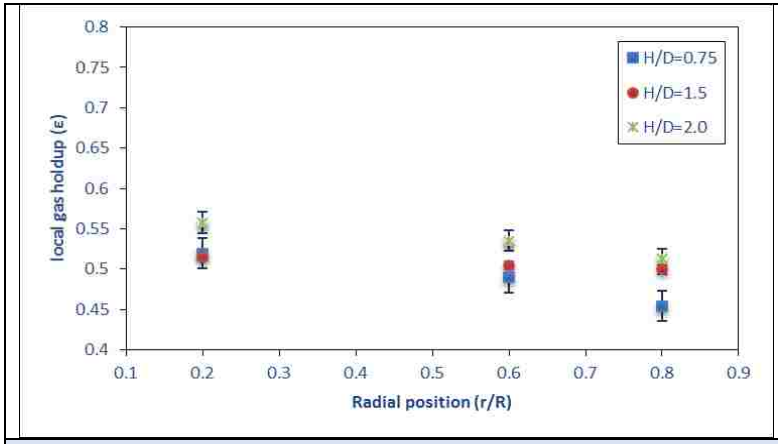

Radial profiles of the gas holdups at different axial heights, where u/u_{mf} = 1.76 for the case without immersed tubes.

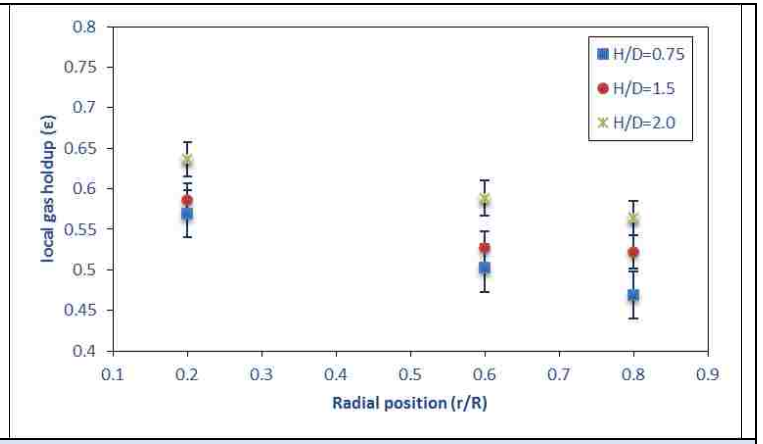

Radial profiles of the gas holdups at different axial heights, where u/u_{mf} = 1.76 for the case with immersed tubes.

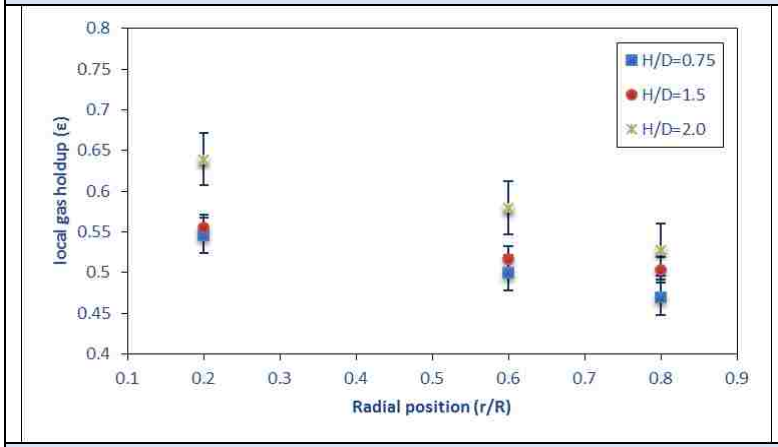

Radial profiles of the gas holdups at different axial heights, where u/u_{mf} = 2.14 for the case without immersed tubes.

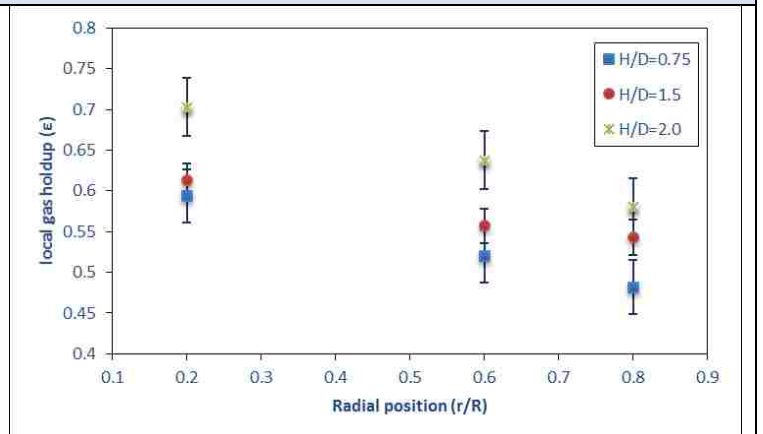

Radial profiles of the gas holdups at different axial heights, where u/u_{mf} = 2.14 for the case with immersed tubes.

Figure 4.8. The radial profiles of gas holdup at different axial heights and three superficial gas velocities in terms of u/u_{mf} for the case without immersed tubes (left side) and with immersed tubes (right side).

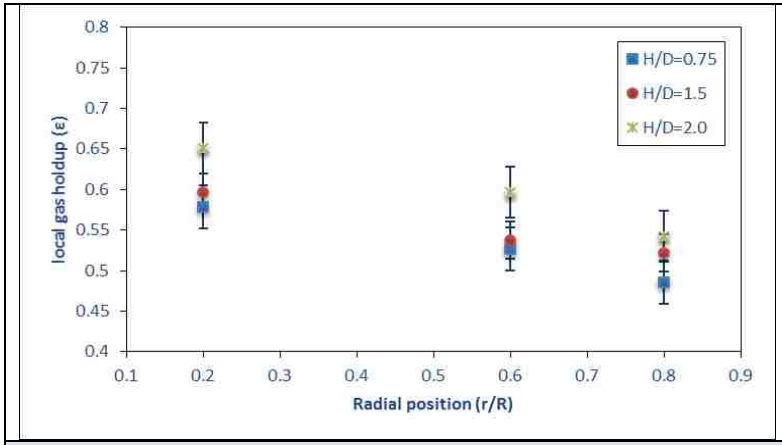

Radial profiles of the gas holdups at different axial heights, where u/u_{mf} = 2.5 for the case without immersed tubes.

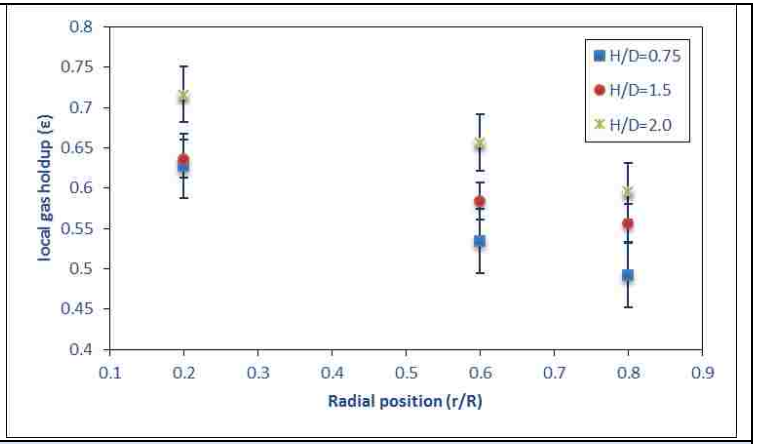

Radial profiles of the gas holdups at different axial heights, where u/u_{mf} = 2.5 for the case with immersed tubes.

Figure 4.8. The radial profiles of gas holdup at different axial heights and three superficial gas velocities in terms of u/u_{mf} for the case without immersed tubes (left side) and with immersed tubes (right side). (cont.)

center region (r/R = 0.2). In which, the percentage of increase of bubble frequency at u/u_{mf} = 2.5 and at r/R =0.8 (near the wall region) is 18%, 30%, and 23% at H/D = 0.75, 1.5, and 2, respectively. While percentage of increase of bubble frequency at u/u_{mf} = 2.5 and at r/R = 0.2 is 16%, 15%, and 15% at H/D = 0.75, 1.5, and 2, respectively. These percentages of increase in the bubble frequency with the presence of vertical internals at different radial position is shown the ability of immersed internals in enhancing the distribution of the gas phase inside the bed for benefiting heat transfer rates. It can be noticed that the percentage increase of bubble frequency at r/R = 0.2 is not noticeable and less than that at r/R= 0.8 at different axial positions.

4.3. THE VIBRATION OF HEAT TRANSFER, BUBBLE FREQUENCY AND LOCAL GAS HOLDUP AT DIFFERENT AXIAL HEIGHTS

Three superficial gas velocities in terms of u/u_{mf} were selected to study the heat transfer and gas hydrodynamics (gas holdup and bubble frequency) in relation to the difference in axial heights (u/u_{mf} = 1.6, 1.96, and 2.3). The axial profiles of the heat transfer coefficients at different radial positions with three superficial gas velocities in terms of u/u_{mf} for the two cases (i.e., with and without immersed tubes) are shown in Figure 4.9. The left side of Figure 4.9 displays the findings for the case without immersed tubes, while the right side illustrates the findings for the case with immersed tubes. As shown in Figure 4.9, the local heat transfer coefficient significantly increased from H/D = 0.75 to H/D = 1.5 and then slightly decreased from H/D = 1.5 to H/D = 2.0. This trend is similar for all the radial positions and superficial gas velocities and for the cases with and without immersed tubes. The incresing in the local heat transfer coefficient at H/D = 1.5 could be explained by the increase in the local bubble frequency and gas holdup, such that when the gas

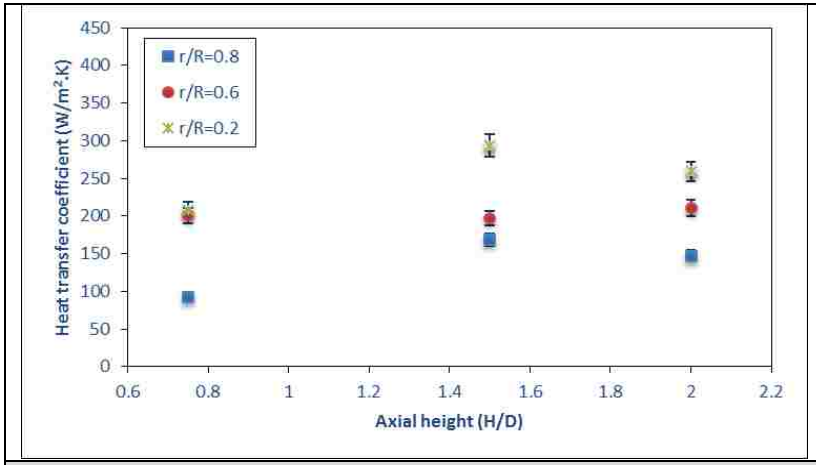

Axial profiles of the heat transfer coefficients at different radial positions, where u/u_{mf} = 1.6 for the case without immersed tubes.

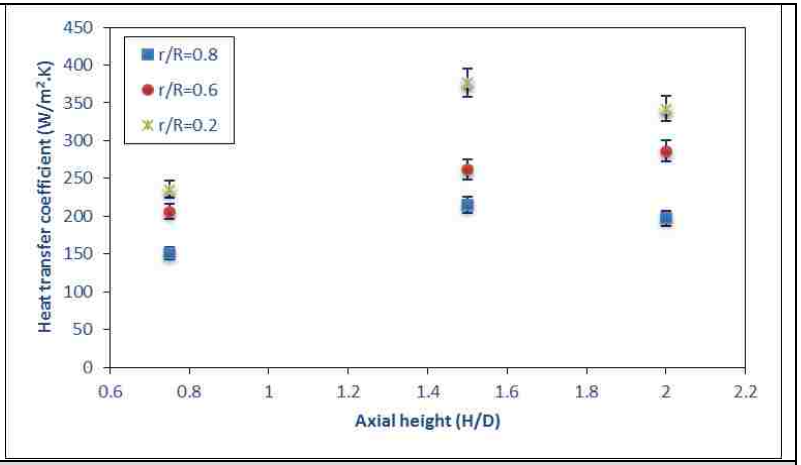

Axial profiles of the heat transfer coefficients at different radial positions, where u/u_{mf} = 1.6 for the case with immersed tubes.

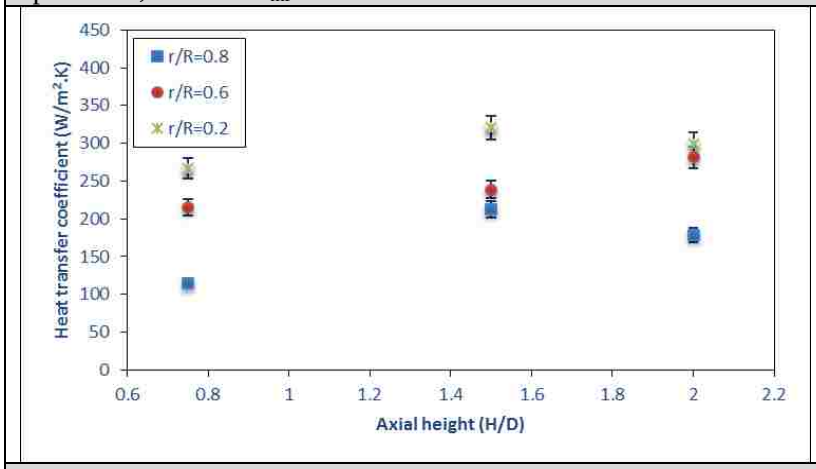

Axial profiles of the heat transfer coefficients at different radial positions, where u/u_{mf} = 1.96 for the case without immersed tubes.

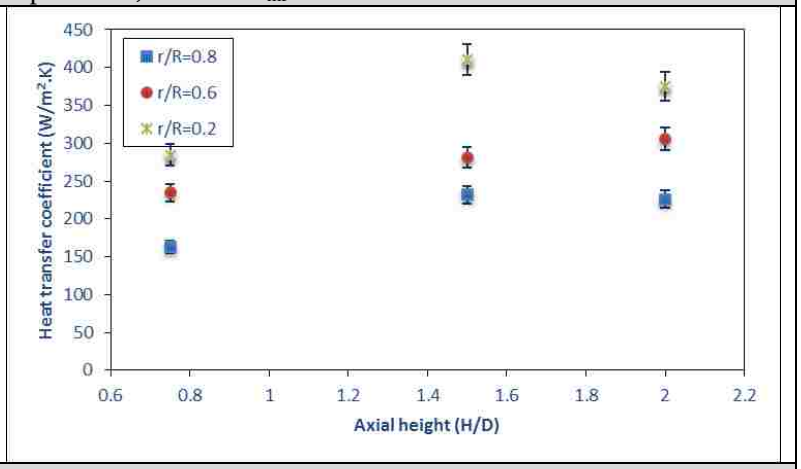

Axial profiles of the heat transfer coefficients at different radial positions, where u/u_{mf} = 1.96 for the case with immersed tubes.

Figure 4.9. Axial profiles of heat transfer coefficients at different radial positions and three superficial gas velocities in terms of u/u_{mf} for the case without immersed tubes (left side) and with immersed tubes (right side).

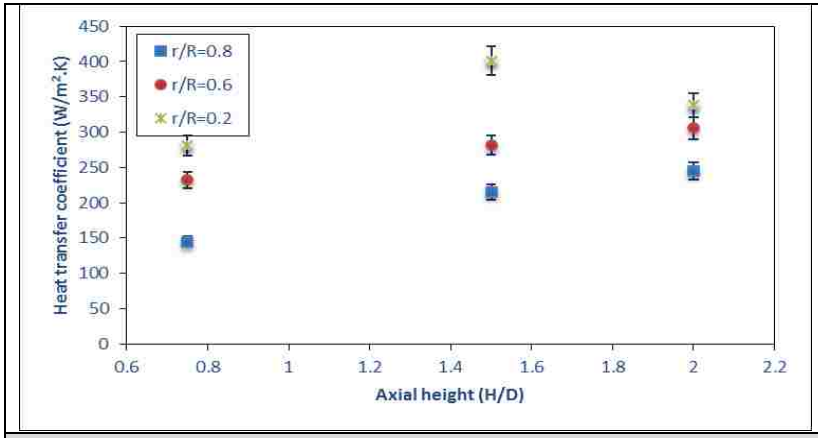

Axial profiles of the heat transfer coefficients at different radial positions, where u/u_{mf} = 2.3 for the case without immersed tubes.

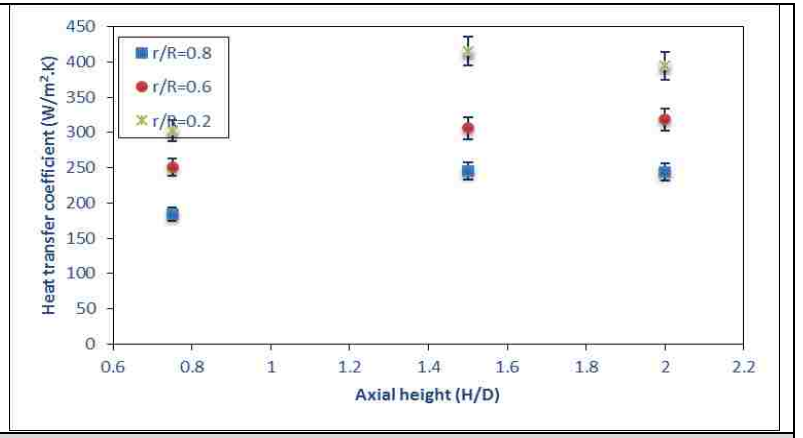

Axial profiles of the heat transfer coefficients at different radial positions, where u/u_{mf} = 2.3 for the case with immersed tubes.

Figure 4.9. Axial profiles of heat transfer coefficients at different radial positions and three superficial gas velocities in terms of u/u_{mf} for the case without immersed tubes (left side) and with immersed tubes (right side). (cont.)

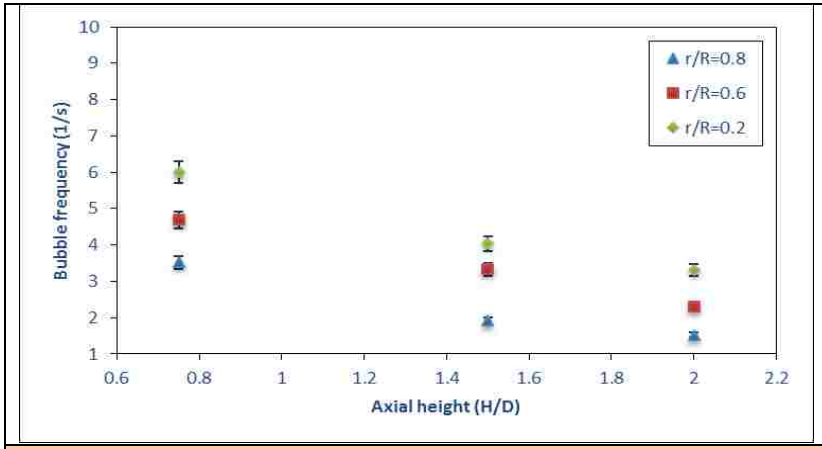

Axial profiles of the bubble frequency at different radial positions, where u/u_{mf} = 1.6 for the case without immersed tubes.

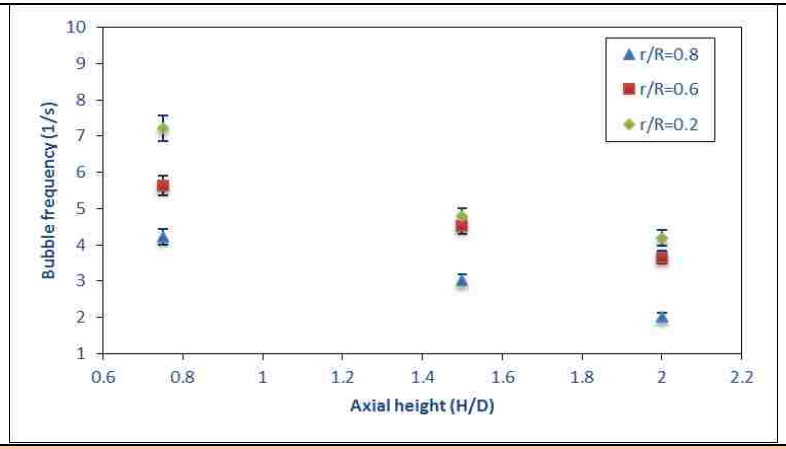

Axial profiles of the bubble frequency at different radial positions, where u/u_{mf} = 1.6 for the case with immersed tubes.

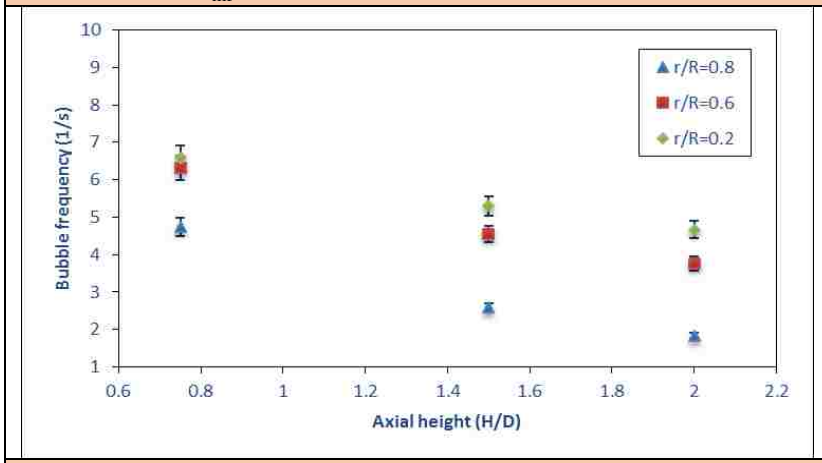

Axial profiles of the bubble frequency at different radial positions, where u/u_{mf} = 1.96 for the case without immersed tubes.

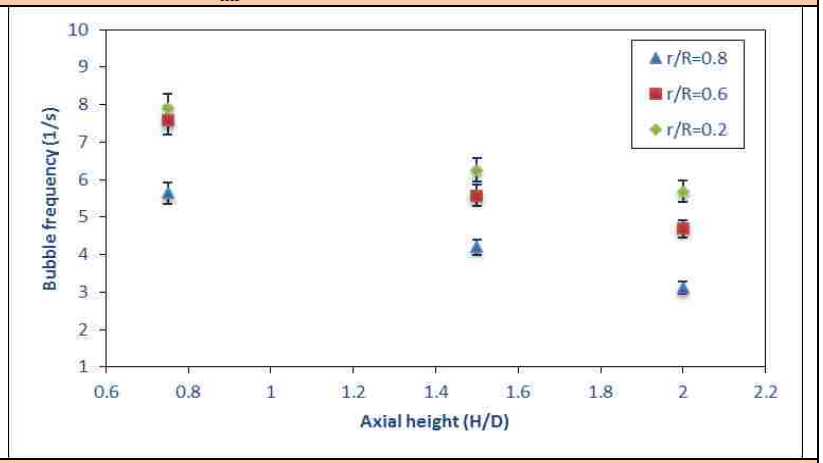

Axial profiles of the bubble frequency at different radial positions where u/u_{mf} = 1.96 for the case with immersed tubes.

Figure 4.10. The axial profiles of bubble frequency at different radial positions and three superficial gas velocities in terms of u/u_{mf} for the case without immersed tubes (left side) and with immersed tubes (right side).

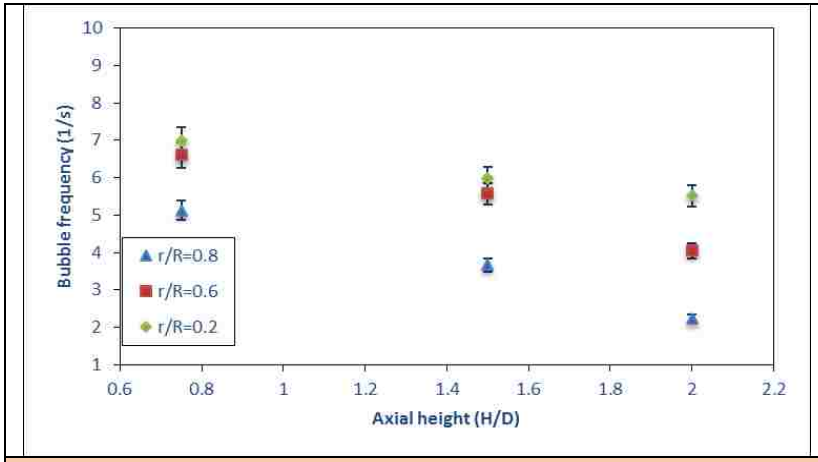

Axial profiles of the bubble frequency at different radial positions, where u/u_{mf} = 2.3 for the case without immersed tubes.

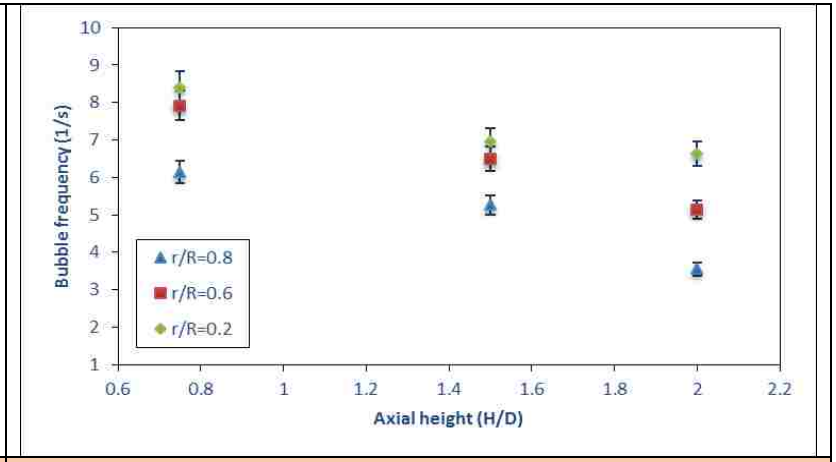

Axial profiles of the bubble frequency at different radial positions, where u/u_{mf} = 2.3 for the case with immersed tubes.

Figure 4.10. The axial profiles of bubble frequency at different radial positions and three superficial gas velocities in terms of u/u_{mf} for the case without immersed tubes (left side) and with immersed tubes (right side). (cont.)

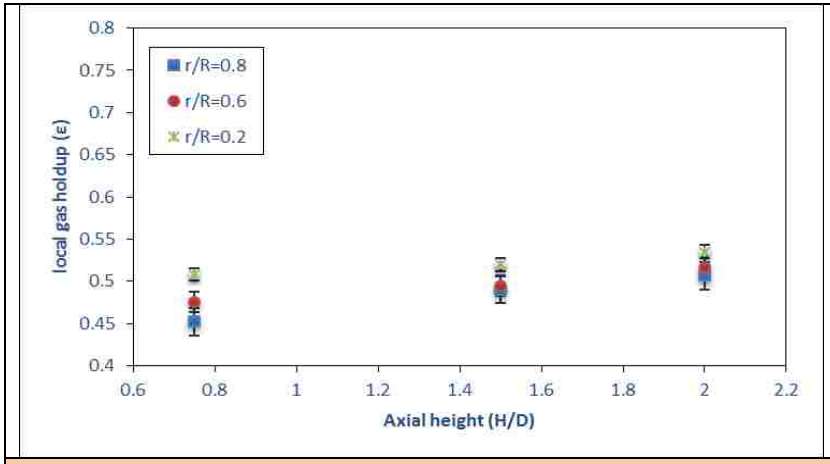

Axial profiles of the gas holdups at different radial positions, where u/u_{mf} = 1.6 for the case without immersed tubes.

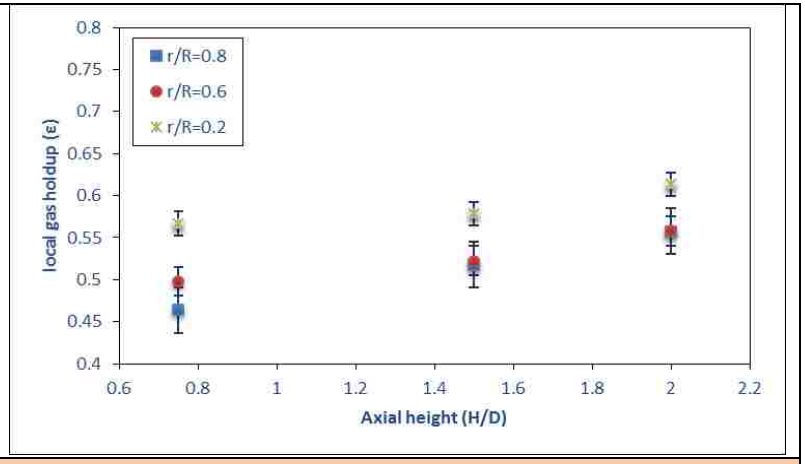

Axial profiles of the gas holdups at different radial positions, where u/u_{mf} = 1.6 for the case with immersed tubes.

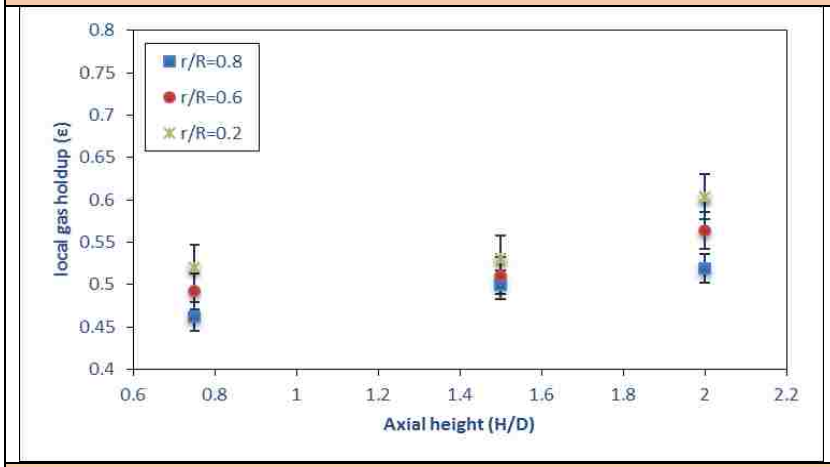

Axial profiles of the gas holdups at different radial positions, where u/u_{mf} = 1.96 for the case without immersed tubes.

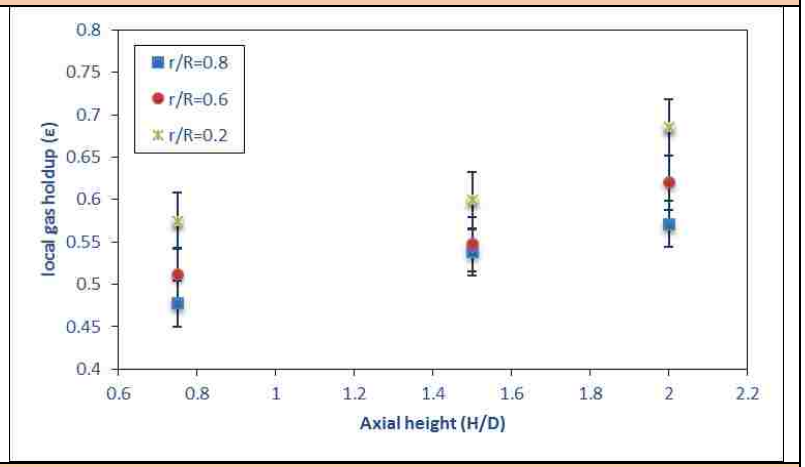

Axial profiles of the gas holdups at different radial positions, where u/u_{mf} = 1.96 for the case with immersed tubes.

Figure 4.11. The axial profiles of gas holdup at different radial positions and three superficial gas velocities in terms of u/u_{mf} for the case without immersed tubes (left side) and with immersed tubes (right side).

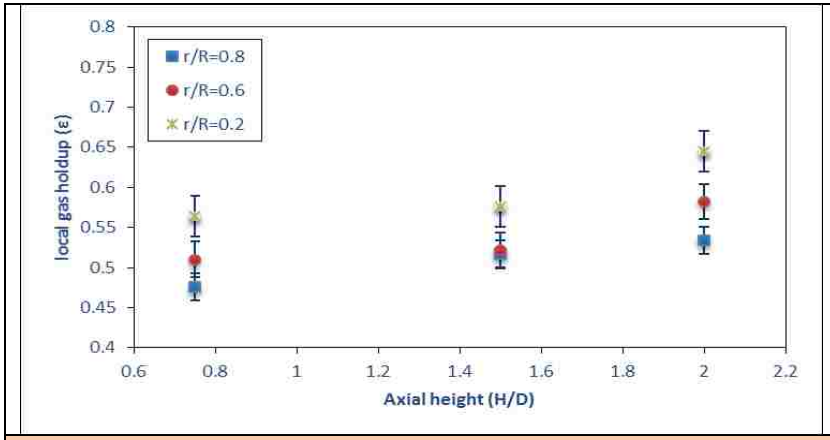

Axial profiles of the gas holdups at different radial positions, where u/u_{mf} = 2.3 for the case without immersed tubes.

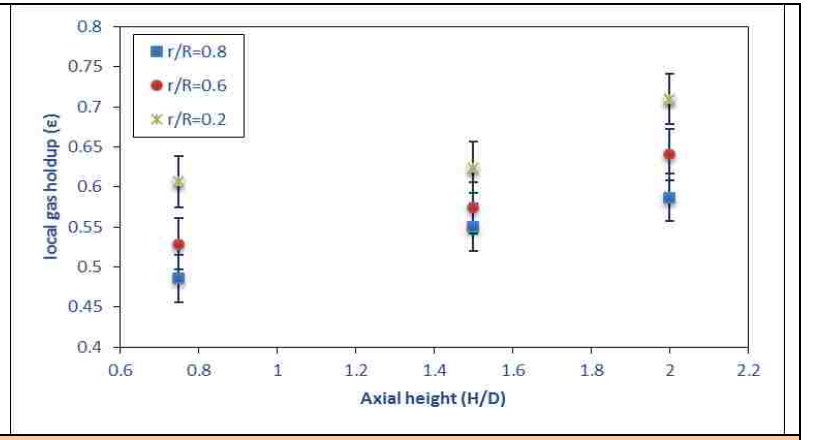

Axial profiles of the gas holdups at different radial positions, where u/u_{mf} = 2.3 for the case with immersed tubes.

Figure 4.11. The axial profiles of gas holdup at different radial positions and three superficial gas velocities in terms of u/u_{mf} for the case without immersed tubes (left side) and with immersed tubes (right side). (cont.)

bubbles passed the lower end of the immersed tubes located at H/D = 0.25, the larger bubbles split into two or more smaller bubbles; therefore, both the local bubble frequency and the bubble elongation increased due to the small space between the immersed tubes. This led to an increase in the local gas holdup in comparison with the case without immersed tubes. Thus, the increase in the local bubble frequency due to the splitting mechanism and in the local gas holdup due to the elongation behavior of the bubbles led to an increase in the percentage of the surface area of the heating probe that was exposed to both gas and solid particles that moved frequently; this caused the local heat transfer coefficient to increase accordingly, as shown in Figures 4.10 and 4.11. Such increse in the local heat transfer coefficents with axial height has been reported in litreture by many experimental works (Kim et al. 2003, Pisters and Prakash (2011). Furthermore, as the bubbles rose until they reached H/D = 2.0, they tended to coalescence, creating large bubbles, resulting in a slight decrease in the local bubble frequency and an increase in the local gas holdup, as seen in Figures 4.10 and 4.11. It is worth noting that the local bubble frequency and local gas holdup are a function of the superficial gas velocity and the radial level near the freeboard of the column due to the effect of the back-mixing of the solid particles. At u/u_{mf} = 1.4 and r/R = 0.2, it was found that the heat transfer coefficient has been increased when the axial height is increased from H/D = 0.75 to H/D = 1.5 by 43% and 20%, respectively for the case of with and without internals. It is clearly shown that the percentage increase in the local heat transfer coefficient with axial height is higher in the presence of vertical immersed tubes.

4.4. HEAT TRANSFER COEFFICIENTS OSCILLATIONS AND LOCAL GAS HOLDUP FLUCTUATIONS

The effect of the vertical immersed tubes on heat transfer coefficients inside the gas-solid fluidized bed was analyzed using heat transfer oscillations. The heat transfer oscillations are represented by the heat transfer coefficient signals recorded through a specific time span. Analyzing heat transfer oscillations provides a vehicle for comprehending the instantaneous impact of the vertical immersed tubes on the efficiency of the heat transfer through the time-dependent heat transfer coefficient. To compare the two signals for the two cases (i.e., with and without immersed tubes), the mean and standard deviation of each signal was estimated. Three superficial gas velocities in terms of u/u_{mf} were selected 1.6, 1.96, and 2.5 as well as one axial height (H/D = 1.5), and one radial position (r/R = 0.2), where, at these positions, the heat transfer coefficient reached its maximum value compared with other axial and radial positions. The heat transfer coefficient oscillations are illustrated in Figure 4.12 for both cases (i.e., with and without immersed tubes), with the left side representing the case without internals and the right side illustrating the case with internals. As can be seen in Figure 4.12, the values of both the average and standard deviation of the case with immersed tubes are higher than those of the case without immersed tubes, except for the value of the average at u/umf = 2.5 for the case with immersed tubes, in which a small decrease in the heat transfer coefficient magnitude occurred. This small reduction can be explained in relation to the value of u (non-dimensionalized superficial gas velocity in m/s), for which, at this superficial gas velocity (u/umf = 2.5), the value was 0.40 m/s. This velocity indicates the start of the slow bubble sub-regime, which is the flow regime that follows the fast bubble flow regime in the Geldart A particles. In general, these two sub-regimes combine to form the bubble flow

regime as reported by Nedeltchev et al. (2012). Furthermore, the average value (μ) indicates the magnitude of the heat transfer coefficient, while the standard deviation (σ) represents the variations of the heat transfer coefficients with respect to the aveage value. The values of the average and standard deviation of the heat transfer coefficient obtained from there signals indicate that the heat transfer coefficient increased in the case of vertical immersed tubes due to the hydrodynamics effects that occurred in the immersed tubes, such as increased bubble frequency and gas holdup. Moreover, the values of the standard deviation significantly increased in the case of the immersed tubes, as shown in Figure 4.12, which is another indication of the increase in the local oscillation of both the heat transfer and the hydrodynamics due to the presence of the vertical immersed tubes. This increase in the standard deviation values is reflected in the performance of the heat transfer process, in which the local heat transfer coefficient increased accordingly.

In addition to the heat transfer coefficient oscillation, and in order to comprehend the influence of vertical internals of the local gas holdup, the instantaneous fluctuations of the gas holdup at the case of with and without internals that recorded at specific sample time has been presented in form of local gas holdup signals for the case of with and without internals. Thus, to compare the two signals for the two cases (i.e., with and without immersed tubes), the mean and standard deviation of each signal was calculated. Three superficial gas velocities in terms of u/u_{mf} = 1.6, 1.96, and 2.5 were selected as well as one axial height (H/D = 1.5), and one radial position (r/R = 0.2) which are similar to the conditions of the heat transfer oscillation. The local gas holdup fluctuation signals are illustrated in Figure 4.13 for both cases (i.e., with and without immersed tubes), with the left side representing the case without internals and the right side illustrating the case with

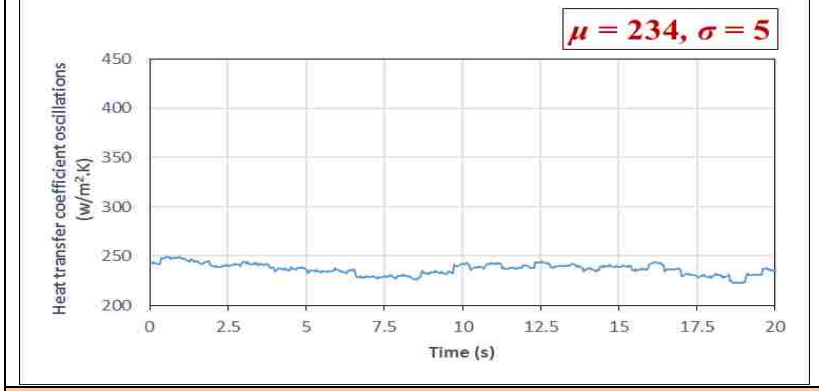

Heat transfer coefficient oscillations, where u/u_{mf} = 1.4 for the case without immersed tubes.

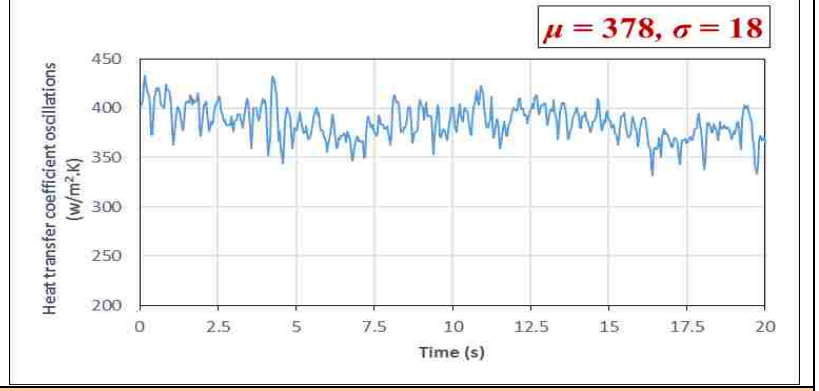

Heat transfer coefficient oscillations, where u/u_{mf} = 1.4 for the case with immersed tubes.

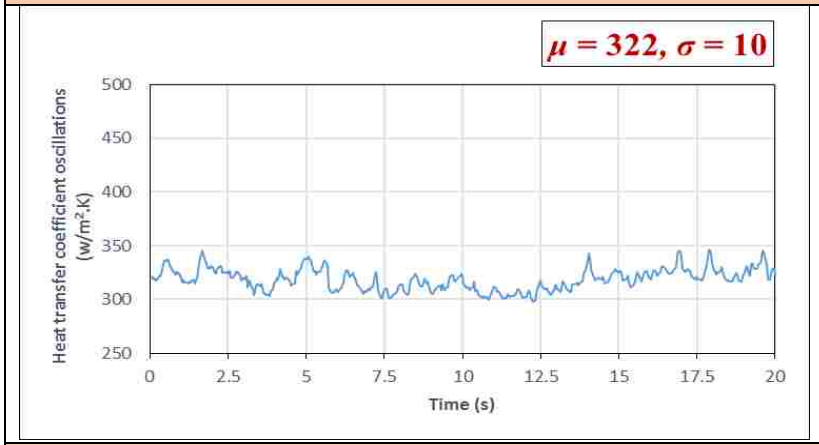

Heat transfer coefficient oscillations, where u/u_{mf} = 1.96 for the case without immersed tubes.

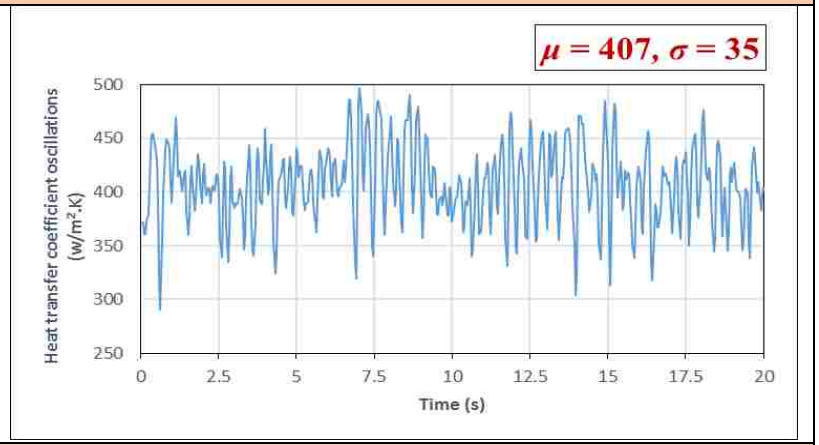

Heat transfer coefficient oscillations, where u/u_{mf} = 1.96 for the case with immersed tubes.

Figure 4.12. Heat transfer coefficient oscillations where H/D = 1.5 and r/R = 0.2, with three superficial gas velocities in terms of u/u_{mf} for the case without immersed tubes (left side) and with immersed tubes (right side), the μ and σ represent the average and standard deviation. The unit of μ is w/m^2. k

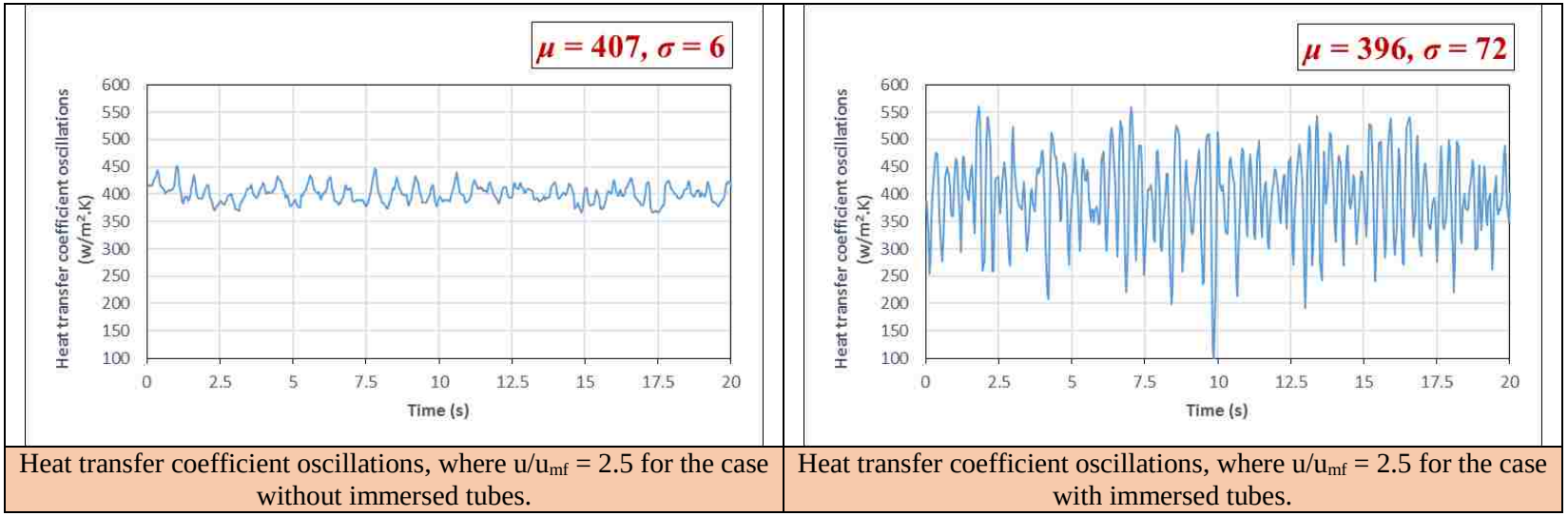

Heat transfer coefficient oscillations, where u/u_{mf} = 2.5 for the case without immersed tubes.	Heat transfer coefficient oscillations, where u/u_{mf} = 2.5 for the case with immersed tubes.

Figure 4.12. Heat transfer coefficient oscillations where H/D = 1.5 and r/R = 0.2, with three superficial gas velocities in terms of u/u_{mf} for the case without immersed tubes (left side) and with immersed tubes (right side), the μ and σ represent the average and standard deviation. The unit of μ is w/m^2. k (cont.)

of the local gas holdup fluctuations are sligthly increased, while the values of standard deviation are sligthly decreased. The increase of the aveage values explain the increase of the gas holdup in the case of vertical internals due to the reduction in cross-sectional area avilable from flowing gas, since the average value of the gas holdup fluctuation signal is represented the gas holdup. The sligthly decrease in the values of standard deviation reflects the decrease in the local gas holdup fluctuation in which the existing of vertical internals reduce the bed fluctuation and make the fluidization process or the contact between the solid phase and gas phase more smoother.

4.5. COMPARISON WITH LITERATURE STUDIES

The experimental results of the heat transfer coefficients are compared with the most common predicted correlations available in the literature listed in Table 4.1. In order to do so, the radial-average heat transfer coefficient has been estimated at different axial position and superficial gas velocity in the form of u/u_{mf} as well as for the case of with and without vertical internals as follows:

$$h = \frac{2}{R^2} \int_0^R h(r) r \, dr \tag{4}$$

The average absolute relative error (AARE) between the experimental and predicted data has been estimated as follows:

$$AARE = \frac{1}{N} \sum_{i=1}^{N} \left| \frac{h_{exp(i)} - h_{pred(i)}}{h_{exp(i)}} \right| \tag{5}$$

where N is the data point number

The experimental data of the heat transfer coefficient from this work and the predicted data from the correlations listed in Table 4.1 have been demonstrated in Figure 4.14 for the case of with and without vertical internals and at different axial heights. The

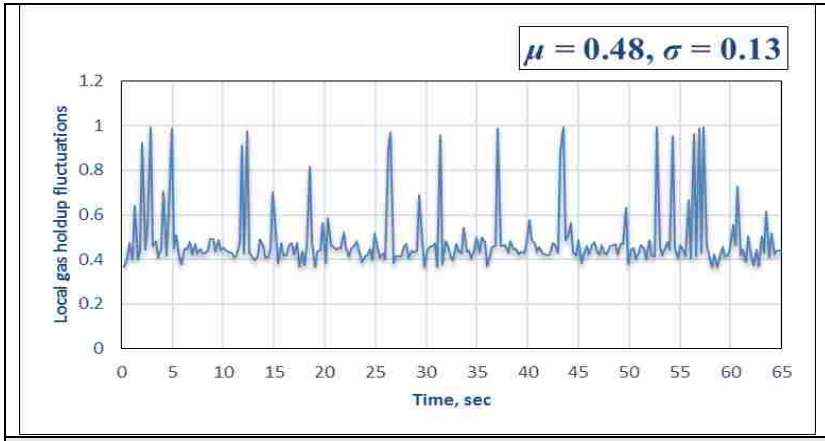

Local gas holdup fluctuations, where u/u_{mf} = 1.4 for the case without immersed tubes.

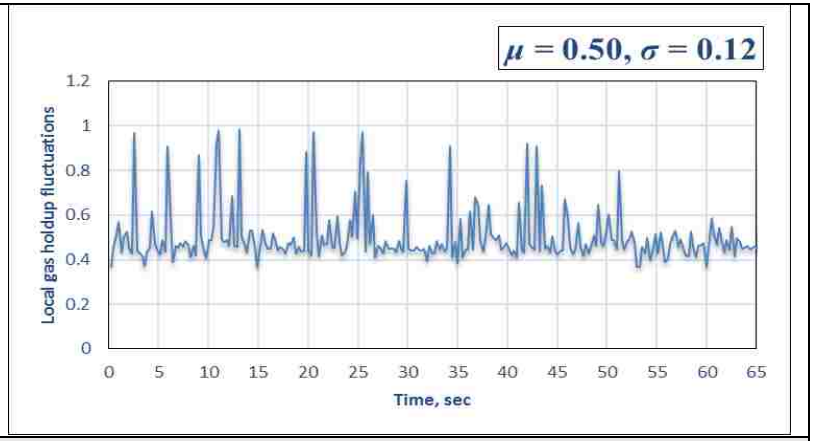

Local gas holdup fluctuations, where u/u_{mf} = 1.4 for the case with immersed tubes.

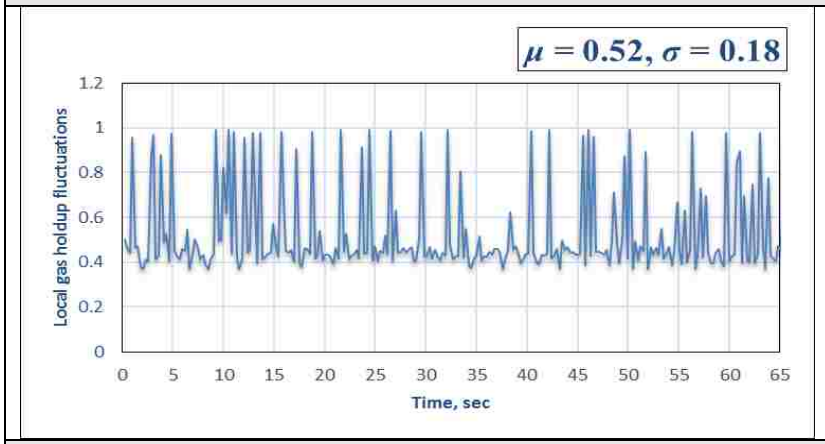

Local gas holdup fluctuations, where u/u_{mf} = 1.96 for the case without immersed tubes.

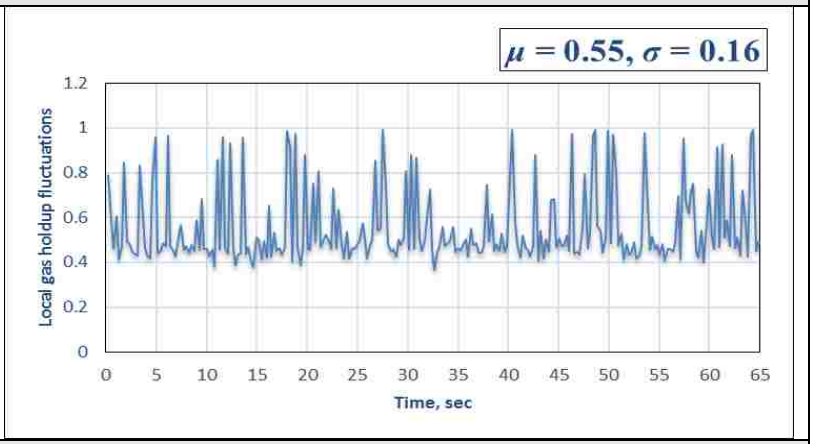

Local gas holdup fluctuations, where u/u_{mf} = 1.96 for the case with immersed tubes.

Figure 4.13. Local gas holdup fluctuations where H/D = 1.5 and r/R = 0.2, with three superficial gas velocities in terms of u/u_{mf} for the case without immersed tubes (left side) and with immersed tubes (right side), the μ and σ represent the average and standard deviation.

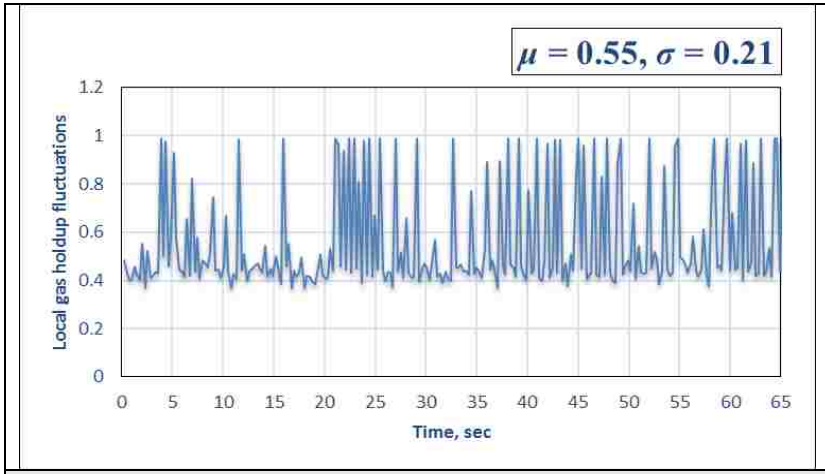

Heat transfer coefficient oscillations, where $u/u_{mf} = 2.5$ for the case without immersed tubes.

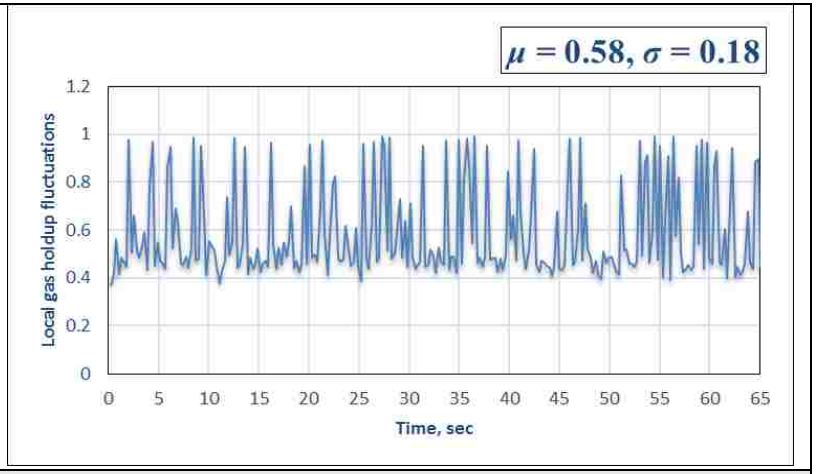

Heat transfer coefficient oscillations, where $u/u_{mf} = 2.5$ for the case with immersed tubes.

Figure 4.13. Local gas holdup fluctuations where H/D = 1.5 and r/R = 0.2, with three superficial gas velocities in terms of u/u_{mf} for the case without immersed tubes (left side) and with immersed tubes (right side), the μ and σ represent the average and standard deviation. (cont.)

left side of Figure 4.14 illustrates the results for the case without vertical internals, while the right side displays the findings for the case with vertical internals. Additionally, the average absolute relative error between the experimental and predicted values of heat transfer coefficient are listed in Table 4.1.

As shown in Figure 4.15 and Table 4.1, there is a big difference between the experimental and predicated heat transfer coefficients for both cases of with and without vertical internals and at all the axial height except the predicated results by Leva and Grumme's correlation (1952) at H/D = 0.75 and for case of without internals where the AARE is 6%. The reasons of this big difference are some of these correlations are developed for the case of horizontal immersed heat surfaces inside the gas-solid fluidized beds as in the case of correlations predictaed by Vreedenberg (1958); Andeen and Glicksman (1976). Additionally, in these predicated correlations, the impact of the hydrodynamic parameters such as gas holdup and bubble frequency has not implemented in these correlations. Therefore, there is a need to develop a correlation that includes the gas holdup and/or bubble frequency and relate them to the heat transfer coefficient in the form of relevant dimensionless groups. The development of the correlation in the form of related dimensionless groups is discussed in the next section.

4.6. THE DEVELOPED HEAT TRANSFER CORRELATION FOR GAS-SOLID FLUIDIZED BED WITH INTERNALS

The correlation was developed based on relevant dimensionless groups involving related parameters such as the design parameter (column diameter), operating condition (superficial gas velocity), physical properties of the gas and solid particles (gas density, gas viscosity, gas thermal conductivity, and solid particle size), and bubble

Table 4.1. Correlations available in literature for estimating the average heat transfer coefficient

References	Correlations	Scope of use	% Average Absolute Relative Error (without internals) at different axial heights			% Average Absolute Relative Error (with internals) at different axial heights		
			H/D= 0.75	H/D= 1.5	H/D= 2	H/D= 0.75	H/D= 1.5	H/D= 2
Leva and Grumme (1952)	$\frac{hd_p}{k_g} = 0.525\ Re_p^{0.75}$	Heat trasfer from vertical surfaces	16%	36%	34%	6%	31%	30%
Vreedenberg (1958)	$\frac{h\ D_t}{k_g} = 0.66 Pr_g^{0.3} \left(\frac{\rho_{s(1-\varepsilon)}}{\rho_g \varepsilon}\right)^{0.44} Re_D^{0.44}$	Heat trasfer from horizontal surfaces	85%	41%	47%	77%	22%	13%
Andeen and Glicksman (1976)	$\frac{hD_t}{k_g} = 900\ (1\text{-}\varepsilon)\left(\frac{\rho_s}{\rho_g} Pr_g \left(\frac{\mu_g^2}{g\rho_s^2 d_p^3}\right)\right)^{0.3} Re_D^{0.3}$	Heat trasfer from horizontal surfaces	184%	108%	101%	155%	72%	54%
Borodulya et al. (1991)	$\frac{hd_p}{k_g} = 0.74\ Ar^{0.1}\left(\frac{\rho_s}{\rho_g}\right)^{0.14}\left(\frac{Cp_s}{Cp_g}\right)^{0.24}(1\text{-}\varepsilon)^{2/3} + 0.46 Re_p Pr_g \frac{(1\text{-}\varepsilon)^{2/3}}{\varepsilon}$	Heat trasfer from Vertical and horizontal surfaces	155%	87%	82%	136%	59%	44%

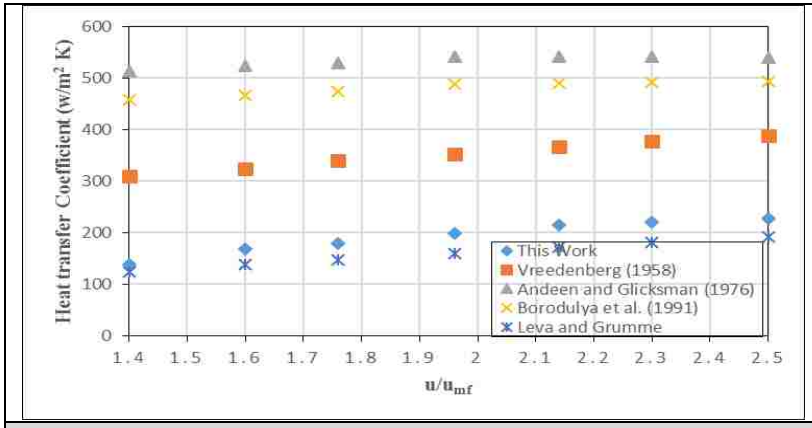

Comparison between the experimental and predicted values of the heat transfer coefficient at H/D = 0.75

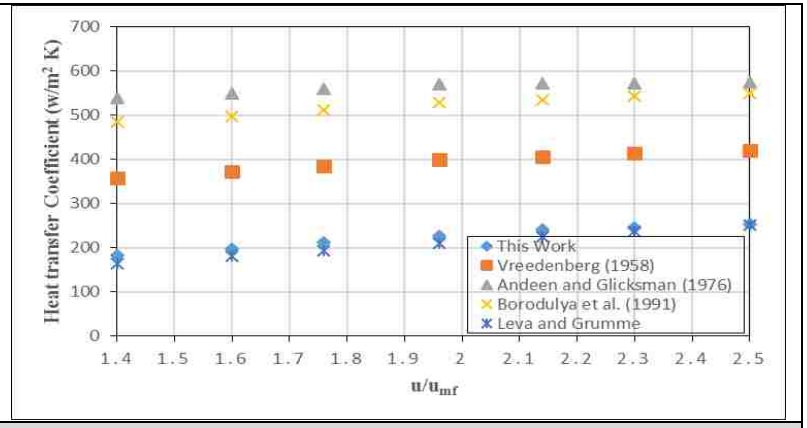

Comparison between the experimental and predicted values of the heat transfer coefficient at H/D = 0.75

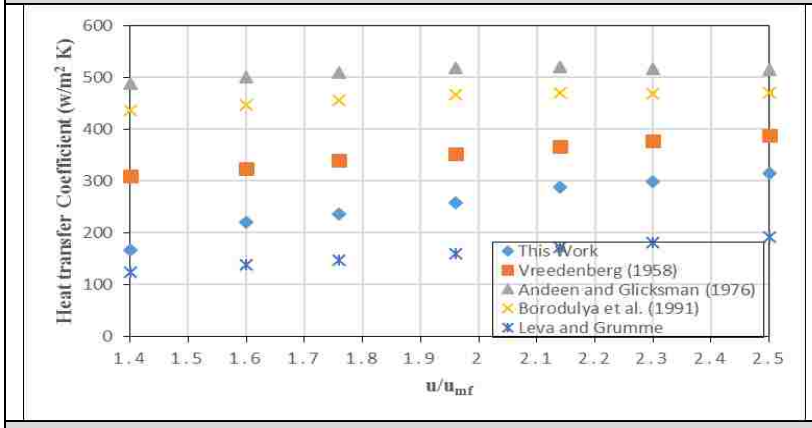

Comparison between the experimental and predicted values of the heat transfer coefficient at H/D =1.5

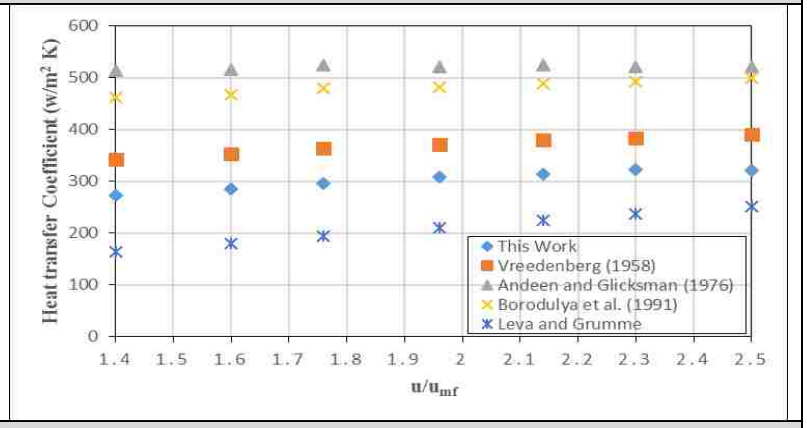

Comparison between the experimental and predicted values of the heat transfer coefficient at H/D =1.5

Figure 4.14. Comparison between the experimental and predicted values of the heat transfer coefficient at different superficial gas velocities superficial gas velocities in terms of u/u_{mf} and axial heights for the case without immersed tubes (left side) and with immersed tubes (right side).

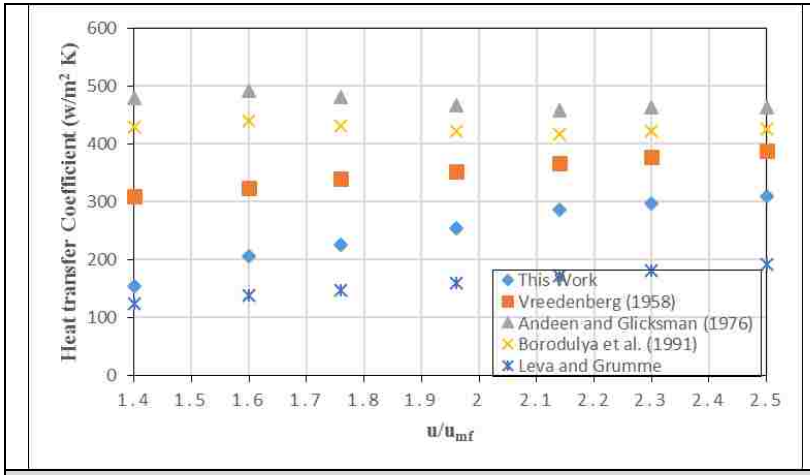

Comparison between the experimental and predicted values of the heat transfer coefficient at H/D = 2

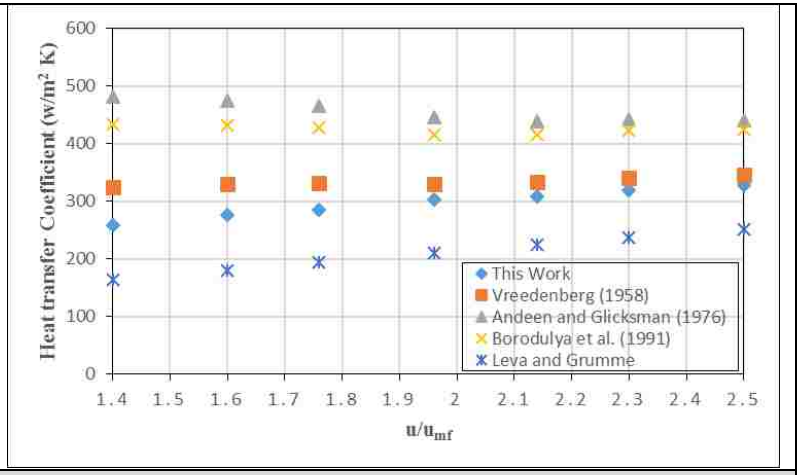

Comparison between the experimental and predicted values of the heat transfer coefficient at H/D = 2

Figure 4.14. Comparison between the experimental and predicted values of the heat transfer coefficient at different superficial gas velocities superficial gas velocities in terms of u/u_{mf} and axial heights for the case without immersed tubes (left side) and with immersed tubes (right side). (cont.)

hydrodynamic characteristics (gas holdup (ε) and bubble frequency (B_f)). It is worth to mention that the heat transfer coefficient, gas holdup and bubble frequency used here are radial-averaged values that calculated using Equation 4. A dimensional analysis approach was employed, in which the system parameters were classified into the following dimensionless groups:

1) Operating parameter: Reynolds number based on the particle diameter (Re_p).

2) Operating, Design, and Bubble hydrodynamic parameters: ratio of superficial gas velocity to the column diameter (u_g/D_c) multiply by the bubble frequency.

3) gas holdup in form of ($1-\varepsilon/\varepsilon$)

3) Measurement position parameter: axial positions of measurement H/D.

The heat transfer coefficient (h) correlation related to the above parameters is as follows:

$$\mathrm{Nu_p} = \mathrm{K}\left(\mathrm{Re_p}\right)^{\mathrm{a}} \left(\frac{\mathrm{u_g}}{\mathrm{D_c{*}B_f}}\right)^{\mathrm{b}} \left(\frac{1-\varepsilon}{\varepsilon}\right)^{\mathrm{c}} \left(\frac{\mathrm{H}}{\mathrm{D}}\right)^{\mathrm{d}} \qquad (6)$$

where

Nu_p is the Nusselt number based on the tube diameter ($\frac{\mathrm{hd_p}}{\mathrm{k_g}}$);

Re_p is the Reynolds number based on the particle diameter $\left(\frac{\rho_g \mathrm{U d_p}}{\mu_g}\right)$;

d_p is the particle size and k_g is the thermal conductivity of the gas; K is the coefficient; and a, b, c, and d are the exponents.

To perform a multiple linear regression using the experimental data, Eq. 4 was reformulated to a linear formula by taking the natural logarithm (Eq. 7):

$$\ln(\mathrm{Nu_t}) = \ln(\mathrm{K}) + \mathrm{a}\ln\left(\mathrm{Re_p}\right) + \mathrm{b}\ln\left(\frac{\mathrm{u_g}}{\mathrm{D_c{*}B_f}}\right) + \mathrm{c}\ln\left(\frac{1-\varepsilon}{\varepsilon}\right) + \mathrm{d}\ln\left(\frac{\mathrm{H}}{\mathrm{D}}\right) \qquad (7)$$

The coefficient K and the exponents a, b, c, and d were estimated. The values of ln(K) and the exponents a, b, c, and d are listed in Table 4.2, and the regression statistic data together with the analysis of variance (ANOVA) for the selected dimensionless groups are illustrated in Table 4.2. The developed correlation equation obtained for the Nusselt number using multiple linear regression in JMP®12 is presented in Eq. 8, with an R^2 value of 0.91 and an average error of 0.069 as illustrated in Table 4.3. From the probability factor of each dimensionless group that listed in Table 4.2, it shown that all the parameters in form of their dimensionless groups have a significant effect on the radial-averaged heat transfer coefficient in form of Nusselt number

$$\mathrm{Nu_t} = 0.3719\left(\mathrm{Re_p}\right)^{0.8675}\left(\frac{u_g}{D_c{*}B_f}\right)^{-0.4592}\left(\frac{1\text{-}\varepsilon}{\varepsilon}\right)^{0.501}\left(\frac{H}{D}\right)^{0.6547} \qquad (8)$$

The mean relative deviation (MRD) between the experimental and predicted results was obtained as follows:

$$\mathrm{MRD\%} = \left[\sum_{i=1}^{42}\left|\frac{Eu_{i,exp}\text{-}Eu_{i,pred}}{Eu_{i,exp}}\right|\right]*\frac{100}{42} = 4.84\% \qquad (9)$$

The MRD of 4.84%, shows a good agreement between the values of the averaged-radial heat transfer coefficient predicted by Eq. 8 and the experimental data. Figure 4.15 presents the plot of the experimental data versus the predicted values of the Nusselt number.

It has been found from Equation 8 that the Reynold number of the solid particles which represent the ratio of inertial forces of the solids particles to viscous force of the fluidizing fluid has a significant impact on the heat transfer coefficient inside the bed. The positive sign of Reynold number in Equation 8 indicates that the increase of Reynold number (superficial gas velocity) leads to increase the heat transfer coefficient accordingly. Moreover, the bubbles hydrodynamic characteristics of gas holdup and bubble frequency

Table 4.2. Parameter estimates from analysis of variance of the parameters used in Eq. 3. using JMP statistical software

Term	**Estimate**	**Std Error**	**t Ratio**	**Prob > |t|**
Intercept	Ln(K) = -0.989	0.1516	-6.52	<.0001
Re_p	a = 0.8675	0.0881	9.85	<.0001
$U_g/Dc*B_f$	b = -0.4592	0.0934	-4.92	<.0001
$(1-\varepsilon)/\varepsilon$	c = 0.501	0.1624	3.08	0.0038
H/D	d = 0.6547	0.0706	9.26	<.0001

Table 4.3. Regression statistic data (summary of fit)

RSquare	0.9151
RSquare Adj	0.906
Root Mean Square Error	0.0693
Mean of Response	0.6811
Observations	42

together with the measurement positions (axial position) have a considerable effect on the heat transfer coefficient inside the gas-solid fluidized bed with and without vertical internals. The negative sign of the term $(\frac{u_g}{D_c*B_f})$ indicates that combination of the superficial gas velocity together with the bubble frequency have an opposite effect on the heat transfer

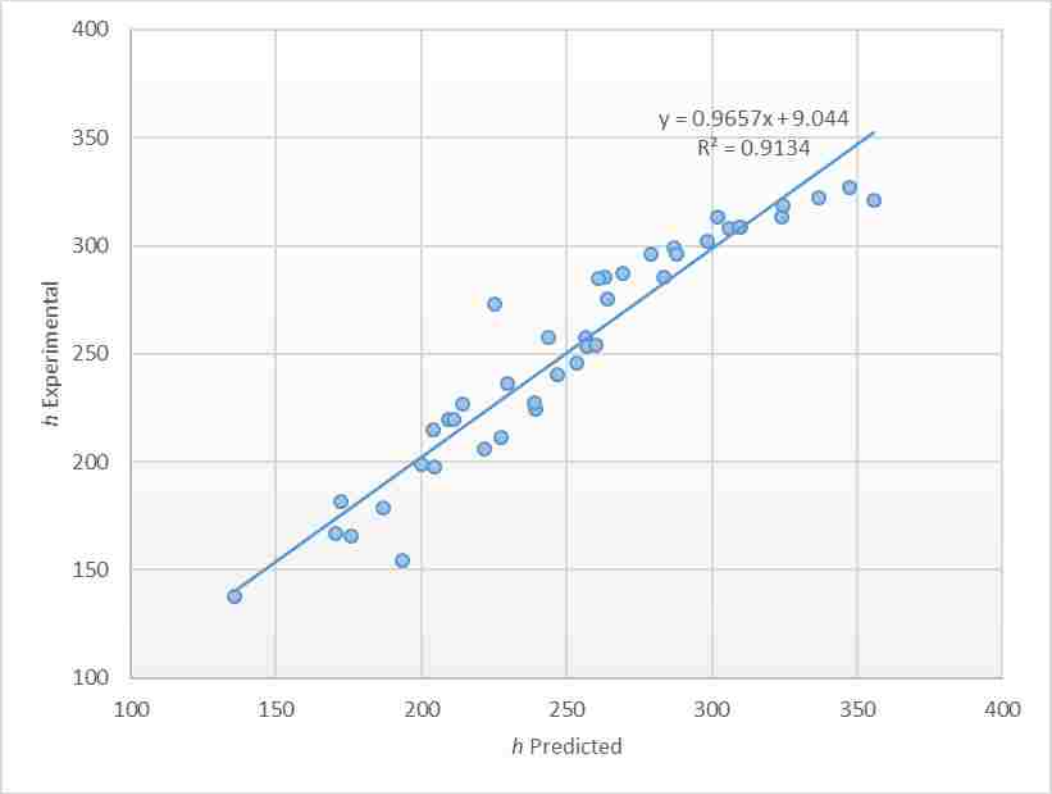

Figure 4.15. Comparison between the experimental and predicted values of the heat transfer coefficient.

coefficient inside the gas-solid fluidized bed. As well it indicates that the bubble frequency has more effect on the heat transfer coefficient when it compares with the superficial gas velocity, since the bubble frequency in dominator and both of them has a positive effect on the heat transfer coefficient as discussed earlier. The positive sign of the terms $(\frac{1-\varepsilon}{\varepsilon})$ is indicates that the increasing of gas holdup leads to increase the heat transfer coefficient as mentioned and discussed earlier. Additionally, the axial height of the measurement has a positive sign as shown in Equation 6, this indicates that the heat transfer coefficient increases with increasing the axial height (away from the distributor plate) and these indications has been demonstrated earlier in the results discussion and analysis. The results of Equation 6 are agreed with experimental results reported in literature by Kim et al.

(2003), Rasouli et al. (2005), Stefanova et al. (2007), Stefanova et al. (2011), Pisters and Prakash (2011), and Yao et al. (2015) with regard to the importance of the effect of bubbles hydrodynamics (local gas holdup and bubble frequency) and measurement positions as well as the superficial gas velocity and Reynolds number of the solids particle on the heat transfer coefficients inside the gas-solid fluidized bed with heat immersed surfaces.

5. REMARKS

The impact of a bundle of intense vertical immersed tubes on the heat transfer, bubble frequency and gas holdup was studied in a gas-solid fluidized bed of 0.14 m inside diameter. The heat transfer coefficient measurements were carried out with a non-invasive fast response heat transfer probe, which used the advanced flash mounted Micro-Foil® sensor. In addition, the optical fiber probe was used as a sophisticated technique to measure the local gas holdup and bubble frequency since these two hydrodynamic properties have a considerable relation to the heat transfer coefficient inside gas-solid fluidization systems. A circular arrangement of vertical immersed tubes was employed to represent the vertical heat exchanger tubes inside gas-solid fluidized bed reactors. Different superficial gas velocities (u/u_{mf}) of bubbling flow regime, radial positions (r/R), and axial heights (H/D) were used. Glass beads were the solid particles of Geldart A, with 210 μm average particle size and 2,500 Kg/m^3 solids density, along with a 0.35 m static bed height. It was demonstrated experimentally that the local heat transfer coefficient was enhanced when using vertical immersed tubes for all the studied conditions and locations inside the bed. The local heat transfer has found to be directly related to bubble frequency and gas holdup, such that the increases in the bubble frequency and gas holdup using vertical immersed

tubes led to an increase in the heat transfer coefficients. The experimental results of heat transfer coefficient in the form of the Nusselt number (Nu) were correlated with the related dimensionless groups to properly predict our results. The developed correlation was in a good agreement with experimental results with mean relative deviation of 4.84%. Additionally, the experimental values of the heat transfer coefficient have been compared with the prediction of the most common correlations and it was found that there is a big difference between the experimental and predicted heat transfer coefficients since these correlations do not account for the effect of the bubble dynamics especially the bubble frequency and local gas holdup on the heat transfer coefficient inside the gas-solid fluidized bed.

ACKNOWLEDGEMENTS

The authors would like to thank the Multiphase Reactors Engineering and Applications Laboratory (mReal) for funding and support.

NOMENCLATURE

B_f	bubble frequency (1/s)
Cp_g	heat capacity of fluidizing gas (J/Kg. K)
Cp_s	heat capacity of solid particles (J/Kg. K)
D	inside column diameter (m)
d_p	particles diameter (m)
D_t	tube diameter (m)
H	axial height (m)
h	heat transfer coefficient (W/m^2. K)

k_g	thermal conductivity of the fluidizing gas (W/m. k)
Pr_g	Prandtl number of the fluidizing gas
r	radial position (m)
R	radius of the column (m)
Re_D	Reynolds number based on tube dimeter
Re_p	Reynolds number based on particle diameter
u	superficial gas velocity (m/s)
u_{mf}	minimum fluidized velocity (m/s)

Greek Letters

ε	gas holdup
μ_g	gas viscosity (Pa. s)
ρ_g	gas density (Kg/m^3)
ρ_s	solids density (Kg/m^3)

Subscripts and Superscripts

mf	minimum fluidization
p	particle

REFERENCES

A. Pinto. 1978. Ammonia Production Process, issued 1978.

Abdulmohsin, Rahman S., Balasim A. Abid, and Muthanna H. Al-Dahhan. 2011. "Heat Transfer Study in a Pilot-Plant Scale Bubble Column." *Chemical Engineering Research and Design* 89 (1). Institution of Chemical Engineers: 78–84. doi:10.1016/j.cherd.2010.04.019.

Abdulmohsin, Rahman S., and Muthanna H. Al-Dahhan. 2012. "Impact of Internals on the Heat-Transfer Coefficient in a Bubble Column." *Industrial and Engineering Chemistry Research* 51 (7): 2874–81. doi:10.1021/ie2018096.

Al-Dahhan, Muthanna, Shreekanta Aradhya, and Haidar Taofeeq. 2017. "Prediction of Spout Diameter in Gas-Solid Spouted Beds Using Factorial Design of Experiments Approach with the Aid of Advanced Optical Fibre Probe." *The Canadian Journal of Chemical Engineering* 95 (8): 1463–70. doi:10.1002/cjce.22817.

Andeen, B.R., and L.R. Glicksman. 1976a. "Heat Transfer to Horizontal Tubes in Shallow Fluidized Beds." In *ASME AIChE Heat Transfer Conference*.

Andeen, B.R., and L.R. Glicksman. 1976. 1976b. "HEAT TRANSFER TO HORIZONTAL TUBES IN SHALLOW FLUIDIZED BEDS." *American Society of Mechanical Engineers (Paper)*, no. 76-NaN-67.

Aradhya, Shreekanta, Haidar Taofeeq, and Muthanna Al-Dahhan. 2016. "A New Mechanistic Scale-up Methodology for Gas-Solid Spouted Beds." *Chemical Engineering and Processing: Process Intensification* 110. Elsevier B.V.: 146–59. doi:10.1016/j.cep.2016.10.005.

Aradhya, Shreekanta, Haidar Taofeeq, and Muthanna Al-Dahhan. 2017. "Evaluation of the Dimensionless Groups Based Scale-up of Gas–solid Spouted Beds." *International Journal of Multiphase Flow* 94 (September): 209–18. doi:10.1016/j.ijmultiphaseflow.2017.04.006.

Baeyens, J., and W.R.A. Goossens. 1973. "Some Aspects of Heat Transfer between a Vertical Wall and a Gas Fluidized Bed." *Powder Technology* 8: 91–96.

Bartholomew, Calvin H., and Robert J. Farrauto. 2010. *Fundamentals of Industrial Catalytic Processes: Second Edition*. *Fundamentals of Industrial Catalytic Processes: Second Edition*. doi:10.1002/9780471730071.

Borodulya, V.A., Yu.S. Teplitsky, I.I. Markevich, A.F. Hassan, and T.P. Yeryomenko. 1991. "Heat Transfer between a Surface and a Fluidized Bed: Consideration of Pressure and Temperature Effects." *International Journal of Heat and Mass Transfer* 34 (1): 47–53. doi:10.1016/0017-9310(91)90171-A.

Borodulya, V. A., V.L. Ganzha, A.I. Podberezsky, S. N. Upadhyay, and S. C. Saxena. 1984. “Heat Transfer Berween Fluidized Bed of Large Particles and Horizontal Tube Bundles at High Pressures.” *International Journal of Heat and Mass Transfer* 27 (8): 1219–25.

Doherty, J. A., R. S. Verma, S. Shrivastava, and S. C. Saxena. 1986. “Heat Transfer from Immersed Horizontal Tubes of Different Diameter in a Gas-Fluidized Bed.” *Energy* 11 (8): 773–83. doi:10.1016/0360-5442(86)90016-2.

Efhaima, Abdelsalam. 2016. “Scale-up Investigation and Hydrodynamics Study of Gas-Solid Fluidized Bed Reactor Using Advanced Non- Invasive Measurement Techniques.” PhD Thesis, Missouri University of Science and Technology.

Fox, W.B., N.S. Grewal, and D.a. Moen. 1999. “Wall-to-Bed Heat Transfer in Circulating Fluidized Beds.” *International Communications in Heat and Mass Transfer* 26 (4): 499–508. doi:10.1016/S0735-1933(99)00035-4.

Glass, D. H., and D. Harrison. 1964. “Flow Patterns near a Solid Obstacle in a Fluidized Bed.” *Chemical Engineering Science* 16 (12): 1001–2. doi:10.1016/0009-2509(64)85112-5.

Grace, J. R., and D. Harrison. 1968. “The Effect of Internal Baffles in Fluidized Beds: A Guide to Design.” In *Inst. Chem. Eng. Symp. Ser.*

HU, Gouxin, Huier Cheng, and Haojie Fan. 1998. “Particle-Fluid Transfer in a Circulation Fluidized Bed.” In *Energy and Enviroment: Proceedings of the International Conference on Energy*, 553–59.

Kagumba, Moses. 2013. “Heat Transfer and Bubble Dynamics in Bubble and Slurry.” PhD Thesis, Missouri University of Science and Technology.

Kim, Sang Done Sung Won Sang Done Sung Won, Jung Yeul Ahn, Sang Done Sung Won Sang Done Sung Won Kim, and Dong Hyun Lee. 2003. “Heat Transfer and Bubble Characteristics in a Fluidized Bed with Immersed Horizontal Tube Bundle.” *International Journal of Heat and Mass Transfer* 46 (3): 399–409. doi:10.1016/S0017-9310(02)00296-X.

Kim, Sung Won, Jung Yeul Ahn, Sang Done Kim, and Dong Hyun Lee. 2003. “Heat Transfer and Bubble Characteristics in a Fluidized Bed with Immersed Horizontal Tube Bundle.” *International Journal of Heat and Mass Transfer* 46 (3): 399–409. doi:10.1016/S0017-9310(02)00296-X.

Krishna, R., J. Ellenberger, and D. E. Hennephof. 1993. “Analogous Description of the Hydrodynamics of Gas-Solid Fluidized Beds and Bubble Columns.” *The Chemical Engineering Journal and The Biochemical Engineering Journal* 53 (1): 89–101. doi:10.1016/0923-0467(93)80010-T.

Law, Chung Lim, Siti Masrinda Tasirin, Wan Ramli Wan Daud, and Derek Geldart. 2003. "Effect of Vertical Baffles on Particle Mixing and Drying in Fluidized Beds of Group D Particles." *China Particuology* 1 (3): 115–18. doi:10.1016/S1672-2515(07)60121-3.

Lechner, Stefan, Matthias Merzsch, and Hans Joachim Krautz. 2014. "Heat-Transfer from Horizontal Tube Bundles into Fluidized Beds with Geldart A Lignite Particles." *Powder Technology* 253. Elsevier B.V.: 14–21. doi:10.1016/j.powtec.2013.10.041.

Leming, Cheng, Mingjiang Ni, Zhongyang Luo, and P. Basu. 1995. "Heat Transfer in Circulating Fluidized Bed and Its Modeling." *Fluidized Bed Combustion* 1: 487–97.

Leva, M., and M. A Grumme. 1952. "Correlation of Solids Turnovers in Fluidized Systems." In *Chem Eng Progr 48*, 307–313.

Li, Hong Shun, Wen Di Huang, and Ren Zhang Qian. 1995. "An Instrumented Cylinder for Simultaneous Measurements of Instantaneous Local Heat Transfer Coefficients and Hydrodynamics in High-Temperature Fluidized Beds." *Powder Technology* 83 (3): 281–85. doi:10.1016/0032-5910(94)02968-T.

Martin, Holger. 1984. "Heat Transfer between Gas Fluidized Beds of Solid Particles and the Surfaces of Immersed Heat Exchanger Elements, Part I." *Chemical Engineering and Processing: Process Intensification* 18 (3): 157–69. doi:10.1016/0255-2701(84)87003-8.

Maurer, Simon, Evert C Wagner, Tilman J Schildhauer, J. Ruud van Ommen, Serge M A Biollaz, and Robert F Mudde. 2015. "X-Ray Measurements of Bubble Hold-up in Fluidized Beds with and without Vertical Internals." *International Journal of Multiphase Flow* 74. Elsevier Ltd: 118–24. doi:10.1016/j.ijmultiphaseflow.2015.03.009.

Maurer, Simon, Evert C Wagner, J. Ruud van Ommen, Tilman J Schildhauer, Sinan L Teske, Serge M A Biollaz, Alexander Wokaun, and Robert F Mudde. 2015. "Influence of Vertical Internals on a Bubbling Fluidized Bed Characterized by X-Ray Tomography." *International Journal of Multiphase Flow* 75. Elsevier Ltd: 237–49. doi:10.1016/j.ijmultiphaseflow.2015.06.001.

Mickley, H S, and D F Fairbanks. 1955. "Mechanism of Heat Transfer to Fluidized Beds." *AIChE Journal* 1 (3): 374–84. doi:10.1002/aic.690010317.

Nedeltchev, Stoyan, Shreekanta Aradhya, Faraj Zaid, and Muthanna Al-Dahhan. 2012. "Flow Regime Identification in Three Multiphase Reactors Based on Kolmogorov Entropies Derived from Gauge Pressure Fluctuations." *Journal of Chemical Engineering of Japan* 45 (9): 757–64. doi:10.1252/jcej.12we075.

Pisters, K., and A. Prakash. 2011. “Investigations of Axial and Radial Variations of Heat Transfer Coefficient in Bubbling Fluidized Bed with Fast Response Probe.” *Powder Technology* 207 (1–3). Elsevier B.V.: 224–31. doi:10.1016/j.powtec.2010.11.003.

Ramamoorthy, S., and N. Subramanian. 1981. “Axial Solids Mixing and Bubble Characteristics in Gas-Fluidized Beds with Vertical Internals.” *Chemical Engineering Journal* 22 (3): 237–42.

Rasouli, S., M. R. Golriz, and A. A. Hamidi. 2005. “Effect of Annular Fins on Heat Transfer of a Horizontal Immersed Tube in Bubbling Fluidized Beds.” *Powder Technology* 154 (1): 9–13. doi:10.1016/j.powtec.2005.02.008.

Rüdisüli, Martin, Tilman J. Schildhauer, Serge M. A. Biollaz, and J. Ruud Van Ommen. 2012a. “Radial Bubble Distribution in a Fluidized Bed with Vertical Tubes.” *Industrial and Engineering Chemistry Research* 51 (42): 13815–24. doi:10.1021/ie3004418.

Rüdisüli, Martin, Tilman J Schildhauer, Serge M A Biollaz, and J. Ruud Van Ommen. 2012b. “Bubble Characterization in a Fluidized Bed with Vertical Tubes.” *Industrial and Engineering Chemistry Research* 51 (12): 4748–58. doi:10.1021/ie2022306.

Schweitzer, J. M., J. Bayle, and T. Gauthier. 2001. “Local Gas Hold-up Measurements in Fluidized Bed and Slurry Bubble Column.” *Chemical Engineering Science* 56 (3): 1103–10. doi:10.1016/S0009-2509(00)00327-4.

Seo, Myung Won, Young Ho Suh, Sang Done Kim, Sunwon Park, Dong Hyun Lee, and Byung Ho Song§. 2011. “Cluster and Bed-to-Wall Heat Transfer Characteristics in a Dual Circulating Fluidized Bed.” *Industrial & Engineering Chemistry Research* 51 (6): 2048–61. doi:10.1007/BF02706030.

Stefanova, A., H. T. Bi, C. J. Lim, and J. R. Grace. 2007. “Heat Transfer from Immersed Vertical Tube in a Fluidized Bed of Group A Particles near the Transition to the Turbulent Fluidization Flow Regime.” *International Journal of Heat and Mass Transfer* 51 (7–8): 2020–28. doi:10.1016/j.ijheatmasstransfer.2007.06.005.

Stefanova, A., H. T. Bi, J. C. Lim, and J. R. Grace. 2011. “Local Hydrodynamics and Heat Transfer in Fluidized Beds of Different Diameter.” *Powder Technology* 212 (1): 57–63. doi:10.1016/j.powtec.2011.04.026.

Stefanova, A., John R. Grace, C. Jim Lim, J. Sanderson, Xiaotao T. Bi, and K.S. Lim. 2007. “New Horizons in Fluidization Scale-Up Effect on Heat Transfer in a Fluidized Bed Near the Onset of Turbulent Fluidization.” In *The 12th International Conference on Fluidization*, 272–80.

Sundaresan, R, and AK Kolar. 2002. “Core Heat Transfer Studies in a Circulating Fluidized Bed.” *Powder Technology* 124: 138–51. http://www.sciencedirect.com/science/article/pii/S0032591001004831.

Sunderesan, Suresh R., and Nigel N. Clark. 1995. “Local Heat Transfer Coefficients on the Circumference of a Tube in a Gas Fluidized Bed.” *Int. J. Multiphase Flow* 21 (6): 1003–24.

Taofeeq, Haidar, Shreekanta Aradhya, and Muthanna Al-Dahhan. n.d. “Simple Calibration Methodologies for Simultaneous Measurements and Investigations of Solids Holdup and Particles Velocity in Gas-Solid Fluidization Systems.”

Tijm, P. J A, F. J. Waller, and D. M. Brown. 2001. “Methanol Technology Developments for the New Millennium.” *Applied Catalysis A: General* 221 (1–2): 275–82. doi:10.1016/S0926-860X(01)00805-5.

Vreedenberg, H. 1958. “Heat Transfer between a Fluidized Bed and a Horizontal Tube.” *Chemical Engineering Science* 9 (1): 52–60. doi:10.1016/0009-2509(58)87007-4.

White, T. R., A. Mathur, and S. C. Saxena. 1986. “Effect of Vertical Boiler Tube Diameter on Heat Transfer Coefficient in Gas-Fluidized Beds.” *The Chemical Engineering Journal* 32 (1): 1–13. doi:10.1016/0300-9467(86)85001-8.

Wiman, J., and A. E. Almstedt. 1997. “Hydrodynamics, Erosion and Heat Transfer in a Pressurized Fluidized Bed: Influence of Pressure, Fluidization Velocity, Particle Size and Tube Bank Geometry.” *Chemical Engineering Science* 52 (16): 2677–95. doi:10.1016/S0009-2509(97)00096-1.

Wu, R.L., C.J. Lim, J.R. Grace, and C.M.H. Brereton. 1991. “Instantaneous Local Heat Transfer and Hydrodynamics in a Circulating Fluidized Bed.” *International Journal of Heat and Mass Transfer* 34 (8): 2019–27. doi:10.1016/0017-9310(91)90213-X.

Yao, Xiuying, Yongmin Zhang, Chunxi Lu, and Xiao Han. 2015. “Systematic Study on Heat Transfer and Surface Hydrodynamics of a Vertical Heat Tube in a Fluidized Bed of FCC Particles.” *AICHE* 61: 68–83. doi:10.1002/aic.

Zhang, H., P. M. Johnston, J. X. Zhu, H. I. De Lasa, and M. A. Bergougnou. 1998. “A Novel Calibration Procedure for a Fiber Optic Solids Concentration Probe.” *Powder Technology* 100 (2–3): 260–72. doi:10.1016/S0032-5910(98)00147-8.

III. FLOW REGIMES IN GAS-SOLID FLUIDIZED BED WITH VERTICAL INTERNALS

Haidar Taofeeq[1] and Muthanna Al-Dahhan[2*]

Multiphase Reactors Engineering and Applications Laboratory (mReal)

Department of Chemical & Biochemical Engineering, Missouri University of Science & Technology, Rolla, MO-65409 USA

ABSTRACT

In this work, the impact of the vertical internals on the flow regimes and their transition velocities has been studied in a 0.14 m inside diameter gas-solid fluidized bed. The identification of the flow regimes was accomplished statistically (standard deviation) and chaotically (Kolmogorov entropy) analyzing the pressure drop fluctuations. Circular configurations of vertical tubes with two different sizes (0.0254 and 0.0127 m diameter), two kinds of solid particles of Geldart B type (glass beads and aluminum oxide), and a wide range of superficial gas velocities (0.15-1.2 m/s) have been implemented in this study. Generally, it was demonstrated that the vertical internals have a significant effect on the flow regimes, transition velocities, and transition velocity ranges of each individual flow regime. However, such effect is a function of the physical properties of the used solid particles in which the turbulent transition velocity (U_c) decreased in the case of glass beads and increased in the case of aluminum oxide for both of the configuration designs of vertical internals used in the present work. In addition, the 0.0254 m vertical internals type has been shown to be more efficient either in minimizing the turbulent transition velocity (U_c) and superficial gas velocity within the range of slugging flow regime and increase the

range of the superficial gas velocity within the range of bubbling flow regime or in reducing the pressure drop and pressure fluctuations inside the bed.

Keywords: Vertical internals, flow regimes, transition velocities, pressure drop fluctuation, gas-solid fluidized bed

* Corresponding Author: aldahhanm@mst.edu

1. INTRODUCTION

The gas-solid fluidization beds with different design and operating conditions have been applied in many industrial processes such as fluid catalytic cracking, solid particles drying, waste combustion, and biomass gasification. The use of these types of beds in several manufacturing applications was due to their many advantageous and efficient properties. They were characterized as having excellent heat and mass transfer rates, good mixing between gas and solid particles, and uniform temperature distribution. But even though the use of these beds has many benefits in commercial processes, their hydrodynamic behavior and the gas-solid flow circulation patterns are still very complicated due to the perplexing contact among solid particles, gas phase and solid particles, and between each solids particle with their surrounding fluidizing medium and the wall of the column or the wall of the immersed surfaces. The effectiveness of the gas-solid fluidization systems is highly dependent on the flow regime, or the way that the gas and solid particles contact together inside the bed. It has been reported by many researchers in the literature that the main flow regimes that exist in different gas-solid fluidization systems are bubbling fluidization, slugging fluidization, turbulent fluidization, fast fluidization, and pneumatic conveying (Arnaldos and Casal 1996; Zijerveld et al. 1998; Bai, Issangya, and Grace 1999). It has been noted by Nedeltchev, Ahmed, and Al-Dahhan (2012) that the two most common flow regimes used in industrial applications in fixed gas-solid fluidizing beds are the bubbling and turbulent flow regimes. The flow regimes and their transition velocities can be affected by different factors, which can be classified into three main types (Yerushalmi et al. 1978; Lim, Zhu, and Grace 1995; Bai et al. 1996;

Zijerveld et al. 1998; Trnka et al. 2000; Andreux et al. 2005; Nedeltchev, Ahmed, and Al-Dahhan 2012):

1- Operating conditions: superficial gas velocity, pressure, temperature, and solid circulation rate (as in the case of circulating fluidized beds).
2- Physical properties: solid particles size, shape, density, and solid particles sphericity. Geldart type, gas density and viscosity, and solids size distribution.
3- Design parameters: static bed height, column geometry and size, gas distributor design, and the existence of different types of immersed surfaces.

In addition to the factors mentioned above, Andreux et al. (2005) indicated that the measured transition velocity from bubbling to the turbulent flow regime is strongly dependent on the type of measurement techniques. There have been several studies in the literature reporting the use of different kinds of measurement techniques to identify the flow regimes in gas-solid fluidization systems with and without different configurations of immersed surfaces, such as high speed camera (Yerushalmi et al. 1978; Johnsson et al. 2000), optical fiber probe (Bai, Issangya, and Grace 1999; Andreux et al. 2005), electrical capacitance tomography (Makkawi and Wright 2002; Qiu et al. 2014), gamma-ray densitometry (Nedeltchev, Ahmed, and Al-Dahhan 2012; Nedeltchev 2015), fast X-ray tomography (Saayman et al. 2013), differential pressure measurement techniques including manometers and transducers (Yerushalmi and Cankurt 1979; Jin et al. 1986; Olsson, Wiman, and Almstedt 1995; Smolders and Baeyens 2001; Shaul, Rabinovich, and Kalman 2012), absolute pressure transducers (Zijerveld et al. 1998; Bai, Issangya, and Grace 1999; Nedeltchev et al. 2012), and probe-absolute pressure transducer either in the vertical way (Trnka et al. 2000) or in the horizontal way (Johnsson et al. 2000). Table 1.1 lists some the

sources of experimental data for the flow regime identification in gas–solid fluidization systems with and without immersed surfaces.

Among all the above measurement techniques, is the use of pressure fluctuations measurement devices which to have many advantages over other techniques and are considered the most common techniques that have been used in gas–solid fluidized beds. The pressure transducers mounted at the wall are simple and easy to implement even under severe conditions, and they are a relatively inexpensive, durable, and noninvasive technique at the wall to avoid any disturbance that can happen to the gas–solid flow patterns (Van Ommen et al. 2011). During operation, some hydrodynamic behaviors can be indicated from the measurements of the pressure fluctuations within the bed (Trnka et al. 2000).

The flow regime in the gas–solid fluidized beds has been experimentally investigated by many researchers using several kinds of measurement techniques, and the collected experimental data has been analyzed using different types of data analysis methods (Tayebi et al. 1999; Trnka et al. 2000; Johnsson et al. 2000; Van Ommen et al. 2011). These experimental investigations were conducted in gas-solid fluidized beds without immersed surfaces. These types of studies and data analyses can be generally categorized into:

1- Flow regime mapping: The map represents the relationship between the Reynolds number and Archimedes number of the system (Yerushalmi et al. 1978; Rhodes 1989; Bi and Grace 1995; Smolders and Baeyens 2001; Shaul, Rabinovich, and Kalman 2012). Recently, Kuwagi, Kogane, Hirano, Bin Alias, and Takami (2014) used numerical simulation to predict a three-dimensional flow regime map that relates the Reynolds

number and Archimedes number together with density ratio ρ^* (ratio between solid particles density and gas density).

2- Time domain analysis (or statistical analysis of the time series): this method includes mean or average, standard deviation, skewness, flatness, auto-correlation function, intermittency indices, average absolute deviation, and probability distribution function (Zijerveld et al. 1998; Bai, Issangya, and Grace 1999; Johnsson et al. 2000; Van Ommen et al. 2011).

3- Frequency domain analysis (or spectral analysis of the time series): this method includes power spectrum, power spectral density distribution, and wavelets (Olsson, Wiman, and Almstedt 1995; Andreux et al. 2005; Qiu et al. 2014).

4- State space analysis (or chaos analysis of time series): this methods includes Kolmogorov entropy (KE), Hurst exponent, correlation dimension and Lyapunov exponent (Zijerveld et al. 1998; Bai, Issangya, and Grace 1999; Van Ommen et al. 2011). Recently, new methods of state space analysis have been implemented using maximum information entropy and entropy that represent the extent of order and disorder to identify the flow regimes and their transition velocities in conventional fluidized bed using Gamma-ray densitometry (Nedeltchev, Ahmed, and Al-Dahhan 2012; Nedeltchev 2015).

Immersed surfaces with different sizes, configurations, and orientations have been employed inside the gas solid fluidized beds for many purposes. It has been demonstrated by many experimental works (Volk, Johnson, and Stotler 1962; Grace and Harrison 1968; Olowson 1994; Mathew, Begum, and Anantharaman 2014; Rüdisüli et al. 2012b) that these immersed surfaces have the ability to improve the fluidization quality by reducing the

Table 1.1: Some of the sources of experimental data for flow regime identification in gas–solid fluidization systems with and without immersed surfaces (internals)

Year	Author	Technique used	Analysis method	Solid Material	Particle Diameter (d_p)	Particle Density (ρ_p)	Internals used	Geldart type	Measuring System
1978	Yerushalmi et al.	High-speed photography & pressure drop measurements	Flow regime map	-FCC -Dicalite 4200	49 µm 33 µm	1070 kg/m^3 1670 kg/m^3	-	A A	Gas-solid riser of 15.2 cm ID
1979	Yerushalmi and Cankurt	Dynamic and pressure drop measurements	Flow regime map & pressure fluctuation peak	- Dicalite 4200 -FCC -HFZ-20 -Hydrated alumina -Sand -Glass	33 µm 49 µm 49 µm 103 µm 268 µm 157 µm	1670 kg/m^3 1070 kg/m^3 1450 kg/m^3 2460 kg/m^3 2650 kg/m^3 2420 kg/m^3	-	A A A B B B	Gas-solid riser of 15.2 cm ID
1986	Jin et al.	Inductive transducer	Mean amplitude and nonuniformity coefficient of pressure fluctuations signal	-Silica gel -Resin -FCC	165 µm 476 µm 1057 µm 566 µm 52.7 µm 65.3 µm	711 kg/m^3 834 kg/m^3 844 kg/m^3 1330 kg/m^3 1667 kg/m^3 1172 kg/m^3	Vertical tubes	A A B B A A	Fluidized bed with a cross-section of 0.28 * 0.28 m
1989	Rhodes	-	Flow regime map	FCC	50 µm	1020 kg/m^3	-	A	Gas-solid riser of 15.2 cm ID

Table 1.1: Some of the sources of experimental data for flow regime identification in gas–solid fluidization systems with and without immersed surfaces (internals) (cont.)

1995	Bi and Grace	-	Flow regime map	-	-	-	-	A	Different fluidized-bed systems
1995	Olsson et al.	Differential pressure transducer	Power spectral density distribution	Silica sand	700 μm	2600 kg/m^3	Horizontal tubes of 20 mm diameter and three different configurations of (14.6%, 12.5% and 24% cross sectional area)	B/D	Pressurized fluidized bed with a cross-section of 0.2 * 0.3 m
1996	Bai et al.	Differential pressure transducer	Statistical analysis (Standard deviation)	FCC Silica sand	51.9 μm 166 μm	1623 kg/m^3 2220 kg/m^3	-	A B	Riser of 97 mm ID
1998	Zijerveld et al.	Absolute pressure transducer	-Statistical analysis (average absolute deviation) -Spectral analysis (power spectral density) -Chaos analysis (Kolmogorov entropy)	Silica sand	300 μm	2600 kg/m^3	-	B	Four circulating fluidized beds of different size and design

Table 1.1: Some of the sources of experimental data for flow regime identification in gas–solid fluidization systems with and without immersed surfaces (internals) (cont.)

1999	Bai et al.	Optical fiber probe, differential and absolute pressure transducers	-Statistical analysis (average, standard deviation, intermittency indices, probability distribution, amplitude spectra and cycle frequencies) -Chaos analysis (Hurst exponent, correlation dimension and Kolmogorov entropy)	FCC particles	70 μm	1600 kg/m^3	-	A	High-density circulating fluidized bed of 76.2 mm ID
2000	Trnka et al.	Pressure probe (vertical probe-pressure transducer)	Spectral analysis (Fast discrete Fourier transform to obtain amplitude spectrum)	-Glass beads -Bentonite -Glass beads -Bentonite -Ceramsite -Ceramsite	(0.1-0.12) (0.4-0.6) (0.6-0.9) (0.8-1.2) (0.4-2.4) (1.8-3.6) mm	- - - - - 1570	-	A A/B B B/D B/D D	Cylindrical glass column of 8 cm ID
2000	Johansson et al.	-High speed camera -Differential pressure transducer -probe-single ended pressure transducer	-Time domain analysis (standard deviation, skewness, flatness and auto-correlation function) -Frequency domain analysis (power spectrum) -State-space analysis (correlation dimension and Kolmogorov entropy)	Silica sand	310 μm	2600 kg/m^3	-	B	Circulating fluidized bed with a cross-section of 0.12 * 0.7 m

Table 1.1: Some of the sources of experimental data for flow regime identification in gas–solid fluidization systems with and without immersed surfaces (internals) (cont.)

2001	Smolders and Baeyens	Water manometer and a solid-state pressure transducer	Flow regime map	-Sand -FCC particles	90 μm 70 μm	2600 kg/m^3 2700 kg/m^3	-	- -	Circulating fluidized bed with 100 mm ID
2002	Makkawi and Wright	Electrical capacitance tomography and pressure drop measurements	-Average and standard deviation analysis - Amplitude analysis - Frequency analysis - Power spectra analysis	glass ballotini	530 μm	2600 kg/m^3	-	B	Conventional fluidized bed with 15 cm ID
2005	Andreux et al.	Pressure drop probes and bi-optical fiber probes	-Statistical analysis (standard deviation, time averaged values and probability density function distributions) -Dominant frequencies of the local voidage fluctuations	Sand particles	250 μm	2585 ± 35 kg/m^3	-	B	Fluidized bed with 152 mm ID

Table 1.1: Some of the sources of experimental data for flow regime identification in gas–solid fluidization systems with and without immersed surfaces (internals) (cont.)

2011	Van Ommen et al.	Probe-single ended pressure transducer	-Time domain methods (standard deviation, probability distribution function, autoregressive models and rescaled range analysis) -Frequency domain methods (power spectrum and wavelets) -State-space methods (correlation dimension, Kolmogorov entropy and Lyapunov exponents)	Silica sand	310 µm	2600 kg/m^3	-	B	Circulating fluidized bed with a cross-section of 0.12 * 0.7 m
2012a	Nedeltchev et al.	Gamma-Ray Densitometry	Maximum information entropy and Kolmogorov entropy	polyethylene	675 µm	755 kg/m^3	-	A	Gas-solid fluidized bed of 0.438 m ID
2012b	Nedeltchev et al.	Single-ended pressure transducer	Kolmogorov entropy	Glass beads	(150-210) µm	2500 kg/m^3	-	A	Gas-solid fluidized bed of 0.14 m in ID

Table 1.1: Some of the sources of experimental data for flow regime identification in gas–solid fluidization systems with and without immersed surfaces (internals) (cont.)

2012	Shaul et al.	Pressure drop meter	Flow regime diagram	-Tubular alumina (A1) -Glass beads (A2) -Glass Beads (A3) -Tubular alumina (B1) -Glass beads (B2) -Sand (B3) -Tubular alumina (B4) -Glass Beads (D1) -Steel beads (D2) -Zirconium (D3) -Zirconium (D4)	36 μm 41.6 μm 69.5 μm 109 μm 250 μm 350 μm 578 μm 855 μm 1000 μm 1100 μm 1500 μm	3600 kg/m^3 2500 kg/m^3 2500 kg/m^3 3600 kg/m^3 2500 kg/m^3 2495 kg/m^3 3600 kg/m^3 2500 kg/m^3 7500 kg/m^3 5983 kg/m^3 5983 kg/m^3	-	A A A B B B B D D D D	Fluidized beds of four different Column diameters (15 mm, 42 mm, 50 mm and 80 mm)
2013	Saay man et al.	Fast X-ray tomography and absolute-pressure sensor	Standard deviation of pressure signals and mean of the cross-sectional solids fraction and void rise velocity	Sand	101 μm	2530 kg/m^3	-	B	Gas-solid fluidized bed of 0.14 m in ID

Table 1.1: Some of the sources of experimental data for flow regime identification in gas–solid fluidization systems with and without immersed surfaces (internals) (cont.)

2014	Qiu et al.	Electrical capacitance tomography and differential pressure transducer	standard deviation, autocorrelation function and power spectrum of solids volume fraction and pressure fluctuations	Sand	469 μm	1608 kg/m^3	-	B	Gas-solid circulating fluidized bed of different diameter (10, 12 and 15 cm)
2015	Nedeltchev	Nuclear gauge densitometry	Entropy and information entropy	polyethylene	675 μm	755 kg/m^3	-	A	Gas-solid fluidized bed of 0.438 m ID

bubble size and the coalescence between them, minimizing the solids circulation patterns, reducing the pressure drop through the bed, decreasing the channelling and slugging flow regime (which exist in Geldart B particles and small size vessels), improving the heat and mass transfer rates, increasing the chemical reaction conversion by increasing the residence time of the gas inside the bed. Moreover, the scale-up process from small to large size bed would also affected with implementing of vertical immersed internals (Volk, Johnson, and Stotler 1962). Additionally, it was found that the vertical internals can reduce the horizontal tube erosion by 50% comparing with that of vertical internals as well as the vertical internals can reduce the pressure drop, bed expansion and fluctuation, and minimize the coalescence between the bubbles in their vertical pathways inside the bed (Rüdisüli et al. 2012b). Jin et al. (1986) studied the effect of vertical internals on the transition velocity (U_c). They reported that, the transition velocity in beds with vertical internals from bubbling to turbulent flow regime occurred at lower transition U_c. The experimental data of Jin et al. (1986) was predicted as follows:

$$\frac{U_c}{\sqrt{gd_p}} = \left[\frac{k_{DF}}{d_p} * \frac{(\rho_p - \rho_f)}{\rho_f}\right]^n \quad (1)$$

where n=0.27 and K_{DF} is a parameter called performance diameter which has length dimension. The K_{DF} is found to characterize the geometric structure of the beds and its value is obtained as follows:

K_{DF} =0.00367 for free bed

K_{DF} =0.00232 for bed with vertical tubes

K_{DF} =0.00342 for bed with pagoda types internals baffles.

Olsson et al. (1995) examined the effect of different configurations of horizontal tube banks on the flow regime inside the pressurized fluidized bed. They used horizontal

tubes of 20 mm in diameter and three different configurations in a rectangular bed of 0.2 m× 0.3 m in which the percentage of cross-sectional area of the three configurations of horizontal tubes are (14.6%, 12.5% and 24%). They found that the horizontal tube banks reduced the bubbles size by splitting them as well as the transition from bubbling to turbulent flow regime occurred at lower pressure and superficial gas velocity compared to the case without tube bundles.

Because of a significant number of preferences from claiming the use of vertical internals inside the fluidized beds specified above, the hydrodynamic research in understanding the flow regime behavior inside distinctive types of fluidized bed reactors with vertical internals needs to expand. Furthermore, the unpredictability of the fluidization framework with vertical internals has been acknowledged as a huge challenge and needs more comprehension. The flow structures in various hydrodynamic regimes and their impact by vertical internals are also still not well understood. Furthermore, the experimental data available in the literature on studying the effect of immersed vertical internals on the flow regimes and their transition velocities inside the fluidized-beds is limited, particularly for Geldart B particles and vertical tube types.

In the present work, the effect of different configurations and sizes of vertical immersed tubes on the flow regimes and their transition velocities in the system of gas–solid fluidized bed has been examined by experimental studies in a gas–solid fluidized bed using a differential pressure transducer technique. The time series of the pressure drop fluctuation signals have been analyzed using two types of data analysis, time domain method (standard deviation) and state space method (Kolmogorov entropy).

2. EXPERIMENTAL SETUP

The experimental setup consisted of a fluidized bed column with 0.14 m inside diameter and 1.84 m height. The column was constructed from Plexiglas, and the plenum was manufactured from rigid aluminum metal. The column and the plenum were based on the top of a stainless-steel base. The industrial scale compressors were used for supplying compressed air to the column at pressures up to 1.38 MPa. The Omega type flow meters were used to control the flow rate of the inlet gas to the plenum section. A schematic diagram of the fluidized bed column with vertical internals is illustrated in Figure 2.1.a. The gas phase was introduced through a sparger tube in the plenum and then through a distributor plate placed between the fluidized bed column and the plenum section. The gas distributor plate was made of a porous polyethylene sheet and had a pore size of 15–40 μm. The sparger tube was plugged at one end and had fourteen holes, all facing downward with respect to the fluidized bed column (opposite to the gas flow direction to make the gas distribution more homogenous). The column was electrically grounded to minimize electrostatic effects. A rigid metallic structure was used to support the column and eliminate the mechanical vibrations as shown in Figure 2.1.b.

In the current study, two different diameter sizes (0.0254 and 0.0127 m) of circular configurations of internals have been used. The schematic and configuration arrangement diagrams of the two types of the vertical internals are shown in Figure 2.2 and 2.3. The circular arrangement features uniformly distributed the internals over the cross-sectional area of the fluidized bed column. These circular configurations of the internals were performed to maintain equal spacing between the internals and the wall of the fluidized bed column. The internal configurations and their supports are shown in Figure 2.4. The

configuration of the 0.0127 m internals consists of 30 Plexiglas vertical internals with 1.84 m height and this configuration represents the dense vertical internals used in gas-solid

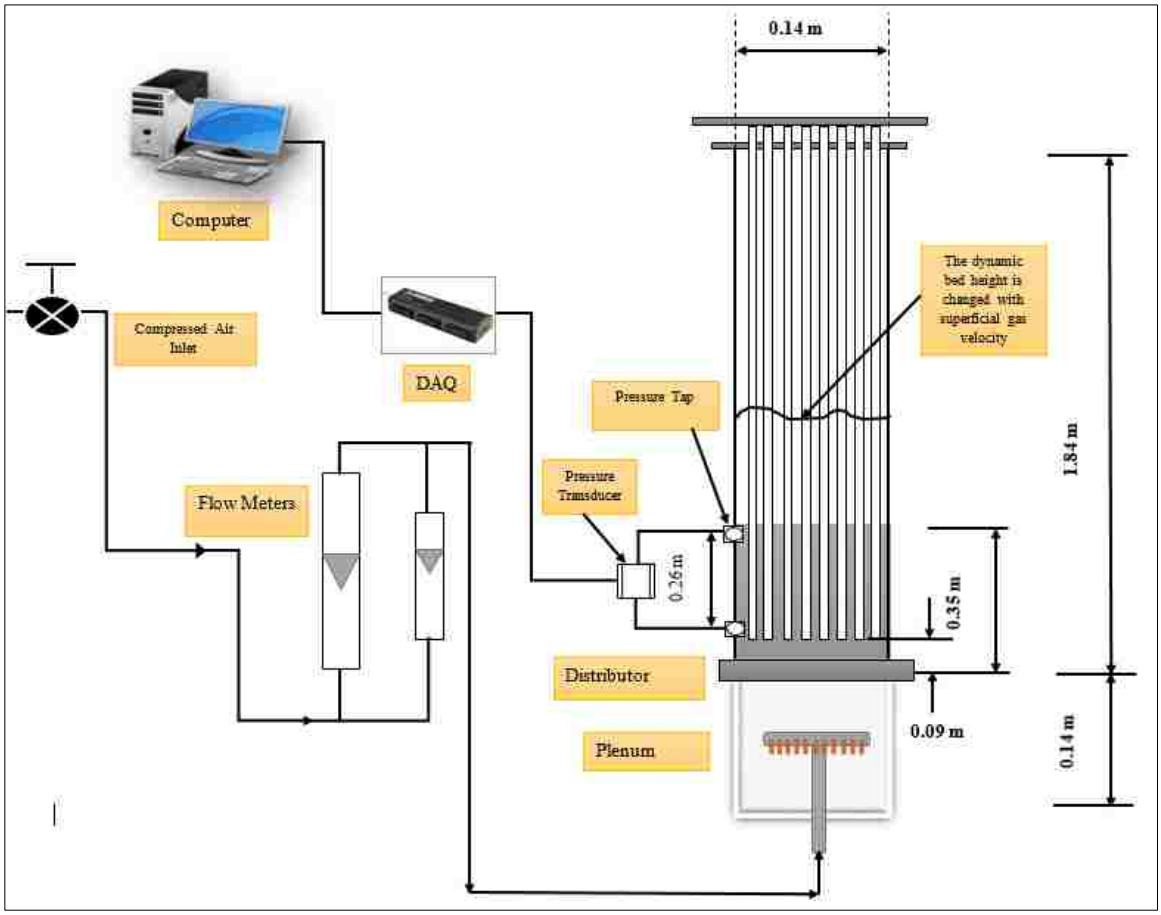

Figure 2.1.a. Schematic diagram of the experimental setup (flow meters, fluidized bed column with vertical internals and differential pressure transducer accessories).

fluidized bed, while the arrangement of the 0.0254 m internals which represents less dense vertical internals, consists of 8 Plexiglas vertical internals. Both of the configurations covered 25% of the column cross-sectional area. These intense internals have been used in high exothermic reaction processes where intense heat exchanging surfaces are needed to control the reaction temperature in high temperature industrial processes such as Fisher-

Figure 2.1.b. Photo for the fluidized-bed column with internals.

Tropsch, Ammonia synthesis, and methanol synthesis (Bartholomew and Farrauto 2010; A. Pinto 1978; Tijm, Waller, and Brown 2001). The internals were secured in the column by using four supports (honeycombs), which also minimized internal vibration during the experiments. The distance between the distributor plate and the lower end of the vertical internals was 0.09 m. The differential pressure transducer ends were connected to the

pressure taps that mounted on the column wall, which were located at 0.26 m height differences (the lower tap and the upper tap were at the height of 0.045 m and 0.305 m above the distributor). The locations of the lower and upper taps have been selected to cover the zone before the lower end of the vertical internals (0.09 m above the distributor plate) and the zone before the freeboard of the column.

It was found experimentally that the minimum fluidization velocities with and without internals were the same for all cases (different solid particles used and two types of internals), as listed in Table 2.1. Therefore, the experiments were conducted at superficial gas velocities ranging from 0.15 to 1.2 m/s instead of the relative gas velocity (U_0/U_{mf}), which were permanently used in order to compare the experiment results between the column with and without internals. Consequently, the superficial gas velocity of the column without internals was calculated based on the cross-sectional area of the column when it was not occupied with internals. For the cases with internals, the superficial gas velocity was calculated based on the free cross-sectional area available, for the gas to flow which represented 75% of the cross-sectional area of the column.

The solid particles used in this work were glass beads of 365 μm average particle size and 2500 Kg/m^3 in density and aluminum oxide of 255 μm average particle size and 3900 Kg/m^3 in density. The static bed height for both types of solid particles were 0.35 m. The minimum fluidization velocities for the case of with and without vertical internals and for the two types of solids particles were estimated using the pressure drop measurements versus the superficial gas velocity since the differential pressure transducer used in this work measures the pressure drop at different operating conditions, in which the pressure drop has been increased with increasing the superficial gas velocity until it reaches the

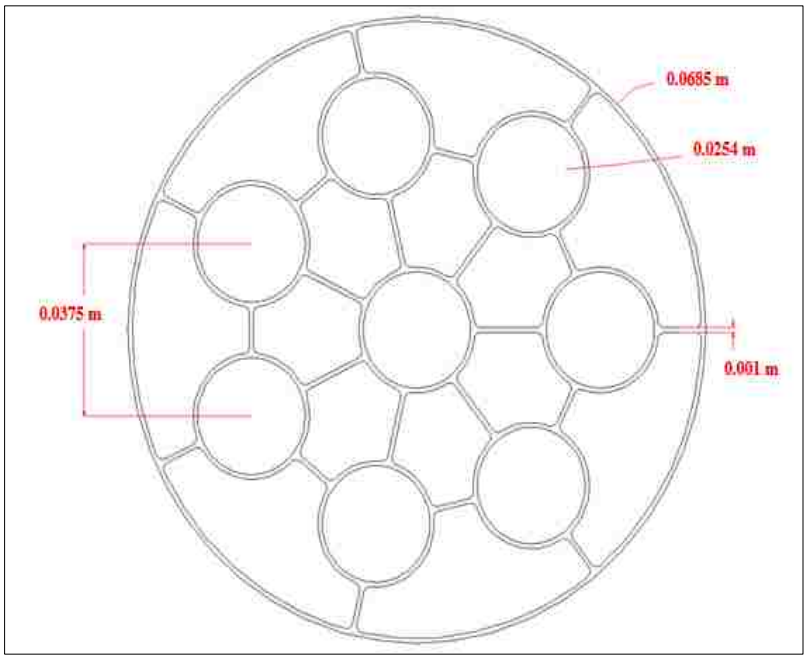

(a)

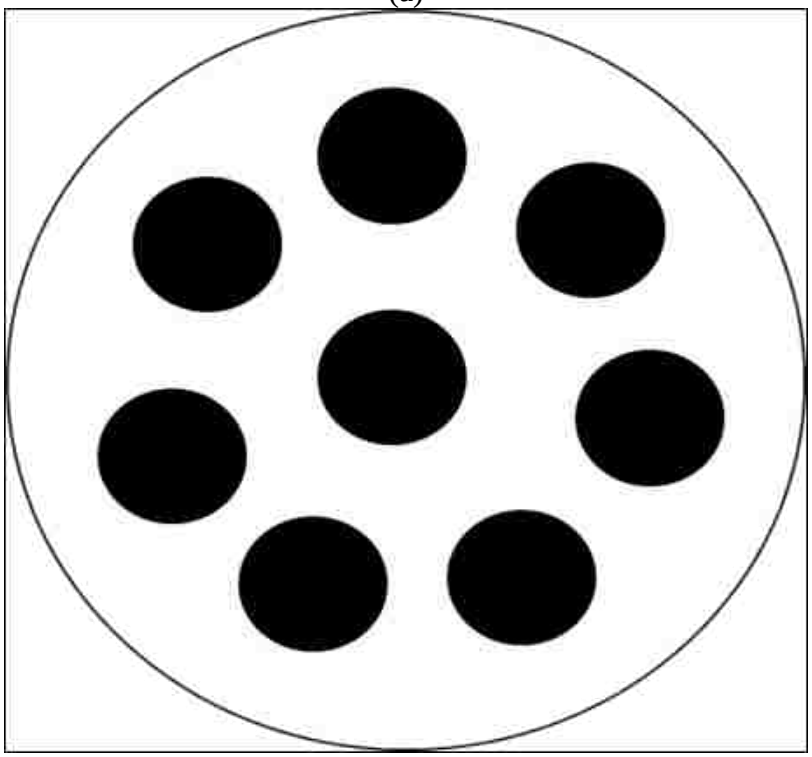

(b)

Figure 2.2. (a) Schematic of 0.0254 m internals support (honey comb), all the dimensions in meter, (b) the configuring arrangement of the 0.0254 m internals, the 8 tubes internals covered 25% of the total cross-sectional area of the column.

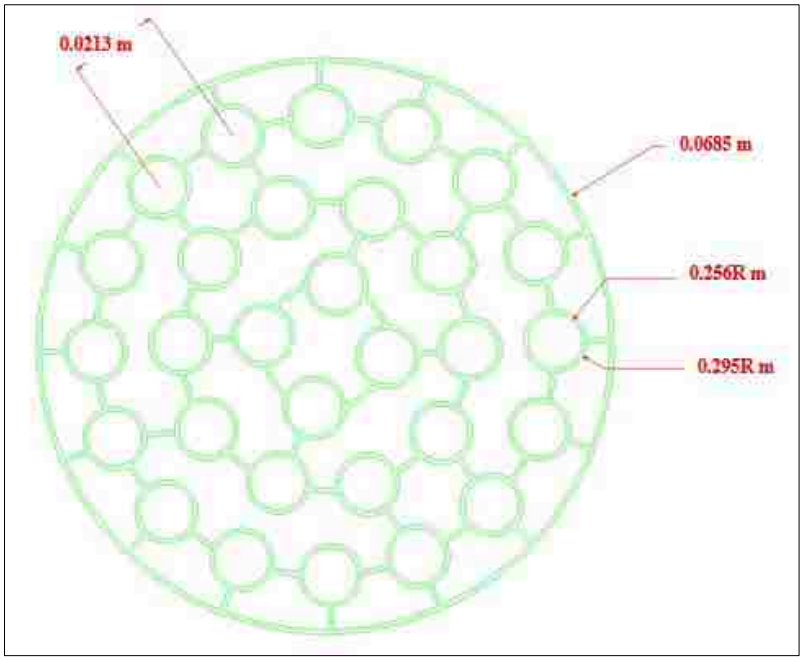

(a)

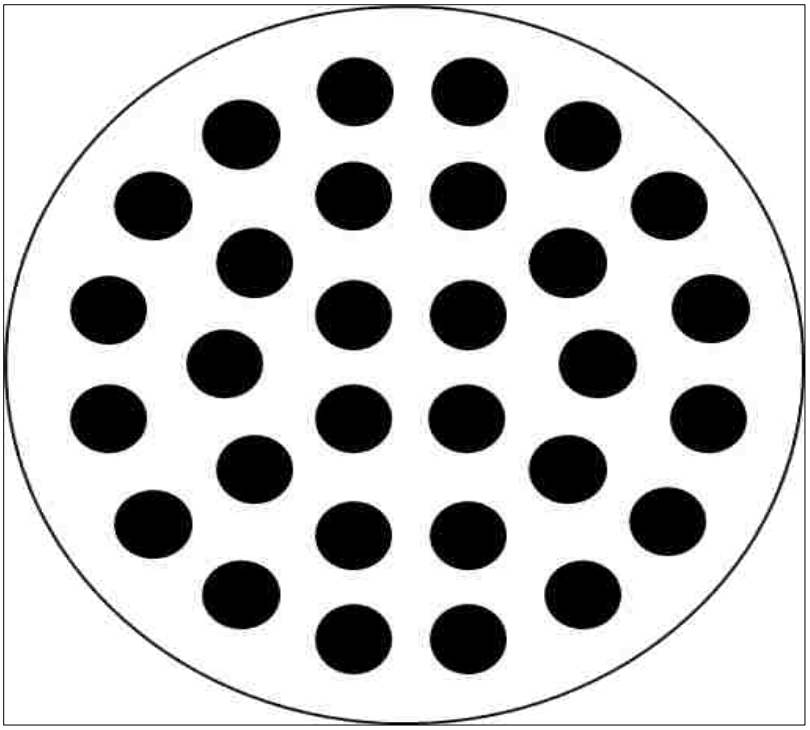

(b)

Figure 2.3. (a) Schematic of 0.0127 m internals support (honey comb), all the dimensions in meter, (b) the configuring arrangement of the 0.0127 m internals, the 30 tubes internals covered 25% of the total cross-sectional area of the column.

(a)

(b)

Figure 2.4. (a) Photo of 0.0127 m vertical internals configuration and its support (b) Photo of 0.0254 m vertical internals configuration and its support.

maximum value and then start to be constant. The corresponding superficial gas velocity at the point when the pressure drop reach its maximum value is represented the minimum fluidization velocity. This experiment was done for both the cases of with and without internals. More details about the particles used and the minimum fluidization velocity for each condition are illustrated in Table 2.1. As illustrated in Table 2.1, both solid particles have same minimum fluidization velocity while they are different in their physical properties and this could be the combination effect of particles size and density.

Table 2.1. The physical properties of different solid particles and the minimum fluidization velocities with and without internals for each solid particles.

Conditions	Glass Beads	Aluminum Oxide
Particles mean diameter (μm)	365	255
Particle density (Kg/m^3)	2500	3900
Static bed height (m)	0.35	0.35
sphericity factor (φ)	0.90	0.74
Particle size distribution (μm)	300-430	165-406
Minimum fluidized velocity without internals (m/s)	0.4	0.4
Minimum fluidized velocity with 0.0254 m internals (m/s)	0.4	0.4
Minimum fluidized velocity with 0.0127 m internals (m/s)	0.4	0.4

3. DIFFERENTIAL PRESSURE TRANSDUCER

3.1 DIFFERENTIAL PRESSURE TRANSDUCER TECHNIQUE

The differential pressure transducer (Omega Inc. of model PX-409-015 DDUV) was used to measure the time series of the pressure drop fluctuation signals along the bed height of the fluidized bed and covered a pressure range from 0–102 kPa. The pressure

transducer was connected to a DC power supply, which provides a voltage proportional to the measured differential pressure along the bed. The signal is received by the data acquisition (DAQ) system from Omega Inc. model OMB-DAQ-3000, which has high speed capability in collecting data up to 10^6 Hz. The DAQ converts the electrical voltage signal to a digital signal and feeds it to the computer. The DAQ-View software was used to control the DAQ system, which included DaqCal software application for easy user calibration. The signals were recorded for 40 s at a rate of 100 Hz and repeated three times to ensure that the reproducibility of the results. The reproducibility of the results was found to be less than of 2%. As well, the error bars were shown for each measurement. It is worthy to note that a wide range of sampling frequency (25 to 500 Hz) was used to estimate which sampling rate suitable for estimating the Kolmogorov entropy measurements (Van Ommen et al., 2011). The two ends of the pressure transducer were connected to the pressure taps mounted at the wall of the column. The distance between the two taps was 0.26 m (the lower and the upper taps were at a height of 0.045 and 0.305 m above the distributor). As the transducer is very sensitive, copper meshes were connected in the transducer taps to prevent the particles from getting inside the transducer. The time series of the pressure drop fluctuation signals were used to identify the flow regimes and their transition velocities in the case of with and without vertical internals.

To ensure that the differential pressure transducer measures properly the pressure drop, the overall gas holdup that can be measured by the pressure drop measurements has been compared with the gas holdup measured by the bed height expansion. The overall gas holdup can be estimated from the measured pressure drop as follows:

$$\varepsilon_g = 1\text{-}\frac{\Delta p}{\rho_s\, g\, \Delta z} \qquad (2.\ a)$$

Where Δp = the overall pressure drop and Δz = the bed height.

Also, the overall gas holdup can be measured by measuring the bed expansion after sparged the gas through the bed as follows:

$$\varepsilon_g = \frac{H_e - H_s}{H_e} \qquad (2.\ b)$$

where H_e: the bed height after the gas is sparger or expansion bed height and H_s: is the static bed height.

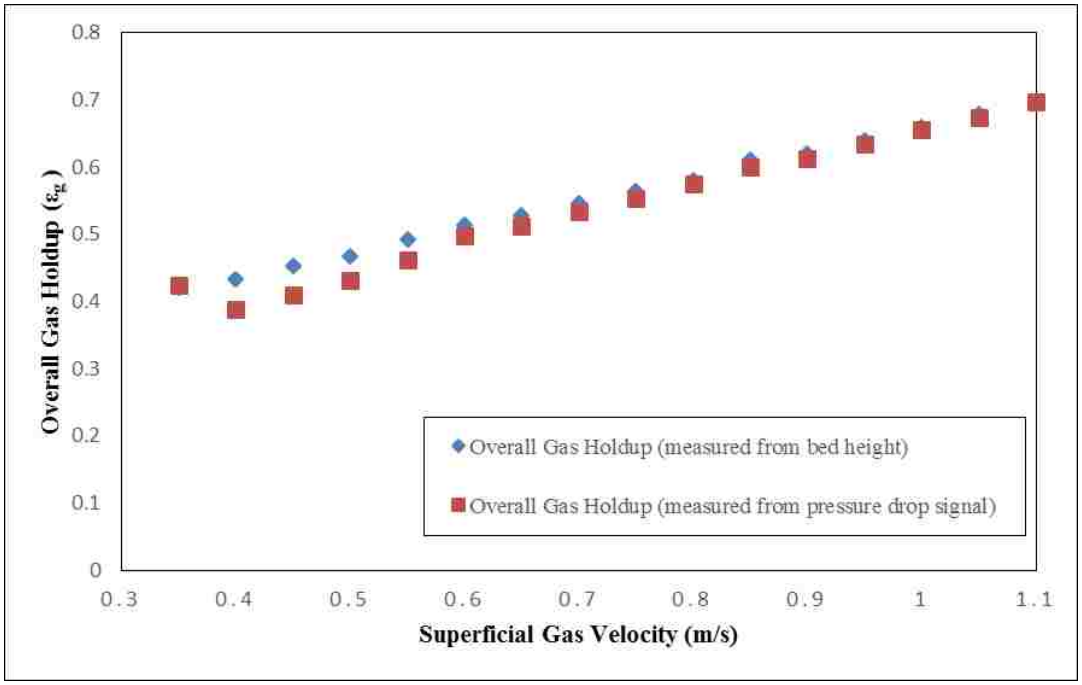

Figure 3.1. Overall gas holdup estimated from pressure drop fluctuation signals and bed height at different superficial gas velocities, for the case of without internals and glass beads solids particles

The overall gas holdup measured from pressure drop fluctuation signal (Equation 2. a) and overall gas holdup measured from the bed height (Equation 2. b) were compared in Figure 3.1 for the case of without vertical internals in a bed of glass beads solid particles

and for a range of superficial gas velocity (0.35 to 1.1 m/s). It was found that the relative percentage difference in the overall gas holdup is of 3.38 % between the two methods. This confirms that the differential pressure transducer was installed properly and provides indicative signals of the pressure drop and the flow regime conditions.

4. DATA ANALYSIS METHODS

4.1. STATISTICAL ANALYSIS (STANDARD DEVIATION)

The approach of standard deviation has been widely used for identifying the flow regimes and their transition velocities in the gas–solid fluidization systems (Johnsson et al. 2000). The maximum in the standard deviation value as a function of the superficial gas velocity demonstrates the transition velocity (Van Ommen et al. 2011). This means that the criteria of indicating the flow regime is that the standard deviation of the pressure drop fluctuation signal starts to increase with increasing the superficial gas velocity due to the change of the flow structure until it reaches its maximum value at the transition velocity from flow regime to another. However, if the standard deviation decreases after the transition velocity and then starts to increase again to its new maximum value, this represents another transition velocity which could be another flow structure within the same flow regime or a new flow regime.

The standard deviation (SD) of the time series of pressure drop fluctuation signals has been calculated as follows:

$$SD = \sqrt{\frac{\sum_{i=1}^{N}(x_i - \bar{x})^2}{(N-1)}} \qquad (3)$$

where x_i represents each point in the time series, N is the total number of the data points (which is 4000 and $\bar{x}$ is the mean of the time series, which can be calculated as follows:

$$\bar{x} = \frac{\sum_{i=1}^{N} x_i}{N} \quad (4)$$

4.2. STATE SPACE ANALYSIS (KOLMOGOROV ENTROPY)

The dynamic behavior of the fluidized beds is considered one of the most chaotic systems among the various types of multiphase flows. The chaotic feature of these types of beds returns to the complex interaction between the gas phase and its surroundings (solid particles, vessel wall, and the wall of the immersed surfaces if it exists inside the bed). The degree of the chaotic system of the fluidized beds can be affected by many parameters such as operating conditions, design parameters, and physicochemical properties of the solid particles. Consequently, the flow regime inside the fluidized beds is a function of the chaotic degree of the system. Many analysis methods have been used to represent the chaotic degree or the chaos state of the systems of gas–solid fluidized bed, such as attractor reconstruction, correlation dimension, entropy, and Kolmogorov entropy. Van Ommen et al. (2011) have shown that the Kolmogorov entropy is considered the more appropriate way to explain the chaotic degree or the system disorder of the gas–solid fluidization systems compared to other methods. Because it is easy to calculate and the analysis of pressure drop fluctuation time series data using KE gives a clear picture about the chaos behavior of the system, KE is the obvious choice for identifying the regime transitions in gas–solid fluidized beds.

Kolmogorov entropy is considered a useful tool for identifying and distinguishing the flow regime and their transition velocities in gas–solid fluidized systems, as indicated by many researchers (Zijerveld et al. 1998; Bai, Issangya, and Grace 1999; Van Ommen et al. 2011; Nedeltchev, Ahmed, and Al-Dahhan 2012; Nedeltchev et al. 2012; Nedeltchev

2015). Kolmogorov Entropy represents the degree of disorder or the rate of information loss in the system. In this study, the method used to calculate the KE is based on the approach of maximum likelihood estimation of entropy that was proposed by Schouten et al. (1994). The KE algorithm was developed at a multiphase engineering and applications laboratory (mReal) (Nedeltchev et al. (2012a), Nedeltchev et al. (2012), and Toukan et al. (2017).

5. RESULTS AND DISCUSSION

5.1. PRESSURE DROP FLUCTUATION SIGNALS

5.1.1. Pressure Drop Fluctuation Signals in Case of Without Internals. The pressure drop fluctuation signals at different flow regimes have been illustrated for the two types of solid particles, as shown in Figures 5.1 and 5.2. For glass beads solid particles (Figure 5.1), the pressure drop fluctuations increase with increasing the superficial gas velocity for all flow regimes except turbulent flow regime because the pressure drop fluctuations in terms of standard deviation reached its maximum point at the transition velocity (U_c) and then started to decrease after this point (Johnsson et al. 2000; Van Ommen et al. 2011; Saayman et al. 2013). For aluminum oxide (Figure 5.2), the pressure drop fluctuations increase from packed bed flow regime to bubbling flow regime due to the movement of the gas bubbles through the bed; then, the pressure drop fluctuations decrease with increasing the superficial gas velocity in the slugging flow regime, and consequently the pressure drop fluctuation reached its maximum value in the turbulent flow regime. It worthy to mention that the slugging flow regime is occurred in our system due to the small size of the bed and the using of relatively large solids particles size (Geldart B particles) as

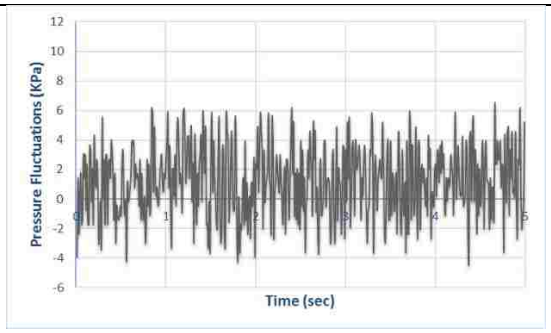

(a). Pressure drop fluctuations signal at gas velocity of 0.25 m/s (packed bed flow regime)

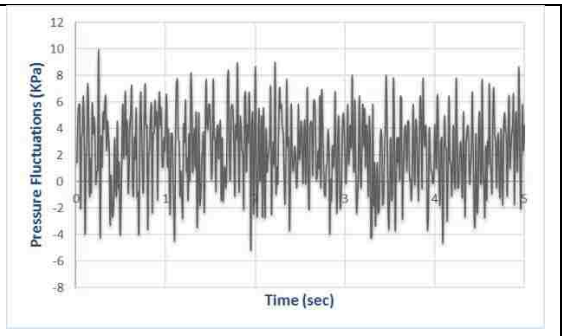

(b). Pressure drop fluctuations signal at gas velocity of 0.5 m/s (bubbling flow regime)

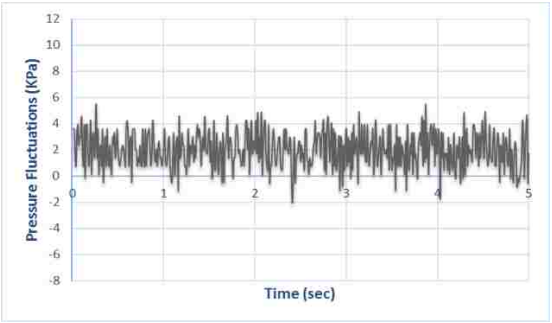

(c). Pressure drop fluctuations signal at gas velocity of 0.80 m/s (slugging flow regime)

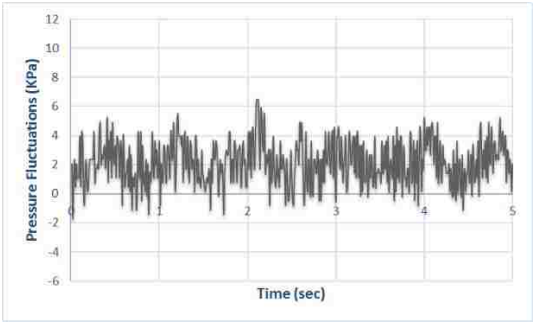

(d). Pressure drop fluctuations signal at gas velocity of 1.05 m/s (turbulent flow regime)

Figure 5.1. Pressure drop fluctuations signals at different flow regimes for glass beads solid particles without internals.

mentioned and reported by Olsson et al., (1995), Arnaldos and Casal (1996), Makkawi and Wright (2002) and others. The difference in the behavior of the aluminum oxide compared with the glass beads (whose pressure drop fluctuations with different flow regimes represent the normal behavior of Geldart B solid particles) could be due to the difference in the solid densities, solid particles shapes, and solid particles sphericity since these factors affect the flow regime as mentioned previously (Yerushalmi et al. 1978; Lim, Zhu, and Grace 1995; Bai et al. 1996; Zijerveld et al. 1998; Trnka et al. 2000; Andreux et al. 2005).

The shape of the glass beads is almost a sphere with sphericity factor of 0.9, whereas the aluminum oxide particles have an angular shape with a sphericity factor of 0.74.

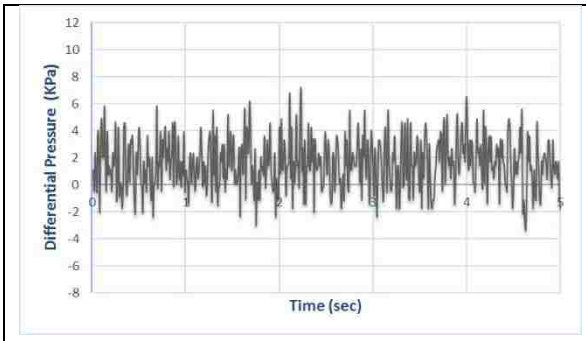

(a). Pressure drop fluctuations signal at gas velocity of 0.25 m/s (packed bed flow regime)

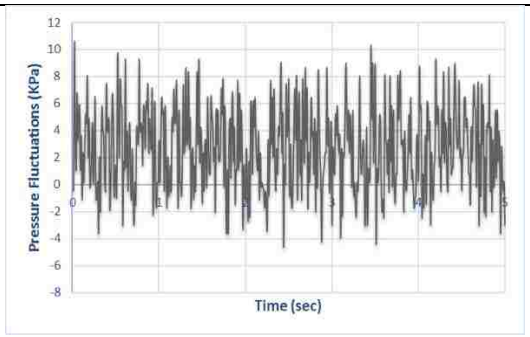

(b). Pressure drop fluctuations signal at gas velocity of 0.5 m/s (bubbling flow regime)

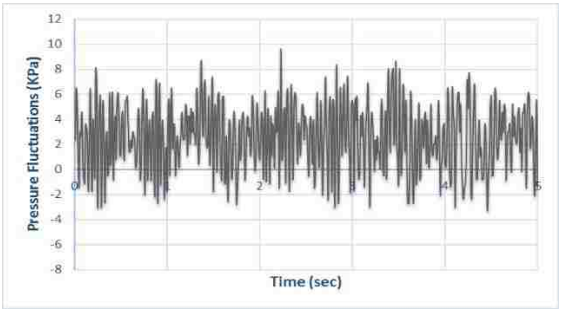

(c). Pressure drop fluctuations signal at gas velocity of 0.80 m/s (slugging flow regime)

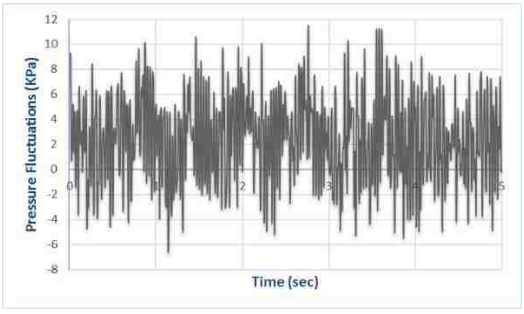

(d). Pressure drop fluctuations signal at gas velocity of 1.05 m/s (turbulent flow regime)

Figure 5.2. Pressure drop fluctuations signals at different flow regimes for aluminum oxide solid particles without internals.

5.1.2. Pressure Drop Fluctuation Signals in Case of With Internals. The immersed vertical internals have a significant impact on the pressure drop fluctuations inside the gas–solid fluidized bed (Rüdisüli et al. 2012b). It has been demonstrated by Rüdisüli et al. (2012a) that the vertical internals can reduce the amplitude of the pressure

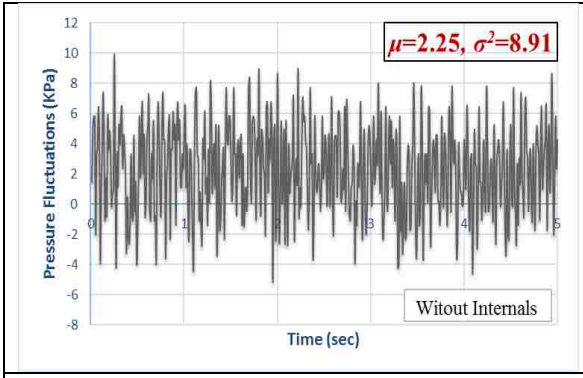

Pressure drop fluctuations signal at gas velocity of 0.5 m/s (bubbling flow regime) without internals

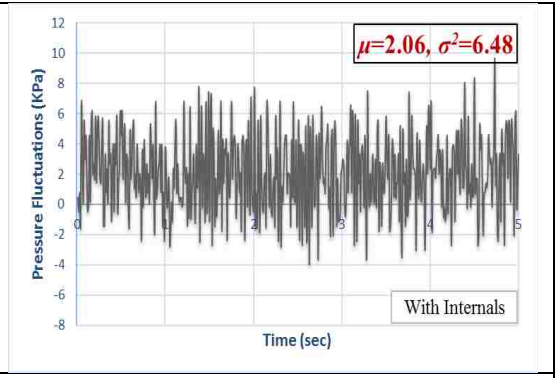

Pressure drop fluctuations signal at gas velocity of 0.5 m/s (bubbling flow regime) with 0.0254 m internals

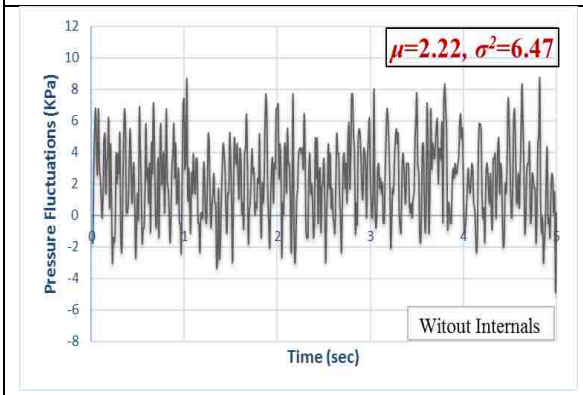

Pressure drop fluctuations signal at gas velocity of 0.7 m/s (slugging flow regime) without internals

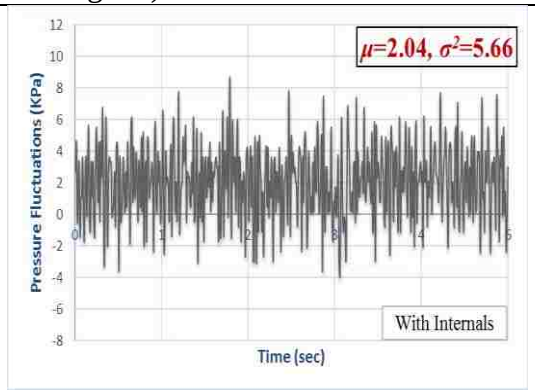

Pressure drop fluctuations signal at gas velocity of 0.7 m/s (slugging flow regime) with 0.0254 m internals

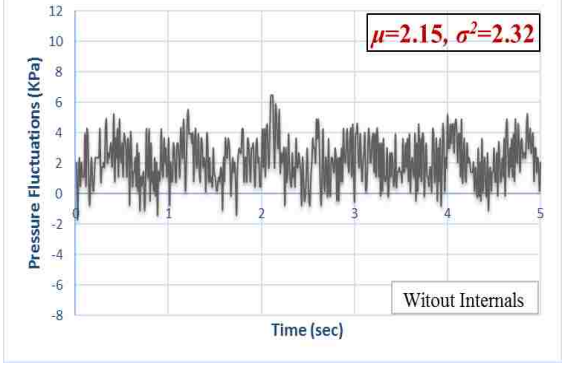

Pressure drop fluctuations signal at gas velocity of 1.05 m/s (turbulent flow regime) without internals

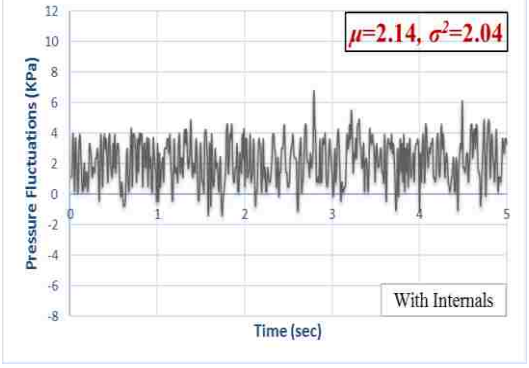

Pressure drop fluctuations signal at gas velocity of 1.05 m/s (turbulent flow regime) with 0.0254 m internals

Figure 5.3. Pressure drop fluctuations signals at different flow regimes for glass beads solid particles with 0.0254 m diameter internals (right side) and without internals (left side).

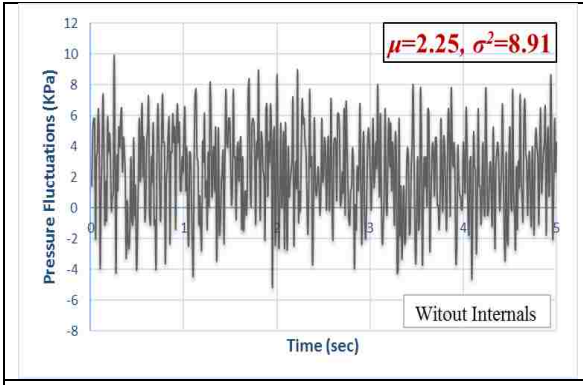

Pressure drop fluctuations signal at gas velocity of 0.5 m/s (bubbling flow regime) without internals

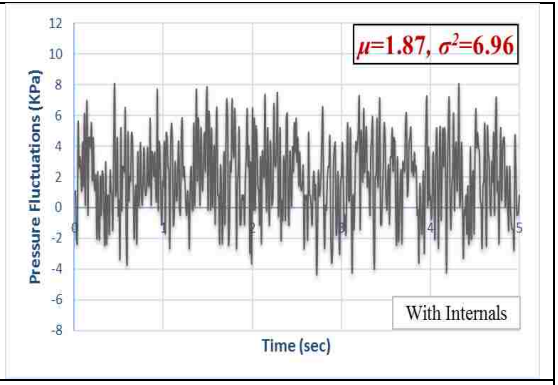

Pressure drop fluctuations signal at gas velocity of 0.5 m/s (bubbling flow regime) with 0.0127 m internals

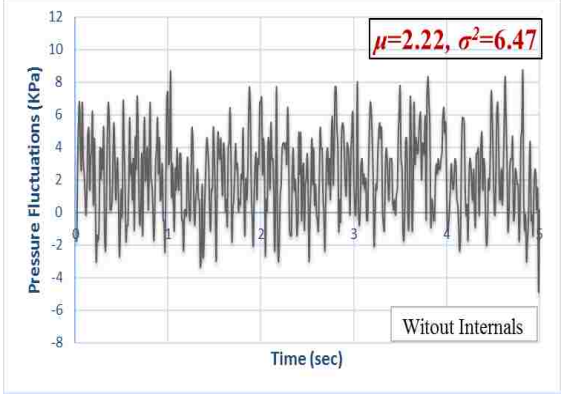

Pressure drop fluctuations signal at gas velocity of 0.7 m/s (slugging flow regime) without internals

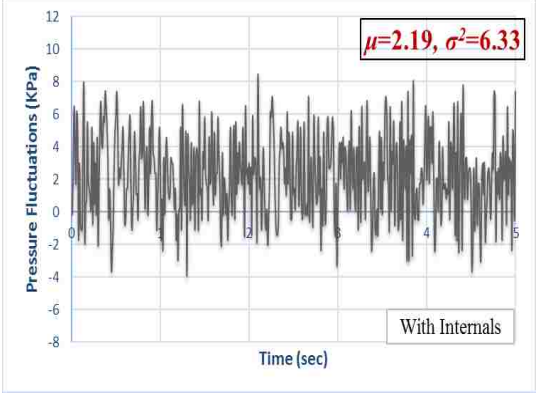

Pressure drop fluctuations signal at gas velocity of 0.7 m/s (slugging flow regime) with 0.0127 m internals

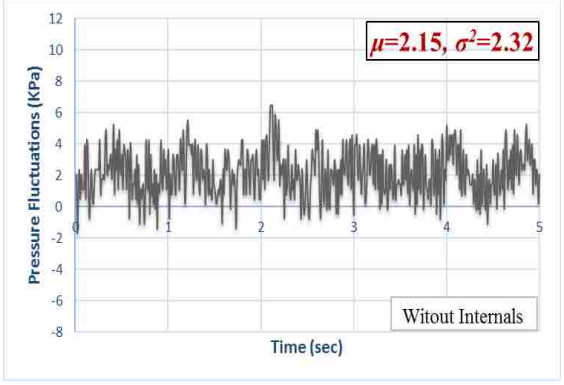

Pressure drop fluctuations signal at gas velocity of 1.05 m/s (turbulent flow regime) without internals

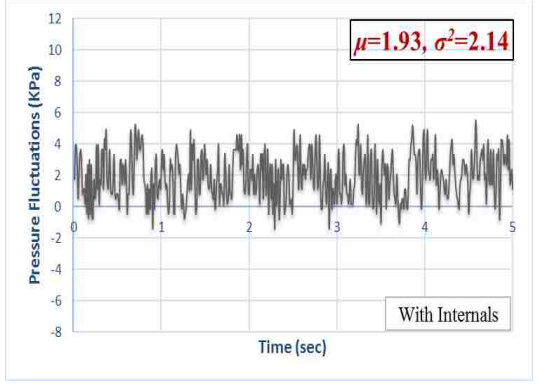

Pressure drop fluctuations signal at gas velocity of 1.05 m/s (turbulent flow regime) with 0.0127 m internals

Figure 5.4. Pressure drop fluctuations signals at different flow regimes for glass beads solid particles with 0.0127 m diameter internals (right side) and without internals (left side).

drop fluctuations and minimize slugging inside the bed. The pressure drop fluctuation signals at different flow regimes for the cases without internals and with two types of internals are presented in Figure 5.2 (0.0254 m internals and without internals) and Figure 5.4 (0.0127 m internals and without internals). The left side of Figure 5.3 and 5.4 represents the pressure drop fluctuation signals at different flow regimes without internals, while the right side of Figure 5.3 and 5.4 represents the pressure drop fluctuation signals at different flow regimes with internals. Apparently, the pressure drop fluctuations with 0.025 and 0.0127 m internals are less alike; the mean and variance values of the pressure fluctuation signals are lower than those without internals.

Table 5.1. The mean and variance of the pressure drop fluctuation signals at different flow regimes with and without internals for glass beads solid particles.

Conditions	**Without internals**		**With internals**			
Vertical internals size	**-**		**0.0254 m**		**0.0127 m**	
Data analysis method	Mean	Variance	Mean	Variance	Mean	Variance
Bubbling flow regime at gas velocity of 0.5 m/s	2.25	8.91	2.06	6.48	1.87	6.96
Slugging flow regime at gas velocity of 0.8 m/s	2.22	6.47	2.04	5.66	2.19	6.33
Turbulent flow regime at gas velocity of 1.05 m/s	2.15	2.32	2.14	2.04	1.93	2.14

The values of the mean and variance of the pressure fluctuation signals for the cases without and with two types of internals are illustrated in Table 5.1. The mean and variance of the pressure fluctuations are lesser with the existence of vertical internals. As well, the 0.0254 m internals give less pressure fluctuation than that of the 0.0127 m internals, and this reduction in pressure fluctuations by means of 0.0254 m internals demonstrates their

ability in minimizing the slugging transition velocity range and maximizing the range of bubbling and turbulent flow regimes, as mentioned previously. In general, it can be deduced that both types of vertical internals can reduce bed fluctuations, slugging behavior, bubble size and the coalescence between them, which reduces the slugging behavior inside the bed and makes the fluidization process smoother.

In order to make a clear picture about the effect of the vertical internals on the flow behavior of the aluminum oxide solid particles and extend the knowledge of the hydrodynamics of the gas–solid fluidized beds with the vertical tubes and how these immersed surfaces affect the behavior of various flow regimes, the impact of both types of vertical internals on the different flow regimes has been represented by means of pressure drop fluctuation signals. As mentioned earlier, the vertical tubes can minimize the pressure fluctuations inside the gas–solid fluidized beds. This idea has been supported by many experimental works (Grace and Harrison 1968; Ramamoorthy and Subramanian 1981; Law et al. 2003; Rüdisüli et al. 2012b; Mathew, Begum, and Anantharaman 2014). The time series of the pressure drop fluctuations at various flow regimes for the cases without internals and with the effect of two types of internals is displayed in Figure 5.5 (0.0254 m internals and without internals) and Figure 5.6 (0.0127 m internals and without internals). The left side of Figure 5.5 and 5.6 shows the pressure drop fluctuation signals at different flow regimes without internals, while, the right side of Figure 5.5 and 5.6 represents the pressure drop fluctuation signals at different flow regimes with internals. Figure 5.5 and 5.6 clearly show that the pressure fluctuations in cases without internals (left sides of both figures) have been minimized due to the implementation of both types of vertical internals (right sides of both figures). The mean and variance of the pressure drop fluctuation signals

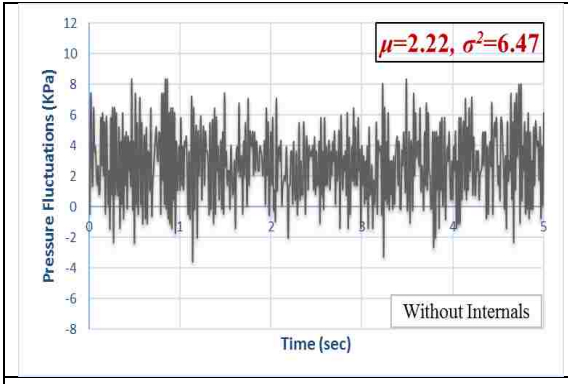

Pressure drop fluctuations signal at gas velocity of 0.6 m/s (bubbling flow regime) without internals

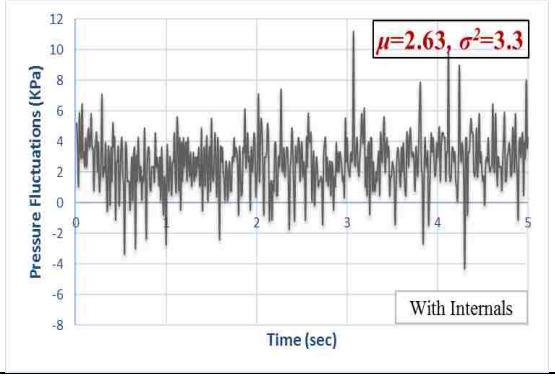

Pressure drop fluctuations signal at gas velocity of 0.6 m/s (bubbling flow regime) with 0.0254 m internals

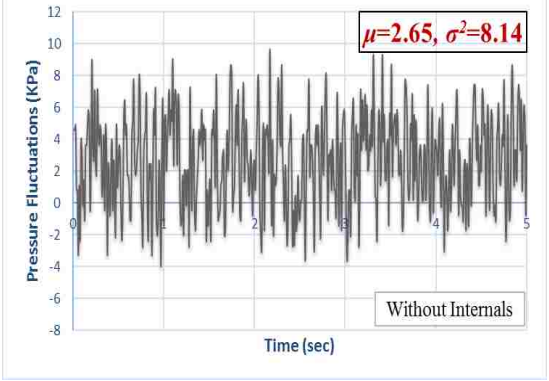

Pressure drop fluctuations signal at gas velocity of 0.9 m/s (slugging flow regime) without internals

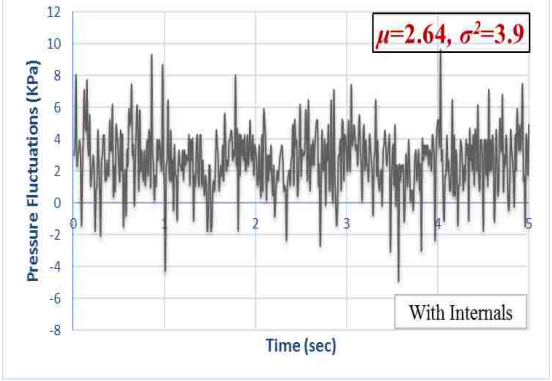

Pressure drop fluctuations signal at gas velocity of 0.9 m/s (slugging flow regime) with 0.0254 m internals

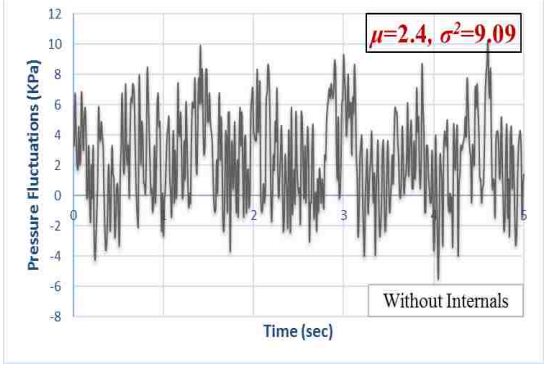

Pressure drop fluctuations signal at gas velocity of 1.2 m/s (turbulent flow regime) without internals

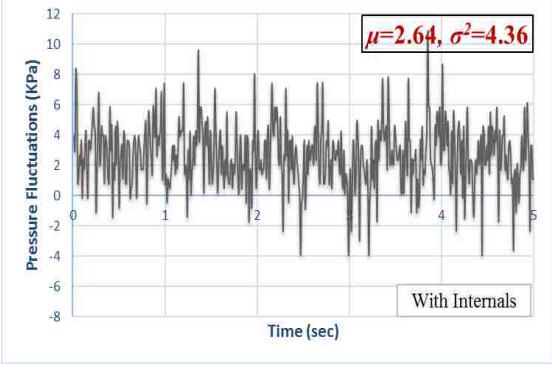

Pressure drop fluctuations signal at gas velocity of 1.2 m/s (turbulent flow regime) with 0.0254 m internals

Figure 5.5. Pressure drop fluctuations signals at different flow regimes for aluminum oxide solid particles with 0.0254 m diameter internals (right side) and without internals (left side).

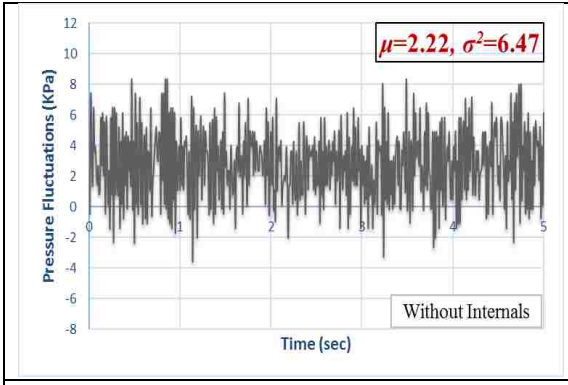

Pressure drop fluctuations signal at gas velocity of 0.6 m/s (bubbling flow regime) without internals

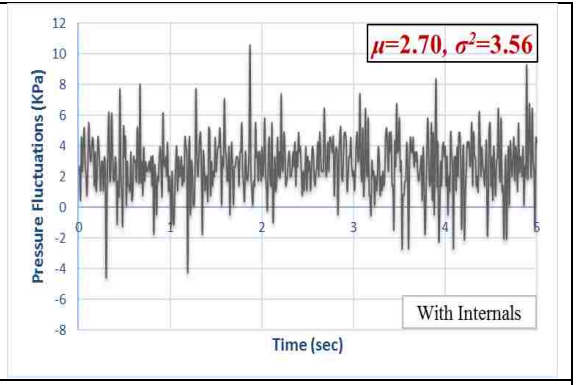

Pressure drop fluctuations signal at gas velocity of 0.5 m/s (bubbling flow regime) with 0.0127 m internals

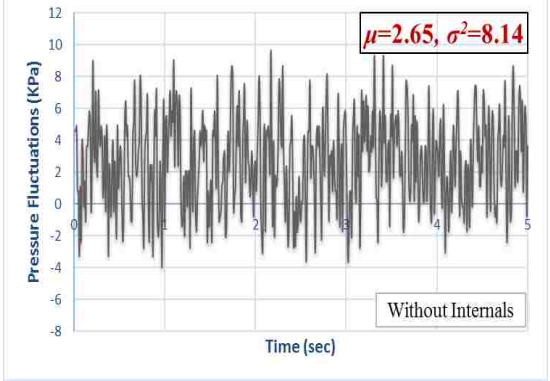

Pressure drop fluctuations signal at gas velocity of 0.9 m/s (slugging flow regime) without internals

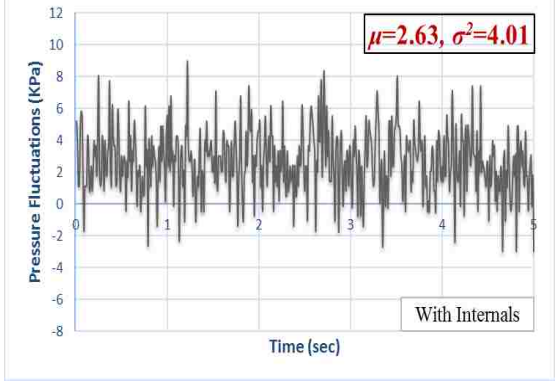

Pressure drop fluctuations signal at gas velocity of 0.9 m/s (slugging flow regime) with 0.0127 m internals

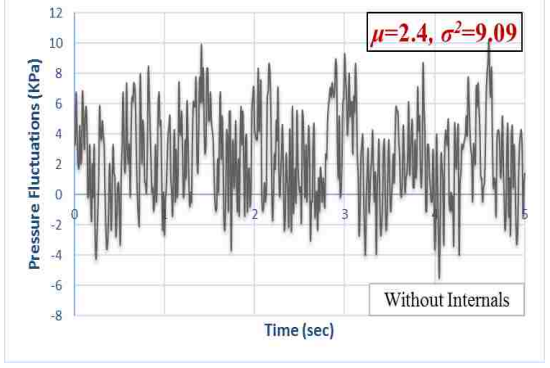

Pressure drop fluctuations signal at gas velocity of 1.2 m/s (turbulent flow regime) without internals

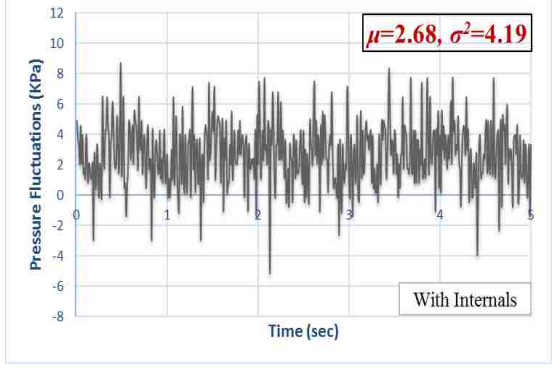

Pressure drop fluctuations signal at gas velocity of 1.2 m/s (turbulent flow regime) with 0.0127 m internals

Figure 5.6. Pressure drop fluctuations signals at different flow regimes for aluminum oxide solid particles with 0.0127 m diameter internals (right side) and without internals (left side).

have been estimated and are listed in Table 5.2 for cases with and without internals. The values of the variance of the pressure fluctuations in the case of vertical internals are lesser than with the cases without internals.

Table 5.2. The mean and variance of the pressure drop fluctuation signals at different flow regimes with and without internals for aluminum oxide solid particles.

Conditions	**Without internals**		**With internals**			
Vertical internals size	**-**		**0.0254 m**		**0.0127 m**	
Data analysis method	Mean	Variance	Mean	Variance	Mean	Variance
Bubbling flow regime at gas velocity of 0.6 m/s	2.22	6.47	2.63	3.3	2.7	3.56
Slugging flow regime at gas velocity of 0.9 m/s	2.65	8.14	2.64	3.9	2.63	4.01
Turbulent flow regime at gas velocity of 1.2 m/s	2.4	9.09	2.64	4.36	2.68	4.19

The reduction in the values of variance demonstrates the capability of the vertical internals in minimizing the pressure fluctuations inside the gas–solid fluidized bed and makes the fluidization process more uniform. In the meantime, the mean values of the pressure fluctuations for vertical internals have been increased compared to the cases without internals. The reason for the increase in the mean values of pressure fluctuations with the immersed vertical internals is due to the nature of the aluminum oxide solid particles. This type of solid particle has an angular shape (irregular shape) with 0.74 sphericity factor that would increase the pressure drop inside the gas–solid fluidized bed as compared to the glass beads solid particles, which have a sphericity factor of 0.9. To clarify the difference in mean values of the pressure fluctuation which represent the pressure drop inside the bed as shown in Figure 5.7 for the case of with and without internals. The values of pressure drop after the minimum fluidization velocity increase for

both types of vertical internals, particularly for the case of 0.0127 m diameter internals, which supports the idea that the 0.0254 m diameter internals have the greater capability in improving the fluidization process by reduce the bed fluctuation and slugging inside the bed more than that of the 0.0127 m diameter internals as in the case of the glass beads solid particles.

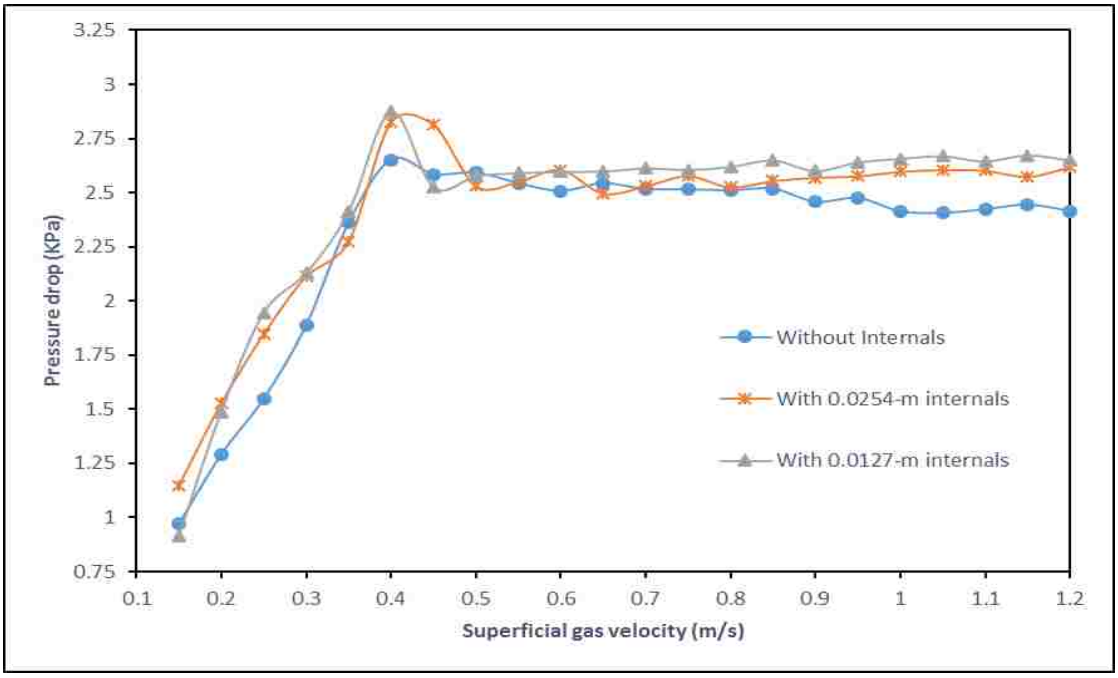

Figure 5.7. Pressure drop vs. superficial gas velocity with and without internals for aluminum oxide solid particles.

5.2. FLOW REGIMES WITH-OUT INTERNALS

The standard deviation and Kolmogorov entropy of the pressure drop fluctuations at different superficial gas velocities range from 0.15 to 1.1 m/s for the glass beads, and aluminum oxide solid particles are plotted in Figure 5.8 through 5.11. For statistical

analysis (standard deviation), the maximum values of the standard deviation of pressure drop fluctuations are referred to the transition velocities as reported by Andreux et al. (2005), Johnsson et al. (2000), and Van Ommen et al. (2011). For state space analysis (Kolmogorov entropy), the minimum values of the Kolomogrov entropy of the pressure drop fluctuations are referred to as the transition velocities, as indicated by Nedeltchev (2015), Nedeltchev et al., (2012), and Nedeltchev et al. (2012). In which, the Kolmogorov entropy starts to increase with increasing the superficial gas velocity as an indicator of increasing the disorder of the system (chaotic behavior) until it reaches its maximum value which represents the starting of instability of the system or transition regime. Then after such maximum value the Kolmogorov entropy decreases to minimum value within the same flow regime at which the contact between the gas and solid phases starts to be more organized.

For the range of superficial gas velocity used, four different flow regimes have been identified using the two methods of pressure drop fluctuations data analysis (packed bed, bubbling fluidization, slugging fluidization, and turbulent fluidization). Three distinguishable transition velocities have been recognized: minimum fluidized velocity (U_{mf}) or minimum bubbling velocity (U_{mb}), minimum slugging velocity (U_{slug}), and the transition velocity (turbulent transition velocity) from slugging to turbulent flow regime (U_c). The minimum fluidized velocity is equal to the minimum bubbling velocity in Geldard B type solid particles, while it is different in Geldard A type solid particles (Nedeltchev et al. 2012). In current study, both of the solid particles are Geldard B type, and thus we use the minimum fluidized velocity (U_{mf}) to refer to the transition velocity from packed bed to bubbling fluidization flow regime.

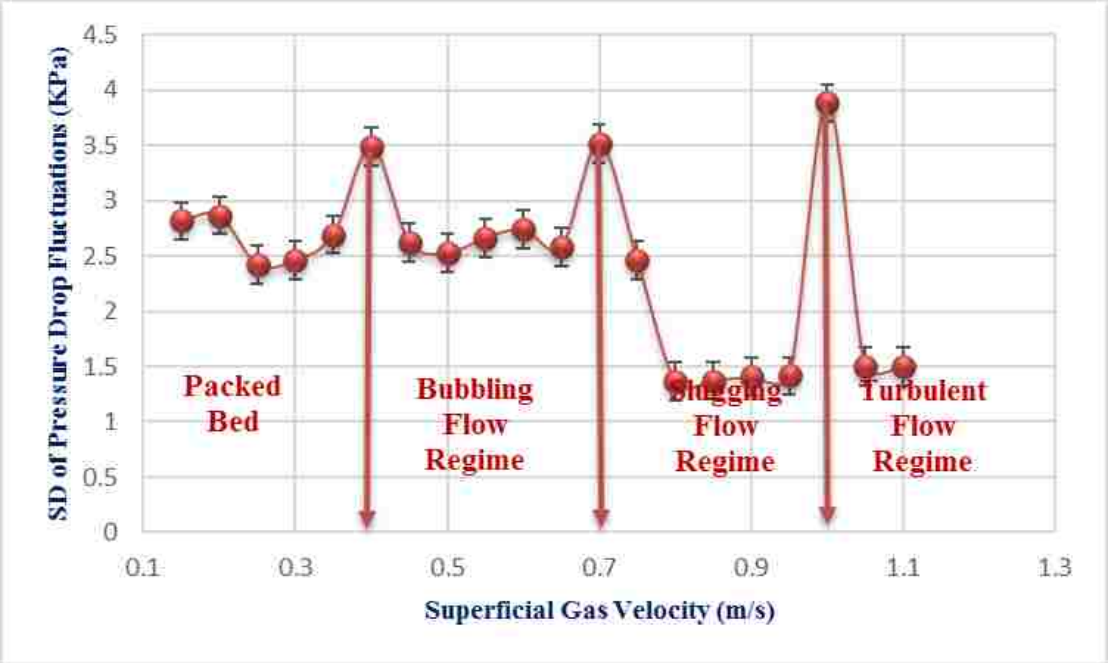

Figure 5.8. Standard deviation of pressure drop fluctuations vs. superficial gas velocity for the glass beads solid particles without internals.

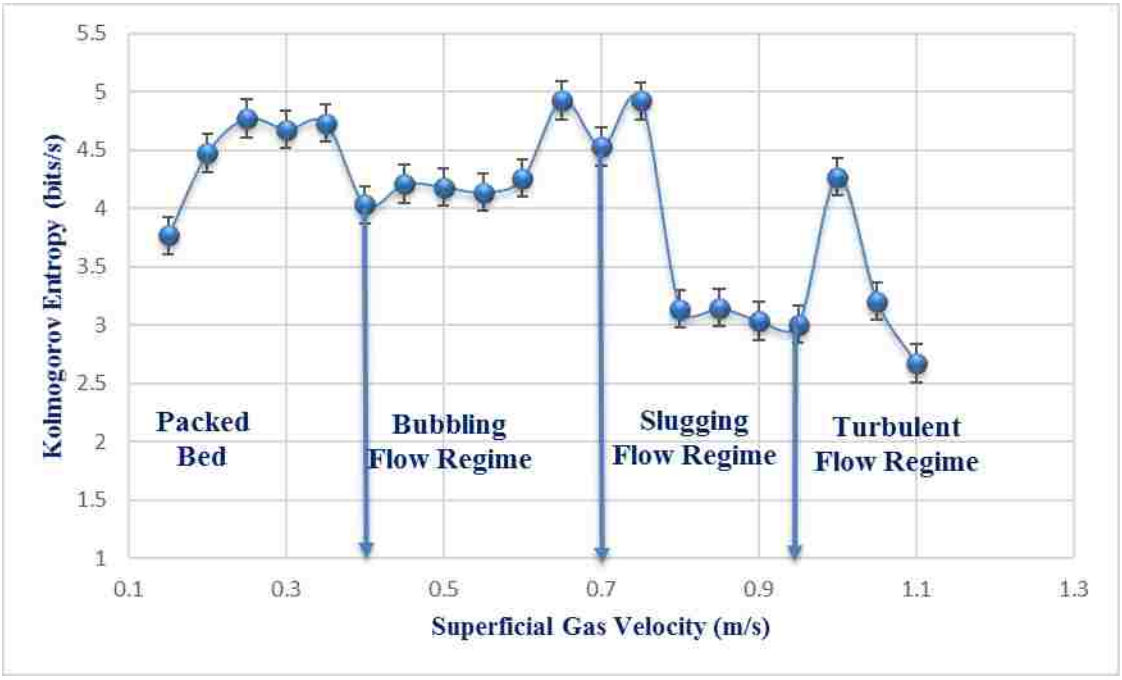

Figure 5.9. Kolmogorov entropy of pressure drop fluctuations vs. superficial gas velocity for the glass beads solid particles without internals.

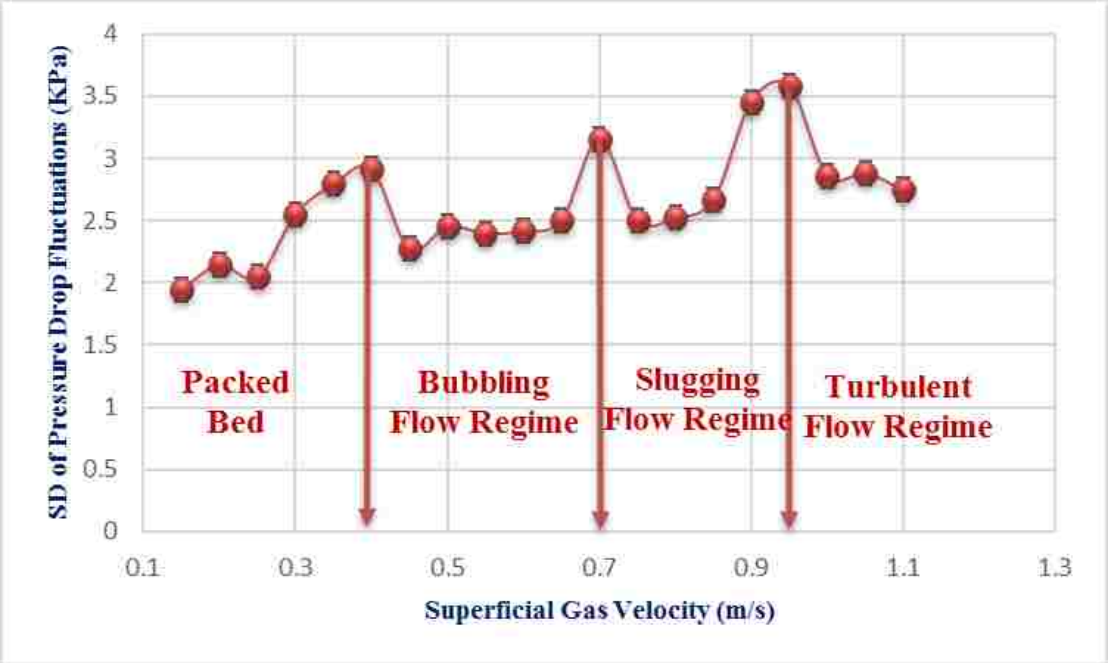

Figure 5.10. Standard deviation of pressure drop fluctuations vs. superficial gas velocity for the aluminum oxide solid particles without internals.

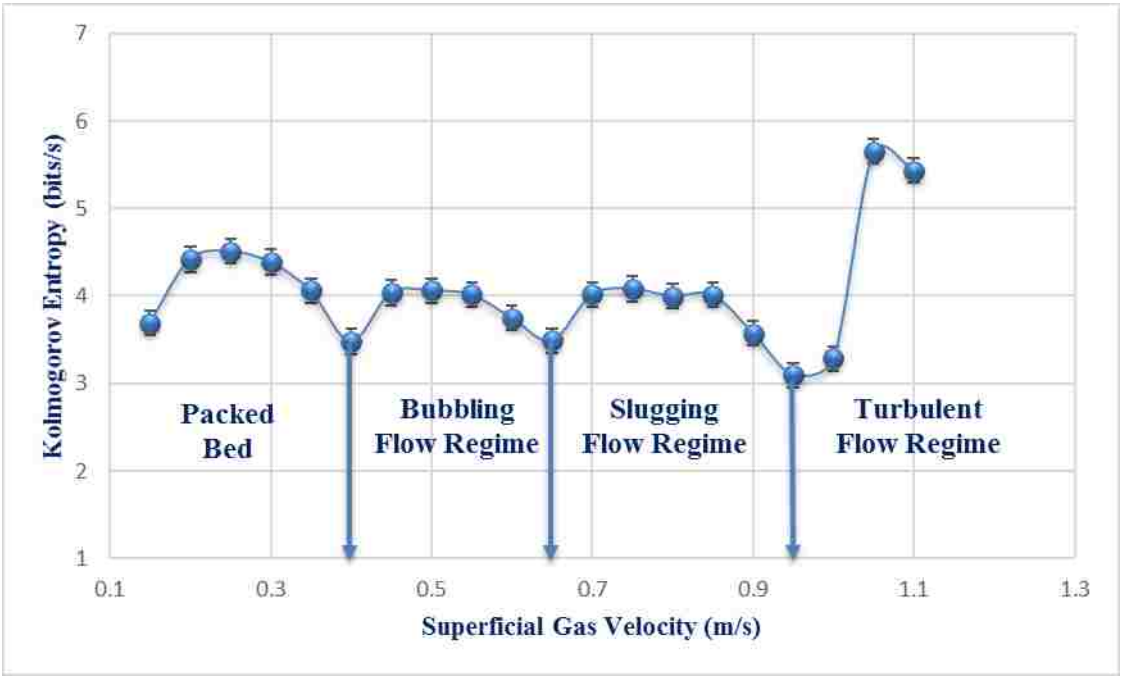

Figure 5.11. Kolmogorov entropy of pressure drop fluctuations vs. superficial gas velocity for the aluminum oxide solid particles without internals.

As shown in Figure 5.9 to 5.11 and for all the flow regimes that indicated in these figures, the Kolmogorov entropy starts to increase with increasing the superficial gas velocity as an indicator of increasing the disorder of the system (chaotic contact between the gas-solid phases) and then the Kolmogorov entropy values begin to be almost constant in which the system of gas-solid start to behave in more organized way. Thereafter, with increasing the superficial gas velocity the values of the Kolmogorov entropy start to decrease until reach its minimum value where the gas-solid flow patterns behave in an order way within the flow regime or it indicates the transition region or the beginning of another flow regime.

As demonstrated from Figures 5.8 through 5.11, the ability of both statistical analysis (standard deviation) and state space analysis (Kolmogorov entropy) in identifying different flow regimes from the data of pressure drop fluctuations is in good agreement with the measurements of different transition velocities regardless of the physical properties of solid particles (particles size, particles shape, and particles density). The transition velocities and the superficial gas velocity within the range for each flow regime for both solid particles using the two methods of data analysis are listed in Table 5.3. The two important transition velocities are minimum fluidized velocity and transition velocity because most industrial applications operate at bubbling and turbulent flow regimes (Nedeltchev, Ahmed, and Al-Dahhan 2012). The values of minimum fluidized velocities and transition velocities for both solid particles were compared with available correlations in the literature and the results are listed in Tables 5.4 and 5.5. It has been found that most of the transition velocities reported in Table 5.4 and 5.5 are in good agreement with the predicted correlations available in the literature.

Table 5.3. The transition velocities & the Superficial gas velocity within the range of each flow regime for both solid particles with the two types of data analysis.

Conditions	**Glass Beads**		**Aluminum Oxide**	
Data analysis method	SD	KE	SD	KE
Minimum fluidized velocity U_{mf} (m/s)	0.4	0.4	0.4	0.4
Minimum slugging velocity U_{slug} (m/s)	0.7	0.7	0.7	0.65
Transition velocity U_c (m/s)	1.0	0.95	0.95	0.95
Packed bed velocity range (m/s)	≥ 0.4	≥ 0.4	≥ 0.4	≥ 0.4
Superficial gas velocity within the range of bubbling regime (m/s)	0.4-0.7	0.4-0.7	0.4-0.7	0.4-0.65
Superficial gas velocity within the range of slugging regime (m/s)	0.7-1.0	0.7-0.95	0.7-0.95	0.65-0.95
Superficial gas velocity within the range of turbulent flow regime (m/s)	≤ 1.0	≤ 0.95	≤ 0.95	≤ 0.95

Table 5.4. Comparison between minimum fluidized velocity U_{mf} (m/s) measured by this work and the minimum fluidized velocity predicted from the available correlations in the literature.

Conditions	Glass Beads	Aluminum oxide
Data analysis method (SD & KE)	0.4	0.4
Experimentally measured by this work	0.4	0.4
$\mathrm{Re_{mf}} = 0.000955\ \mathrm{Ar}^{0.96}$ (Shaul, Rabinovich, and Kalman 2012)	0.42	0.37
$\mathrm{Re_{mf}} = \sqrt{(27.2)^2 + 0.0408\mathrm{Ar}}$-27.2 (Bi and Grace 1995)	0.42	0.38
%Relative error with respect to (Shaul, Rabinovich, and Kalman 2012)	4.76	7.5
%Relative error with respect to (Bi and Grace 1995)	4.76	5

Table 5.5. Comparison between transition velocity U_c (m/s) measured by this work and the transition velocity U_c (m/s) predicted from the available correlations in the literature.

Conditions	Glass Beads	Aluminum oxide
Kolmogorov Entropy (KE)	0.95	0.95
Standard deviation (SD)	1.0	0.95
$\frac{U_c}{\sqrt{gd_p}} = \left[\frac{k_{DF}}{d_p} * \frac{(\rho_p - \rho_f)}{\rho_f}\right]^n$ Where n=0.27 K_{DF}=0.00367 (for free bed) (Jin et al. 1986)	0.86	0.89
%Relative error of KE with respect to (Jin et al. 1986)	9.4	6.3
%Relative error of SD with respect to (Jin et al. 1986)	16.2	6.3
$Re_c = 0.57\ Ar^{0.46}$ (Lim, Zhu, and Grace 1995)	1.01	1.05
%Relative error of KE with respect to (Lim, Zhu, and Grace 1995)	5.9	9.5
%Relative error of SD with respect to (Lim, Zhu, and Grace 1995)	1	9.5

5.3. FLOW REGIMES WITH INTERNALS

5.3.1. Glass Beads Solid Particles. The two different tube sizes (0.0254 and 0.0127 m) of the circular-shape configurations of vertical internals have been used to study the impact of the vertical tubes on the flow regimes and their transition velocities for the case of glass beads solid particles in the current gas–solid fluidized bed. The identified flow regimes and their transition velocities using the two methods of data analysis are shown in Figures 5.12 through 5.15. These figures show the capability of the two methods of analysis (statistical method and state space method) in specifying different flow regimes and their transition velocities with good agreement in the case of vertical internals inside the gas–solid fluidized bed.

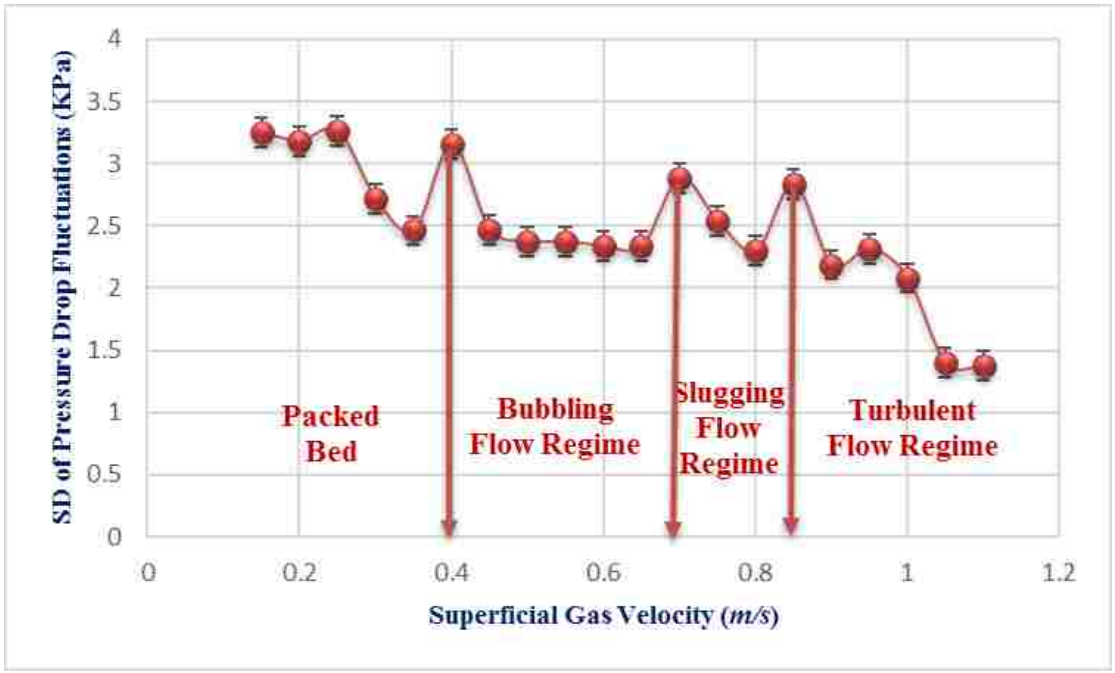

Figure 5.12. Standard deviation of pressure drop fluctuations vs. superficial gas velocity for the glass beads solid particles with 0.0254 m internals.

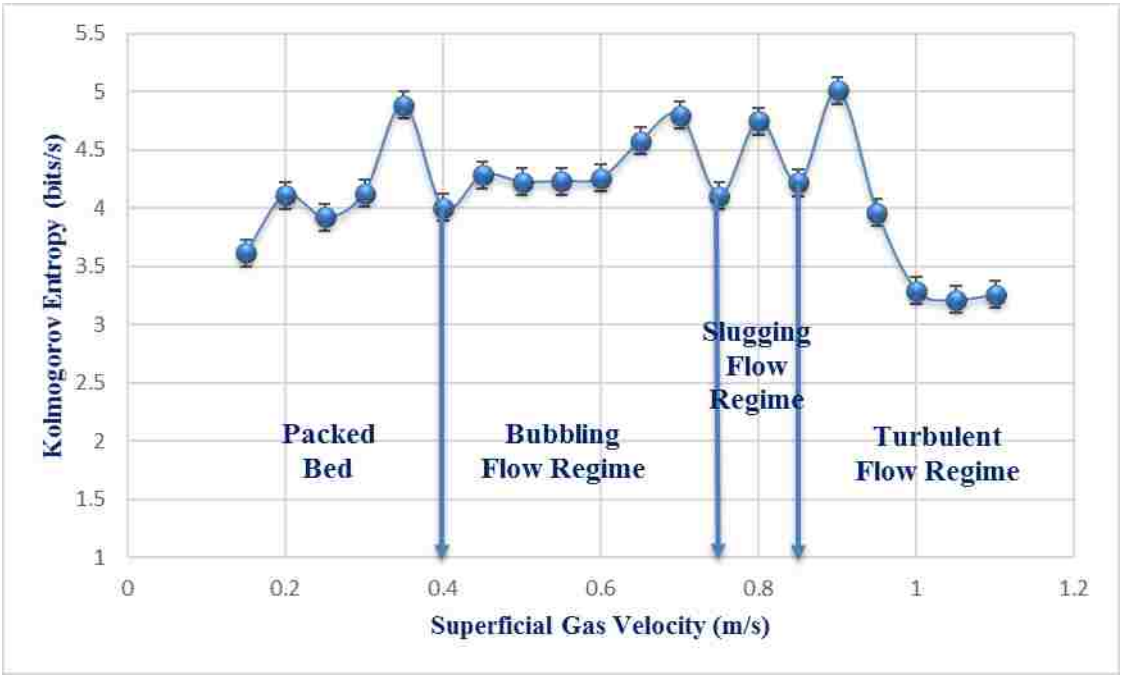

Figure 5.13. Kolmogorov entropy of pressure drop fluctuations vs. superficial gas velocity for the glass beads solid particles with 0.0254 m internals.

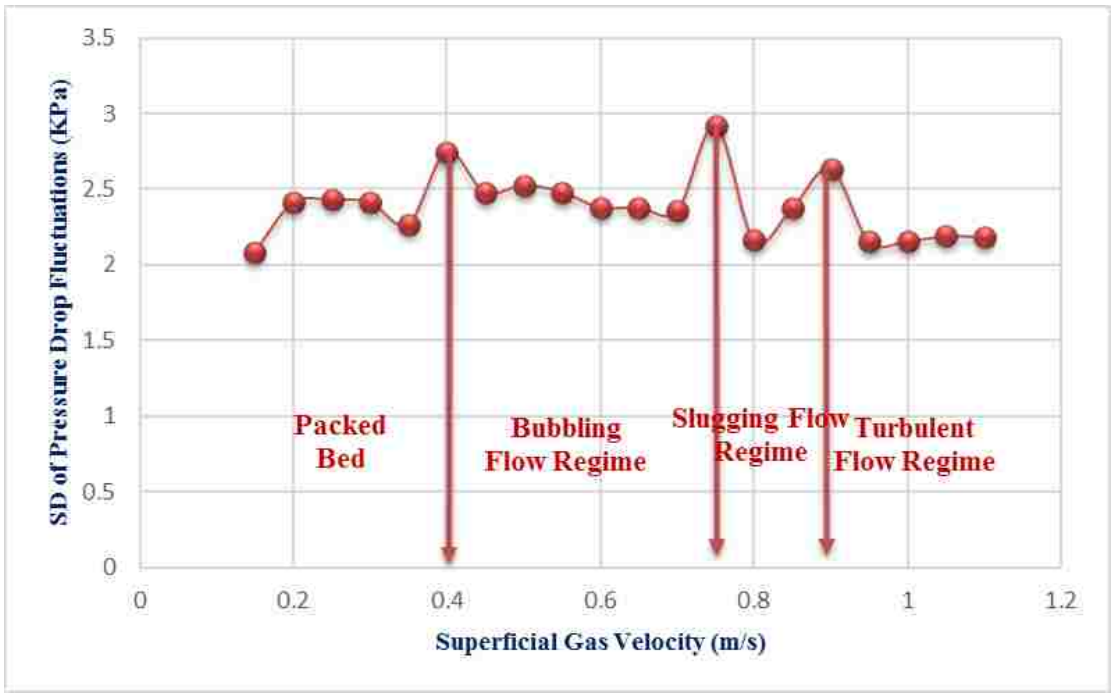

Figure 5.14. Standard deviation of pressure drop fluctuations vs. superficial gas velocity for the glass beads solid particles with 0.0127 m internals.

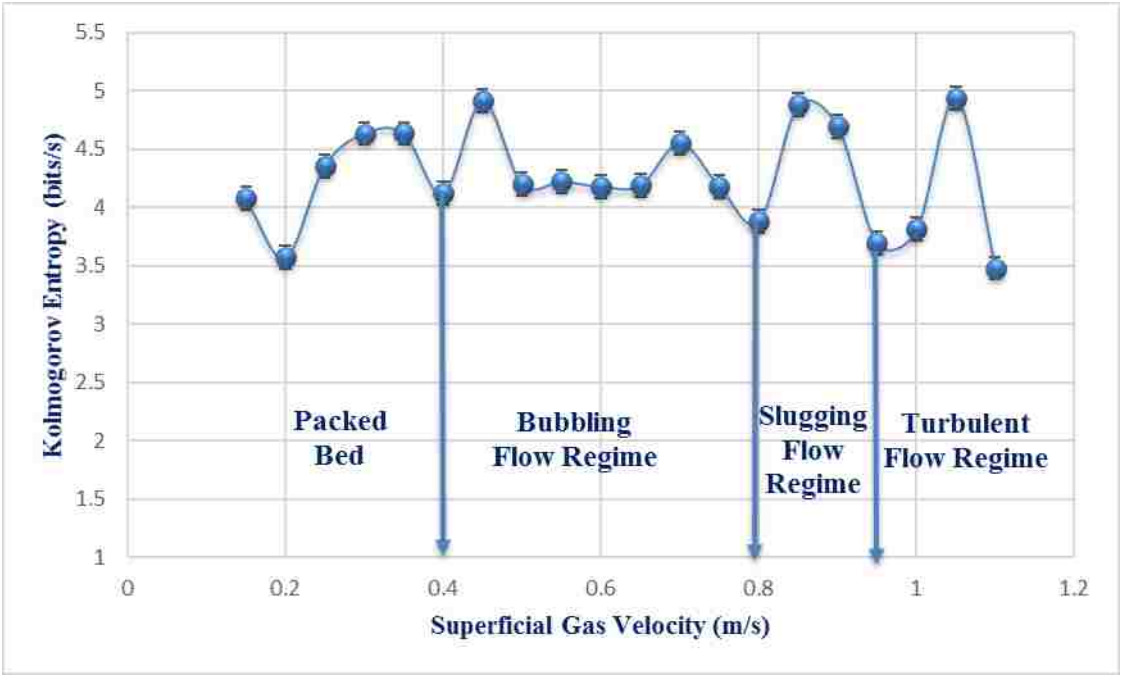

Figure 5.15. Kolmogorov entropy of pressure drop fluctuations vs. superficial gas velocity for the glass beads solid particles with 0.0127 m internals.

Four distinct flow regimes and three distinguished transition velocities have been identified for each type of the implemented vertical internal. The various transition velocities (U_{mf}, U_{slug}, and U_c) and the superficial gas velocity within the range of each flow regime for both vertical internals in glass beads solid particles bed using the two methods of data analysis are listed in Table 5.6. The data illustrated in Table 5.6 indicate a good agreement between the two methods of data analysis methods in specifying the values of different transition velocities for both types of vertical internals implemented inside the fluidized bed that occupied with glass beads solid particles.

Table 5.6. The transition velocities & superficial gas velocity within the range of each flow regime for both immersed vertical internals in glass beads solid particles with the two types of data analysis.

Conditions	**0.0254 m**		**0.0127 m**	
Data analysis method	SD	KE	SD	KE
Minimum fluidized velocity U_{mf} (m/s)	0.4	0.4	0.4	0.4
Minimum slugging velocity U_{slug} (m/s)	0.7	0.75	0.75	0.8
Transition velocity U_c (m/s)	0.85	0.85	0.9	0.95
Packed bed velocity range (m/s)	≥ 0.4	≥ 0.4	≥ 0.4	≥ 0.4
Superficial gas velocity within the range of bubbling regime (m/s)	0.4-0.7	0.4-0.75	0.4-0.75	0.4-0.8
Superficial gas velocity within the range of slugging regime (m/s)	0.7-85	0.75-0.85	0.75-0.9	0.8-0.95
Superficial gas velocity within the range of turbulent regime (m/s)	≤ 0.85	≤ 0.85	≤ 0.9	≤ 0.95

The turbulent transition velocity (U_c) measured by our experimental work for both types of vertical internals has been compared to the correlation equation predicted by Jin et al. (1986) which was show earlier (Equation 1), since it is the only predicted correlation available in the literature that has studied the effect of vertical tubes on the flow regimes of gas–solid fluidized bed. The values of the turbulent transition velocity that were measured experimentally for the two vertical internals sizes (1 and 0.5) are 0.85 and 0.95 m/s, respectively. The value of predicted turbulent transition velocity has been found to be 0.76 m/s, which is in relatively good agreement with the transition velocity of the 0.0254 m vertical internals with 10.5% relative error.

In order to show the effect of the two types of vertical internals on the flow regimes and their transition velocities, the data of the transition velocity and Superficial gas velocity within the range of each flow regime are illustrated in Table 5.7 for both cases (with and without internals) for glass beads solid particles. It appears from Table 5.7 that the minimum slugging velocity (U_{slug}) or the transition velocity from bubbling flow regime to slugging flow regime has been increased with the two types of vertical internals compared to the case without internals, as well this transition velocity was occurred at higher superficial gas velocity within the case of 0.0127 m internals compared to the 0.0254 m internals due to at 0.0127 m where intense distribution of internals that enhance flow distribution of gas and solids compared to that of 0.0254 m internals. The turbulent transition velocity (U_c) has been decreased with the two types of vertical internals compared to the case without internals and the decrease in the case of 0.0254 m internals is relatively less than that of 0.0127 m internals. This approach is satisfied with what has been mentioned in the literature by Jin et al. (1986) and Olsson et al. (1995). In which, they

Table 5.7. The transition velocities & the transition velocity range for each flow regime for cases of with and without immersed vertical internals in glass beads solid particles with the two types of data analysis.

Conditions	**With internals**				**Without internals**	
Vertical internals size	**0.0254 m**		**0.0127 m**		**-**	
Data analysis method	SD	KE	SD	KE	SD	KE
Minimum fluidized velocity U_{mf} (m/s)	0.4	0.4	0.4	0.4	0.4	0.4
Minimum slugging velocity U_{slug} (m/s)	0.7	0.75	0.75	0.8	0.7	0.7
Transition velocity U_c (m/s)	0.85	0.85	0.9	0.95	1.0	0.95
Packed bed velocity range (m/s)	≥ 0.4	≥ 0.4	≥ 0.4	≥ 0.4	≥ 0.4	≥ 0.4
Superficial gas velocity within the range of bubbling regime (m/s)	0.4-0.7	0.4-0.75	0.4-0.75	0.4-0.8	0.4-0.7	0.4-0.7
Superficial gas velocity within the range of slugging regime (m/s)	0.7-0.85	0.75-0.85	0.75-0.9	0.8-0.95	0.7-1.0	0.7-0.95
Superficial gas velocity within the range of turbulent regime (m/s)	≤ 0.85	≤ 0.85	≤ 0.9	≤ 0.95	≤ 1.0	≤ 0.95

have indicated that the implementation of different types of immersed tube bank orientations (vertical or horizontal) can reduce the turbulent transition velocity. In other words, the immersed internals can cause the turbulent flow regime to occur at lower superficial gas velocity. Consequently, the phenomenon of increasing the minimum slugging velocity and decreasing the turbulent transition velocity with the enforcement of vertical internals inside the fluidized bed can be represented more clearly when we compare the superficial gas velocity within the range of each flow regime reported in Table 5.7 with and without internals based on the data of Kolmogorov entropy. For 0.0254 m internals, the superficial gas velocity within the range of bubbling flow regime is 0.4–0.75 m/s, the superficial gas velocity within the range of slugging flow regime is 0.75–0.85 m/s, and the

superficial gas velocity within the range of turbulent flow regime is ≤ 0.85 m/s. For 0.0127 m internals, the superficial gas velocity within the range of bubbling flow regime is 0.4–0.8 m/s, the superficial gas velocity within the range of slugging flow regime is 0.8–0.95 m/s, and the superficial gas velocity within the range of turbulent flow regime is ≤ 0.95. For the cases without internals, the superficial gas velocity within the range of bubbling flow regime is 0.4–0.7 m/s, the superficial gas velocity within the range of slugging flow regime is 0.7–0.95 m/s, and the superficial gas velocity within the range of turbulent flow regime is ≤ 0.95 m/s. Table 5.7 clearly shows that the superficial gas velocity within the range of the bubbling flow regime increases with the implementation of both types of internals which can be explained by the reduced bubbles size, and coalescence between the bubbles due to the existing of vertical internals (Rüdisüli et al. 2012b; Mathew, Begum, and Anantharaman 2014). Additionally, superficial gas velocity within the range of the slugging flow regime decreases with the effectuation of internals, and this can be elucidated by the inhibition of the slugging phenome due to the presence of vertical internals (Ramamoorthy and Subramanian 1981). In addition, the superficial gas velocity within the range of the turbulent flow regime increases with the influence of internals due to the increase in turbulent behavior of the fluidized bed with the presence of immersed internals (Yang 2003). It is noteworthy to mention that the 0.0254 m internals minimize the superficial gas velocity within the range of slugging and maximize the superficial gas velocity within the range of turbulent transition velocity range more than that of 0.0127 m internals as shown in Table 5.7. This difference may be due to the differences in the tube size and tube-to-tube space, both of which have a significant effect on the hydrodynamic behavior of the gas–solid fluidized bed with immersed vertical internals (Rüdisüli et al. 2012a).

5.3.2. Aluminum Oxide Solid Particles. The influence of the two types of vertical internals on the flow regimes and their transition velocities has been studied using aluminum oxide solid particles. The aluminum oxide is B type particles according to the Geldart classification of solid particles, which is a function of the average particles size and solid density (Geldart 1973). The reason of utilizing another solid type of Geldart B particles is to extend the knowledge about the effect of the vertical internals on the flow behavior of gas–solid fluidized bed with solid particles of different physical properties and to investigate the effect of different physical properties (solid density, particles sizes, and particles shape) on the various flow patterns of the gas–solid fluidized bed. The density of the aluminum oxide is 3900 Kg/m^3, the average particle size is 255 μm, and the particle shape is angular (irregular shape) with a sphericity factor of 0.74. The flow regimes and their transition velocities verses the superficial gas velocity using the two methods of pressure fluctuation analysis and the two types of immersed vertical internals are represented in Figure 5.16–5.19. It important to note that the range of superficial gas velocity with the immersed vertical internals has been extended to be (0.15–1.2 m/s) instead of (0.15–1.1 m/s) as in the case without internals (of aluminum oxide) and glass beads solid particles due to the effect of the vertical internals, in which led to minimizing the bubbling transition velocity range, maximizing the slugging transition velocity range, and increasing the transition velocity (U_c).

It can be noticed from Figure 5.16–5.19 that four distinguished flow regimes and three featured transition velocities have been identified for each type of the implemented vertical internal. Moreover, three transition velocities (U_{mf}, U_{slug}, and U_c) and the superficial gas velocity within the range of each flow regime for both immersed vertical internals in the

Figure 5.16. Standard deviation of pressure drop fluctuations vs. superficial gas velocity for the aluminum oxide solid particles with 0.0254 m internals.

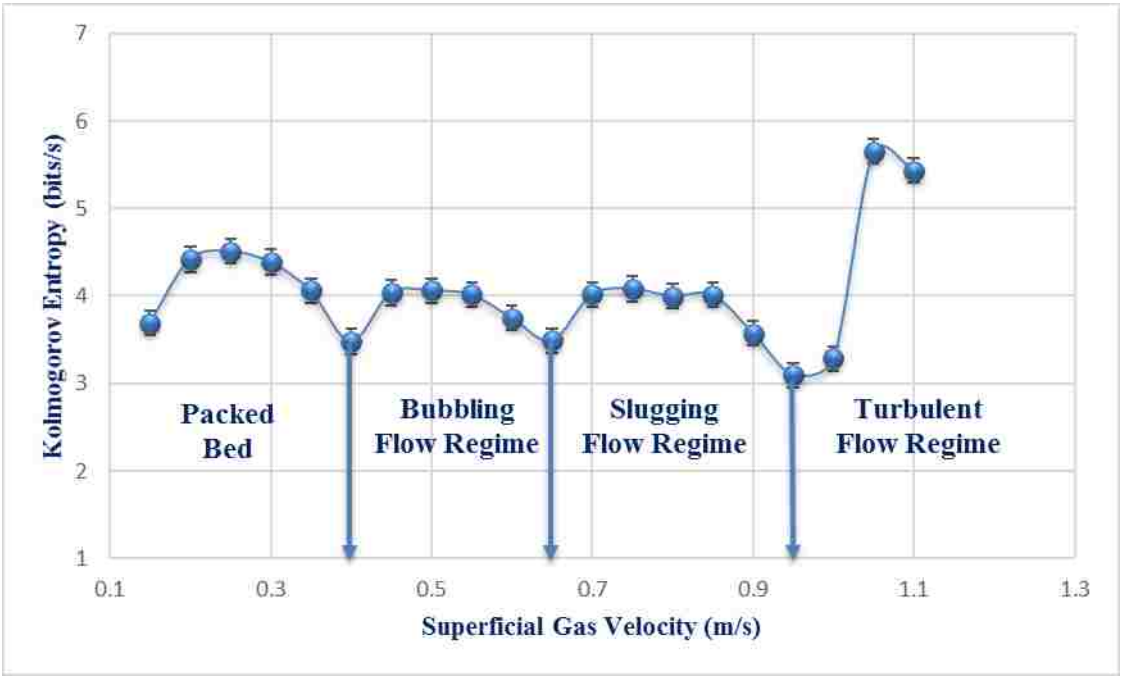

Figure 5.17. Kolmogorov entropy of pressure drop fluctuations vs. superficial gas velocity for the aluminum oxide solid particles with 0.0254 m internals.

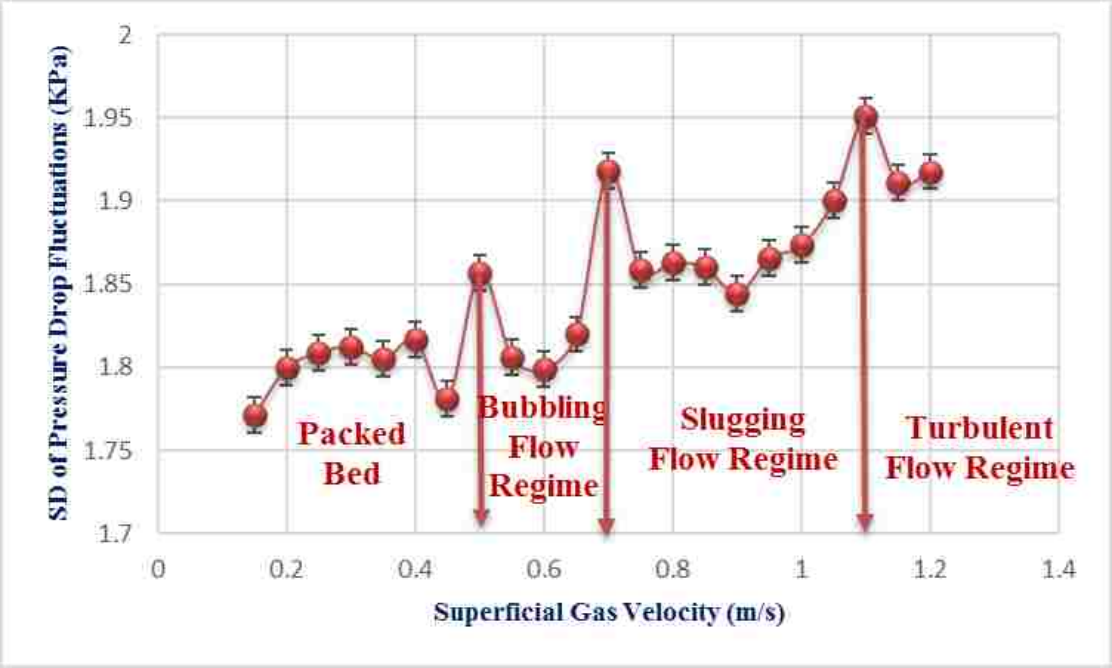

Figure 5.18. Standard deviation of pressure drop fluctuations vs. superficial gas velocity for the aluminum oxide solid particles with 0.0127 m internals.

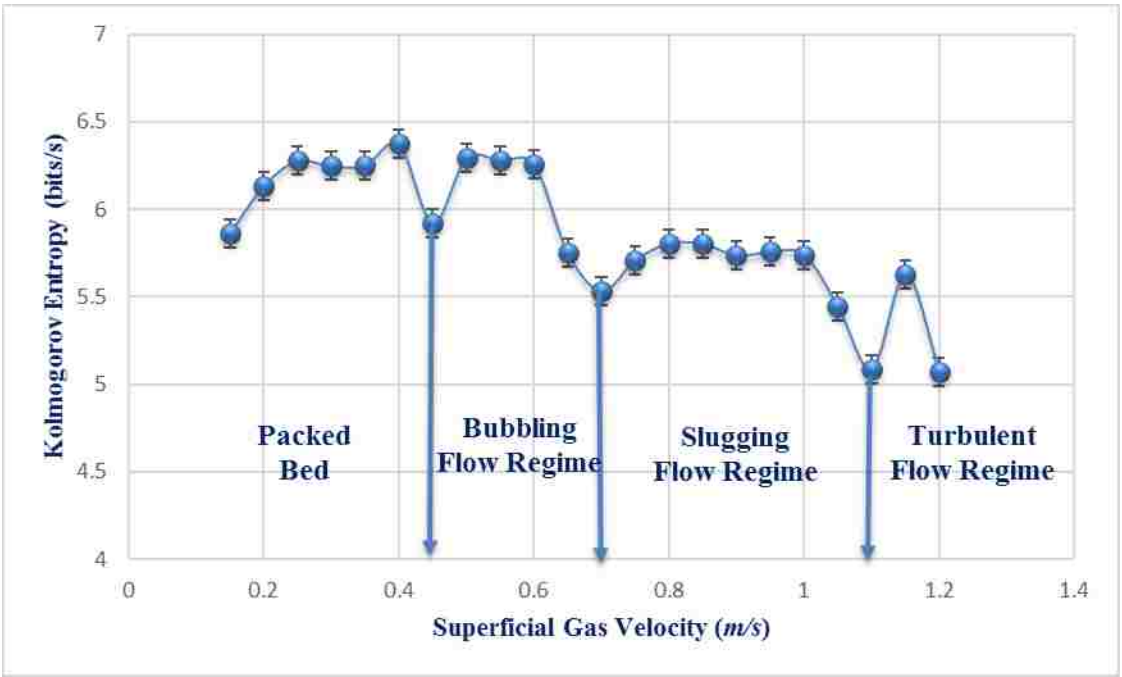

Figure 5.19. Kolmogorov entropy of pressure drop fluctuations vs. superficial gas velocity for the aluminum oxide solid particles with 0.0254 m internals.

Table 5.8. The transition velocities & the transition velocity range for each flow regime for both immersed vertical internals in aluminum oxide solid particles with the two types of data analysis.

Conditions	**0.0254 m**		**0.0127 m**	
Data analysis method	SD	KE	SD	KE
Minimum fluidized velocity U_{mf} (m/s)	0.45	0.5	0.5	0.45
Minimum slugging velocity U_{slug} (m/s)	0.85	0.8	0.7	0.7
Transition velocity U_c (m/s)	1.15	1.15	1.1	1.1
Packed bed velocity range (m/s)	≥ 0.45	≥ 0.5	≥ 0.5	≥ 0.45
Superficial gas velocity within the range of bubbling regime (m/s)	0.45-0.85	0.5-0.8	0.5-0.7	0.45-0.7
Superficial gas velocity within the range of Slugging regime (m/s)	0.85-1.15	0.8-1.15	0.7-1.1	0.7-1.1
Superficial gas velocity within the range of turbulent regime (m/s)	≤ 1.15	≤ 1.15	≤ 1.1	≤ 1.1

aluminum oxide solid particles bed using two methods of data analysis are listed in Table 5.8. The data illustrated in Table 5.8 indicate a good agreement between the two methods of analysis used to identify the values of different transition velocities for both types of vertical internals carried out inside the fluidized bed with aluminum oxide solid particles.

The transition turbulent velocity (U_c) estimated for both vertical internals has been compared with the predicted correlation of Jin et al. (1986), which was illustrated earlier (Equation 1). The experimental values of U_c for the two types of internals (0.0254 and 0.0127 m) are 1.15 m/s and 1.1 m/s, respectively. The value of predicted U_c has been found to be 0.79 m/s, which is too far from the experimental values of the U_c of both types of vertical internals. The large difference between the predicted and experimental data can be attributed to the lack of important parameters such solid particles sphericity, vertical

internals size, and vertical internals configuration in the prediction equation of Jin et al. (1986).

Table 5.9. The transition velocities & the transition velocity range for each flow regime for cases of with and without immersed vertical internals in aluminum oxide solid particles with the two types of data analysis.

Conditions	**With internals**				**Without internals**	
Vertical internals size	**0.0254 m**		**0.0127 m**		**-**	
Data analysis method	SD	KE	SD	KE	SD	KE
Minimum fluidized velocity U_{mf} (m/s)	0.45	0.5	0.5	0.45	0.4	0.4
Minimum slugging velocity U_{slug} (m/s)	0.85	0.8	0.7	0.7	0.7	0.65
Transition velocity U_c (m/s)	1.15	1.15	1.1	1.1	0.95	0.95
Packed bed velocity range (m/s)	≥ 0.45	≥ 0.5	≥ 0.5	≥ 0.45	≥ 0.4	≥ 0.4
Superficial gas velocity within the range of bubbling regime (m/s)	0.45-0.85	0.5-0.8	0.5-0.7	0.45-0.7	0.4-0.7	0.4-0.65
Superficial gas velocity within the range of slugging regime (m/s)	0.85-1.15	0.8-1.15	0.7-1.1	0.7-1.1	0.7-0.95	0.65-0.95
Superficial gas velocity within the range of turbulent regime (m/s)	≤ 1.15	≤ 1.15	≤ 1.1	≤ 1.1	≤ 0.95	≤ 0.95

The influence of the two types of vertical internals on the flow regimes and their transition velocities is represented by means of transition velocity and superficial gas velocity within the range of each flow regime as shown in Table 5.9. The data of both cases (with and without internals) of aluminum oxide solid particles are compared in Table 5.9. For vertical internals, three transition velocities (U_{mf}, U_{slug}, and U_c) have clearly increased for both types of vertical internals compared to those without internals based on

Kolmogorov entropy data. The superficial gas velocity within the range of bubbling and slugging flow regimes are almost constant for the case of 0.0254 m internals, but with a little shifting towered larger values of gas velocity; For 0.0127 m internals, the superficial gas velocity within the range of bubbling transition is constant and the superficial gas velocity within the range of slugging is increased. Accordingly, it was noticed that the 0.0254 m internals kept the superficial gas velocity within the range of slugging constant, while the 0.0127 m internals increased the superficial gas velocity within the range of slugging regime, as shown in Table 5.9. The difference in the influence of the two internals may be represented by the difference in tube size, tube-to-tube space, and tube bundle arrangements (Rüdisüli et al. 2012a).

Compared to glass beads solid particles, the change in the transition velocities and the superficial gas velocity within the range of each flow regime for the case of aluminum oxide solid particles is due to several factors, including particles shape, solid particles density, solid particles size distribution, and particles size. It has been mentioned by Yerushalmi & Cankurt (1979) that the physical properties of the solids has a considerable effect on the flow regimes and their transition velocities. Yerushalmi and Cankurt (1979) studied the impact of physical properties such as solid density, solid particles size, and solid sphericity of several solid particles on the flow regimes in circulating fluidized bed. The shape factor number was optically measured, and the inverse of the shape factor represented the sphericity of the solid particles. Consequently, they reported that the turbulent transition velocity (U_c) increases with increasing the solids density and particle size concurrently with the particle shape.

6. REMARKS

The flow regimes and their transition velocities of a 0.14 m inside diameter gas-solid fluidized bed were studied using two sizes (0.0254 and 0.0127 m) of circular configuration vertical internals in a gas-solid fluidized bed of 0.14 m inside diameter. The time series of the pressure drop fluctuation signals was analyzed using two methods of data analysis: statistical analysis (standard deviation) and state space analysis (Kolmogorov entropy). The results of the two methods for all the cases (with and without vertical internals, vertical internal sizes, and solid particle types) used in the present work were in good agreement. Two solid particles (glass beads and aluminum oxide) of various physical properties and a broad range of operating superficial gas velocities (0.15–1.2 m/s) were used to extend the knowledge of the influence of these parameters together with vertical internal arrangement designs on the identification of flow regime inside the gas–solid fluidized bed.

The key remarks that have been deduced from the findings are summarized as follows:

1) From the studying of the pressure fluctuation signals inside the bed (their mean and variance values), the 0.0254 m diameter vertical internals have been found to be more efficient in improving the fluidization inside the bed by minimizing the slugging phenomena and bed fluctuations and makes the fluidization behave more smoothly.
2) Both types of vertical internals reduce the slugging behavior and its fluidization velocity range and lowered the transition velocity (U_c) as well as increase the superficial gas velocity within the range of bubbling flow regime for the case of glass beads solid particles.

3) For aluminum oxide solid particles, the implementation of the two types of vertical internals has an opposite effect on the good hydrodynamic behavior of the glass beads solid particles. In which, the range of superficial gas velocity within the bubbling flow regime has been reduced and increased for that of slugging flow regime. The transition velocity from slugging to turbulent flow regime was occurred at higher superficial gas velocity for both types of internals.

ACKNOWLEDGEMENTS

The authors would like to thank the multiphase reactors engineering and applications laboratory (mReal) for funding and support.

NOMENCLATURE

d_p	particle mean diameter or average particle diameter (μm)
ρ_p	solid particle density or solid density (Kg/m^3)
U_{mb}	minimum bubbling velocity (m/s)
U_{mf}	minimum fluidization velocity (m/s)
U_{slug}	minimum slugging velocity (m/s)
U_c	transition velocity or turbulent transition velocity (m/s)
g	acceleration gravity (m/s^2)
ρ_f	fluid density (Kg/m^3)
Re_{mf}	Reynolds number of solid particle at minimum fluidized velocity (U_{mf})
Re_c	Reynolds number of solid particles at transition fluidized velocity (U_c)
Ar	Archimedes number of the solid particles

Greek Letters

ρ	density (Kg/m^3)
φ	sphericity factor

Subscripts and Superscripts

c	minimum turbulent fluidization
mb	minimum bubbling
mf	minimum fluidization
p	particle
f	fluid
slug	minimum slugging

Abbreviations

FCC	fluid catalytic cracking
ID	inside diameter
KE	Kolmogorov entropy
SD	standard deviation

REFERENCES

A. Pinto. 1978. Ammonia Production Process, issued 1978.

Andreux, R., T. Gauthier, J. Chaouki, and O. Simonin. 2005. "New Description of Fluidization Regimes." *AIChE Journal* 51 (4): 1125–30. doi:10.1002/aic.10380.

Arnaldos, Josep, and Joaquim Casal. 1996. "Prediction of Transition Velocities and Hydrodynamical Regimes in Fluidized Beds." *Powder Technology* 86 (3): 285–98. doi:10.1016/0032-5910(95)03054-9.

Bai, D., a. S. Issangya, and J. R. Grace. 1999. "Characteristics of Gas-Fluidized Beds in Different Flow Regimes." *Industrial & Engineering Chemistry Research* 38 (3): 803–11. doi:10.1021/ie9803873.

Bai, D., E. Shibuya, N. Nakagawa, and K. Kato. 1996. "Characterization of Gas Fluidization Regimes Using Pressure Fluctuations." *Powder Technology* 87 (2): 105–11. doi:10.1016/0032-5910(95)03072-7.

Bartholomew, Calvin H., and Robert J. Farrauto. 2010. *Fundamentals of Industrial Catalytic Processes: Second Edition*. *Fundamentals of Industrial Catalytic Processes: Second Edition*. doi:10.1002/9780471730071.

Bi, H. T., and J. R. Grace. 1995. "Flow Regime Diagrams for Gas-Solid Fluidization and Upward Transport." *Int. J. Multiphase Flow* 21 (6): 1229–36.

Geldart, D. 1973. "Types of Gas Fluidization." *Powder Technology* 7 (5): 285–92. doi:10.1016/0032-5910(73)80037-3.

Grace, J. R., and D. Harrison. 1968. "The Effect of Internal Baffles in Fluidized Beds: A Guide to Design." In *Inst. Chem. Eng. Symp. Ser.*

Jin, Yong, Zhiqing Yu, Zhanweng Wang, and Ping Cai. 1986. "A Criterion for Transition from Bubbling to Turbulent Fluidization." In *Fluidization 5*, 289–96.

Johnsson, F., R. C. Zijerveld, J. C. Schouten, C. M. Van den Bleek, and B. Leckner. 2000. "Characterization of Fluidization Regimes by Time-Series Analysis of Pressure Fluctuations." *International Journal of Multiphase Flow* 26 (4): 663–715. doi:10.1016/S0301-9322(99)00028-2.

Kuwagi, Kenya, Atsuto Kogane, Hiroyuki Hirano, Azri Bin Alias, and Toshihiro Takami. 2014. "Non-Dimensionalization and Three-Dimensional Flow Regime Map for Fluidization Analyses." *Chemical Engineering Science* 119. Elsevier: 199–211. doi:10.1016/j.ces.2014.08.006.

Law, Chung Lim, Siti Masrinda Tasirin, Wan Ramli Wan Daud, and Derek Geldart. 2003. "Effect of Vertical Baffles on Particle Mixing and Drying in Fluidized Beds of Group D Particles." *China Particuology* 1 (3): 115–18. doi:10.1016/S1672-2515(07)60121-3.

Lim, K.S., J. X. Zhu, and J. R. Grace. 1995. "Hydrodynamics of Gas-Solid Fluidization." *Int. J. Multiphase Flow* 21: 141–93.

Makkawi, Y. T., and P. C. Wright. 2002. "Fluidization Regimes in a Conventional Fluidized Bed Characterized by Means of Electrical Capacitance Tomography." *Chemical Engineering Science* 57 (13): 2411–37. doi:10.1016/S0009-2509(02)00138-0.

Mathew, Ronnie Kiran, K. M Meera Sheriffa Begum, and N. Anantharaman. 2014. "Hydrodynamic Studies on Fluidized Beds with Internals: Experimental and ANN Approach." *Powder Technology* 264. Elsevier B.V.: 423–29. doi:10.1016/j.powtec.2014.06.001.

Nedeltchev, Stoyan. 2015. "New Methods for Flow Regime Identification in Bubble Columns and Fluidized Beds." *Chemical Engineering Science* 137. Elsevier: 436–46. doi:10.1016/j.ces.2015.06.054.

Nedeltchev, Stoyan, Fadha Ahmed, and Muthanna Al-Dahhan. 2012. "A New Method for Flow Regime Identification in a Fluidized Bed Based on Gamma-Ray Densitometry and Information Entropy." *Journal of Chemical Engineering of Japan* 45 (3): 197–205. doi:10.1252/jcej.11we189.

Nedeltchev, Stoyan, Shreekanta Aradhya, Faraj Zaid, and Muthanna Al-Dahhan. 2012. "Flow Regime Identification in Three Multiphase Reactors Based on Kolmogorov Entropies Derived from Gauge Pressure Fluctuations." *Journal of Chemical Engineering of Japan* 45 (9): 757–64. doi:10.1252/jcej.12we075.

Olowson, P.A. 1994. "Influence of Pressure and Fluidization Velocity on the Hydrodynamics of a Fluidized Bed Containing Horizontal Tubes." *Chemical Engineering Science* 49 (15): 2437–46.

Olsson, S. E., J. Wiman, and A. E. Almstedt. 1995. "Hydrodynamics of a Pressurized Fluidized Bed with Horizontal Tubes: Influence of Pressure, Fluidization Velocity and Tube Bank Geometry." *Chemical Engineering Science* 50 (4): 581–92.

Qiu, Guizhi, Jiamin Ye, Haigang Wang, and Wuqiang Yang. 2014. "Investigation of Flow Hydrodynamics and Regime Transition in a Gas-Solids Fluidized Bed with Different Riser Diameters." *Chemical Engineering Science* 116. Elsevier: 195–207. doi:10.1016/j.ces.2014.05.006.

Ramamoorthy, S., and N. Subramanian. 1981. “Axial Solids Mixing and Bubble Characteristics in Gas-Fluidized Beds with Vertical Internals.” *Chemical Engineering Journal* 22 (3): 237–42.

Rhodes, M. J. 1989. “The Upward Flow of Gas/solid Suspensions. II: A Practical Quantitative Flow Regime Diagram for the Upward Flow of Gas/solid.” *Chemical Engineering Research and Design* 67 (1): 30–37.

Rüdisüli, Martin, Tilman J. Schildhauer, Serge M. A. Biollaz, and J. Ruud Van Ommen. 2012a. “Radial Bubble Distribution in a Fluidized Bed with Vertical Tubes.” *Industrial and Engineering Chemistry Research* 51 (42): 13815–24. doi:10.1021/ie3004418.

Rüdisüli, Martin, Tilman J Schildhauer, Serge M A Biollaz, and J. Ruud Van Ommen. 2012b. “Bubble Characterization in a Fluidized Bed with Vertical Tubes.” *Industrial and Engineering Chemistry Research* 51 (12): 4748–58. doi:10.1021/ie2022306.

Saayman, Jean, Willie Nicol, J. Ruud Van Ommen, and Robert F. Mudde. 2013. “Fast X-Ray Tomography for the Quantification of the Bubbling-, Turbulent- and Fast Fluidization-Flow Regimes and Void Structures.” *Chemical Engineering Journal* 234. Elsevier B.V.: 437–47. doi:10.1016/j.cej.2013.09.008.

Schouten, Jaap C., Floris Takens, and Cor M. Van Den Bleek. 1994. “Maximum-Likelihood Estimation of the Entropy of an Attractor.” *Physical Review E* 49 (1): 126–29. doi:10.1103/PhysRevE.49.126.

Shaul, Semion, Evgeny Rabinovich, and Haim Kalman. 2012. “Generalized Flow Regime Diagram of Fluidized Beds Based on the Height to Bed Diameter Ratio.” *Powder Technology* 228. Elsevier B.V.: 264–71. doi:10.1016/j.powtec.2012.05.029.

Smolders, K., and J. Baeyens. 2001. “Gas Fluidized Beds Operating at High Velocities: A Critical Review of Occurring Regimes.” *Powder Technology* 119 (2–3): 269–91. doi:10.1016/S0032-5910(01)00267-4.

Tayebi, Davoud, Hallvard F Svendsen, Arne Grislinga, Thor Mejdell, and Kjetil Johannessen. 1999. “Dynamics of Fluidized-Bed Reactors . Development and Application of a New Multi- Fiber Optical Probe.” *Chemical Engineering Science* 54: 2113–22.

Tijm, P. J A, F. J. Waller, and D. M. Brown. 2001. “Methanol Technology Developments for the New Millennium.” *Applied Catalysis A: General* 221 (1–2): 275–82. doi:10.1016/S0926-860X(01)00805-5.

Toukan, A., V. Alexander, H. AlBazzaz, and M.H. Al-Dahhan. 2017. “Identification of Flow Regime in a Cocurrent Gas – Liquid Upflow Moving Packed Bed Reactor Using Gamma Ray Densitometry.” *Chemical Engineering Science* 168. Elsevier Ltd: 380–90. doi:10.1016/j.ces.2017.04.028.

Trnka, O, V Vesely, M Hartman, and Z Beran. 2000. “Identification of the State of a Fluidized Bed by Pressure Fluctuations.” *AIChE Journal* 46 (3): 509–14. doi:10.1002/aic.690460309.

Van Ommen, J. Ruud, Srdjan Sasic, John Van der Schaaf, Stefan Gheorghiu, Filip Johnsson, and Marc Olivier Coppens. 2011. “Time-Series Analysis of Pressure Fluctuations in Gas-Solid Fluidized Beds - A Review.” *International Journal of Multiphase Flow* 37 (5). Elsevier Ltd: 403–28. doi:10.1016/j.ijmultiphaseflow.2010.12.007.

Volk, W., C. A. Johnson, and H. H. Stotler. 1962. “Effect of Reactor Internals on Quality of Fluidization.” *Chemical Engineering Progress* 58 (3): 44–47.

Yang, Wen-Ching. 2003. *Handbook of Fluidization and Fluid-Particle Systems*. *Chemical Engineering*. doi:10.1016/S1672-2515(07)60126-2.

Yerushalmi, J., and N. T. Cankurt. 1979. “Further Studies of the Regimes of Fluidization.” *Powder Technology* 24 (2): 187–205. doi:10.1016/0032-5910(79)87036-9.

Yerushalmi, J., N. T. Cankurt, D. Geldart, and B. Liss. 1978. “Flow Regimes in Vertical Gas-Solid Contact Systems.” In *Fluidization CONF-761109-8*. New York (USA); Bradford Univ.(UK); Coalcon, New York (USA).

Zijerveld, Robert C., Filip Johnsson, Antonio Marzocchella, Jaap C. Schouten, and Cor M. Van Den Bleek. 1998. “Fluidization Regimes and Transitions from Fixed Bed to Dilute Transport Flow.” *Powder Technology* 95 (3): 185–204. doi:10.1016/S0032-5910(97)03336-6.

IV. EFFECT OF VERTICAL INTERNALS ON THE PRESSURE DROP IN GAS–SOLID FLUIDIZED

Haidar Taofeeq[1] and Muthanna Al-Dahhan[2*]

Multiphase Reactors Engineering and Applications Laboratory (mReal)
Department of Chemical & Biochemical Engineering
Missouri University of Science & Technology, Rolla, MO-65409 USA

ABSTRACT

In this work, the pressure drop at the wall and radial profiles of pressure drop along the bed height have been measured using a differential pressure transducer and pressure probe-differential pressure transducer in the a gas–solid fluidized bed with a 0.14 m inside diameter. Two types of circular arrangements of intense vertical internals (0.0254 m and 0.0127 m diameter), two kinds of solid particles of Geldart B type (glass beads and aluminum oxide), and four selected superficial gas velocities in terms of u/u_{mf} have been used to study the impact of these different design as well as the physical and operating variables on the pressure drop measured at the wall of the bed and the radial pressure drop inside the fluidized bed. It has been experimentally demonstrated that the 0.0254 m internals can reduce the pressure drop at the wall and the radial pressure drop inside the bed by about 10% when compared to without internals, and this result holds true for both kinds of solids used. However, the implementation of 0.0127 m internals inside the gas–solid fluidized bed leads to a decrease in the pressure drop and radial pressure drop in the case of glass beads solid particles and an increase in the pressure drop in the case of aluminum oxide solid particles. The experimental results in the form of relevant dimensionless groups have been correlated using JMP 12 due to the big difference between

the experimental results of this work and the predicted values from the available correlations in the literature. The new correlation have been developed with a good mean relative deviation value of 1.08% between the experimental and predicted values.

Keywords: Pressure drop, Vertical internals, Pressure probe, Pressure transducer, Gas–solid fluidized bed.

* Corresponding Author: aldahhanm@mst.edu

1. INTRODUCTION

Gas–solid fluidized beds have been widely utilized in many industrial applications, such as drying of solids, combustion, fluid catalytic reactions, gasification, coating, and many other processes (Mohanty et al. 2009). They possess several advantages: (1) Good gas–solid particles mixing, which leads to high contact efficiency between gas and solid phases. This characteristic is substantial especially in the case of gas–solid catalyzed reactions to obtain high catalyst utilization, drying, and coating, (2) Good local temperature distribution and high heat transfer rate. These excellent thermal properties are essential in the chemical processes where highly exothermic or endothermic reactions are involved, because they improve the reaction yield and better control the reaction temperature, and (3) The particle size used is much smaller than that which is used in fixed-bed systems yielding larger catalyst effectiveness factors and larger surface areas for a high mass transfer. Additionally, the transportation of the solid particles to or from the reaction bed is considered more accessible, particularly in the systems that used short-time active catalyst (Padhi, Singh, and Agrawal 2010).

Despite all the advantages mentioned above, the efficiency and operation of gas–solid fluidized beds still suffer from many inherent drawbacks like bubbling, channeling, and slugging (Kar and Roy 2000; Sau, Mohanty, and Biswal 2008a; Mathew, Begum, and Anantharaman 2014). These drawbacks would result in a poor homogeneity between the gas and solid phases, which would then lower the efficiency of heat and mass transfer rates and reduce the overall fluidization quality (Krishnamurty et al. 1981; Kumar and Roy 2002; Sau, Mohanty, and Biswal 2008b). Specifically, the formation of bubbles and slugs can

increase the bed expansion, pressure drop, and fluctuations of the bed (Mathew, Begum, and Anantharaman 2014).

Various methods have been used to overcome the drawbacks of the gas–solid fluidized beds, and these include using a secondary fluidizing medium (Mohanty et al. 2009), implementing mechanical stirrers promoters (Abanti Sahoo 2011) and baffled promoters (Krishnamurty et al. 1981; Kaza 2008), operating in multistage units (Sau, Mohanty, and Biswal 2008a), vibration of the bed and modification in bed geometry (Sau, Mohanty, and Biswal 2008a; Sau, Mohanty, and Biswal 2008b), and using different types and configurations of internals (Ramamoorthy and Subramanian 1981; Mathew, Begum, and Anantharaman 2014). Among all of the above, various kinds of methods are used to enhance the fluidization quality and to minimize the problems associated with the operating of the gas–solid fluidized beds. Among these methods is the usage of internals with different configurations to enhance the fluidization quality and the reduction of pressure drop, bed expansion, and fluctuations of the bed, as well as providing the improvement of the gas–solid mixing inside the bed (Mathew, Begum, and Anantharaman 2014). Furthermore, for exothermic and endothermic reactions where the temperature needs to be controlled, vertical internals are used as heat exchange tubes. It has been proven by many researchers that the implementation of various internal surfaces in the fluidized beds can control the size of bubbles by splitting and breaking them up, as well as by reducing the coalescence phenomenon between the small bubbles, which leads to minimizing the slugging behavior inside the bed (Volk, Johnson, and Stotler 1962; Grace and Harrison 1968). The internals can also reduce the cross-circulation of solid patterns and make the fluidization smoother (Olowson 1994). Additionally, the internal surfaces can reduce

channeling and improve the heat and mass transfer rates (Ramamoorthy and Subramanian 1981; Mathew, Begum, and Anantharaman 2014).

Pressure drop in fluidized beds is an important hydrodynamic parameter for design, scaleup, and operation (A. Sahoo and Roy 2005; Kaza 2008; Mathew et al., 2014). It indicates any malfunctioning if it happens during operation. Effects of different types, configurations, and orientations of internal surfaces on pressure drop were investigated in conventional gas–solid fluidized beds. Table 1.1 summarizes the studies related to the effect of different types and arrangements of internals, promoters, and baffles on the pressure drop inside different sizes and configurations of gas–solid fluidized bed vessels. As listed in Table 1.1, several kinds of internals have been implemented, and these include vertical and horizontal rods with baffles (Krishnamurty et al. 1981), vertical wires and coils (Ramamoorthy and Subramanian 1981), different shapes of co-axial promoters (rods, blades, and discs) (Kar and Roy 2000; Kumar and Roy 2002; A. Sahoo and Roy 2005), vertical rods with different baffle configurations (circular, squared, and triangular) (Kaza 2008), vertical twisted baffles (Padhi, Singh, and Agrawal 2010), mechanically stirred promoters (Abanti Sahoo 2011), and vertical internal rods (Rüdisüli, Schildhauer, Biollaz, and Van Ommen 2012a; Mathew, Begum, and Anantharaman 2014).

Among all of the kinds of internal surfaces mentioned above, many researchers have reported that the vertical internal tubes are considered the most important type of internals, especially, when the configuration is a circular cross section (Kaza 2008). This importance is due to the many advantages that come with the use of these types of internals, such as reduction of bubble size, simplicity of the design, easy to installstion and removal, elimination of the dead zones, less tube erosion, reduction of pressure drop, limitation of

Table 1.1: Summery of the studies of the effect of different types and configurations of internals on the pressure drop in gas–solid fluidized beds

Year	Author	Internals Configuration and Orientations	Internals Types	Internals size	Materials of Internals	Solid Material	Particle Diameter (d_p)	Particle Density (ρ_p)	Measuring System & Vessel Size
1981	Krishna murty et al.	Vertical and horizontal rods with different types of baffles	Vertical & horizontal rods	3 mm 5 mm 12.5 mm	Mild steel	Glass beads Ilmenite	851 µm 486 µm	2600 kg/m^3 4200 kg/m^3	Fluidized bed column of 7.62 cm ID
1999	Kar and Roy	Co-axial promoters	-Vertical rods -Vertical discs	0.6 cm 4.4 cm	-	Coal Coal+Dolomite Sand Dolomite Manganese	925 µm 780 µm 605 µm 428 µm -	1430 kg/m^3 1950 kg/m^3 2610 kg/m^3 2760 kg/m^3 4836 kg/m^3	Batch fluidized bed
2002	Kumar and Roy	Co-axial promoters	-Vertical rods -Vertical blades	0.6 cm 4.4 cm	-	Coal+Dolomite Sand Dolomite Manganese	925 µm 780 µm 605 µm 428 µm	1950 kg/m^3 2610 kg/m^3 2760 kg/m^3 4836 kg/m^3	Fluidized bed column of 5.0 cm ID
2005	Sahoo and Roy	Co-axial promoters	Vertical discs	4.4 cm	-	Glass beads	1.7 mm 1.125 mm 0.725 mm 0.55 mm	2860 kg/m^3 2250 kg/m^3 1528 kg/m^3	Squared fluidized bed (0.83 m x 0.83 m)
2008	Kaza	Vertical rods with circular, squared and triangular baffles	Vertical rods	12 mm	Copper	Sand	930 µm	2520 kg/m^3	Squared fluidized bed (0.9 m x 0.9 m)

Table 1.1: Summery of the studies of the effect of different types and configurations of internals on the pressure drop in gas–solid fluidized beds (cont.)

2010	Padhi et al.	Vertical baffles	Vertical twisted tape	Different sizes	-	Dolomite	0.605 mm	-	Fluidized bed column of 5.0 cm ID
2011	Shaoo	Vertical Stirrers	- Vertical discs -Vertical rods	-10 cm (disc) -6.25 cm (rod) -6.25 cm central rod	-	Dolomite Iron particle	2.40 mm 1.85 mm 1.55 mm 1.29 mm	2940 kg/m^3 4760 kg/m^3	Fluidized bed column of 14 cm ID
2014	Mathe w et al.	Vertical Internals	Vertical rods	2 mm		Raagi	1.708 mm	1172 kg/m^3	Fluidized bed columns of (25.4, 38.1 and 50.8) mm ID

the channeling and slugging, and improvement of the heat transfer efficiency (Volk, Johnson, and Stotler 1962; Grace and Harrison 1968; Rüdisüli, Schildhauer, Biollaz, and Van Ommen 2012c).

In the literature the pressure drops were measured using manometers (Krishnamurty et al. 1981; Kar and Roy 2000; Kumar and Roy 2002; A. Sahoo and Roy 2005; Kaza 2008; Padhi, Singh, and Agrawal 2010). The weakness of this type of measurement is not accurate to indicate the mean level at each level particularly when there are high pressure fluctuations inside the bed as well as the pressure fluctuations cannot be recorded. Additionally, they didn't use intense vertical internals that represented the needs of vertical internals for high exothermic reaction where intense heat exchanging surfaces are required to control the reaction temperature inside the gas-solid fluidized beds (A. Pinto 1978; Tijm, Waller, and Brown 2001; Bartholomew and Farrauto 2010). Hence, there is no work has been done to measure the pressure drop at the wall of gas-solid fluidized bed with intense vertical internals or at different radial profiles along the bed height using pressure probe-differential pressure transducer. Therefore, there is a need to use a technique that can provide a detailed knowledge about the hydrodynamic behavior inside the gas-solid fluidized bed such as pressure transducer which considered as best choice for these requirements. As well, develop a pressure probe that connected to the differential pressure transducer to measure the radial profiles of pressure drop along the bed height since the using of pressure probe has been done in the literature works just for measuring the gauge/dynamic pressure inside the bed (Xie and Geldart 1997; Van Ommen et al. 1999). Additionally, the configuration of the vertical internals should mimic the type of intense internals used in the chemical processes that implement the gas-solid fluidized bed

reactor with high exothermic reaction such as Ammonia synthesis, methanol production, and other catalytic processes (A. Pinto 1978; Tijm, Waller, and Brown 2001; Bartholomew and Farrauto 2010).

The hydrodynamics behavior of the fluidized beds with vertical internals is very complicated due to the complex interactions between solid particles (catalyst particles) and their contacts with the surroundings (gas phase in the form of bubbles, vertical internal surfaces, and the wall of the column). Unfortunately, the flow structures of the fluidized bed with vertical internals are still not well understood, and therefore the proper understanding of flow patterns and hydrodynamics is an important task in the design, scale-up, and operation of gas–solid fluidized beds with vertical internals. In the meantime, the experimental data available in the literature that study the effect of the vertical internals on pressure drop are rare. The knowledge of pressure drop in gas–solid fluidized beds is considered crucial and plays a role in the design, especially in the computation of bed height (Mohanty et al. 2009), and energy required for gas phase pumping and circulation. Various correlations have been developded and reported in the literature to correlate the pressure drop in gas-solid fluidized beds with different operating, design, and physical parameters for the case of with and without immersed surfaces (Kar and Roy 2000; Padhi et al., 2010; Mathew et al., 2014).

Accordingly, the present work focuses on studying the pressure drop measured at the wall and the radial pressure drop along the bed height and its fluctuations inside the gas–solid fluidized bed using differential pressure transducer. Different powder types of Geldart B that have various solid particle densities were used. This study also examines the effect of two different sizes of circular-configuration of vertical internals on the

pressure drop and radial profiles of the pressure drop inside a gas–solid fluidized bed. The measuremnts of pressure drop along the bed height at different radial positions have been performed to examine if there is any channaling or maldistribution inside the bed for both cases of with and without internals. The predictions of selected pressure drop correlations have been evaluated using our data and a new correlation has been developed.

2. EXPERIMENTAL SETUP

The experimental setup consists of a fluidized bed column with a 0.14 m inside diameter and 1.84 m height. The column was made from Plexiglas, and the plenum was manufactured from rigid aluminum metal. The column and the plenum were positioned on top of a stainless-steel base. Compressed air was supplied by compressors operated at pressures up to 1.38 MPa. The Omega-type flow meters were used to control the flow rate of the inlet gas to the plenum section. A schematic diagram of the fluidized bed column with vertical internals is illustrated in Figure 2.1. The gas phase was introduced through a sparger tube in the plenum and then through a distributor plate, which was placed between the fluidized bed column and the plenum section. The gas distributor plate was made of a porous polyethylene sheet and had a pore size of 15–40 μm. The sparger tube was plugged at one end and had fourteen holes along its length, all facing downward with respect to the fluidized bed column, which opposite to the gas flow direction to make the gas distribution more homogenous. The column was electrically grounded in order to minimize electrostatic effects. A rigid metallic structure was used to support the column and eliminate the mechanical vibrations, as shown in the photo of the column that is presented in Figure 2.2.

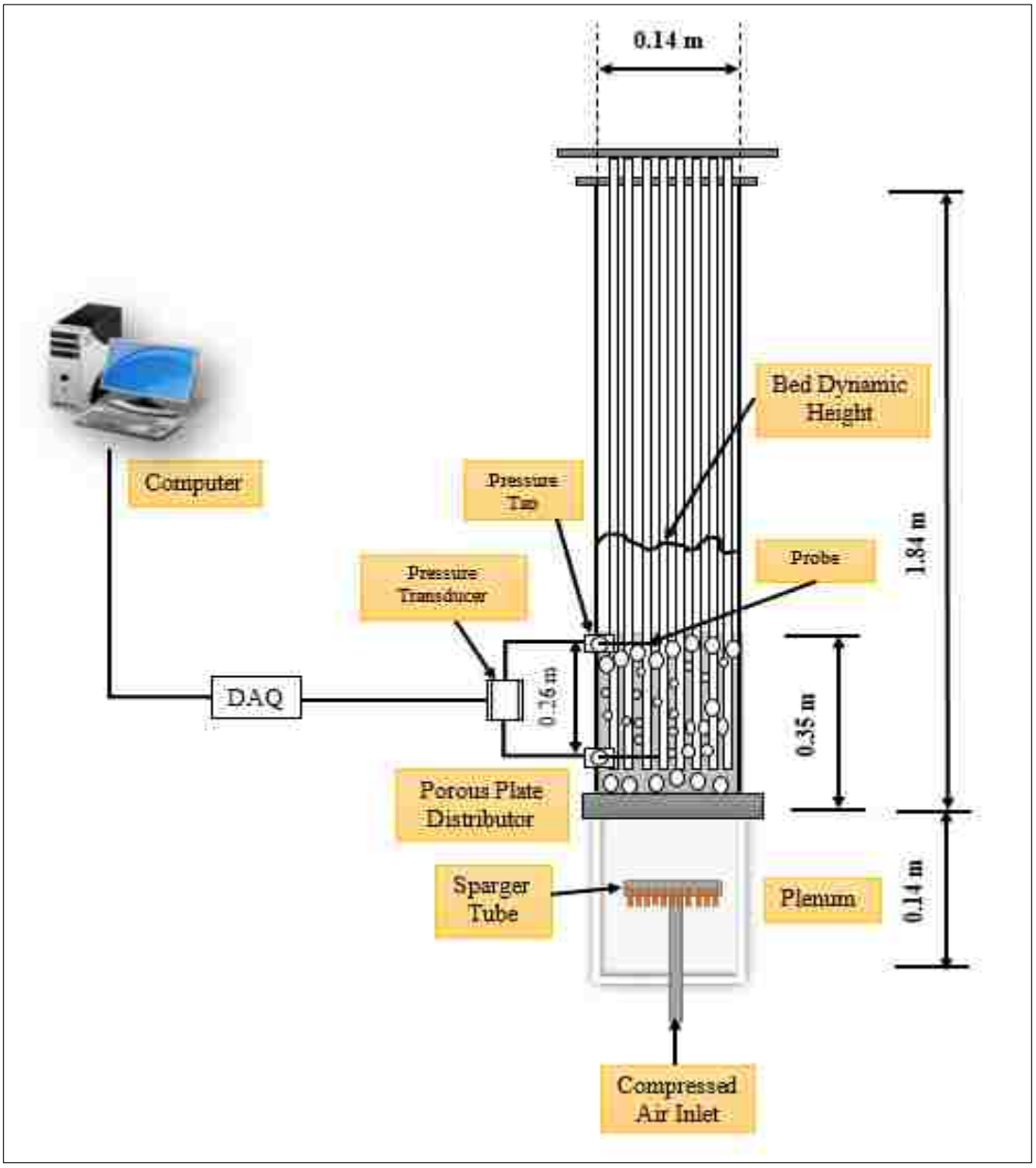

Figure 2.1. Schematic diagram of 0.14 m inside diameter fluidized bed column with vertical internals used in present work.

In the current study, two different diameters of 0.0127 and 0.0254 m of a circular shape configurations of the internals have been used. The schematic diagrams with dimensions of the internal supports are shown in Figures 2.3 and 2.4. The circular arrangement features uniformly distributed internals over the cross-sectional area of the

fluidized bed column. This circular configuration of the internals was constructed to maintain equal spacing between the internals and the wall of the fluidized bed column. The photos of the internal configurations and their supports are shown in Figures 2.5 and 2.6. The arrangement of the 0.0127 m internals consisted of 30 Plexiglas vertical internals with 1.84 m heights while the arrangement of the 0.0254 m internals consisted of 8 Plexiglas vertical internals. Both configurations covered %25 of the column cross-sectional area. These intense internals have been used to represent the need for high exothermic reaction where intense heat exchanging surfaces are required to control the reaction temperature in order to keep the operating fluidized bed reactor under the desired operation conditions and to control the reaction rate of the operating process. It is worth to mention that most of the

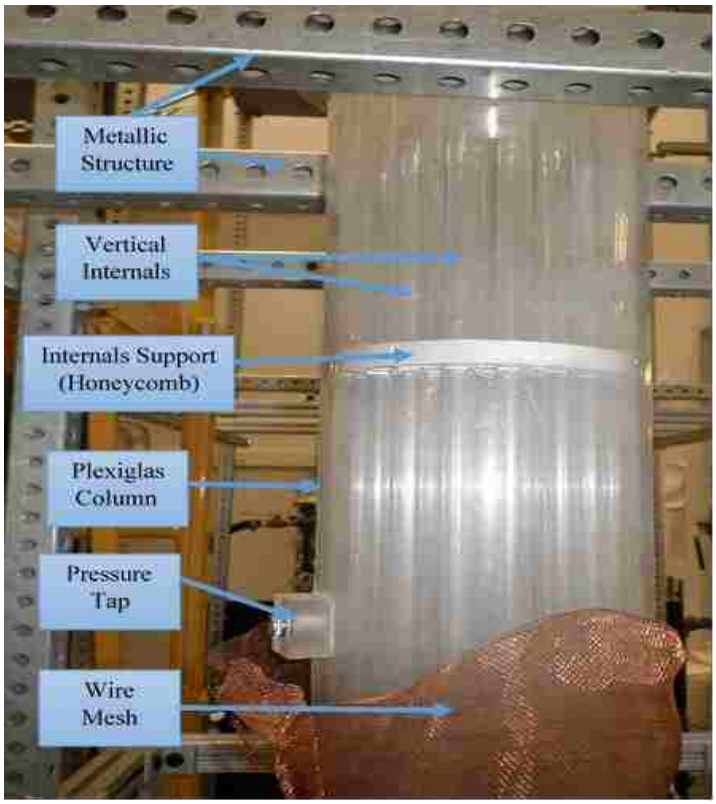

Figure 2.2. Photo for the fluidized-bed column with internals.

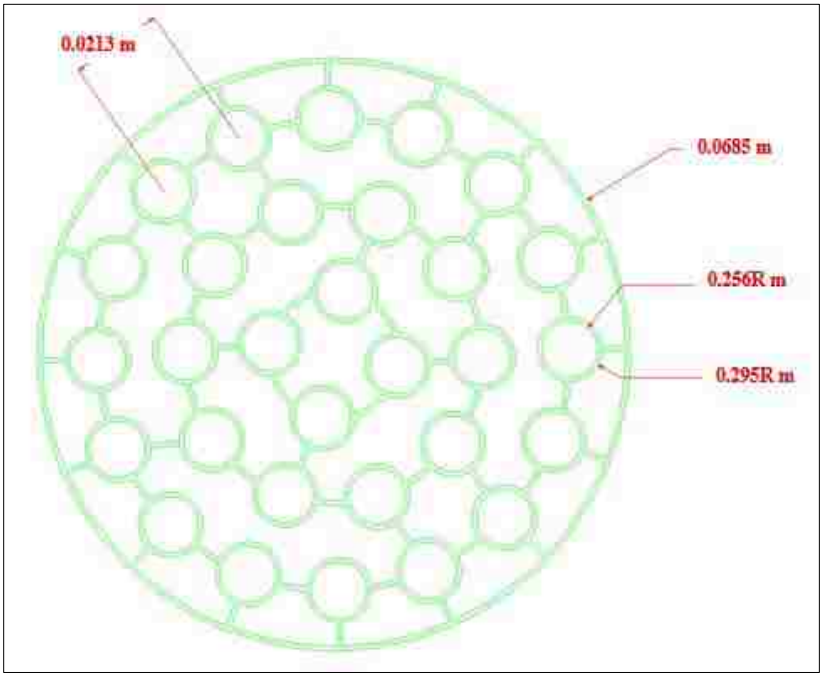

(a)

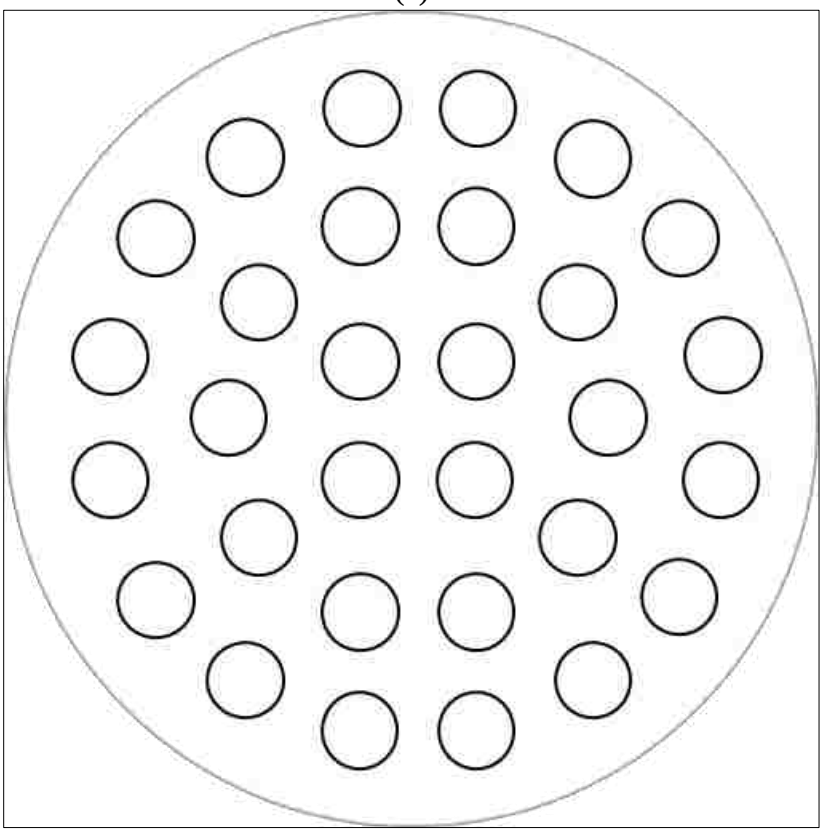

(b)

Figure 2.3. (a) Schematic of 0.0127 m internals support (honey comb), all the dimensions in meter, (b) the arrangement of the 0.0127 m internals.

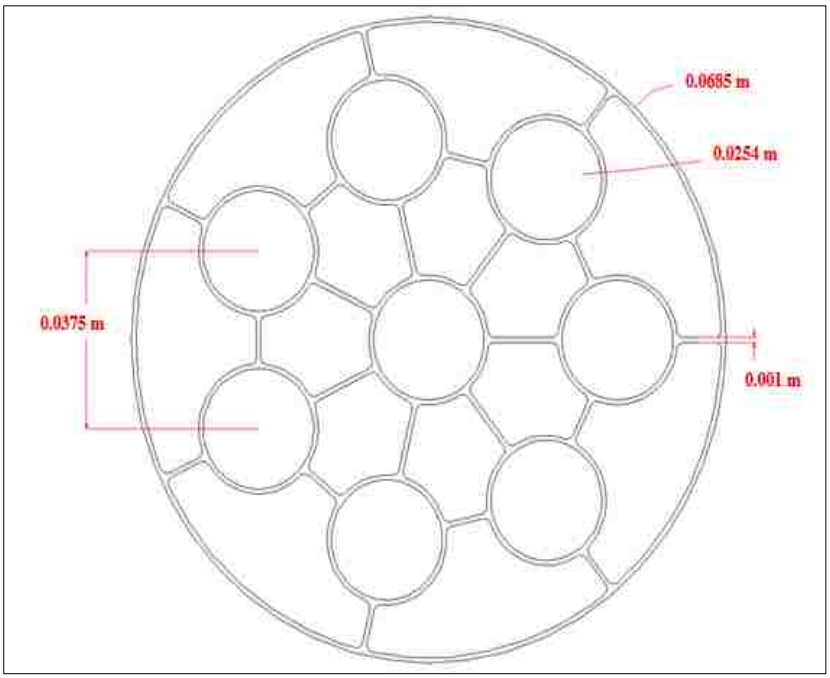

(a)

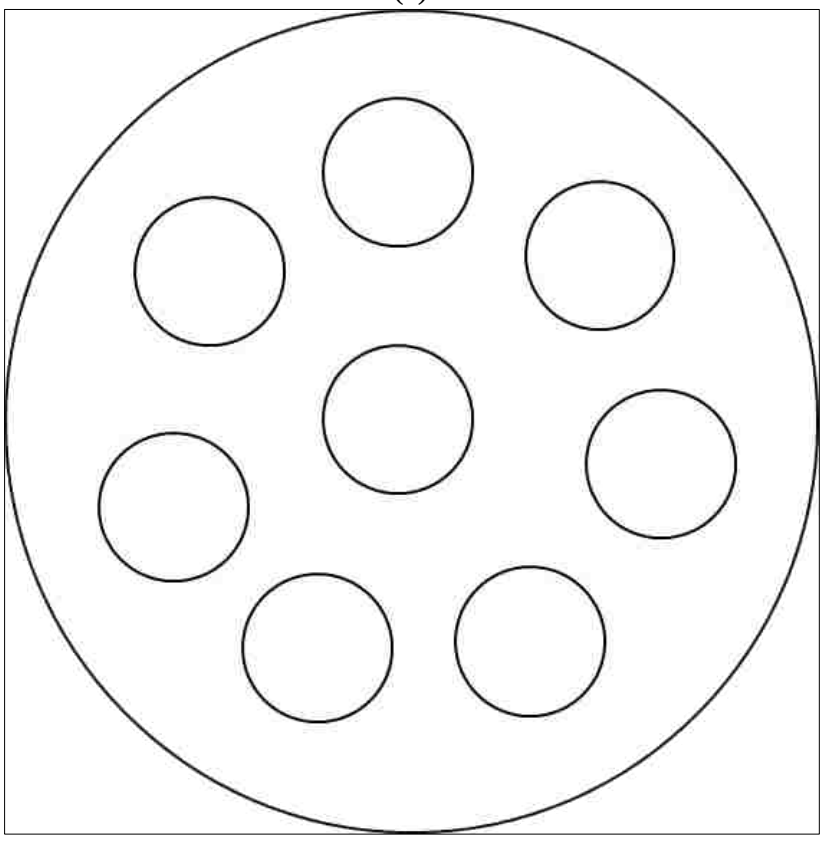

(b)

Figure 2.4. (a) Schematic of 0.0254 m internals support (honey comb), all the dimensions in meter, (b) the arrangement of the 0.0254 m internals.

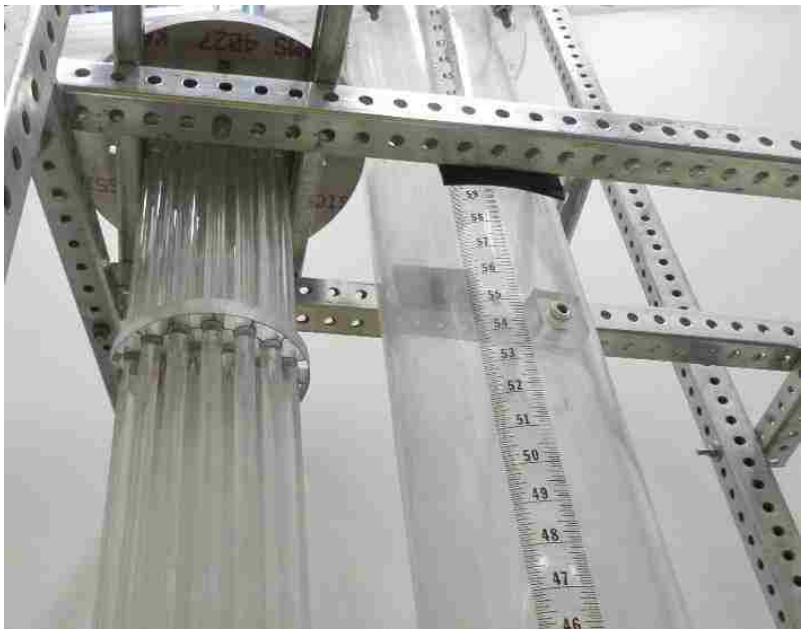

Figure 2.5. Photo of 0.0127 m vertical internals and its support.

Figure 2.6. Photo of 0.0254 m vertical internals and its support.

vertical immersed surfaces used in the literature have percentage cross-sectional range from 21% to 26% (Volk, Johnson, and Stotler 1962; Grace and Harrison 1968; Rüdisüli, Schildhauer, Biollaz, and Van Ommen 2012c; Maurer, Wagner, Schildhauer, et al. 2015). The internals were secured in the column by using four supports (honeycombs), which also minimized internal vibration during the experiments. The distance between the distributor plate and the lower end of vertical internals was 0.09 m.

The experiments were conducted at the u/u_{mf} of 1.6, 1.78, 1.96, and 2.14, the u_{mf} for each condition (whether with or without internals) depends on the type of solid particles used, and u is the superficial gas velocity that is adjusted to obtain these ratios based on the free cross-sectional are for the gas to flow. In order to compare the experimental results between the cases with and without internals, as well as with different particles types, the ratio of u/u_{mf} has been maintained hydrodynamically similar. Consequently, the superficial gas velocity of the column without internals was estimated based on the cross-sectional area of the column when it was not occupied with internals. In the case of internals, the superficial gas velocity was calculated based on the free cross-sectional area available for the flow, which represented 75% of the cross-sectional area of the column.

The solid particles used in this work were glass beads of 365 μm average particle size and 2500 Kg/m^3 density and aluminum oxide particles of 355 μm average particle size and 3900 Kg/m^3 density. Both solid particles are of Geldart B type since these types of solid particles were used in many industrial processes such as chemical, food processing, drying processes and others. The static bed height for both types of solid particles was 0.35 m. The minimum fluidization velocities in the case of with and without vertical internals were estimated from the data of the pressure drop versus different superficial gas, in which

the measured pressure drop is gradually increased with increasing the superficial gas velocity until it reaches the maximum value and then start to be constant with increasing the superficial gas velocity. The superficial gas velocity at the maximum value of the pressure drop is represents the minimum fluidization velocity. More details about the physical properties of solid particles used and the minimum fluidization velocity for each condition are illustrated in Table 2.1.

Table 2.1. Physical properties of different solid particles and the minimum fluidization velocities with and without internals for each solid particle.

Conditions	**Glass Beads**	**Aluminum Oxide**
Particles mean diameter (μm)	365	356
Particle density (Kg/m^3)	2500	3900
Static bed height (m)	0.35	0.35
Particles sphericity (φ)	0.9	0.74
Particle size distribution (μm)	300-430	241-559
Minimum fluidized velocity without internals (m/s)	0.4	0.5
Minimum fluidized velocity with 0.0254 m internals (m/s)	0.4	0.53
Minimum fluidized velocity with 0.0127 m internals (m/s)	0.4	0.53

3. EXPERIMENTAL TECHNIQUE

3.1. DIFFERENTIAL PRESSURE TRANSDUCER

A differential pressure transducer, Omega Inc. model PX-409-015DDUV, was used to measure the pressure fluctuation signals and the pressure drop at the wall of the fluidized bed. The measured differential pressures ranging from 0 to 102 kPa. The pressure

transducer was connected to a DC power supply that provided a voltage proportional to the measured differential pressure along the bed. The signals were received by the data acquisition (DAQ) system from Omega Inc., model OMB-DAQ-3000, which has the high-speed capability of collecting data with up to 10^6 Hz and was connected to the computer. The pressure transducer ends were connected to the pressure taps that mounted on the column wall, which were located at 0.26 m height differences (the lower tap and the upper tap were at the height of 0.045 m and 0.305 m, respectively above the distributor). The locations of lower and upper taps have been selected to cover the zone before the lower end of the vertical internals (0.09 m above the distributor plate) and the zone before the freeboard of the column.

Figure 3.1. Photo of the differential pressure transducer (Omega Inc.) used in the present work.

The DAQ-View software was used to perform the DAQ system, which included a DaqCal software application for easy user calibration. The signals were recorded for 40 s at a rate of 100 Hz, and this process was repeated five times in order to ensure that the results were reproducible. Additionally, the reproducibility was found to be less than of 5% and the error bars were shown for each measurement. Because the transducer is very sensitive, aluminum meshes were connected to the transducer taps to prevent the particles from getting inside. The photo of the pressure transducer used in the present work is shown in Figure 3.1 while Figure 2.1 show schematically the measuring of pressure drop on the column.

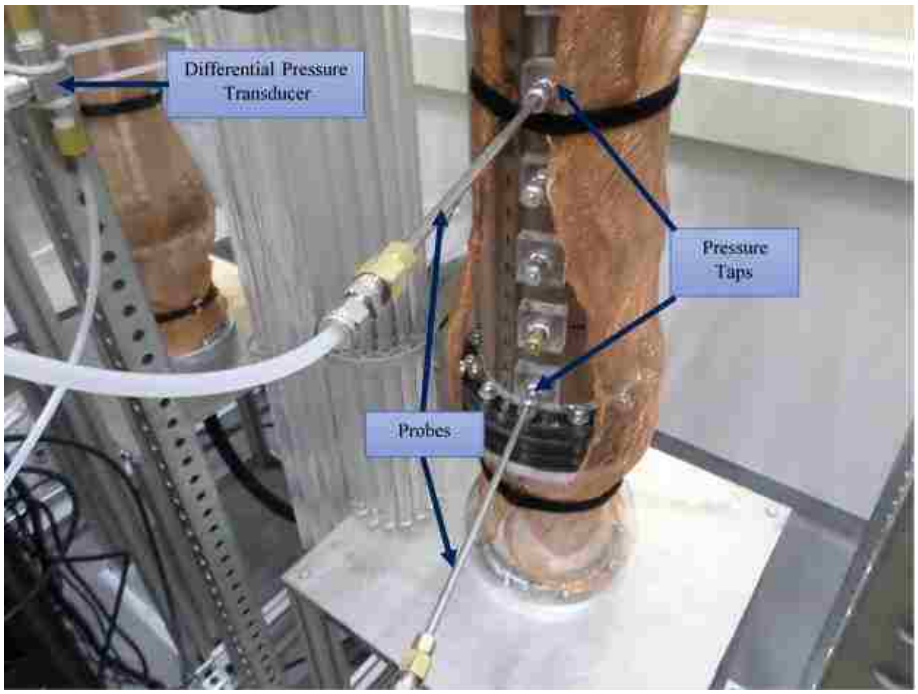

Figure 3.2. The pressure probe for pressure drop measurements at various radial locations connected to the differential pressure transducer.

3.2. PRESSURE PROBE-DIFFERENTIAL PRESSURE TRANSDUCER FOR PRESSURE DROP MEASUREMENT MOUNTED AT VARIOUS RADIAL LOCATIONS

In the recent decades, the pressure probe connected to the pressure transducers have been applied in gas-solid fluidized beds. Xie and Geldart (1997) studied the effect of probe size on the measurements of the bubble properties in a fluidized bed of 0.15 m diameter. They proposed that the 4.0 mm inside diameter probes is consider as a better choice to eliminate the disruption of the probe on the flow patterns inside the bed as well as bubble properties measurements. Van Ommen et al. (1999) studied the influence of probe dimensions (probe length and inside diameter) on the outcomes of different data analysis methods for gas-solid fluidized pressure signals such as statistical analysis, spectral analysis, and chaos analysis. They found that the using of pressure probe with 2.5 m length and inside diameter ranging from 2 to 5 mm don't hardly effect the analysis results. Also, the collecting pressure fluctuation signals has shown no damping or resonance due to the effect of inside diameter of the pressure probe. Van Ommen et al. (2004) examined the effect of the local placement of the pressure probe using pressure probe of 4 mm dimeter that connected to gauge pressure transducer on the accuracy of the measurement of dynamic pressure inside bubbling fluidized bed of 0.8 m inside diameter that occupied with Geldart B solid particles. They mentioned that the local measurement of gauge (dynamics) pressure fluctuation at a certain location in fluidized bed may be due to bubble passage and compression waves (bubble coalescence and bubble eruption). Thus, they found that the compression waves with high amplitude which represent the coherent part of the dynamic pressure signal can be measured everywhere inside the bed. While, the compression waves

with low amplitude which represent the incoherent part of the dynamics pressure signal can only measured close to their origin.

Figure 3.3. Photo of the probe.

Hence, in this work, two probes of 2.5 mm inside diameter and 0.25 m length that were made from stainless steel were connected to the two ends of the differential pressure transducer in order to measure the pressure drop along the bed at different radial locations inside the fluidized bed, as shown in Figure 3.2. The inside diameter of the probes were chosen as per the finding of (Xie and Geldart 1997; Ommen et al. 1999) to ensure that the pressure fluctuation signals were collected without any damping caused by the small inside diameter of the probe (less than 2 mm) or by any resonance that may happen as a result of using a probe with a long inside diameter (higher than 5 mm), as mentioned and

recommended by Van Ommen et al. (1999); Van Ommen et al. (2004) and Van Ommen et al. (2011). The end tips of the probes were covered with a wire mesh to prevent the solid particle from entering inside the probe and blocking the tips, which could have disturbed the measurements. The wire meshes used were made from stainless steel with 80 µm mesh diameter and 40 µm wire diameter, and the open area of the wire mesh was 46% of the total area, which has no considerable effect on the pressure fluctuations (Van Ommen et al. 1999). A photo of the probe used in this work is shown in Figure 3.3.

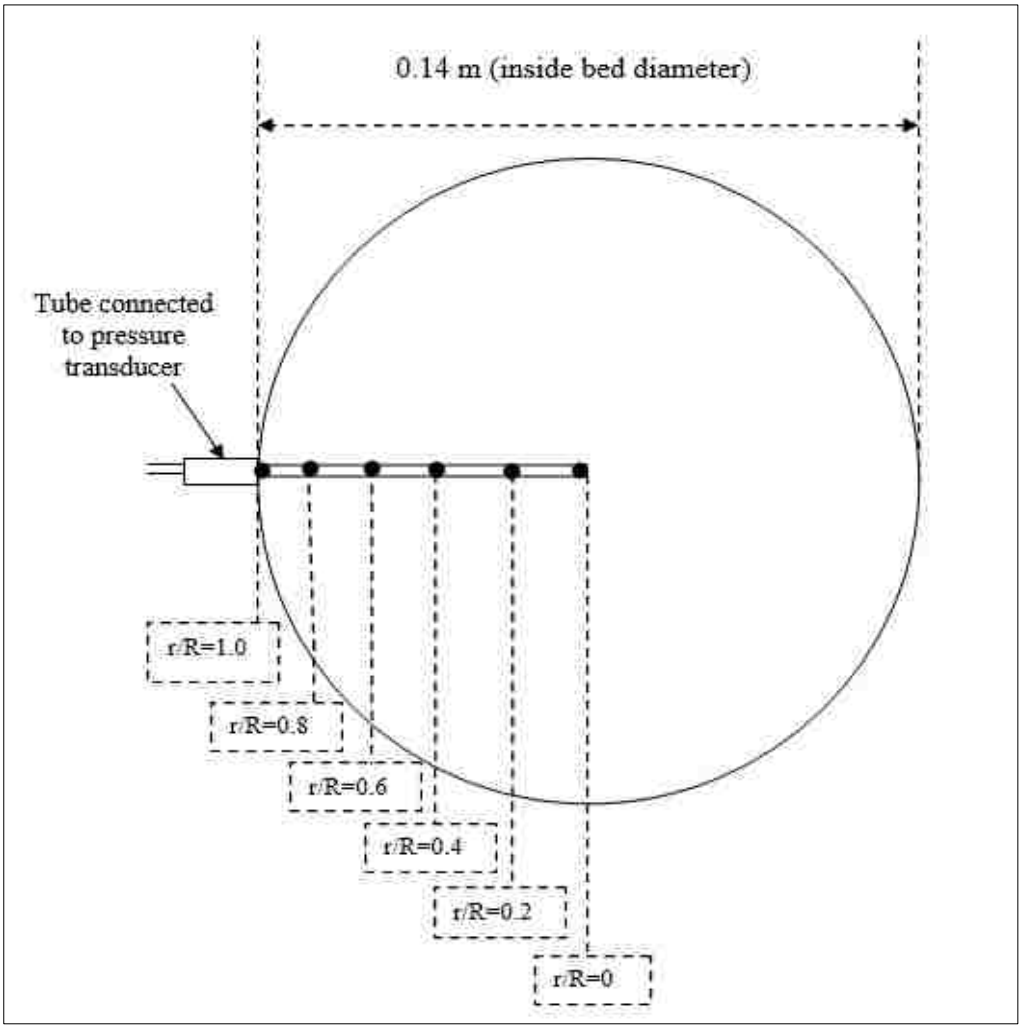

Figure 3.4. Radial positions for the pressure drop measurements with 0.0127 m vertical internals.

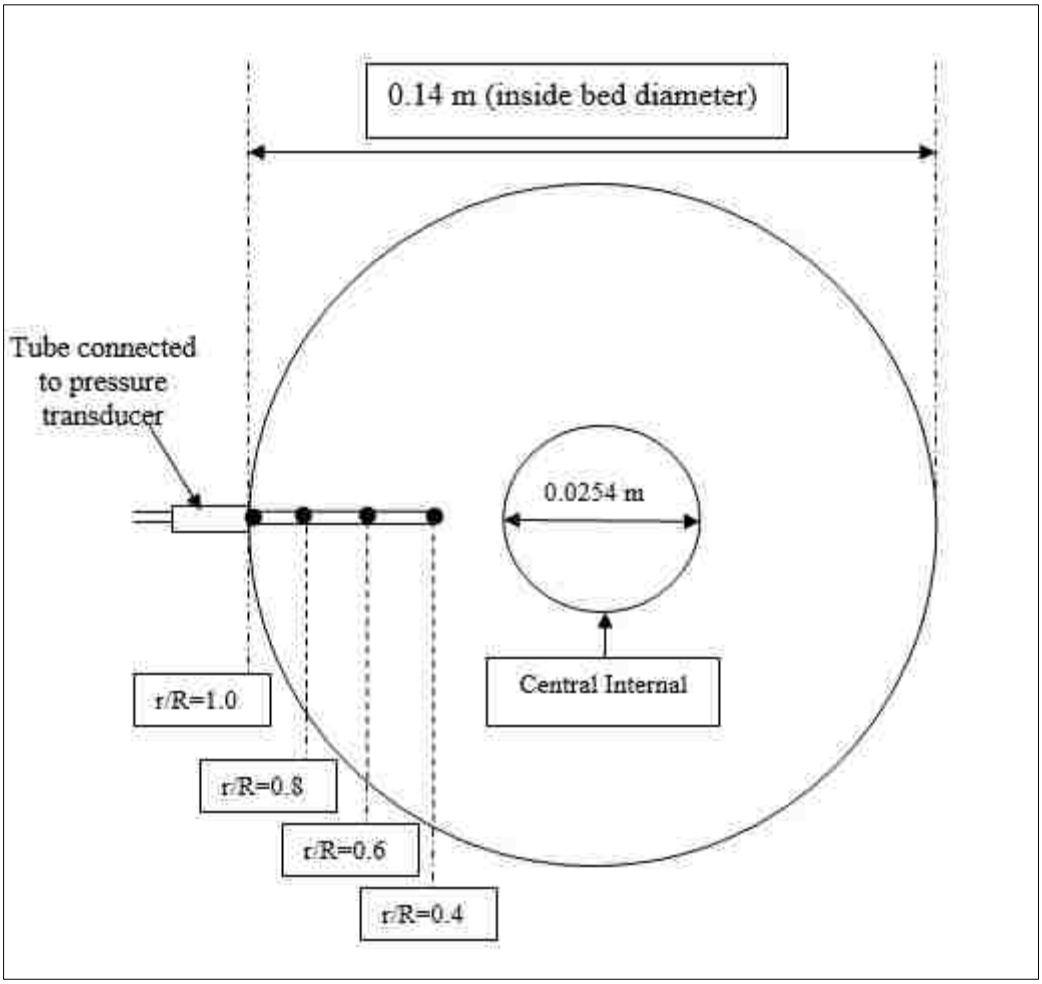

Figure 3.5. Radial positions for the pressure drop measurements with 0.0254 m vertical internals.

The pressure drop measurements along the bed height of 0.26 m were carried out at six radial positions (r/R = 0.0, 0.2, 0.4, 0.6, 0.8, and 1.0) for the 0.0127 m internals, as shown in Figure 3.4. Both the lower and upper probe are mounted through the pressure taps at the wall at similar radial locations. For the 0.0254 m internals, only four radial positions (r/R = 0.0, 0.2, 0.4, and 0.6) were available for the measurements due to the existence of one of the internals in the center of the column for the configuration used, as shown in Figure 3.5.

4. RESULTS AND DISCUSSION

4.1. PRESSURE DROP AT THE WALL OF THE BED USING GLASS BEADS SOLID PARTICLES

The pressure drop at the wall of the bed with different u/u_{mf} for the cases of with and without vertical internals were demonstrated in Figure 4.1. It is clearly shown in Figure 4.1 that the pressure drop has been slightly decreased with increasing the superficial gas velocity (u/u_{mf}) for the case of with and without internals. In which, the pressure drop in the case of without vertical internals is 2.74 KPa at u/u_{mf} = 1.6, while it is 2.7 KPa at u/u_{mf} = 2.4. Moreover, the percentage of decrease of the pressure drop when the superficial gas velocity (u/u_{mf}) increase from u/u_{mf} = 1.6 to u/u_{mf} = 2.4 is about 2.5% and 4.5% for the case of 0.0254 m and 0.0127 m vertical internals, respectively. Additionally, it can be indicated from Figure 4.1 that the pressure drop has been decreased in the case of both vertical internals used in this wok.

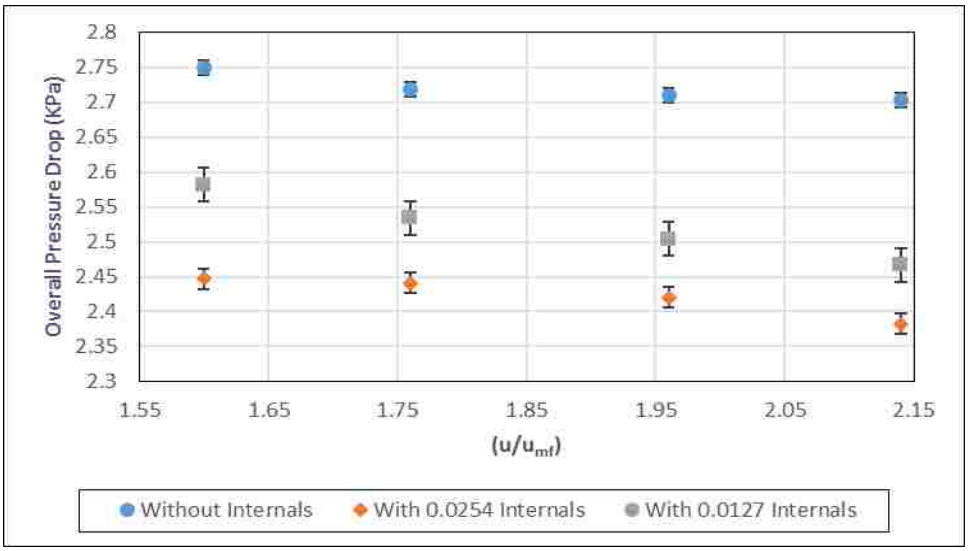

Figure 4.1. Effect of superficial gas velocity in terms of u/u_{mf} on the pressure drop at the wall of the bed for the case of with and without vertical internals in glass beads solid particles.

In order to measure the percentage of pressure reduction (%PR) or sometimes is named as the drag reduction in the case of vertical internals (Shanshool and Al-Qamaje 2008). Equation 1 is used to measure the pressure reduction (%PR) when the vertical internals are implemented inside the bed.

$$\%PR = \frac{\Delta P_{without} - \Delta P_{with}}{\Delta P_{without}} * 100 \quad (1)$$

where $\Delta P_{without}$: pressure drop without internals, and ΔP_{with}: pressure drop with internals.

The (%PR) for the case of both vertical internals used in this work has been estimated versus u/u_{mf} different as shown in Figure 4.2. Apparently, the %PR is higher in the case of 0.0254 m vertical internals with the different superficial gas velocities, in which the %PR is about 11%. While, for case of 0.0127 m vertical internals, the %PR is lesser than that for the case of 0.0254 m vertical internals and it has been increases with increasing the superficial gas velocity, in which the %PR is increased from 6% to about 9% when the superficial gas velocity increase from 1.6 to 2.4. The different in behavior of the two vertical internals with respect to the %PR is related to the difference in the tube size, tube to tube space and the existing of the central tube in the configuration of 0.0254 m vertical internals which can affect the flow behavior of the bubbles in the central region of column by reduce the bubble size and increase the bubble frequency, as well reduce the coalescence between the bubbles. Thus, the pressure of the gas phase (bubbles) would decrease accordingly (Rüdisüli, Schildhauer, Biollaz, and Van Ommen 2012a; Rüdisüli, Schildhauer, Biollaz, and Van Ommen 2012c; Mathew, Begum, and Anantharaman 2014).

The time series of differential pressure drop fluctuations along the bed with and without the vertical internals have been illustrated in Figures. The mean (μ) and the variance (σ^2) of the pressure drop fluctuation signals have been estimated which represent

the amplitude and frequency of these time series signals, respectively. Figure 4.3 illustrates the pressure drop fluctuation signals for the cases of with and without internals at three different gas velocities (u/u_{mf} = 1.76, 1.96 and 2.14) using glass beads particle. As appear in Figure 4.3, the mean of the pressure drop fluctuations has been decreased with the existing of both sizes of vertical internals and for all the superficial gas velocities. This reduction in the mean values of the pressure drop fluctuation signals reflects the reduction in the pressure drop due to the existing of vertical internals since the mean value or the amplitude of the differential pressure drop fluctuation is represented the pressure drop inside the bed. In the meantime, the decreasing in the mean value (amplitude) is found to be higher in the case of 0.0254 m internals and in comparing with case of 0.0127 m internals. Additionally, it has been clearly shown in Figure 4.3 that the values of variance of the pressure drop fluctuation signals have been increased in the case of vertical internals

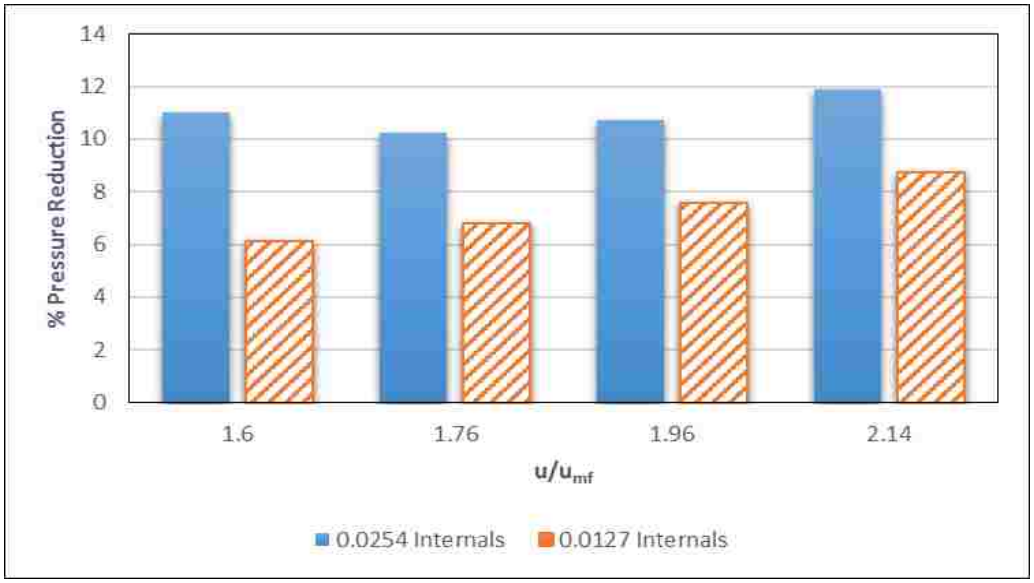

Figure 4.2. The percentage pressure reduction (%PR) at the wall of the column, at different superficial gas velocities in terms of u/u_{mf} for the case of with vertical internals and for the case of glass beads solid particles.

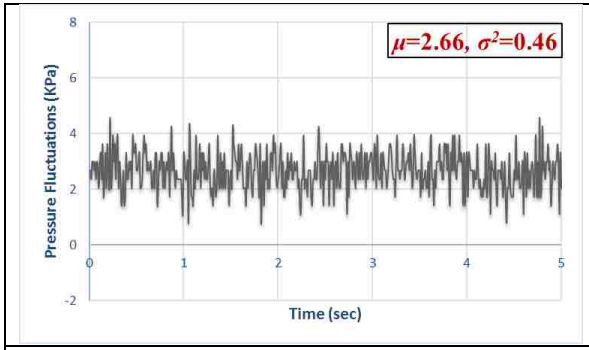

Pressure drop fluctuations without internals at (u/u_{mf} = 1.76)

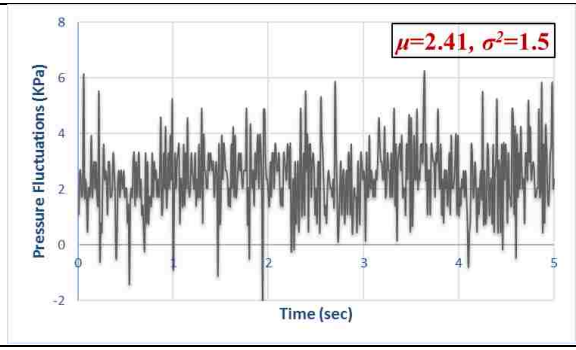

Pressure drop fluctuations with 0.0127 m internals at (u/u_{mf} = 1.76)

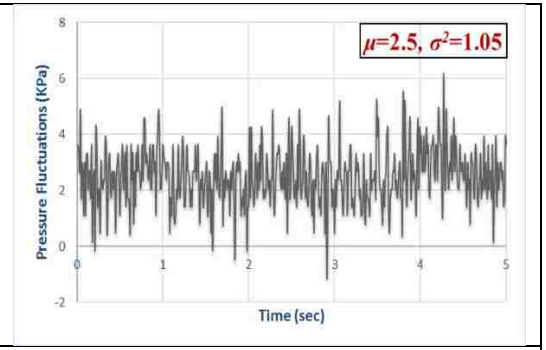

Pressure drop fluctuations with 0.0254 m internals at (u/u_{mf} = 1.76)

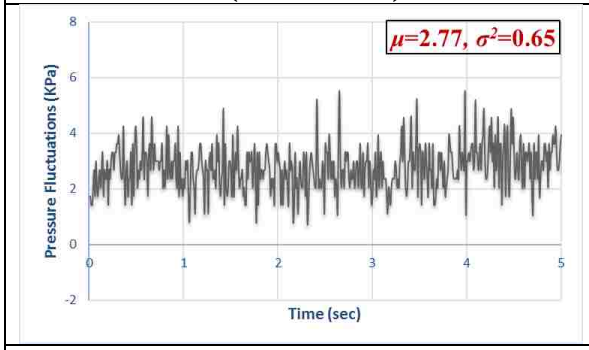

Pressure drop fluctuations without internals at (u/umf = 1.96)

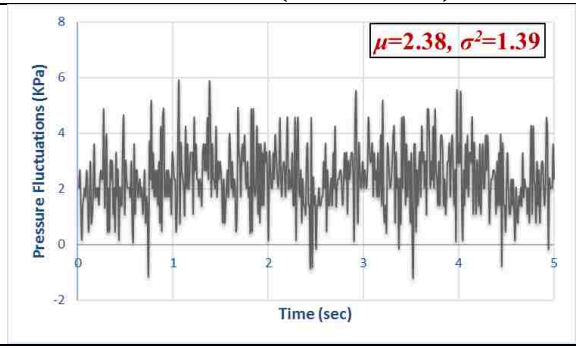

Pressure drop fluctuations with 0.0127 m internals at (u/u_{mf} = 1.96)

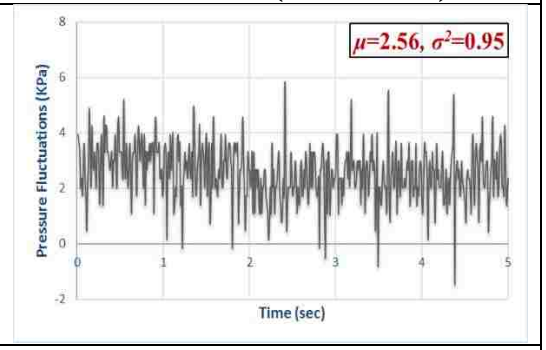

Pressure drop fluctuations with 0.0254 m internals at (u/u_{mf} = 1.96)

Figure 4.3. Pressure drop fluctuations for the cases of with and without internals at the wall of the column, at different superficial gas velocities in terms of u/u_{mf} and in glass beads solid particles.

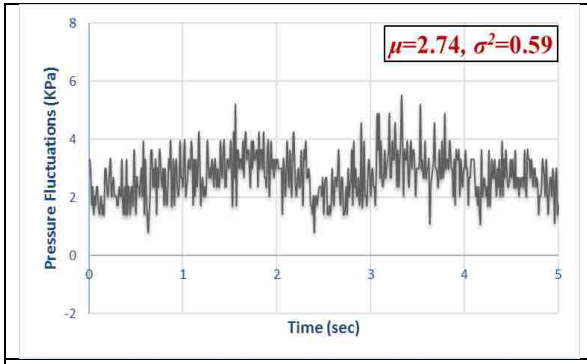	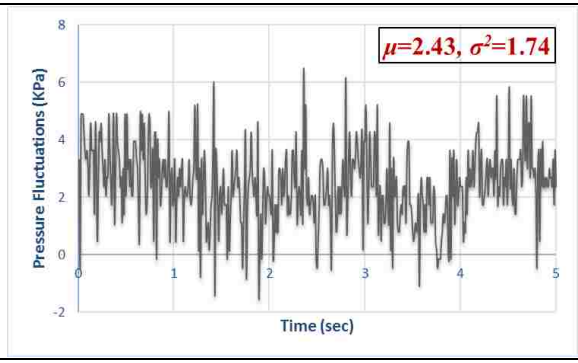	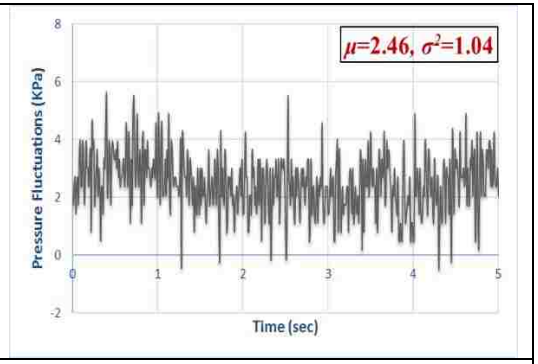
Pressure drop fluctuations without internals at (u/umf = 2.14)	Pressure drop fluctuations with 0.0127 m internals at (u/u_{mf} = 2.14)	Pressure drop fluctuations with 0.0254 m internals at (u/u_{mf} = 2.14)

Figure 4.3. Pressure drop fluctuations for the cases of with and without internals at the wall of the column, at different superficial gas velocities in terms of u/u_{mf} and in glass beads solid particles. (cont.)

and for all the superficial gas velocities. The variance is represented the frequency or the fluctuation of the of differential pressure fluctuation signal inside the bed. Moreover, the increasing of the variance value with the existence of vertical internals is a function of the vertical internals size and configuration, in which the variance has been increase with increase the size of internals as in the case of 0.0254 m internals. Furthermore, it can be indicated that the existing of central tube in the 0.0254 m internals configuration works to reduce the pressure drop fluctuation as shown in Figure 4.3 (less variance value comparing with that of 0.0127 m internals) inside the bed since the gas phase in form of bubbles tend to move toward the center of the bed and away from the column wall.

It worthy to noting, that the analysis of pressure drop fluctuation signals in terms of amplitude (mean) and frequency (variance) for the case of with and without internals demonstrates the ability of the vertical internals in reduce the pressure drop inside the bed due to the many advantages that can be obtained in the case of vertical internals that mentioned earlier such as the reduction of bubble size, increase bubble frequency and reduce coalescence between the bubbles in their vertical pathways. These benefits would lead to reduce the pressure drop and increase the local and overall pressure fluctuations inside the bed with acceptable level. The pressure drop fluctuations would indicate effects on the overall heat transfer and mass transfer inside the bed since the heat and mass transfers is a function of the solid particles and bubbles hydrodynamic characteristics.

4.2. PRESSURE DROP AT THE WALL OF THE BED USING ALUMINUM OXIDE SOLID PARTICLES

The variations of the pressure drop for the case of aluminum oxide solid particles with different superficial gas velocities in terms of u/u_{mf} and with and without vertical

internals are illustrated in Figure 4.4. Apparently, the pressure drop has been gradually decreased with increasing the u/u_{mf} for the case of without internals, which is one of the good hydrodynamic characteristic of the typical type of the gas-solid fluidized bed as mentioned by Mathew et al., (2014). It is worthy to mention that the trend of the pressure drops with the different superficial gas velocities in terms of u/u_{mf} for the case of without internals (shown in Figure 4.4) is different about that in the case of glass beads solid particles, in which the pressure drop was decreased with increasing the superficial gas

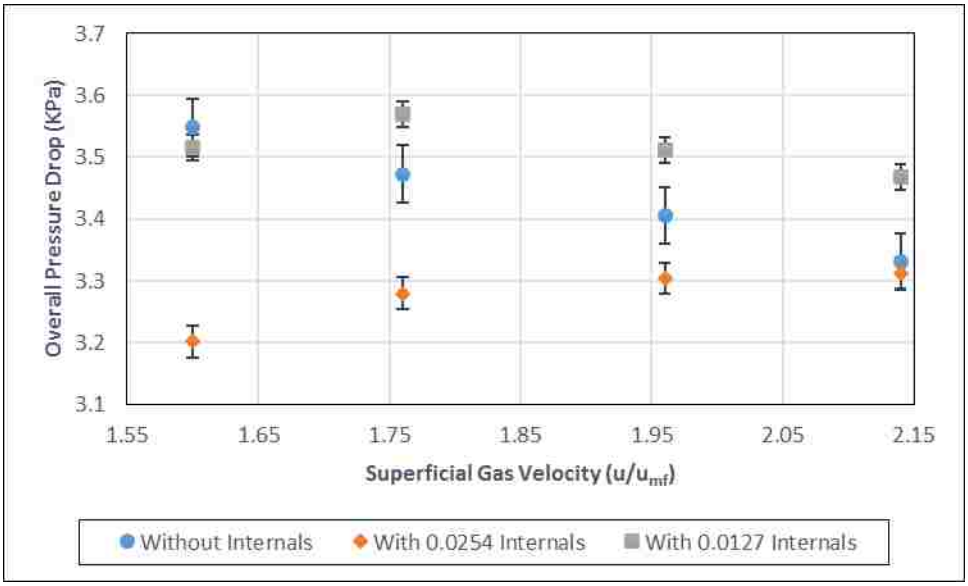

Figure 4.4. Effect of superficial gas velocity in terms of u/u_{mf} on the pressure drop at the wall of the bed for the case of with and without vertical internals in aluminum oxide solid particles.

velocity in the case of glass beads solid particles. The difference between the trends of the pressure drops with different superficial gas velocities of the two solids is return to the fact that although these two solids have almost the same particles average size but they are

different in some other physical properties such as solids density and solids sphericity as illustrated in Table 2.1. Moreover, the pressure drop in the case of without vertical internals is 3.54 KPa at u/u_{mf} = 1.6, while it is 3.33 KPa at u/u_{mf} = 2.4. Furthermore, the profiles of pressure drop for the case of 0.0127 m vertical internals has been relatively increased and then gradually decreased with increasing the u/u_{mf} in which the percentage of increase of the pressure drop when the u/u_{mf} increase from u/u_{mf} = 1.6 to u/u_{mf} = 2.4 is about 1.42%, while for case of 0.0254 m vertical internals, the pressure drop has been progressively increased with increasing the superficial gas velocity in terms of u/u_{mf}, in which the percentage of increase of the pressure drop when the superficial gas velocity increase from u/u_{mf} = 1.6 to u/u_{mf} = 2.4 is about 3.32%.

Additionally, it is clearly appeared from the profiles of the pressure drop with different superficial gas velocities in terms of u/u_{mf} illustrated in Figure 4.4, that the pressure drop is increased for the case of 0.0127 m vertical internals and decreased for the case of 0.0254 m vertical internals with respect to the case of without internals. The variation in the behavior of these two vertical internals with respect to the pressure drop in the case of without internals can be explained by the difference in the design parameters of the two configurations of vertical internals used such as tube size, tube-to-tube space and tube configuration. It is true that both configurations are of circular arrangement but the exitance of center tube in the arrangement of 0.0254 m vertical internals together with other difference in design parameters makes the pressure drop is different since the pressure drop is a function of these design parameters. In addition, these design parameters can significantly affect the hydrodynamic characteristics of the gas phase, solid phase and the gas-solid flow patterns inside the bed and the pressure drop would be effected accordingly.

The (%PR) for the case of both vertical internals used in this work has been estimated using Equation 1 and plotted versus the different u/u_{mf} in Figure 4.5. As appear in Figure 4.5, the %PR is positive in the case of 0.0254 m vertical internals and it decreased with increasing u/u_{mf}. This indicates that the 0.0254 m vertical internals can gives a reduction in the pressure drop when it used inside the bed. The %PR is about 10% at u/u_{mf} = 1.6 and decreased to about 0.5% at u/u_{mf} = 2.4. For the case of 0.0127 m inside diameter, the % PR is positive at u/u_{mf} = 1.6 and then it becomes negative for the whole range of the u/u_{mf} used. The %PR is about 1% at u/u_{mf} = 1.6 while it is about -4.1 at u/u_{mf} = 2.4. It is worthy to noting that for both types of vertical internals, the pressure drop is increased with increasing u/u_{mf}, the idea here is the occurrence of different flow regime with increasing the u/u_{mf} started from bubbling flow regime until reach slugging or turbulent flow regime at higher superficial gas velocity (u/u_{mf} = 2.4), and since the flow regime is the way that solid and gas phases interacts inside the bed. Therefore, the flow regime is significantly affect the pressure drop inside the gas-solid fluidized bed.

Additionally, the physical properties such as solid particles sphericity, density and particle size distribution of the aluminum oxide (Table 2.1) which are different from that of the glass beads have a considerable impact on both of the flow regime and pressure drop as mentioned by Yerushalmi et al., (1978) and Yerushalmi and Cankurt (1979). These physical properties of the solid particles were found to influence the solid circulation, gas solid flow patterns and the gas-solid hydrodynamic characteristics such as solids holdup and velocity, gas holdup and velocity, as well as bubble frequency, bubble size and bubble rise velocity as mentioned by (Rüdisüli, Schildhauer, Biollaz, and Van Ommen 2012b; Rüdisüli, Schildhauer, Biollaz, and Ruud van Ommen 2012; Rüdisüli, Schildhauer,

Biollaz, and Van Ommen 2012c; Maurer, Wagner, Schildhauer, et al. 2015). Therefore, these is an obvious difference in the pressure drop and %PR of the two solid particles (aluminum oxide and glass beads) when the vertical internals are implemented inside the bed.

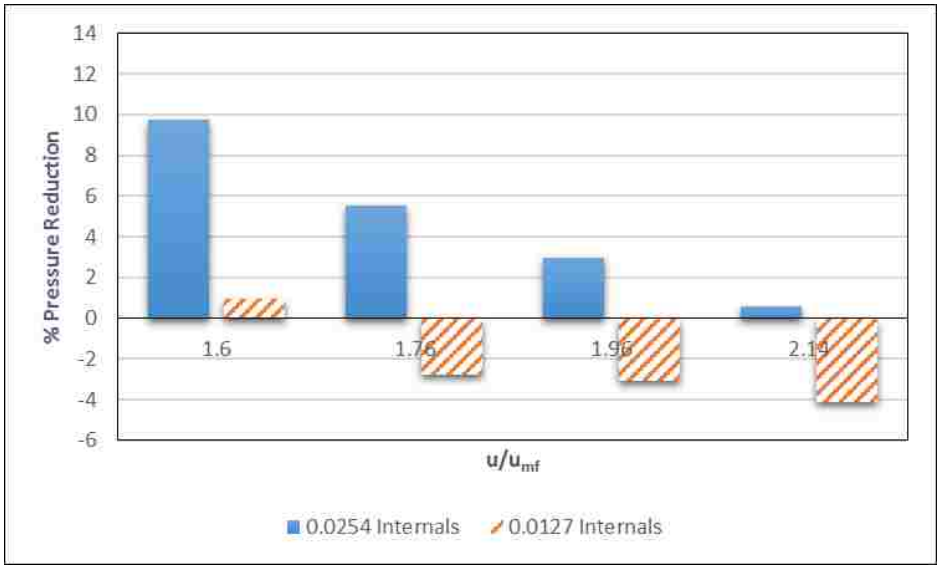

Figure 4.5. The percentage pressure reduction (%PR) at the wall of the column, at different superficial gas velocities in terms of u/u_{mf} for the case of with vertical internals and for the case of glass beads solid particles.

As in the case of glass beads, the differential pressure fluctuation signals have been demonstrated in Figure 4.6. The differential pressure drops fluctuation signals and their values of mean and variance are estimated. Figure 4.6 shows the pressure drop fluctuation signals for the cases of with and without internals at three different superficial gas velocities (u/u_{mf} = 1.76, 1.96 and 2.14). As appears in Figure 4.6, the mean values of the drop pressure fluctuations have been decreased in the case of 0.0254 m vertical internals

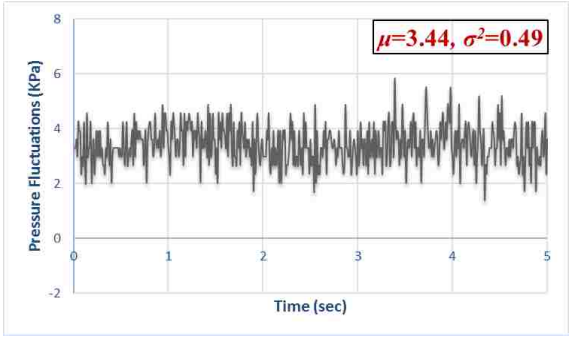

Pressure drop fluctuations without internals at (u/u_{mf} = 1.76)

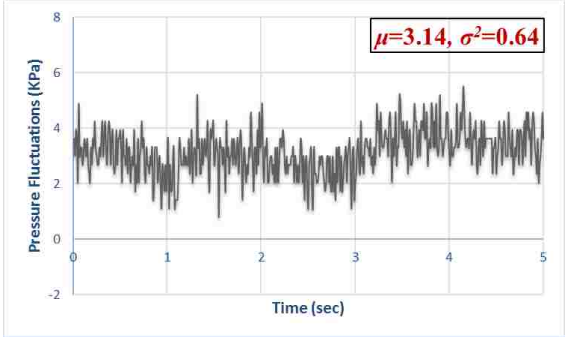

Pressure drop fluctuations with 0.0127 m internals at (u/u_{mf} = 1.76)

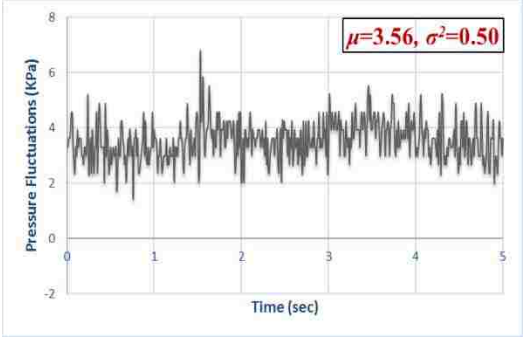

Pressure drop fluctuations with 0.0254 m internals at (u/u_{mf} = 1.76)

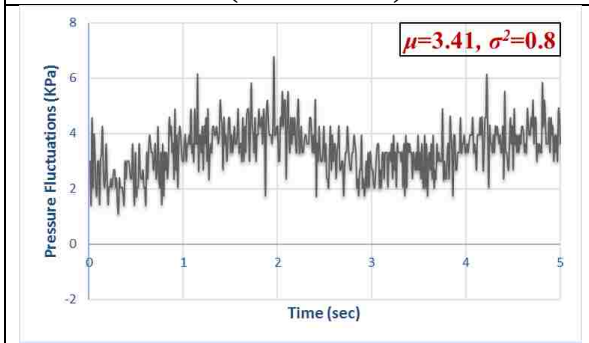

Pressure drop fluctuations without internals at (u/umf = 1.96)

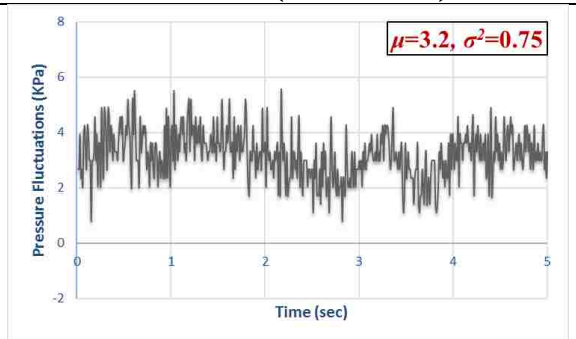

Pressure drop fluctuations with 0.0127 m internals at (u/u_{mf} = 1.96)

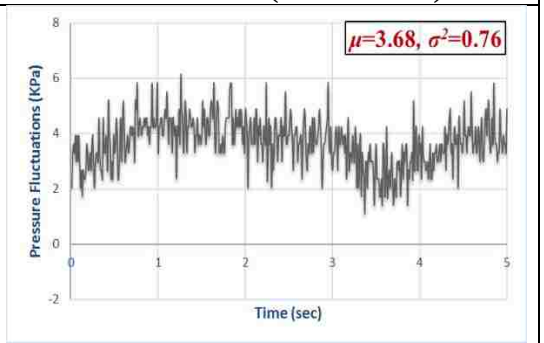

Pressure drop fluctuations with 0.0254 m internals at (u/u_{mf} = 1.96)

Figure 4.6. Pressure drop fluctuations for the cases of with and without internals at the wall of the column, at different superficial gas velocities in terms of u/u_{mf} and in aluminum oxide solid particles.

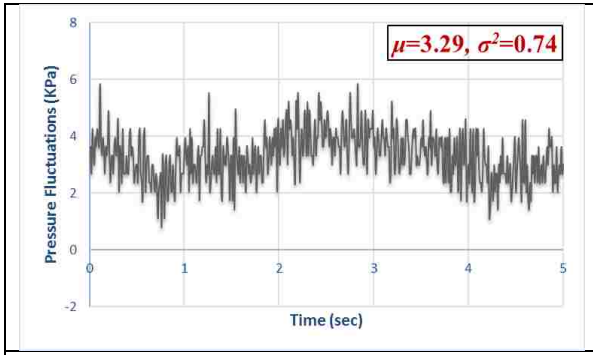

Pressure drop fluctuations without internals at (u/umf = 2.14)

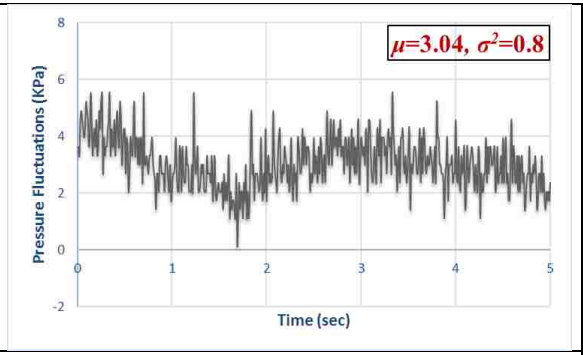

Pressure drop fluctuations with 0.0127 m internals at (u/u_{mf} = 2.14)

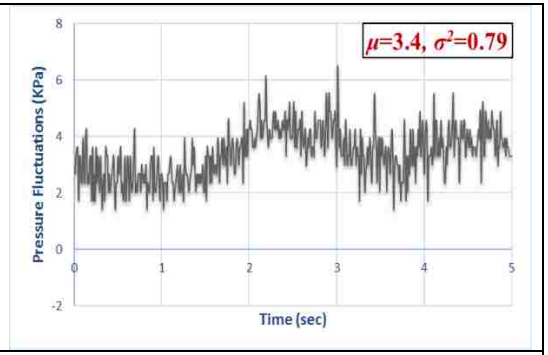

Pressure drop fluctuations with 0.0254 m internals at (u/u_{mf} = 2.14)

Figure 4.6. Pressure drop fluctuations for the cases of with and without internals at the wall of the column, at different superficial gas velocities in terms of u/u_{mf} and in aluminum oxide solid particles. (cont.)

and increased in the case of 0.0127 m vertical internals. The reduction in the mean values of pressure drop fluctuations in the case of 0.0254 m vertical internals confirms the ability of this configuration in reduce the pressure drop inside the gas-solid fluidized bed of aluminum oxide solid particles as in the case of glass beads solid particles. While, for the case of 0.0127 m vertical internals, the increasing of mean values reflects the negative effect of this configuration of vertical internals on the pressure drop inside the bed as clearly shown earlier in the %PR calculations (Figure 4.6). In the meantime, it is clearly shown from Figure 4.6 that the variance values of the pressure drop fluctuations in the case of with and without internals are almost same for all the three superficial gas velocities in terms of u/u_{mf} listed in Figure 4.6. The values of variance are used to represent the frequency or fluctuation of the pressure drop fluctuation signals as shown earlier. Therefore, it clearly shown that the implemented of the two types of vertical internals in the case of aluminum oxide has no effect on the pressure drop fluctuations inside the bed.

4.3. COMPARISON OF PRESSURE REDUCTION OF THE TWO SOLID PARTICLES

The %PR at different superficial gas velocity in terms of u/u_{mf} have been compared for the two solid particles used in this work (glass beads and aluminum oxide), as shown in Figure 4.18 for the case of 0.0254 m internals. Since the 0.0254 m internals have been proven to have less pressure drop in both solid particles when compared to the case without internals, the %PR have been plotted against the superficial gas velocity in terms of u/u_{mf}, as mentioned earlier for the case of 0.0254 m internals. The following can be concluded from Figure 4.7:

1- The %PR in the case of glass beads are higher than those of the aluminum oxide for all superficial gas velocities used.

2- The difference between the two cases in terms of %PR becomes bigger with an increase in superficial gas velocity.

3- The %PR in the case of glass beads is slightly increased with the superficial gas velocity, while in the case of aluminum oxide, it has been decreased with increasing the superficial gas velocity.

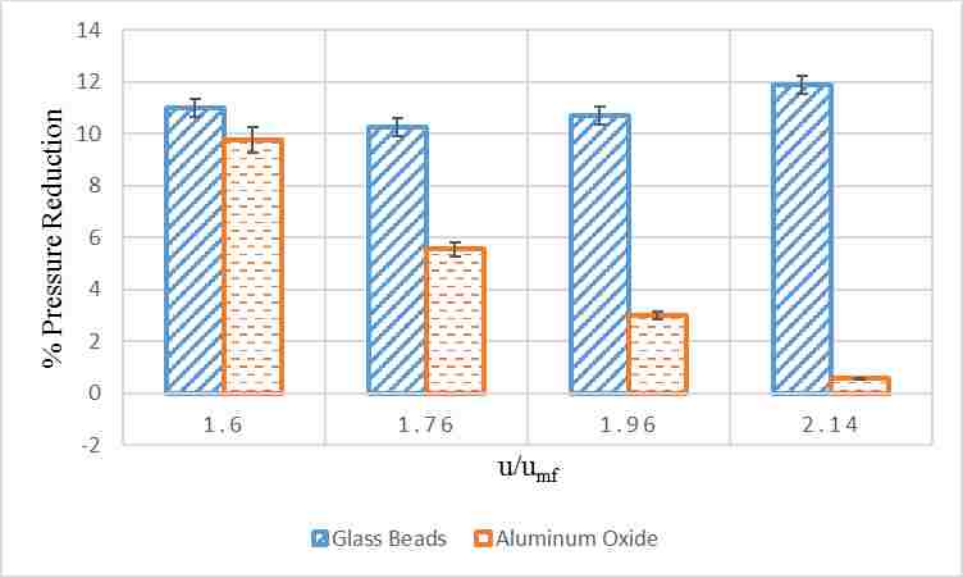

Figure 4.7. Comparsion between the %pressure reduction for 0.0254 m internals at different superficial gas velocities in both solid particles used in current work.

4- The difference in the performance of the 0.0254 m internals due to the type of solid particles used is based on the difference in physical properties of the two solid particles. These physical properties are solid particle shape (the glass beads have a spherical shape and the aluminum oxide has an angular, or irregular shape) and the solid density

(the density of glass beads is 2500 Kg/m^3 and the density of the aluminum oxide is 3900 Kg/m^3). These physical properties can affect the pressure drop inside the bed, as indicated by many experimental works (A. Sahoo and Roy 2005; Kaza 2008; Abanti Sahoo 2011; Mathew, Begum, and Anantharaman 2014).

5- In general, the 0.0254 m internals can reduce the pressure drop inside the conventional gas–solid fluidized bed by about 10%. This reduction can minimize the power consumption through the operation of this type of chemical reactor, and it can also improve the hydrodynamic characteristics of the fluidized bed reactor when implementing such vertical internals inside the bed.

4.4. COMPARISON WITH LITERATURE STUDIES

The experimental results of the pressure drop measured at the wall of the bed that measured in this work is compared with the predicted correlations available in literature that listed in Table 4.1. The comparison is including the data of the pressure drop that has been estimated at different superficial gas velocity in the form of u/u_{mf} as well as for the case of with vertical internals and for the two types of solid particles.

The average absolute relative error (AARE) between the experimental and predicted data has been estimated as follows:

$$\mathrm{AARE} = \frac{1}{N}\sum_{i=1}^{N}\left|\frac{h_{exp(i)}-h_{pred(i)}}{h_{exp(i)}}\right| \qquad (2)$$

where N is the data point number

The average absolute relative error between the experimental and predicted values of the pressure drop for both sizes of vertical internals and solid particles are listed in Table 4.1. As shown in Table 4.1, there is a big difference between the experimental and

Table 4.1. Correlations available in literature for estimating the pressure drop in gas-solid fluidized bed

References	Correlations	% Average Absolute Relative Error (without internals) for the case of glass beads solid particles		% Average Absolute Relative Error (with internals) for the case of aluminum oxide	
		0.0254 m internals	0.0127 m internals	0.0254 m internals	0.0127 m internals
Kar and Roy (2000)	$\frac{\Delta p}{\rho_f u^2} = 0.003 \left(\frac{h_s}{D}\right)^{2.19} \left(\frac{H_e}{D}\right)^{-2.15} \left(\frac{d_p}{D}\right)^{-1.3} \left(\frac{\rho_s}{\rho_f}\right)^{1.02}$ where H_e is the expansion bed height	752%	693%	218%	205%
Padhi et al., (2010)	$\Delta p = 956.07 \left(\frac{h_s}{D}\right)^{0.876} (y)^{0.876} \left(\frac{G_f}{G_{mf}}\right)^{-1.5049}$ Where y is the twist ratio of the internals	73%	75%	64%	66%
Mathew et al., (2014)	$\frac{\Delta p}{\rho_f u^2} = 6762.3\ Fr^{-0.96} \left(\frac{D_c}{d_p}\right)^{-0.12} \left(\frac{h_s}{D}\right)^{1.24} \left(\frac{w}{s}\right)^{-0.14}$ where w is internal width and s is the internal spacing	98%	98%	76%	77%

predicated values of the pressure drop for both sizes of vertical internals and both solid particles used in this work. The reasons of this big difference are some of these correlations were developed for the case of different configurations and shapes of immersed surfaces inside the gas-solid fluidized beds as in the case of correlation developed by Padhi et al., (2010). Additionally, these correlations have been predicted in gas-solid fluidized beds with different design parameters , operating conditions and physical properties of gas and solid particles as in the case of correlation developed by (Kaza 2008; Mathew, Begum, and Anantharaman 2014). Therefore, the need is to predict a correlation that relates the pressure drop in case of vertical internals with the other parameters that used in this work based on the relevant dimensionless groups. The developing of the in the form of related dimensionless groups correlation would be discussed in the next section.

4.5. CORRELATION DEVELOPMENT

The correlation has been developed with the help of relevant dimensionless groups involving cooperating factors; these factors are design parameter (size of internals and column diameter), operating condition (superficial gas velocity), and physical properties of the gas and solid particles (gas density, gas viscosity, and solid density). It is worthy to noting that the dimensionless groups are selected in this work based on the developed correlations available in literature. In which, the developers of these correlations have been reported that these dimensionless groups have a significant effect on the pressure drop inside the gas-solid fluidized beds in the case of with and without immersed surfaces (Sahoo and Roy, 2005; Kaza, 2008; Sahoo, 2011; Mathew et al., 2014).

Hence, the dimensional analysis approach has been used, in which the system variables have been classified into the following dimensionless parameters:

- Operating parameters: Froude number (*Fr*) and Reynolds number (Re_p)
- Material physical parameter: Archimedes number (*Ar*)
- Internal design parameter: ratio of internal diameter to column diameter (D_i/D_c)

The pressure drops (Δp) can be related to the above different parameters as follows:

$$\mathrm{Eu} = \mathrm{C}(\mathrm{Fr})^{\mathrm{a}}\left(\mathrm{Re_p}\right)^{\mathrm{b}}(\mathrm{Ar})^{\mathrm{c}}\left(\frac{\mathrm{D_i}}{\mathrm{D_c}}\right)^{\mathrm{d}} \quad (3)$$

where,

Eu Euler number = $(\frac{\Delta \mathrm{p}}{\rho_g U^2})$,

Fr Froude number = $\left(\frac{U^2}{g d_p}\right)$,

Re_p Reynolds number = $\left(\frac{\rho_g U d_p}{\mu_g}\right)$,

Ar Archimedes number = $\left(\frac{\rho_g(\rho_s-\rho_g)g d_p^3}{\mu_g^2}\right)$,

D_i internal diameter,

D_c column diameter,

C coefficient, and

a, b, c, d exponents.

The analysis of variance (ANOVA) were performed using JMP12 to verify that all the parameters that are involved in Equation 3 are significant. The ANOVA results are illustrated in Tables 4.2 and 4.3. The estimate column in Table 4.3 represents the values of the coefficient C and the exponents of Equation 3. The Pro column represent the probability values (P value) of each dimensionless group listed in Equation 3. It is clearly shown from

the P values listed in Table 4.3 that the Reynolds number (Re_p) is not significant because the P value is either unpredictable or higher than 0.05. The physical meaning of the statistical results is that the Froude number which represents the ratio of the inertial force to the gravitational force is more significant than the Reynolds number (Rep) which represents the ratio of the inertial force to the viscous force. In which, the gravitational forces of the solids particles are different (different physical properties in terms of solids density and particles sphericity) are affected the pressure drop (Euler number) while the viscous force is constant since just one type of fluidizing gas was used. Hence, the Reynolds number (Re_p) has been removed from Equation 3 and rewritten in Equation 4, due to the insignificant effect of this parameter on Euler number.

$$\mathrm{Eu} = \mathrm{C}(\mathrm{Fr})^{\mathrm{a}}(\mathrm{Ar})^{\mathrm{b}}\left(\frac{\mathrm{D_i}}{\mathrm{D_c}}\right)^{\mathrm{c}} \quad (4)$$

Table 4.2. Analysis of Variance (ANOVA) of the parameters used in Equation 4.

Source	DF	Sum of Squares	Mean Square	F Ratio
Model	3	4.458	1.4862	5498.839
Error	12	0.003	0.0002	Prob > F
Total	15	4.461		<0.0001

Table 4.3. Parameter Estimates from Analysis of Variance of the parameters used in Equation 4.

Term	Estimate	Std Error	Prob>|t|
Intercept	Ln(c) = 5.8804	0.4644	<0.0001
Fr	a = -1.0229	0.0191	<0.0001
Rep	b = 0	0	.
Ar	c = 0.7782	0.0058	<0.0001
Di/Dc	d = -0.0802	0.01185	<0.0001

The multiple linear regression has been performed on the experimental data to estimate the values of the coefficient (C) and the exponents (a, b, and c). The values of Ln (C) and the exponents (a, b, and c) have been listed in Table 4.4, and the regression statistic data has been illustrated in Table 4.5. The predicted correlation equation obtained for the pressure drop using multiple linear regression in JMP12 has been presented in Equation 5 with R^2 value of 0.999 and an average error of 0.016.

$$\mathrm{Eu} = 357.9523\ (\mathrm{Fr})^{-1.0229}(\mathrm{Ar})^{0.7782}\left(\frac{\mathrm{D_i}}{\mathrm{D_c}}\right)^{-0.0802} \qquad (5)$$

The mean relative deviation (MRD) from experimental and predicted results then:

$$\mathrm{MRD\%} = \left[\sum_{i=1}^{16}\left|\frac{\mathrm{Eu_{i,exp}}-\mathrm{Eu_{i,pred}}}{\mathrm{Eu_{i,exp}}}\right|\right]*\frac{100}{16} = 1.08\% \qquad (6)$$

The mean relative deviation (MRD) value of %1.08, obtained from Equation 6, shows a good agreement between the values of the Euler number predicted by Equation 5 and of the experimental data. The plot of experimental data against predicted values of the Euler number (pressure drop) is plotted in Figure 4.8.

Table 4.4. Parameter Estimates from Analysis of Variance of the parameters used in Equation 5.

Term	**Estimate**	**Std Error**	**Prob>|t|**
Intercept	Ln(c) = 6.7660	0.1822	<0.0001
Fr	a = -0.9717	0.0115	<0.0001
Ar	b = 0.6605	0.0244	<0.0001
Di/Dc	c = -0.0714	0.0072	<0.0001

Table 4.5. Regression statistic data (Summary of Fit)

RSquare	0.9993
RSquare Adj	0.9990
Root Mean Square Error	0.0164
Mean of Response	8.3786
Observations	16

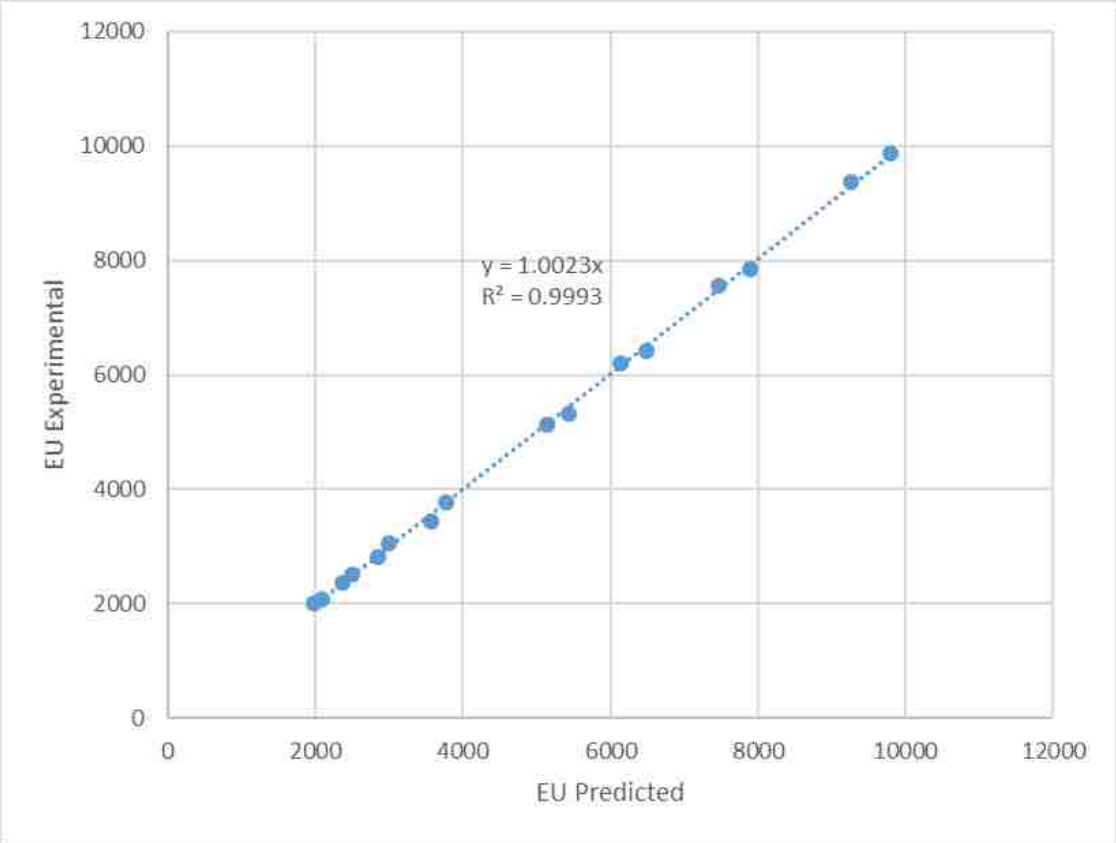

Figure 4.8. Comparison between experimental and predicted values of pressure drop measured at the wall of the bed in terms of Euler number.

4.6. PRESSURE DROP AT VARIOUS RADIAL LOCATIONS ALONG THE BED USING GLASS BEADS SOLID PARTICLES

The measurements of the pressure drop at various radial locations along the bed have been done using the pressure probe-differential pressure transducer that described earlier. Figures 4.9 shows the plot of the radial profiles of pressure drop, both with and without the two types of vertical internals, that occurred at different superficial gas velocities (u/u_{mf}) in the case of glass beads solid particles. Apparently, the radial profiles of pressure drop have decreased with the implementation of both types of vertical internals. However, the pressure drop reduction is relatively higher in the case of 0.0254 m internals when compared to the case of 0.0127 m internals. The decrease in radial profiles of pressure drop with vertical internals utilized inside the bed is due to the many advantages of implementing such vertical internals, as mentioned previously. One of these benefits is the pressure drop reduction, which was initially reported by Mathew et al. (2014) and Ramamoorthy and Subramanian (1981).

As mentioned earlier, only four radial positions (1, 0.8, 0.6, 0.4) were used to measure the radial profiles of pressure drop in the case of 0.0254 m internals due to the existence of the central internal in this configuration type. In order to compare the reduction in pressure drop in the cases with and without two types of vertical internals used, the pressure drop reduction or drag reduction was calculated using Equation 1.

The %PR at the four radial positions for the two types of vertical internals that used four different superficial gas velocities (u/u_{mf}) have been shown in Figure 4.10. Figure 4.10 confirms that the %PR of the 0.0254 m internals is higher than that of the 0.0127 m internals for most of the radial positions and superficial gas velocities. The difference in the results of these two types of vertical internals when reducing pressure drop, which is

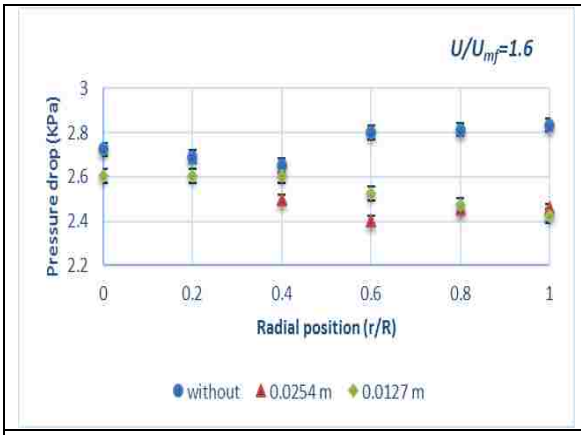

Radial profiles of pressure drop with and without internals at (u/u_{mf} =1.6)

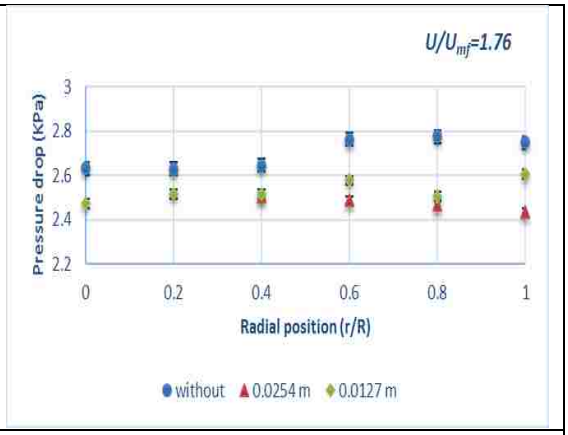

Radial profiles of pressure drop with and without internals at (u/umf =1.76)

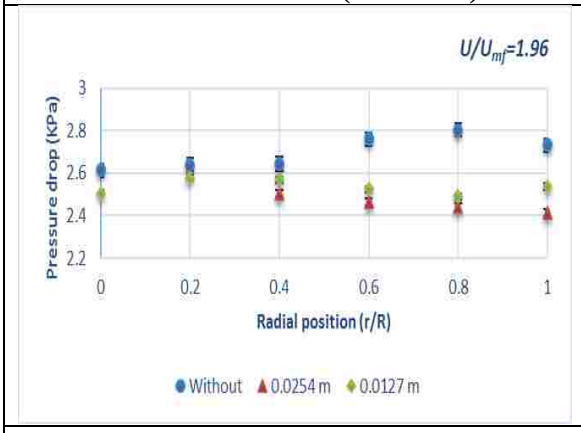

Radial profiles of pressure drop with and without internals at (u/u_{mf} =1.96)

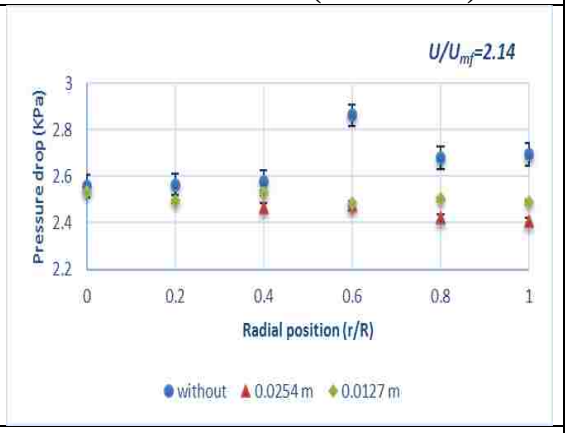

Radial profiles of pressure drop with and without internals at (u/u_{mf} =2.14)

Figure 4.9. Radial profiles of pressure drop with and without internals at different superficial gas velocities in glass beads solid particles.

represented by %PR, is due to the difference in distance between the internal tubes (tube to tube space), the arragement and size of internals, and these factors have a significant impact on the hydrodynamics behavior and flow patterns of the gas and solid phases inside the fluidized bed vessel (Rüdisüli, Schildhauer, Biollaz, and Van Ommen 2012c; Rüdisüli, Schildhauer, Biollaz, and Van Ommen 2012a; Mathew, Begum, and Anantharaman 2014). Additionally, Figure 4.10 shows that the %PR is high near the wall region and is reduced toward the center of the column for both types of vertical internals and all superficial gas

velocities (u/u_{mf}). Furthermore, the movement of the gas phase can explain this phenomenon: the gas bubbles move near the center of the column and away from the wall region, in which more drag forces are applied. The effect of the superficial gas velocity (u/u_{mf}) on the %PR is represented in Figure 4.11, in which the radial profiles of %PR of each type of vertical internal in Figure 4.10 have been averaged and plotted against their superficial gas velocities (u/u_{mf}). It should be noted that the %PR decreased when u/u_{mf}

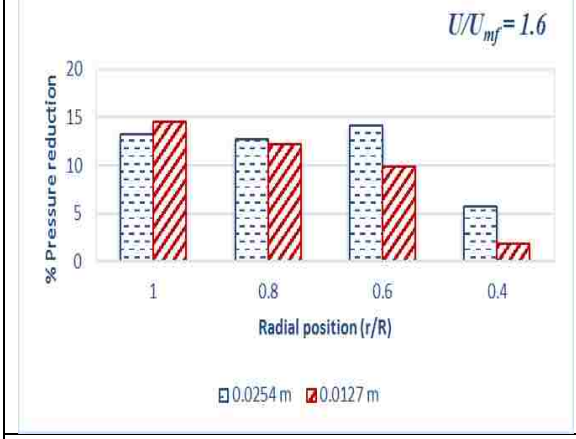

Radial profiles of % pressure reduction with and without internals at (u/u_{mf} =1.6)

Radial profiles of % pressure reduction with and without internals at (u/u_{mf} =1.76)

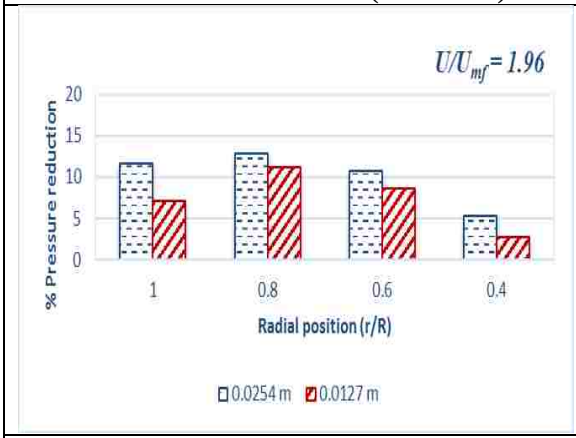

Radial profiles of % pressure reduction with and without internals at (u/u_{mf} =1.96)

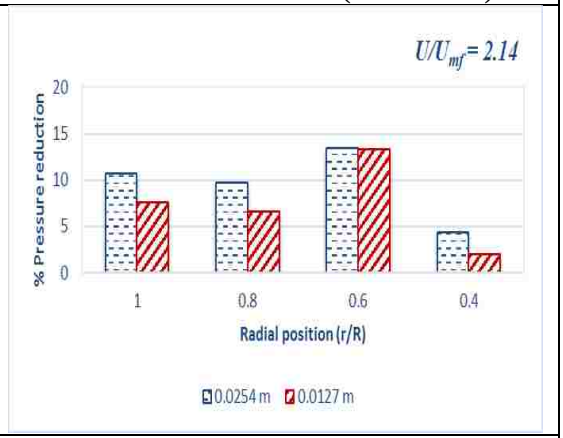

Radial profiles of % pressure reduction with and without internals at (u/u_{mf} =2.4)

Figure 4.10. Radial profiles of %pressure reduction with internals at different superficial gas velocities (u/u_{mf}) in the case of glass beads solid particles.

increased from 1.6 to 1.76 and that the values of %PR are almost constant when the superficial gas velocity (u/u_{mf}) increases.

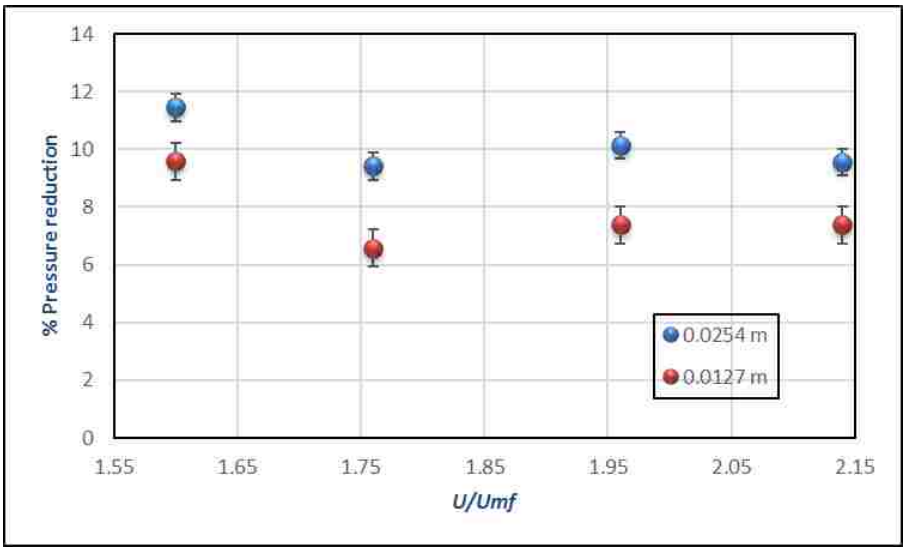

Figure 4.11. Effect of superficial gas velocity in terms of u/u_{mf} on the radial averaged %PR for the two types of vertical internals used in this work and for the case of glass beads solid particles.

As mentioned previously, the pressure drop experiments have been carried out using pressure probe transducer to measure the pressure drop fluctuation inside the bed. Figures 4.12 and 4.13 show the pressure drop fluctuation signals and their mean and variance values for cases with and without the two types of internals (0.0254 and 0.0127 m) at r/R = 1.0 and r/R = 0.4 with three different superficial gas velocities (1.76, 1.96, and 2.14). Both Figures 4.12 and 4.13 indicate that the mean of the pressure drop fluctuation signals is reduced in the case of both types of internals when compared to the case without internals. Moreover, because the mean of the pressure drop fluctuation signals represents the pressure drop measured at a certain operating condition and at a specific radial position,

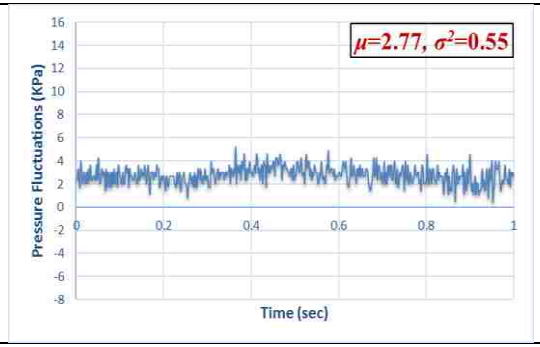	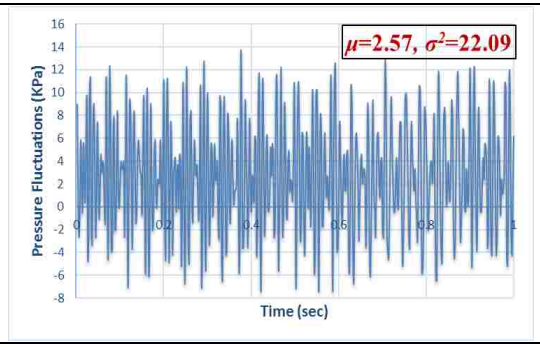	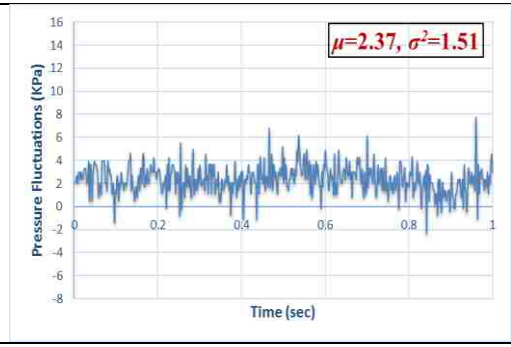
Pressure drop fluctuations without internals at (u/u_{mf} = 1.76)	Pressure drop fluctuations with 0.0127 m internals at (u/u_{mf} = 1.76)	Pressure drop fluctuations with 0.0254 m internals at (u/u_{mf} = 1.76)
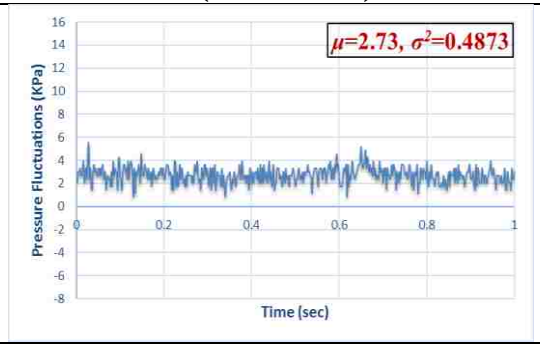	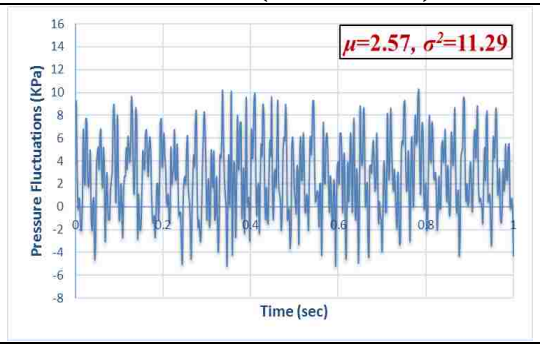	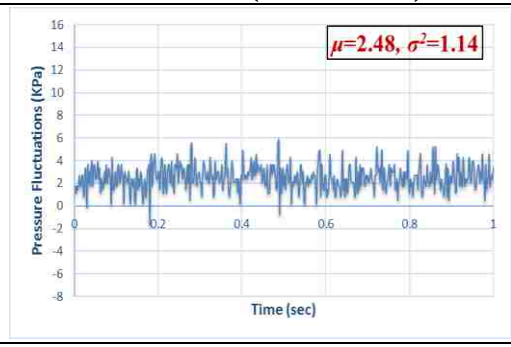
Pressure drop fluctuations without internals at (u/umf = 1.96)	Pressure drop fluctuations with 0.0127 m internals at (u/u_{mf} = 1.96)	Pressure drop fluctuations with 0.0254 m internals at (u/u_{mf} = 1.96)

Figure 4.12. Pressure drop fluctuations at (r/R= 1.0) for the cases of with and without internals at three different superficial gas velocities (u/u_{mf}) and in glass beads solid particles.

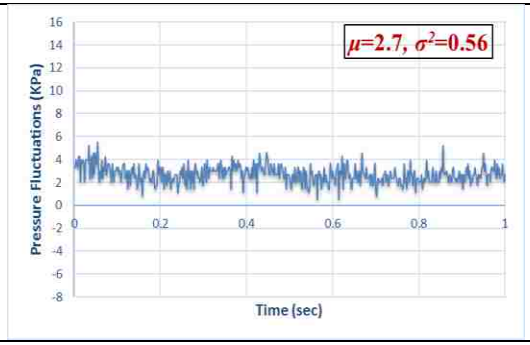

Pressure drop fluctuations without internals at (u/umf = 2.14)

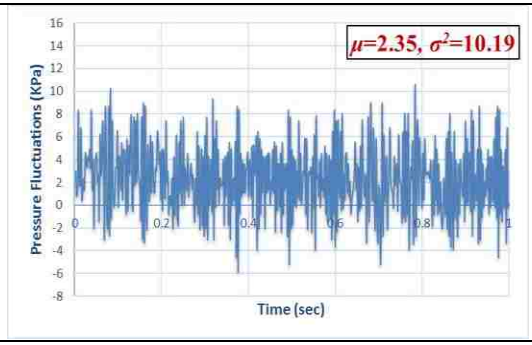

Pressure drop fluctuations with 0.0127 m internals at (u/u_{mf} = 2.14)

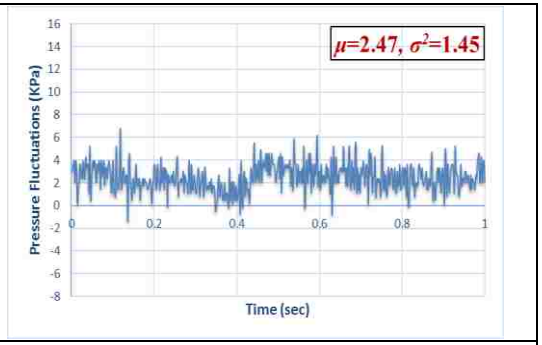

Pressure drop fluctuations with 0.0254 m internals at (u/u_{mf} = 2.14)

Figure 4.12. Pressure drop fluctuations at (r/R= 1.0) for the cases of with and without internals at three different superficial gas velocities (u/u_{mf}) and in glass beads solid particles. (cont.)

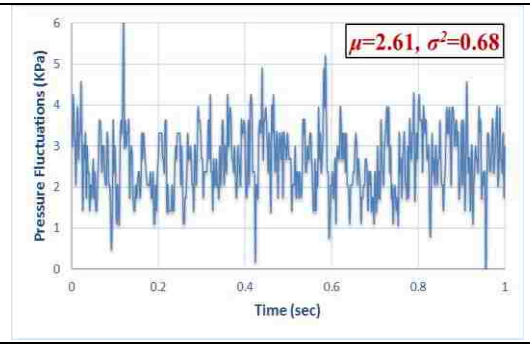

Pressure drop fluctuations without internals at (u/u_{mf} = 1.76)

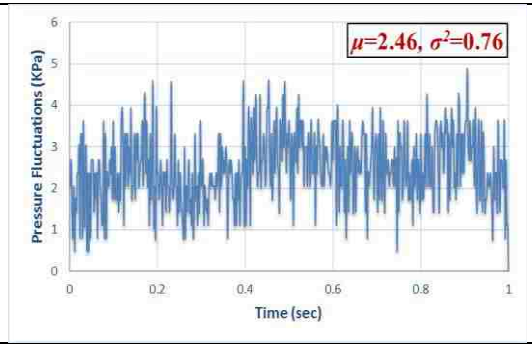

Pressure drop fluctuations with 0.0127 m internals at (u/u_{mf} = 1.76)

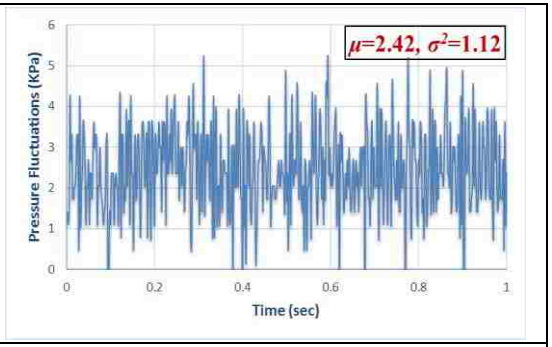

Pressure drop fluctuations with 0.0254 m internals at (u/u_{mf} = 1.76)

Figure 4.13. Pressure drop fluctuations at (r/R= 0.4) for the cases of with and without internals at three different superficial gas velocities (u/u_{mf}) and in glass beads solid particles.

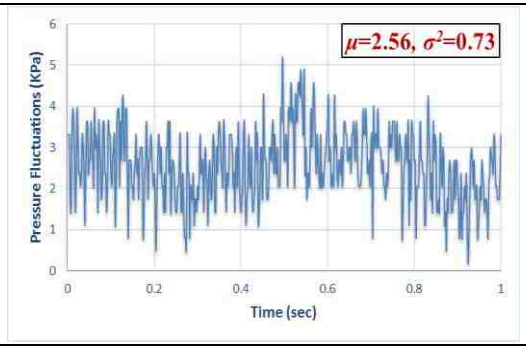	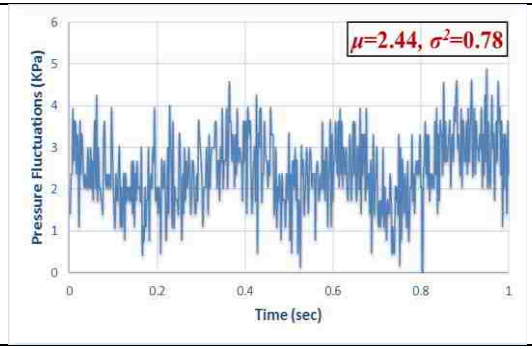	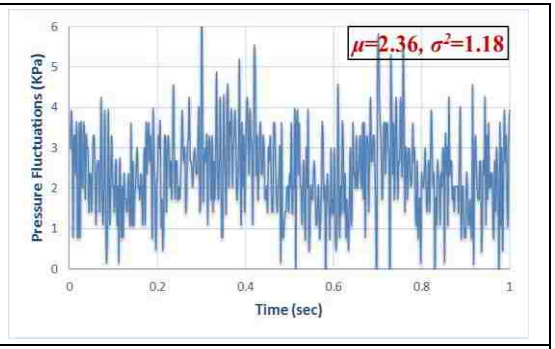
Pressure drop fluctuations without internals at (u/umf = 1.96)	Pressure drop fluctuations with 0.0127 m internals at (u/u_{mf} = 1.96)	Pressure drop fluctuations with 0.0254 m internals at (u/u_{mf} = 1.96)
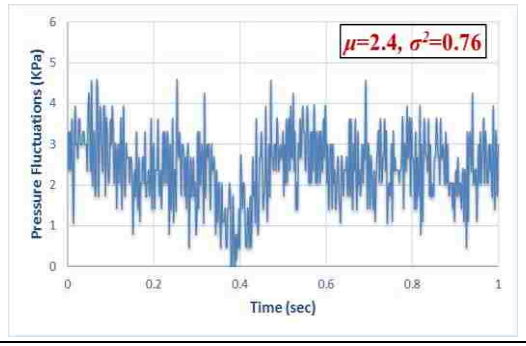	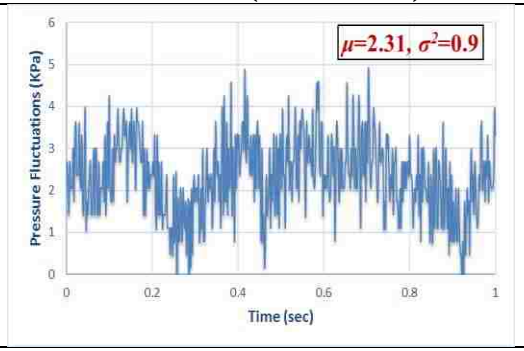	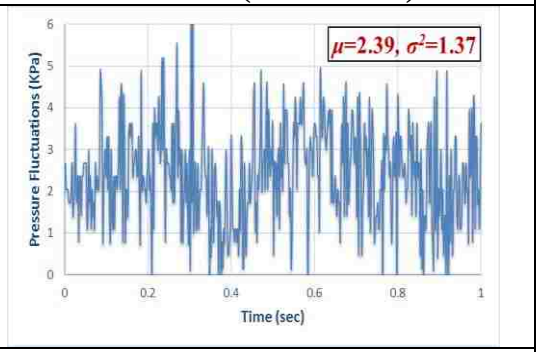
Pressure drop fluctuations without internals at (u/umf = 2.14)	Pressure drop fluctuations with 0.0127 m internals at (u/u_{mf} = 2.14)	Pressure drop fluctuations with 0.0254 m internals at (u/u_{mf} = 2.14)

Figure 4.13. Pressure drop fluctuations at (r/R= 0.4) for the cases of with and without internals at three different superficial gas velocities (u/u_{mf}) and in glass beads solid particles. (cont.)

the decrease in the mean values of the pressure drop fluctuation signals due to the presence of the vertical internals supports the finding of pressure drop reduction as a result of using vertical internals as shown the case of pressure drop measured at the wall of the bed that discusses earlier. Additionally, the decrease in mean values of the pressure drop fluctuation signals is higher in the case of 0.0254 m internals when compared to the case of 0.0127 m internals. Alternatively, at the wall region (r/R = 1.0), as in Figure 4.12, the frequency (variance) value of the pressure drop fluctuation signals has been increased with the implementation of two types of the vertical internals. This is especially true in the case of 0.0127 m internals. This increase in the variance values is due to the increase in the pressure fluctuations, and this is considered a useful phenomenon because it would lead to an increase in the local heat and mass transfer rates, an increase in the residence time of the gas phase inside the bed, and a reduction of the solid circulation by dividing the fluidized bed to multiple small fluidized bed sections (Law et al. 2003). Likewise, the enhancement in the variance values of the pressure drop fluctuations should be with the limit, as in the case of 0.0254 m internals, while for the case of 0.0127 m internals, the variance of the pressure drop fluctuations is considered overly high, which leads to an increase in the bed expansion and a reduction of the heat and mass transfer rates. Additionally, the residence time of the gas phase inside the bed would decreased, as shown in Figure 4.23. However, near the center region (r/R = 0.4), as in Figure 4.13, the frequency (variance) values of the pressure drop fluctuation signals have been relatively increased due to the use of both types of vertical internals, and this increase is higher in the case of 0.0254 m internals when compared to that of the 0.0127 m internals. In general, the 0.0254 m internals have shown an improvement in the performance of the selected gas–solid fluidized bed, in which the

use of this type of internals has offered lower pressure drop and higher pressure drop fluctuations when compared to the case without internals.

4.7. RADIAL PROFILES OF PRESSURE DROP USING ALUMINUM OXIDE SOLID PARTICLES

The radial measuremnts of the pressure drop along bed height for the case of aluminum oxide solids particles are carried out using pressure probe-differential pressure transducer at different superficial gas velocities in terms of u/u_{mf}. The radial profiles of pressure drop with and without vertical internals and of four different superficial gas velocities in terms of u/u_{mf}, in the case of aluminum solid particles, have been illustrated in Figure 4.14. As shown in Figure 4.14, the radial profiles of pressure drop have been reduced with the use of both types of vertical internals at low superficial gas velocity (u/u_{mf} =1.6). However, the reduction of the pressure drop is higher in the case of 0.0254 m internals comparing with that of 0.127 m vertical internal. The radial profile of the 0.0127 m internals increased when the superficial gas velocity increased, as in the case of u/u_{mf} =1.76 and 1.96, which means that the pressure drop increased with the use of this vertical internal (0.0127 m) with respect to the case without internals. While, the radial profiles of the pressure drop of 0.0254 m internals still showns less pressure drop when compared to the case without internals. The variation in the behavior of the two vertical internals may be explained by the difference in the vertical internals design parameters such as tube-to-tube space, tube sizes and configurations. Accordingly, the 0.0254 m internals have the ability to split the big bubbles in the system and reduce the slugging behavior because of the internals tubes of large size (0.0254 m) and because of the existence of the central

internal tube, which serves as an inhibitor of the formation of large bubbles and also makes the bubbles distribute more uniformly through the radial profiles inside the bed.

At high superficial gas velocity (u/u_{mf} =2.4), the radial profiles of both types of internals have been increased when compared to the case without internals, in which the radial profiles of pressure drop increased for both types of vertical internals used. In other words, the implementation of both types of the vertical internals would lead to an increase in the pressure drop at this high superficial gas velocity. Consequently, to explain the effect of the superficial gas velocity in terms of u/u_{mf} on the performance of the vertical internals with respect to the pressure drop inside the bed at different radial positions, the radial profiles of pressure drop have been averaged and plotted against the superficial gas velocity in terms of u/u_{mf}, as shown in Figure 4.15. Apparently, for the range of the superficial gas velocity used, the averaged pressure drop of the case without internals has gradually decreased along with an increase in the superficial gas velocity, which is one of the good characteristics of the conventional gas–solid fluidized bed (Mathew, Begum, and Anantharaman 2014).The same findings has been found in the case of pressure drop measured at the wall of the bed. Moreover, the average pressure drop of the 0.0127 m internals becomes stabilized after increasing the superficial gas velocity of u/u_{mf} =1.6 with higher pressure drop than in the case without internals, as mentioned above. However, for the case of 0.0254 m internals, the average pressure drops progressively increased with an increase in the superficial gas velocity until the gas velocity reached its maximum value at (u/u_{mf} =2.4). The superficial gas velocity, at the point when the average pressure drops of the cases both with 0.0254 m internals and without internals are equal, is about (u/u_{mf} =2.12), and the superficial gas velocity (u) of the case of 0.0254 m internals is 1.12 m/s at

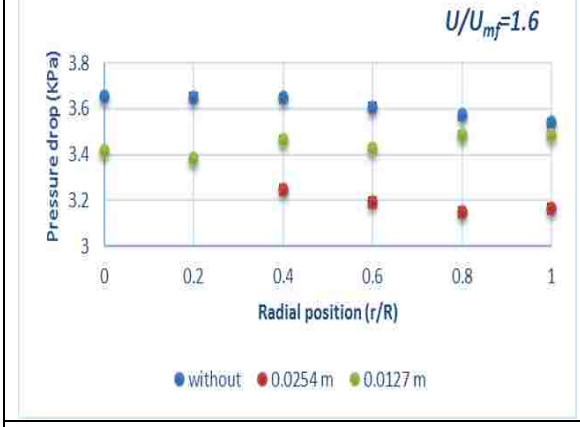

Radial profiles of pressure drop with and without internals at (u/u_{mf} =1.6)

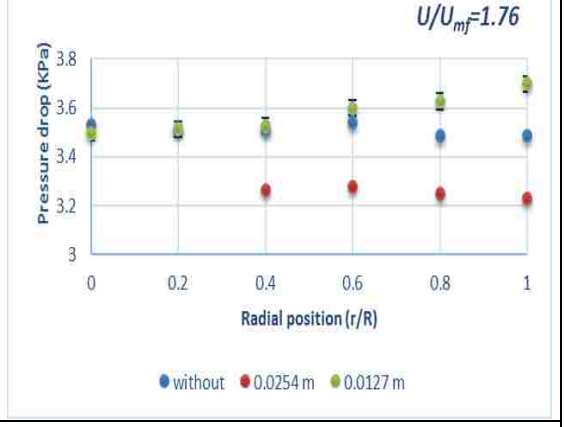

Radial profiles of pressure drop with and without internals at (u/u_{mf} =1.76)

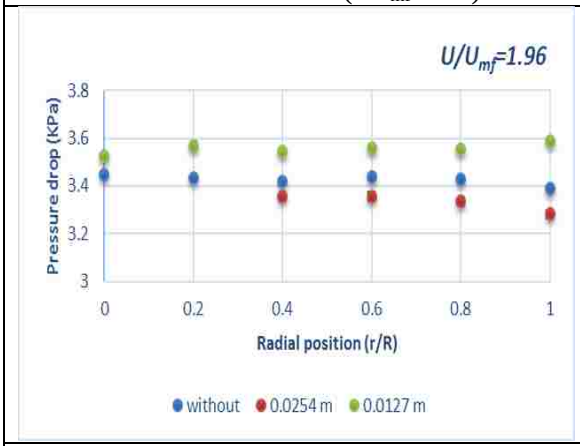

Radial profiles of pressure drop with and without internals at (u/u_{mf} =1.96)

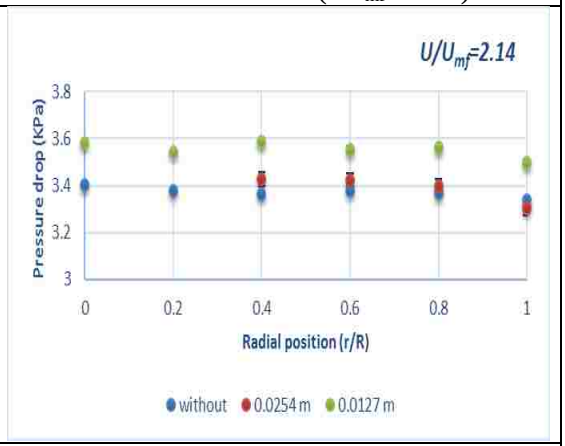

Radial profiles of pressure drop with and without internals at (u/u_{mf} =2.4)

Figure 4.14. Radial profiles of pressure drop with and without internals at different superficial gas velocities in aluminum oxide solid particles.

this point. The minimum fluidizing velocity in the case of aluminum oxide is 0.53 and 0.5 m/s for the cases with and without both types of vertical internals, as shown in Table 2.1. Thus, this point is more likely to represent slugging or even turbulent flow regime, and the change in the flow regime from bubbling to slugging or turbulent can explain why the pressure drop increased in the case of 0.0254 m internals at high superficial gas velocity (u/u_{mf} =2.14). The same trends of pressure drop with different superficial gas velocities has

been found in the case of pressure drop measured at the wall of the bed and for both cases of vertical internals used.

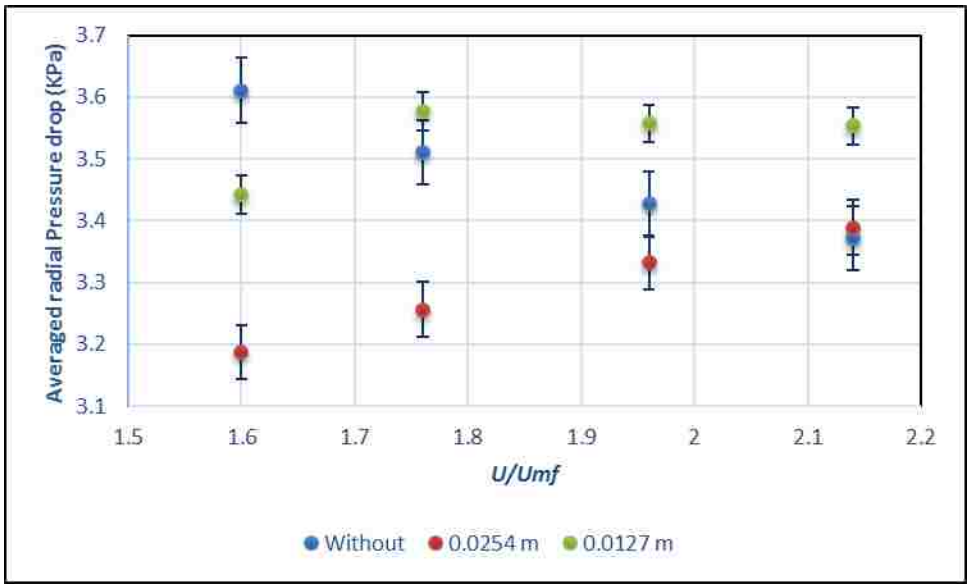

Figure 4.15. Effect of superficial gas velocity (u/u_{mf}) on the averaged radial pressure drop with and without for the case of glass beads solid particles.

The percentage of pressure reduction has been calculated using Equation 1, and it has been plotted in Figure 4.16 for the cases with two types of vertical internals at four radial positions (r/R = 1.0, 0.8, 0.6, and 0.4) and with four different superficial gas velocities in terms of u/u_{mf}. As shown in Figure 4.16, the %PR is higher in the case of 0.0254 m internals at low superficial gas velocity (u/u_{mf} =1.6) than that of 0.0127 m internals. As the superficial gas velocity increases, the %PR is decreased in the case of 0.0254 m internals, while for the case of 0.0127 m internals, the %PR starts to become negative (increasing the pressure drop inside the bed). As mentioned earlier, the divergence in the performance of the two types of internals is based on the difference in the design

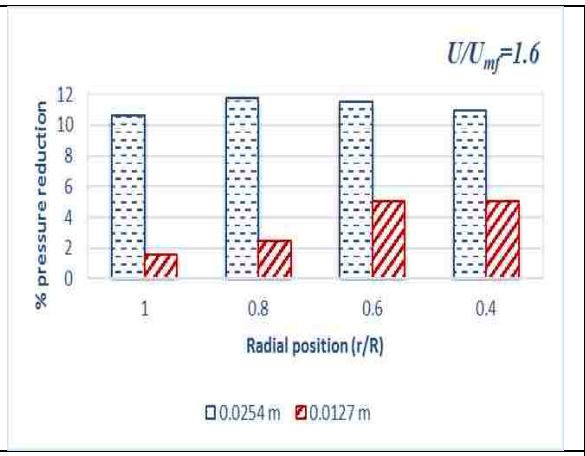

Radial profiles of % pressure reduction with and without internals at (u/u_{mf} =1.6)

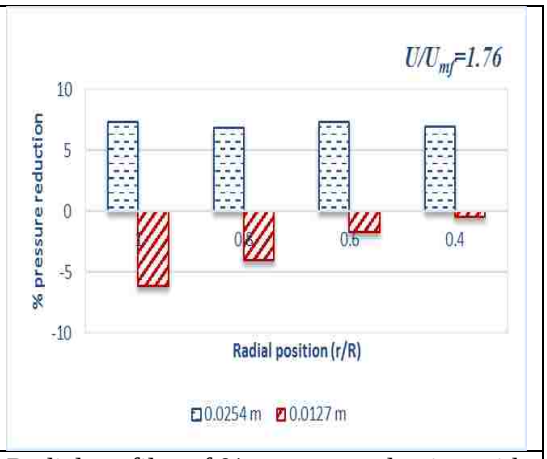

Radial profiles of % pressure reduction with and without internals at (u/u_{mf} =1.76)

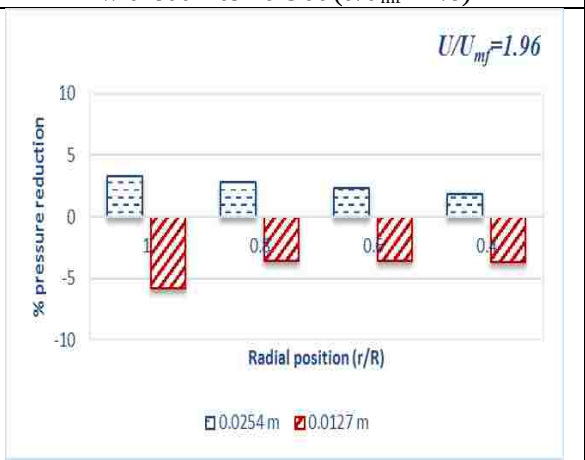

Radial profiles of % pressure reduction with and without internals at (u/u_{mf} =1.96)

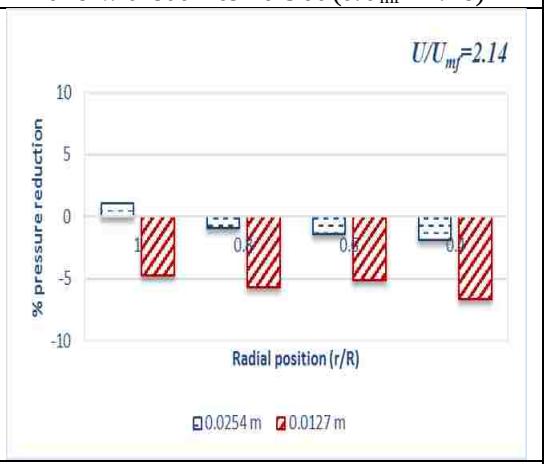

Radial profiles of % pressure reduction with and without internals at (u/u_{mf} =2.4)

Figure 4.16. Radial profiles of %pressure reduction with internals at different superficial gas velocities in aluminum oxide solid particles.

parameters of these two types. This variation can affect the solid circulation and gas–solid flow patterns as well as the hydrodynamic properties of both of solid and gas phases, such as bubble size, bubble frequency, bubble velocity, holdup, and velocity of solids (Rüdisüli, Schildhauer, Biollaz, and Van Ommen 2012c; Rüdisüli, Schildhauer, Biollaz, and Van Ommen 2012a; Maurer, Wagner, van Ommen, et al. 2015; Maurer, Wagner, Schildhauer, et al. 2015). Additionally, Figure 4.16 shows that the %PR is high near the center region

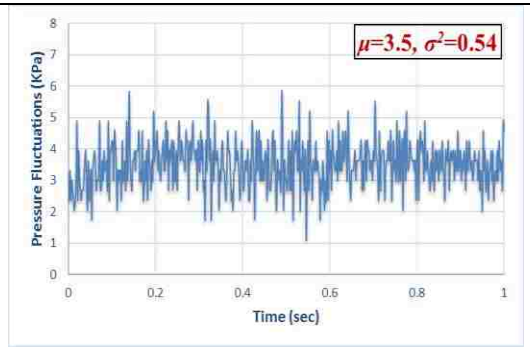

Pressure drop fluctuations without internals at (u/u_{mf} = 1.76)

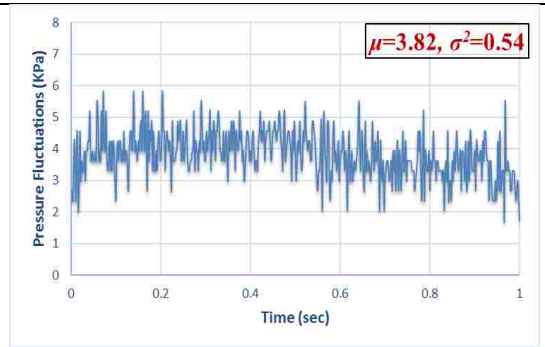

Pressure drop fluctuations with 0.0127 m internals at (u/u_{mf} = 1.76)

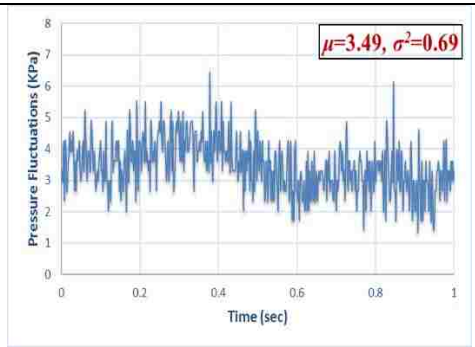

Pressure drop fluctuations with 0.0254 m internals at (u/u_{mf} = 1.76)

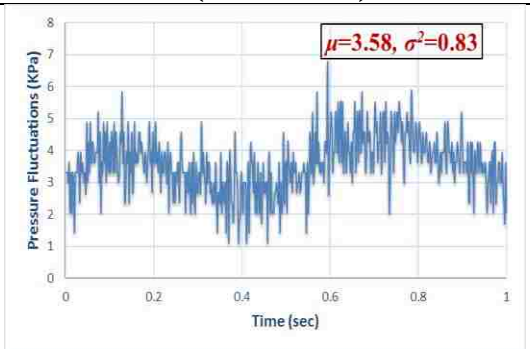

Pressure drop fluctuations without internals at (u/umf = 1.96)

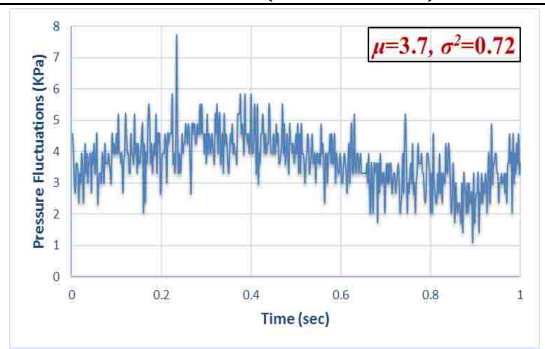

Pressure drop fluctuations with 0.0127 m internals at (u/u_{mf} = 1.96)

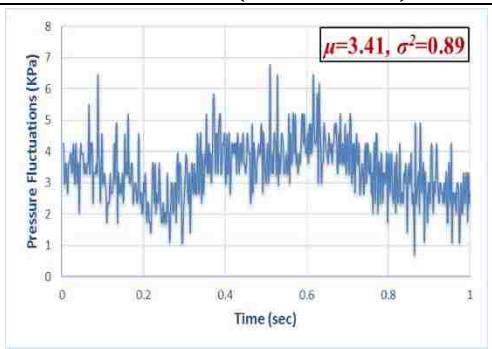

Pressure drop fluctuations with 0.0254 m internals at (u/u_{mf} = 1.96)

Figure 4.17. Pressure drop fluctuations at (r/R= 1.0) for the cases of with and without internals at three different superficial gas velocities in terms of u/u_{mf} and in aluminum oxide solid particles.

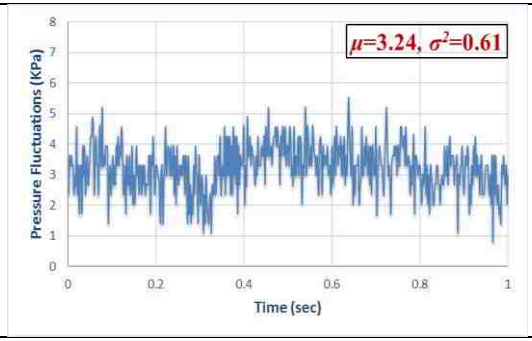

Pressure drop fluctuations without internals at (u/umf = 2.14)

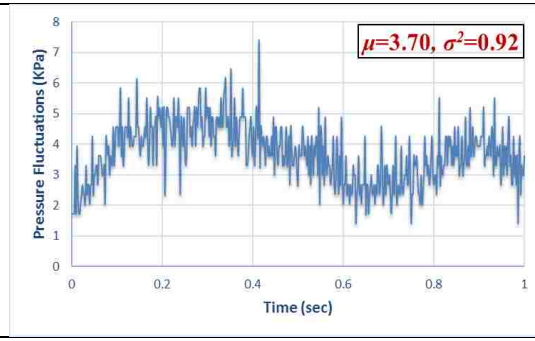

Pressure drop fluctuations with 0.0127 m internals at (u/u_{mf} = 2.14)

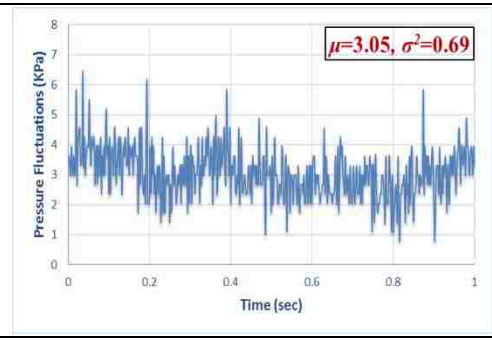

Pressure drop fluctuations with 0.0254 m internals at (u/u_{mf} = 2.14)

Figure 4.17. Pressure drop fluctuations at (r/R= 1.0) for the cases of with and without internals at three different superficial gas velocities in terms of u/u_{mf} and in aluminum oxide solid particles. (cont.)

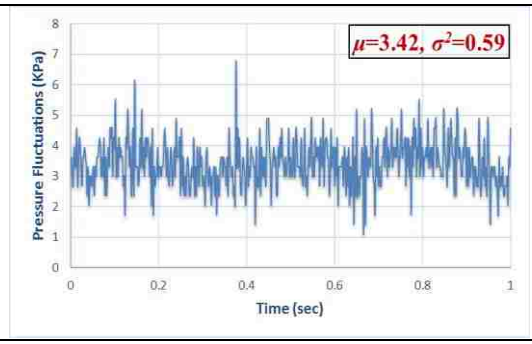

Pressure drop fluctuations without internals at (u/u_{mf} = 1.76)

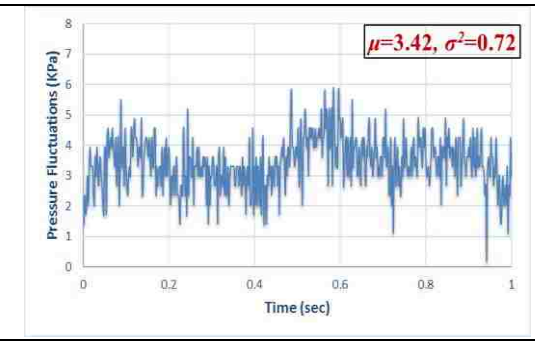

Pressure drop fluctuations with 0.0127 m internals at (u/u_{mf} = 1.76)

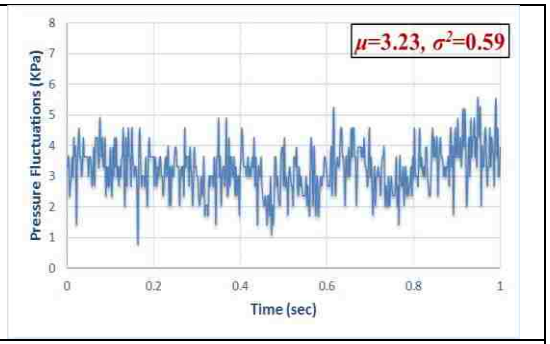

Pressure drop fluctuations with 0.0254 m internals at (u/u_{mf} = 1.76)

Figure 4.18. Pressure drop fluctuations at (r/R= 0.4) for the cases of with and without internals at three different superficial gas velocities in terms of u/u_{mf} and in aluminum oxide solid particles.

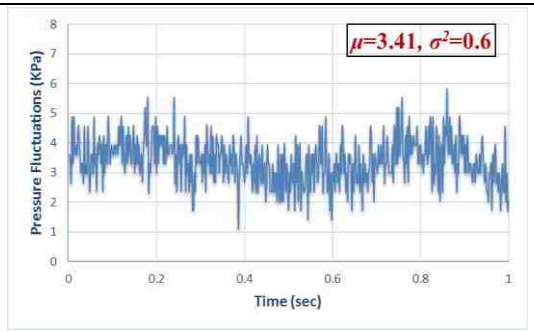	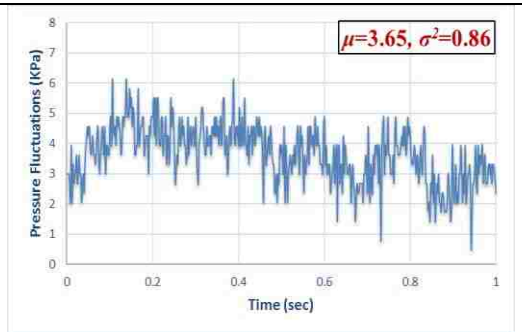	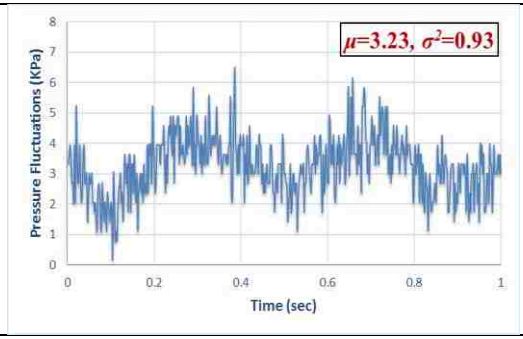
Pressure drop fluctuations without internals at (u/umf = 1.96)	Pressure drop fluctuations with 0.0127 m internals at (u/u_{mf} = 1.96)	Pressure drop fluctuations with 0.0254 m internals at (u/u_{mf} = 1.96)
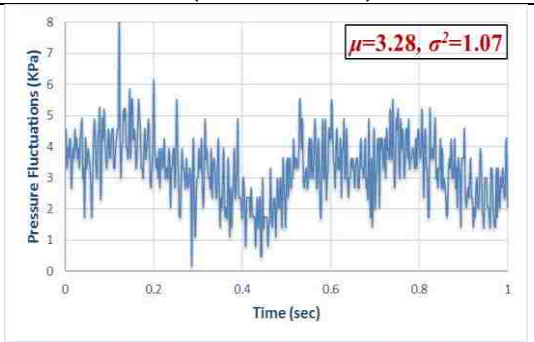	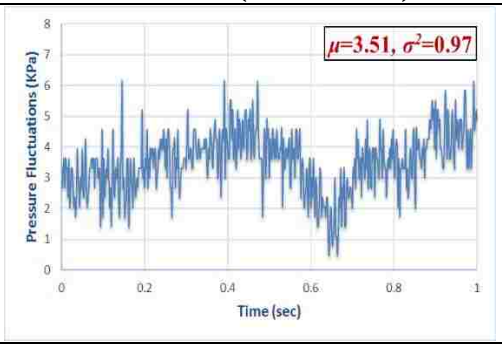	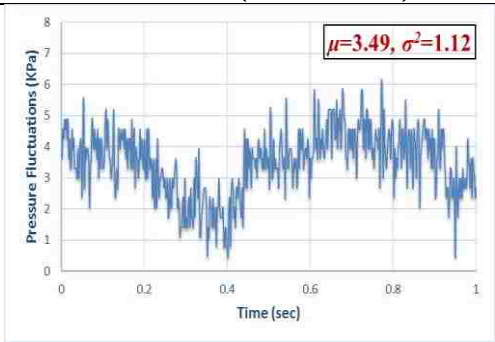
Pressure drop fluctuations without internals at (u/umf = 2.14)	Pressure drop fluctuations with 0.0127 m internals at (u/u_{mf} = 2.14)	Pressure drop fluctuations with 0.0254 m internals at (u/u_{mf} = 2.14)

Figure 4.18. Pressure drop fluctuations at (r/R= 0.4) for the cases of with and without internals at three different superficial gas velocities in terms of u/u_{mf} and in aluminum oxide solid particles. (cont.)

and decreases toward the wall of the column for the 0.0127 m internals at low superficial gas velocities (u/u_{mf}), while it almost constant for case of 0.0254 m internals at all superficial gas velocities used in this work.

The pressure drop fluctuation signals have been plotted and compared in terms of their amplitude (mean) and frequency (variance) values for different superficial gas velocities and in cases with and without internals. As in the case of glass beads solid particles, two radial positions were selected for the comparison of radial position, and these were selected near the center of the column ($r/R = 0.4$) and at the wall region ($r/R = 1.0$). The pressure drop fluctuation signals have been presented in Figures 4.17 and 18 for the cases with and without internals at three different superficial gas velocities ($u/u_{mf} = 1.76$, 1.96, and 2.14). Figure 4.17 shows the pressure fluctuation signals at the wall region, while Figure 4.18 illustrates the pressure fluctuation signals near the center of the bed. Figure 4.17 and 4.18 also show that the mean values of the pressure drop fluctuation signals (local pressure drop) increase in the case of 0.0127 m internals at both radial positions. Additionally, the mean values of the pressure drop fluctuation signals are shown to decrease in the case of 0.0254 m internals for both of the selected radial positions. Accordingly, the pressure drop reduction, which is represented by decreasing the mean values of the pressure drop fluctuations due to the presence of the 0.0254 m internals, confirms the results of lowering the pressure drop with the existence of this type of internal that was mentioned earlier. Furthermore, Figures 4.17 and 4.18 indicate that the values of variance of the pressure drop fluctuation signals have increased in the case of 0.0254 m internals when compared to the case without internals, for all superficial gas velocities used and at both radial positions. This increment would lead to enhancement of the contact

between the gas and solid phases, increase the gas residence time, and improve the fluidization quality. However, the values of the variance of the 0.0127 m internals have shown irregular attitudes compared to the case without internals. In these cases, the variance value decreased when the superficial gas velocity increased from 1.76 to 1.96, and the variance value increased when the superficial gas velocity increased from 1.96 to 2.14 at (r/R = 1.0). Alternatively, the variance value increased when the superficial gas velocity increased from 1.76 to 1.96, and it decreased when the superficial gas velocity increased from 1.96 to 2.14 at (r/R = 0.4).

4.8. COMPARISON OF RADIAL PRESSURE REDUCTION OF THE TWO SOLID PARTICLES

The radial profiles of %PR have been compared for the two solid particles used in this work (glass beads and aluminum oxide) and for different superficial gas velocities (u/u_{mf}), as shown in Figure 4.19 for the case of 0.0254 m internals. Since the 0.0254 m internals have been proven to have less pressure drop in both solid particles when compared to the case without internals, the radial profiles of %PR have been plotted against four radial positions, as mentioned earlier for the case of 0.0254 m internals. The following can be concluded from Figure 4.19:

1. The radial profiles of %PR in the case of glass beads are higher than those of the aluminum oxide for all superficial gas velocities and for most of the radial positions.
2. The difference between the two cases in terms of %PR becomes bigger with an increase in superficial gas velocity.

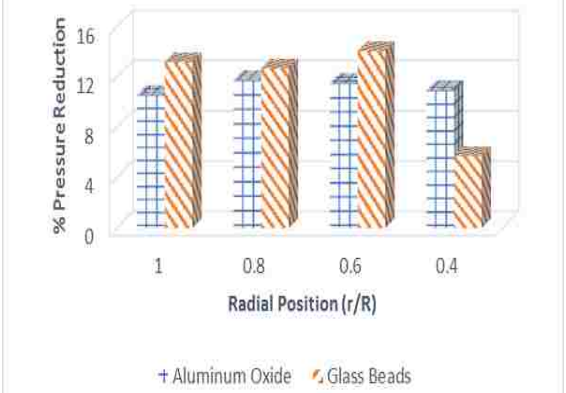

Radial profiles of %PR for both solids at (u/u_{mf} =1.6)

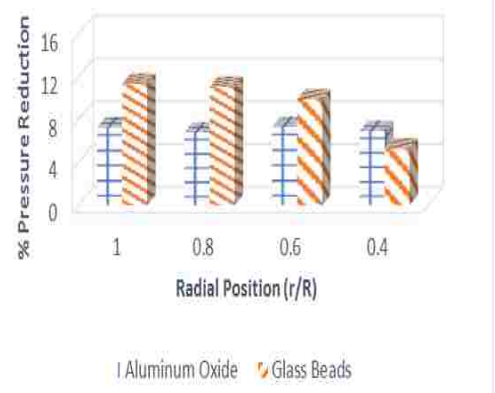

Radial profiles of %PR for both solids at (u/u_{mf} =1.76)

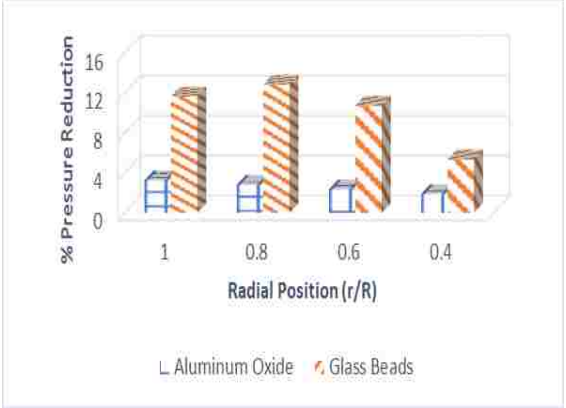

Radial profiles of %PR for both solids at (u/u_{mf} =1.96)

Radial profiles of %PR for both solids at (u/u_{mf} =2.4)

Figure 4.19. Radial profiles of %pressure reduction for 0.0254 m internals at different superficial gas velocities in both solid particles used in current work.

3. The %PR in the case of aluminum oxide is almost constant with radial position, while in the case of glass beads, it is higher near the wall and lower near the center.
4. The difference in the performance of the 0.0254 m internals due to the type of solid particles used is based on the difference in physical properties of the two solid particles. These physical properties are solid particle shape (the glass beads have a spherical shape and the aluminum oxide has an angular, or irregular shape) and the solid density (the density of glass beads is 2500 Kg/m^3 and the density of the

aluminum oxide is 3900 Kg/m^3). These physical properties can affect the pressure drop inside the bed, as indicated by many experimental works (A. Sahoo and Roy 2005; Kaza 2008; Abanti Sahoo 2011; Mathew, Begum, and Anantharaman 2014).

5. In general, the 0.0254 m internals can reduce the pressure drop inside the conventional gas–solid fluidized bed by about 16%. This reduction can minimize the power consumption through the operation of this type of chemical reactor, and it can also improve the hydrodynamic characteristics of the fluidized bed reactor when implementing such vertical internals inside the bed.

5. REMAKES

The pressure drop measured at the wall of the bed and the radial profiles of pressure drop along the bed height have been measured using differential pressure transducer and pressure probe-differential pressure transducer in a gas–solid fluidized bed of 0.14 m inside diameter. The impacts of two types of circular configurations of intense vertical internals (0.0254 m and 0.0127 m diameter) on the pressure drop measured at the wall and the radial pressure drop along the bed height have been studied in this work. Two types of solid particles of Geldart B type (glass beads and aluminum oxide) with the same average particle size, different solid densities, solid shapes, and sphericity factor as well as four different superficial gas velocities (u/u_{mf} = 1.6, 1.76, 1.96, and 2.14) have been used to study the effect of the physical and operating parameters on the pressure drop measured at the wall of the bed and radial pressure drops measured along the bed height. The following have been concluded:

- The pressure drop measured at the wall and the radial profiles of pressure drop in the case of glass beads were found to decrease with both types of internals.
- In the case of aluminum oxide, the pressure drop measured at the wall and the radial profiles of pressure drop decreased with the 0.0254 m internals and increased with 0.0127 m internals due to the reduction in spaces between the internals, the internal tube sizes, the nature of the aluminum oxide solid particles (irregular particle shapes, while the glass beads are spherical particles), and the difference in the solid densities.
- The experimental results of the pressure drop measured at the wall of the bed are compared with the correlations available in literature and a big difference was found between the predicated and experimental results. Therefore, a new correlation was developed using JMP 12 statistical software that based on relevant dimensionless groups and using the multiple linear regression method. These dimensionless groups represent the operation, design, and physical parameters of the gas–solid fluidized bed system used in the present work. The predicted correlation was in good agreement with experimental results with a mean relative deviation value of 1.08%.
- The dimensionless groups of the Froude number (Fr), Archimedes number (Ar) and the diameter ratio (D_i/D_c) have been found to significantly affect the pressure drop in terms of Euler number inside the used gas–solid fluidized bed.
- The percentage pressure reduction (%PR) in the cases of pressure drop measured at the wall and the radial pressure drop measured along the bed height are generally

decreases with an increase in the superficial gas velocity for both types of solid particles.

- The radial profiles of the %PR in the case of aluminum oxide with 0.0254 m internals was almost constant for all radial positions, while in the case of glass beads it was high near the wall and became lower toward the center of the bed.

ACKNOWLEDGEMENTS

The authors would like to thank the Multiphase Reactors Engineering and Applications Laboratory (mReal) for funding and support.

NOMENCLATURE

D_c	Column diameter (m)
D_i	Internal diameter (m)
d_p	Particle diameter (μm)
g	gravitational force (m/s^2)
r	Radial position (m)
R	Radius of the column (m)
u	superficial gas velocity (m/s)
u_{mf}	minimum fluidized velocity (m/s)
Δp	pressure drop (KPa)
μ_g	gas viscosity (Kg/m.s)
ρ	gas density (Kg/m^3)
ρ_s	Solid particle density (Kg/m^3)

Greek Letters

μ	Viscosity (Kg/m.s)
ρ	Density (Kg/m3)

Subscripts and Superscripts

g	gas
p	Particle
s	solid

Abbreviations

%PR	Percentage pressure drop
Ar	Archimedes number
Eu	Euler number
Fr	Froude number
MRD	Mean relative deviation

REFERENCES

A. Pinto. 1978. Ammonia Production Process, issued 1978.

Bartholomew, Calvin H., and Robert J. Farrauto. 2010. *Fundamentals of Industrial Catalytic Processes: Second Edition*. *Fundamentals of Industrial Catalytic Processes: Second Edition*. doi:10.1002/9780471730071.

Grace, J. R., and D. Harrison. 1968. "The Effect of Internal Baffles in Fluidized Beds: A Guide to Design." In *Inst. Chem. Eng. Symp. Ser.*

Kar, Sudakhina, and G. K. Roy. 2000. "Effect of Co-Axial Rod Promoters on the Dynamics of a Batch Gas-Solid Fluidized Bed." *Indian Chemical Engineers* 42 (3): 170–74.

Kaza, Srinivasa Rao Venkata Naga. 2008. "Effect of Various Parameters on the Solids Holdup in a Liquid-Solid Circulating Fluidized Bed Effect of Various Parameters on the Solids Holdup in a Liquid-Solid Circulating Fluidized Bed." *International Journal of Chemical Reactor Engineering* 6.

Krishnamurty, S, J S N Murty, G K Roy, Associate Member, and V S Pakala. 1981. "Gas-Solids Fluidization in Baffled Beds." *Journal of the Institution of Engineers (India)* 61 (February).

Kumar, A, and G K Roy. 2002. "Influence of Coaxial-Rod- and Coaxial-Blade-Type Baffles on Bed Expansion in Gas – Solid Fluidization." *Powder Technology* 126: 91–95.

Law, Chung Lim, Siti Masrinda Tasirin, Wan Ramli Wan Daud, and Derek Geldart. 2003. "Effect of Vertical Baffles on Particle Mixing and Drying in Fluidized Beds of Group D Particles." *China Particuology* 1 (3): 115–18. doi:10.1016/S1672-2515(07)60121-3.

Mathew, Ronnie Kiran, K. M Meera Sheriffa Begum, and N. Anantharaman. 2014. "Hydrodynamic Studies on Fluidized Beds with Internals: Experimental and ANN Approach." *Powder Technology* 264. Elsevier B.V.: 423–29. doi:10.1016/j.powtec.2014.06.001.

Maurer, Simon, Evert C Wagner, Tilman J Schildhauer, J. Ruud van Ommen, Serge M A Biollaz, and Robert F Mudde. 2015. "X-Ray Measurements of Bubble Hold-up in Fluidized Beds with and without Vertical Internals." *International Journal of Multiphase Flow* 74. Elsevier Ltd: 118–24. doi:10.1016/j.ijmultiphaseflow.2015.03.009.

Maurer, Simon, Evert C Wagner, J. Ruud van Ommen, Tilman J Schildhauer, Sinan L Teske, Serge M A Biollaz, Alexander Wokaun, and Robert F Mudde. 2015. "Influence of Vertical Internals on a Bubbling Fluidized Bed Characterized by X-Ray Tomography." *International Journal of Multiphase Flow* 75. Elsevier Ltd: 237–49. doi:10.1016/j.ijmultiphaseflow.2015.06.001.

Mohanty, Y. K., B. P. Mohanty, G. K. Roy, and K. C. Biswal. 2009. "Effect of Secondary Fluidizing Medium on Hydrodynamics of Gas-Solid Fluidized Bed-Statistical and ANN Approaches." *Chemical Engineering Journal* 148 (1): 41–49. doi:10.1016/j.cej.2008.07.037.

Olowson, P.A. 1994. "Influence of Pressure and Fluidization Velocity on the Hydrodynamics of a Fluidized Bed Containing Horizontal Tubes." *Chemical Engineering Science* 49 (15): 2437–46.

Ommen, J Ruud Van, Jaap C Schouten, Michel L M Stappen, and Cor M Van Den Bleek. 1999. "Response Characteristics of Probe – Transducer Systems for Pressure Measurements in Gas – Solid Fluidized Beds : How to Prevent Pitfalls in Dynamic Pressure Measurements." *Powder Technology* 106: 199–218. doi:10.1016/S0032-5910(99)00078-9.

Padhi, S. K., R. K. Singh, and S. K. Agrawal. 2010. "Effect of Twisted Tape Baffles on Pressure Drop, Fluctuation and Expansion Ratios in Gas - Solid Fluidized Bed." *Iranian Journal of Chemistry and Chemical Engineering* 29 (1): 33–40.

Ramamoorthy, S., and N. Subramanian. 1981. "Axial Solids Mixing and Bubble Characteristics in Gas-Fluidized Beds with Vertical Internals." *Chemical Engineering Journal* 22 (3): 237–42.

Rüdisüli, Martin, Tilman J. Schildhauer, Serge M. A. Biollaz, and J. Ruud Van Ommen. 2012a. "Radial Bubble Distribution in a Fluidized Bed with Vertical Tubes." *Industrial and Engineering Chemistry Research* 51 (42): 13815–24. doi:10.1021/ie3004418.

Rüdisüli, Martin, Tilman J. Schildhauer, Serge M A Biollaz, and J. Ruud Van Ommen. 2012b. "Scale-up of Bubbling Fluidized Bed Reactors - A Review." *Powder Technology* 217. Elsevier B.V.: 21–38. doi:10.1016/j.powtec.2011.10.004.

Rüdisüli, Martin, Tilman J Schildhauer, Serge M A Biollaz, and J. Ruud van Ommen. 2012. "Bubble Characterization in a Fluidized Bed by Means of Optical Probes." *International Journal of Multiphase Flow* 41: 56–67. doi:10.1016/j.ijmultiphaseflow.2012.01.001.

Rüdisüli, Martin, Tilman J Schildhauer, Serge M A Biollaz, and J. Ruud Van Ommen. 2012c. “Bubble Characterization in a Fluidized Bed with Vertical Tubes.” *Industrial and Engineering Chemistry Research* 51 (12): 4748–58. doi:10.1021/ie2022306.

Sahoo, A., and G. K. Roy. 2005. “Bed Expansion of a Squared Gas-Solid Promoted Fluidized Bed By Modified Godard - Richardson Equation.” *Indian Chemical Engineers* 47 (2).

Sahoo, Abanti. 2011. “Bed Expansion and Fluctuation in Cylindrical Gas Solid Fluidized Beds with Stirred Promoters.” *Advanced Powder Technology* 22 (6). The Society of Powder Technology Japan: 753–60. doi:10.1016/j.apt.2010.10.019.

Sau, D. C., S. Mohanty, and K. C. Biswal. 2008a. “Correlations for Critical Fluidization Velocity and Maximum Bed Pressure Drop for Binary Mixture of Regular Particles in Gas-Solid Tapered Fluidized Beds.” *Chemical Engineering and Processing: Process Intensification* 47 (12): 2114–20. doi:10.1016/j.cep.2007.10.022.

Sau, D. C., S. Mohanty, and K. C. Biswal. 2008b. “Critical Fluidization Velocities and Maximum Bed Pressure Drops of Homogeneous Binary Mixture of Irregular Particles in Gas-Solid Tapered Fluidized Beds.” *Powder Technology* 186 (3): 241–46. doi:10.1016/j.powtec.2007.12.008.

Shanshool, Jabir, and Haider Al-Qamaje. 2008. “Effect of Molecular Weight on Turbulent Drag Reduction with Polyisobutylene.” In *NUCEJ Spatial*, 11:52–59.

Tijm, P. J A, F. J. Waller, and D. M. Brown. 2001. “Methanol Technology Developments for the New Millennium.” *Applied Catalysis A: General* 221 (1–2): 275–82. doi:10.1016/S0926-860X(01)00805-5.

Van Ommen, J. Ruud, Srdjan Sasic, John Van der Schaaf, Stefan Gheorghiu, Filip Johnsson, and Marc Olivier Coppens. 2011. “Time-Series Analysis of Pressure Fluctuations in Gas-Solid Fluidized Beds - A Review.” *International Journal of Multiphase Flow* 37 (5). Elsevier Ltd: 403–28. doi:10.1016/j.ijmultiphaseflow.2010.12.007.

Van Ommen, J. Ruud, Jaap C. Schouten, Michel L M Vander Stappen, and Cor M. Van Den Bleek. 1999. “Response Characteristics of Probe-Transducer Systems for Pressure Measurements in Gas-Solid Fluidized Beds: How to Prevent Pitfalls in Dynamic Pressure Measurements.” *Powder Technology* 106 (3): 199–218. doi:10.1016/S0032-5910(99)00078-9.

Van Ommen, J. Ruud, John Van Der Schaaf, Jaap C. Schouten, Berend G M Van Wachem, Marc Olivier Coppens, and Cor M. Van Den Bleek. 2004. “Optimal Placement of Probes for Dynamic Pressure Measurements in Large-Scale Fluidized Beds.” *Powder Technology* 139 (3): 264–76. doi:10.1016/j.powtec.2003.12.009.

Volk, W., C. A. Johnson, and H. H. Stotler. 1962. “Effect of Reactor Internals on Quality of Fluidization.” *Chemical Engineering Progress* 58 (3): 44–47.

Xie, H.-Y, and D Geldart. 1997. “The Response Time of Pressure Probes.” *Powder Technology* 90 (2): 149–51. doi:10.1016/S0032-5910(96)03218-4.

Yerushalmi, J., and N. T. Cankurt. 1979. “Further Studies of the Regimes of Fluidization.” *Powder Technology* 24 (2): 187–205. doi:10.1016/0032-5910(79)87036-9.

Yerushalmi, J., N. T. Cankurt, D. Geldart, and B. Liss. 1978. “Flow Regimes in Vertical Gas-Solid Contact Systems.” In *Fluidization CONF-761109-8*. New York (USA); Bradford Univ.(UK); Coalcon, New York (USA).

V. COMPARISON BETWEEN THE NEW MECHANISTIC AND THE CHAOS SCALE-UP METHODS FOR GAS-SOLID FLUIDIZED BEDS

Haidar Taofeeq[1] and Muthanna Al-Dahhan[2]*

Multiphase Reactors Engineering and Applications Laboratory (mReal)

Department of Chemical & Biochemical Engineering

Missouri University of Science & Technology, Rolla, MO 65409 USA

ABSTRACT

The chaotic scale-up approach by matching the Kolmogorov entropy (KE) proposed by Schouten et al. (1996) was assessed in two geometrically similar scales of gas-solid fluidized bed columns of 0.14 and 0.44 m diameter. we used four conditions of our validated new mechanistic scale-up method based on matching the radial profiles of gas holdup where the local dimensionless hydrodynamic parameters were similar as measured by advanced measurement techniques. These experimental conditions were used to evaluate the validity of the chaotic scale-up method, which were selected based on our new mechanistic scale-up methodology that is built on matching radial profiles of the gas holdup between the fluidized beds. Pressure gauge transducer measurements at the wall and inside the bed at various local radial locations and at three axial heights were used to estimate KE. It was found that the experimental conditions with similar or close radial profiles of the Kolmogorov entropy and with similar or close radial profiles of the gas holdup achieve similarity in local dimensionless hydrodynamics parameters. While, the experimental conditions with non-similar radial profiles of the KE and of the gas holdup have non-similar local dimensionless hydrodynamic parameters.

Keywords: Scale-up, chaotic analysis approach, new scale-up methodology, Kolmogorov entropy, gas-solid fluidized bed.

* Corresponding author: aldahhanm@mst.edu

1. INTRODUCTION

The fluidized bed is considered one of the most important solid-gas reaction and contacting systems with a vast number of industrial applications, such as catalyst regeneration, drying, catalytic cracking, Fischer-Tropsch synthesis, gas-solid polymerization (Kelkar and Ng 2002; Rüdisüli et al. 2012) and many others. Gas-solid fluidized bed reactors are characterized by many advantages compared with the other types of reactors (e.g., fixed bed reactors) which include simple to construct; relative low operating and maintenance expenses; low pressure drop; approximately isothermal temperature distribution, excellent contact and good mixing between the gas and solid particles, good mass and heat transfer rates; and have ability to handle a large quantity of solid particles even with a continuous process rate (Horio et al. 1986).

Despite all these advantages, due to the complexity of the flow structure and the multifaceted interaction between the phases of gas-solid fluidized beds, it has been challenging to understand and quantify their hydrodynamics, design, scale-up, and performance. In addition, the gas-solid mixing behavior is poorly understood (Bisio and Kabel 1985). These drawbacks make it difficult to scale up gas-solid fluidized bed reactors from small-scale (laboratory- or pilot plant-scale) to industrial-scale. Rüdisüli et al. (2012) reported some of the pitfalls that could be associated with poor scale-up, such as gas bypassing, gas channeling, partial defluidization, erosion and damage to immersed surfaces, elutriation of solid particles, a reduction in the heat and mass transfer rate performance, and insufficient solid particle mixing.

Many experimental and numerical studies related to scale-up of gas-solid fluidized beds have been reported in the open literature (Knowlton 2013; Zaid 2013; Efhaima 2016;

Efhaima and Al-Dahhan 2016). As a result, various scaling methods have been proposed to maintain hydrodynamics similarity in scaling up of the gas-solid fluidizing beds (Zaid 2013; Efhaima 2016; Efhaima and Al-Dahhan 2016). These scale-up methods for geometrically similar gas-solid fluidized beds can be characterized as follows: (1) matching key dimensionless groups (Glicksman 1984; Nicastro and Glicksman 1984; Horio et al. 1986; Glicksman 1988; Glicksman et al., 1993; Stein et al., 2002), (2) matching chaotic behavior by estimating Kolmogorov Entropy (KE) of the pressure signal to describe the order/disorder of the system (Van Den Bleek and Schouten 1993; Van den Bleek, Schouten, and Bleek 1993; J. C. Schouten, Vander Stappen, and Van Den Bleek 1996), and (3) matching the radial or diameter profiles of the gas holdups as a mechanistic new method since the gas phase dictate the dynamics of these beds (Zaid 2013; Al-Dahhan et al. 2014; Efhaima 2016; Efhaima and Al-Dahhan 2016)

In our research group, we have assessed the scaling up method based on matching dimensionless groups using advanced measurement techniques of optical fiber probe, radioactive particle tracking (RPT), gamma ray computed tomography (CT), and gamma ray densitometry (GRD). We found that the used dimensionless groups are not sufficient to maintain hydrodynamics similarity and it will become difficult to apply if the number of the dimensionless groups to match increase (Zaid (2013); Efhaima (2016); Efhaima and Al-Dahhan (2016). Al-Dahhan et al. (2014) proposed a new mechanistic methodology for scaling up gas-solid fluidized beds to achieve hydrodynamics similarity in beds that are geometrically similar. This method is based on matching the radial or diameter profiles of the gas phase holdup at a height within the bed that could represent the hydrodynamics of the bed. Advanced measurement techniques have been used to validate this method by

measuring local detailed hydrodynamics using optical fiber probes, gamma ray computed tomography (CT), radioactive particle tracking (RPT), and gamma ray densitometry (GRD) techniques (Zaid 2013; Efhaima 2016; Efhaima and Al-Dahhan 2016). However, the method that is based on matching Kolmogorov entropy (KE) (Schouten et al.,1996) of the pressure signal measured at the wall has not been evaluated by measuring the detailed local hydrodynamic parameters using the above-mentioned techniques. Schouten et al. (1996) proposed matching Kolmogorov entropy (KE) estimated from the pressure drop signal measured at the wall to scale-up and maintain hydrodynamics similarity of gas-solid fluidized beds. In this case, KE represents the degree of freedom of the system or in other words the degree of the order/disorder behavior of the system. The basic concept of this chaos analysis based method is that the rate of information loss should be kept similar when scaling up a fluidized bed from small-scale to the large-scale, to ensure the hydrodynamics similarity between the two scaled beds. The advantage of this method as stated by Schouten et al., (1996) is that the KE is explicitly linked to the bed diameter and hence same solid particles can be used in both scales of the fluidized beds. Thus, the problem of finding appropriate solid particles is averted as in the case of matching dimensionless groups. In addition, the dimensionless entropy group number (KE d_p/u) is directly proportional to the Froude number ($u_g^2/g\ d_p$) and the ratio between the static bed height and the bed diameter. Van Den Bleek and Schouten (1993a, b) claimed that when the dimensionless entropy group number is matched in the two scales of a fluidized bed, the matching of dimensionless scaling groups in terms of the Froude number and H/D_c ratio are enough to have matching cases.

Accordingly, the foucs of this work is to assess the scale-up of a gas-solid fluidized bed based on the chaos analysis based methodology proposed by Schouten et al. (1996), by applying their methodology using pressure signal on the matching cases of our new mechanistic scale-up methodology which is based on matching the radial profiles of the gas holdup between two fluidized beds with geometrical similarity where the similarirty detailed hydrodynamic parameters have been measured and confirmed using the above mentioned advanced measurements techniques. In this case, at these conditions we will assess if the estimated KE from the measured pressure signal at the wall and inside the bed at various axial and radial locations will be matched or not.

2. DESCRIPTION OF THE APPROACH FOR THE ASSESSMENT OF THE CHAOTIC METHOD FOR SCALE-UP OF FLUIDIZED BED

The chaotic based scale-up methodology was assessed using the experimental conditions that we used for validating our new mechanistic scale-up methodology, that is based on matching the radial profiles of the gas holdup between two scales of gas-solid fluidized beds that are geometrically similar. Therefore, the experimental conditions used by Zaid (2013), Efhaima (2016), and Efhaima and Al-Dahhan (2016) were used in the present study, as illustrated in Table 2.1. In this table, there are conditions of Case B with respect to the conditions of the reference case (Case A) that provide similar gas holdup radial profiles as we confirmed and measured by optical fiber probe and gamma ray computed tomography (CT) techniques measurement in these two beds. The local hydrodynamic parameters such as dimensionless solids velocity, gas/solid holdups, dimensionless turbulent parameters (stresses and turbulent kinetic energy) have been measured using radioactive particle tracking, gamma ray computed tomography and

Table 2.1. Conditions that provide similar gas holdup radial profiles that give similarity in local hydrodynamics and non-similar gas holdup radial profiles that give non-similarity in local hydrodynamics

Condition	Reference Case (Case A)	Condition for similar ($\varepsilon_{g,r}$) (Case B)	Condition for non-similar ($\varepsilon_{g,r}$) (Case C)	Condition for non-similar ($\varepsilon_{g,r}$) (Case D)
D_c (m)	0.44	0.14	0.14	0.14
Particle types	Glass Beads	Glass Beads	Glass Beads	Glass Beads
L (m)	4.877	4.775	4.775	4.775
H (m)	0.88	0.28	0.28	0.28
T (K)	298	298	298	298
P (Kpa)	101	101	101	101
d_p (µm)	210	70	70	210
ρ_s (Kg/m^3)	2500	2500	2500	2500
ρ_f (kg/m^3)	1.21	1.21	1.21	1.21
µ (Kg·s m^{-2})	1.81E-05	1.81E-05	1.81E-05	1.81E-05
U_{mf} (m/s)	0.105	0.06	0.06	0.12
U_g (m/s)	0.36	0.25	0.2	0.2
***Φ* (sphericity)**	0.95	0.95	0.95	0.95
Dc/dp	2095.24	2000	2000	666.67
H/D_c	2	2	2	2
ρ_s/ρ_f	2066.12	2066.12	2066.12	2066.12
U/U_{mf}	3.42	4.1666	3.3333	1.666
$Fr=U^2/(g*H)$	0.015	0.0227	0.0145	0.0145
$Fr=U_{mf}^2/(g*H)$	0.0011	0.0013	0.0013	0.0052
e_{ss}	0.9	0.9	0.9	0.9

optical fiber probe techniques. We found that these hydrodynamic parameters are similar or close to each other when the radial profiles of the gas holdup are close to each other. The question then will the Kolmogorov entropy (KE) of the pressure signal measured at the wall or inside the bed be similar or close to each other or not in these beds identical to cases A and B. This has been assessed here by adopting the conditions of Case A and the conditions of Case B for similar ($\varepsilon_{g,r}$). Since we have already approved similarity of these mentioned local parameters that have been reported in Zaid (2013), Al-Dahhan et al. (2014), Efhaima (2016), and Efhaima and Al-Dahhan (2016), we are not going to report these results rather that we state that if KEs are similar or not when these local hydrodynamic parameters are similar and vice versa. Same approach will be applied to the cases where the hydrodynamic parameters are not similar which are for the cases of Case C and Case D with respect to the reference Case A. We will see in this assessment if KE will be also non-similar and the magnitude of its non-similarity proportional to the magnitude of the non-similarity of the measured hydrodynamic parameters that reported by our work mentioned above.

In this approach, Case A was selected as a reference condition, while Case B was identified (matching conditions) to have similar or close radial profiles of the gas holdup. Cases C and D were selected as mismatching conditions because they have different radial profiles of radial gas holdup compared with the reference condition (Case A). In this work, both Cases A and B were considered matching cases, while Cases C and D were considered mismatching cases. It is worth mentioning that the new scale-up methodology was validated using both invasive and noninvasive techniques mentioned above. We confirmed that Cases A and B have the same radial profiles of dimensionless particles velocity in the

form of (V_p/u_{mf}), where u_{mf} is the minimum fluidization velocity. Additionally, the radial profiles of the dimensionless turbulent parameters with respect to the minimum fluidization velocities (e.g., dimensionless shear stresses, dimensionless turbulent kinetic energy, and dimensionless eddy diffusivity,) were matched for Cases A and B (Zaid 2013; Al-Dahhan et al. 2014; Efhaima 2016; Efhaima and Al-Dahhan 2016).

3. EXPERIMENTAL SETUP

The experimental setup consisted of two fluidized bed columns of 0.14 m and 0.44 m inside diameters, with similar geometries. Both columns were constructed from Plexiglas®, and the plenums were made from aluminum. The columns and plenums were placed on the top of a stainless steel base. Industrial-scale compressor was used to supply compressed air to the columns at pressures up to 1.38 MPa. Omega flow meters controlled the gas flow rate entering the columns. Schematic diagrams of the two fluidized bed columns are shown in Figures 3.1 and 3.2. The 0.14 m inside diameter column was 1.84 m high and connected from the top with an upper section that had a larger diameter of 0.42 m. It was 0.84 m high to disengage the solid particles from the flowing gas by reducing the superficial gas velocity and hence the terminal velocity of the solids. The gas phase was introduced through a sparger tube inside the plenum section and then through a distributor affixed between the column and plenum sections. The gas distributor was manufactured of a porous polyethylene sheet and had a pore size of 15-40 μm. The sparger tube was plugged at one end and had 14 holes, all facing downward with respect to the column. This sparger construction makes the gas distribution more homogenous. The 0.44 m inside diameter fluidized bed column closely resembled the 0.14 m inside diameter fluidized bed column.

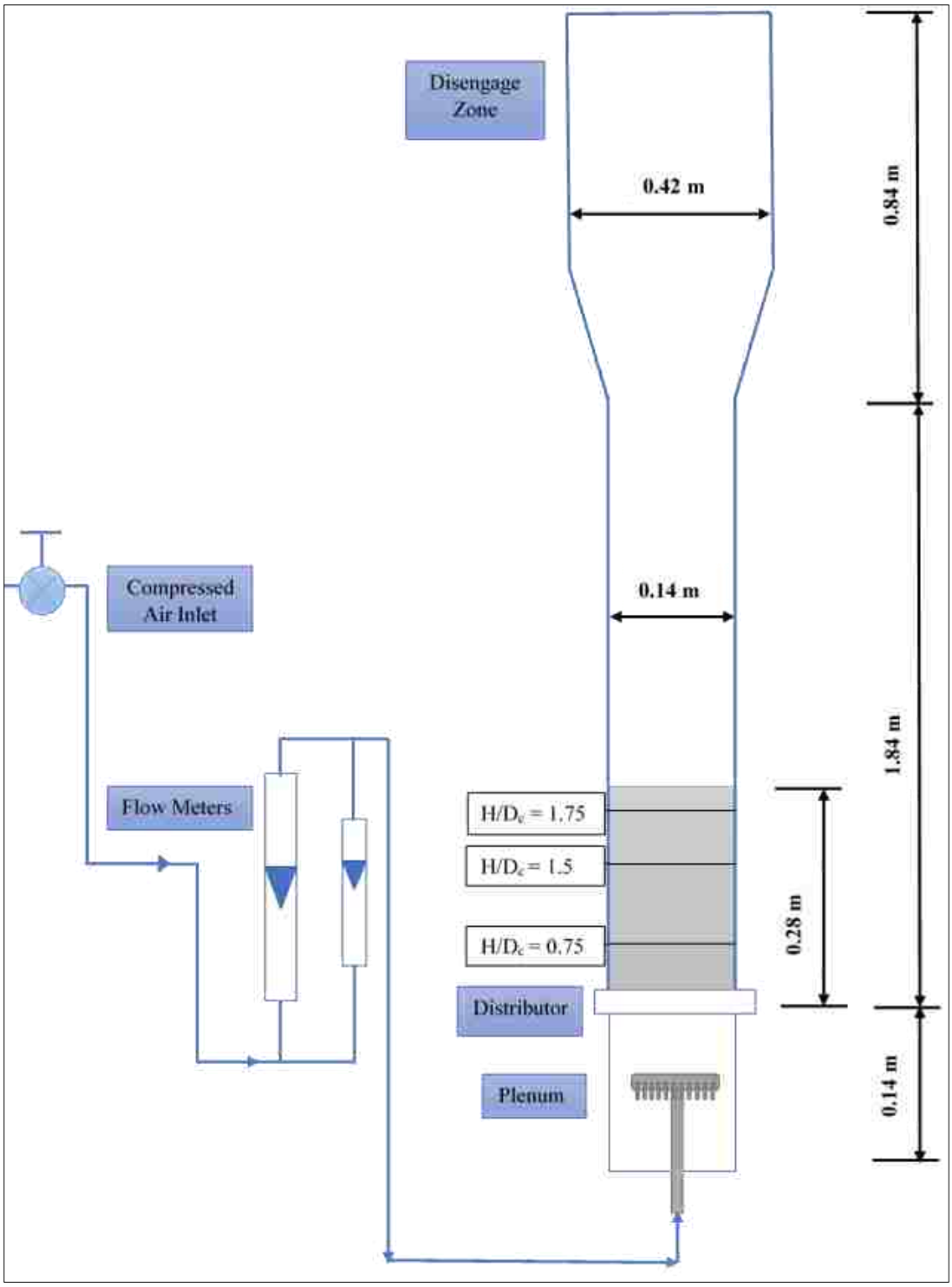

Figure 3.1. Schematic diagram of 0.14 m inside diameter fluidized bed column.

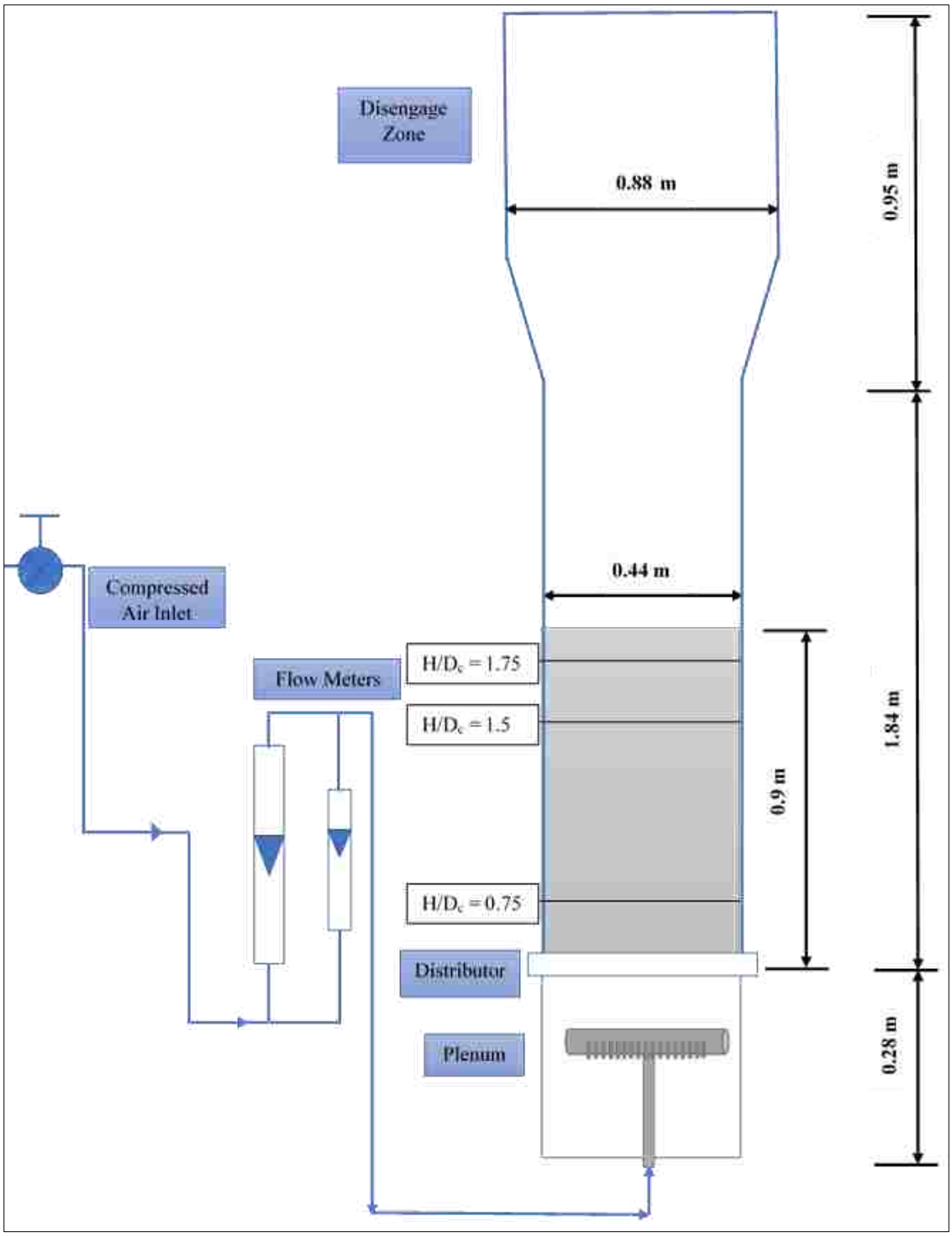

Figure 3.2. Schematic diagram of 0.44 m inside diameter fluidized bed column.

Figure 3.3. Photo of the two fluidized bed columns.

The shape of the upper section was similar, but it had an inside diameter of 0.88 m and was 0.95 m high. The distributor design was also similar to that used in the 0.14 m diameter fluidized bed column, and the plenum consisted of a sparger tube, which had 20 holes, all facing downward with respect to the column. Both fluidized bed columns were electrically grounded to minimize the electrostatic effects. A photo of the two fluidized bed columns is shown in Figure 3.3.

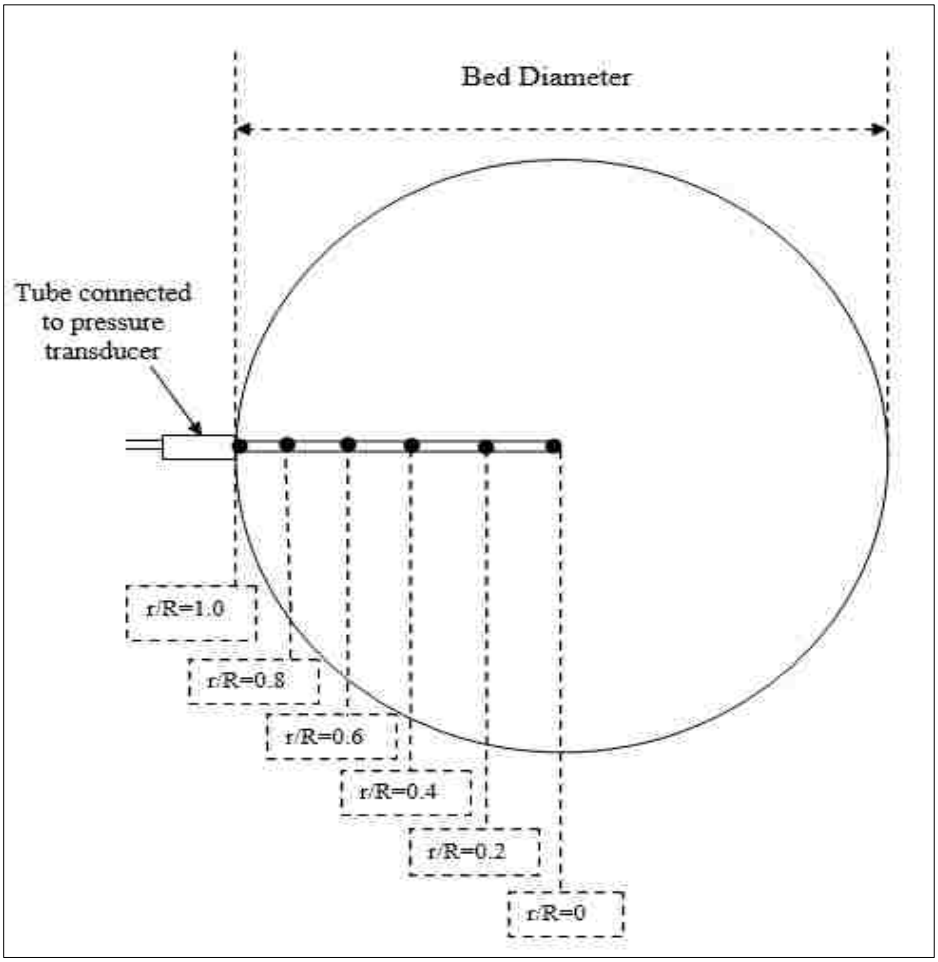

Figure 3.4. Local measurements at six radial positions for all three heights: H/D_c = 0.75, 1.5, and 1.75 of both columns.

The gauge-pressure transducer measurements were acquired at H/D_c = 0.75, 1.5, and 1.75 above the gas distributor for both fluidized bed columns. The selection of three axial heights was made to cover three important axial zones inside the fluidized bed: (1) H/D_c = 0.75, which represents the axial zone near the distributor plate, when the bubbles first form and rise through the dense phase; (2) H/D_c = 1.5, which represents the axial zone that is located approximately in the middle of the fluidizing bed which is the region that represent the bed hydrodynamics; (3) H/D_c = 1.75, which represents the axial zone near the

freeboard of the column, when the bubbles and their wake start to disengage and leave the bed.

In addition, local measurements using a tube connected to the pressure transducer and it is called here pressure probe were taken at six radial positions (r/R = 0.0, 0.2, 0.4, 0.6, 0.8, and 1.0) and at the same mentioned H/D_c, as shown in Figure 3.4. The solid particles used in this work were similar to the cases listed in Table 2.1 and were glass beads with two average particle sizes (70 μm and 210 μm) and a particle density of 2500 Kg/m^3.

4. EXPERIMENTAL TECHNIQUE

4.1. SINGLE-ENDED PRESSURE TRANSDUCER

A single-ended pressure transducer (Omega Inc., model PX-409-050GV) was used to measure the pressure fluctuation signals at three axial heights and six radial positions of the fluidized beds mentioned before, covering the gauge pressure range from 0-345 kPa. The pressure transducer was connected to an AC power supply, which provided a voltage proportional to the measured pressure. The signal was received by the data acquisition (DAQ) system (Omega Inc., model OMB-DAQ-3000), which has high-speed capability in collecting data up to 10^6 Hz, and was connected to the computer. The signals were recorded for 100 s at a rate of 100 Hz and repeated five times to ensure the reproducibility of the results which was found to be less than 5%. The error bars in terms of standard deviation were found to be within the data point. It is worthy to mention that a wide range of sampling frequency (25 to 500 Hz) was used to estimate which sampling rate properly provide the Kolmogorov entropy KE since the KE estimation is highly depended on the sampling rate as stated by Van Ommen et al. (2011). The number of data points for each signal was 10^4,

as recommended by Schouten et al. (1994) to be an adequate measurement of the Kolmogorov Entropy estimation.

4.2. A TUBE AS A LOCAL PRESSURE PROBE CONNECTED TO THE PRESSURE TRANSDUCER

Local pressure probe of 2.5 mm inside diameter and lengths of 0.2 m and 0.3 m tubes made from stainless steel were connected to a single-ended pressure transducer to measure the local pressure fluctuations at a number of radial and axial locations inside the used fluidized beds as shown in Figures 4.1 and 4.2.

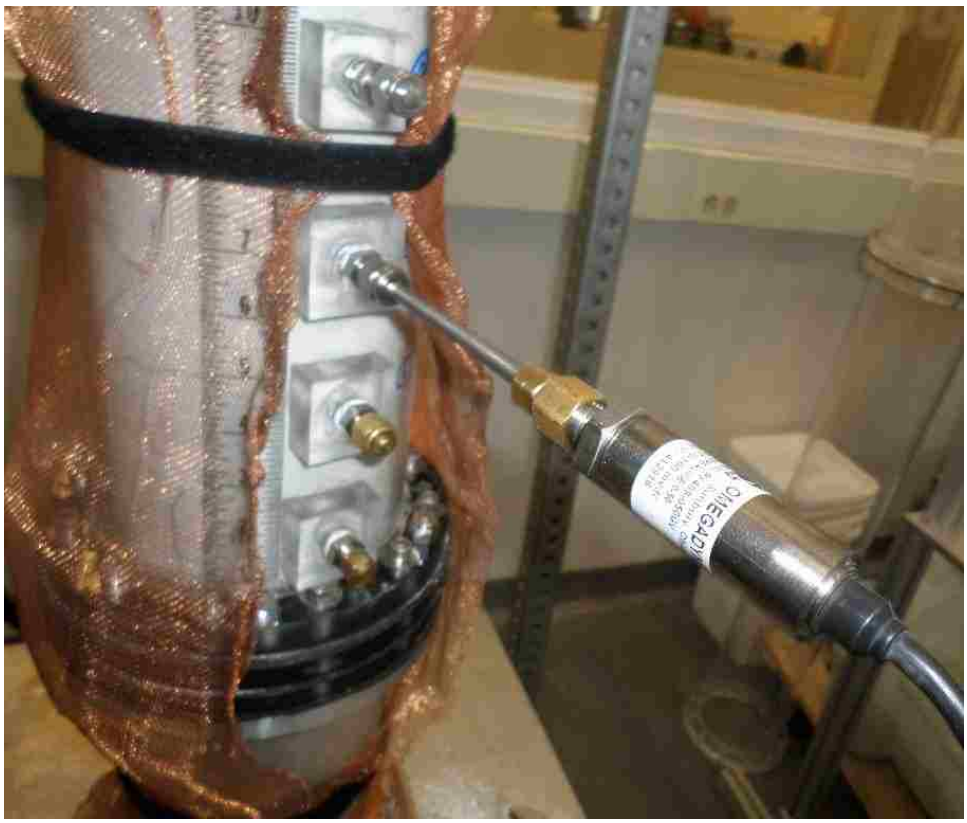

Figure 4.1. The local pressure probe connected to a single-ended pressure transducer (0.14 m inside diameter fluidized bed column).

Figure 4.2. The local pressure probe connected to a single-ended pressure transducer (0.44 m inside diameter fluidized bed column).

The local pressure probe of 0.2 m length tube was used for the column of 0.14 m diameter, while the probe of 0.3 m length tube was used for the column of 0.44 m diameter. The inside diameter of the probes was chosen to ensure that the pressure fluctuation signals were collected without any damping due to the small inside diameter of the probe (which was reported to be less than 2 mm) or any resonance that could occur as a result of using a probe with a large inside diameter (which was reported to be higher than 5 mm), as stated and recommended by Van Ommen et al. (1999, 2004, 2011). They reported that the inside

diameter of the probe should be kept between 2 and 5 mm. The end tips of the probes were covered with a wire mesh to prevent solid particles from entering the probes and blocking the tips or damping the pressure transducer, which would disturb the measurements. The wire mesh was stainless steel, with a 30 μm mesh diameter and 20 μm wire diameter and the open area of the wire mesh was 36% which had no considerable effect on the pressure fluctuations (Van Ommen et al. 1999).

5. OUTLINE OF THE KOLMOGOROV ENTROPY (KE) ESTIMATION

Fluidized beds have been characterized with dynamic behavior that is considered chaotic. The chaotic characteristics of these types of reactors results from the complex interaction between the gas phase and its surroundings (e.g., solid particles; the vessel wall; and the wall of the immersed surfaces, if it exists inside the bed). The degree of the chaotic system of gas-solid fluidized beds can be affected by many parameters, such as operating conditions, design parameters, and the physicochemical properties of the solid particles. Consequently, the rate of the loss of the information inside fluidized beds which represent the degree of order and disorder of the dynamics of the system is a function of many hydrodynamic parameters, such as voidage, solids velocity and turbulent parameters, bubble size, bubble rise velocity, bubble frequency and others. Many analytical methods have been used to represent the chaotic degree or the chaos state of the systems in a gas-solid fluidized bed, such as attractor reconstruction, correlation dimension, entropy, and the Kolmogorov entropy (KE). Van Ommen et al. (2011) showed that the Kolmogorov entropy is considered the most appropriate way to explain the chaotic degree of gas-solid fluidization systems. Because it is easy to calculate and the analysis of the time series of

the pressure fluctuation using the KE gives a clear picture about the chaos behavior of the system. Hence, the KE becomes the obvious choice for estimating the chaotic degree or loss of information in gas-solid fluidized beds.

Additionally, it has been found that the Kolmogorov entropy is considered a useful tool for identifying and distinguishing the flow regimes and their transition velocities in gas-solid fluidized systems and other multiphase flows, in which flow regimes play an important role in the scale-up process because they identify the way that both solids and gases interact inside the bed with different operating and design conditions (Zijerveld et al. 1998; Bai, Issangya, and Grace 1999; Van Ommen et al. 2011; Nedeltchev, Ahmed, and Al-Dahhan 2012; Nedeltchev et al. 2012; Nedeltchev 2015). In this study, the method used to calculate the KE is based on the maximum likelihood estimation of entropy proposed by Schouten et al. (1994) and used by (Nedeltchev et al. 2012a; Nedeltchev et al., 2012b), as shown in Eq. 4. The algorithm and its program were developed by Toukan et al., (2017) in our Multiphase Reactors Engineering and Applications Laboratory (mReal):

$$KE = -f_s \ln\left[1-\frac{1}{b_m}\right] \quad (4)$$

where $b_m = \frac{1}{M}\sum_{i=1}^{M} b_i$, and f_s = signal frequency (Hz).

6. RESULTS AND DISCUSSION

The statistical differences in the measurements of the Kolmogorov entropy profiles between the conditions illustrated in Table 2.1 are represented in terms of the percentage change in the average absolute relative difference (AARD) of all the local measurements and the percentage change in the absolute relative difference (ARD) of each individual local point as follows:

$$\text{AARD} = \frac{1}{\text{N}} \sum_{1}^{\text{N}} \left[\frac{\text{x(r)-y(r)}}{\text{x(r)}} \right] \times 100 \quad (5)$$

$$\text{ARD} = \left[\frac{\text{x(r)-y(r)}}{\text{x(r)}} \right] \times 100 \quad (6)$$

where x and y are the measured local Kolmogorov entropies at the radial locations for the cases outlined in Table 2.1, and N is the total number of the local data points. The reproducibility of the experiments is one of the most crucial factors to consider before taking any measurements. To check the reproducibility of the pressure fluctuation, measurements were repeated five times at each local position and for each experimental condition. The local averaged Kolmogorov entropy values were almost identical with few differences were within about a 5% margin of difference. The error bars shown in each figure represent the standard deviation around the mean and they were found to be within the data points.

6.1. RADIAL PROFILES OF THE KOLMOGOROV ENTROPY FOR MATCHING CASES (CASES A AND B)

Figure 6.1 illustrates the radial profiles of the Kolmogorov entropy of the pressure signal measured at the wall and at the earlier mentioned radial locations using local pressure probes at three axial heights for the experimental conditions of matching hydrodynamics with similar or close radial profiles of gas holdup of Cases A and B as listed in Table 2.1. As shown in the figure, the local Kolmogorov entropy is illustrated with respect to the dimensionless radius (r/R) at three axial levels. The radial profiles of the Kolmogorov entropy (KE) for similar local hydrodynamics of Cases A and B were close or similar for all axial and radial locations within the bed.

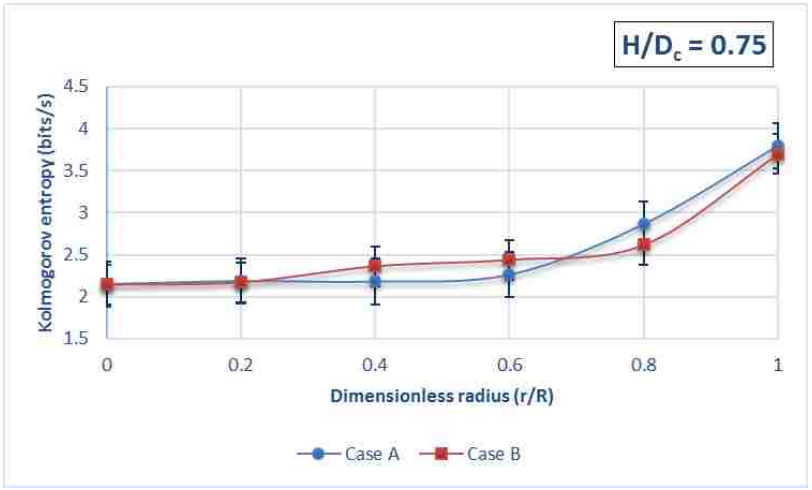

(a)

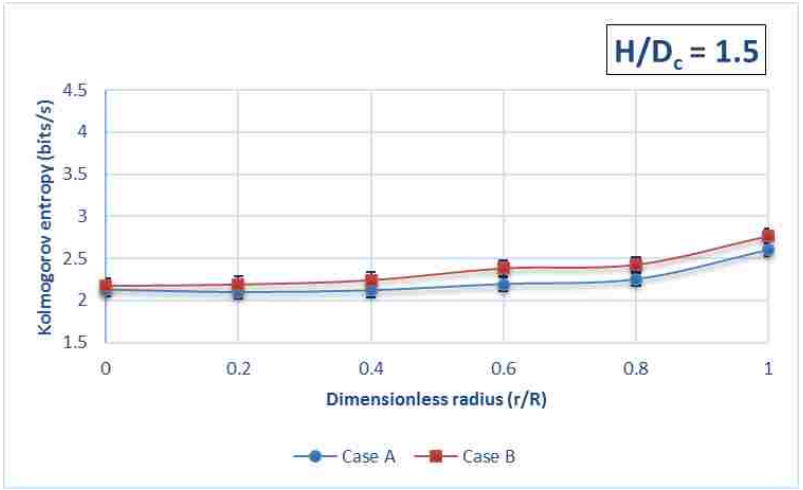

(b)

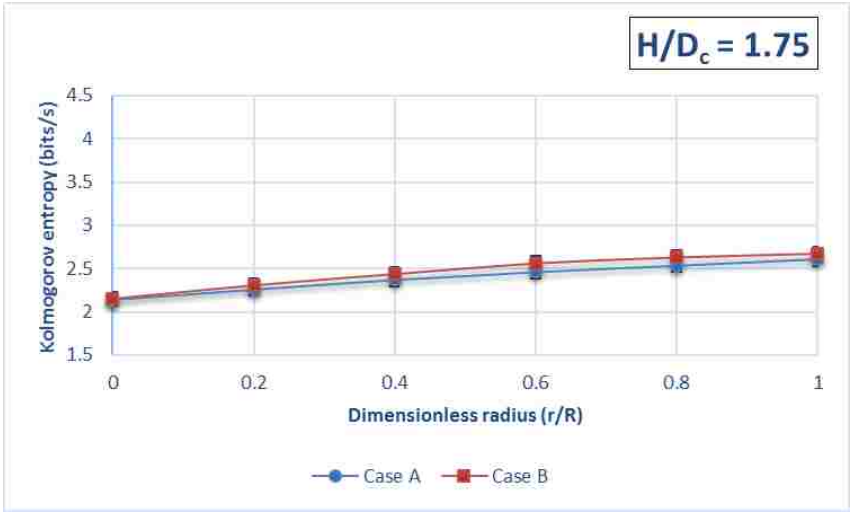

(c)

Figure 6.1. Radial profiles of the Kolmogorov entropy for Cases A and B of similar hydrodynamics with matching radial profiles of gas holdup at different axial levels, (a) $H/D_c = 0.75$, (b) $H/D_c = 1.5$, and (c) $H/D_c = 1.75$.

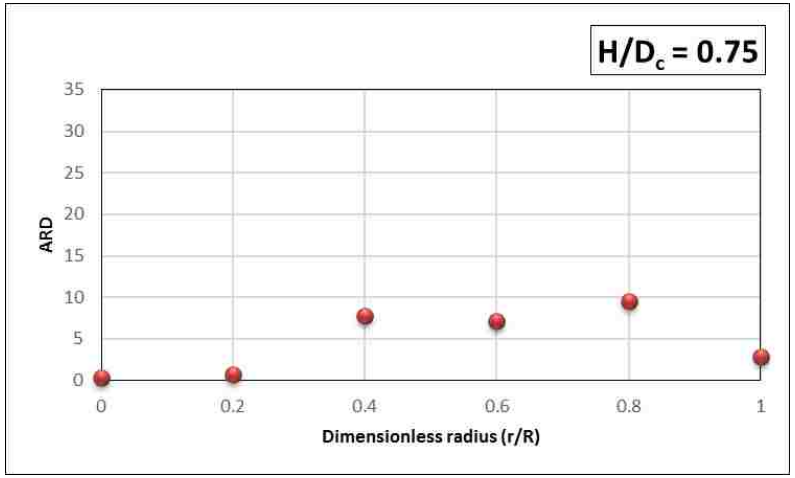

(a)

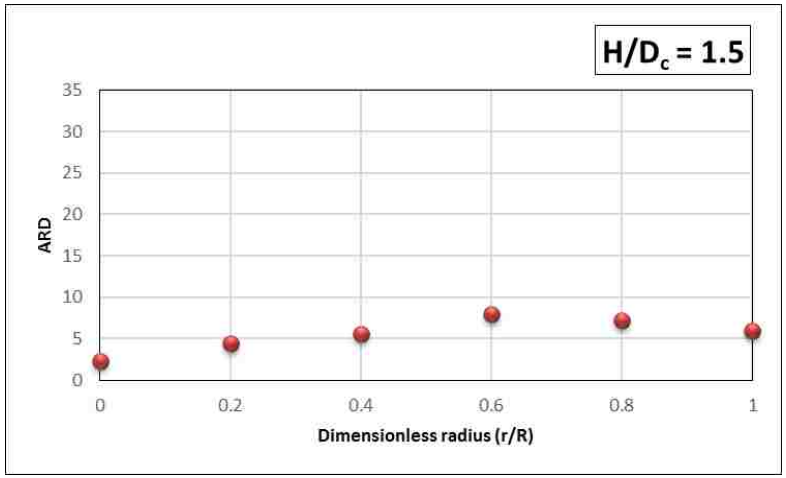

(b)

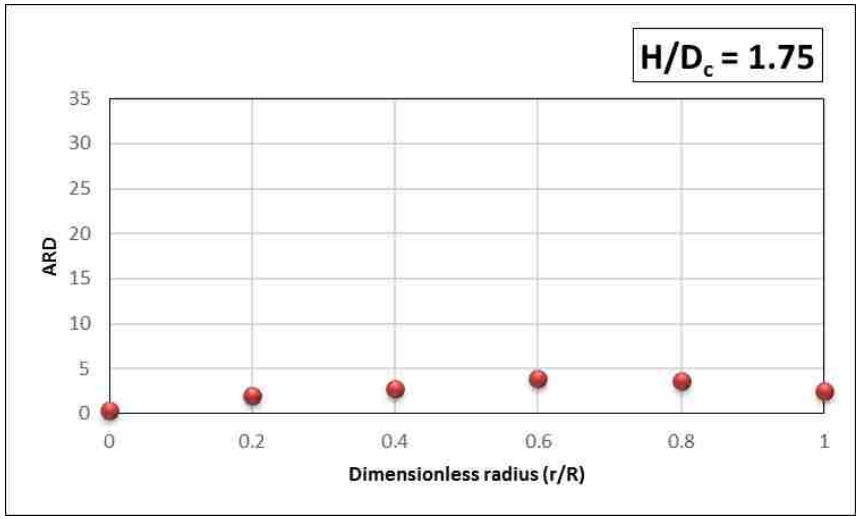

(c)

Figure 6.2. Radial variations of the ARD in the Kolmogorov entropy for Cases A and B of similar hydrodynamics with matching radial profiles of gas holdup at different axial levels, (a) $H/D_c = 0.75$, (b) $H/D_c = 1.5$, and (c) $H/D_c = 1.75$.

The percentage change in the average absolute relative difference (AARD) was 4.7% at $H/D_c = 0.75$; and the percentage change in the absolute relative difference (ARD) was about 2.85% at the wall region (r/R = 1.0); 9.58% at r/R = 0.8; 7.17% at r/R = 0.6; 7.7% at r/R = 0.4; 0.67% at r/R = 0.2; and 0.28% at r/R = 0 (central region). The results were not much different when H/D_c changed from 0.75 to 1.5. The percentage change in the average absolute relative difference (AARD) was about 5.5% at $H/D_c = 1.5$; and the percentage change in the absolute relative difference (ARD) was about 5.9% at the wall region (r/R = 1.0); 7.25% at r/R = 0.8; 8.01% at r/R = 0.6; 5.58% at r/R = 0.4; 4.38% at r/R = 0.2; and 2.26% at r/R = 0 (central region). The same trend of similar or close radial profiles of the Kolmogorov entropy was obtained at $H/D_c = 1.75$, where the percentage change in the average absolute relative difference (AARD) was about 2.5% at $H/D_c = 0.75$, and the percentage change in the absolute relative difference (ARD) was about 2.49% at the wall region (r/R = 1.0); 3.36% at r/R = 0.8; 3.93% at r/R = 0.6; 2.75% at r/R = 0.4; 1.99% at r/R = 0.2; and 0.4% at r/R = 0 (central region). The radial variations of the percentage change in the absolute relative difference (ARD) of the Kolmogorov entropy between Cases A and B at three axial heights above the distributor are shown in Figure 6.2, where the trends in the radial variations of the ARD were generally the same at different axial levels and local values of the ARD variation, as well, the value of ARD is decreased with an increase in the ratio H/D_c. It is worth to mention that the ARD values are relatively larger within the range of r/R = 0.4-0.8 and this is could be due to the inversion point of the time averaged solids velocity from positive to negative values occur at about r/R = 0.65-0.68 where the fluctuations at these points need to be recorded for longer time or due to the nature of such local locations. The differences attained between the studied cases are

reasonable which indicates also the similarity in the chaotic behavior. As mentioned earlier, for Cases A and B, the local dimensionless hydrodynamic parameters are similar (Zaid 2013; Al-Dahhan et al. 2014; Efhaima 2016; Efhaima and Al-Dahhan 2016). Therefore, we can conclude that similar to our validated mechanistic scale-up methodology when KE of the pressure signal measured at the wall or inside the bed of two scales is maintained similar or close to each other, the local hydrodynamics similarity in terms of dimensionless parameters are similar or close to each other in the targeted two scales.

6.2. RADIAL PROFILES OF THE KOLMOGOROV ENTROPY FOR (CASES A, C, AND D)

The radial profiles of the Kolmogorov entropy for the cases of the experimental conditions (Cases C and D) that have non-similar radial profiles of gas holdup with respect to the reference case (Case A) are demonstrated in Figures 6.3 and 6.4. For these conditions, the local hydrodynamics are not similar as reported earlier and the details can be found in Zaid, (2013), Al-Dahhan et al., (2014) Efhaima, (2016) Efhaima and Al-Dahhan (2016). Figure 6.3 shows the radial profiles of the Kolmogorov entropy for Cases A and C, while Figure 6.4 shows the radial profiles of the Kolmogorov entropy for Cases A and D. In Figures 6.3 and 6.4, the local Kolmogorov entropy at three axial heights is demonstrated with respect to the dimensionless radial positions. Figures 6.3 and 6.4 show a large difference between the radial profiles of the Kolmogorov entropy for the non-similar cases (Cases C and D) with respect to the reference case as compared to Figure 6.1. These differences are comparable with the differences in gas holdup profiles and hence in the local hydrodynamic parameters. However, the radial profiles of the Kolmogorov

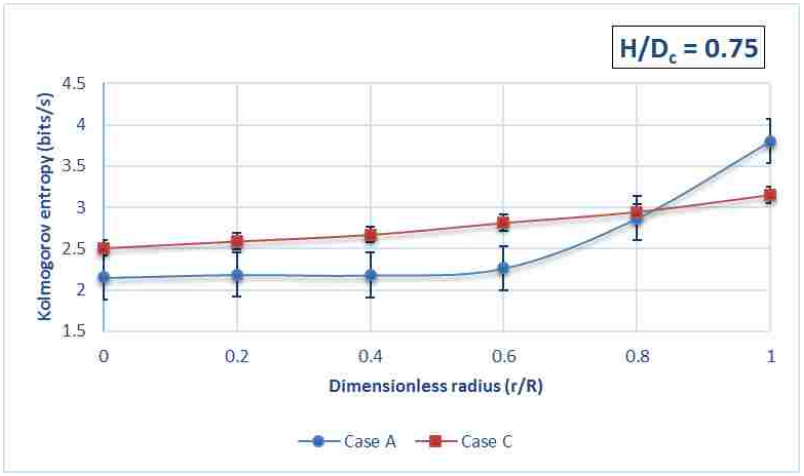

(a)

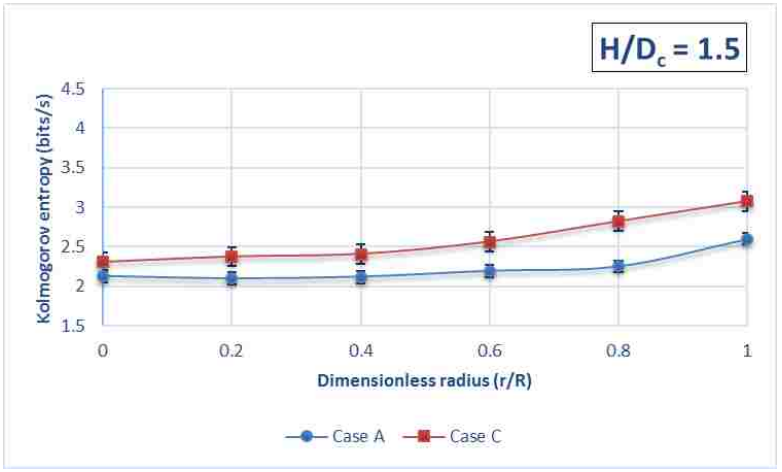

(b)

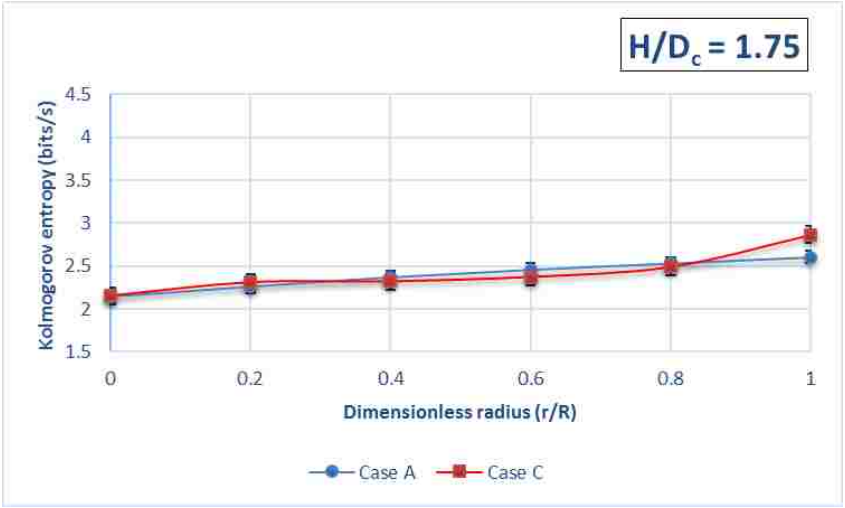

(c)

Figure 6.3. Radial profiles of the Kolmogorov entropy for Cases A and C of non-similar hydrodynamics with mismatching radial profiles of gas holdup at different axial levels, (a) $H/D_c = 0.75$, (b) $H/D_c = 1.5$, and (c) $H/D_c = 1.75$.

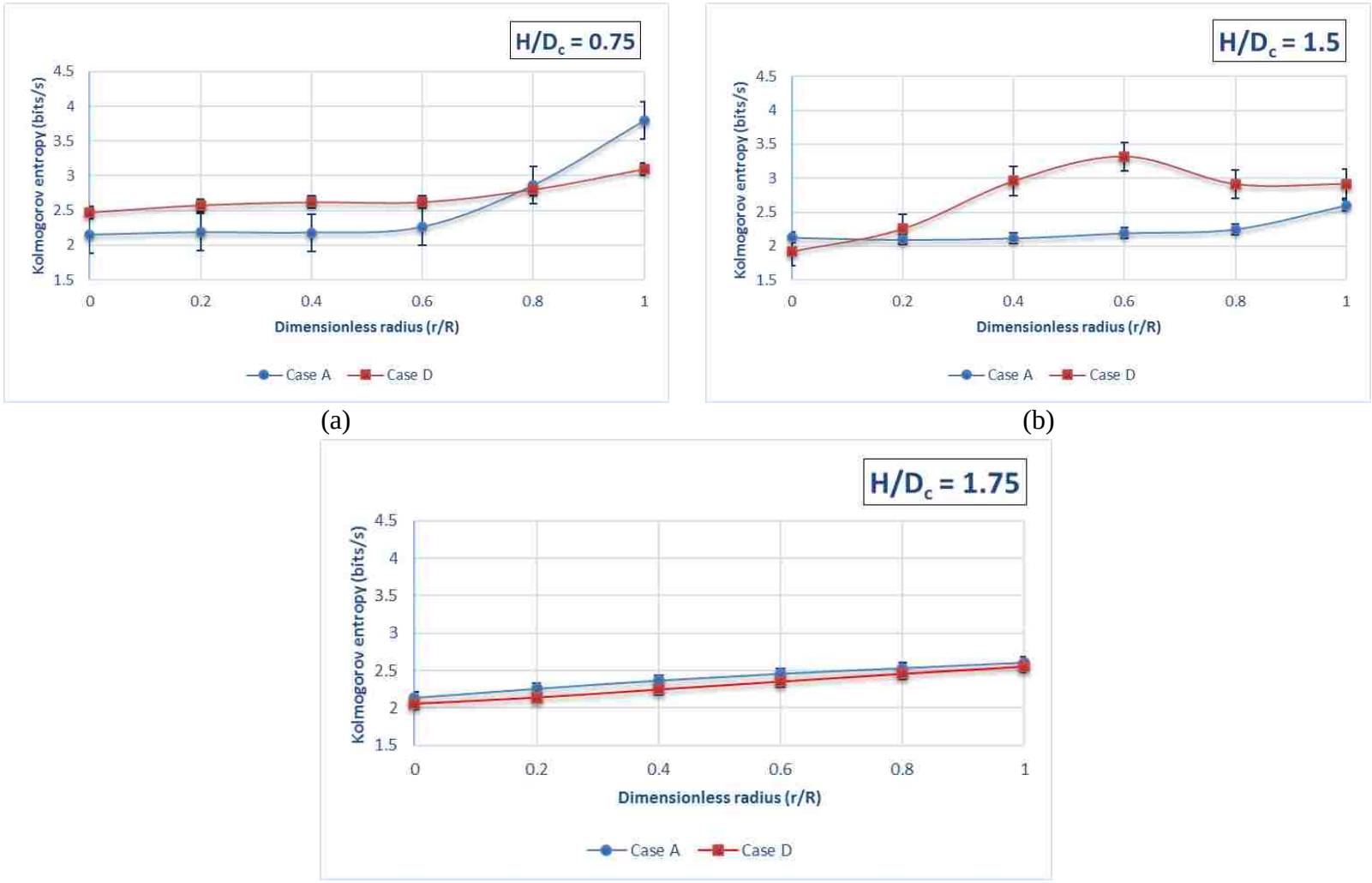

Figure 6.4. Radial profiles of the Kolmogorov entropy for Cases A and D of non-similar hydrodynamics with mismatching radial profiles of gas holdup at different axial levels, (a) $H/D_c = 0.75$, (b) $H/D_c = 1.5$, and (c) $H/D_c = 1.75$.

entropy at $H/D_c = 1.75$ are close, as shown in Figures 6.3 and 6.4. This may be caused by being the measurements are close to the freeboard of the column where the gas phase starts to disengage from the bed. This also could indicate that within the magnitude differences in the radial profile of the gas phase and hence the other local hydrodynamic parameters, the chaotic behavior of the region near the free board and the disengagement region could be not that different. Furthermore, the results indicate that the pressure signal measurements for such analysis should be within the bed away from the disengage and sparger zones.

The percentage change in the average absolute relative difference (AARD) between Cases A and C was about 15.1% at $H/D_c = 0.75$; and the percentage change in the absolute relative difference (ARD) was about 20.63% at the wall region (r/R = 1.0); 2.65% at r/R = 0.8; 19.53% at r/R = 0.6; 18.32% at r/R = 0.4; 15.61% at r/R = 0.2; and 14.29% at r/R = 0 (central region). In addition, the difference became relatively smaller when H/Dc changed from 0.75 to 1.5. The percentage change in the average absolute relative difference (AARD) was about 13.5% at H/Dc = 1.5, while the percentage change in the absolute relative difference (ARD) was about 15.3% at the wall region (r/R = 1.0); 20.18% at r/R = 0.8; 14.4% at r/R = 0.6; 11.95% at r/R = 0.4; 11.65% at r/R = 0.2; 7.61% at r/R = 0 (central region). The same trend of non-similar or not close radial profiles of the Kolmogorov entropy was obtained at $H/D_c = 1.75$ but with less deviation compared with Case A, in which the percentage change in the average absolute relative difference (AARD) was about 3.1% at $H/D_c = 0.75$, and the percentage change in the absolute relative difference (ARD) was about 9.11% at the wall region (r/R = 1.0); 1.71% at r/R = 0.8; 3.64% at r/R = 0.6; 2.09% at r/R = 0.4; 2.14% at r/R = 0.2; and 0.48% at r/R = 0 (central region). The radial

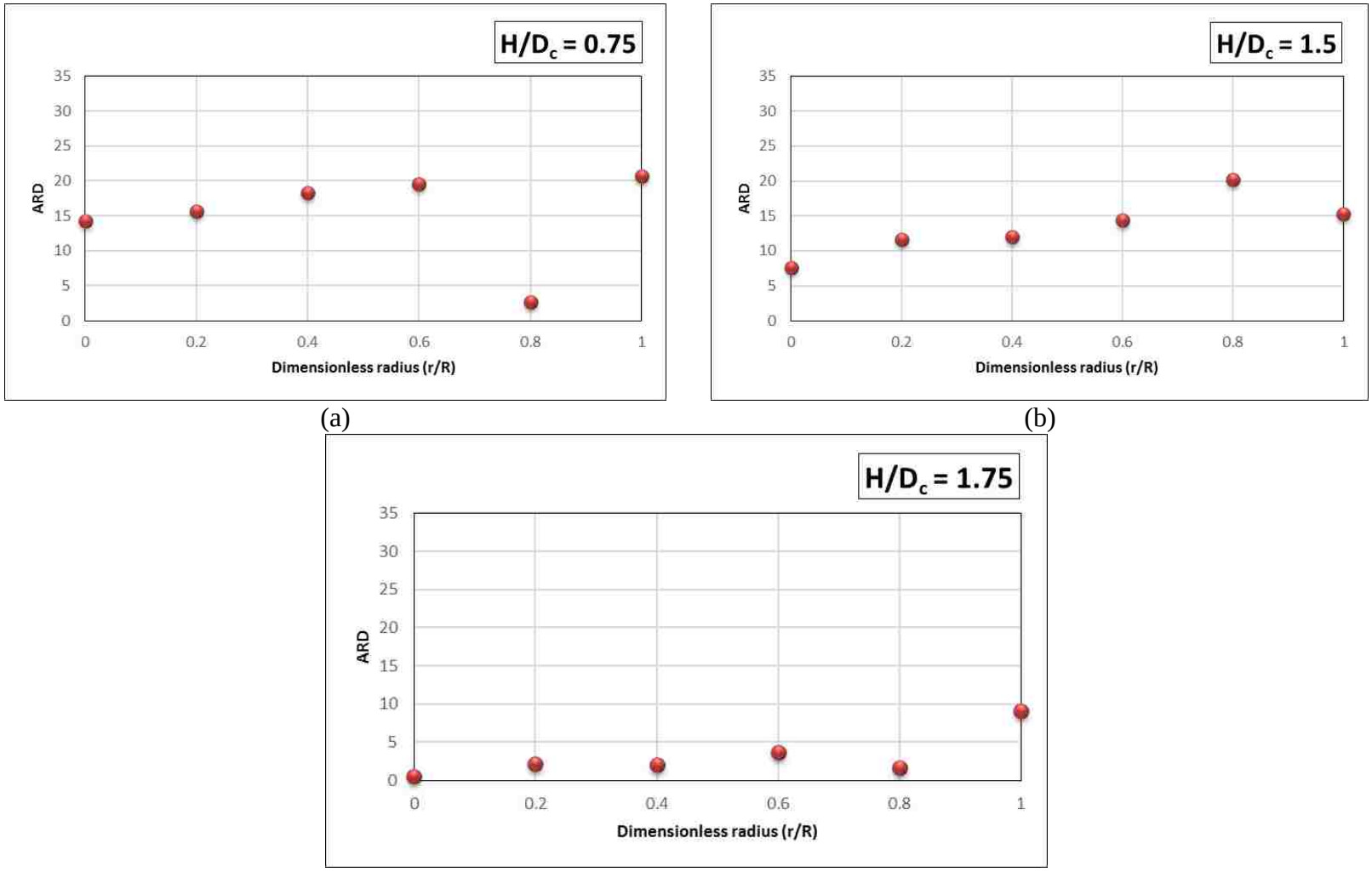

Figure 6.5. Radial variations of the ARD in the Kolmogorov entropy for Cases A and C of non-similar hydrodynamics with mismatching radial profiles of gas holdup at different axial levels, (a) $H/D_c = 0.75$, (b) $H/D_c = 1.5$, and (c) $H/D_c = 1.75$.

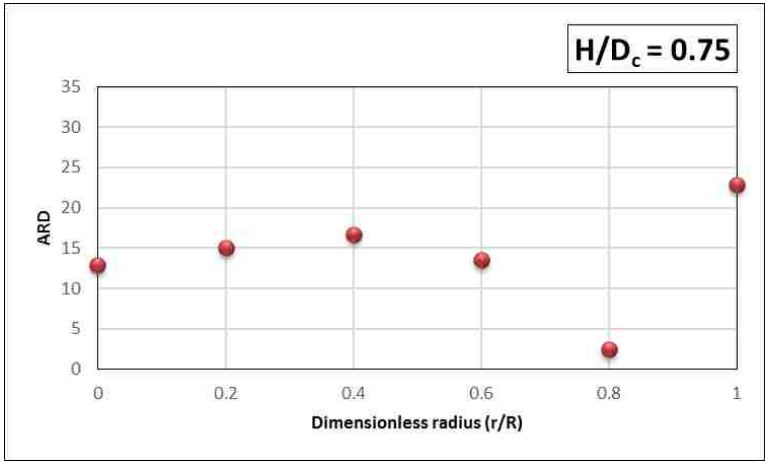

(a)

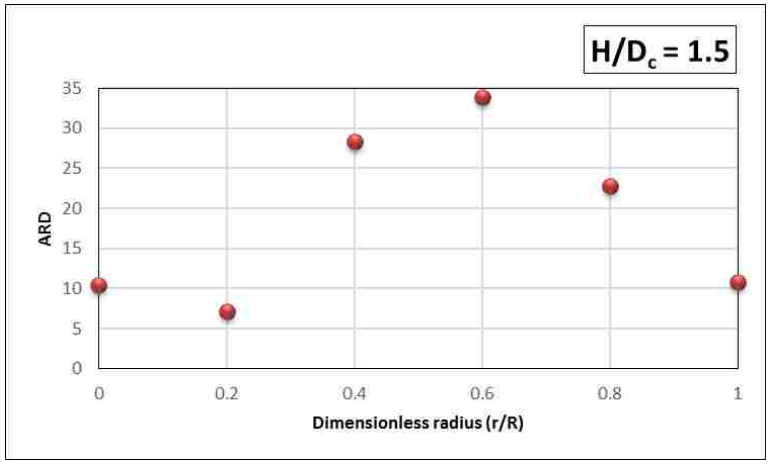

(b)

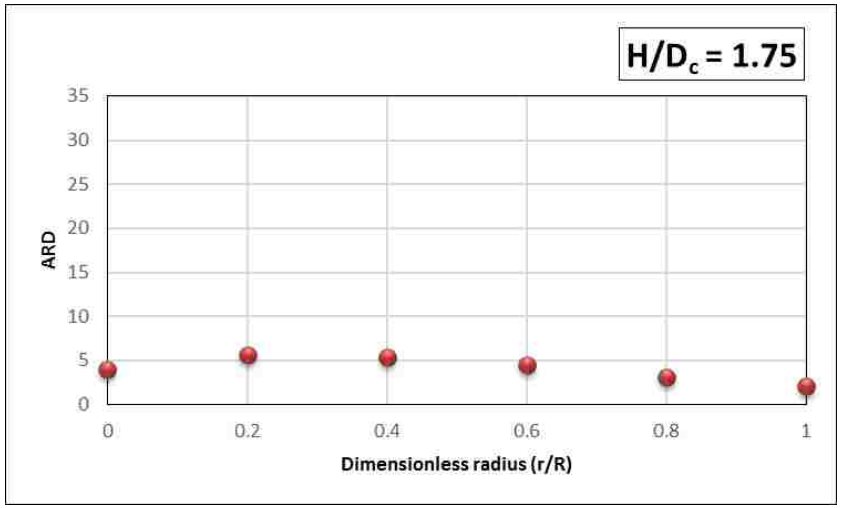

(c)

Figure 6.6. Radial variations of the ARD in the Kolmogorov entropy for Cases A and D of non-similar hydrodynamics with mismatching radial profiles of gas holdup at different axial levels, (a) $H/D_c = 0.75$, (b) $H/D_c = 1.5$, and (c) $H/D_c = 1.75$.

variations of the percentage change in the absolute relative difference (ARD) of the Kolmogorov entropy between Cases A and C at three axial heights above the distributor is shown in Figure 6.5, which shows that the radial variations of the ARD at different axial levels follow no uniform trends either radially or axially for all the local measurements of the Kolmogorov entropy.

The percentage change in the average absolute relative difference (AARD) between Cases A and D was about 13.9% at $H/D_c = 0.75$, and the percentage change in the absolute relative difference (ARD) was about 22.83% at the wall region (r/R = 1.0); 2.43% at r/R = 0.8; 13.52% at r/R = 0.6; 16.7% at r/R = 0.4; 15.05% at r/R = 0.2; and 12.95% at r/R = 0 (central region). In addition, the difference became relatively smaller when H/D_c changed from 0.75 to 1.5. The percentage change in the average absolute relative difference (AARD) was about 18.9% at $H/D_c = 1.5$, and the percentage change in the absolute relative difference (ARD) was about 10.75% at the wall region r/R = 1.0; 22.74% at r/R = 0.8; 33.89% at r/R = 0.6; 28.38% at r/R = 0.4; 7.14% at r/R = 0.2; and 10.49% at r/R = 0 (central region). The same trend (i.e., radial profiles of the Kolmogorov entropy that were not close) was obtained at $H/D_c = 1.75$ but with less deviation compared with Case A, in which the percentage change in the average absolute relative difference (AARD) was about 4.1% at $H/D_c = 0.75$; and the percentage change in the absolute relative difference (ARD) was about 2.11% at the wall region (r/R = 1.0); 3.13% at r/R = 0.8; 4.48% at r/R = 0.6; 5.36% at r/R = 0.4; 5.55% at r/R = 0.2; and 3.96% at r/R = 0 (central region). The radial variations of the percentage change in the absolute relative difference (ARD) of the Kolmogorov entropy between Cases A and D at three axial levels above the distributor plate is shown in Figure 6.6. The same nonuniform behavior of the radial variations of the ARD that was

obtained in Figure 6.5 at different axial levels was also obtained in Figure 6.6 at different radial and axial positions for all the local measurements of the Kolmogorov entropy.

7. REMARKS

The chaotic scale-up approach for the gas-solid fluidized beds proposed by Schouten et al. (1996) that is based on maintaining the same rate of information loss in terms of Kolmogorov entropy between the two scales has been assessed. We used the conditions of using our validated new mechanistic scale-up methodology that based on matching the radial profiles of the gas holdup between the two fluidized beds which ensure similarity in local hydrodynamics measured by advanced techniques. For these conditions, pressure gauge transducer measurements were performed at the wall and using a local pressure probe connected to the pressure transducer to measure the local pressure fluctuation at different radial and axial heights. The following have been found:

(1) When KE is close or matched in two scales or two different conditions with geometrical similarity of gas-solid fluidized beds, the details local dimensionless hydrodynamics parameters will be similar as per the measurements reported by Zaid (2013), Al-Dahhan et al., (2014), Efhaima (2016), Efhaima and Al-Dahhan (2016) using advanced measurement techniques of optical fiber probe, radioactive particle tracking (RPT), gamma ray tomography (CT), and gamma ray densitometry (GRD).

(2) When the KE is not matched or is not close to each other for the two scales and conditions with geometrical similarity of gas-solid fluidized beds, the detailed local dimensionless hydrodynamics parameters will not be similar.

(3) The measurement of the pressure signal for estimating the KE for scale-up should be within the bed away from the freeboard and sparger regions to ensure the hydrodynamics similarity in scale-up by matching KE.

ACKNOWLEDGEMENTS

The authors would like to thank the Multiphase Reactors Engineering and Applications Laboratory (mReal) for funding and support.

NOMENCLATURE

Dc	inside column diameter (m)
dp	particle diameter (μm)
g	gravitational force (m/s2)
H	axial height (m)
r	radial position (m)
R	radius of the column (m)
u	superficial gas velocity (m/s)
u_{mf}	minimum fluidization velocity (m/s)
μ	gas viscosity (Kg/m.s)
ρ_g	gas density (Kg/m3)
ρs	solid particle density (Kg/m3)
L	column height (m)

Greek Letters

ε	gas holdup
μ	viscosity (Kg/m.s)
ρ	density (Kg/m3)
φ	sphericity

Subscripts and Superscripts

g	gas
p	particle
s	solid

REFERENCES

Al-Dahhan, M., S. Aradhya, F. Zaid, N. Ali, and T. Aljuwaya. 2014. "Scale-up and On-Line Monitoring of Gas-Solid Systems Using Advanced and Non-Invasive Measurement Techniques." *Procedia Engineering* 83. Elsevier B.V.: 469–76. doi:10.1016/j.proeng.2014.09.080.

Bai, D., a. S. Issangya, and J. R. Grace. 1999. "Characteristics of Gas-Fluidized Beds in Different Flow Regimes." *Industrial & Engineering Chemistry Research* 38 (3): 803–11. doi:10.1021/ie9803873.

Bisio, Attilio, and Robert L. Kabel. 1985. *Scaleup of Chemical Processes: Conversion from Laboratory Scale Tests to Successful Commercial Size Design*. Wiley-Interscience.

Efhaima, Abdelsalam. 2016. "Scale-up Investigation and Hydrodynamics Study of Gas-Solid Fluidized Bed Reactor Using Advanced Non- Invasive Measurement Techniques." PhD Thesis, Missouri University of Science and Technology.

Efhaima, Abdelsalam, and Muthanna H. Al-Dahhan. 2016. "Assessment of Scale-up Dimensionless Groups Methodology of Gas-Solid Fluidized Beds Using Advanced Non-Invasive Measurement Techniques (CT and RPT)." *The Canadian Journal of Chemical Engineering* 95 (APRIL): 656–69. doi:10.1002/cjce.22745.

Glicksman, L.R. 1984. "Scaling Relationships For Fluidized Beds." *Chemical Engineering Science* 39 (9): 1373–79. doi:10.1016/0009-2509(84)80070-6.

Glicksman, L R, M. Hyre, and K. Woloshun. 1993. "Simplified Scaling Relationships for Fluidized Beds." *Powder Technology* 77: 177–99.

Glicksman, Leon R. 1988. "Scaling Relationships for Fluidized Beds." *Chemical Engineering Science* 43 (6): 1419–21. doi:10.1016/0009-2509(88)85118-2.

Horio, Masayuki, Akira Nonaka, Yoshitaka Sawa, and Iwao Muchi. 1986. "A New Similarity Rule for Fluidized Bed Scaleup." *AIChE Journal* 32 (9): 1466–82. doi:10.1002/aic.690320908.

Kelkar, Vaibhav V., and Ka M. Ng. 2002. "Development of Fluidized Catalytic Reactors: Screening and Scale-Up." *AIChE Journal* 48 (7): 1498–1518. doi:10.1002/aic.690480714.

Knowlton, T.M. 2013. "Fluidized Bed Reactor Design and Scale-Up." In *Fluidized Bed Technologies for Near-Zero Emission Combustion and Gasification*, 481–523. Elsevier. doi:10.1533/9780857098801.2.481.

Nedeltchev, Stoyan. 2015. “New Methods for Flow Regime Identification in Bubble Columns and Fluidized Beds.” *Chemical Engineering Science* 137. Elsevier: 436–46. doi:10.1016/j.ces.2015.06.054.

Nedeltchev, Stoyan, Fadha Ahmed, and Muthanna Al-Dahhan. 2012. “A New Method for Flow Regime Identification in a Fluidized Bed Based on Gamma-Ray Densitometry and Information Entropy.” *Journal of Chemical Engineering of Japan* 45 (3): 197–205. doi:10.1252/jcej.11we189.

Nedeltchev, Stoyan, Shreekanta Aradhya, Faraj Zaid, and Muthanna Al-Dahhan. 2012. “Flow Regime Identification in Three Multiphase Reactors Based on Kolmogorov Entropies Derived from Gauge Pressure Fluctuations.” *Journal of Chemical Engineering of Japan* 45 (9): 757–64. doi:10.1252/jcej.12we075.

Nicastro, M.T., and L.R. Glicksman. 1984. “Experimental Verification of Scaling Relationships for Fluidized Bed.” *Chemical Engineering Science* 39 (9): 1381–91. doi:10.1016/0009-2509(84)80071-8.

Rüdisüli, Martin, Tilman J. Schildhauer, Serge M A Biollaz, and J. Ruud Van Ommen. 2012. “Scale-up of Bubbling Fluidized Bed Reactors - A Review.” *Powder Technology* 217. Elsevier B.V.: 21–38. doi:10.1016/j.powtec.2011.10.004.

Schouten, J. C., M. L. M. Vander Stappen, and C. M. Van Den Bleek. 1996. “Scale-up of Chaotic Fluidized Bed Hydrodynamics.” *Chemical Engineering Science* 51 (10): 1991–2000. doi:10.1016/0009-2509(96)00056-5.

Schouten, Jaap C., Floris Takens, and Cor M. Van Den Bleek. 1994. “Estimation of the Dimension of a Noisy Attractor.” *Physical Review E* 50 (3): 1851–61. doi:10.1103/PhysRevE.50.1851.

Stein, M, Y L Ding, and J P K Seville. 2002. “Experimental Verification of the Scaling Relationships for Bubbling Gas-Fluidised Beds Using the PEPT Technique.” *Chemical Engineering Science* 57: 3649–58. doi:10.1016/S0009-2509(02)00264-6.

Toukan, A., V. Alexander, H. AlBazzaz, and M.H. Al-Dahhan. 2017. “Identification of Flow Regime in a Cocurrent Gas – Liquid Upflow Moving Packed Bed Reactor Using Gamma Ray Densitometry.” *Chemical Engineering Science* 168. Elsevier Ltd: 380–90. doi:10.1016/j.ces.2017.04.028.

Van Den Bleek, Cor M., and Jaap C. Schouten. 1993. “Can Deterministic Chaos Create Order in Fluidized-Bed Scale-Up?” *Chemical Engineering Science* 48 (13): 2367–73. doi:10.1016/0009-2509(93)81058-4.

Van den Bleek, Cor M., Jaap C. Schouten, and Cor M Van Den Bleek. 1993. "Deterministic Chaos: A New Tool in Fluidized Bed Design and Operation." *The Chemical Engineering Journal and the Biochemical Engineering Journal* 53 (1): 75–87. doi:10.1016/0923-0467(93)80009-L.

Van Ommen, J. Ruud, Srdjan Sasic, John Van der Schaaf, Stefan Gheorghiu, Filip Johnsson, and Marc Olivier Coppens. 2011. "Time-Series Analysis of Pressure Fluctuations in Gas-Solid Fluidized Beds - A Review." *International Journal of Multiphase Flow* 37 (5). Elsevier Ltd: 403–28. doi:10.1016/j.ijmultiphaseflow.2010.12.007.

Van Ommen, J. Ruud, Jaap C. Schouten, Michel L M Vander Stappen, and Cor M. Van Den Bleek. 1999. "Response Characteristics of Probe-Transducer Systems for Pressure Measurements in Gas-Solid Fluidized Beds: How to Prevent Pitfalls in Dynamic Pressure Measurements." *Powder Technology* 106 (3): 199–218. doi:10.1016/S0032-5910(99)00078-9.

Van Ommen, J. Ruud, John Van Der Schaaf, Jaap C. Schouten, Berend G M Van Wachem, Marc Olivier Coppens, and Cor M. Van Den Bleek. 2004. "Optimal Placement of Probes for Dynamic Pressure Measurements in Large-Scale Fluidized Beds." *Powder Technology* 139 (3): 264–76. doi:10.1016/j.powtec.2003.12.009.

Zaid, Faraj. 2013. "Gas-Solid Fluidized Bed Reactors: Scale-Up, Flow Regimes Identification and Hydrodynamics." PhD Thesis, Missouri University of Science and Technology.

Zijerveld, Robert C., Filip Johnsson, Antonio Marzocchella, Jaap C. Schouten, and Cor M. Van Den Bleek. 1998. "Fluidization Regimes and Transitions from Fixed Bed to Dilute Transport Flow." *Powder Technology* 95 (3): 185–204. doi:10.1016/S0032-5910(97)03336-6.

SECTION

2. CONCLUSION

The general outcomes of present study can be concluded as follows:

1- The experimental results are demonstrated that the vertical immersed tubes have significant effect on all the hydrodynamic characteristics that investigated in this work. In which, both of solid holdup and bubble mean size have decreased in the case of internals, while the particles velocity, bubble rise velocity and bubble frequency were increased due to the existing of immersed verticals tubes.

2- Regarding the flow regime and their transition velocities, it has been found that the vertical internals have a considerable impact on the flow regimes, transition velocities and transition velocity ranges of each individual flow regime. However, this effectiveness is a function of the physical properties of the used solid particles. In addition, the 1 in vertical internals type has been found to be more efficient either in the minimizing the turbulent transition velocity and slugging transition velocity range or in the reduction of the pressure fluctuations inside the bed.

3- The measurements of pressure drop have been shown that the 1 in internals can reduce the pressure drop inside the bed with about 10% comparing with the case of without internals for both kinds of solids used.

4- It has been demonstrated experimentally that the local heat transfer coefficient is enhanced in the case of vertical immersed tubes as well it is directly related to both gas hydrodynamic characteristics (gas holdup and bubble frequency). In which, increasing the gas holdup and bubble frequency in the case of vertical immersed tubes would lead

to increase the heat transfer area that exposed to both gas bubbles and locally moved solid particles.

5- Concerning the scale-up of two dimensionally identical gas-solid fluidized beds. It was found that the cases with same or close radial profiles of gas holdups (matching cases) were possessed the same or close radial profiles of Kolmogorov entropy and the cases with different radial profiles of gas holdup (mismatching cases) were possessed different radial profiles of Kolmogorov entropy.

APPENDIX A

OPTICAL FIBER PROBE CALIBRATION METHODS FOR SOLIDS HOLDUP AND PARTICLES VELOCITY MEASUREMENTS

A. OPTICAL FIBER PROBE CALIBRATION METHODS FOR SOLIDS HOLDUP AND PARTICLES VELOCITY MEASUREMENTS

A.1. DROPPING/TRAPPING CALIBRATION METHOD OF SOLIDS HOLDUP

The reliability of the optical fiber probe measurements strongly depends upon the accuracy of the calibration process. Moreover, the complexity of fluidized bed systems due to the gas-solid interactions require a reliable calibration method to ensure that the solids concentration measurements are accurate. The dropping/trapping calibration method for solids holdup (Zhang et al. 1998) was performed in our laboratory, with some modifications to calibrate the optical fiber probe, which can be used in gas-solid fluidized beds.

The dropping/trapping calibration apparatus used in this work consisted of the following parts:

1- A syringe motor pump, which is a solids feeder, allowed the solids to flow with a constant mass flow rate and to change the mass flow rate for the solids holdup range from 0 to 0.6.
2- Two solenoid valves were used to trap the solids that passed through the test tube section. The valves were electric-powered and constructed with a durable brass body, a two-way inlet, and outlet ports with a 6.35 inside diameter.
3- The test tube section was made from Plexiglas®, 0.23 m long and with a 6.35 mm inside diameter. The optical fiber probe was fixed in the middle of the test tube, and the two solenoid valves were attached to the two ends (inlet and outlet of the test tube).

The dropping/tapping calibration method was used in the present work to calibrate the optical fiber probe that was 3 mm in diameter, using particles 365 μm in diameter. Glass beads of density 2500 Kg/m^3 were used for this estimation. The experimental setup of the current solid calibration method is shown in Figure A.1.

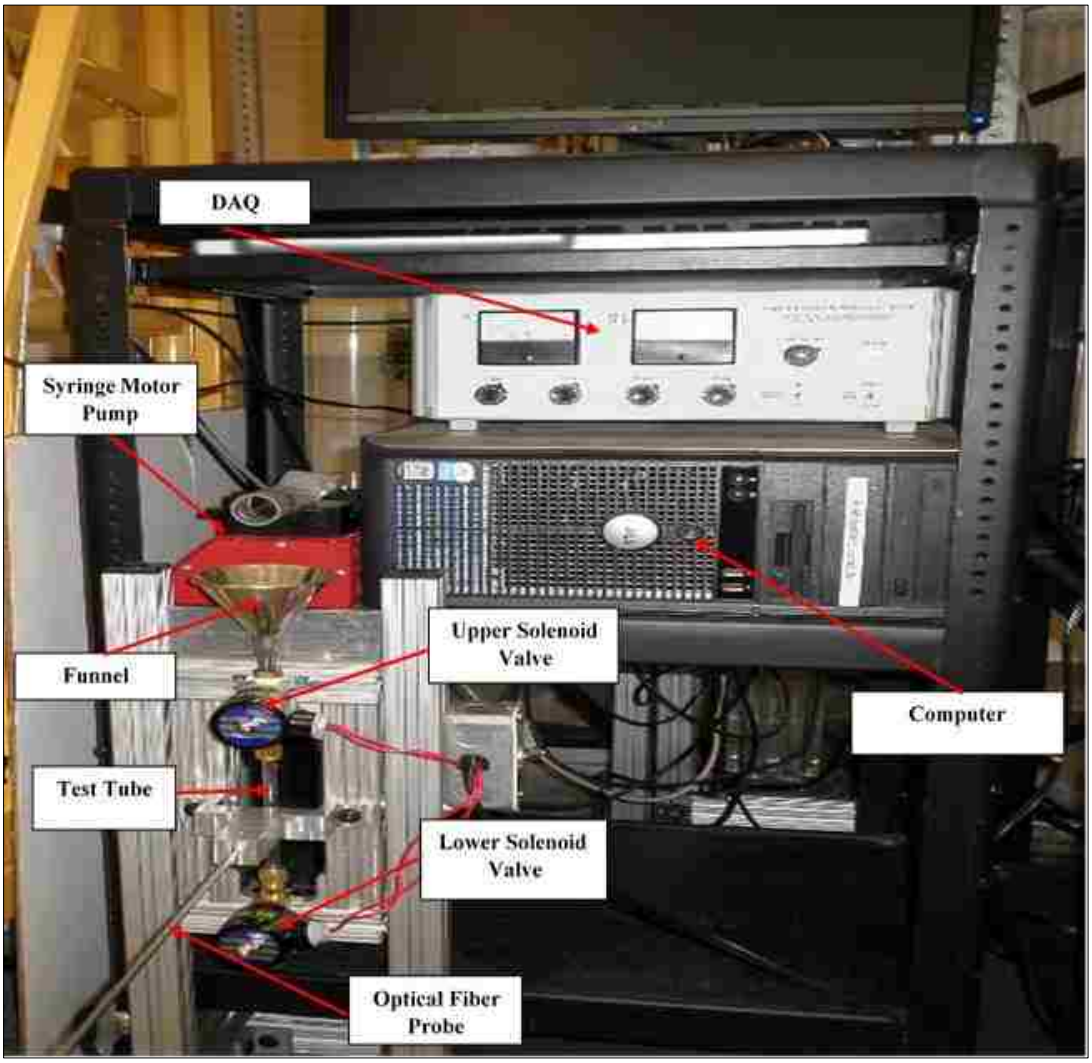

Figure A.1. Dropping/trapping calibration setup.

The solid particles flowed, with a different mass flow rates, from the syringe motor pump and fell in order to pass through the test tube section. The syringe pump can vary the solids mass flow rate to provide different solids holdup in the test tube section. The two solenoid valves were closed simultaneously, and the solid particles were trapped in the test tube. The mass of the trapped solids was determined, thus measuring the solids concentration. The optical fiber probe was located in the middle of the test tube section to generate voltage signals for each related mass flow rate.

The calibration procedure was conducted for 20 mass flow rates, and the solid concentration process was repeated three times to ensure the validity of the measurements. The number of data points for each flow rate was 4,000 points. The entire time series signal was divided into eight parts and analyzed separately. Each part consisted of 500 data points for solids concentration calculation. The signals generated from the optical fiber probe were recorded and converted to a normalized voltage using Eq. 1. Thus, the calibrating curve related the solids holdups to the normalized voltage generated by the probe (Figure A.2).

$$V_{avg} = \frac{1}{n}\sum_{i=1}^{n} V_{i_{norm}} = \frac{V_i - V_{\min}}{V_{\max} - V_{\min}} \qquad (1)$$

A.2 NEW CALIBRATION METHOD AND VALIDATION OF THE SOLIDS VELOCITY

The solid particle velocity is considered an important factor that can affect the hydrodynamic parameters in a gas-solid fluidized bed (Zhu et al. 2008). The precision of the solid particle velocity measurements using an optical fiber probe (Eq. 2) depends on the effective distance between the two light-receiving fibers and the time shift, which can

be measured by analyzing the signals generated from the two tips of the optical fiber probe using a cross-correlation function and cross-correlation coefficients.

$$V_p = \frac{L_e}{\tau} \qquad (2)$$

In this case of this study, the effective distance between the two tips (the distance between the two receiving fibers of the optical probe) was provided by the manufacturer: 2.12 mm for the probe of 3 mm in diameter, which can be used with particles of 20 μm – 400 μm. To ensure that this effective distance was accurate, the optical fiber probe must be calibrated and validated for particle velocity measurements.

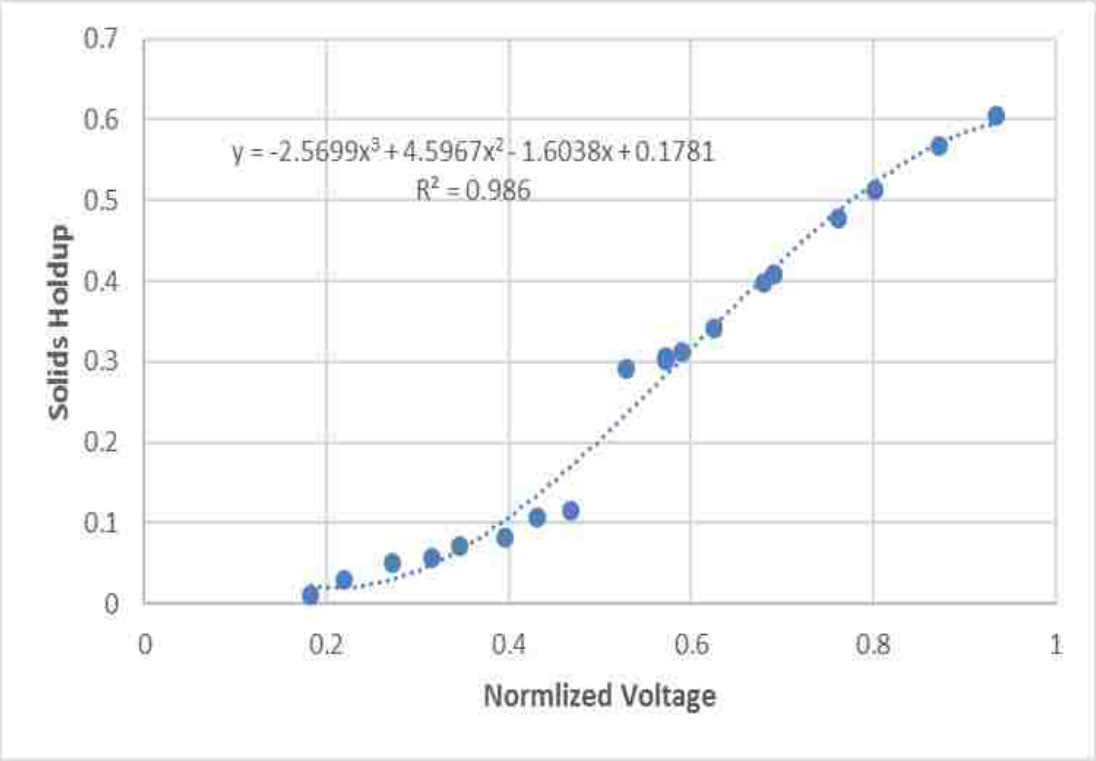

Figure A.2. Calibration curve for glass beads of 365 μm generated using the dropping/trapping method.

This new calibration process was implemented in our laboratory to calibrate and validate the solid particle velocity of fine particles (less than 400 μm). In this calibration process, a belt-driven stepper motor (Velmex Company, model MB 10) (Figure A.3) was used to calibrate the optical fiber probe for the particle velocity measurements. The belt-driven stepper motor was assembled from a gearbox motor that was mounted 90° to the

Figure A.3. Photograph of the belt-driven stepper motor.

traverse. The output of the gearbox motor was directly connected to a stainless steel pulley that drives a steel-strengthened timing belt. The belt drive's high efficiency makes it an

ideal choice for moving light loads at high speed and for continuous duty applications. Speeds as high as 1 m/s can be achieved using direct-drive motors and high-powered controllers. The belt drive can be moved forward and backward up to 1.27 m.

An aluminum plate with glued solid particles (glass beads of 365 μm and density of 2,500 Kg/m^3) was attached to the top of the carriage section of the belt-driven stepper motor (Figure A.4). The optical fiber probe was also fixed perpendicularly to the plate, about 2 mm away from the top of the glued particles, to ensure that the generated voltage signals were accurate (this was the closest distance that could be achieved), and the

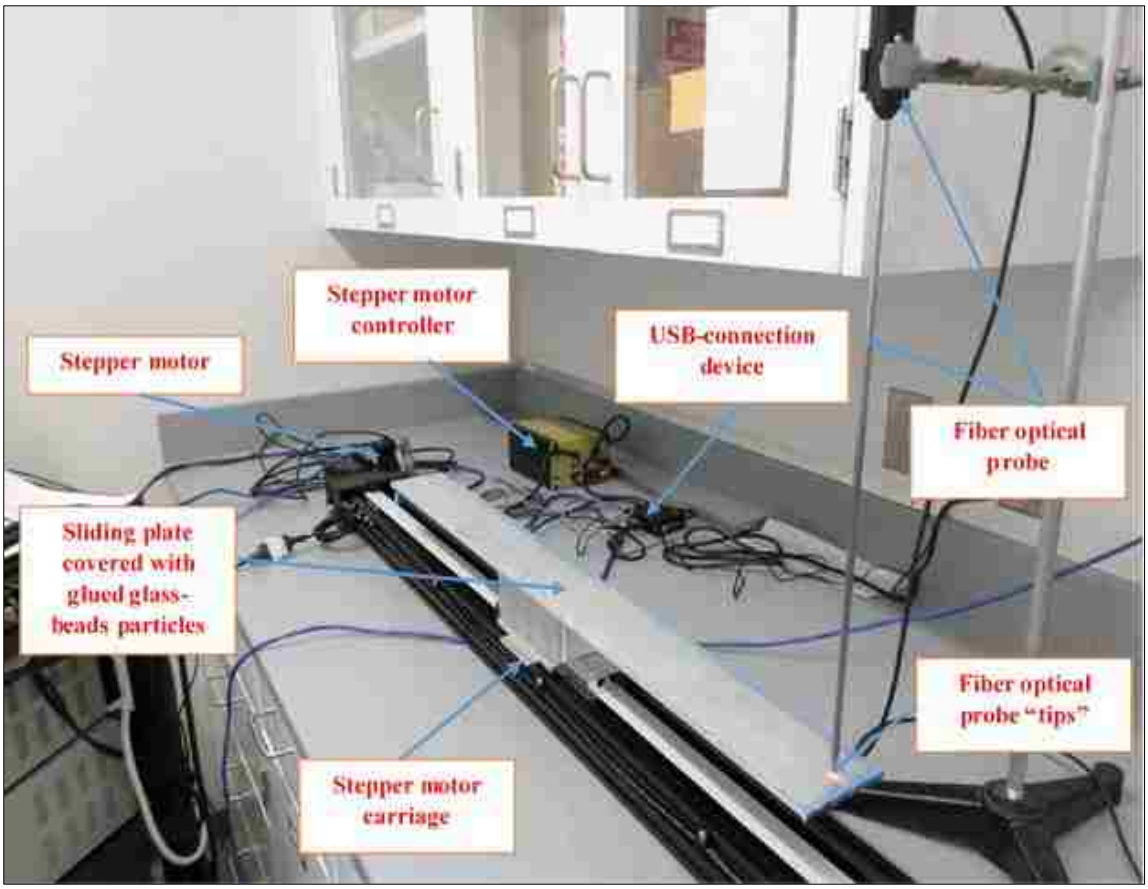

Figure A.4. Optical fiber probe and belt-driven stepper motor calibration setup for the solid particle velocity.

measurements of the optical fiber probe are extremely precise at this distance (Wang, Bi, and Lim 2009), as shown in Figure A.5. The speed of the aluminum plate with the glued particles can be varied from 0 to 0.7 m/s by adjusting the speed of the stepper motor, a range that was chosen to cover the real experimental condition. The particle velocity can be calculated from the voltage signals generated by the two optical fiber probe tips because the effective distance was provided by the manufacturer, and the time shift between the two voltage signals can be calculated using a cross-correlation function.

To validate the particle velocity measured by the optical probe, the optical fiber probe was replaced with a high-speed camera (Figure A.6), using particle image velocimetry (PIV). This technique has been widely used in gas-solid, two-phase flow (Shi 2007) for

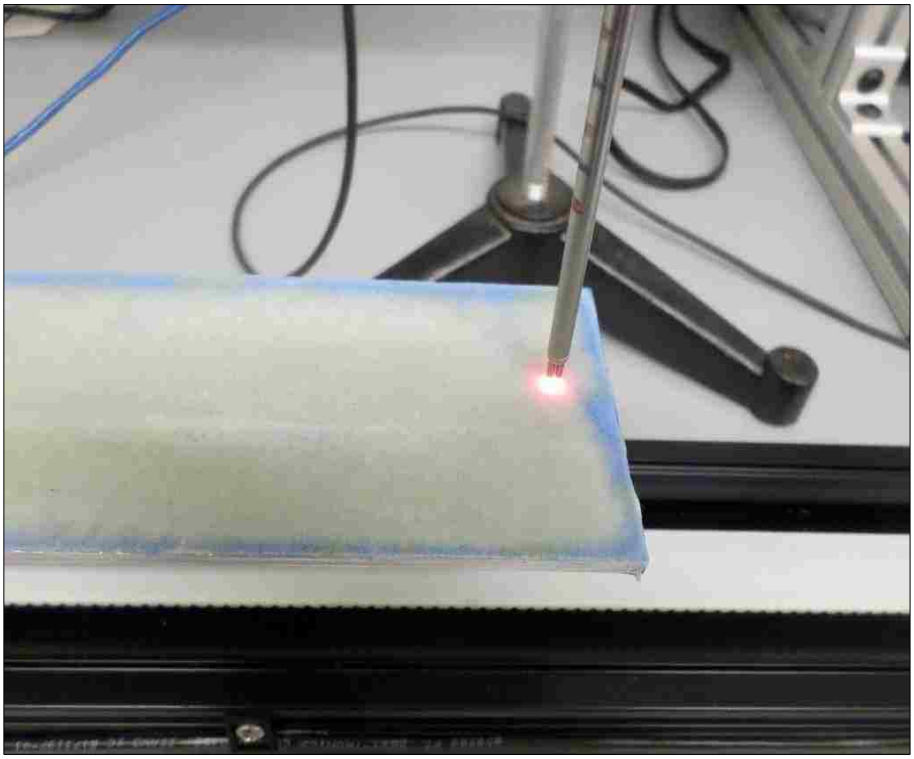

Figure A.5. Optical fiber probe tips at the top of the glued particles.

many purposes, such as visualizing the flow field; measuring the particle velocity and the velocity vectors of these particles; measuring the local holdups and bubble size; and identifying the flow regime (Chen and Fan 1992). The PIV technique consists of three main parts:

1- Video recording system: The high-speed camera (model JVC-GC-PX 100) has a maximum speed of 600 frames per second, with a spatial resolution of 1,920 × 1,080 under 50 frames per second.

2- Light source: Sunlight was used in this experiment as a light source because the intensity of sunlight is adequate for this type of measurement.

3- Image processing and analysis: A two-dimensional, cross-correlation algorithm based on the fast Fourier transform was developed in our laboratory to analyze the image data and to compute the displacement between image pairs. The 2-D, cross-correlation analytical method was chosen because it is considered an appropriate method for measuring the velocity of particles in a high-density solid particle system (Shi 2007).

The same procedure that was used to calibrate the optical fiber probe with the belt-driven stepper motor was repeated but with the high-speed camera. The particle velocity was then calculated by dividing the displacement between image pairs (which was calculated using a 2-D cross-correlation) by the time between each two consecutive pair of images, which can be represented by the adjustable frame per second (fps) of the camera. The results obtained by both techniques (i.e., optical fiber probe and high-speed camera) at the same stepper motor speed are compared in Figure A.7. The values of the particle velocity measured by both techniques were close, with a relative percentage deviation of

Figure A.6. A high-speed camera and belt-driven stepper motor setup for the validation of the solids particle velocity.

1.34% between the two methods. This means that the effective distance supported by the manufacturing company is reliable, and the optical fiber probe can be used in an actual experimental setup for particle velocity measurements.

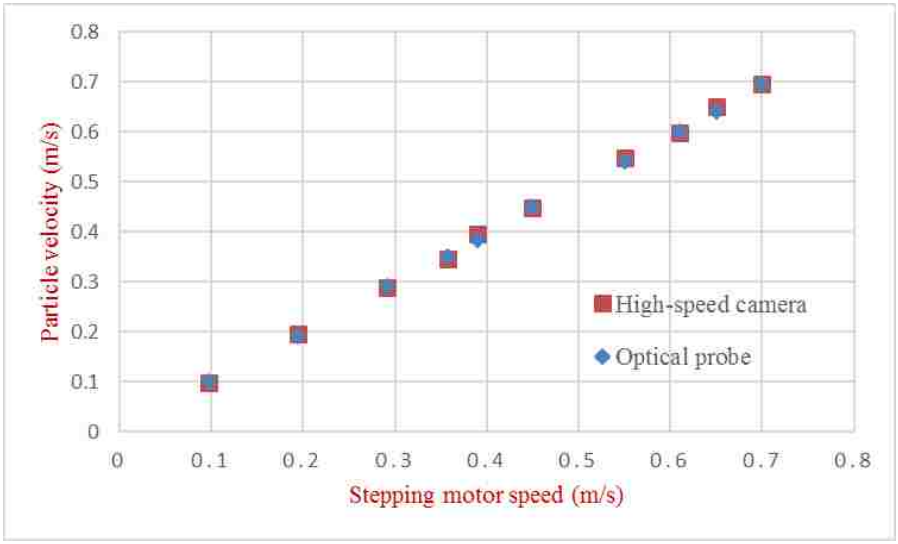

Figure A.7. Solids velocity using the optical fiber probe and high-speed camera at different stepper motor speeds.

APPENDIX B

INVESTIGATION OF THE EFFECT OF VERTICAL IMMERSED TUBE DIAMETER ON HEAT TRANSFER IN A GAS-SOLID FLUIDIZED BED

B. INVESTIGATION OF THE EFFECT OF VERTICAL IMMERSED TUBE DIAMETER ON HEAT TRANSFER IN A GAS-SOLID FLUIDIZED BED

B.1 ABSTRACT

In this work, the influence of the vertical tube diameter on the performance of the heat transfer was conducted in a gas-solid fluidized bed of 0.14 m inside diameter. The heat transfer coefficient was measured using an advanced fast-response heat transfer probe. Two tube diameters (0.0254 and 0.0127 m) were used to study the reliance of the heat transfer coefficient of the immersed vertical tubes on the tube diameter, using glass beads solid particles of 365 μm average size and 2500 Kg/m^3 solid density, with a static bed height of 0.35 m. The experiments were conducted using the bubbling flow regime, with a range of superficial gas velocities (0.45-0.7 m/s), and the measurements of the heat transfer coefficient took place at three axial heights (r/R) and three radial positions (H/D). It was found for all operating conditions and measurement positions inside the bed that the local heat transfer coefficient rose with an increase in the tube diameter such that an enhancement in the heat transfer coefficient occurred when the immersed tube diameter increased from 0.0127 to 0.0254 m. A regression correlation was predicted using JMP®12 statistical software based on relevant dimensionless groups, with a good mean relative deviation value of 4.59% between the experimental and predicted data.

B.2. INTRODUCTION

Gas-solid fluidized beds are extensively employed as a part of numerous industrial applications, such as petroleum refining, chemical synthesis, industrial food production, and power generation. Moreover, due to their high heat transfer efficiency and good particle mixing, fluidized bed reactors have been applied in many chemical commercial processes, including catalytic cracking, drying, coating, and combustion (Martin 1984; White, Mathur, and Saxena 1986; Hu, Cheng, and Fan 1998; Stefanova et al. 2011). Furthermore, many studies state that heat transfer plays a key role in the operation and performance of these types of processes (Sunderesan and Clark 1995; Cui and Chaouki 2004; Chen, Grace, and Golriz 2005; Stefanova et al. 2007a; Pisters and Prakash 2011; Yao et al. 2015).

Fluidized bed reactors are generally classified into two main types: gas-solid fluidized and catalytic fluidized. The main difference between the two is the behavior of the solid particles through the chemical reactions. In gas-solid fluidized bed reactors, the solid particles are involved in the chemical reaction, as in the case of biomass and coal gasification or combustion processes, while in catalytic fluidized bed reactors, the solid particles do not engage in the chemical reaction (e.g., the chemical cracking of oil to produce different chemical substances). The addition or removal of heat in both types of gas-solid fluidized beds is essential for controlling the temperature and maintaining high efficiency and good performance. Therefore, immersed surfaces are required to control the heat transfer rate inside both types of fluidizing reactors.

The three forms of heat transfer between the bed (either gas phase or solid particles) and the heat exchanger surface are solid particle convection, gas convection, and radiation heat transfer, especially when the fluidized bed reactor operates above 500 °C. Many

chemical processes using fluidized beds operate at temperatures below 500 °C, where the radiation is negligible (Stefanova et al. 2007a, b). These three forms of heat transfer are considered components in the overall heat transfer coefficient for a gas-solid fluidized bed, which is usually written as follows:

$$h = \delta_d\, h_p + (1-\delta_d) h_g + h_{rad} \quad (1)$$

where δ_d is a fraction of time during which any point on the heat transfer surface is occupied by particle packets, $\delta_d\ h_p$ is the particle convection component, $(1-\delta_d)h_g$ is the gas convection component, and h_{rad} is the radiation component (Kim et al. 2003; Stefanova et al. 2011).

Many researchers have investigated the behavior of heat transfer in relation to various factors in gas-solid fluidized beds. Moreover, to investigate the impact of these factors on the heat transfer coefficient inside the gas-solid fluidizing systems, several theoretical and experimental studies have been conducted using different designs, operating conditions, and physical parameters as well as various configurations of gas-solid fluidized bed vessels (Wu et al. 1991; Li, Huang, and Qian 1995; Seo et al. 2011). Much research (Vreedenberg 1958; Doherty et al. 1986; Rasouli, Golriz, and Hamidi 2005; Masoumifard et al. 2008; Merzsch, Lechner, and Krautz 2013) has reported that the heat transfer coefficient is significantly affected by the following parameters:

1) Physical properties of the fluidizing gas and solid particles: gas density, gas viscosity, gas thermal conductivity, specific heat capacity, solid particle size, solid density, specific heat capacity, and the thermal conductivity of the solid.
2) Operating conditions: superficial gas velocity, operating temperature, and pressure.

3) Design parameters: distributor design, heat transfer surface geometry, radial and axial positions as well as the orientation of the heated surface inside the bed.

In addition to the design factors mentioned above, one of the most important design factors affecting the heat transfer inside the gas-solid fluidized bed is the tube diameter (D_T) (White, Mathur, and Saxena 1986). Therefore, many experimental works have been performed to study the impact of the tube diameter on the heat transfer coefficients inside the different sizes and configurations of gas-solid fluidizing media (Vreedenberg 1958; Grewal and Saxena 1980; Doherty et al. 1986; Merzsch, Lechner, and Krautz 2013). It is worth mentioning that these works were conducted to study the influence of the tube diameter on the performance of the heat transfer in gas-solid fluidized beds having a horizontal orientation, which is also the case with most of the experimental research in the literature that studied the effect of the tube diameter. It has been stated and recommended by many researchers that using vertical tubes as heat exchanger surfaces has many benefits compared with tubes in a horizontal orientation; for example, the design and scale-up of a fluidized bed with vertical internals poses less problems; the installation, removal, and emptying of the bed is physically easier; channeling and dead zones are eliminated; the occupied volume of the vertical orientation is lower; the heat transfer efficiency is higher; and the tube erosion is 50% less than that of a horizontal arrangement (Volk, Johnson, and Stotler 1962; Grace and Harrison 1968; Rüdisüli et al. 2012a).

The many above mentioned benefits of using vertical tubes inside gas-solid fluidized beds have increased the interest in studying the effect of the tube diameter of the vertical heat exchanger internals on the heat transfer coefficient inside the gas-solid fluidized bed, prompting this research. In addition, the heat transfer mechanism inside gas-

solid fluidization systems with vertical tubes is still considered a big challenge that needs more study. Furthermore, there is little experimental data available in the literature studying the influence of the tube diameter of the vertical heat exchanger internals on the performance of the heat transfer inside the gas-solid fluidized beds. Accordingly, in the present work, the impact of the vertical heat exchanger tube diameter on the local heat transfer coefficient inside a laboratory-scale gas-solid fluidized bed was examined using an advanced fast-response heat transfer probe. Two heat transfer probes with different tube diameters were employed as a part of the vertical immersed tubes, and the local heat transfer coefficient measurements were taken at different axial and radial positions inside the bed, after which, the experimental was correlated based on relevant dimensionless groups using multiple linear regressions with JMP®12 statistical software.

B.3. EXPERIMENTAL SETUP

The experimental setup consisted of a laboratory-scale fluidized bed column with 0.14 m inside diameter and 1.84 m height. The column was constructed from Plexiglas®, and the plenum was made from aluminum. The column and plenum were placed on the top of a stainless steel base. The compressed air was fed to the column using industrial-scale compressors with pressure up to 1.38 MPa. A pressure stabilizer regulated the inlet pressure because the flow meters operate at 0.69 MPa. Omega flow meters controlled the flow rate. A schematic diagram of the fluidized bed column with vertical internals is provided in Figure B.1. The gas phase was introduced through a sparger tube in the plenum section and then through a distributor sheet mounted between the column and plenum. The gas distributor was made of a porous polyethylene sheet, with a pore size of 15-40 μm. The

sparger tube was plugged at one end and had 14 holes, all facing downward with respect to the column. The column was electrically grounded using copper wire mesh to minimize electrostatic effects. A rigid metallic structure was used to support the column and eliminate the mechanical vibrations, as shown in Figure B.2.

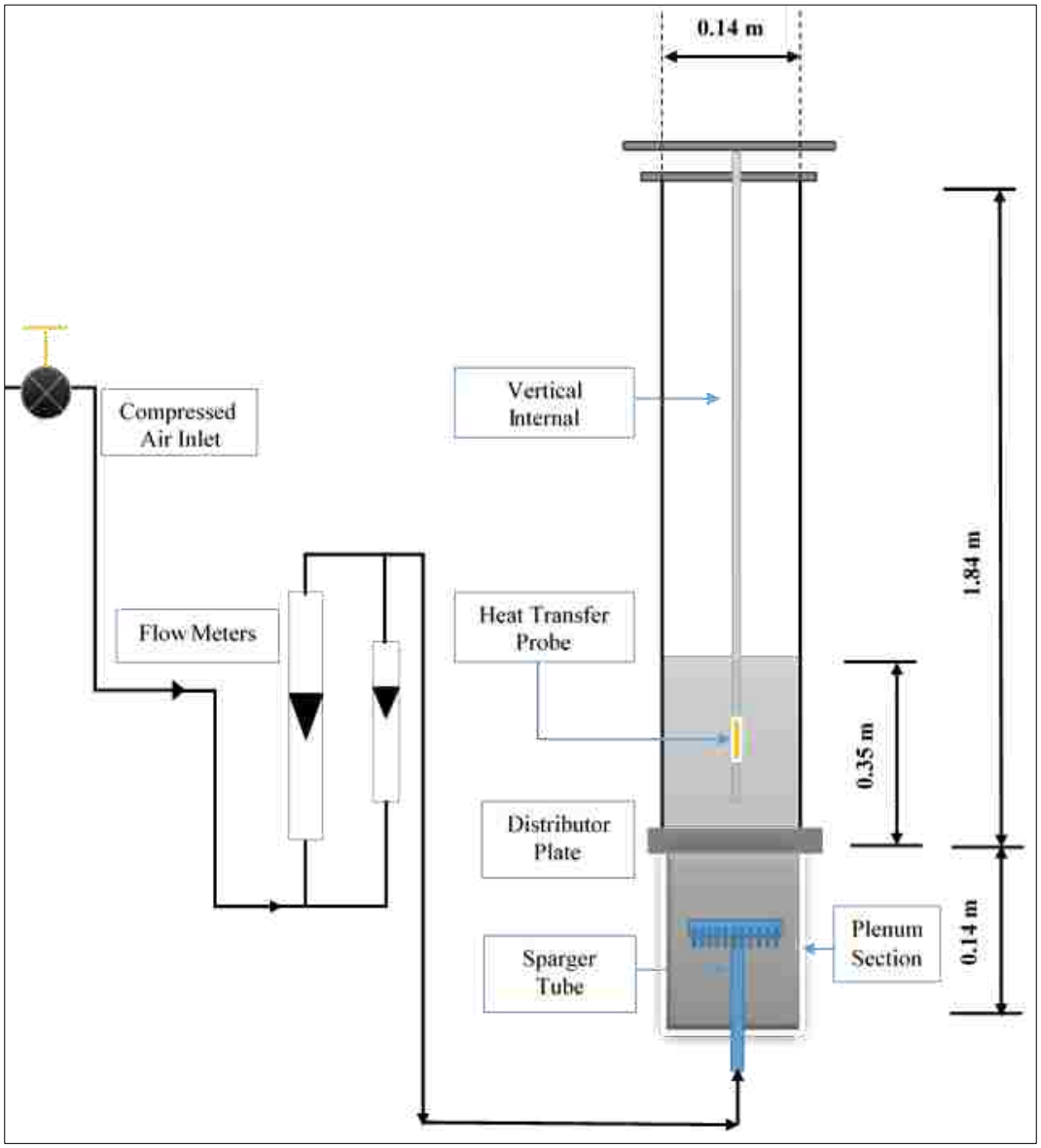

Figure B.1. Schematic diagram of 0.14 m inside diameter, laboratory-scale fluidized bed column.

Figure B.2. Fluidized bed column with metallic structure and copper wire mesh.

The experiments were conducted at superficial gas velocities of 0.45, 0.5, 0.55, 0.6, 0.65, and 0.7 m/s. The analysis of the pressure fluctuations was recorded by a differential pressure transducer. The literature indicates that the bed should be in the bubbling flow regime and that the solid particles should be well mixed (White, Mathur, and Saxena 1986). Furthermore, the heat transfer measurements were acquired at three axial heights (H/D = 0.75, 1.5, and 2.0) above the gas distributor and at three radial positions (r/R = 0.0, 0.5, and

0.8), according to the radial locations of the heat transfer probe. The solid particle used in this work was glass beads of Geldart B type, with 365 μm average particle size and 2500 Kg/m^3 density, and the static bed height was 0.35 m. The minimum fluidized velocity, measured experimentally using a differential pressure transducer, was 0.4 m/s.

B.4. ADVANCED FAST RESPONSE HEAT TRANSFER PROBE TECHNIQUE

The measurements of the local heat transfer coefficients were made using heat transfer probes of two sizes (0.0127 and 0.0254 mm), with a length of 0.062 and 0.095 m, respectively. Both heat transfer probes were built as a part of the vertical internals, as shown in Figure B.3. As mentioned earlier, the measurements were taken at different axial positions (H/D = 0.75, 1.5, and 1.75), and each internal was moved to three radial positions (r/R = 0.0, 0.5, and 0.8), as shown in Figure B.4. The heat transfer probe consisted of a MicroFoil™ heat transfer sensor (RDF Corp., model 27134-1). The MicroFoil™ sensor was flash mounted on the outer surface of a brass cylinder. It is noteworthy that the new generation of MicroFoil™ sensor used in this work has more active surface area for heat flux and surface temperature measurements than the old generation, which consisted of a point measurement in the center of the foil; in the new generation, the microsensor wires covered most of the MicroFoil™ surface area. Furthermore, the MicroFoil™ sensor is considered one of the most accurate techniques for measuring the heat transfer coefficient due to its many beneficial characteristics, such as fast response, high sensitivity, low thermal impedance, thin size (least disturbance to heat flow), flexibility, and wide temperature range. The MicroFoil™ sensor includes a built-in heat flux sensor and thermocouple to measure the local heat flux (q_i) and the surface temperature (T_{si}) of the

a b

Figure B.3. Heat transfer probes: (a) 0.0127 m outer diameter, and (b) 0.0254 m outer diameter.

heat transfer probe simultaneously. The heat element cartridge (Chromalox, model CIR-1012) was installed inside the brass cylinder, which is a heat source. Electric power was supplied to the heating element through a DC power supply. The bed temperature was measured using five copper-constantan thermocouples (Omega Inc., model TQSS-18U-12), one of which was contiguous to the heat probe, while the other was installed at various axial and radial positions. The heat flux voltage signal was generated in the micro-voltage range, so an amplifier (JH Technology, Inc., model JH4300) was connected to the heat flux sensor before the voltage signal was received by the data acquisition system (DAQ, model

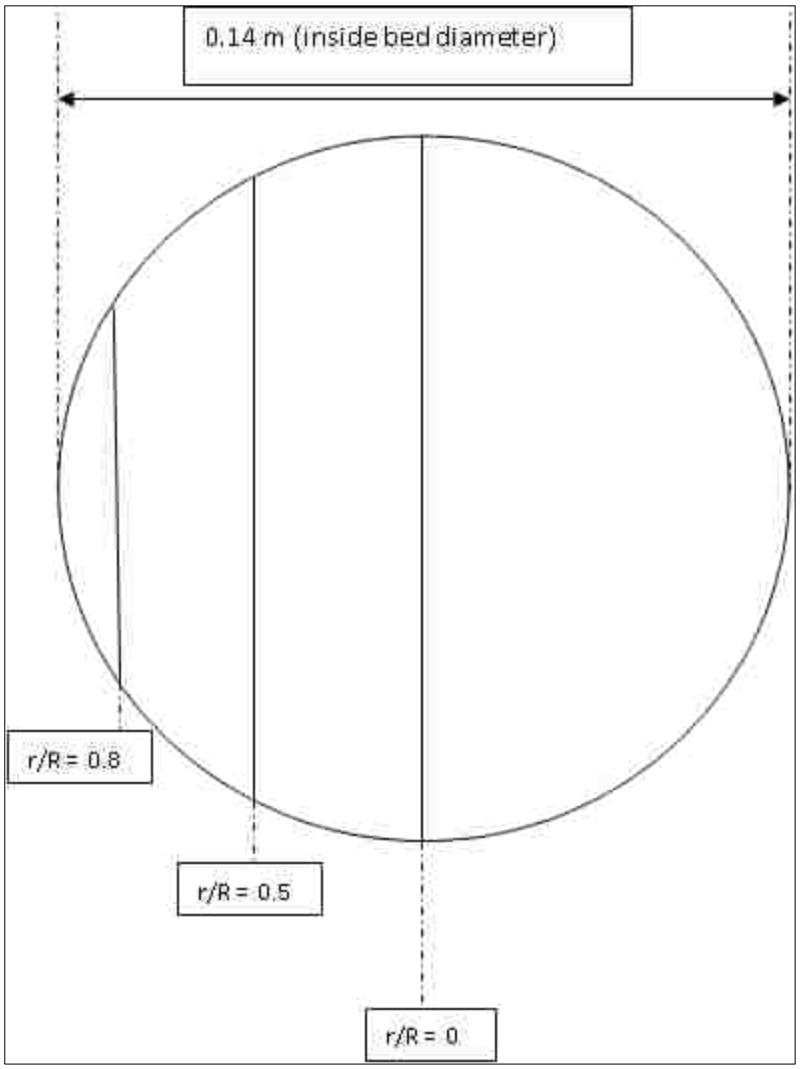

Figure B.4. Three radial positions of the heat transfer measurements.

NI-9205). The surface temperature sensor and the bed thermocouples were connected to another data acquisition system (DAQ, model NI-9213). The heat transfer measurement system is shown in Figure B.5. LabVIEW™ software was used to control the experimental measurements and data recording of the heat transfer coefficients, including the foil-sensor measurement (heat flux voltage signal and surface temperature signal) as well as the bed temperature signals, using five thermocouples located at different radial and axial

positions. The heat flux signals and the signals from the thermocouples were recorded at 25 Hz for about 160 s and repeated five

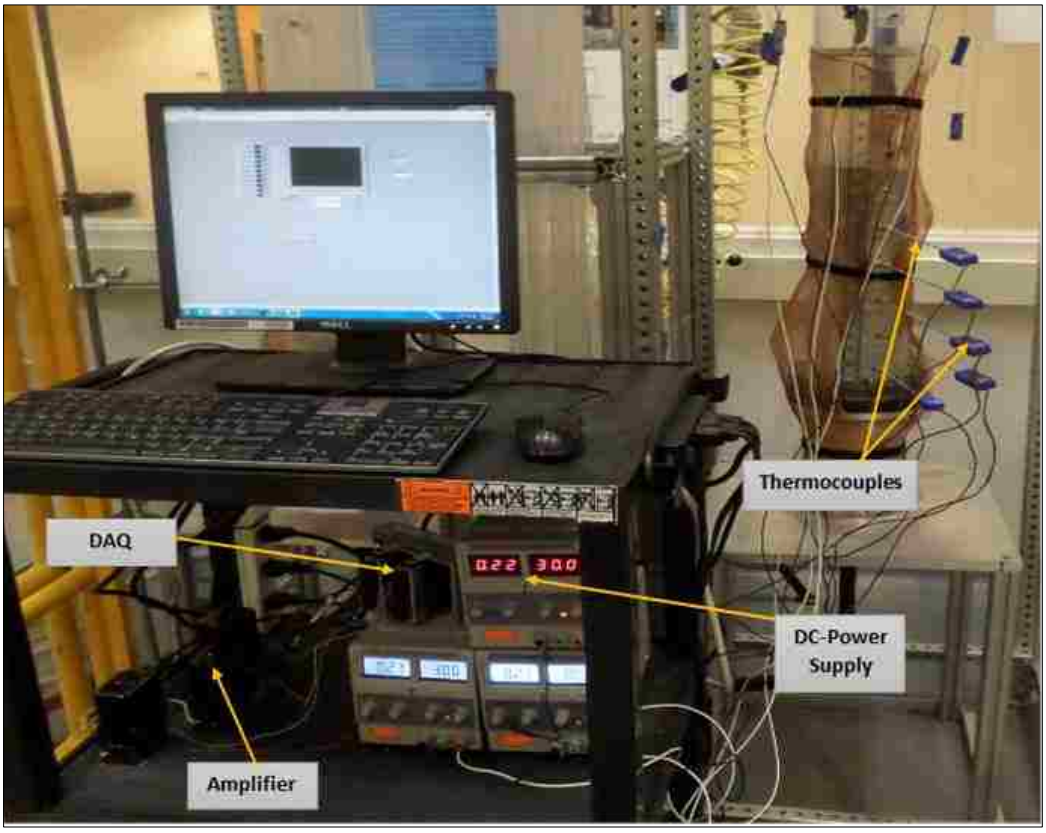

Figure B.5. Heat transfer measurement device and its accessories.

times to ensure the validity of the measurements. The instantaneous local heat transfer coefficient is determined by the direct measurement of the heat flux and the difference between the surface and the bulk temperatures at a given time, as follows (Abdulmohsin, Abid, and Al-Dahhan 2011; Abdulmohsin and Al-Dahhan 2012):

$$h_i = \frac{q_i}{T_{si} - T_{bi}} \qquad (2)$$

where h_i is the instantaneous local heat transfer coefficient ($W/m^2.K$), q_i is the instantaneous heat flux across the sensor (W/m^2), T_{si} is the instantaneous surface temperature of the heat transfer probe (K), and T_{bi} is the instantaneous bulk temperature of the bed (K). The time-averaged heat transfer coefficient (h_{ave}) at a given location was then calculated by averaging the instantaneous heat transfer coefficient measurements over the sampling period of 160 s:

$$h_{ave} = \frac{1}{n}\sum_{i=1}^{n}\frac{q_i}{T_{si}-T_{bi}} \quad (3)$$

where n is the total number of the sampled data points (n = 4000 over the sampling period).

B.5. RESULTS AND DISCUSSION

The measurements of the heat transfer coefficient were performed using an advanced fast-response heat transfer probe with two tube diameters to investigate the effect of the tube diameter (D_T) on the performance of the heat transfer inside the gas-solid fluidized bed. Furthermore, the experiments were conducted at different superficial gas velocities and various axial heights and radial positions. As mentioned earlier, the superficial gas velocities were selected so that the column operated in the bubbling flow regime when the gas-solid fluidized bed worked in the bubbling flow regime, the solid particles were well mixed, and the distribution of the gas phase in the form of bubbles was uniform, and the fluidization process operated smoothly. Moreover, the three axial heights were chosen to cover three key zones inside the bed: H/D = 0.75, near the distributor plate, where the bubbles first form and start to rise; H/D = 1.5, the axial level that almost represents the middle of the fluidizing bed, where the bubbles continue to move up and tend to coalesce with each other in their vertical pathways, and H/D = 2.0, the axial height

that represents the area near the freeboard of the column where the bubbles reach their maximum size and then break up when they reach the upper level of the bed. In addition, three radial positions were selected to study the local heat transfer coefficients within the bed: r/R = 0.8, near the wall region of the column; r/R = 0.0, the central region of the column, and r/R = 0.5, the middle of the column radius.

B.5.1. EFFECT OF SUPERFICIAL GAS VELOCITY

The influence of the superficial gas velocity on the heat transfer coefficients measured at different axial heights and radial positions for both tube diameters is illustrated in Figures b.6-b.8, demonstrating that the heat transfer coefficients increased with increases in the superficial gas velocity for all radial heights and axial positions. Moreover, the heat transfer coefficients were higher in the case of the larger tube diameter (D_T = 0.0254) compared with the case of the smaller tube diameter (D_T = 0.0127) for all the superficial gas velocities tested. In addition, it is clear that the increment of change in the heat transfer coefficient is a function of the axial height and radial position, in which the percentage of change in the increment increased radially from the zone near the wall region toward the central region of the bed and increased axially with an increase in the value of H/D. The heat transfer coefficient was enhanced due to the increase in the superficial gas velocity because that improves the gas convection heat transfer fraction due to the increase in the bubble frequency and the gas concentration near the heat transfer surface. Furthermore, the frequency of replacing the gas film that contacts the heat transfer surface is a function of the superficial gas velocity; therefore, increasing the gas velocity replaces the gas film more frequently (Doherty et al. 1986). It was also found that the heat transfer coefficient

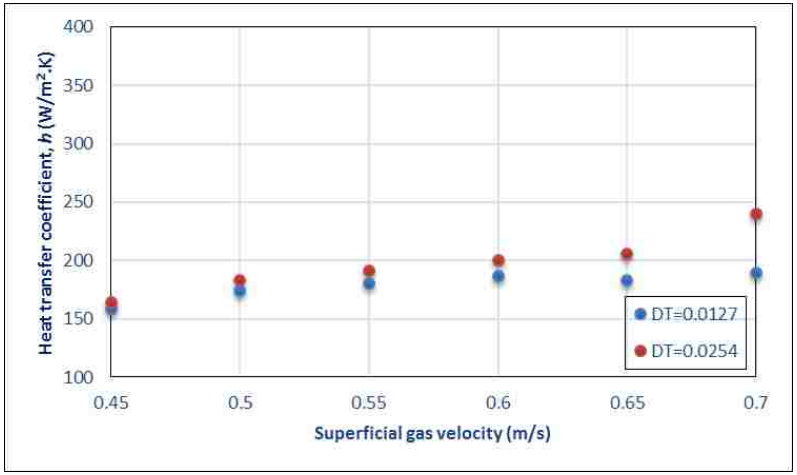

(a)

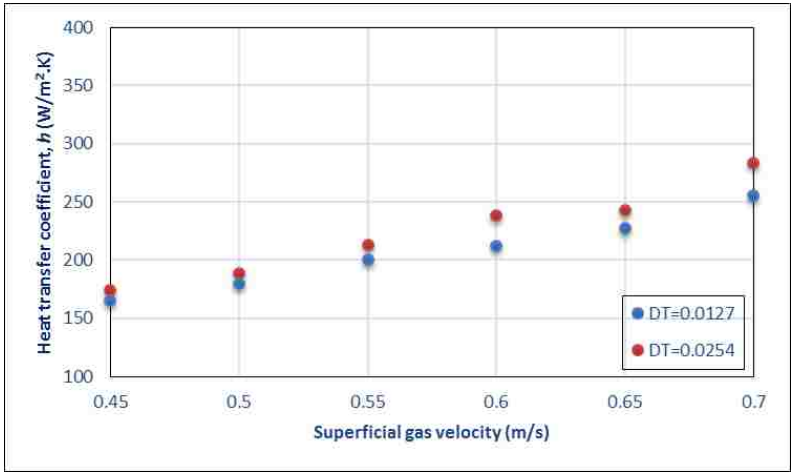

(b)

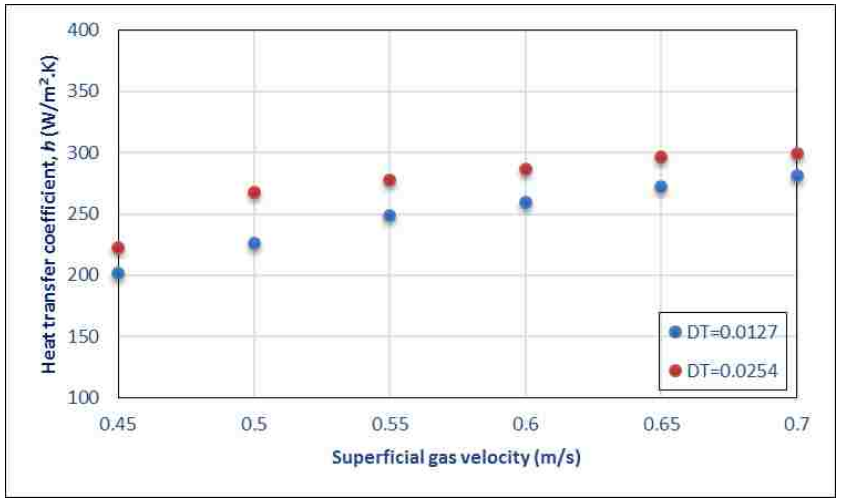

(c)

Figure B.6. Heat transfer coefficient at different superficial gas velocities at H/D = 0.75 and both tube diameters: (a) r/R = 0.8, (b) r/R = 0.5, and (c) r/R = 0.0.

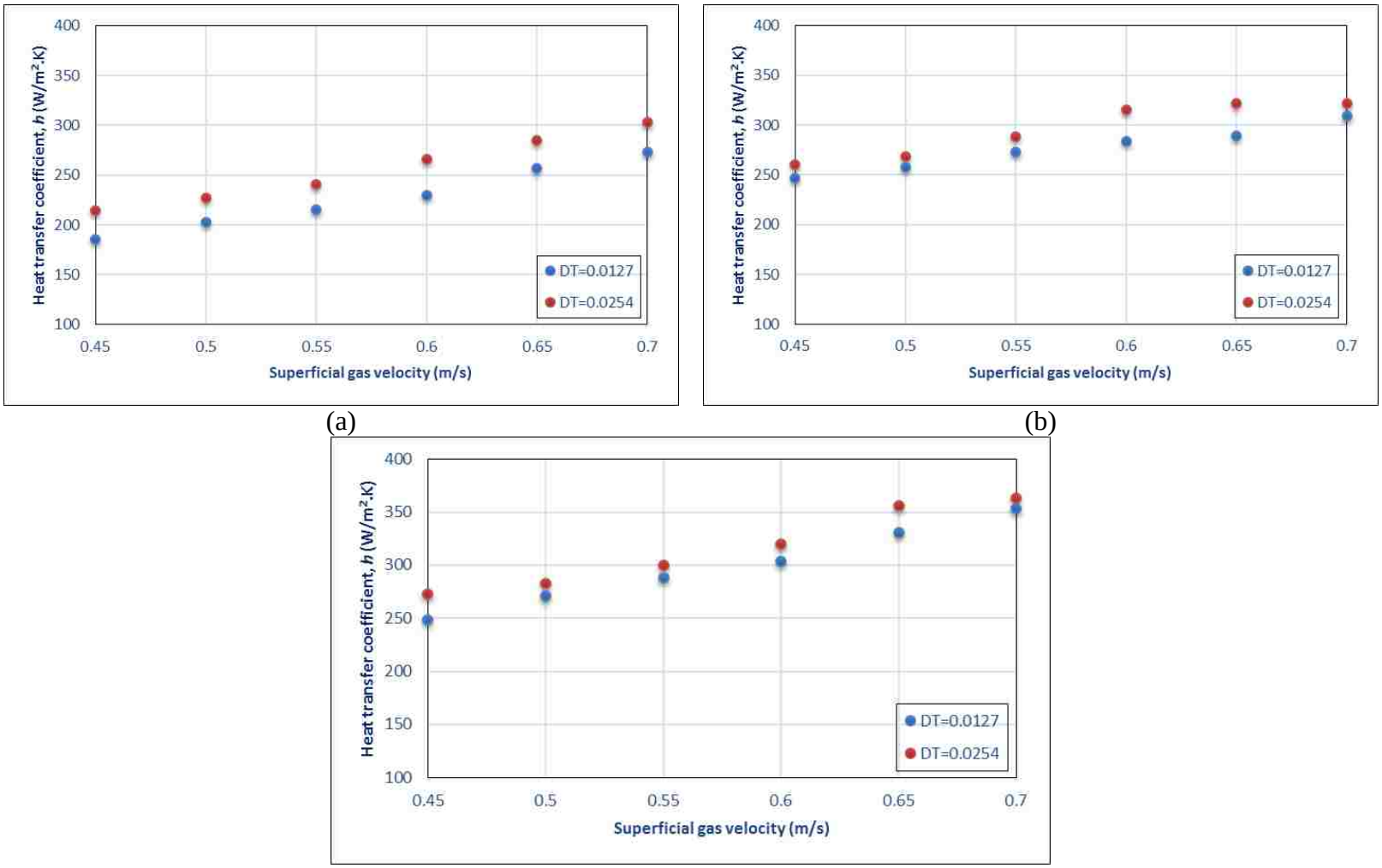

Figure B.7. Heat transfer coefficient at different superficial gas velocities at H/D = 1.5 and both tube diameters: (a) r/R = 0.8, (b) r/R = 0.5, and (c) r/R = 0.0.

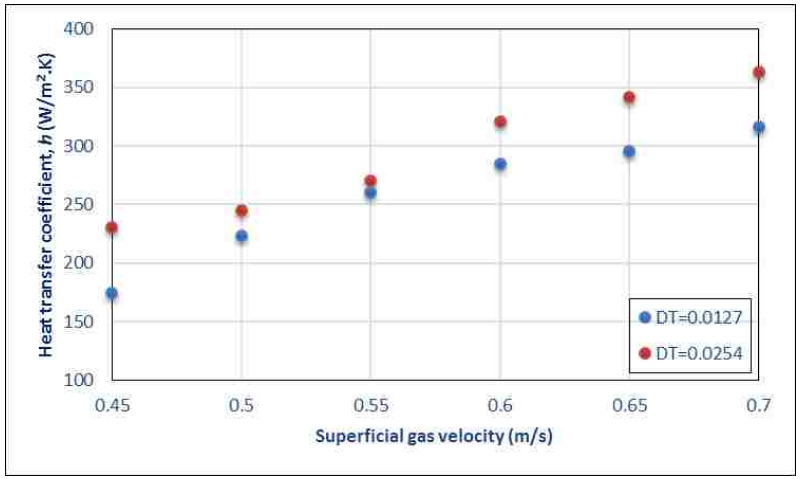

(a)

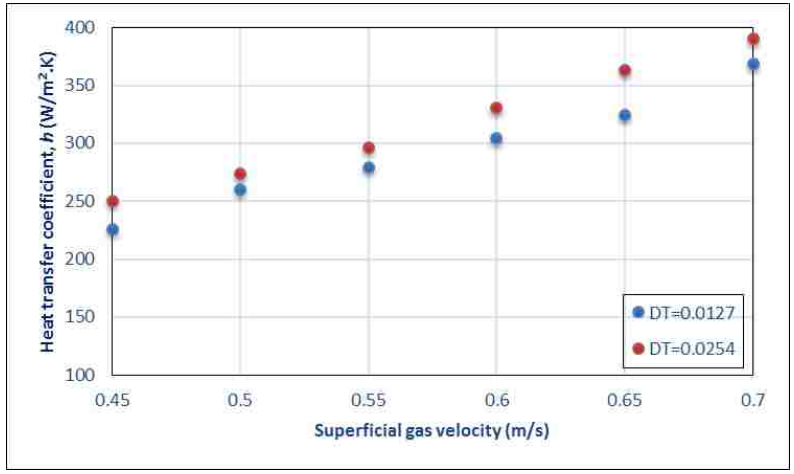

(b)

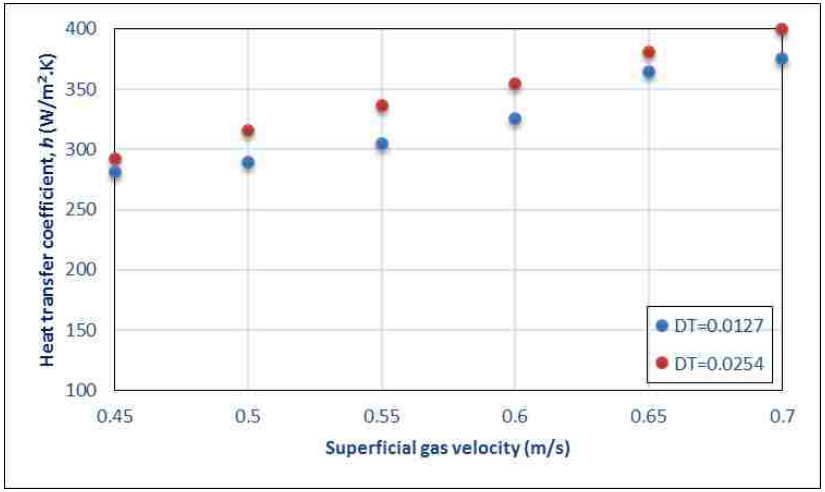

(c)

Figure B.8. Heat transfer coefficients at different superficial gas velocities at H/D = 2.0 and both tube diameters: (a) r/R = 0.8, (b) r/R = 0.5, and (c) r/R = 0.0.

rose with an increase in D_T for all the superficial gas velocities, axial heights, and radial positions tested in the present work, and the performance of the heat transfer between the immersed tube and the fluidized bed improved with the larger heat transfer tube surface area: $D_T = 0.0254$. The increase in the heat transfer coefficient with an increase in D_T can be explained by referring to the two predominant heat transfer forms between the immersed tube and the gas-solid fluidized bed, especially when the fluidized bed operates under relatively low temperature. These two forms are solid particle heat convection and gas film heat convection. Furthermore, the solid particle heat convection is controlled by the solid particle residence time and the solid particle concentration near the heat transfer surface. Therefore, an increase in D_T leads to a decrease in the particle residence time, causing the heat transfer coefficient to increase accordingly. The decrease in the particle residence time produces an increase in the temperature difference between the tube surface and the particles; hence, the driving force increases, which enhances the heat transfer flux, particularly when the tube surface and bed temperatures remain constant (Baskakov et al. 1973). Moreover, it has been stated by White, Mathur, and Saxena (1986) that the gas film residence time is significantly influenced by the curvature of the tube surfaces or the surface area of the tube such that the gas residence time rises with increases in D_T, which causes the heat transfer coefficient to increase.

B.5.2. HEAT TRANSFER COEFFICIENT AT DIFFERENT RADIAL POSITIONS

As mentioned before, the local heat transfer coefficient measurements were conducted at three radial positions. These radial positions were selected to cover three key radial positions of the bed: near the column wall region ($r/R = 0.8$), at the middle of the

radius (r/R = 0.5), and in the central region of the bed (r/R = 0.0), as shown in Figure B.4. Three superficial gas velocities were chosen to investigate the heat transfer behavior with a change in radial profiles (0.45, 0.55, and 0.65 m/s). The radial profiles of the heat transfer coefficients at different axial heights and for both tube sizes are shown in Figure B.9. The left side of Figure B.9 represents the radial profiles of the heat transfer coefficient at three axial levels (H/D = 0.75, 1.5, and 2.0) for the tube diameter of 0.0127 m, while the right side of Figure B.9 represents the radial profiles of the heat transfer coefficient at three axial levels (H/D = 0.75, 1.5, and 2.0) for the tube diameter of 0.0254 m. It can be seen from Figure B.9 that the local heat transfer coefficients increased from the wall region toward the central region of the bed for all the axial heights and the selected superficial gas velocities. This result is compatible with the experimental results reported in the literature (Pisters and Prakash 2011; Stefanova et al. 2007a, 2011). Furthermore, Figure B.9 illustrates that the local values of the heat transfer coefficients in the case of D_T = 0.0127 m were higher than for D_T = 0.0254 m for all the axial heights and selected superficial gas velocities. The results indicate that the increment of change in the heat transfer coefficients with D_T agrees with the results of White, Mathur, and Saxena (1986), who reported an increase in the heat transfer coefficient when the vertical immersed tube diameter increased from 0.0254 m to 0.0603 m.

B.5.3. HEAT TRANSFER COEFFICIENT AT DIFFERENT AXIAL HEIGHTS

As mentioned earlier, the three selected axial heights were chosen because they represent three significant axial levels inside the gas-solid fluidized bed: H/D = 0.75, near the distributor plate; H/D = 1.5, in the middle of the fluidizing bed; and H/D = 2.0, near the

freeboard of the column. Also, three superficial gas velocities (0.5, 0.6, and 0.7 m/s) were chosen to study the influence of tube diameter at different axial heights on the local heat transfer coefficients. The axial profiles of the heat transfer coefficients at different radial positions, three superficial gas velocities, and for both tube diameters are shown in Figure B.10. The left side of Figure B.10 illustrates the axial profiles of the heat transfer coefficients for D_T = 0.0127 m, while the right side of Figure B.10 illustrates the axial profiles of the heat transfer coefficients for D_T = 0.0254 m. As shown in Figure B.10, the local heat transfer coefficient significantly increased with an increase in the axial level (H/D) inside the bed for all the radial positions and selected superficial gas velocities as well as for both tube diameters. In addition, the local heat transfer coefficients at different axial heights were higher in the case of D_T = 0.0254 for all conditions.

The increment of change in the local heat transfer coefficient with the axial height (H/D) in the case of a vertical immersed tube can be explained by increases in the local bubble frequency and the local gas holdup such that when the gas bubbles pass the lower end of the immersed tube (which is located at H/D = 0.25), the larger bubbles will split into two or more smaller bubbles; therefore, the number of bubbles and the gas concentration around the vertical immersed tube will increase. Thus, the increase in the local bubble frequency and the local gas holdup due to the splitting mechanism leads to an increase in the percentage of the surface area of the heating probe that is exposed to both gas and solid particles that move frequently, causing the local heat transfer coefficient to rise, consequently (Kim et al. 2003; Stefanova et al. 2011). Furthermore, the splitting mechanism of the bubbles and the resulting bubble sizes are a function of the vertical internal tube diameter (Rüdisüli et al. 2012a, b). Rüdisüli et al. (2012a) found a significant

Radial profiles of the heat transfer coefficients at different superficial gas velocities and H/D = 0.75 for the case D_T = 0.0127.

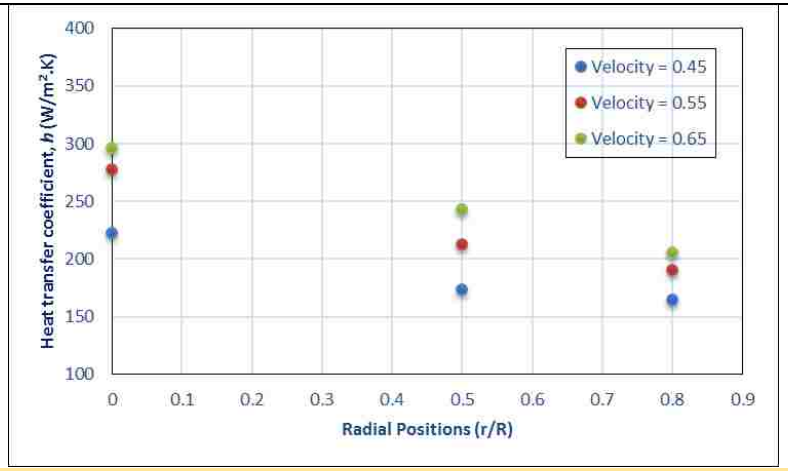

Radial profiles of the heat transfer coefficients at different superficial gas velocities and H/D = 0.75 for the case D_T = 0.0254.

Radial profiles of the heat transfer coefficients at different superficial gas velocities and H/D = 1.5 for the case D_T = 0.0127.

Radial profiles of the heat transfer coefficients at different superficial gas velocities and H/D = 1.5 for the case D_T = 0.0254.

Figure B.9. Radial profiles of the heat transfer coefficients at three superficial gas velocities and different axial heights for the case D_T = 0.0127 (left side) and D_T = 0.0254 (right side).

Radial profiles of the heat transfer coefficients at different superficial gas velocities and H/D = 2.0 for the case D_T = 0.0127.

Radial profiles of the heat transfer coefficients at different superficial gas velocities and H/D = 2.0 for the case D_T = 0.0254.

Figure B.9. Radial profiles of the heat transfer coefficients at three superficial gas velocities and different axial heights for the case D_T = 0.0127 (left side) and D_T = 0.0254 (right side). (cont.)

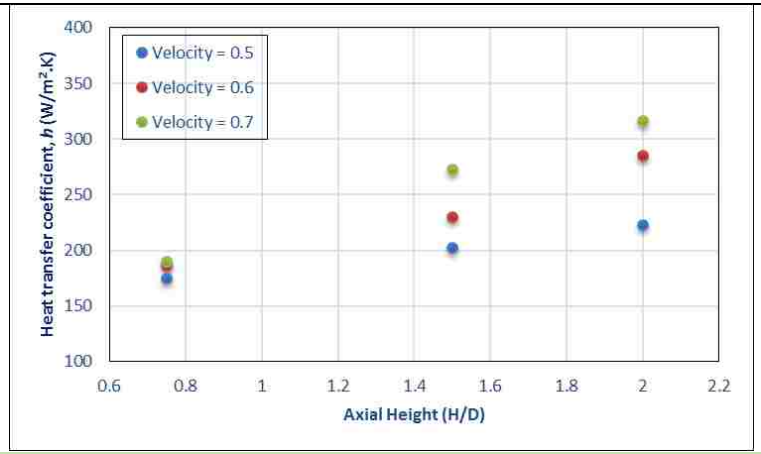

Axial profiles of the heat transfer coefficients at different superficial gas velocities and r/R = 0.8 for the case D_T = 0.0127.

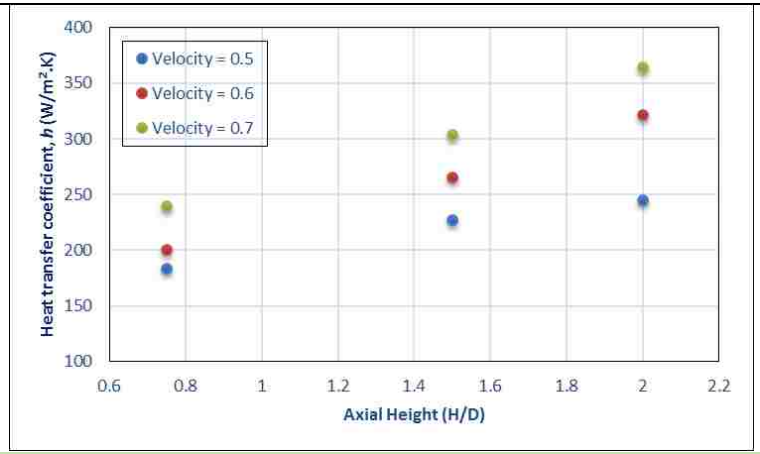

Axial profiles of the heat transfer coefficients at different superficial gas velocities and r/R = 0.8 for the case D_T = 0.0254.

Axial profiles of the heat transfer coefficients at different superficial gas velocities and r/R = 0.5 for the case D_T = 0.0127.

Axial profiles of the heat transfer coefficients at different superficial gas velocities and r/R = 0.5 for the case D_T = 0.0254.

Figure B.10. Axial profiles of the heat transfer coefficients at three superficial gas velocities and different radial positions for the case D_T = 0.0127 (left side) and D_T = 0.0254 (right side).

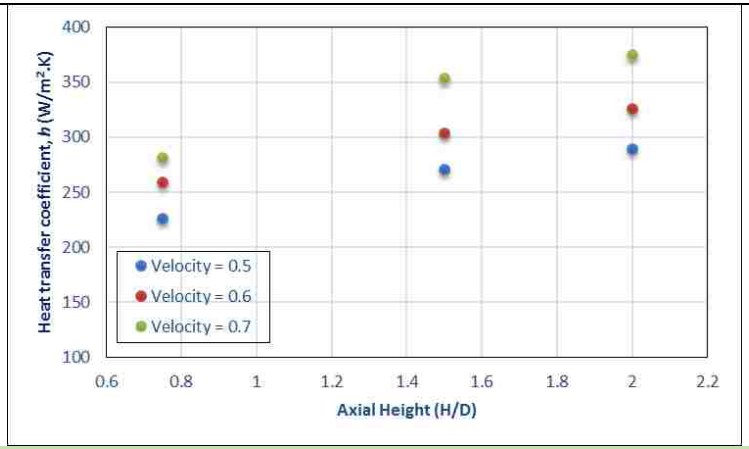

Axial profiles of the heat transfer coefficients at different superficial gas velocities and r/R = 0 for the case of D_T = 0.0127.

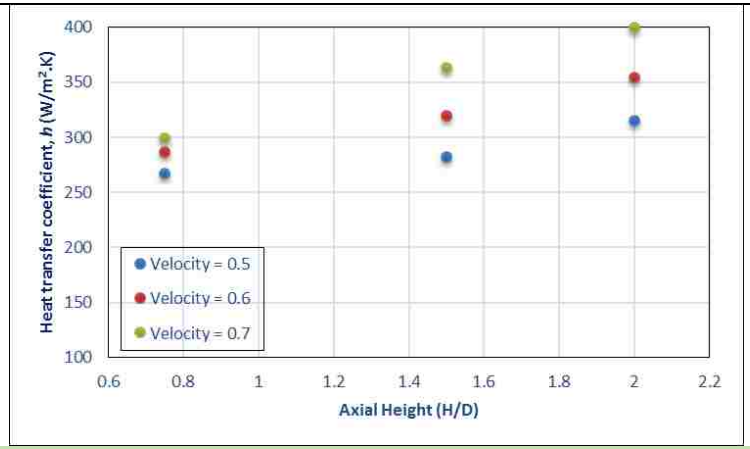

Axial profiles of the heat transfer coefficients at different superficial gas velocities and r/R = 0 for the case of D_T = 0.0254.

Figure B.10. Axial profiles of the heat transfer coefficients at three superficial gas velocities and different radial positions for the case D_T = 0.0127 (left side) and D_T = 0.0254 (right side). (cont.)

relationship between the vertical immersed tube diameter and the bubble characteristics, such as the number of bubbles and the bubble size. They also reported that the splitting mechanism is a function of the bubble size prior to splitting. In addition, they concluded that the larger tube diameter can enhance the behavior of bubble splitting and reduce the bubble size significantly. Consequently, it can be concluded that the larger tube diameter can give higher bubble frequency, smaller bubble size, and larger gas concentration; all of these improvements in the bubble parameters would positively influence the heat transfer coefficient.

B.5.4. HEAT TRANSFER OSCILLATIONS

The influence of the diameter of the tube on the performance of the heat transfer inside the gas-solid fluidized bed was investigated using heat transfer oscillations. The heat transfer oscillations or heat transfer fluctuations can be represented by the heat transfer coefficient signals recorded through a certain period. Studying the heat transfer oscillations provides an added understanding of the instantaneous impact of the diameter of the tube on the heat transfer efficiency through the time-dependent heat transfer coefficient. To compare the two signals for the cases of two tube diameters, the mean and standard deviation of each signal were estimated, such that the average value (μ) indicated the magnitude of the heat transfer coefficient, and the standard deviation (σ) represented the oscillations of the heat transfer coefficient. Therefore, three superficial gas velocities were selected (0.5, 0.6, and 0.7 m/s) as well as one axial height (H/D = 2), and one radial position (r/R = 0.0) because at these positions, the heat transfer coefficient reaches its maximum value compared with other axial and radial positions. The heat transfer coefficient

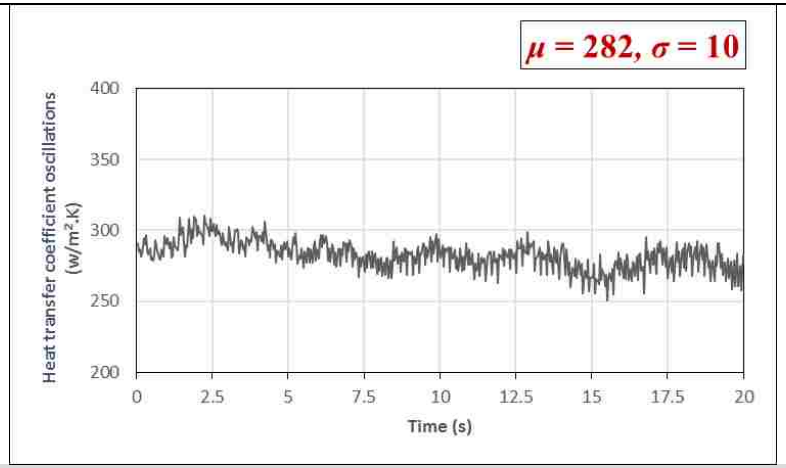

Heat transfer coefficient oscillations at u = 0.5 m/s for the case D_T = 0.0127 m.

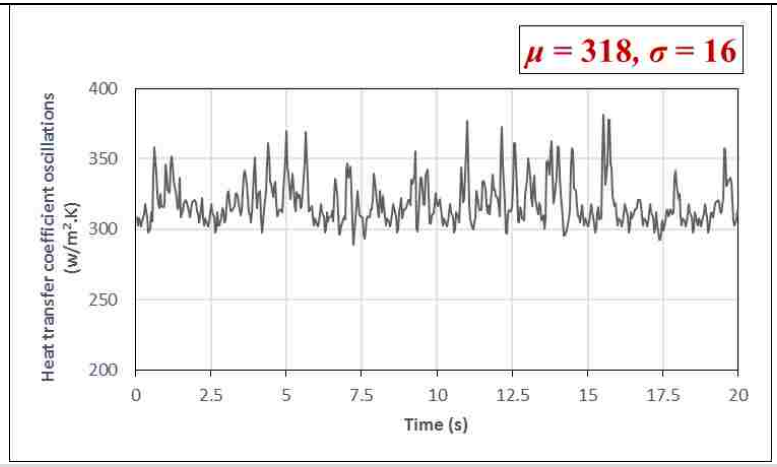

Heat transfer coefficient oscillations at u = 0.5 m/s for the case D_T = 0.0254 m.

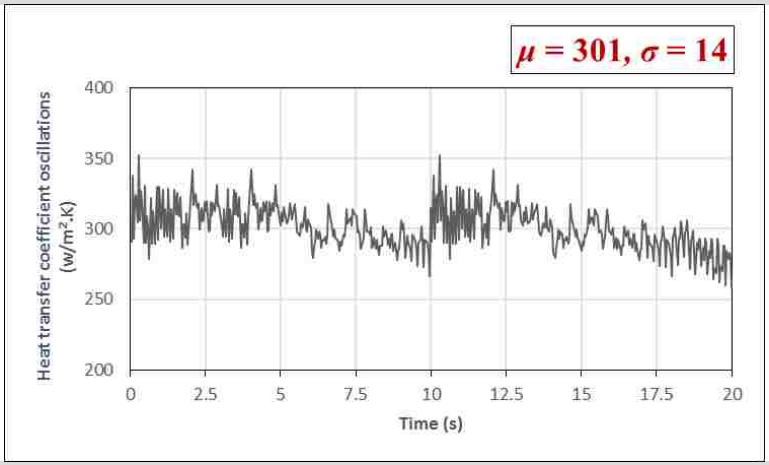

Heat transfer coefficient oscillations at u = 0.55 m/s for the case D_T = 0.0127 m.

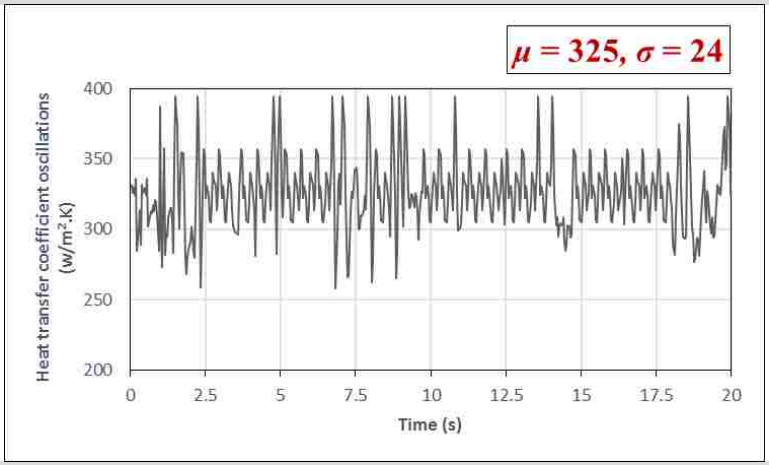

Heat transfer coefficient oscillations at u = 0.55 m/s for the case of D_T = 0.0254 m.

Figure B.11. Heat transfer coefficient oscillations at H/D = 2, r/R = 0.0, and three superficial gas velocities for D_T = 0.0127 m (left side) and D_T = 0.0254 m (right side).

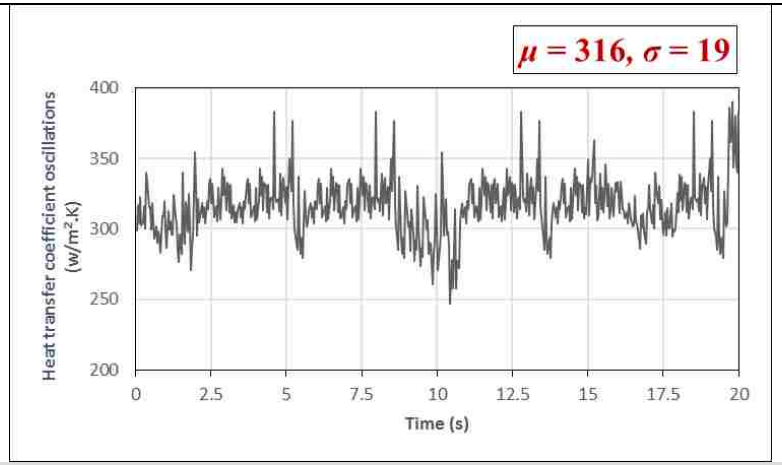

Heat transfer coefficient oscillations at u = 0.6 m/s for the case D_T = 0.0127 m.

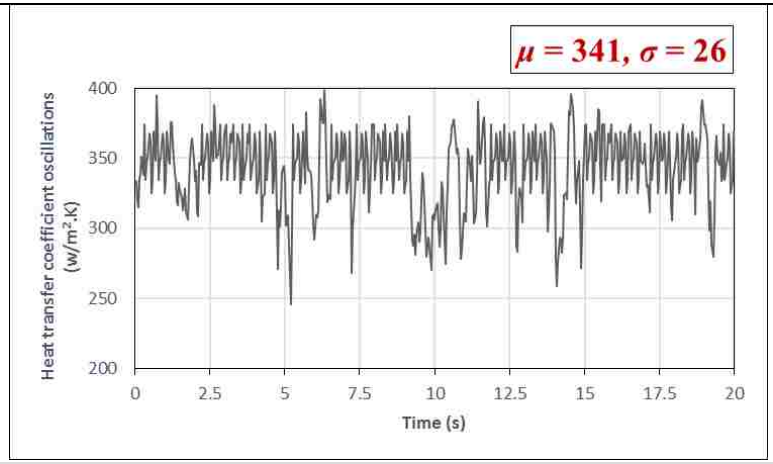

Heat transfer coefficient oscillations at u = 0.6 m/s for the case D_T = 0.0254 m.

Figure B.11. Heat transfer coefficient oscillations at H/D = 2, r/R = 0.0, and three superficial gas velocities for D_T = 0.0127 m (left side) and D_T = 0.0254 m (right side). (cont.)

oscillations are illustrated in Figure B.11 for both tube diameters: the left side illustrates the case D_T = 0.0127 m, while the right side illustrates the case of D_T = 0.0254 m.

Figure B.11 shows that the values of both the average and standard deviation of the case of D_T = 0.0254 m are higher than for D_T = 0.0127 m for all three selected superficial gas velocities. The values of the average and standard deviation of the heat transfer coefficient signals indicate that the heat transfer coefficient was enhanced in the case of D_T = 0.0254 m due to the effect of the gas-solid hydrodynamics that occur with the presence of vertical internals with different tube diameters: the larger tube diameter made some dynamic changes in the gas-solid flow patterns and gas-solid hydrodynamic characteristics, such as increasing the number of bubbles and the gas concentration. Furthermore, the values of the standard deviation increased in the case of D_T = 0.0254 m, as shown in Figure B.11; this increment of change in the standard deviation of the heat transfer oscillation signal indicates an increase in the local fluctuations of both the heat transfer coefficient and the hydrodynamics due to the presence of a larger vertical immersed tube diameter. This increase in the standard deviation is reflected in the performance of the heat transfer process such that the local heat transfer coefficient increased.

B.5.5. PREDICTED CORRELATION

The predicted correlation was developed based on relevant dimensionless groups involving related parameters; these parameters are the design parameter (tube diameter), operating condition (superficial gas velocity), physical properties of the gas and solid particles (gas density, gas viscosity, gas thermal conductivity, and solid particle size). A

dimensional analysis approach was employed, in which the system parameters were classified into the following dimensionless groups, as follows:

1) Operating parameter: Froude number (*Fr*), Reynolds number based on the particle diameter (Re_p), and Reynolds number based on the tube diameter (Re_t).

2) Design and physical parameter: the ratio of tube diameter to the solid particle size (D_T/d_p).

3) Measurement position parameter: radial and axial positions of measurement r/R and H/D.

The tube diameter (D_T) and heat transfer coefficient (h) relate to the above parameters as follows:

$$Nu_t = K(Re_t)^a \left(\frac{D_T}{d_p} . \frac{F_r}{Re_p^2}\right)^b \left(\frac{r}{R}\right)^c \left(\frac{H}{D}\right)^d \quad (4)$$

where Nu_t is the Nusselt number based on the tube diameter ($\frac{hD_T}{k_g}$); Fr is the Froude number $\left(\frac{U^2}{gd_p}\right)$; Re_p is the Reynolds number based on the particle diameter $\left(\frac{\rho_g U d_p}{\mu_g}\right)$; Re_t is the Reynolds number based on the tube diameter = $\left(\frac{\rho_g U D_T}{\mu_g}\right)$; D_T is the tube diameter, d_p is the particle size; K is the coefficient; and a, b, c, and d are the exponents.

The expression $\frac{F_r}{Re_p^2}$ represents the ratio of the Froude number and the square of the Reynolds number based on the particle diameter (Re_p), which can be written as $\frac{\mu_g^2}{d_p^3 \rho_s^2 g}$. This ratio was introduced in the present correlation because Vreedenberg (1958) proved that in the case of coarse and heavy particles (Geldart B type), the group $\frac{\mu_g^2}{d_p^3 \rho_s^2 g}$ affects the stirring factor introduced by Mickley and Fairbanks (1955).

To perform a multiple linear regression on the experimental data, Eq. 1 was reformulated to a linear formula by taking the natural logarithm (Eq. 5):

$$\ln(Nu_t) = \ln(K) + a\ln(Re_t) + b\ln\left(\frac{D_T}{d_p}.\frac{F_r}{Re_p^2}\right) + c\ln\left(\frac{r}{R}\right) + d\ln\left(\frac{H}{D}\right) \quad (5)$$

A multiple linear regression was performed on the experimental data to estimate the values of the coefficient K and the exponents a, b, c, and d. The values of ln(K) and the exponents a, b, c, and d are listed in Table B.1, and the regression statistic data is illustrated in Table B.2. The predicted correlation equation obtained for the Nusselt number using multiple linear regression in JMP®12 is presented in Eq. 6, with an R^2 value of 0.98 and an average error of 0.06.

Table B.1. Parameter estimates from analysis of variance of the parameters used in Eq. 3.

Term	Estimate	Std Error	t Ratio	Prob > |t|
Intercept	-1.8398	0.1806	-16.93	<.0001
Re_t	1.4469	0.0507	28.50	<.0001
(Dt/Dp*Fr/Re_p^2)	-0.3190	0.0417	-7.64	<.0001
r/R	-0.4158	0.0235	-17.69	<.0001
H/D	0.3316	0.014	23.64	<.0001

Table B.2. Regression statistic data (summary of fit)

RSquare	0.982843
RSquare Adj	0.982177
Root Mean Square Error	0.060012
Mean of Response	5.197704
Observations	108

$$Nu_t = 0.1588\,(Re_t)^{1.4469}\left(\frac{D_T}{d_p}.\frac{F_r}{Re_p^2}\right)^{-0.319}\left(\frac{r}{R}\right)^{-0.4158}\left(\frac{H}{D}\right)^{0.3316} \quad (6)$$

The mean relative deviation (MRD) from the experimental and predicted results was obtained as follows:

$$MRD\% = \left[\sum_{i=1}^{108}\left|\frac{Eu_{i,exp}-Eu_{i,pred}}{Eu_{i,exp}}\right|\right] * \frac{100}{108} = 4.59\% \quad (7)$$

The MRD of 4.59%, obtained from Eq. 7, shows a good agreement between the values of the Nusselt number predicted by Eq. 6 and the experimental data. Figure B.12 presents the plot of the experimental data versus the predicted values of the Nusselt number.

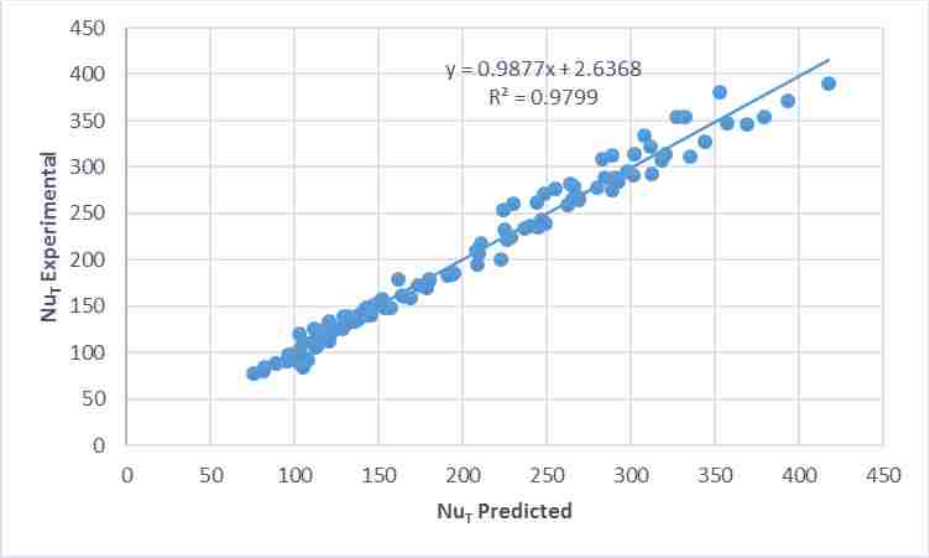

Figure B.12. Comparison between the experimental and predicted values of the Nusselt number.

B.6. REMARKS

The relation between the heat transfer and vertical immersed tube diameter was studied in a gas-solid fluidization system of 0.14 m inside diameter. The heat transfer experimental investigation was conducted using advanced fast-response heat transfer probes of two tube diameters (0.0254 and 0.0127 m). The fast-response heat transfer probe used a MicroFoil™ sensor, which has the ability to measure the heat flux and the probe's surface temperature simultaneously. The solid particles were glass beads of 365 μm mean particle size, 2500 Kg/m^3 density, in a static bed of 0.35 m. The fluidized bed was operated in the bubbling flow regime, with a superficial gas velocity range of 0.45 to 0.7 m/s, along with measurements performed at different axial and radial positions inside the bed, to give a clear picture of the behavior of the local heat transfer coefficient of the immersed tubes with two diameters. It was found that the heat transfer coefficient increased with the tube diameter for the entire range of fluidizing gas velocities and all locations of the local heat transfer coefficients inside the bed. Heat transfer improvement with increasing tube diameter was confirmed and validated with the heat transfer oscillations, in which the magnitude and frequency of the heat transfer coefficient signals, which were represented by the average and the standard deviation, increased more in the case of the 0.0254 m tube diameter than with the smaller tube diameter of 0.0127 m. Ultimately, the regression correlation formula suggested using a multi-linear regression to correlate the relevant parameters in the form of a pertinent dimensionless group, and the predicted values were in good agreement with the experimental data, with a mean relative deviation of 4.59%.

ACKNOWLEDGEMENTS

The authors would like to thank the Multiphase Reactors Engineering and Applications Laboratory (mReal) for funding and support.

NOMENCLATURE

D	inside column diameter (m)
d_p	particle diameter (μm)
D_T	tube diameter (m)
g	gravitational force (m/s2)
H	axial height (m)
h	heat transfer coefficient ($W/m^2.K$)
r	radial position (m)
R	radius of the column (m)
u	superficial gas velocity (m/s)
μ_g	gas viscosity (Kg/m.s)
ρ_g	gas density (Kg/m3)
ρs	solid particle density (Kg/m3)

Greek Letters

ε	gas holdup
μ	viscosity (Kg/m.s)
ρ	density (Kg/m3)

Subscripts and Superscripts

g	gas
p	particle
s	solid

REFERENCES

Abdulmohsin, Rahman S., Balasim A. Abid, and Muthanna H. Al-Dahhan. 2011. "Heat Transfer Study in a Pilot-Plant Scale Bubble Column." Chemical Engineering Research and Design 89 (1). Institution of Chemical Engineers: 78–84. doi:10.1016/j.cherd.2010.04.019.

Abdulmohsin, Rahman S., and Muthanna H. Al-Dahhan. 2012. "Impact of Internals on the Heat-Transfer Coefficient in a Bubble Column." Industrial and Engineering Chemistry Research 51 (7): 2874–81. doi:10.1021/ie2018096.

Baskakov, A. P., B. V. Berg, O. K. Vitt, N. F. Filippovsky, V. A. Kirakosyan, J. M. Goldobin, and V. K. Maskaev. 1973. "Heat Transfer to Objects Immersed in Fluidized Beds." Powder Technology 8 (5–6): 273–82. doi:10.1016/0032-5910(73)80092-0.

Chen, John C., John R. Grace, and Mohammad R. Golriz. 2005. "Heat Transfer in Fluidized Beds: Design Methods." Powder Technology 150 (2 SPEC. ISS.): 123–32. doi:10.1016/j.powtec.2004.11.035.

Chen, R.C., and L.S. Fan. 1992. "Particle Image Velocimetry for Characterizing the Flow Structure in Three-Dimensional Gas-Liquid-Solid Fluidized Beds." Chemical Engineering Science 47: 3615–22. doi:10.1017/CBO9781107415324.004.

Cui, Heping, and Jamal Chaouki. 2004. "Effects of Temperature on Local Two-Phase Flow Structure in Bubbling and Turbulent Fluidized Beds of FCC Particles." Chemical Engineering Science 59 (16): 3413–22. doi:10.1016/j.ces.2004.05.006.

Doherty, J. A., R. S. Verma, S. Shrivastava, and S. C. Saxena. 1986. "Heat Transfer from Immersed Horizontal Tubes of Different Diameter in a Gas-Fluidized Bed." Energy 11 (8): 773–83. doi:10.1016/0360-5442(86)90016-2.

Glass, D. H., and D. Harrison. 1964. "Flow Patterns near a Solid Obstacle in a Fluidized Bed." Chemical Engineering Science 16 (12): 1001–2. doi:10.1016/0009-2509(64)85112-5.

Grace, J. R., and D. Harrison. 1968. "The Effect of Internal Baffles in Fluidized Beds: A Guide to Design." In Inst. Chem. Eng. Symp. Ser.

Grewal, N. S., and S. C. Saxena. 1980. "Heat Transfer Between a Horizontal Tube and a Gas-Solid Fluidized Bed." International Journal of Heat and Mass Transfer 23 (11): 1505–19. doi:10.1016/0017-9310(80)90154-4.

Halvorsen, B. 2005. "An Experimental and Computational Study of Flow Behaviour in Bubbling Fluidized Beds." PhD thesis, The Norwegian University of Science and Technology, Norway. http://teora.hit.no/dspace/handle/2282/301.

HU, Gouxin, Huier Cheng, and Haojie Fan. 1998. “Particle-Fluid Transfer in a Circulation Fluidized Bed.” In Energy and Environment: Proceedings of the International Conference on Energy, 553–59.

Kim, Sang Done Sung Won Sang Done Sung Won, Jung Yeul Ahn, Sang Done Sung Won Sang Done Sung Won Kim, and Dong Hyun Lee. 2003. “Heat Transfer and Bubble Characteristics in a Fluidized Bed with Immersed Horizontal Tube Bundle.” International Journal of Heat and Mass Transfer 46 (3): 399–409. doi:10.1016/S0017-9310(02)00296-X.

Law, Chung Lim, Siti Masrinda Tasirin, Wan Ramli Wan Daud, and Derek Geldart. 2003. “Effect of Vertical Baffles on Particle Mixing and Drying in Fluidized Beds of Group D Particles.” China Particuology 1 (3): 115–18. doi:10.1016/S1672-2515(07)60121-3.

Li, Hong Shun, Wen Di Huang, and Ren Zhang Qian. 1995. “An Instrumented Cylinder for Simultaneous Measurements of Instantaneous Local Heat Transfer Coefficients and Hydrodynamics in High-Temperature Fluidized Beds.” Powder Technology 83 (3): 281–85. doi:10.1016/0032-5910(94)02968-T.

Martin, Holger. 1984. “Heat Transfer between Gas Fluidized Beds of Solid Particles and the Surfaces of Immersed Heat Exchanger Elements, Part I.” Chemical Engineering and Processing: Process Intensification 18 (3): 157–69. doi:10.1016/0255-2701(84)87003-8.

Masoumifard, Nima, Navid Mostoufi, Ali-Asghar Hamidi, and Rahmat Sotudeh-Gharebagh. 2008. “Investigation of Heat Transfer between a Horizontal Tube and Gas–solid Fluidized Bed.” International Journal of Heat and Fluid Flow 29 (5): 1504–11. doi:10.1016/j.ijheatfluidflow.2008.06.004.

Mathew, Ronnie Kiran, K. M Meera Sheriffa Begum, and N. Anantharaman. 2014. “Hydrodynamic Studies on Fluidized Beds with Internals: Experimental and ANN Approach.” Powder Technology 264. Elsevier B.V.: 423–29. doi:10.1016/j.powtec.2014.06.001.

Maurer, Simon, Evert C Wagner, J. Ruud van Ommen, Tilman J Schildhauer, Sinan L Teske, Serge M A Biollaz, Alexander Wokaun, and Robert F Mudde. 2015. “Influence of Vertical Internals on a Bubbling Fluidized Bed Characterized by X-Ray Tomography.” International Journal of Multiphase Flow 75. Elsevier Ltd: 237–49. doi:10.1016/j.ijmultiphaseflow.2015.06.001.

Maurer, Simon, Evert C Wagner, Tilman J Schildhauer, J. Ruud van Ommen, Serge M A Biollaz, and Robert F Mudde. 2015. “X-Ray Measurements of Bubble Hold-up in Fluidized Beds with and without Vertical Internals.” International Journal of Multiphase Flow 74. Elsevier Ltd: 118–24. doi:10.1016/j.ijmultiphaseflow.2015.03.009.

Merzsch, Matthias, Stefan Lechner, and Hans Joachim Krautz. 2013. “Heat-Transfer from Single Horizontal Tubes in Fluidized Beds: Influence of Tube Diameter, Moisture and Diameter-Definition by Geldart C Fines Content.” Powder Technology 235. Elsevier B.V.: 1038–46. doi:10.1016/j.powtec.2012.12.002.

Mickley, H S, and D F Fairbanks. 1955. “Mechanism of Heat Transfer to Fluidized Beds.” AIChE Journal 1 (3): 374–84. doi:10.1002/aic.690010317.

Mohanty, Y. K., B. P. Mohanty, G. K. Roy, and K. C. Biswal. 2009. “Effect of Secondary Fluidizing Medium on Hydrodynamics of Gas-Solid Fluidized Bed-Statistical and ANN Approaches.” Chemical Engineering Journal 148 (1): 41–49. doi:10.1016/j.cej.2008.07.037.

Olowson, P.A. 1994. “Influence of Pressure and Fluidization Velocity on the Hydrodynamics of a Fluidized Bed Containing Horizontal Tubes.” Chemical Engineering Science 49 (15): 2437–46.

Ozawa, M, H Umekawa, S Furui, K Hayashi, and N Takenaka. 2004. “Quantitative Flow Visualization of Fluidized-Bed Heat Exchanger by Neutron Radiography.” In Applied Radiation and Isotopes, 61:715–24. doi:10.1016/j.apradiso.2004.03.099.

Ozawa, M, H. Umekawa, S. Furui, K. Hayashi, and N. Takenaka. 2002. “Bubble Behavior and Void Fraction Fluctuation in Vertical Tube Banks Immersed in a Gas-Solid Fluidized-Bed Model.” Experimental Thermal and Fluid Science 26 (6–7): 643–52. doi:10.1016/S0894-1777(02)00178-4.

Pisters, K., and A. Prakash. 2011. “Investigations of Axial and Radial Variations of Heat Transfer Coefficient in Bubbling Fluidized Bed with Fast Response Probe.” Powder Technology 207 (1–3). Elsevier B.V.: 224–31. doi:10.1016/j.powtec.2010.11.003.

Rasouli, S., M. R. Golriz, and A. A. Hamidi. 2005. “Effect of Annular Fins on Heat Transfer of a Horizontal Immersed Tube in Bubbling Fluidized Beds.” Powder Technology 154 (1): 9–13. doi:10.1016/j.powtec.2005.02.008.

Rüdisüli, Martin, Tilman J. Schildhauer, Serge M. A. Biollaz, and J. Ruud Van Ommen. 2012a. “Radial Bubble Distribution in a Fluidized Bed with Vertical Tubes.” Industrial and Engineering Chemistry Research 51 (42): 13815–24. doi:10.1021/ie3004418.

Rüdisüli, Martin, Tilman J Schildhauer, Serge M A Biollaz, and J. Ruud Van Ommen. 2012b. “Bubble Characterization in a Fluidized Bed with Vertical Tubes.” Industrial and Engineering Chemistry Research 51 (12): 4748–58. doi:10.1021/ie2022306.

Ramamoorthy, S., and N. Subramanian. 1981. “Axial Solids Mixing and Bubble Characteristics in Gas-Fluidized Beds with Vertical Internals.” Chemical Engineering Journal 22 (3): 237–42.

Schouten, J. C., M. L. M. Vander Stappen, and C. M. Van Den Bleek. 1996. “Scale-up of Chaotic Fluidized Bed Hydrodynamics.” Chemical Engineering Science 51 (10): 1991–2000. doi:10.1016/0009-2509(96)00056-5.

SHI, Hui xian. 2007. “Experimental Research of Flow Structure in A Gas-Solid Circulating Fluidized Bed Riser by PIV.” Journal of Hydrodynamics 19 (6): 712–19. doi:10.1016/S1001-6058(08)60008-6.

Seo, Myung Won, Young Ho Suh, Sang Done Kim, Sunwon Park, Dong Hyun Lee, and Byung Ho Song§. 2011. “Cluster and Bed-to-Wall Heat Transfer Characteristics in a Dual Circulating Fluidized Bed.” Industrial & Engineering Chemistry Research 51 (6): 2048–61. doi:10.1007/BF02706030.

Stefanova, A., H. T. Bi, C. J. Lim, and J. R. Grace. 2007. “Heat Transfer from Immersed Vertical Tube in a Fluidized Bed of Group A Particles near the Transition to the Turbulent Fluidization Flow Regime.” International Journal of Heat and Mass Transfer 51 (7–8): 2020–28. doi:10.1016/j.ijheatmasstransfer.2007.06.005.

Stefanova, A., H. T. Bi, J. C. Lim, and J. R. Grace. 2011. “Local Hydrodynamics and Heat Transfer in Fluidized Beds of Different Diameter.” Powder Technology 212 (1): 57–63. doi:10.1016/j.powtec.2011.04.026.

Stefanova, A., John R. Grace, C. Jim Lim, J. Sanderson, Xiaotao T. Bi, and K.S. Lim. 2007. “New Horizons in Fluidization Scale-Up Effect on Heat Transfer in a Fluidized Bed Near the Onset of Turbulent Fluidization.” In The 12th International Conference on Fluidization, 272–80.

Sunderesan, Suresh R., and Nigel N. Clark. 1995. “Local Heat Transfer Coefficients on the Circumference of a Tube in a Gas Fluidized Bed.” Int. J. Multiphase Flow 21 (6): 1003–24.

Verma, Vikrant, Tingwen Li, Jean-François Dietiker, and William A. Rogers. 2016. “Hydrodynamics of Gas–solids Flow in a Bubbling Fluidized Bed with Immersed Vertical U-Tube Banks.” Chemical Engineering Journal 287. Elsevier B.V.: 727–43. doi:10.1016/j.cej.2015.11.049.

Volk, W., C. A. Johnson, and H. H. Stotler. 1962. “Effect of Reactor Internals on Quality of Fluidization.” Chemical Engineering Progress 58 (3): 44–47.

Vreedenberg, H. 1958. “Heat Transfer between a Fluidized Bed and a Horizontal Tube.” Chemical Engineering Science 9 (1): 52–60. doi:10.1016/0009-2509(58)87007-4.

Wang, Zhiguo, Hsiaotao T. Bi, and C. Jim Lim. 2009. “Measurements of Local Flow Structures of Conical Spouted Beds by Optical Fibre Probes.” Canadian Journal of Chemical Engineering 87 (2): 264–73. doi:10.1002/cjce.20157.

White, T. R., A. Mathur, and S. C. Saxena. 1986. “Effect of Vertical Boiler Tube Diameter on Heat Transfer Coefficient in Gas-Fluidized Beds.” The Chemical Engineering Journal 32 (1): 1–13. doi:10.1016/0300-9467(86)85001-8.

Wu, R.L., C.J. Lim, J.R. Grace, and C.M.H. Brereton. 1991. “Instantaneous Local Heat Transfer and Hydrodynamics in a Circulating Fluidized Bed.” International Journal of Heat and Mass Transfer 34 (8): 2019–27. doi:10.1016/0017-9310(91)90213-X.

Yates, J.G., D.J. Cheesman, T.A. Mashingaidze, C. Howe, and G Jefferis. 1984. “The Effect of Vertical Rods on Bubbles in Gas Fluidized Beds.” In Engineering Foundation, 103–10. New York.

Yao, Xiuying, Yongmin Zhang, Chunxi Lu, and Xiao Han. 2015. “Systematic Study on Heat Transfer and Surface Hydrodynamics of a Vertical Heat Tube in a Fluidized Bed of FCC Particles.” AICHE 61: 68–83. doi:10.1002/aic.

Yurong, He, Lu Huilin, Sun Qiaoqun, Yang Lidan, Zhao Yunhua, Dimitri Gidaspow, and Jacques Bouillard. 2004. “Hydrodynamics of Gas-Solid Flow around Immersed Tubes in Bubbling Fluidized Beds.” Powder Technology 145 (2): 88–105. doi:10.1016/j.powtec.2004.04.047.

Zhang, H., P. M. Johnston, J. X. Zhu, H. I. De Lasa, and M. A. Bergougnou. 1998. “A Novel Calibration Procedure for a Fiber Optic Solids Concentration Probe.” Powder Technology 100 (2–3): 260–72. doi:10.1016/S0032-5910(98)00147-8.

Zhu, Haiyan, Jesse Zhu, Guozheng Li, and Fengyun Li. 2008. “Detailed Measurements of Flow Structure inside a Dense Gas-Solids Fluidized Bed.” Powder Technology 180 (3): 339–49. doi:10.1016/j.powtec.2007.02.043.

.

VITA

Haidar Taofeeq was born in Baghdad, Republic of Iraq. He received his Bachelor and Master degrees in Chemical Engineering from University of Nahrain-Baghdad, Iraq in 2003 and 2007, respectively. He worked as an assistance lecturer at Nahrain University/Chemical Engineering Department from 2007 until 2011. Through this period, he founded the petroleum characteristics laboratory, published three journal papers, and taught many classes in chemical Engineering. He joined Florida Institute of Technology in Florida, United States in 2011 and got his second Mater degree in Chemical Engineering in Spring 2014.

In Summer of 2014, Haidar Taofeeq joined the Department of Chemical and Biochemical Engineering at Missouri University of Science and Technology. He earned his third Master degree in Chemical Engineering in Summer of 2015. In the meantime, he worked on his PhD degree and his main research area is studying the impact of vertical immersed tubes on the hydrodynamics of gas-solid fluidized bed reactor.

Haidar Taofeeq has participated at many conferences and journal papers. As well, he has been a member of the Iraqi Engineers Association since 2008 and American Institute for Chemical Engineers (AIChE) since 2016.

In December 2017, he received his PhD in Chemical Engineering from Missouri University of Science and Technology.